

Synthesis and Characterization of Neutral Silicon- and Germanium-based Lewis Superacids for Catalytic Applications

Florian Siegfried Tschernuth

Vollständiger Abdruck der von der TUM School of Natural Sciences der Technischen Universität München zur Erlangung eines
Doktors der Naturwissenschaften (Dr. rer. nat.)
genehmigten Dissertation.

Vorsitz: Prof. Dr. Barbara Lechner

Prüfer*innen der Dissertation:

1. Prof. Dr. Shigeyoshi Inoue
2. Priv.-Doz. Dr. Alexander Pöthig
3. Prof. Dr. Lutz Greb

Die Dissertation wurde am 01.09.2023 bei der Technischen Universität München eingereicht und durch die TUM School of Natural Sciences am 03.11.2023 angenommen.

Alle großen Dinge sind einfach, aber zu den einfachsten Erkenntnissen braucht man die längste Zeit.

Justus von Liebig (1803 - 1873)

Die vorliegende Doktorarbeit wurde im Zeitraum von 19.11.2019 bis zum 31.08.2023 an der Technischen Universität München unter Betreuung von Prof. Shigeyoshi Inoue und in enger Zusammenarbeit mit der WACKER Chemie AG angefertigt.

Danksagung

Zuallererst möchte ich mich herzlichst bei meinem Doktorvater Prof. Shigeyoshi Inoue für die Aufnahmen in seinen Arbeitskreis und das Vertrauen bedanken, das er mir im Zuge meiner Forschungen entgegengebracht hat. Seine Förderung und sein wissenschaftlicher Ehrgeiz haben das Beste aus mir herausgeholt und dieses Projekt erfolgreich vorangetrieben.

In diesem Zusammenhang gilt mein besonderer Dank der WACKER Chemie AG für die finanzielle Förderung sowie für den regelmäßigen wissenschaftlichen Austausch, ohne die diese Promotion nicht möglich gewesen wäre. Hier möchte ich mich speziell bei Herrn Dr. Richard Weidner, Herrn Dr. Wolfram Schindler, Herrn Dr. Niklas Wienkenhöver und Herrn Dr. Maximilian Moxter für enge Betreuung in den letzten vier Jahre bedanken.

Während meiner Zeit am Silicium-Institut konnte ich mich stets auf die freundschaftliche Unterstützung und den ungeminderten Humor meiner lieben Kollegen verlassen. Daher möchte ich mich besonders bei Ramona Baiertl, Martin Doleschal, Teresa Eisner, Matthias Nobis, Andreas Saurwein, Daniel Henschel, Jinyu Liu, Moritz Ludwig, Fiona Kiefer, Andreas Hochholzer und Lukas Bichlmaier sowie natürlich dem gesamten Arbeitskreis der Inoue Gruppe bedanken. Darüber hinaus gilt mein besonderer Dank Franziska Hanusch für die hervorragende Betreuung meiner Masterarbeit sowie für die Unterstützung in unzähligen organisatorischen Situationen. Auch bei Dr. Carsten Troll und dem gesamten Rieger Lehrstuhl möchte ich mich untertänigst für die rasche und unkomplizierte Unterstützung bei diversen Reparaturprojekten und Laborangelegenheiten bedanken.

Eine der schönsten und lohnendsten Freuden an meiner Doktorarbeit war die Betreuung von Abschlussarbeiten und Forschungspraktika. Auch hier möchte ich mich für das mir entgegengebrachte Vertrauen, die hohe Arbeitsmoral und die vielen gemeinsamen Stunden bei meinen Studenten Ekaterina Khrameshina, Anna Gradenegger, Lisa Gremmel, Anna Zehrer und Alex Smith bedanken. Mein besonderer Dank gilt hier jedoch Lukas Bichlmaier für seinen unübertroffenen Ehrgeiz bei der Arbeit und die wunderbare Zeit, die wir im Labor hatten.

Wissenschaftliche Exzellenz fällt nicht vom Himmel und daher möchte ich mich bei der Technischen Universität München für die Bereitstellung der hervorragenden Infrastruktur sowie für die wahrhaft exzellente Ausbildungen während meiner Studienjahre bedanken. Auch wenn ich diesem Club inzwischen selbst beigetreten bin, gilt mein besonderer Dank den deutschen Steuerzahlern für die Finanzierung meiner Ausbildung.

Nun komme ich zu meiner Familie, ohne deren ununterbrochenen Rückhalt und finanzielle Förderung mein Studium und die Promotion in München nicht möglich gewesen wären. Ich möchte mich daher ganz besonders bei meinen Eltern Ingrid Tschernuth und Christof

Tschernuth sowie meiner inzwischen verstorbenen Großmutter Helga Tschernuth für die ausdauernde Unterstützung während der letzten neun Jahre bedanken. Darüber hinaus gilt mein besonderer Dank meinem Lebenspartner Emanuel Kring, der mich die letzten sieben Jahre treu unterstützt und während meiner Promotion begleitet hat. Auch seinen Eltern Barbara Rump-Kring und Gerhard Kring möchte ich für die vielen schönen Stunden und aufbauenden Gespräche danken. Darüber hinaus möchte ich mich bei Herrmann und Gerti Rump für die schöne Zeit in Erding und die vielen gemeinsamen Sonntage bedanken. Es war mir eine wahre Freude.

List of Publications and Conference Contributions

Publications that are part of this thesis

- F. S. Tschernuth, T. Thorwart, L. Greb, F. Hanusch and S. Inoue
Angewandte Chemie International Edition **2021**, *60*, 25799–25803
Title: “Bis(perfluoropinacolato)silane: A Neutral Silane Lewis Superacid Activates Si–F Bonds”
DOI: 10.1002/anie.202110980
DOI: 10.1002/ange.202110980 (German version)
- F. S. Tschernuth, L. Bichlmaier, and S. Inoue
ChemCatChem **2023**, *15*, e202300281
Title: “Catalytic Degradation of Aliphatic Ethers using the Lewis Superacidic Bis(perfluoropinacolato)silane”
DOI: 10.1002/cctc.202300281
- F. S. Tschernuth, L. Bichlmaier, S. Stigler, and S. Inoue
Eur. J. Inorg. Chem. **2023**, e202300388
Title: “Tuning the Lewis Acidity of neutral Silanes using perfluorinated Aryl- and Alkoxy Substituents”
DOI: 10.1002/ejic.202300388
- F. S. Tschernuth, A. Kostenko, S. Stigler, A. Gradenegger and S. Inoue
Dalton Trans. **2023**, Accepted Manuscript
Title: “A Neutral Germanium-centered Hard and Soft Lewis Superacid and its Unique Reactivity towards Hydrosilanes”
DOI: 10.1039/D3DT03626J

Publications beyond the scope of this works

- F. S. Tschernuth, F. Hanusch, T. Szilvási, and S. Inoue
Organometallics **2020**, *39*, 4265–4272
Title: “Isolation and Reactivity of Chlorotetryliumylidenes Using a Bidentate Bis(*N*-heterocyclic imine) Ligand”
DOI: 10.1021/acs.organomet.0c00320
- S. V. Hirmer, F. S. Tschernuth, F. Hanusch, R. Baierl, M. Muhr, and S. Inoue
Mendeleev Communications **2022**, *32*, 16–18
Title: “Modification of bidentate bis(*N*-heterocyclic imine) ligands for low-valent main group complexes”
DOI: 10.1016/j.mencom.2022.01.004
- F. S. Tschernuth, X. Shen, A. Rossi, A. Antonelli and H. Goutebroze
CERN IdeaSquare Journal of Experimental Innovation **2023**, *7*, 18-27
Title: “Entrepreneurial tendencies among highly educated students in Germany and Italy - A cross-national study”
DOI: 10.23726/cij.2023.1412

Conference contributions

- F. S. Tschernuth and S. Inoue
Poster: “Bis(perfluoropinacolato)silane – A Novel Lewis Superacid for Catalytic Applications”
19th International Symposium on Silicon Chemistry (ISOS) – July **2021**, Toulouse, France
(Online Conference)
- F. S. Tschernuth and S. Inoue
Oral Lecture: “Bis(perfluoropinacolato)silane – A Silicon Lewis Superacid”
51st Annual Silicon Symposium (SISY) – March **2022**, San Diego, California
- F. S. Tschernuth and S. Inoue
Oral Lecture: “Catalytic Properties of Neutral Si(IV) and Ge(IV) Lewis Superacids with Perfluorinated Pinacolato Substituents”
International Conference on Phosphorus, Boron, and Silicon (PBSi) – March **2023**, Berlin, Germany

List of Abbreviations

BCF	tris(pentafluorophenyl)borane
CIA	chloride ion affinity
DME	dimethoxyethane
FBN	<i>p</i> -fluorobenzonitrile
FIA	fluoride ion affinity
FLP	frustrated Lewis pair
GB	Gutmann-Beckett
HIA	hydride ion affinity
HOMO	highest occupied molecular orbital
HSAB	hard and soft acids and bases
IR	infrared spectroscopy
LA	Lewis acid
LB	Lewis base
LSA	Lewis superacid
LUMO	lowest unoccupied molecular orbital
NMR	nuclear magnetic resonance
OTol ^F	perfluorocresolato group
PEG-DME	polyethyleneglycol dimethyl ether
Ph ^F	perfluorophenyl group
pin ^F	perfluoropinacolato group
ppm	parts per million
SC-XRD	single crystal X-ray diffraction
sLSA	soft Lewis superacid
TEG-DME	tetraethylenegylcol dimethyl ether
Tol ^F	perfluorotolyl group
TON	turnover number
UV-VIS	Ultraviolet and visible light (spectroscopy)
XIA	“X” ion affinity

Abstract

In light of a threatening climate crisis, the importance of transforming energy-consuming and polluting chemical processes towards an eco-friendly and sustainable industry becomes progressively evident. The method of choice to reduce the energy demand for a chemical transformation is the deployment of a catalyst that decreases the activation energy and, therefore, overall energy consumption of a chemical reaction. Most industrial chemical processes rely on catalyst systems based on precious transition metals that are often expensive, toxic, and suffer from limited availability. A possible alternative to overcome those drawbacks is using earth-abundant, inexpensive, and eco-friendly main group element catalysts. Silicon, for example, is the second most abundant element in the earth's crust and is readily available in sand, quartz, and other minerals.

Nevertheless, the catalytic activity of silicon-centered molecules is mainly determined by Lewis acidity as no d-orbitals are available, and low-valent oxidation states are highly disfavored. Tremendously high Lewis acidities were obtained for silyl cations which prove to be potent catalysts in various organic transformations. Another recent strategy is the synthesis of neutral silicon-centered Lewis superacids by the installation of strongly electron-withdrawing substituents. The so-far reported Lewis superacidic silanes were successfully applied in many laboratory-scale reactions. Nonetheless, this research field is still in its infancy.

In this context, the Ph.D. project at hand was dedicated to synthesizing strongly electrophilic silanes and investigating their catalytic potential for industrially relevant reactions. For this purpose, perfluorinated pinacolato groups were chosen as they combine steric protection and substantial electron withdrawal. The consequent bis(perfluoropinacolato)silane was synthesized and isolated as the acetonitrile mono-adduct. Lewis acidity determinations, including fluoride ion affinity calculation and Gutmann-Beckett assessment, revealed a high potential for catalytic use, which was supported by abstraction experiments that outlined Lewis superacidity. Catalytic experiments displayed a high activity for reactions including hydrodefluorination, carbonyl reduction and hydrosilylation, and depolymerization of polyethylene glycols, while outperforming literature-known catalyst systems.

For broadening the scope also for softer substrates, the respective "softer" germanium-centered analog was synthesized and tested for its reactivity. Again, Lewis superacidity could be proven in experiments and by quantum chemical computations revealing a significantly increased affinity for the activation of hydrosilanes.

By abstracting the strongly bound acetonitrile, the liberated bis(perfluoropinacolato)germane was isolated and successfully applied as a pre-catalyst for the important hydrosilylation of

olefins. The active species in this reaction was identified as a germylene complex formed *in situ* by activating the hydrosilane Et_3SiH and subsequent reductive elimination.

Additional Lewis acidic silanes were synthesized by the installation of perfluorotolyl- and perfluorocresolato substituents, as well as a heteroleptic approach using one perfluoropinacolato group and two perfluorophenyl groups. The obtained silanes were comprehensively characterized, and the Lewis acidities were assessed with the Gutmann-Beckett method.

Zusammenfassung

In Anbetracht der aktuellen Klimakrise wird die Notwendigkeit, energieaufwändige chemische Prozesse in umweltfreundlichere Alternativen für eine nachhaltige Industrie umzuwandeln, immer deutlicher. Die wohl am besten geeignete Methode zur Verringerung des Energiebedarfs einer chemischen Reaktion ist der Einsatz von Katalysatoren, welche die Aktivierungsenergie verringern und somit den Energiekonsum eines Gesamtprozesses herabsetzen. Derzeitige chemisch-industrielle Prozesse beruhen meist auf Katalysatorsystemen auf Basis von edlen Übergangsmetallen, die oft sehr teuer, gesundheitsschädlich, und meist nur schwer zugänglich sind. Eine potenzielle Alternative zur Überwindung dieser Nachteile ist die Verwendung von Katalysatoren auf Basis von leicht verfügbaren, kostengünstigen sowie umweltfreundlichen Hauptgruppenelementen. Silizium zum Beispiel ist das zweithäufigste Element in der Erdkruste und kommt sowohl in Sand, Quarz und verschiedenen anderen leicht abbaubaren Mineralien vor.

Die katalytische Aktivität Silizium-zentrierter Moleküle wird jedoch hauptsächlich von der jeweiligen Lewis Säurestärke bestimmt, da keine *d*-Orbitale zur Verfügung stehen und niedervalente Oxidationsstufen für Silizium meist nicht stabil sind. Extrem hohe Lewis Säurestärken wurden zum Beispiel für Silyl-Kationen beobachtet, welche erfolgreich als Katalysatoren bei einer Vielzahl von organischen Umwandlungen eingesetzt werden konnten. Eine weitere neuere Strategie ist die Synthese von neutralen siliziumzentrierten Lewis-Supersäuren, welche durch den Einbau von stark elektronenziehenden Substituenten hergestellt werden können. Die bisher veröffentlichten Lewis-Supersäuren konnten eine Vielzahl von Reaktionen im Labormaßstab erfolgreich katalysieren. Trotz der vielversprechenden Ergebnisse der letzten Jahre steckt dieses Forschungsgebiet allerdings noch in den Kinderschuhen.

Vor diesem Hintergrund widmet sich die vorliegende Doktorarbeit der Synthese von hoch elektrophilen Silanen und der Untersuchung des katalytischen Potenzials dieser Verbindungen für industriell relevante Reaktionen. Zu diesem Zweck wurden perfluorierte Pinakolat-Gruppen ausgewählt, da sie reaktive Silizium-Zentren durch sterische Abstoßung schützen können und gleichzeitig stark elektronenabziehend wirken. Das davon abgeleitete, zweifach substituierte Bis(perfluoropinacolato)silan konnte erfolgreich synthetisiert und als das Acetonitril-Monoaddukt isoliert werden. Die Charakterisierung der Lewis Säurestärke durch Berechnung der Fluoridionenaffinität und dem Einsatz der Gutmann-Beckett-Methode zeigte ein hohes Potenzial für dessen katalytische Anwendbarkeit auf. Dies wurde darüber hinaus mittels Abstraktionsexperimenten bestätigt, die von der Lewis Superazidität der Verbindung zeugten.

Weitere Reaktionsexperimente zeigten eine hohe katalytische Aktivität für ausgewählte Reaktionen, wie der Hydrodefluorierungsreaktion, der Reduktion und Hydrosilylierung von Carbonylen sowie der Depolymerisation von Polyethylenglykolen. Dabei wurde die katalytische Aktivität Literatur-bekannter Systeme deutlich übertroffen.

Um den Anwendungsbereich auch auf weichere Substrate auszudehnen, wurde das entsprechende Germanium-Analogon synthetisiert und hinsichtlich dieser Reaktivitäten getestet. Auch hier konnte in Experimenten und durch quantenchemische Berechnungen eine Lewis-Supersäure nachgewiesen werden, die jedoch eine deutlich erhöhte Affinität zur Aktivierung von Hydrosilanen aufweist.

Durch Abspaltung des molekular gebundenen Acetonitrils konnte das freie Bis(perfluoropinacolato)german isoliert und erfolgreich als Präkatalysator für die Hydrosilylierung von Olefinen eingesetzt werden. Als aktive Spezies in dieser Reaktion wurde ein niedervalenter Germylen-Komplex identifiziert, der *in situ* bei der Aktivierung des Hydrosilans durch das German und anschließender reduktiver Eliminierung gebildet wird.

Weitere Lewis-saure Silane wurden durch den Einbau von Perfluorotolyl- und Perfluorocresolato-Substituenten sowie durch einen heteroleptischen Ansatz mit einer Perfluoropinacolato-Gruppe und zwei Perfluorophenyl-Gruppen synthetisiert. Die erhaltenen Verbindungen wurden umfassend charakterisiert, und die Lewis-Acidität wurde mit der Gutmann-Beckett-Methode bestimmt.

Table of Contents

1	Introduction	1
2	General Concept of Lewis Acidity	3
2.1	The HSAB Principle	3
2.2	Lewis Superacidity	5
2.3	Assessment of Lewis Acidity	6
2.3.1	Ion Affinities	6
2.3.2	Spectroscopic Methods	7
3	Silicon and Germanium Lewis Acids in Catalysis	12
3.1	Lewis acidic silanes acting as catalysts	13
3.1.1	Stoichiometric reactions with hypervalent silicon intermediates	14
3.1.2	Reactions catalyzed by neutral Si(IV)-based Lewis acids	16
3.2	Silylium ions	18
3.3	Silyliumylidene cations	21
3.4	Neutral Lewis Superacidic Silanes	23
3.5	Neutral Germanium Lewis Superacids in Catalysis	32
4	Assignment of the Ph.D. project	38
5	Bis(perfluoropinacolato)silane: A Neutral Silane Lewis Superacid Activates Si–F Bonds .	41
6	Catalytic Degradation of Aliphatic Ethers using the Lewis Superacidic Bis(perfluoropinacolato)silane	47
7	Tuning the Lewis Acidity of neutral Silanes using perfluorinated Aryl- and Alkyl Substituents	53
8	A Neutral Germanium-centered Hard and Soft Lewis Superacid and its unique Reactivity towards Hydrosilanes	61
9	Summary and Outlook	70
10	Bibliography	77
11	Appendix	82
11.1	Supporting Information Chapter 5	82
11.2	Supporting Information Chapter 6	135
11.3	Supporting Information Chapter 7	175
11.4	Supporting Information Chapter 8	196
11.5	Licenses for the reprint of publications	279

1 Introduction

The reduction of global warming caused by anthropogenic CO₂ emissions and its devastating effects on humanity has been one of the most discussed political and societal topics ever since the Paris Climate Agreement in 2015.^[1] As a result, enormous global efforts have been made to reduce the amount of emitted greenhouse gasses, *e.g.*, by advancing the electrification of individual traffic or the massive expansion of renewable energy sources.^[2]

Despite those recent advances, energy-consuming industrial processes account for almost a quarter of global CO₂ emissions (11.95 GT in 2016), with the chemical sector contributing to an overall global emission of 5.8 % alone.^[3] Nevertheless, the chemical industry is an essential part of economic systems and plays a vital role in strategies targeting the implications of climate change with its indispensable products and materials.^[4] However, for a net-zero scenario, carbon emissions need to decline firmly in the foreseeable future while production capacities are predicted to follow an upward trend.^[5] This can only be achieved by providing a sufficient renewable power supply for energy-intensive transformations and further improving the overall efficiency of industrial chemical processes.^[6]

More than 80 % of industrial chemical goods are manufactured by the use of catalysts, bearing a tremendous future potential for carbons reduction through the improvement of catalytic processes.^[7] For reasons of durability, product separation, and in many cases, the possibility of solvent-free conversion, the vast majority of industrial catalysts are heterogeneous.^[8] Especially shape-selective petrochemical transformations are primarily catalyzed using synthetic zeolites. This material comprises microporous acidic aluminosilicates and demonstrates an outstanding success story of main group element catalysts since their introduction into refinery technology in 1962.^[9]

Homogenous catalysts, on the other hand, are industrially applied when milder reaction conditions, high catalyst activities, and selectivity are required.^[10] Transition metal-based homogenous catalysts account for about 15 % of industrial chemical processes and are used to produce bulk-, fine-, and specialty chemicals.^[8, 11] One inherent drawback of homogenous systems is the challenging separation from product material, often leading to significant catalyst losses.^[12] Especially for late transition metal catalysts, this is highly disadvantageous concerning raw material costs and environmental consequences of releasing heavy metals.^[13] The Pt-catalyzed olefin hydrosilylation for curing silicone elastomers is a prominent example of this effect. With the Pt(0) catalyst completely remaining in the product material, the process consumes almost 3 % of the global annual platinum production.^[14] In this regard, developing

innovative catalyst systems by using earth-abundant, inexpensive, and environmentally friendly elements is particularly interesting.

In recent history, main group element-based catalysts have drawn much attention, introducing transition metal-like catalytic properties for a variety of relevant transformations.^[15] Especially, silyl cations and low valent silyliumylidene species have demonstrated tremendous activity for Lewis acid-catalyzed reactions, including *Diels-Alder* additions, C-H arylations and alkylations and even olefin hydrosilylation for siloxane crosslinking.^[16] However, cationic systems (like silyl cations) face immanent drawbacks caused by undesired counter-ion interactions, low functional group tolerance, and limited solubility.^[17]

A recent approach to overcome those limitations is the synthesis of strongly Lewis acidic but neutral main group element compounds that are tested for their catalytic properties. Continuous research in this field could bring earth-abundant and easily accessible group 14 elements into the range of industrial-relevant homogenous catalysis. Nevertheless, this field is in its infancy, and creating a valid alternative for transition metals in homogeneous catalysis will require continuous research.

2 General Concept of Lewis Acidity

The concept of Lewis acidity was introduced in 1923 by Gilbert N. Lewis, defining bases as substances that possess a free pair of electrons that can be donated to form a chemical bond. Conversely, acids are substances that accept such a free pair of electrons.^[18] Consequently, Lewis acids (LAs) form adducts when donor molecules, or in other words, Lewis bases (LBs), are present. The affinity of the two molecules to form a Lewis pair strongly depends on attractive electrostatic, covalent, and dispersive interactions as well as steric repulsion (Figure 1).^[19]

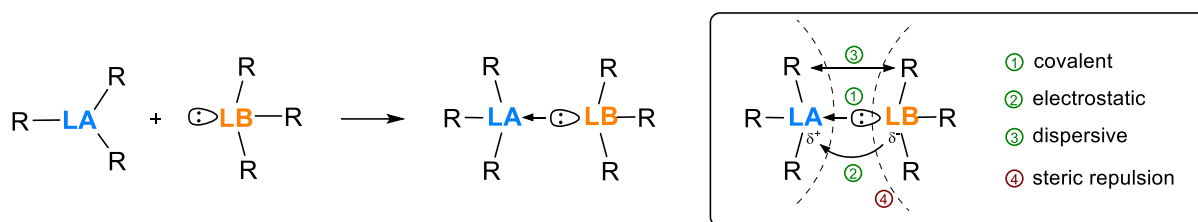


Figure 1: Left: Lewis acid (LA)-base (LB) pair formation; Right: Schematic depiction of attractive and repulsive interactions contributing to Lewis pair formation. Content extracted from reference.^[19]

The affinity of Lewis pairing strongly depends on the nature of the participating molecules, and adduct formation is more favorable if both counterparts share similar characteristics regarding size and polarizability.^[20] Those experimentally found effects led to the development of the hard and soft acids and bases (HSAB) concept.

A slightly different energy scheme was introduced by Drago where both electrostatic (hard) and covalent (soft) interactions contribute to the overall reaction enthalpy. The energetic gain upon Lewis pair formation was described by the following *ECW* formula (I):

$$\Delta H = E_{LA} \cdot E_{LB} + C_{LA} \cdot C_{LB} - W \quad (\text{I})$$

H is the enthalpy, E is the electrostatic interaction of the Lewis Acid LA and Lewis Base LB , C is the covalent interaction, and W is a constant concerning steric repulsion.^[19, 21] Due to the large number of influencing variables, a simple classification of Lewis acids using a general scale for acid strength is impossible.^[19]

2.1 The HSAB Principle

The differing affinities of certain Lewis acids and bases to form specific adducts with each other was discovered by Ralph G. Pearson roughly 60 years ago. In 1963 he published experimental observations as his famous HSAB concept, where a categorization into “hard” and “soft” Lewis acids and bases was made.^[22] According to this concept, hard acids are acceptors that are small-

sized, have a high positive charge, and don't contain free pairs of electrons. Soft acids, on the other hand, are large acceptors with low positive charge and unshared electron pairs. The mentioned determinants sum up to either high electronegativity and low polarizability (hard acids) or low electronegativity and high polarizability (soft acids). A similar classification was made for donor molecules that are defined as hard bases when they are hard to oxidize and possess a high electronegativity as well as low polarizability. Soft bases, consequently, are easy to oxidize and hold a low electronegativity and high polarizability (Figure 2). Pearson's observations conclude, "*Hard acids prefer to bind hard bases, and soft acids prefer to bind soft bases*".

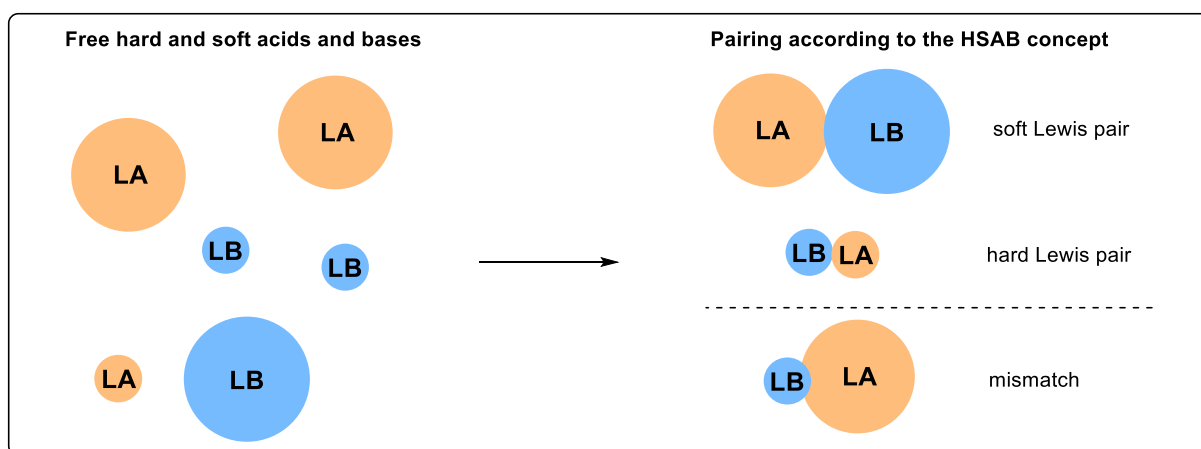


Figure 2: Lewis adduct formation according to the HSAB principle. Orange spheres resemble Lewis acids (LA), and blue disks are Lewis bases (LB).

The initial concept also defines "borderline" acids and bases that do not react as expected and form mismatches due to macroscopic effects.^[20] Even though the concept was initially introduced as a summary of experimental observations, it was soon applied as a theoretical approach to explain chemical reactivity in organic synthesis.^[23] Especially for catalytic applications, the HSAB provided valuable estimations for the selectivity and reactivity of the employed catalysts.^[24] However, as it was rather meant as an qualitative approach to describe the reactivity of certain Lewis acids and bases, the HSAB concept fails to reliably predict chemical transformations.^[25] Nevertheless, the HSAB concept is true for most adduct formations. Yet, it should be used carefully and not overinterpreted, as other influences besides polarizability strongly affect adduct formation and chemical reactivity.^[26] Therefore, it is still valid today in its original denotation but cannot be used as a general measure for the strength of Lewis acids or bases.

2.2 Lewis Superacidity

The term superacids was historically used for Brønsted acids stronger than sulfuric acid.^[27] Not differentiating between Brønsted and Lewis acid, Olah *et al.* generally defined a superacid as a element halide more acidic than anhydrous AlCl_3 .^[28] Apart from this early definition, the term superacid was used in various contexts, including cationic SiF_3^+ species in the gas phase,^[29] silyl cations applied for Diels-Alder reactions,^[30] or Lewis acids obtained from Brønsted superacids,^[31] as summarized in a recent review.^[19] All those definitions seem arbitrary and focused on a specific reactivity or property of a Lewis acid in a particular circumstance rather than giving a general definition. This was changed in 2008 by the Krossing group classifying that “*Molecular Lewis acids, which are stronger than monomeric SbF_5 in the gas phase, are Lewis Superacids*”. To quantitatively measure and compare the strength of Lewis acids, the group used fluoride ion affinity (FIA) values and defined the exceptional Lewis acid SbF_5 as the benchmark for superacidity.^[32] Even though this definition has been widely applied since its introduction, it is still not comprehensive as it excludes multidimensional interactions best described by the HSAB concept. For example, according to the FIA value, $\text{Al}(\text{C}_6\text{F}_5)_3$ is a Lewis superacid (LSA). Still, its affinity towards soft bases like hydride is significantly minor compared to $\text{B}(\text{C}_6\text{F}_5)_3$, which is a much weaker Lewis acid on the FIA scale. The Greb group additionally defined soft Lewis superacids (sLSA) using the hydride ion affinity (HIA) scale to compensate for only considering the affinity towards the hard Lewis base fluoride. As a benchmark for superacidity, the strong hydride acceptor tris(pentafluorophenyl)borane was chosen due to its significance in laboratory catalysis and frustrated Lewis Pair (FLP) chemistry.^[15b, 33] According to Greb’s definition, “*Molecular Lewis acids that have a larger HIA than $\text{B}(\text{C}_6\text{F}_5)_3$ in the gas phase are soft Lewis superacids (sLSA)*”.^[19] This additional classification adds to a more comprehensive definition of Lewis superacids, as depicted in Figure 3.

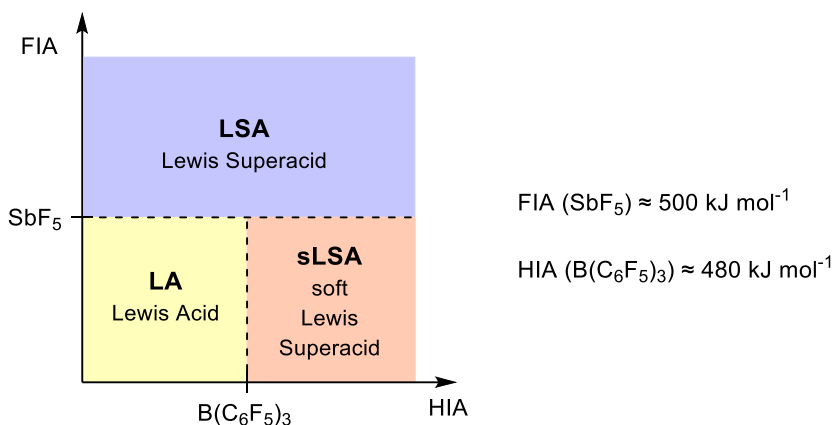


Figure 3: Visual depiction of Crossing's classification of Lewis superacids for molecules with higher FIA values than molecular SbF_5 and Greb's comprehensive addition of soft Lewis superacids for molecules with higher HIA values than $\text{B}(\text{C}_6\text{F}_5)_3$. Content extracted from reference.^[19]

2.3 Assessment of Lewis Acidity

As outlined in the previous sections, a Lewis acid is an electron pair acceptor with the affinity to bind donor molecules, also known as Lewis bases. This affinity strongly depends on the nature of the considered acid molecule and its counterpart, as the adduct formation depends on a multitude of determinants that are not straightforward to predict.^[26, 34] Nevertheless, the emergence of Lewis acids in chemistry and catalysis created a demand for convenient scales to access and compare the strengths of Lewis acids. As a result, a variety of methods were developed and applied trying to gauge Lewis acidities in different contexts. The most applied methods are either based on the thermodynamic energy gain during adduct formation, accessible through ion affinity calculations, or effective electron withdrawal from standardized donor molecules, which are used as probes in spectrometric acidity experiments. Furthermore, less applied intrinsic properties of uncoordinated Lewis acids can also be used to theoretically quantify Lewis acid strength, however they neglect beneficial effects caused by adduct formation.^[35] Section 2.3 summarizes the main methods used in recent years to determine Lewis acid strength in the chemistry of molecular group 13 and 14 compounds.

2.3.1 Ion Affinities

Ion affinity values are a versatile method to access the acidity of an acceptor molecule concerning a defined Lewis base such as fluoride (FIA), hydride (HIA), or chloride (CIA). In principle, the affinity to any ion or substituent can be used to define a one-dimensional measure of Lewis acid strength. The most applied measure for Lewis acids is the FIA, which represents the reaction enthalpy upon molecular adduct formation between the considered Lewis acid and the hard fluoride anion.^[36] It, therefore, can be seen as a determinant for hard Lewis acids concerning the HSAB principle.^[37]

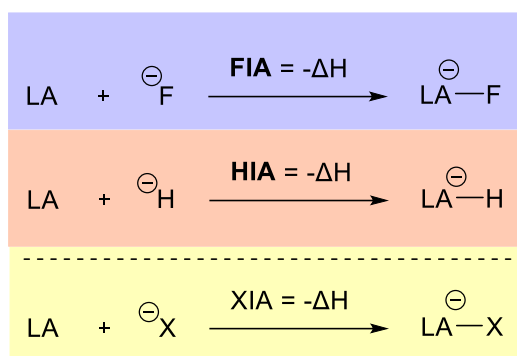


Figure 4: Schematic depiction of ion affinity values derived from the reaction enthalpy of Lewis adduct formation or negative bond dissociation energies of Lewis adducts.

Although different methodologies can be used to obtain FIA values, a computational approach considering isodesmic reactions anchored to experimentally or theoretically known fluoride bond dissociation energies (of $\text{COF}_3^-/\text{COF}_2$ or $\text{Me}_3\text{SiF}/\text{Me}_3\text{Si}^+$) was established (Figure 5).^[36b, 36c] As anions are more challenging to compute than neutral or cationic species, more consistent FIA values were obtained using the Me_3Si^+ system as an anchor point. The final FIA values are calculated by subtracting the heterolytic fluoride bond dissociation enthalpy of Me_3SiF from an isodesmic reaction enthalpy of a given substrate with Me_3SiF . Consequently, FIA values are to be understood as energy values and are usually expressed in kJ mol^{-1} .

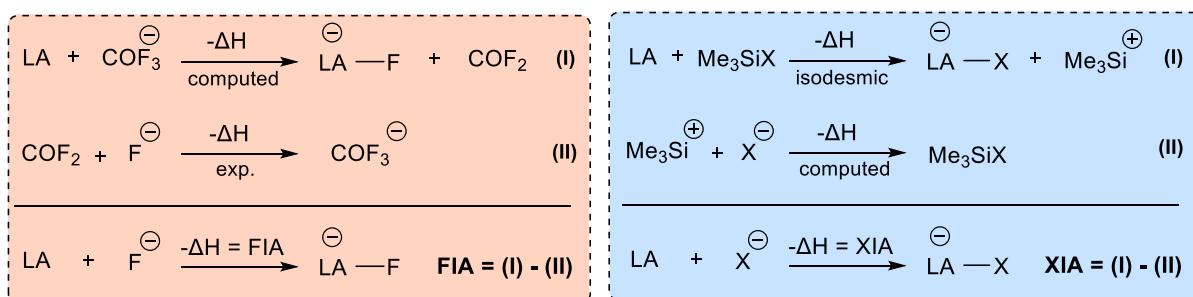


Figure 5: Left: Calculation of the FIA of a LA using an isodesmic reaction approach with the experimentally defined $\text{COF}_3^-/\text{COF}_2$ anchor system; Right: General XIA calculation method using an isodesmic reaction referenced to a $\text{Me}_3\text{SiX}/\text{Me}_3\text{Si}^+$ anchor system. Content obtained from reference.^[35, 38]

The same isodesmic methodology applies to calculating HIA values and other ion affinities. For initial HIA determinations, the experimentally accessible $\text{BH}_4^-/\text{BH}_3$ anchor system was introduced.^[39] However, modern approaches also use the $\text{Me}_3\text{SiX}/\text{Me}_3\text{Si}^+$ anchor system.^[38]

2.3.2 Spectroscopic Methods

Apart from gas phase affinity calculations requiring strong computing power and the right level of theory, a more practical approach is targeting the effective Lewis acidity of an acceptor molecule by adduct formation with certain Lewis bases. The applied donor molecules bind strongly to the investigated Lewis acid and can be analyzed by suitable spectroscopic methods

as the Lewis acid withdraws electron density from the Lewis base.^[35] Potential analytical systems use different probe molecules and spectroscopic techniques such as UV-VIS-, fluorescence-, IR-, and NMR spectroscopy, among others.^[40] The main advantage of those methods is the easy applicability on a laboratory scale. Nevertheless, no global or intrinsic Lewis acid properties are analyzed. Consequently, values obtained depend strongly on the interaction between the studied Lewis acid and the probe molecule used, as well as on the effects of physicochemical conditions such as solvent effects.^[35] The two most popular indirect scales for neutral Lewis acidic molecules (especially boron compounds) are the Gutmann-Beckett and Childs methods using ^{31}P and ^1H probes for NMR spectroscopy.^[41] Recently an additional method was introduced, especially for assessing the Lewis acidity of stabilized silyl cations by ^{19}F NMR spectroscopy presented by the Müller group.^[42]

Gutmann Beckett Method

The Gutmann-Beckett (GB) method is the most popular NMR spectroscopic method for characterizing an acceptor molecule. It uses Et_3PO as a ^{31}P NMR probe that readily undergoes adduct formation with Lewis acids, leading to an electron withdrawal and therefore deshielding of the ^{31}P nucleus. As a result, a distinct downfield shift of the ^{31}P NMR signal can be measured that is characteristic for the investigated Lewis acid.^[35, 41] The method was initially developed by Viktor Gutmann in 1975 for the empirical assessment of the electrophilicity of solvents which affects the reactivity of organometallic compounds.^[43] For the classification of solvent molecules, Gutmann introduced a scale of acceptor numbers (AN) that linearly correlates the $\Delta\delta(^{31}\text{P})$ NMR shift of Et_3PO in the respective solvent to the shifts of Et_3PO in hexane ($\text{AN} = 0$) and a mixture of SbCl_5 in dichloroethane ($\text{AN} = 100$) as defined reference points. The acceptor number is then accessible by the linear equation (II) that, according to Gutmann's original publication, can be further simplified yielding equation (III).^[44]

$$\text{AN} = \frac{\delta(^{31}\text{P}, \text{solvent } x) - \delta(^{31}\text{P}, \text{hexane})}{\Delta\delta(^{31}\text{P}, \text{SbCl}_5)} \cdot 100 \quad (\text{II})$$

$$\text{AN} = \Delta\delta(^{31}\text{P}) \cdot 2.348 \quad (\text{III})$$

The same methodology was then adapted by Michael A. Beckett in 1996 to investigate the Lewis acidity of boron centers and correlated the obtained acceptor numbers to their activity for initiating catalytic epoxide polymerizations.^[45] This adaptation led to the development of the so-called Gutmann-Beckett method, where the Lewis acid of investigation is reacted with Et_3PO , usually in a non-polar solvent like pentane or dichloromethane. Although the concept

of acceptor numbers was of significant relevance for the initial development of the method, modern approaches usually only use the $\Delta\delta(^{31}\text{P})$ NMR shift of the Lewis adduct concerning the shift of uncoordinated Et_3PO (Figure 6).^[41, 46]

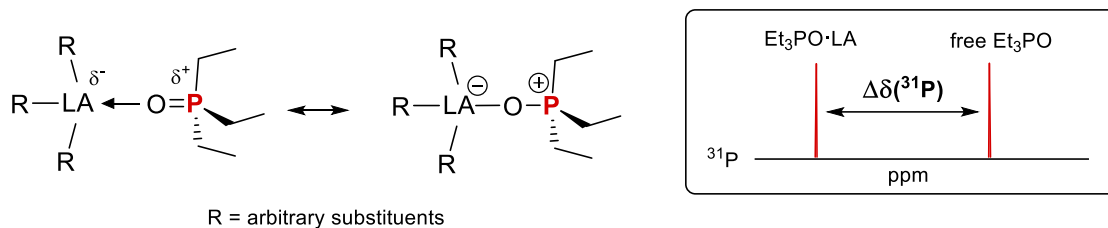


Figure 6: Left: Lewis adduct formation of Et_3PO during GB acidity assessment; Right: Schematic depiction of the resulting NMR downfield shift due to electron withdrawal from the ^{31}P nucleus.

Even though the GB method has been widely applied as a measure for Lewis acidity in recent years, several drawbacks need to be addressed. The very first impediment is that Et_3PO is considered a hard Lewis base due to the strong polarization of the P–O bond.^[35] Therefore, the affinity to bind soft Lewis acids is less pronounced than for hard acids, according to the HSAB principle.^[22] This issue was addressed in the literature using softer NMR probes such as Et_3PS or Me_3PSe .^[44, 47] However, those variants are far less applied than the original GB method. Other factors that impact the Lewis pair formation and, therefore, electron withdrawal from the ^{31}P nucleus, are the adjustment of an association equilibrium, uncorrelated NMR shielding, deformation energies, and London dispersion interactions of the substituents.^[35]

Childs Method

A further method was developed in 1981 by Ronald F. Childs for the empirical classification of Lewis acid catalysts for the complexation of unsaturated nitrile and carbonyl compounds. As the initial formation of a substrate-catalyst Lewis pair is a determinant for the chemoselectivity of specific reactions, the study's goal was to give a scale for Lewis acidity, especially regarding carbonyl substrates. As a result, an NMR spectroscopic method was developed using the H^3 proton signal of *trans*-crotonaldehyde as a suitable NMR probe (Figure 7). For the application of the method, the Lewis acid of investigation is mixed with *t*-crotonaldehyde in the non-polar solvent dichloromethane, and the reaction mixture is analyzed by ^1H NMR spectroscopy. In analogy to the GB method, the $\Delta\delta(^1\text{H}^3)$ NMR shift referenced to free *t*-crotonaldehyde is used as a scale for the Lewis acidity of the acceptor molecule.^[48]

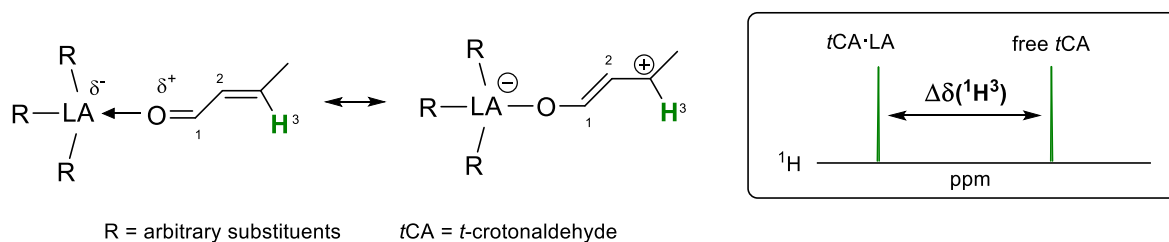


Figure 7: Left: Lewis adduct formation of *trans*-crotonaldehyde with an arbitrary Lewis acid (LA); Right: Schematic depiction of the resulting 1H NMR downfield shift due to electron withdrawal from the H^3 proton.

It could be shown that for a set of common Lewis acid catalysts such as BBr_3 or $TiCl_4$, the observed 1H NMR shifts of the H^3 proton correlate on a linear scale with the employed Lewis acids. Consequently, the method was applied as a convenient additional measure of Lewis acid strengths.^[49] Despite its simple application, the method on its own, though, fails to reliably predict catalyst activity based on the $\Delta\delta(^1H^3)$ NMR shift as physicochemical interactions affect the adduct formation.^[50] The method is also restricted for use on exceptionally weak or strong Lewis acids due to limited association constants or decomposition of the aldehyde.^[51] Because of the more covalent C=O bond, crotonaldehyde is considered a softer Lewis base when compared to Et_3PO , which is why the Childs method can provide a convenient supplementary tool for the assessment of Lewis acidity, especially when HSAB influences come into play.^[52]

Determination with *p*-Fluorobenzonitrile

Recently the Müller group introduced an additional NMR spectroscopic method for the Lewis acidity assessment of stabilized silylium cations. Trivalent silicon cations render among the strongest Lewis acids available for chemical transformations.^[42] Due to their exceptionally high reactivity, they are usually stabilized by weak donor molecules, fine-tuning the Lewis acidity of the resulting complex.^[53] The group initially gauged the Lewis acidity of a set of donor-stabilized silylium cations with the Gutmann-Beckett method and obtained inconsistent results as some of the stabilizing donor molecules were replaced by the strong Lewis base Et_3PO . Because the Childs method could not be applied to silyl cations, the Müller group investigated the use of *p*-fluorobenzonitrile as a weaker ^{19}F NMR probe molecule and obtained suitable results that align well with calculated FIA values. However, no linear correlation was found.^[42]

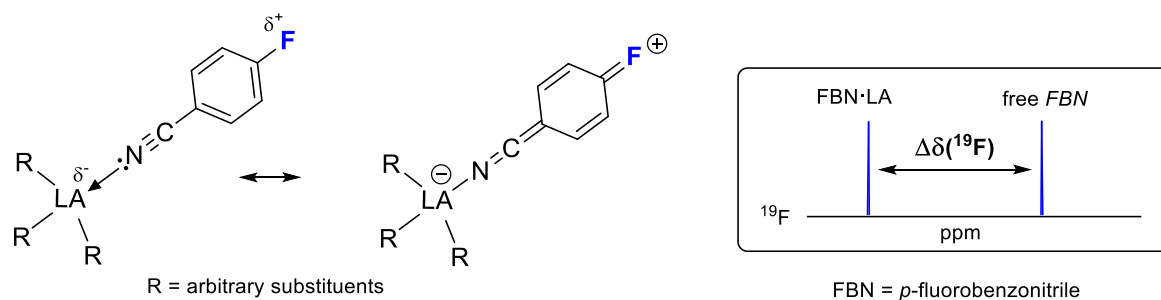


Figure 8: Left: Lewis adduct formation of *p*-fluorobenzonitrile with an arbitrary Lewis acid (LA); Right: Schematic depiction of the resulting ^{19}F NMR downfield shift due to electron withdrawal from the *para*-F substituent.

The method is analogously performed to the previously described NMR experiments as a Lewis adduct is formed between the Lewis acid and the probe molecule in a non-coordinating solvent like dichloromethane leading to a shift of the recorded ^{19}F NMR signal. Also the $^1J_{\text{C-F}}$ coupling constant can be used to gauge the Lewis acidity upon adduct formation.^[42]

3 Silicon and Germanium Lewis Acids in Catalysis

The field of silicon-centered Lewis acids has been of great interest in recent years. Especially silyl cations and Lewis acidic silanes were recognized for their acid strength and applicability for homogenous catalysis on a laboratory scale.^[54] As silicon is the second most abundant element in the earth's crust, this bears great potential for developing sustainable and cost-effective catalyst systems to transition towards an eco-friendly chemical industry.^[55] Because of the tendency to expand its valence shell, forming hypervalent complexes, organosilicon compounds and silicon halides were used in traditional Lewis acid-mediated transformations.^[54b] The catalytic activity of silicon molecules strongly depends on the Lewis acidity and steric accessibility of the central element, which can be boosted by the installation of electron-withdrawing groups such as triflate (OTf^-) or perfluorinated alkyl, alkoxy, or aryl substituents.^[56] Even more vital Lewis acids are formed by the abstraction of those substituents, yielding silylium- or silyliumylidene cations (Si(II) species)^[57] that show tremendous activity for a variety of chemical transformations.^[54a] Silylenes are neutral and ambiphilic silicon(II) species that can oxidatively add small molecules such as H_2 , CO_2 , NH_3 or ethylene among others.^[58] Nevertheless, cationic and low-valent silicon species are highly elusive and difficult to control without the presence of stabilizing donors.^[59]

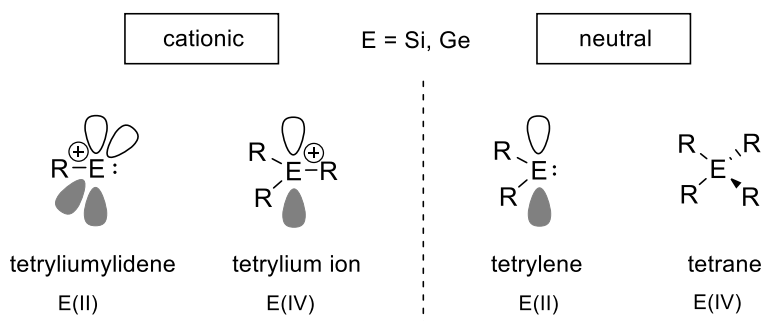


Figure 9: Generalized depiction of silicon- and germanium-centered Lewis acids as low- and tetravalent species with and without positive charge. No stabilizing donor-molecules are depicted.

To overcome this drawback, the synthesis of neutral but highly Lewis acidic silanes, so called Lewis superacids, and their application for catalysis has been an uprising research field in recent history as outlined explicitly in chapter 3.4.

Another potential compound class, which is however less researched, are germanium-centered Lewis superacids. Due to the position in the periodic table, germanium is easier to polarize and more stable in low-valent oxidation states when compared to silicon.^[60] This affects the nature of the corresponding Lewis acids such as germylium ions,^[61] germyliumylidenes,^[62] germylenes^[63] as well as germanes^[64] and enables additional catalytic reactivities that are not accessible with silicon-centered Lewis acids alone.

3.1 Lewis acidic silanes acting as catalysts

As silicon is an element of the 14th group with four electrons in its valence shell, it usually engages bonds to four other atoms to fulfill the Langmuir-Lewis octet rule.^[60, 65] Silicon compounds, however, can expand their coordination sphere by forming hypervalent complexes that are penta-, hexa-, hepta-, and even octa-coordinated.^[66] This effect was first recognized independently by Gay-Lussac and Davis in the early 19th century by the coordination of NH₃ to SiF₄ and the observation of the [SiF₆]²⁻ anion.^[67] Consequently, even neutral silanes with a formally saturated electron octet can act as Lewis acids binding up to four additional donor molecules. This unusual behavior was initially explained by the hybridization of the 3*p*-orbitals with the empty 3*d*-orbitals of silicon.^[68] This theory, however, was discharged as the *d*-orbitals are too diffuse to undergo hybridization within a silicon atom.^[69] More modern approaches explain the affinity to expand the valence shell of late period 3 elements by forming an electron-rich 3-center 4-electron bond involving the silicon *p*-orbitals for each additional substituent. Therefore, the geometric structures of penta- and hexa-coordinated species are explained by sp²- and sp-hybridization of the orbitals involved in the remaining traditional covalent bonds (Figure 10).^[70]

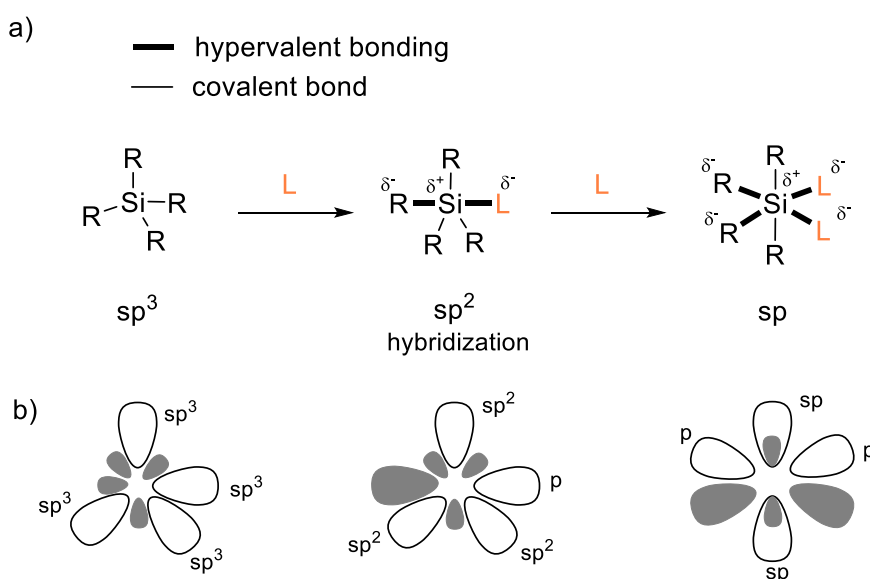


Figure 10: Depiction of hypervalent bonding of silicon(IV) compounds with arbitrary substituents (R) and ligands (L) (a) and the corresponding orbitals (b). Content is taken from literature.^[70-71]

As a result, hypervalent bonds are formed that are linearly oriented around the central silicon atom. The hypervalent bonds are elongated and more polarized with a negative charge distribution on the *p*-orbital of the ligands, causing a nucleophilic character.^[71] The mechanism of hypervalent bonding of group 14 elements is heavily discussed in the literature and generally questions a strict obedience to the octet rule.^[72] Also, heavier group 14 element complexes (E

= Ge, Sn, Pb) show hypervalent tendencies with the same best described by the 3-center 4-electron theory.^[73] Theoretic studies on group 14 halides in the gas phase outline a higher stability for hypervalency (hyper coordination) with heavier central elements, which is explained by lower reorganization energies.^[74] Nevertheless, the ability of neutral silicon molecules to bind additional donors leading to an increased bond polarization of the remaining substituents, was successfully exploited for several catalytic reactivities as outlined in the following chapter.^[70]

3.1.1 Stoichiometric reactions with hypervalent silicon intermediates

Organosilicon molecules, especially those holding organic and halide substituents, can be activated by the additional coordination of a Lewis base.^[70] As discussed in the previous chapter, the electron density is redistributed among the hypervalent bonds, thus leading to an increased nucleophilicity of the attached ligands. This effect was exploited in several reactions in synthetic organic chemistry as demonstrated in the following chapter.^[71] Two major classes of reactions can be divided where stoichiometric amounts of hypervalent silicon intermediates are present:

In the first class, an activated ligand of the silicon intermediate is transferred to an external or coordinated substrate.^[71] In this case, the employed silicon species acts as an activated nucleophile (Figure 11, a). Such reactions include, for instance, the Lewis base-mediated reduction of carbonyls, imines, or nitroaromatic compounds with HSiCl_3 , as demonstrated in Figure 11 b and c.^[75]

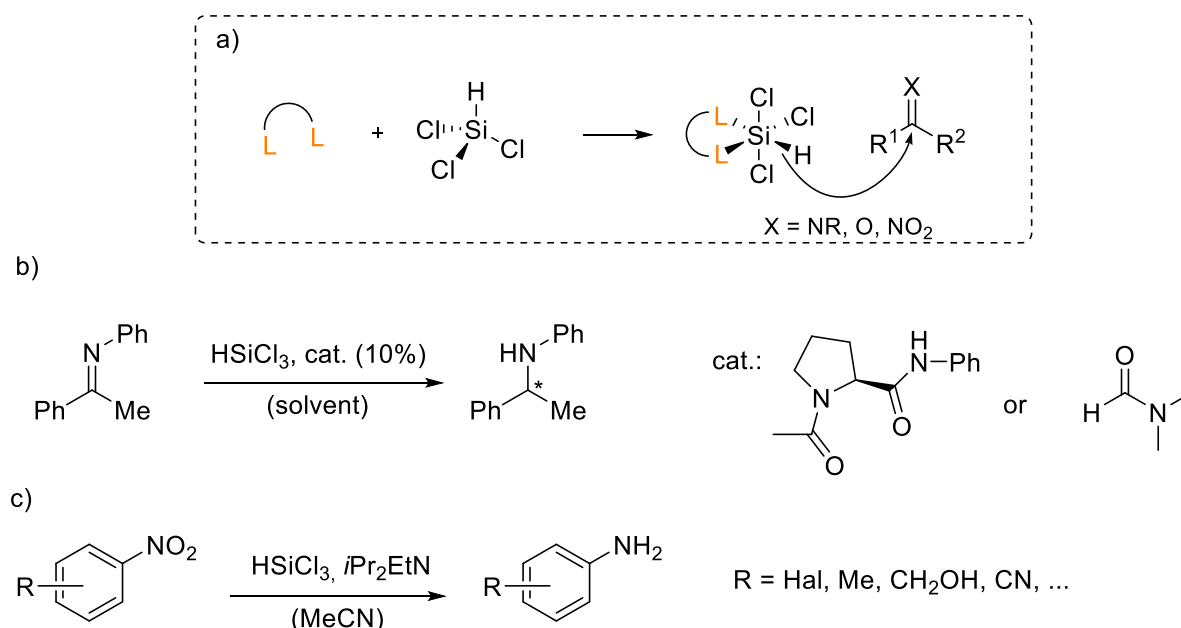


Figure 11: Schematic reduction of carbonyls, ketones, and nitro groups, mediated by the Lewis base activation of HSiCl_3 (a) with specific examples for the reduction of an imine and nitroaromatic

compounds, given in the literature (b and c). Only selected catalysts are shown. Content is taken from literature.^[71]

Furthermore, hydride or chloride substituents of chlorosilanes can be transferred to an electrophilic substrate, enabling selective epoxide openings catalyzed by the coordination of a Lewis basic ligand. The proposed mechanistic cycles of such reactions involve the substrate coordinating to the Lewis acidic silicon atom.^[76] Moreover, catalytic Lewis base activation can achieve the transfer of silicon-bound allyl groups to external carbonyls and imines as well as aldol reactions of enoxysilane derivatives. By employing chiral bases, such as chiral bisphosphoramides for substrate activation, stereoselectivity can be targeted among the reactions mentioned in this paragraph.^[71]

The second class of Lewis base-mediated reactions involving stoichiometric silanes include the prior activation of an electrophilic substrate due to coordination to a hypervalent silicon intermediate. In this regard, allylations and aldol reactions of carbonyl species can be mediated by SiCl_4 in the presence of catalytic Lewis bases. In both cases, the chlorosilane is transferred to the product molecule and subsequently cleaved off upon aqueous workup. Mechanistic investigations for both reaction types outline the coordination of the substrate to the base-activated chlorosilane intermediate, followed by a subsequent attack of the external nucleophile. Figure 12 summarizes the SiCl_4 -mediated allylation of an aromatic carbonyl by forming a hypervalent silyl intermediate, catalyzed by the coordination of a bidentate chiral phosphamide, presented in the literature.^[77]

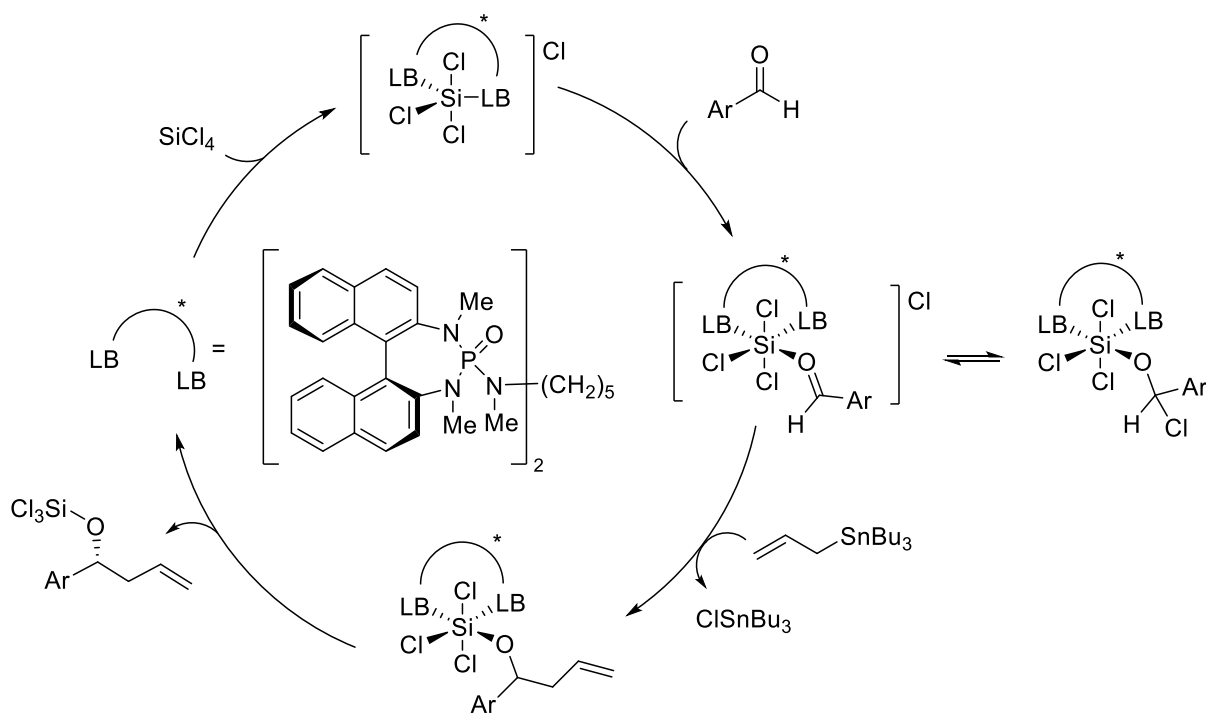


Figure 12: Enantioselective allylation of a carbonyl species mediated by chiral Lewis base-activated SiCl_4 . Content is taken from literature sources.^[71]

Even though these examples demonstrate the necessity of strongly Lewis acidic hypervalent silicon species formed as reaction intermediates, the catalytically active species are the coordinating Lewis bases.^[71]

3.1.2 Reactions catalyzed by neutral Si(IV)-based Lewis acids

Besides stoichiometric reaction intermediates forming upon base coordination, Lewis acidic silanes such as Me_3SiOTf were successfully applied also as catalysts for chemical transformations, including aldol-type and allylation reactions. The Noyori group discovered that Me_3SiOTf catalyzes the stereoselective aldol condensations of acetals and silylenol ethers.^[78] The initially low catalyst activity could be enhanced by the addition of $\text{B}(\text{OTf})_3$, forming a partial silyl cation by triflate abstraction (Figure 13, a).^[79] With $i\text{Pr}_3\text{SiOTf}$ instead of Me_3SiOTf , even higher conversion and stereoselectivity were achieved (Figure 13, b).^[80] Me_3SiOTf was also successfully used for catalytic allylation of acetals and aldol-type condensation between silylenol ethers with imines and carbonyls, without the presence of additional co-catalysts, among other reactions (Figure 13, c).^[81]

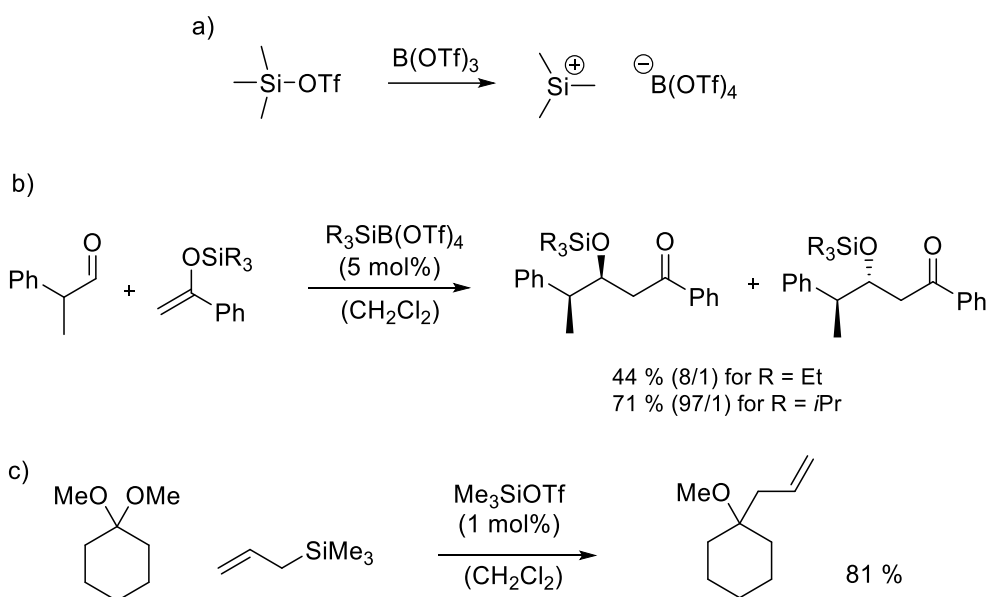


Figure 13: Formation of a silyl cation by the reaction of Me_3SiOTf with $\text{B}(\text{OTf})_3$ (a) which is used for the enantioselective aldol-type condensation between silylenol ethers and aldehydes (b). Reaction (c) demonstrates the application of Me_3SiOTf in the Lewis acid-catalyzed allylation of 1,1-dimethoxycyclohexane. Content is taken from literature sources.^[54b]

Other reactions using silanes for catalysis include Diels-Alder reactions and glycosidations. Even though these reactions are known explicitly for Lewis acid-mediated catalysis, only low conversions were observed.^[54b] Significantly better results for this reaction type were found for silyl cations, which are described in chapter 3.2. Further examples of reactions that were catalyzed by Me_3SiOTf include the reduction of ketones that are masked as acetals in the

presence of hydrosilanes or the Baeyer-Villiger-type oxidations of cyclic ketones using bissilyl peroxides (Figure 14, a-b).^[82] Besides the historic implementation of Lewis acidic triflyl silanes, more recently also genuine SiCl_4 was successfully used in Aza-Michel additions under solvent-free conditions (Figure 14, c).^[83]

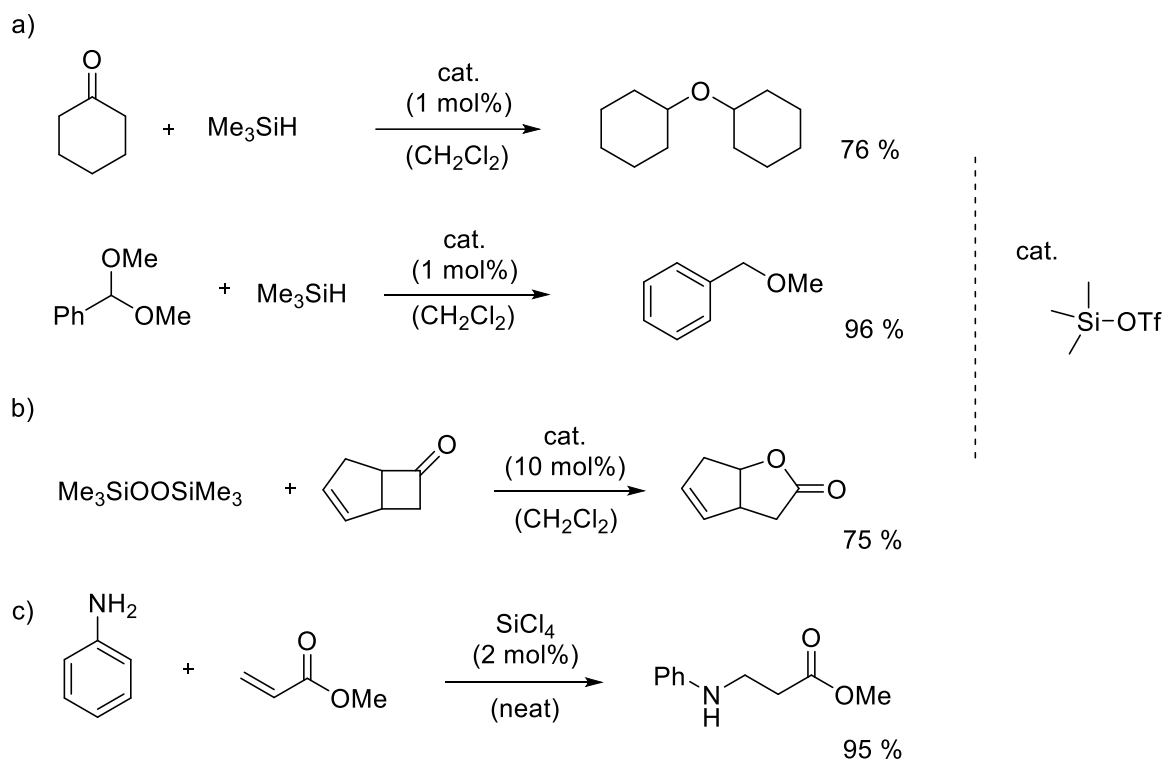


Figure 14: Lewis acid-mediated reduction of ketones and acetal compounds with Me_3SiH (a) and the Baeyer-Villiger-type ketone oxidation with peroxosilanes (b) in the presence of catalytic Me_3SiOTf . Section (c) shows the Aza-Michael addition of aniline and methyl acrylate, catalyzed by SiCl_4 .

Although most of the mentioned stoichiometric and catalytic transformations involving Lewis acidic silanes were studied in the late 20th century, the chemistry of silane-based Lewis acids is experiencing a resurgence in recent years. Silanes containing electron-withdrawing perfluorinated alkyl groups and hypervalent silicon complexes were initially used for the trifluoromethylation of electrophilic organic substances such as aldehydes or ketones.^[84] When multiple trifluoromethyl groups are installed, highly thermolabile compounds were obtained that rapidly decomposed.^[85]

Nevertheless, isolable and highly Lewis acidic silanes were recently obtained by the Hoge group when using perfluoroethyl (CF_3CF_2-) substituents. The group demonstrated the direct synthesis of several perfluoroethyl-substituted silanes and stable fluorosilicate species. The challenging synthesis of the elusive $\text{Si}(\text{CF}_2\text{CF}_3)_4$ was achieved by the direct fluorination of preformed $\text{Si}(\text{C}_2\text{F}_5)_3\text{C}_2\text{H}_5$ with F_2 (Figure 15, a). According to DFT calculations at the B3LYP/6-311+ +G(2d) level of theory, the compound holds an exceptionally high FIA of

420 kJ mol⁻¹.^[56c, 86] With several main group element Lewis acids in hands, the Hoge group investigated the applicability of those compounds for the catalytic hydrogen transfer reaction of 1,3,5-trimethylcyclohexa-1,4-diene, showing significant activity (Figure 15, c).^[87] This catalytic disproportionation reaction is known to be catalyzed by the benchmark Lewis acid B(C₆F₅)₃.^[88] Another strategy to enhance the activity of Lewis acids is the use of frustrated Lewis pairs (FLP), where adduct formation is sterically blocked.^[89] The Mitzel group followed this approach by introducing an alkyl-bridged intramolecular Lewis-pair with an electrophilic silicon center that holds three perfluoroethyl groups (Figure 15, b). The reported FLP compound readily reacted with CO₂ and SO₂ forming a heterocyclic adduct and even activated dihydrogen under ambient conditions.^[56d]

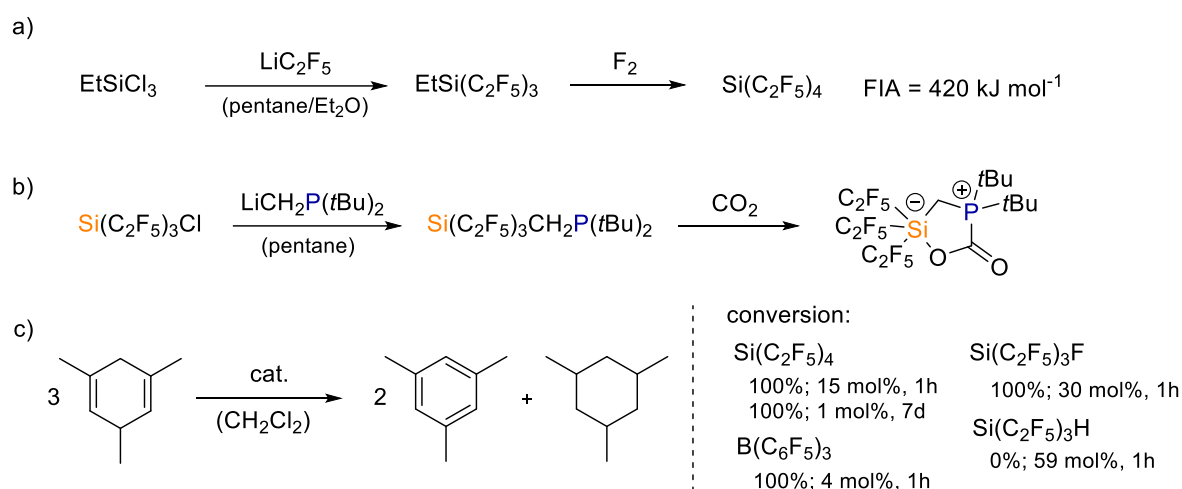


Figure 15: First synthesis of the stable and highly electrophilic Si(C₂F₅)₄ by fluorination (a) and the installation of an intramolecular frustrated Lewis base pair based on a neutral Si(IV) Lewis acid (b). Section (c) shows the catalytic application of perfluoroalkyl substituted silanes for the intermolecular hydrogen transfer reaction of 1,3,5-trimethylcyclohexa-1,4-diene.

3.2 Silylium ions

Silylium ions (R₃Si⁺) are tricoordinate Si(IV) species that hold only six valence electrons and are positively charged. Because of the electron deficiency, the silicon atom is tremendously Lewis acidic.^[54a] In contrast to the well-established carbenium ions (R₃C⁺), the first isolable free silylium ion was reported about two decades ago.^[17, 90] Because of the larger size of the silicon atom and less orbital overlap with its substituents, the positive charge on the silicon center is less stabilized by π- and hyperconjugation compared to the lighter carbenium species.^[16a] As a result, silylium ions readily bind Lewis bases, even when they are non-nucleophilic or only weakly coordinating. For this reason, the solvent and counter ion choice as well as the steric protection of the silyl center are substantial for synthesizing donor-free

silylium cations. Without steric protection, intra- or intermolecularly stabilized silyl cations form *via* Lewis pairing with present donor molecules (Figure 16).^[54a]

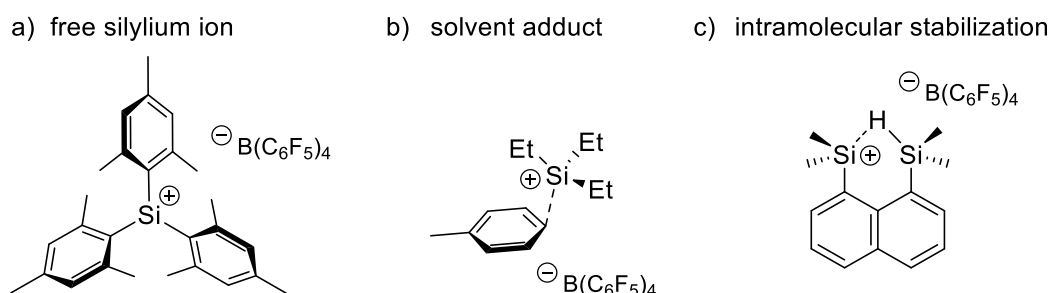


Figure 16: Examples of free silylium ions without donor-acceptor interaction (a), π -type solvent coordination (b), and intramolecular σ -type stabilization (c). Content is taken from literature sources.^[16a]

The Lewis acidity of the resulting donor-stabilized silyl cations is, however, diminished when compared to free ions due to the partial electron transfer of the donor molecule to the vacant p -orbital of the silicon atom. The magnitude of this effect strongly depends on the respective donor-acceptor interaction.^[91] An experimental scale for assessing the resulting Lewis acid strength of donor-stabilized silyl cations was recently introduced by the Müller group using p -fluorobenzonitrile as an NMR probe (Chapter 2.3.2).^[42] Donor-stabilized silyl cations are still highly electrophilic complexes with tremendous activity for catalytic transformations in various Lewis acid-mediated reactions.^[54a, 92]

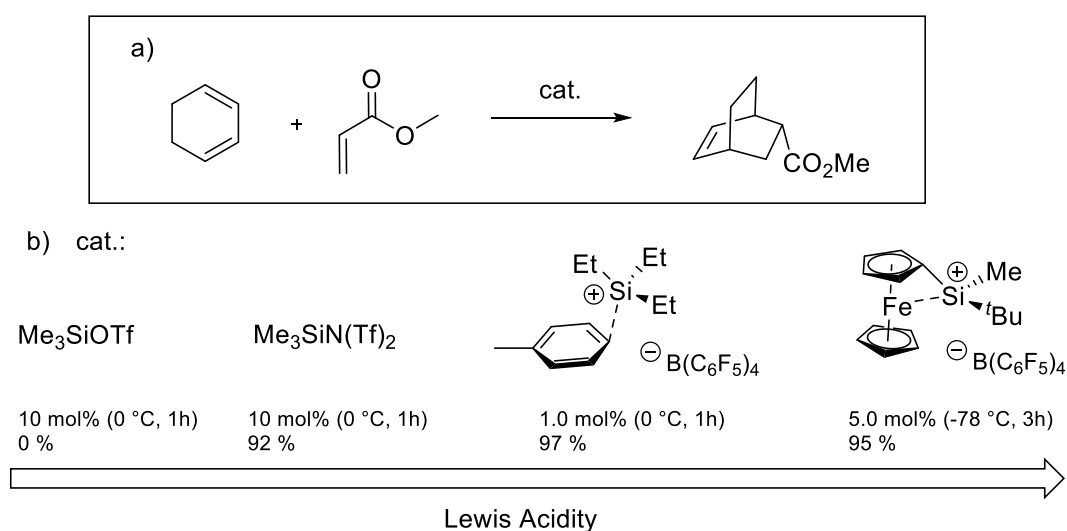


Figure 17: Increasing catalyst activity for the Diels-Alder addition of methyl acrylate and cyclohexa-1,3-diene (a) with increasing Lewis acidity of neutral Lewis acidic silanes and stabilized silyl cations, used as the reaction catalyst (b). Figure inspired by literature source.^[16a]

The potential of silyl cations to outperform well-established neutral silane-based catalysts can be illustrated by the challenging Diels-alder cycloaddition of methyl acrylate and 1,3-

cyclohexadiene (Figure 17). The reactivity for this reaction increases with the increasing Lewis acidity of the employed catalyst molecule.^[16a] While only minor reactivity for this reaction was obtained using neutral Lewis acidic silanes Me_3SiOTf and $\text{Me}_3\text{SiN}(\text{Tf})_2$,^[93] low catalyst loadings of donor-stabilized silyl cations furnished fast and quantitative conversion, even at low temperatures.^[94]

Other testimonial applications display the self-regeneration of the silyl cation from stoichiometrically employed hydrosilanes. Such catalytic reactions include the C-F hydrodefluorination of sp^3 carbons with hydrosilanes (Figure 18, a),^[95] the hydrosilylation of olefins (Figure 18, b),^[96] carbonyls and imines,^[97] aldol-type Mukaiyama-Michael as well as Hosomi-Sakurai reactions.^[98] Beyond that, the challenging $\text{C}(\text{sp}^2)\text{-F}$ activation is also accessible with silyl cations, allowing for selective catalytic intramolecular C-H arylation reactions (Figure 18, c).^[99] Intermolecular C-H arylation and alkylation reactions can also be successfully catalyzed by self-regenerating silyl cations (Figure 18, d).^[100] A unique reaction exclusively catalyzed by silyl cations is the disilylation of alkenes with Me_6Si_2 yielding 1,2-bissilylated products (Figure 18, e).^[101]

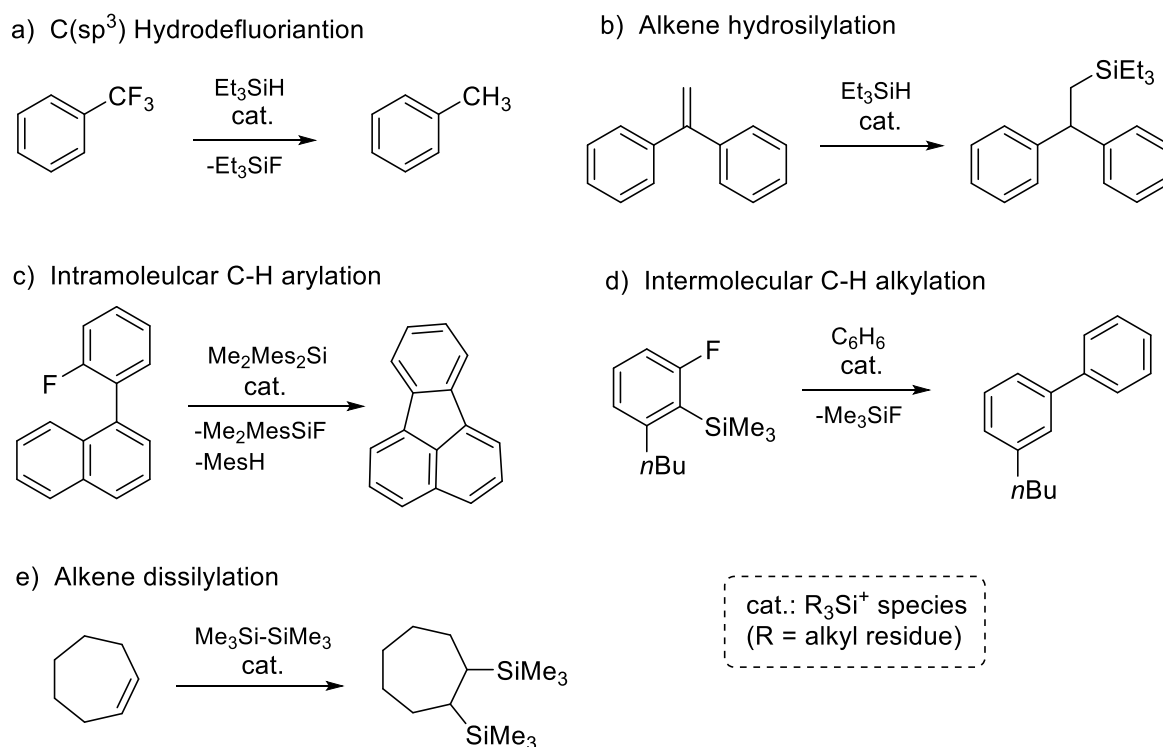


Figure 18: Selected examples of organic reactions catalyzed by self-generating silylium ions, including C-F hydrodefluorination (a), C-H arylation (b) and alkylation (c), olefin hydrosilylation (d), and alkene disilylation (e). Content is taken from literature sources.^[16a]

Illustrated by those examples, it is evident that the catalyst activity correlates strongly with the Lewis acidity of the employed catalyst. Consequently, potent catalyst molecules could be

obtained by further increasing the electrophilicity of neutral, so-called Lewis superacidic silanes.

3.3 Silyliumylidene cations

Another highly Lewis acidic compound class that was successfully used for catalysis are silyliumylidene cations.^[102] As indicated by their names, silyliumylidenes are a chimera of divalent silylenes (Si(II) species) and silylium ions. Therefore, the resulting central Si(II) atom is mono-valent and holds one additional lone pair of electrons and a cationic charge. The highly electrophilic silicon center bears two additional vacant *p*-orbitals, usually coordinated by donor molecules such as *N*-heterocyclic carbenes (NHCs) for stabilization. As low valent Si(II) centers are elusive species due to the undesired oxidation state,^[103] the first silyliumylidene species **L-1** was only isolated in 2004 by the Jutzi group,^[57] which was about two decades after the synthesis of the respective germanium derivative **L-2** (Figure 19).^[104]

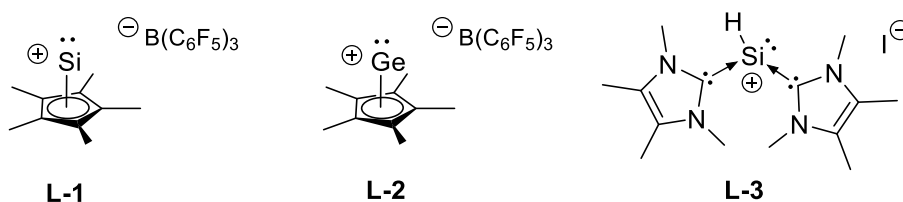


Figure 19: First reported isolable silyliumylidene species **L-1** and the related germylium ylidene species **L-2** that was isolated 24 years earlier in 1980, as well as NHC-stabilized parent silyliumylidene **L-3** synthesized in 2017.^[57, 104-105]

The remarkable catalytic properties of silyliumylidene **L-1** were first reported in 2011 for the C-O ring-closing metathesis of ethyleneglycol diethers.^[106] In this reaction, catalytic amounts between 0.5 – 10 mol% were sufficient for the oligoether fragmentation yielding 1,4-dioxane as the main reaction product. A proposed mechanistic cycle suggested the coordination of two ether fragments to the strongly electrophilic silicon center. This further leads to the cleavage of the aliphatic ether bonds and yields the formation of cyclic 1,4-dioxane units (Figure 20, c).^[106] The tremendous catalytic potential of silyliumylidenes was further recognized by the WACKER Chemie AG, that recently reported on the applicability of **L-1** for the hydrosilylation of olefins and alkynes, which are essential reactions for the industrial curing of silicone elastomers. In a model reaction setup with terminal α -methylstyrene and pentamethyl disiloxane as hydride sources, catalyst loadings of only 0.013 mol% of **L-1** efficiently catalyzed the quantitative formation of the *anti*-Markovnikov hydrosilylation product. This translates to a turnover number (TON) of about 80,000, which ranges among the TONs of industrially applied Pt-catalysts. In the presence of siloxane species, **L-1** additionally showed reactivity for the Piers-

Rubinsztajn reaction at slightly elevated temperatures (Figure 20, e). Exploiting both reactivities, silyliumylidene **L-1** was introduced as an efficient catalyst for the temperature-induced crosslinking of silicone elastomers.

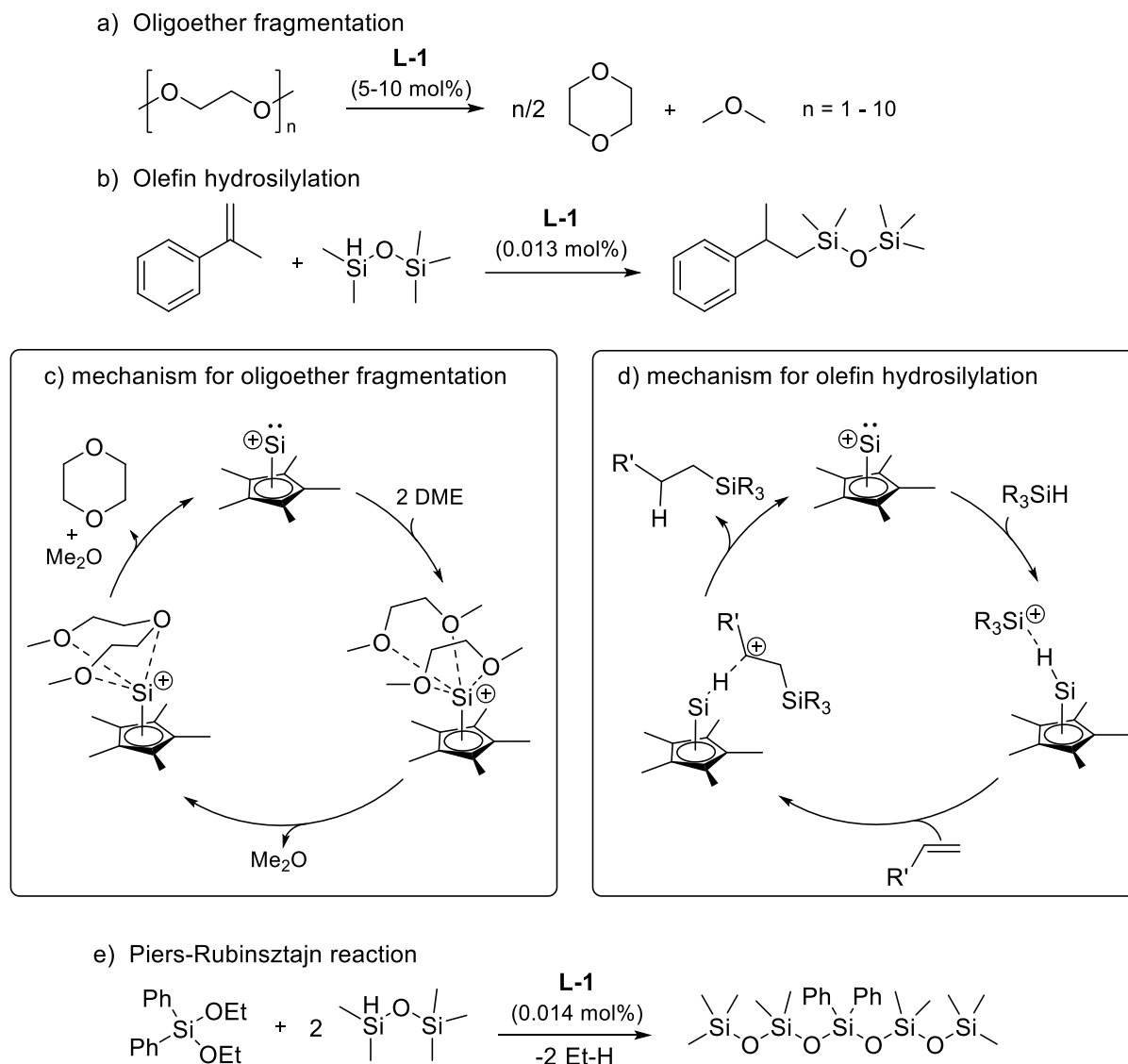


Figure 20: Exemplary catalytic applications of Jutzi's silyliumylidene species **L-1** for the C-O metathesis of oligoethers (a), the hydrosilylation of alkenes (b), and the Piers-Rubinsztajn reaction or siloxanes (e). The figure further shows the proposed mechanistic cycles for the C-O metathesis of dimethoxyethane (DME) (c) as well as for the olefin hydrosilylation (d).^[16b, 106]

A recent publication even demonstrates the outstanding applicability of the air-stable germylium ylide species **L-2** and related derivatives for the catalytic olefin hydrosilylation in the presence of oxygen.^[62a] Other silicone cross-linking strategies using main group element catalysts **L-1** and **L-2** include the oxidative hydrosilane coupling with stoichiometric carbonyls or ketones present.^[107] Apart from highly versatile silyliumylidene **L-1**, also the NHC-stabilized parent silyliumylidene **L-3** was successfully applied for the catalytic reduction of carbonyls,

ketones, pyridine derivatives, and even carbon dioxide with borohydrides. While hydroboration of a variety of carbonyl substrates with pinacol borane (HBpin) was accomplished with catalyst loadings of 10 mol% at ambient conditions, hydroboration of ketones, substituted pyridines, and CO₂ required reaction temperatures of 90 °C.^[108]

Those examples outline the tremendous catalytic potential of low valent Si(II) cations. However, the low stability of silyliumylidenes against moisture and air, and the immanent drawbacks that come along with ionic compounds, hamper the potential application on an industrial scale. As discussed in the following chapter, a possible alternative is synthesizing highly Lewis acidic but neutral Si(IV) Lewis superacids.

3.4 Neutral Lewis Superacidic Silanes

Bis(perfluorocatecholato)silane

The journey of Lewis superacidic silanes started just recently with the synthesis of the bis(perfluorocatecholato)silane **L-4** and its implementation for the catalytic hydrosilylation and silyl cyanation of electron-deficient aldehydes by the groups of Tilley and Bergman in 2015. In their publication, the groups gauged the Lewis acidity of **L-4** with the Gutmann-Beckett method, revealing a $\Delta\delta(^{31}\text{P})$ chemical shift of 35.9 ppm. This shift is only minorly increased compared to the non-fluorinated derivative **L-5** ($\Delta\delta(^{31}\text{P}) = 32.5$ ppm).^[109]

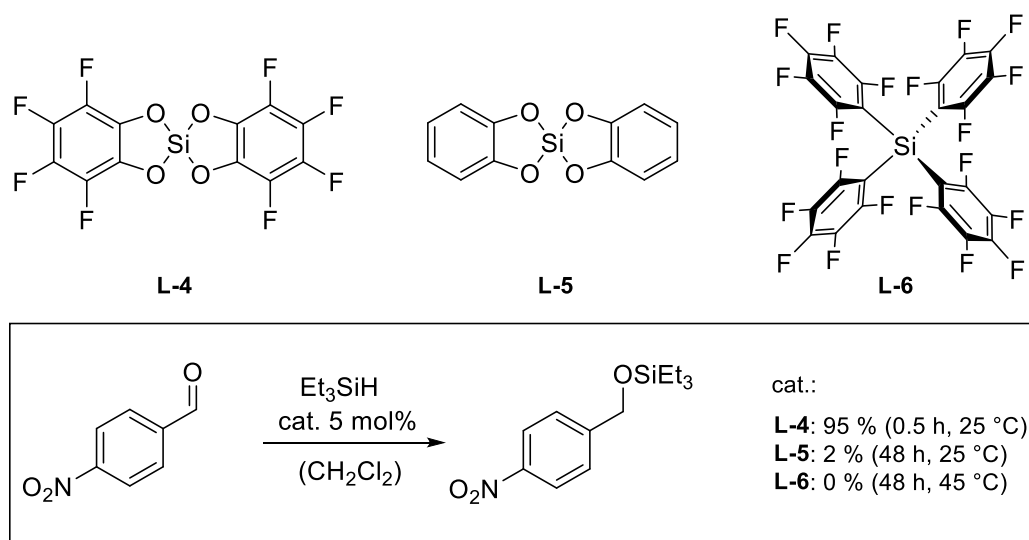


Figure 21: Si(C₆F₅)₄ and catecholato-based Lewis acidic silanes investigated by the groups of Tilley and Bergman for the hydrosilylation of electron-deficient carbonyls.^[109]

Nevertheless, **L-4** demonstrated remarkable activity for the catalytic hydrosilylation of *p*-nitrobenzaldehyde with Et₃SiH, while no considerable conversion was obtained for **L-5** and the silicon derivative of famous tris(pentafluorophenyl)borane **L-6** (Figure 21). A consecutive reactivity study outlined the applicability of **L-4** for a broad substrate scope, including sterically

congested silanes, such as *i*Pr₃SiH, that are inactive in case of B(C₆F₅)₃-mediated catalysis.^[109-110] Reactivity experiments with hydrosilanes revealed no interaction of the Lewis acid with the soft hydride moiety, as it is the case for B(C₆F₅)₃. Consequently, the proposed hydrosilylation mechanism starts with activating the carbonyl substrate by coordinating the Lewis acidic silicon center. This hypothesis was additionally supported by a reactivity study on the hydrosilylation of *p*-nitrobenzaldehyde with enantiopure *R*-methyl-(1-naphthyl)phenylsilane. While predominant stereochemical retention was observed in benzene (70 % *ee*), racemization facilitated in more polar solvents, such as *o*-dichlorobenzene (40 % *ee*) and dichloromethane (12 % *ee*). The additional use of the phase transfer catalyst [NBu₄][BAr^F] further amplified this effect. Consequently, two competing mechanistic cycles were proposed, depending on the polarity of the employed chemical environment (Figure 22).^[109]

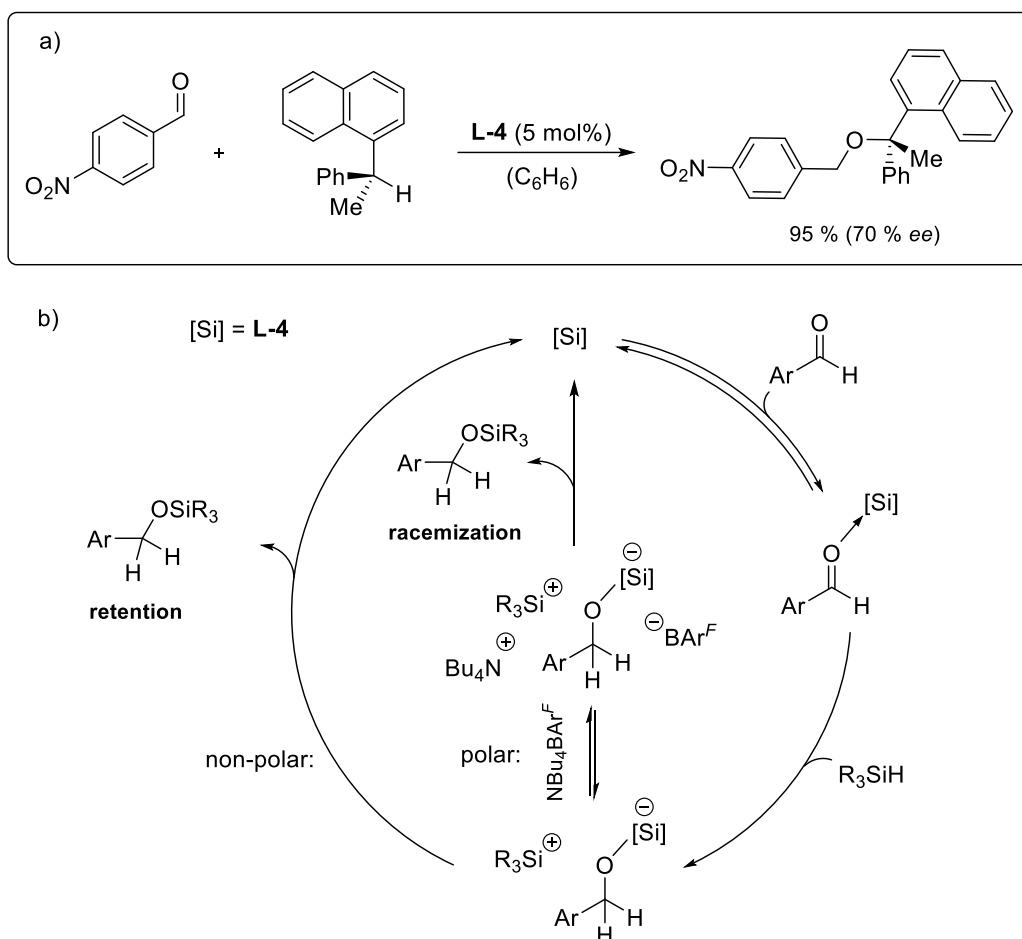


Figure 22: Enantioselective hydrosilylation of *p*-nitrobenzaldehyde with *R*-methyl-(1-naphthyl)phenylsilane catalyzed by L-4 (a) and the proposed mechanistic cycles in polar and non-polar environments (b). Figure inspired by literature source.^[109]

The cycles involve the formation of an alkoxy silicate intermediate with a silylium counter ion. In a non-polar environment, the catalyst is cleaved off by forming a new Si–O bond before a

rotation of the silyl group, which leads to the retention of the stereo center. In a more polar environment, the rotation of the silyl group causes racemization.^[109]

Bis(perchlorocatecholato)silane

Despite this tremendous catalytic activity, **L-4** does formally not justify as a Lewis superacid by Krossing's definition^[32] as quantum chemical calculation revealed only an FIA value of 490 kJ mol⁻¹ that is below molecular SbF₅ (FIA: 501 kJ mol⁻¹).^[111] To further enhance the Lewis acidity of this compound class, the Greb group replaced the fluoride substituents on the catecholato fragments with less electron back-donating chlorides and obtained the first true Lewis superacidic silane **L-7** with a calculated FIA of 507 kJ mol⁻¹. The compound was synthesized from perchlorinated catechol (H₂cat^{Cl}) and HSiCl₃ in acetonitrile solution. Because of the enhanced Lewis acidity, compound **L-7** could only be obtained as the acetonitrile bis-adduct *via* this route (Figure 23). The donor-free form **L-7*** was isolated by an alternative strategy, using the Oestreich SiH₄ surrogate (**L-8**) in a toluene solution.^[111] A recent publication furthermore reports the successful synthesis of **L-7*** from H₂cat^{Cl} and HSiCl₃ in dichloromethane solution by employing substoichiometric amounts of *n*-butylsulfone to facilitate the elimination of H₂ and HCl.^[112]

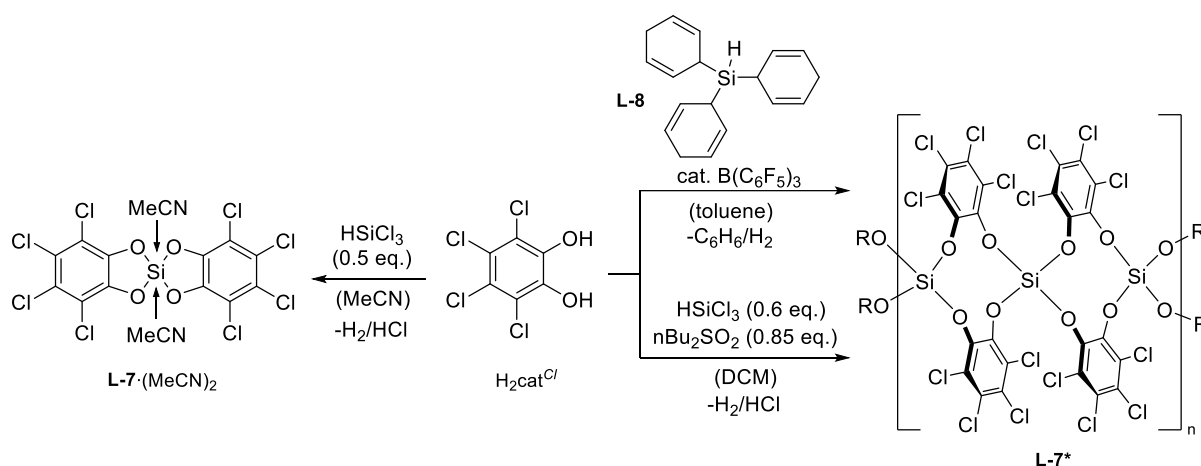


Figure 23: Synthesis of Lewis superacid **L-7** as the acetonitrile bis-adduct and donor-free synthesis routes for polymeric **L-7*** reported by the Greb group.^[111-112]

An in-depth structural study on catecholato silanes using advanced analytical techniques and high-level quantum chemical calculations revealed an oligomeric to polymeric appearance of the donor-free Lewis acid **L-7*** (Figure 23).^[113] Experimental Lewis acidity assessments were conducted with the monomeric **L-7**·(MeCN)₂ for solubility reasons. The Gutmann-Beckett method revealed a $\Delta\delta(^{31}\text{P})$ shift of 35.0 ppm for the Et₃PO mono-adduct, which is slightly diminished compared to **L-4** (35.9 ppm).^[109, 111] In a subsequent publication, a slightly increased $\Delta\delta(^{31}\text{P})$ shift of 36.7 ppm was found for **L-7** in the same solvent.^[114] The ultimate proof for the

compounds' superacidity was provided experimentally by the abstraction of a fluoride substituent from $[\text{SbF}_6]^-$ in a dichloromethane solution (Figure 24, a). While this reaction is, of course, affected by solvent interactions, the results align well with the computed superacidity for the single molecule, according to Krossing's definition.^[32] Further abstraction experiments with KF , Ph_3CCl , and $[\text{Me}_3\text{SiF}_2]^-$ demonstrated the formidable Lewis acidity of **L-7**, yielding mono- and bis-substituted silicate species **L-9** – **L-11** that were characterized by SC-XRD structure analysis. The tremendous FIA of compound **L-7** was successfully used for the catalytic hydrodefluorination of 1-adamantylfluoride with Et_3SiH or PMHS (Figure 24, b). This reaction proceeds *via* the initial activation of the $\text{C}(\text{sp}^3)\text{-F}$ bond by the Lewis superacid. Complete conversion was obtained after 15 hours at room temperature, using catalyst loadings of 10 mol% in tetrachloroethane solution.

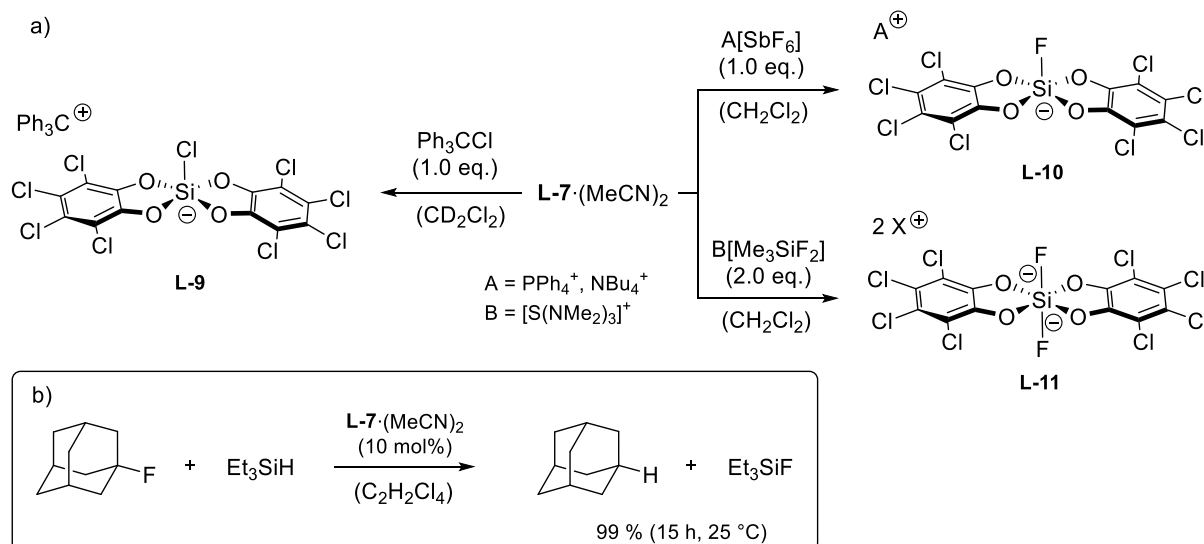


Figure 24: Abstraction experiment with **L-7·(MeCN)₂** proofing tremendous Lewis acidity by the formation of mono- and bis-substituted silicate addition products (a) and catalytic hydrodefluorination of 1-fluoroadamantane with Et_3SiH using 10 mol% of **L-7·(MeCN)₂** as catalyst (b).^[111]

Despite the catalytic applicability for the hydrodefluorination of sp^3 carbons, the acetonitrile bis-adduct **L-7·(MeCN)₂** was further successfully employed to capture CO_2 by carbamate formation in the presence of amines. Penta- or hexa-oxo-coordinate silicon complexes were obtained depending on the engaged base.^[115]

The catalytic C-O ring-closing metathesis of ethylene glycol diethers with donor-free **L-7*** further highlighted the catalytic applicability of neutral Lewis superacids. Complete conversion of 1,5-dimethoxypentane to the cyclization product tetrahydropyran and dimethylether was observed by using a catalyst loading of 5 mol% **L-7*** at 115 °C in *o*-dichlorobenzene solution (Figure 25, a).^[116] The activity significantly outperformed the benchmark system $\text{Fe}(\text{OTf})_3$, given in the literature, which achieved a conversion of only 85 % by using a catalyst loading of

20 %.^[117] A similar trend was observed for the more challenging substrate diglyme, which leads to catalyst deactivation by chelating the active Lewis acidic center. Quantitative conversion to the cyclization product 1,4-dioxane was observed with a catalyst loading of 10 mol% of **L-7***. With 5 mol% of the catalyst, the reaction stopped at a conversion of 43 %, indicating the deactivation of the active species. Further reactivity screenings also demonstrated the applicability of **L-7*** for the degradation of polymeric ethyleneglycol dimethylether (PEG-DME) with a molar mass of ~2000 g/mol. Again, catalyst loadings of 5 – 10 mol% were sufficient to afford conversions of 84 – 99 % at 60 °C within 19 h in dichloromethane solution, thus successfully introducing neutral Lewis acidic silanes for the degradation catalysis of commodity plastics.^[116] Even for the more challenging polypropyleneglycol derivative, a conversion of about 25 % was achieved, which is remarking as no reactivity with secondary ethers was reported for Fe(OTf)₃.^[117]

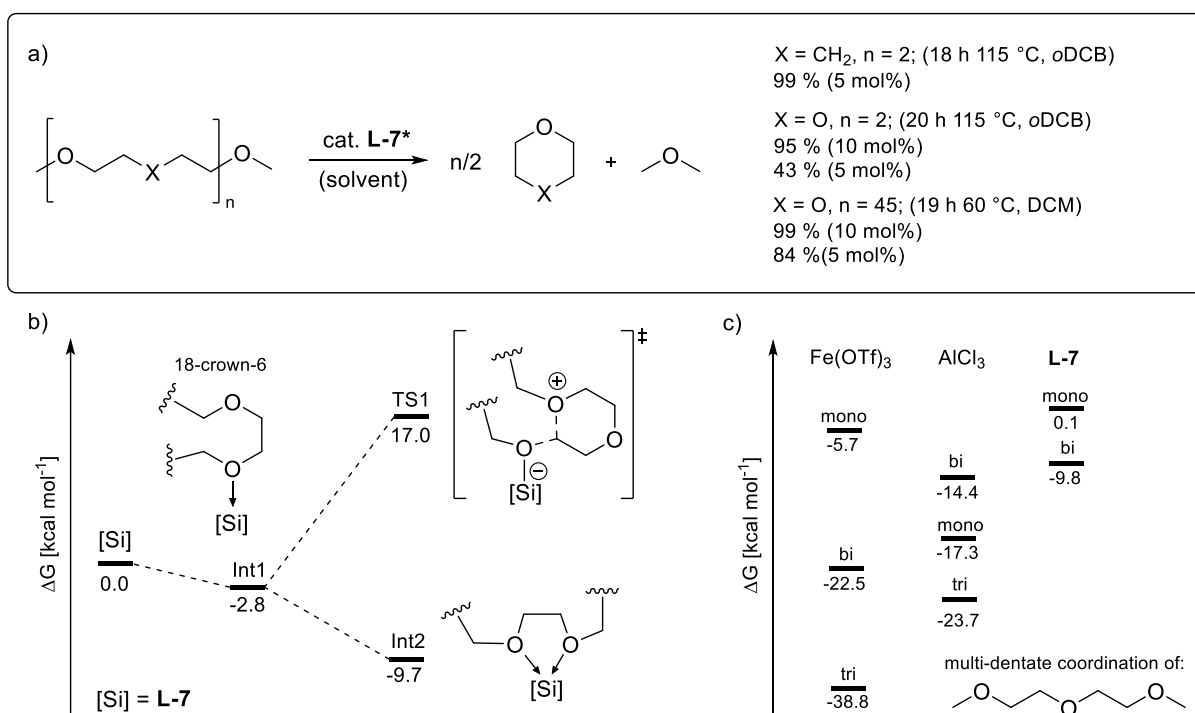


Figure 25: C-O ring-closing metathesis of 1,5-dimethoxypentane, diglyme, and PEG-DME, catalyzed by **L-7** (a). Energetic profile of the initiating degradation cascade by mono- and bi-coordination of 18-crown-6 to **L-7** (b) and stabilization energies of mono- and multi-dentate coordination of diglyme (c).^[116]

To understand the high reactivity of **L-7***, quantum chemical calculations were performed for the degradation of 18-crown-6 with formal monomeric **L-7**. These insightful computations suggested a monodentate coordination of one etheric oxygen to the Lewis acidic silicon center before a zwitterionic transition state is formed that initiates fragmentation cascade by an intramolecular S_N2 attack. The activation barrier between the mono-coordinated adduct and the zwitterionic transition state has a ΔG of 19.8 kcal mol⁻¹ and is, therefore, energetically

accessible (Figure 25, b). However, the competing twofold coordination, or chelation, of the silicon center by two etheric oxygen moieties leads to increased adduct stabilization. In this case, the energy barrier between the chelated adduct and the zwitterionic transition state is significantly enlarged ($\Delta G = 26.9 \text{ kcal mol}^{-1}$), causing decreased catalyst activity. Further calculation on multidentate coordination of diglyme to Lewis acids including **L-7**, $\text{Fe}(\text{OTf})_3$, and AlCl_3 , revealed a strong tendency for bi- and tridentate substrate coordination. This leads to heavily stabilized adducts in the case of $\text{Fe}(\text{OTf})_3$ and AlCl_3 , explaining the poor catalyst performance compared to **L-7** (Figure 25, c).^[116]

Bis(perbromo)- and bis(pertrifluoromethylcatecholato) silanes

According to the Hammett theory, less π -overlap of the halide substituents on the catechol ring should furnish even more electrophilic silicon centers.^[118] Therefore the Lewis acidity of fully substituted bis(catecholato)silanes should be further enhanced by replacing chloride ($\sigma_m = 0.37$) with even less electron back-donating bromide ($\sigma_m = 0.39$) or CF_3 groups ($\sigma_m = 0.43$).^[119] Following this theory, the Greb group successfully synthesized both compounds, **L-12** and **L-13**, as the respective solvent adducts and found Lewis acidity values exceeding those of **L-7** in terms of FIA and the Gutmann-Beckett assessment.^[114, 120] Compound **L-12** was synthesized in analogy to **L-7** from perbrominated catechol and HSiCl_3 in acetonitrile. Consequently, the Lewis acid was obtained as the twofold coordinated solvent-adduct **L-12** $\cdot(\text{MeCN})_2$.^[114]

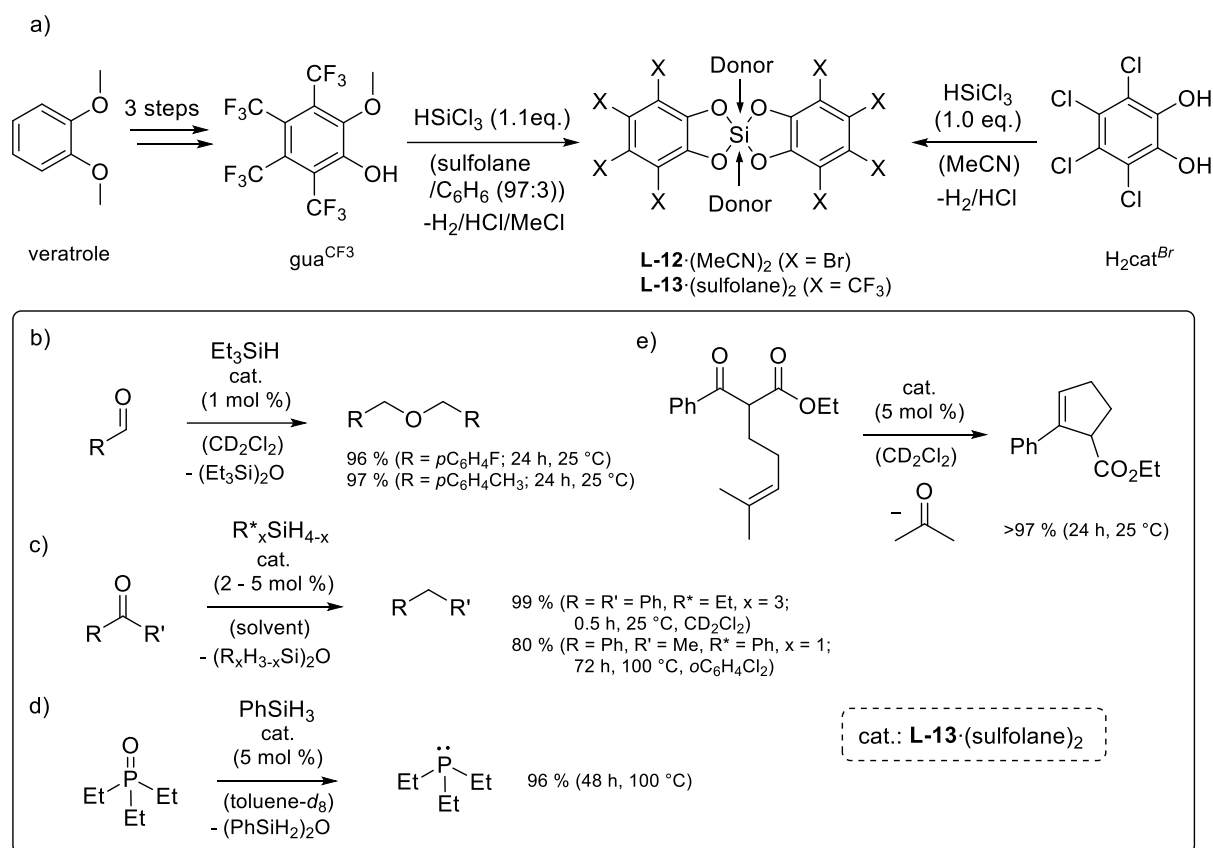


Figure 26: Synthesis of Lewis superacids **L-12**·(MeCN)₂ and of **L-13**·(sulfolane)₂ as the solvent bis-adducts (a) and experimentally confirmed Lewis superacidity by ion abstraction experiments yielding fluoride and chloride substituted pentavalent silicate species **L-14** and **L-15** (b).^[114, 120]

For **L-13**, the synthesis started from veratrole, which was converted into tetrakis(trifluoromethyl)guaiaicol (gua^{CF_3}) in a 3-step synthesis. A subsequent conversion with HSiCl_3 in a mixture of sulfolane and benzene furnished the successful synthesis of **L-13**·(sulfolane)₂ (Figure 26, a).^[120] No isolation of the donor-free form was reported in both cases.

Lewis acidity determination by the Gutmann-Beckett method revealed a slightly increased shifts of the phosphorus signal in the region of Lewis superacidic **L-7**. For mono-coordinated **L-12**· OPeT_3 , a chemical shift of $\Delta\delta(^{31}\text{P}) = 36.8$ ppm was detected (36.7 ppm for **L-7**· OPeT_3). The obtained shift for **L-12** corresponds well with the calculated FIA value of 538 kJ mol^{-1} , which easily surpasses the fluoride affinity of the first reported neutral Lewis superacid **L-7** (507 kJ mol^{-1}).^[114] Even stronger Lewis acidity values were observed for **L-13**, which holds a $\Delta\delta(^{31}\text{P})$ shift of 38.9 ppm and a computed FIA of 584 kJ mol^{-1} . Interestingly, **L-13** also displays a tremendously high affinity for softer hydride ions, outlined by a calculated HIA of 559 kJ mol^{-1} . This value exceeds the hydride affinity of $\text{B}(\text{C}_6\text{F}_5)_3$ (HIA: 471) and is therefore considered a hard and soft Lewis superacid, according to the definition given by Greb.^[19, 120] While no further reactivity investigations were conducted for **L-12**, the Lewis superacidity of

L-13·(sulfolane)₂ was again demonstrated by successful abstraction experiments with [Ph₄P][SbF₆] and Ph₃CCl, yielding the respective fluoride- and chloride substituted pentavalent silicate anions **L-14** and **L-15** (Figure 26, b).^[120]

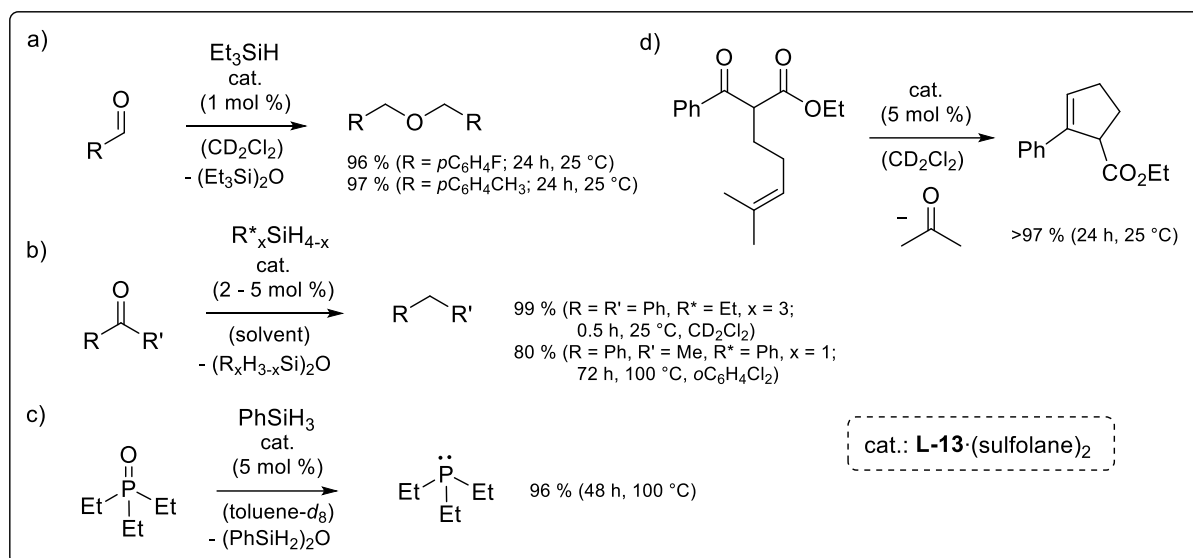


Figure 27: Selected reactions successfully catalyzed by **L-13**·(sulfolane)₂, including reductive ether formation of carbonyls (b), ketone and phosphine oxide defunctionalization (c and d), as well as a carbonyl-olefin metathesis reaction (e).^[120]

When tested for its activity to catalyze the literature-known hydrosilylation of carbonyls, **L-13**·(sulfolane)₂ selectively furnished the reduction of electron-deficient as well as electron-rich carbonyls, yielding the respective dialkyl ethers. Already a catalyst loading of 1 mol% was sufficient to give quantitative yields at ambient conditions using Et₃SiH as a reducing agent. The same conditions applied for benzophenone led to efficient defunctionalization of the ketone, giving the 1,1-diphenylmethane as the reaction product (Figure 27, b). Even more challenging substrates such as acetophenone, cyclohexanone, Et₃PO, and Ph₃PO led to efficient defunctionalization with **L-13**·(sulfolane)₂ as a catalyst, but with access of the PhSiH₃ and harsher reaction conditions required (Figure 27, b-c). A further testimonial of the versatile applicability of neutral Lewis acid catalysts was given by a successful carbonyl-olefin metathesis (Figure 27, d), which success critically depends on a sufficient Lewis acidity of the employed catalyst.^[120]

Bis(perfluoro-*N*-phenyl-*o*-amidophenolato)silane

Another goal for relevant catalytic applicability is the activation of dihydrogen. This was achieved using the Lewis acidic bis(perfluoro-*N*-phenyl-*o*-amidophenolato)silane in an FLP-type reaction approach.^[121] The perfluorinated ortho-aminophenol ligand was chosen to prevent the silicon center from oligomerization while providing sufficient electron withdrawal to form a neutral Lewis superacid. The silane was synthesized as the donor-adduct **L-16**·NHMe₂ from

$\text{HSi}(\text{NMe}_2)_3$ and perfluoro(*N*-phenyl-*o*-aminophenol) ($\text{am}^{\text{F}}\text{Ph}^{\text{F}}\text{H}_2$) which was prepared from perfluorobenzene in three reaction steps. The abstraction of NHMe_2 to form the monomolecular **L-16** was ultimately achieved by the abstraction with HNTf_2 in toluene (Figure 28, a).

Contrastingly to the previously described catecholato silanes, compound **L-16** possesses an excellent solubility in non-polar solvents. It therefore could be characterized including ^{29}Si NMR spectroscopy giving a ^{29}Si shift at $\delta = -40.6$ ppm. Ion affinity calculations showed an FIA of 494 kJ mol^{-1} and HIA of 449 kJ mol^{-1} , which is close to superacidity in both cases. Lewis acidity assessment by the Gutmann-Beckett method revealed a ^{31}P NMR shift of $\Delta\delta(^{31}\text{P}) = 32.8$ ppm for the monocoordinated Et_3PO adduct, which is slightly decreased but in the range as for the parent biscatecholatosilane **L-5** (32.5 ppm).^[109] Nevertheless, the manuscript stated that superacidity could be confirmed by the fluoride abstraction from $[\text{PPh}_4][\text{SbF}_6]$ in dichloromethane. However, only the chloride abstraction from Ph_3CCl is found in the provided supporting information.^[121]

Due to the steric protection, **L-16** was successfully applied for the cleavage of H_2 in the presence of sterically congested 1,2,2,6,6-pentamethylpiperidine (pmp) (Figure 28, b) to form the ionic activation product **L-17**. No interaction with H_2 was found for other bases such as NTBu_3 , NiPr_2Et , 2,2,6,6-pentamethylpiperidine, and the *N*-heterocyclic carbenes at various conditions.^[121] The catalytic applicability of **L-16** as a superacid was further demonstrated for the C-O ring-closing metathesis of diglyme, showing a conversion of 81 % with a catalyst loading of only 3 mol% (Figure 28, c). Compared to benchmark system **L-7***, the enhanced reactivity of **L-16** was explained by the silane center's steric protection, blocking undesired catalyst deactivation due to substrate chelation.^[116]

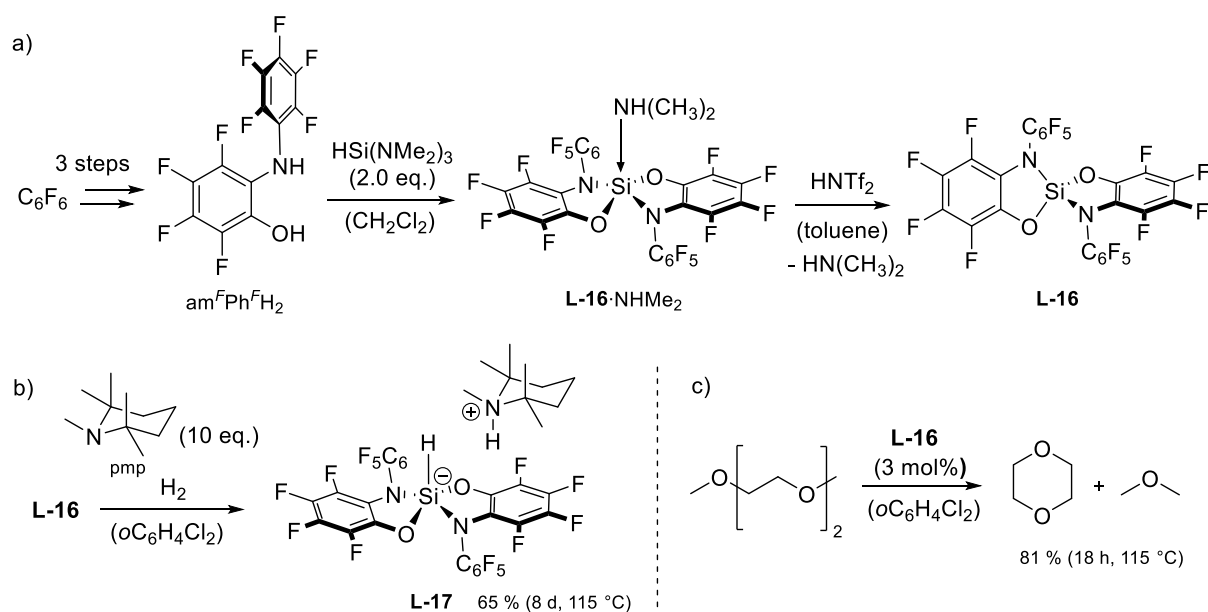


Figure 28: Synthesis of donor-free Lewis superacid **L-17** (a) and its implementation for the FLP-type activation of H₂ in the presence of pmp (b), as well as for the catalytic C-O ring-closing metathesis of diglyme (c).^[116, 121]

Silicon tetrakis(trifluoromethanesulfonate)

Another strategy that yielded an exceptionally strong hard and soft Lewis superacidic silane was the installation of four OTf⁻ groups on a silicon center. The respective Si(OTf)₄ (**L-18**) was obtained from the reaction of SiI₄ and AgOTf in dichloromethane on a multi-gram scale. The Gutmann-Beckett assessment revealed a tremendous $\Delta\delta(^{31}\text{P})$ shift of 51.2 ppm for the monocoordinated Et₃PO adduct. Further characterization by ion affinity calculations showed FIA of 521 kJ mol⁻¹ and HIA of 547 kJ mol⁻¹, surpassing the border for Lewis superacidity in both cases. The calculated affinity values were additionally confirmed by abstraction experiments with [Ph₄P][SbF₆] and even [HPMes₃][HB(C₆F₅)₃], proofing a hard and soft Lewis superacidic nature. Because of the lability of the Si–OTf bond, only stoichiometric substitution reactions with CF₃-substituted benzenes were carried out, demonstrating the exchange of fluoride and triflate groups. Despite the extraordinary high $\Delta\delta(^{31}\text{P})$ GB shift and Lewis acidity by FIA and HIA values, no catalytic transformations were reported for **L-18** due to the lability of the complex. The currently reported neutral Si(IV) Lewis superacids are summarized in Figure 29.

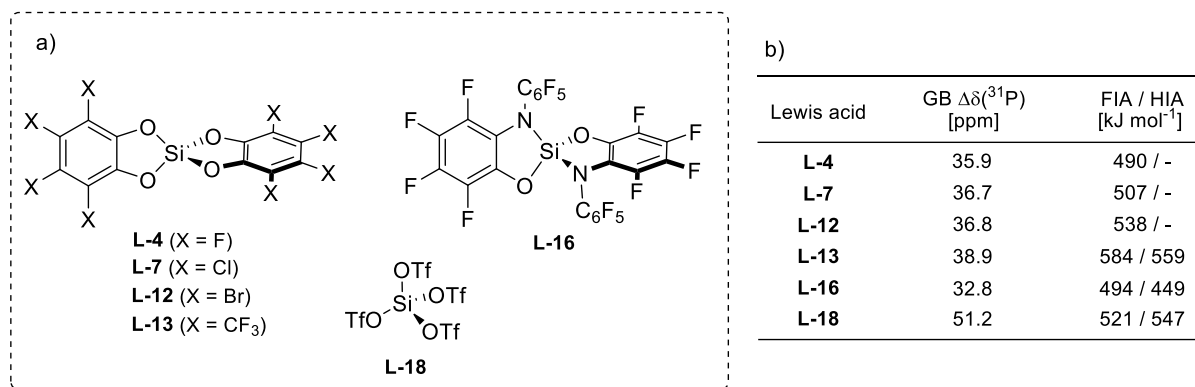


Figure 29: Summary of Lewis superacids reported before and during this Ph.D. project (a), the obtained Gutmann-Beckett shifts, and the calculated FIA and HIA values collected in table (b).^[109, 111, 114, 120-122]

3.5 Neutral Germanium Lewis Superacids in Catalysis

While the catalytic applications of low-valent germynes,^[63] germylene-metal complexes,^[123] germylumylidene cations,^[62, 107] as well as germylum cations^[61] have attracted much attention in recent years (Figure 30), the research on neutral Lewis acidic germanes has hardly been touched so far.

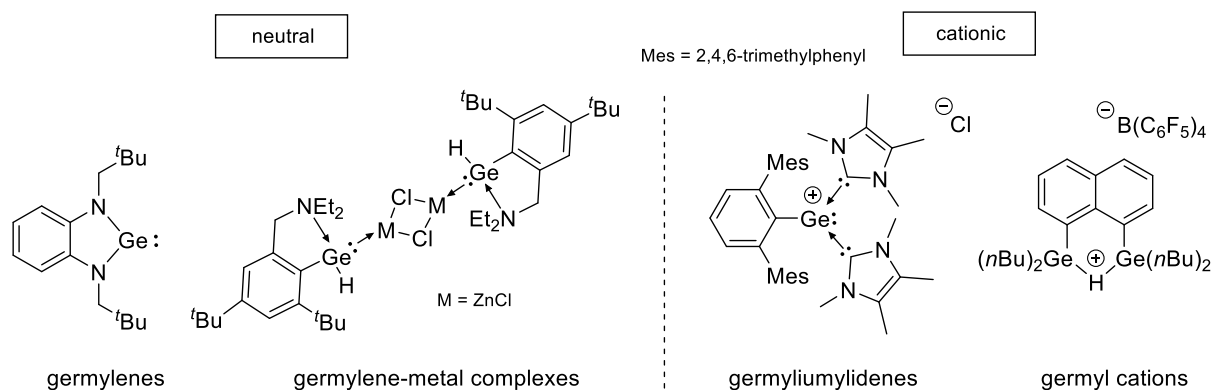


Figure 30: Selected examples of germylenes, germylene-metal complexes, germyliumylidenes and germylium cations successfully tested for catalytic applications in the literature.^[61c, 62b, 63a, 123c]

Nevertheless, the Greb group recently published Lewis superacidic germane **L-19**, holding two perchlorinated catecholato substituents.^[64b] In contrast to the respective silane homolog, **L-19** showed unlimited stability in water, which is impressively demonstrated by its synthesis from GeO_2 and $\text{H}_2\text{cat}^{\text{Cl}}$ in H_2O at ambient reaction conditions. The corresponding Lewis acid was isolated in almost quantitative yields (94 %) as the H_2O -adduct **L-19**·(H_2O)₄ after solvent removal and purification in dichloromethane (Figure 31, a). SC-XRD structure analysis of **L-19** recrystallized from H_2O solution gave the bis-aqua complex with two H_2O molecules in the *trans*-position and two co-planar perchlorocatecholato groups. The unit cell contained four additional water molecules bound *via* hydrogen bridges forming two (H_2O)₃ clusters. Storing **L-19**·(H_2O)₄ in acetonitrile/dichloromethane or acetone solution over molecular sieves (3 Å) yielded the water-free, but bis-solvent-coordinated complexes **L-19**·(MeCN)₂ and **L-19**·(acetone)₂. In contrast to the related silicon derivative **L-7**·(MeCN)₂, Lewis acidity determination by the Gutmann-Beckett method was hampered by the favored formation of the Et_3PO -bis-adduct **L-19**·(OPEt_3)₂, which gave $\Delta\delta(^{31}\text{P})$ shifts of 24.6 ppm and 20.1 ppm for the *cis*- and *trans*-coordination product.^[64b] In a subsequent publication, the Bains group achieved the formation of the monocoordinated product **L-19**· OPEt_3 showing an associated $\Delta\delta(^{31}\text{P})$ shift of 37.7 ppm.^[64a]

The calculation of the ion affinity values revealed an FIA of 504 kJ mol^{-1} and an HIA of 555 kJ mol^{-1} , justifying **L-19** as the first hard and soft Lewis superacid based on a neutral germane. Lewis superacidity was further demonstrated also in experiment by the formal fluoride abstraction of **L-19**·(MeCN)₂ from $[\text{PPh}_4][\text{SbF}_6]$ and hydride abstraction from $[\text{tBu}_3\text{PH}][\text{HB}(\text{C}_6\text{F}_5)_3]$ (Figure 31, b).^[64b]

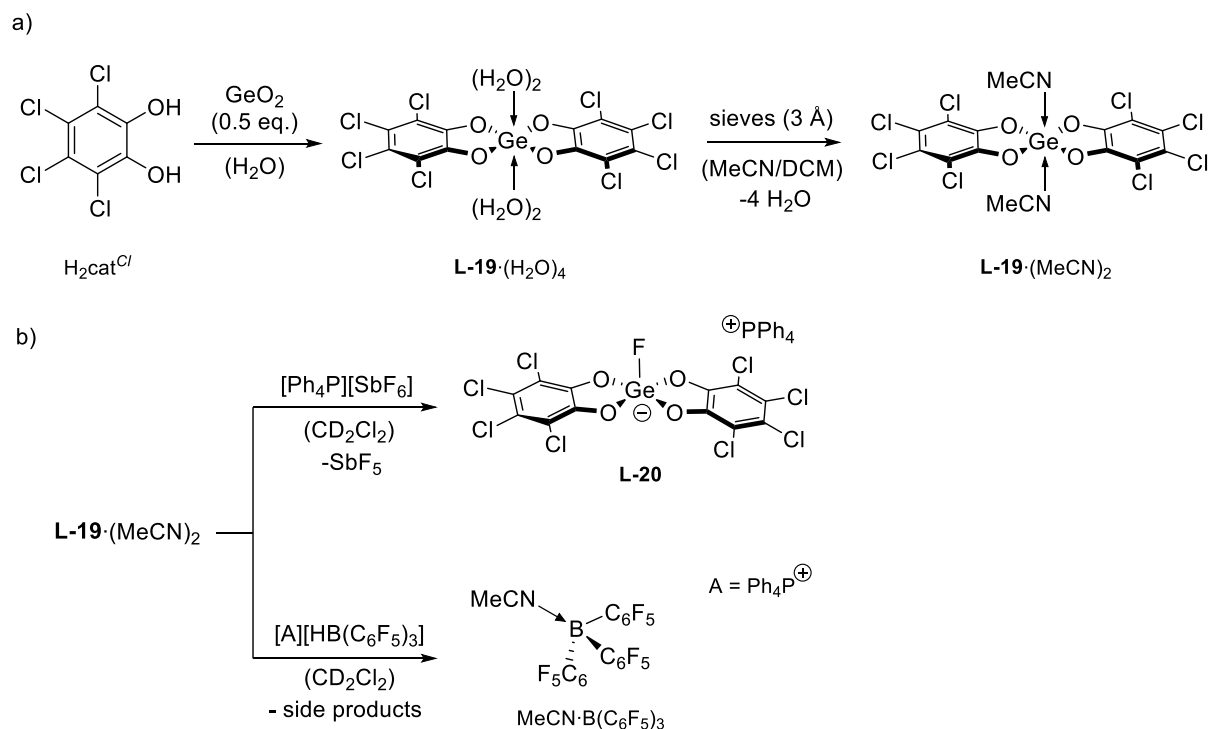


Figure 31: Synthesis of Lewis superacid $\text{L-19}\cdot(\text{H}_2\text{O})_4$ and $\text{L-19}\cdot(\text{MeCN})_2$ from GeO_2 and $\text{H}_2\text{cat}^{\text{Cl}}$ in water (a) and experimentally confirmed Lewis superacidity by fluoride and hydride ion abstraction from $[\text{PPh}_4][\text{SbF}_6]$ and $[\text{tBu}_3\text{PH}][\text{HB}(\text{C}_6\text{F}_5)_3]$ (b).^[64b]

The reaction progress was traced by multinuclear NMR spectroscopy, suggesting the formation of the respective fluoride-substituted pentavalent germanate species **L-20** in the case of $[\text{PPh}_4][\text{SbF}_6]$. This was proven by the selective formation of the same germanate anion from the reaction of $\text{L-19}\cdot(\text{MeCN})_2$ with KF and 18-crown-6. In the case of $[\text{tBu}_3\text{PH}][\text{HB}(\text{C}_6\text{F}_5)_3]$, the successful hydride abstraction was traced by the formation of the acetonitrile-BCF adduct.^[64b]

Because of the tremendous Lewis acidity, water-free $\text{L-19}\cdot(\text{MeCN})_2$ was successfully tested for various catalytic reactions. For the hydrodefluorination of 1-fluoroadamantane catalyst loadings down to only 0.05 mol% were sufficient to catalyze quantitative conversion at ambient conditions, translating to a formidable TON of almost 1,900 (Figure 32, a). When tested for the hydrosilylation of aliphatic and aromatic aldehydes, $\text{L-19}\cdot(\text{MeCN})_2$ efficiently catalyzed the formation of the respective hydrosilylation product with Et_3SiH (Figure 32, b). No reductive ether formation was observed, as it was the case for $\text{L-13}\cdot(\text{sulfolane})_2$. However, an analogous reactivity was found for the catalytic olefin-carbonyl metathesis reaction of a β -ketoester, yielding the respective cyclization product in quantitative yield after 20 h at room temperature (Figure 32, c). In addition, the Friedel-Crafts type dimerization of 1,1-diphenylethylene was found for $\text{L-19}\cdot(\text{MeCN})_2$, showing almost 50 % conversion after 24 h at 50 °C when using a catalyst loading of 5 mol% (Figure 32, d). In the presence of the dihydrogen surrogate 1,4-

cyclohexadiene, no Friedel-Crafts dimerization, but reduction of 1,1-diphenylethylene was observed, quantitatively yielding 1,1-diphenylmethane after 1 h at room temperature with a catalyst loading of 10 mol% (Figure 32, e).

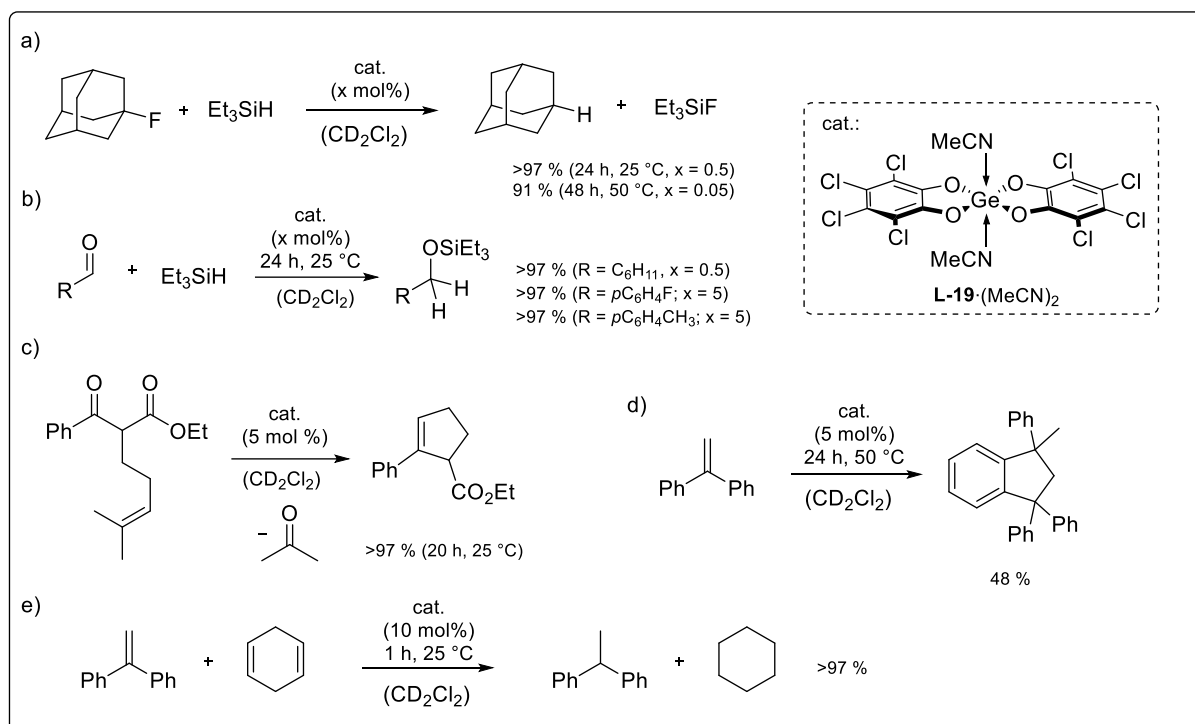


Figure 32: Selected reaction catalyzed by the Lewis superacidic germane **L-19**·(MeCN)₂ including hydrodefluorination of 1-fluoroadamantane (a), carbonyl hydrosilylation of aromatic and aliphatic carbonyls (b), an olefin-carbonyl metathesis reaction (c), the Friedel-Crafts dimerization (d) and transfer hydrogenation (e) of 1,1-diphenylethylene.^[64b]

An additional research article contributed to this compound class with an in-depth study on the Friedel-Crafts dimerization of α -methylstyrene catalyzed by Lewis superacidic germanes.^[64a] For this purpose, different solvent-coordinated bis(perchlorocatecholato)germanes **L-19**·(Donor)₂, as well as the brominated derivatives **L-21**·(Donor)₂, were synthesized from perchlorinated quinone and GeCl₂·dioxane, or from H₂cat^{Br} and GeCl₄ (Figure 33, a) and comprehensively analyzed regarding their Lewis acidity and catalytic potential. Additionally, the 3,5-di-tert-butyl-substituted derivative **L-22**·(Donor)₂ was synthesized, but no catalytic reactivity investigations were conducted for this compound due to its insufficient Lewis acidity. Calculations revealed FIA values of 508, 513, and 433 kJ mol⁻¹ for **L-19**, **L-21**, and **L-22**, respectively.^[64a] For **L-19**, the value is slightly shifted compared to the preceding article published by the Greb group (FIA: 504 kJ mol⁻¹), which is explained by a different calculation method.^[64b] Non-halogenated **L-22** possessed only a diminished Lewis acidity, which ranks among the value calculated for the parent bis(catecholato)germane (FIA: 415 kJ mol⁻¹).

Lewis acidity determination using the Gutmann-Beckett method demonstrated the influence of the adduct-forming donor-molecule (MeCN or THF) on the obtained $\Delta\delta(^{31}\text{P})$ shift. It was shown

that substoichiometric amounts of Et_3PO lead to the substitution of only one donor-molecule, yielding an octahedral complex, with one Et_3PO and one solvent molecule coordinating to the germanium center. The obtained Gutmann-Beckett shifts for the monocoordinated adducts with remaining MeCN were $\Delta\delta(^{31}\text{P}) = 37.7$ ppm, 37.9 ppm, and 32.3 ppm for **L-19**, **L-21**, and **L-22**, respectively.

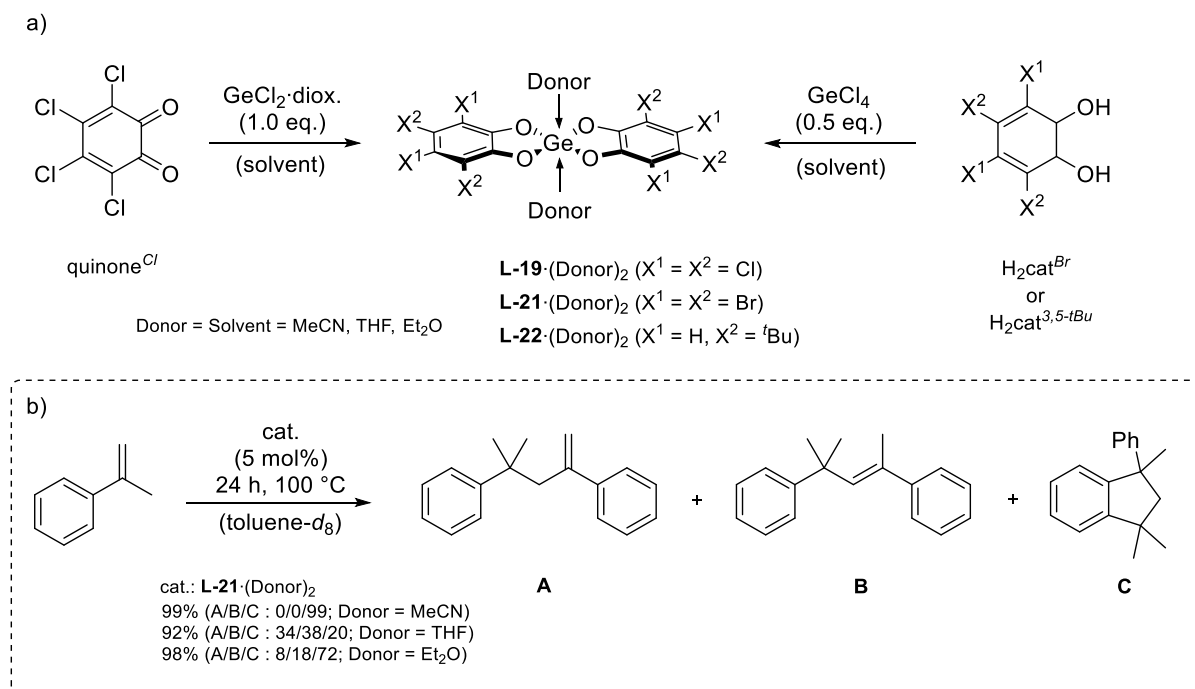


Figure 33: Water-free synthesis routes for the donor-coordinated Lewis acidic germanes **L-19**·(Donor)₂, **L-21**·(Donor)₂, and **L-22**·(Donor)₂ (a) and Friedel-Crafts dimerization of α -methylstyrene efficiently catalyzed by **L-22**·(Donor)₂ (b). (Donor = MeCN, THF, Et₂O).^[64a]

As already demonstrated by the Greb group **L-19**·(MeCN)₂ efficiently catalyzed the Friedel-Crafts dimerization of 1,1-diphenylethylene. This reactivity was now analyzed for the dimerization of α -methylstyrene, as the intended hydrosilylation with Et_3SiH was not successful. Instead, rapid dimerization of the olefin occurred. Targeted catalytic studies using **L-19**·(Donor)₂ and **L-21**·(Donor)₂ with loadings of 5 mol% in toluene-*d*₈ revealed the efficient dimerization of α -methylstyrene to the three structural isomers **A**, **B**, and **C**.^[64a] The observed catalyst activity for this reaction was comparable to that of transition metal-based systems presented in the literature.^[124] The best result was obtained for Lewis superacid **L-21**·(MeCN)₂, selectively forming dimerization product **C** in quantitative yields. For **L-21**·(THF)₂ and **L-21**·(Et₂O)₂ as well, sufficient conversion was detected; however, different ratios of the dimerization products were obtained (Figure 33, b). The presence of additional Et_3SiH severely affected the conversion but increased the selectivity for product **A**. DFT calculations were performed to understand the product formation, suggesting three different mechanisms involved, where the monocoordinated Lewis acid acts as the active species.^[64a]

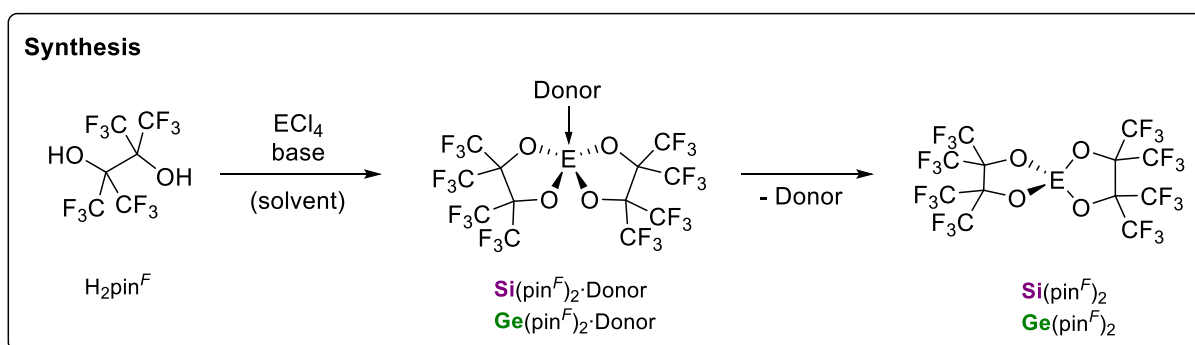
Another publication analyzed the catalytic photoredox alkylation of primary amines using Lewis acidic germanes such as Ph_2GeCl_2 as effective co-catalysts facilitating the reaction. Despite the reactivity of chlorogermanes, only trace amounts to no conversion was obtained when compound **L-19** $\cdot(\text{H}_2\text{O})_n$ was used as a co-catalyst.^[125] Nevertheless, the potential applicability of Lewis superacidic germanes for catalytic transformations remains a promising research field, that together with silicon-based Lewis superacids will contribute to the development of efficient and industrially relevant catalytic processes for a more sustainable future.

4 Assignment of the Ph.D. project

As outlined in the previous chapters, the synthesis of neutral Lewis superacidic silanes as well as germanes and their application for homogenous catalysis is an emerging research field that contributes with fundamental research to developing sustainable industrial processes. To date, this research is predominantly defined by perhalocatecholato-based Lewis acids that, lack sufficient solubility in most used non-polar solvents and require donor-stabilization to prevent oligo- or polymerization.^[113] As outlined by the Greb group, however, an ideal Lewis superacid catalyst should feature a set of defined characteristics that include the following selection.^[19]

- Superior Lewis acidity
- Thermal stability
- Strongly bound and inert ligands
- Solubility and solvent tolerance
- Tunable steric properties

In this context, we aimed to install perfluorinated pinacolate (pin^F) as a potent alternative to catecholates, enabling the formation of highly electron-deficient silanes while providing sufficient kinetic stabilization by steric protection.



Broadening to other substituents

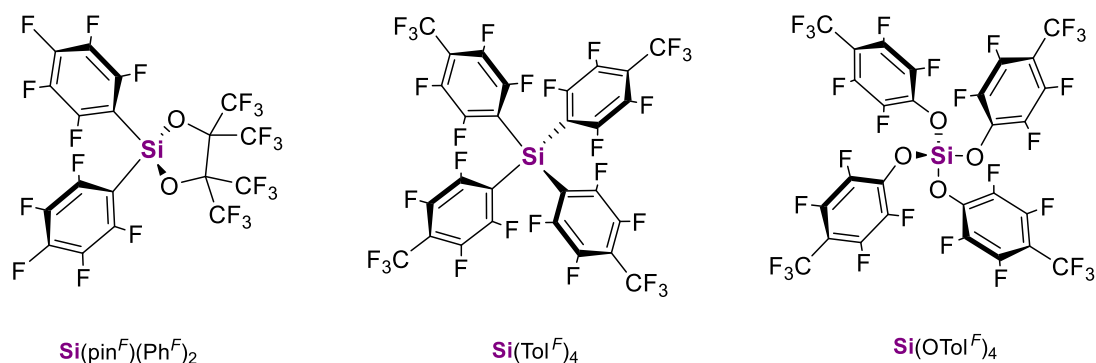


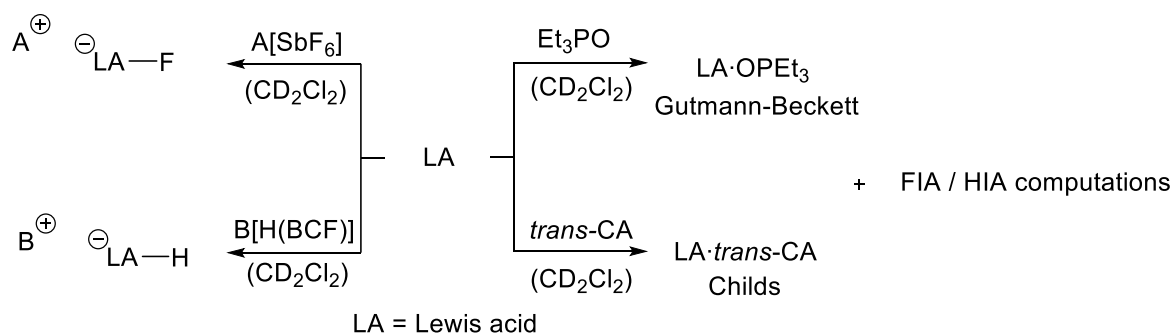
Figure 34: Targeted Lewis acids that should be synthesized and analyzed in this Ph.D. project.

The synthesis strategy should start from perfluorinated pinacol (H_2pin^F) and SiCl_4 , as a direct synthesis from poisonous perfluoro acetone appeared too dangerous. Consequently, the

synthesis of the bis-substituted Lewis superacid $\text{Si}(\text{pin}^F)_2$ and its consecutive analysis regarding its Lewis acidity was the first target of this Ph.D. project. In addition to the bidentate pinacolato-based systems also monodentate perfluorotolyl- (ToI^F) and perfluorocresolato (OToI^F) groups should be investigated for the synthesis of Lewis acidic silanes (Figure 34).

Due to the strong coordination of polar solvent molecules, reaction optimization and solvent abstraction is a significant challenge in synthesizing strongly Lewis superacidic compounds. With a reliable synthetic protocol at hand, the obtained Lewis acids should be prepared on a gram-scale, comprehensively analyzed, and tested for their catalytic potential. The obtained reactivities should be compared to the perhalocatecholato-based benchmark systems, researched within the groups of Tilley and Berman,^[109] Baines,^[64a] and Greb.^[64b, 111, 114, 116, 120-121]

Lewis acidity accessment



Screening for catalytic potential

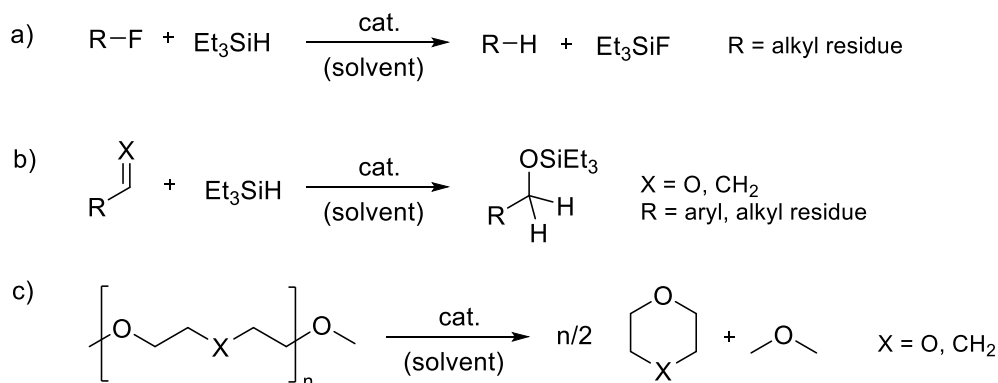


Figure 35: Additional scope of this project, including a consecutive Lewis acidity assessment in experiment and by computational methods, and the screening for potential applicability in relevant catalytic transformations (a-c).

The primary reactions of interest include $\text{C}(\text{sp}^3)\text{-H}$ hydrodefluorination reactions, carbonyl hydrosilylation, defunctionalization of ketones with hydrosilanes, and the degradation of oligo and polyethylene glycol diethers. In addition, the obtained catalysts should be scouted for olefin hydrosilylation activity in analogy to Jutzi's famous silyliumylidene cation, as this challenging reaction was not yet achieved with neutral Lewis acidic silanes.^[16b, 57]

Because of well-known HSAB influences on the reactivity of Lewis acids for hard and soft substrates, additionally, the germanium-centered derivatives should be synthesized, starting with $\text{Ge}(\text{pin}^F)_2$, and tested for their catalytic potential. Due to the “softer” germanium atom, the obtained germanes should significantly differ in terms of reactivity when compared to their respective silicon analogs. As a benchmark reactivity in this regard, the activation of fluoro- and hydrosilanes should be tested for the obtained Lewis superacids.

! ATTENTION !

The perfluoropinacol (H_2pin^F) majorly used as a precursor to perfluoropinacolato substituents in this work is ACUTELY TOXIC by SKIN CONTACT and INHALATION.^[126]



Lithiated perfluoropinacol (Li_2pin^F) appeared to be explosive by applying mechanical stress (scratching with a spatula) when residual amounts of *n*-butyllithium were present.



5 Bis(perfluoropinacolato)silane: A Neutral Silane Lewis Superacid Activates Si–F Bonds

Journal: *Angewandte Chemie International Edition*, **2021**, *60*, 25799–25803.
Publisher: Wiley-VCH GmbH
Authors: Florian S. Tschernuth, Thaddäus Thorwart, Lutz Greb, Franziska Hanusch, and Shigeyoshi Inoue*
Status: Communication, published 27. September 2021
DOI: 10.1002/anie.202110980 (Original Version)^[127]
10.1002/ange.202110980 (German Version)^[128]

Reproduced with open access permission.

Content: In this publication, perfluoropinacol ($\text{H}_2\text{pin}^{\text{F}}$) was used to form a novel Lewis superacidic silane. The synthesis strategy started from the reaction of lithiated perfluoropinacol ($\text{Li}_2\text{pin}^{\text{F}}$) with SiCl_4 in acetonitrile solution leading to the initial formation of the pentavalent lithium chlorosilicate salt $\text{Li}[\text{Si}(\text{pin}^{\text{F}})_2\text{Cl}]$. A similar result was obtained when HSiCl_3 was used instead of SiCl_4 . However, the respective hydrosilicate species $\text{Li}[\text{HSi}(\text{pin}^{\text{F}})_2]$ was formed in this case. Heating the obtained $\text{Li}[\text{Si}(\text{pin}^{\text{F}})_2\text{Cl}]$ to 110 °C led to the liberation of the neutral silane by LiCl elimination. The liberated Lewis acid was collected by sublimation at 0.02 mbar as the acetonitrile mono-adduct $\text{Si}(\text{pin}^{\text{F}})_2 \cdot \text{MeCN}$.

With the synthetic strategy at hand, $\text{Si}(\text{pin}^{\text{F}})_2 \cdot \text{MeCN}$ was synthesized on a gram-scale and analyzed for its Lewis acidity and catalytic behavior. Consecutive ATR-IR and Gutmann-Beckett analysis revealed a Lewis acidity in the range of literature-known perfluoro- and perchlorocatecholato-based Lewis superacids **L-4** and **L-7**. Lewis superacidity was proven in experiment by the successful fluoride abstraction from $\text{Ag}[\text{SbF}_6]$, forming a stable pentavalent fluorosilicate species $[\text{FSi}(\text{pin}^{\text{F}})_2]^-$. Ultimately the superior Lewis acidity of $\text{Si}(\text{pin}^{\text{F}})_2 \cdot \text{MeCN}$ was demonstrated by the fluoride abstraction from Et_3SiF , leading to the formation of acetonitrile-stabilized silyl cation, which was confirmed by crystal structure analysis. Additionally, calculated FIA and HIA values supported the experiments.

Furthermore, $\text{Si}(\text{pin}^{\text{F}})_2 \cdot \text{MeCN}$ was successfully tested for the catalytic hydrodefluorination of 1-fluoroadamantane with Et_3SiH , the hydrosilylation of electron-deficient benzaldehydes, the reductive ether formation of methylated benzaldehydes, and the reductive defunctionalization of benzo- and acetophenone with Et_3SiH .

*Florian S. Tschernuth planned and prepared all synthesis and experiments for this publication and wrote the manuscript and Supporting Information. Franziska Hanusch was responsible for the SC-XRD measurement and refinement of the crystal data. Thaddäus Thorwart and Lutz Greb provided quantum chemical computations. The research was performed under the direct supervision of Prof. Shigeyoshi Inoue.

Si–F Bond Activation

How to cite: *Angew. Chem. Int. Ed.* **2021**, *60*, 25799–25803
International Edition: doi.org/10.1002/anie.202110980
German Edition: doi.org/10.1002/ange.202110980

Bis(perfluoropinacolato)silane: A Neutral Silane Lewis Superacid Activates Si–F Bonds

Florian S. Tschernuth, Thaddäus Thorwart, Lutz Greb, Franziska Hanusch, and Shigeyoshi Inoue*

Dedicated to Professor Holger Braunschweig on the occasion of his 60th birthday

Abstract: Despite the earth abundance and easy availability of silicon, only few examples of isolable neutral silicon centered Lewis superacids are precedent in the literature. To approach the general drawbacks of limited solubility and unselective deactivation pathways, we introduce a Lewis superacid, based on perfluorinated pinacol substituents. The compound is easily synthesized on a gram-scale as the corresponding acetonitrile mono-adduct **1**-(MeCN) and was fully characterized, including single crystal X-ray diffraction analysis (SC-XRD) and state-of-the-art computations. Lewis acidity investigations by the Gutmann-Beckett method and fluoride abstraction experiments indicate a Lewis superacidic nature. The challenging Si–F bond activation of Et₃SiF is realized and promising catalytic properties are demonstrated, consolidating the potential applicability of silicon centered Lewis acids in synthetic catalysis.

The investigations of molecular main group element Lewis acids for bond activation and catalysis has drawn much attention.^[1] Especially cationic silylium ions and silyliumylidene have demonstrated exceptional catalytic abilities including hydrosilylation^[2] or hydrodefluorination reactions,^[3] thus moving the second most abundant element of the earth's crust into the reach of industrial relevance.^[4] To overcome the poor functional group tolerance and mostly limited solubility of cationic silicon reagents, the use of neutral, silicon-centered Lewis acids is highly desirable. Initial reports inspired by the research of Denmark and co-workers revealed the suitability of SiCl₄ as a potent co-catalyst for specific reactivities including aldol additions^[5] and aza-

Michael additions.^[6] However, due to the easily cleaved Si–Cl bond, examples of SiCl₄-catalyzed reactions remained rather rare. To prevent bond cleavage and elimination reactions, neutral, silicon-centered Lewis acids were realized by the installation of strongly electron withdrawing, mostly aryl and alkyl, substituents.^[7] Using a perfluorinated catecholato ligand, Tilley and Bergmann et al. were able to isolate a strongly Lewis acidic silane that was successfully applied in the hydrosilylation catalysis of electron deficient aldehydes.^[8] By a slight variation of the catecholato system using less π-back donating chloride and bromide substituents, the isolation of the first Lewis superacidic silanes was achieved (Figure 1),^[9] which possess formal fluoride ion affinities (FIAs) exceeding that of SbF₅ (definition of Lewis superacidity).^[10] The very recently reported bis(pertrifluoromethylcatecholato)silane displayed an even stronger Lewis acidity and broadened the catalytic portfolio of Lewis acidic silanes by the reductive dialkyl ether formation, deoxygenation of several substrates and a carbonyl-olefin metathesis reaction.^[11b] Still, this compound class suffers from poor solubility. This issue was addressed by the hard and soft Lewis superacidic silicon tetrakis(trifluoromethanesulfonate).^[11a] Despite its remarkable reactivity and improved solubility, so far no catalytic but only stoichiometric reactions were reported for this compound, potentially caused by the rather labile Si–OTf bond nature.

To overcome undesired side reactions and to stabilize the highly electron deficient Si^{IV} center by steric protection, we investigated the incorporation of bulky as well as strongly electron-withdrawing perfluoropinacolato groups as suitable substituents for the synthesis of Lewis acids. In this regard, we present the straight-forward synthesis and characterization of a novel and easy to handle, neutral silicon-centered Lewis superacid, its exceptional catalytic activity, and its ability to

*F. S. Tschernuth, F. Hanusch, Prof. Dr. S. Inoue
Department of Chemistry, WACKER-Institute of Silicon Chemistry and Catalysis Research Center, Technische Universität München Lichtenbergstraße 4, 85748 Garching (Germany)
E-mail: s.inoue@tum.de

T. Thorwart, Dr. L. Greb
Anorganisch-Chemisches Institut, Universität Heidelberg
Im Neuenheimer Feld 270, 69120 Heidelberg (Germany)

Supporting information and the ORCID identification number(s) for the author(s) of this article can be found under:
<https://doi.org/10.1002/anie.202110980>.

© 2021 The Authors. *Angewandte Chemie International Edition* published by Wiley-VCH GmbH. This is an open access article under the terms of the Creative Commons Attribution Non-Commercial License, which permits use, distribution and reproduction in any medium, provided the original work is properly cited and is not used for commercial purposes.

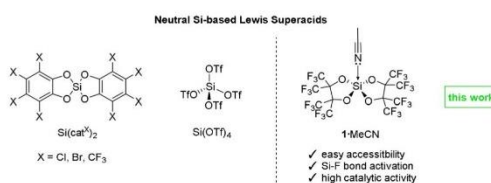


Figure 1. Literature known neutral, silicon-centered Lewis superacids (left)^[9,11] and the catalytically active Lewis superacid **1**-(MeCN), presented in this work.

abstract fluorides even from neutral fluorosilanes. State-of-the-art computations support the experimental findings.

In a first reaction, perfluoro pinacol (H_2pin^f) was lithiated by deprotonation with $nBuLi$ to obtain the more nucleophilic lithium salt Li_2pin^f . For the introduction of the strongly electron withdrawing perfluoro pinacol moiety onto a Si^{IV} center, Li_2pin^f was reacted with $SiCl_4$ and $HSiCl_3$, respectively, in acetonitrile solution. In both cases the precipitation of $LiCl$ was observed shortly after the silane was added. The reaction mixtures were stirred at $85^\circ C$ for three hours to ensure the complete formation of the monomeric reaction products. Subsequent filtration, and solvent removal in vacuo in both cases yielded colorless solids that could be assigned to the ionic compounds $Li[1-Cl]$ (for $SiCl_4$) and $Li[1-H]$ (for $HSiCl_3$), coordinated by residual acetonitrile.

The obtained pentavalent silicate species were characterized using NMR spectroscopic methods. The 1H NMR spectrum of $Li[1-Cl] \cdot (MeCN)_2$ in CD_3CN gave a singlet at $\delta = 1.96$ ppm that was attributed to the coordinating non-deuterated solvent. Two multiplets in the ^{19}F NMR spectrum at $\delta = -69.0$ to -69.2 ppm and $\delta = -69.9$ to -70.2 ppm indicated the presence of diastereotopic CF_3 moieties, in line with the symmetry of a pentacoordinate state. The ^{29}Si NMR spectrum gave a singlet at $\delta = -93.26$ ppm matching chemical shifts of related pentavalent chloride-substituted silicate species, obtained by Greb and co-workers,^[9,11b] showing a distinct downfield-shift compared to penta-alkoxy substituted silicates given in the literature.^[12]

The 1H NMR spectrum of $Li[1-H] \cdot (MeCN)_2$ gave an additional multiplet at $\delta = 4.52$ to 4.45 ppm that was attributed to the hydride substituent on the silicon center. The integral ratio between the acetonitrile proton and the hydride signal suggested a twofold coordination by the solvent. The ^{19}F NMR spectrum showed a similar but distinctively up-field shifted pattern, compared to $Li[1-Cl] \cdot (MeCN)_2$, by giving two multiplets at $\delta = -69.9$ to -70.2 ppm and $\delta = -70.7$ to -70.9 ppm. The singlet in the ^{29}Si NMR spectrum at $\delta = -90.19$ ppm was slightly shifted, but still within the expected range for pentavalent silicate species. Both structural motifs were supported by ^{29}Si NMR shift computations and ultimately confirmed by SC-XRD analysis. (see the supporting information). The formal activation of $LiCl$ in $Li[1-Cl]$, and LiH in $Li[1-H]$, salts of high lattice energy, indicates a strong Lewis acidity of the targeted neutral bis(perfluoropinacolato)silane **1**. In particular, the stability of $Li[1-H]$ renders remarkable, in light of the instability of hydrosilicates based on the catecholate ligand.^[14]

By the sublimation of $Li[1-Cl] \cdot (MeCN)_2$ at elevated temperatures in fine vacuo, the neutral silane was released as the acetonitrile adduct **1**·(MeCN), which was isolated in moderate to good yields (Figure 2). Attempts to remove the residual coordinating solvent by additional sublimation or azeotropic distillation with less coordinating solvents, however, remained unsuccessful so far. The obtained **1**·(MeCN) was well soluble in CD_3CN and could be characterized using NMR spectroscopic methods. The 1H NMR spectrum gave a singlet that was attributed to the solvent molecule. Further NMR experiments revealed two partially overlaying broad

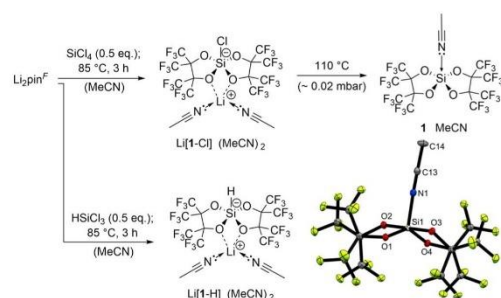


Figure 2. Left: Performed synthesis strategy yielding pentavalent silicate species $Li[1-Cl] \cdot (MeCN)_2$ and $Li[1-H] \cdot (MeCN)_2$ and the neutral Lewis superacidic silane **1**·(MeCN) as the acetonitrile mono-adduct. Right: Molecular structure of **1**·(MeCN) obtained by SC-XRD analysis (ellipsoids at 50% probability level). Selected bond lengths (Å): Si1–N1 1.8412(16), Si1–O1 1.6745(14), Si1–O2 1.7223(14), Si1–O3 1.7234(14), Si1–O4 1.6886(14).^[13]

multiplets at $\delta = -69.5$ to -70.6 ppm in the ^{19}F spectrum and a singlet at $\delta = -110.34$ ppm in the ^{29}Si spectrum.

The solid-state IR spectrum revealed two strongly overlapping signals at 2358 cm^{-1} and 2329 cm^{-1} that are assigned to the $C\equiv N$ stretching coupled to CH_3 -deformation vibrations of strongly coordinating acetonitrile. The coordinating CH_3CN was substituted with CD_3CN leading to only one sharp signal at 2352 cm^{-1} , that could be assigned to the blue-shifted $C\equiv N$ stretching vibration. The observed shift of 94 cm^{-1} with respect to the free CD_3CN (2258 cm^{-1})^[15] indicated an outstandingly high Lewis acidity, even exceeding literature known examples of acetonitrile adducts of Lewis superacids $Si(cat^f)_2$,^[9a] $Al(OTeF_5)_3$,^[15] and SbF_5 .^[16]

To further investigate the Lewis acidity by the Gutmann-Beckett method, **1**·(MeCN) was reacted with stoichiometric amounts of Et_3PO in non-polar solvent CD_2Cl_2 . Subsequent ^{31}P NMR analysis revealed the formation of the phosphine oxide monoadduct **1**- OPe_3 with a ^{31}P shift of $\Delta\delta = 35.8$ ppm. This result is in good agreement with literature-known electron deficient silanes like $Si(cat^f)_2$ ($\Delta\delta = 36.1$ ppm) and even the Lewis superacidic $Si(cat^f)_2$ ($\Delta\delta = 36.7$ ppm).^[9b] In contrast to related silanes holding halogenated catechol derivatives or triflate substituents, no bis-adduct formation was observed in case of **1**·(MeCN),^[9,11] even when surplus Et_3PO amounts were added (up to 3.0 equiv.).

For a closer structural investigation, single crystals suitable for SC-XRD analysis were obtained by recrystallization from toluene.^[13] The obtained structure shows a pentavalent, square pyramidal coordination of Si1 by two pinacolato groups and a terminal acetonitrile molecule. The extreme close Si1–N1 bond length of $1.8412(16)$ Å surpasses literature known acetonitrile adducts of aluminum-based Lewis superacid $Al(OCaF_3)_3$ ($1.9431(11)$ Å)^[17] and matches bond lengths reported for silylium ion-MeCN adducts (1.864 to 1.847 Å).^[18] To our knowledge, this represents the first MeCN-adduct of a neutral silicon-based Lewis acid confirmed by SC-XRD. The steric protection of the pinacolato groups is demonstrated by a slightly bent geometry with

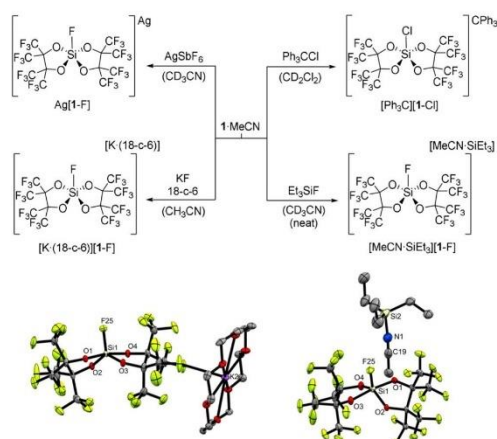


Figure 3. Top: Reactivity experiments of **1** showing the successful fluoride abstraction from AgSbF_6 confirming formal Lewis superacidity. Halide abstraction was also observed for KF , Et_3SiF and trityl chloride. Bottom: Crystal structures (50% probability level) obtained by diffraction analysis of reaction products with KF and Et_3SiF .^[13]

diagonal bond angles O1-Si1-O4 and O2-Si1-O3 of $136.31(7)^\circ$ and $179.60(7)^\circ$.

To investigate potential Lewis super acidity, **1**·(MeCN) was reacted with AgSbF_6 in acetonitrile solution (Figure 3 top). Already after 10 minutes at room temperature the ^{19}F NMR spectrum showed nearly quantitatively consumption of the starting material. Instead, the formation of the pentavalent $[\text{I-F}]^-$ anion was observed, thus confirming Lewis superacidity by experiment ($\text{FIA} > \text{SbF}_5$). The computed FIA (474 kJ mol^{-1} , DLPNO-CCSD(T)/aug-cc-pVQZ) did not exceed that of SbF_5 , but suggested additional effects are supporting the thermodynamics of this reaction in experiment. Still, **1**·(MeCN) thus extends the rare class of experimentally confirmed neutral Si^{IV} Lewis superacids by a well-defined and well-soluble derivative. The pentavalent $[\text{I-F}]^-$ silicate species was additionally synthesized by the reaction of **1**·(MeCN) with KF in the presence of the crown ether 18-c-6. The ^{19}F NMR spectrum matched the pattern obtained from isolated $\text{Ag}[\text{I-F}]^-$ showing two split multiplets at $\delta = -69.8$ to -70.1 ppm and $\delta = -70.8$ to -71.1 ppm for the CF_3 moieties as well as a smaller multiplet at $\delta = -138.6$ to -138.9 ppm corresponding to the silicon bound fluoride. The ^{29}Si NMR spectrum gave a doublet at $\delta = -108.37$ ppm with a silicon-fluoride coupling constant of $J_{\text{Si,F}} = 179.8$ Hz. Single crystals suitable for SC-XRD analysis were obtained from a saturated solution in chloroform at -30°C .^[13] The $[\text{I-F}]^-$ anion shows a pentavalent square pyramidal structure of the central silicon atom by two perfluoropinacolato groups and one fluoride with bond lengths of $1.592(2)$ Å for the Si–F bond and 1.698 to 1.740 Å for the Si–O bonds. The pinacolato substituents are slightly bent towards each other with bond angles of $169.82(11)^\circ$

(O1-Si1-O4) and $133.11(11)^\circ$ (O2-Si1-O3) in the *trans* position, respectively.

The addition of Ph_3CCl to a CD_2Cl_2 solution of **1**·(MeCN) immediately led to the formation of a triphenyl carbenium ion, which was indicated by rapid color change yielding a luminous yellow solution. ^{19}F and ^{29}Si NMR spectroscopic analyses of the reaction mixture after 24 hours revealed the quantitative formation of the pentavalent $[\text{I-Cl}]^-$ species, matching the pattern of previously synthesized $\text{Li}[\text{I-Cl}]^-$ ·(MeCN)₂.

The most remarkable testimonial of the high fluoride ion affinity was provided by the neat reaction of **1**·(MeCN) with stoichiometric Et_3SiF . After 10 minutes at room temperature complete conversion was observed in the ^{19}F NMR spectrum showing quantitative formation of the $[\text{I-F}]^-$ pattern. The ^{29}Si NMR analysis gave the characteristic doublet at $\delta = -108.37$ ppm and an additional singlet at $\delta = +36.63$ ppm that was assigned to the Et_3Si^+ ion coordinated by acetonitrile.^[19] This observation was confirmed by SC-XRD analysis of single crystals obtained from saturated CH_2Cl_2 solution at -30°C (Figure 3 bottom).^[13] The crystal structure reveals the presence of the $[\text{I-F}]^-$ anion located directly next to a Et_3Si^+ cation, that is coordinated by an acetonitrile molecule with a Si–N bond length of $1.826(3)$ Å. As already indicated by NMR, the anion showed the exact same pentavalent binding motif that was already observed for the potassium derivative $[\text{K-18-c-6}][\text{I-F}]^-$. The abstraction of the fluoride to form a silylium ion coordinated by acetonitrile confirms an exceptionally high Lewis acidity of **1**·(MeCN). Although the FIA of **1** is lower than those of silylium ions (see SI), the overall process is driven by the favorable thermodynamics of the binding of the silylium ion to acetonitrile, and the salt formation between $[\text{I-F}]^-$ and $[\text{MeCN:SiEt}_3]^+$. This was additionally confirmed by favorable solvation corrected DSD-BLYP-D3/def2-QZVPP computed thermodynamics for the reaction (see section 3 in the SI). Si–F bonds are among the most stable single bonds, and their activation

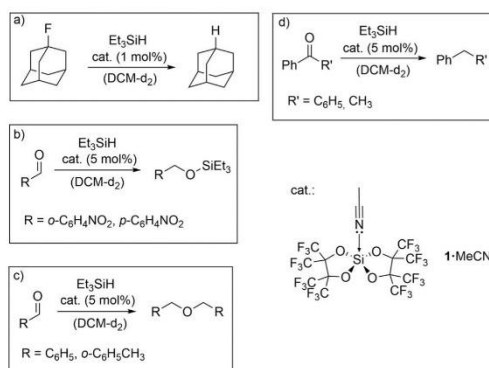


Figure 4. Reactivity investigations using **1**·(MeCN) as Lewis acid catalyst showing successful hydrodefluorination of 1-fluoroadamantane (a), hydrosilylation of *o*- and *p*-nitrobenzaldehyde (b), reductive dialkyl ether formation of benzaldehyde and *o*-methyl benzaldehyde (c) and deoxygenation of benzophenone and acetophenone (d).

represents a formidable challenge, even for transition metal complexes.^[20]

Inspired by the strong fluoride affinity, compound **1**-(MeCN) was investigated as potential catalyst for the stoichiometric hydrodefluorination (HDF) of 1-fluoroadamantane with Et₃SiH using low catalyst loadings of 1 mol% (Figure 4a). After two hours at room temperature quantitative conversion was observed in the ¹⁹F NMR spectrum by the absence of the fluoroadamantane signal and the selective formation of Et₃SiF. While this reaction is well known for silylium cations,^[3,21] examples for neutral Lewis acidic silanes as a catalyst are rare. To our knowledge, only the perhalogenated Lewis superacids Si(cat^X)₂ (X = Cl, Br) show a comparable reactivity, but with longer reaction periods required.^[9] The observed reactivity prompted us to further investigate the HDF reactivity by using the terminal 1-fluoropentane as a substrate. In this case, however, fluoride abstraction led to dehydrodefluorination indicated by immediate hydrogen evolution. Subsequent isomerization led to an unselective mixture of pentene isomers and unreacted starting material. No HDF could be observed, as it was also reported for Si(cat^C)₂.^[9a]

In analogy to previously reported Si(cat^F)₂, **1**-(MeCN) was investigated as catalyst (5 mol%) for the hydrosilylation of electron deficient *p*- and *o*-nitrobenzaldehyde using Et₃SiH (Figure 4b). In both cases complete silane conversion was observed already after 20 minutes at room temperature in CD₂Cl₂, selectively yielding the respective hydrosilylation products. After longer reaction periods, a subsequent reaction occurred, partially turning the hydrosilylation products into the respective dialkyl ethers.^[22] As the side product hexaethyldisiloxane was liberated during this reaction.

When using non-electron-deficient benzaldehyde and *o*-methylbenzaldehyde in the same experimental setup but with 1.5 equiv. of Et₃SiH, no hydrosilylation could be observed at all (Figure 4c). Instead, the immediate selective formation of the respective dialkyl ethers was favored. A similar reactivity was observed for the recently published Si(cat^{CF₃})₂.^[11b]

Reaction with benzophenone and even acetophenone rapidly yielded deoxygenation products when 3.0 equiv. of Et₃SiH and 5 mol% of catalyst **1**-(MeCN) were used (Figure 4d). In case of benzophenone nearly complete and selective conversion was detected in the ¹H NMR spectrum already after 2 hours at room temperature using only a catalyst loading of 1 mol%. For more challenging acetophenone a catalyst loading of 5 mol% led to quantitative conversion within 1 hour at room temperature.

In summary, we have extended the exclusive club of silicon-centered Lewis superacids by the straightforward synthesis of **1**-(MeCN), which was successfully tested for the fluoride abstraction from SbF₆⁻. The compound holds the rare ability to bind hydrides, granting access to the respective tetraoxy-substituted hydrosilicate. Further experiments revealed the fluoride abstraction from stoichiometric Et₃SiF in the presence of acetonitrile. Si–F bond activation in tetravalent fluorosilanes remains a significant challenge, ironically now achieved with a silicon-based Lewis acid. Finally, **1**-(MeCN) was successfully tested in the catalytic hydrodefluorination of 1-fluoroadamantane, hydrosilylation

of electron deficient aldehydes, reductive dialkyl ether formation of benzaldehydes and deoxygenation of ketones. With its easy accessibility and catalytic versatility **1**-(MeCN) represents a highly promising reagent that once again contributes to the overall aim of transition metal-free catalysis for a more ecological future.

Acknowledgements

We are exceptionally grateful to the WACKER Chemie AG for the idealistic and financial support, as well as contributions in guidance and discussions, which enabled us to carry out this research project. We also thank Lena Staiger (Prof. R. A. Fischer) for conducting IR measurements. Open Access funding enabled and organized by Projekt DEAL.

Conflict of Interest

The authors declare no conflict of interest.

Keywords: main-group catalysis · perfluoropinacol · Si–F activation · silicon Lewis superacid · silicon mediated catalysis

- [1] a) H. Yamamoto, *Silicon(IV) Lewis Acids*, Wiley-VCH, Weinheim, **2000**; b) A. G. Davies, *Appl. Organomet. Chem.* **2002**, *16*, 65–65; c) M. Rubin, T. Schwier, V. Gevorgyan, *J. Org. Chem.* **2002**, *67*, 1936–1940; d) C. B. Caputo, L. J. Hounjet, R. Dobrovetsky, D. W. Stephan, *Science* **2013**, *341*, 1374–1377; e) L. J. Hounjet, C. Bannwarth, C. N. Garon, C. B. Caputo, S. Grimme, D. W. Stephan, *Angew. Chem. Int. Ed.* **2013**, *52*, 7492–7495; *Angew. Chem.* **2013**, *125*, 7640–7643; f) M. Pérez, L. J. Hounjet, C. B. Caputo, R. Dobrovetsky, D. W. Stephan, *J. Am. Chem. Soc.* **2013**, *135*, 18308–18310; g) T. Stahl, H. F. T. Klare, M. Oestreich, *ACS Catal.* **2013**, *3*, 1578–1587; h) H. Böhler, N. Trapp, D. Himmel, M. Schleep, I. Krossing, *Dalton Trans.* **2015**, *44*, 7489–7499; i) M. Yang, D. Tofan, C.-H. Chen, K. M. Jack, F. P. Gabbaï, *Angew. Chem. Int. Ed.* **2018**, *57*, 13868–13872; *Angew. Chem.* **2018**, *130*, 14064–14068; j) A. Roy, M. Oestreich, *Chem. Eur. J.* **2021**, *27*, 8273–8276.
- [2] E. Fritz-Langhals, *Org. Process Res. Dev.* **2019**, *23*, 2369–2377.
- [3] a) V. J. Scott, R. Çelenligil-Çetin, O. V. Ozerov, *J. Am. Chem. Soc.* **2005**, *127*, 2852–2853; b) C. Douvris, O. V. Ozerov, *Science* **2008**, *321*, 1188–1190.
- [4] H. F. T. Klare, L. Albers, L. Süsse, S. Keess, T. Müller, M. Oestreich, *Chem. Rev.* **2021**, *121*, 5889–5985.
- [5] a) S. E. Denmark, T. Wynn, *J. Am. Chem. Soc.* **2001**, *123*, 6199–6200; b) S. E. Denmark, G. L. Beutner, T. Wynn, M. D. Eastgate, *J. Am. Chem. Soc.* **2005**, *127*, 3774–3789; c) L. Palombi, M. R. Accocella, N. Celenta, A. Massa, R. Villano, A. Scettri, *Tetrahedron: Asymmetry* **2006**, *17*, 3300–3303; d) S. E. Denmark, W.-j. Chung, *J. Org. Chem.* **2008**, *73*, 4582–4595.
- [6] N. Azizi, R. Baghi, H. Ghafuri, M. Bolourtchian, M. Hashemi, *Synlett* **2010**, 379–382.
- [7] a) S. Steinhauer, J. Bader, H.-G. Stammer, N. Ignat'ev, B. Hoge, *Angew. Chem. Int. Ed.* **2014**, *53*, 5206–5209; *Angew. Chem.* **2014**, *126*, 5307–5310; b) S. Steinhauer, T. Böttcher, N. Schwarze, B. Neumann, H.-G. Stammer, B. Hoge, *Angew. Chem. Int. Ed.* **2014**, *53*, 13269–13272; *Angew. Chem.* **2014**, *126*, 13485–13488; c) N. Schwarze, B. Kurscheid, S. Steinhauer, B.

- Neumann, H.-G. Stammler, N. Ignat'ev, B. Hoge, *Chem. Eur. J.* **2016**, *22*, 17460–17467.
- [8] A. L. Liberman-Martin, R. G. Bergman, T. D. Tilley, *J. Am. Chem. Soc.* **2015**, *137*, 5328–5331.
- [9] a) R. Maskey, M. Schädler, C. Legler, L. Greb, *Angew. Chem. Int. Ed.* **2018**, *57*, 1717–1720; *Angew. Chem.* **2018**, *130*, 1733–1736; b) D. Hartmann, M. Schädler, L. Greb, *Chem. Sci.* **2019**, *10*, 7379–7388.
- [10] L. O. Müller, D. Himmel, J. Stauffer, G. Steinfeld, J. Slattery, G. Santiso-Quiñones, V. Brecht, I. Krossing, *Angew. Chem. Int. Ed.* **2008**, *47*, 7659–7663; *Angew. Chem.* **2008**, *120*, 7772–7776.
- [11] a) A. Hermannsdorfer, M. Driess, *Angew. Chem. Int. Ed.* **2021**, *60*, 13656–13660; *Angew. Chem.* **2021**, *133*, 13769–13773; b) T. Thorwart, D. Roth, L. Greb, *Chem. Eur. J.* **2021**, *27*, 10422–10427.
- [12] K. C. Kumara Swamy, V. Chandrasekhar, J. J. Harland, J. M. Holmes, R. O. Day, R. R. Holmes, *Phosphorus Sulfur Silicon Relat. Elem.* **1995**, *99*, 239–256.
- [13] Deposition numbers 2102990 I-(MeCN), 2102991 [I-Cl]⁻, 2102992 Li[I-H](MeCN)₂, 2102993 [K(18-c-6)][I-F], and 2102994 [MeCN·SiEt₃][I-F] contain the supplementary crystallographic data for this paper. These data are provided free of charge by the joint Cambridge Crystallographic Data Centre and Fachinformationszentrum Karlsruhe Access Structures service.
- [14] M. Kira, K. Sato, H. Sakurai, *J. Org. Chem.* **1987**, *52*, 948–949.
- [15] A. Wiesner, T. W. Gries, S. Steinhauer, H. Beckers, S. Riedel, *Angew. Chem. Int. Ed.* **2017**, *56*, 8263–8266; *Angew. Chem.* **2017**, *129*, 8375–8378.
- [16] B. v. Ahlsen, B. Bley, S. Proemmel, R. Wartchow, H. Willner, F. Aubke, *Z. Anorg. Allg. Chem.* **1998**, *624*, 1225–1234.
- [17] J. F. Kögel, A. Y. Timoshkin, A. Schröder, E. Lork, J. Beckmann, *Chem. Sci.* **2018**, *9*, 8178–8183.
- [18] a) N. Masaaki, F. Tomohide, S. Akira, *Chem. Lett.* **2004**, *33*, 38–39; b) C. Gerdes, W. Saak, D. Haase, T. Müller, *J. Am. Chem. Soc.* **2013**, *135*, 10353–10361; c) S. S. Chitnis, F. Krischer, D. W. Stephan, *Chem. Eur. J.* **2018**, *24*, 6543–6546.
- [19] S. R. Bahr, P. Boudjouk, *J. Am. Chem. Soc.* **1993**, *115*, 4514–4519.
- [20] a) H. Kameo, T. Kawamoto, S. Sakaki, D. Bourissou, H. Nakazawa, *Chem. Eur. J.* **2016**, *22*, 2370–2375; b) H. Kameo, H. Yamamoto, K. Ikeda, T. Isasa, S. Sakaki, H. Matsuzaka, Y. García-Rodeja, K. Miqueu, D. Bourissou, *J. Am. Chem. Soc.* **2020**, *142*, 14039–14044.
- [21] C. Douvris, C. M. Nagaraja, C.-H. Chen, B. M. Foxman, O. V. Ozerov, *J. Am. Chem. Soc.* **2010**, *132*, 4946–4953.
- [22] J. Chen, L. Dang, Q. Li, Y. Ye, S. Fu, W. Zeng, *Synlett* **2012**, *23*, 595–600.
- Manuscript received: September 24, 2021
Accepted manuscript online: September 27, 2021
Version of record online: November 5, 2021

6 Catalytic Degradation of Aliphatic Ethers using the Lewis Superacidic Bis(perfluoropinacolato)silane

Journal: *ChemCatChem*, **2023**, *15*, e202300281.^[129]
Publisher: Wiley-VCH GmbH
Authors: Florian S. Tschernuth, Lukas Bichlmaier, and Shigeyoshi Inoue*
Status: Research Article, published 21. March 2023
DOI: 10.1002/cctc.202300281

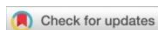
Reproduced with open access permission.

Content: In this study, the previously synthesized Lewis superacid $\text{Si}(\text{pin}^F)_2 \cdot \text{MeCN}$ (*vide supra*) was tested for the catalytic C-O ring-closing metathesis to degrade oligo- and polyethyleneglycol diethers and derivatives. The research was inspired by a preceding work of the Greb group that demonstrated the importance of selective mono-coordination of the etheric substrate to the Lewis acidic center for the catalyst activity.^[116] The study showed that in the case of di- and polydentate chelation, the reaction conversion is significantly decreased due to strong thermodynamic stabilization of the catalyst molecule.

According to that reasoning, $\text{Si}(\text{pin}^F)_2 \cdot \text{MeCN}$ should exhibit increased activity for the catalytic ether fragmentation because the sterically congested Lewis acidic center only enables monodentate donor coordination. In fact, the reactivity assessment for the C-O bond metathesis of 1,5-dimehtoxypentane and diglyme displayed an excellent catalytic behavior, selectively yielding the respective cyclization products in quantitative yields while outperforming literature-known catalyst systems. Nevertheless, further studies with tetra- and polyethyleneglycol dimethylether (TEG-DME / PEG-DME) revealed fast catalyst deactivation, which was explained by competing nucleophilic attacks during the fragmentation cycle that either led to reaction progress or irreversible side-reactions. Deactivation was more pronounced in the case of longer-chained substrates because the catalytic process involves nucleophilic attacks on less favored secondary carbon centers instead of the more accessible primary carbons.

Furthermore, a potential penta-oxo-coordinated reaction intermediate was synthesized by the cleavage of Et_2O in the presence of $\text{Si}(\text{pin}^F)_2 \cdot \text{MeCN}$. The formed silicate species was obtained as the respective triethyloxonium and *N*-ethyl acetonitrilium species and comprehensively characterized, including multinuclear NMR and SC-XRD analysis.

*Florian S. Tschernuth planned and prepared all synthesis experiments for this publication and wrote the manuscript as well as Supporting Information. Lukas Bichlmaier contributed by the reliable execution of repetitive catalytic fragmentation experiments, which was part of his master's thesis. Prof. Shigeyoshi Inoue directly supervised the research.



Catalytic Degradation of Aliphatic Ethers using the Lewis Superacidic Bis(perfluoropinacolato)silane

Florian S. Tschernuth,^[a] Lukas Bichlmaier,^[a] and Shigeyoshi Inoue^{*,[a]}

The exceptional catalytic activity of a neutral Si(IV) Lewis superacid was highlighted on the degradation of oligo- and polyethers *via* ring closing metathesis. Model reaction experiments with diglyme and 1,5-dimethoxypentane outlined a significantly increased reactivity surpassing comparable Lewis acid catalyst presented in the literature. The high observed activity was explained by the kinetic effect of the bulky perfluorinated substituents, blocking a second coordination site

that is responsible for catalyst deactivation by substrate chelation. Further experiments with aliphatic oligoethers outlined a gradual activity loss of the catalyst due to mechanistic disparities favoring side-reactions when more than one internal product unit is present. The extraordinary affinity for the cleavage of etheric C–O bonds was ultimately demonstrated by the reaction with diethylether, producing a pentavalent silicate species that was fully characterized including SC-XRD analysis.

Introduction

The demand for sustainable products and environmentally friendly industrial processes increased significantly in recent years, leading to challenging changes but also opportunities especially in the chemical and polymer industry.^[1] For the production of plastic commodities, for instance, a clear tendency towards circular and recyclable materials can be traced. Nevertheless, this transition is rather slow and the majority of plastic waste still ends up in landfills or is thermally converted for energy recovery.^[2] In this regard chemical depolymerization introduces an alternative solution to recover valuable building blocks and chemicals from waste-materials.^[3] Especially aliphatic polyethers are produced on a megatong scale and can be found in a wide range of commodities as well as functionalized materials like fibers, foams, or medical surfactants.^[4] The predominant repeating units of those polymers are composed of aliphatic ethers, that can be degraded in the presence of strong Lewis acids thus enabling a strategy for targeted depolymerization.^[5] The early work of Enthaler *et al.* demonstrated that Lewis acidic iron and zinc catalysts successfully convert various oligo- and poly(ethylene)glycols with stoichiometric amounts of acyl chlorides.^[6] Additional studies

showed the suitability of various Lewis and Brønsted acids for the degradation of poly(THF) substrates with no additional reactants, but harsh reaction conditions required.^[7] The Morandi group investigated Fe(OTf)₃ for the catalytic ring-closing metathesis of 1,5-dimethoxypentane and resembling aliphatic ethers to form cyclic reaction products.^[8] A metal-free version of this reaction was further outlined by Liu *et al.* using imidazolium-based ionic liquids as catalysts under biphasic and solvent-free conditions.^[9] Pursuing an environmentally friendly polymer degradation, Cantat and coworkers applied the multi-talent B(C₆F₅)₃ as well as transition-metal catalysts for the reductive degradation of polyethers, polyesters and polycarbonates with hydrosilanes.^[10] As shown by the Jutzi group also low-valent silicon cations can be used for the C–O metathesis of oligo(ethylene glycol)diethers (Figure 1, b), thus introducing the second most abundant

[a] F. S. Tschernuth, L. Bichlmaier, Prof. S. Inoue
TUM School of Natural Sciences
Department of Chemistry
WACKER-Institute of Silicon Chemistry and Catalysis Research Center
Technical University of Munich
Lichtenbergstraße 4
85748 Garching (Germany)
E-mail: s.inoue@tum.de

Supporting information for this article is available on the WWW under
https://doi.org/10.1002/cctc.202300281

© 2023 The Authors. ChemCatChem published by Wiley-VCH GmbH. This is an open access article under the terms of the Creative Commons Attribution Non-Commercial License, which permits use, distribution and reproduction in any medium, provided the original work is properly cited and is not used for commercial purposes.

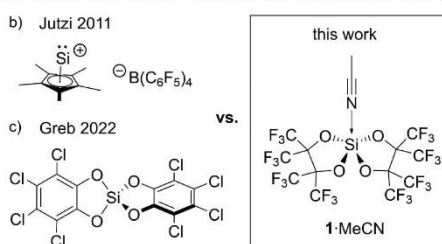
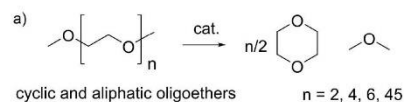


Figure 1. (a) Reported ring closing metathesis of oligoethers catalysed by the low-valent Si(II) cation (b) and the neutral Lewis superacidic Si(cat)₂ (c), compared to the catalyst system studied in this work.^[11–12]

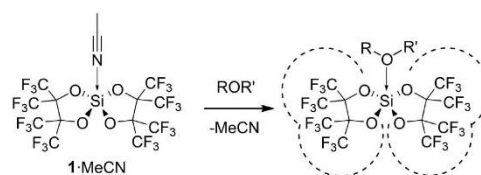
element of the earth's crust as a potential catalyst for polymer degradation.^[11]

A recent study from the Greb group comprehensively investigated the catalytic C–O metathesis reactions of oligo- and polyethers using the neutral Si(IV) Lewis superacid $[\text{Si}(\text{cat}^{\text{Cl}})_2]$ that possesses a polymeric structure $([\text{Si}(\text{cat}^{\text{Cl}})_2]_n)$.^[12] The compound catalytically converted chelating substrates like 1,5-dimethoxypentane, diglyme and crown ethers while outperforming previously established catalysts with ease (Figure 1, c). Even polymeric ethylene- and propyleneglycol diethers could be degraded, however high catalyst loadings were required. Our group published a related acetonitrile-adduct of a Lewis superacidic silane ($\text{Si}(\text{pin}^{\text{F}})_2 \cdot \text{MeCN}$) that showed significant catalytic behavior for carbonyl reduction reactions and even activated Si–F bonds.^[13] In this study we present the compound's tremendous activity in the degradation of oligo- and polyethers and discuss reaction differences for etheric substrates that affect the catalyst's performance. We additionally give a full characterization of a penta-coordinate silicate species as a potential reaction intermediate derivative that was isolated by the cleavage of diethyl ether.

Results and Discussion

In 2021 we presented the synthesis and characterization of bis(perfluoropinacolato)silane as its acetonitrile mono-adduct $\text{Si}(\text{pin}^{\text{F}})_2 \cdot \text{MeCN}$ (1·MeCN).^[13] Lewis acidity investigations by competitive abstraction experiments outlined a Lewis superacidic nature and several reactions like hydrodefluorination or carbonyl reduction were successfully catalyzed by 1·MeCN. While assessing the Lewis acidity by the Gutmann-Beckett (GB) method only mono-coordinated Lewis pairs were formed and no double-coordinated product could be observed, even when surplus Et_3PO was present. This inclination is rather uncommon among Lewis acids like in the case of catecholato silanes and related systems, where twofold coordination is the prevalent structural motif.^[14] An explanation for this phenomenon can be found in the steric bulk of the perfluorinated pinacolato groups that shield a second coordination site when one donor molecule is already attached to the silicon center. The resulting pentacoordinate geometry was already visualized in case of the acetonitrile-coordinated 1·MeCN by SC-XRD analysis.^[13]

Due to this geometric effect, the pinacolato silane could act as a potent catalyst for the ring closing metathesis of oligoethers, as recently published mechanistic investigations for the related Lewis superacid $[\text{Si}(\text{cat}^{\text{Cl}})_2]_n$ would suggest.^[12] In that study the catalytic ether degradation initiated via the mono-coordination of one etheric oxygen followed by the cleavage of a C–O bond while forming a zwitterionic intermediate. As reported, a twofold coordination by the chelating reactant, however, leads to catalyst deactivation because of the strong thermodynamic stabilization.^[12] For this reason, catalysts with two or three potential coordination sites for multidentate substrates were found less active for the ring-closing metathesis, whereas catalysts with blocked or less favorable multi-



Scheme 1. Schematic depiction of catalyst mono-coordination by etheric substrate substituting acetonitrile in solution.

ple-coordination sites showed increased activity. This was underpinned by an experiment with bis(perfluoro-*N*-phenylamidophenolato)silane,^[15] where the double coordination of diglyme is even less stabilized as for $[\text{Si}(\text{cat}^{\text{Cl}})_2]_n$.^[12] Following this reasoning, we expected that our pinacolato silane 1·MeCN shows even higher reactivity as acetonitrile should be exchanged in solution with the employed etheric substrate (Scheme 1) Furthermore, the liberated silane 1 possesses a similar Lewis acidity compared to $[\text{Si}(\text{cat}^{\text{Cl}})_2]_n$ in case of fluoride ion affinity calculations (FIA: 474 kJ mol^{-1} (1) vs. 507 kJ mol^{-1}) as well as GB measurements ($\Delta\delta(^1\text{P}) = 35.8 \text{ ppm}$ (1) vs. 35 ppm).^[13,14e] Deactivating effects caused by twofold coordination of the substrate should be sufficiently diminished by steric protection of the perfluoropinacolato groups.

In fact, reactions with 1,5-dimethoxypentane and diglyme revealed an outstanding performance of 1·MeCN for the catalytic C–O metathesis reaction under mild condition and low catalyst loadings, thus outperforming established catalyst systems (Table 1).^[8,12] For both substrates full conversion was observed quantitatively yielding the cyclic reaction products already after 1 hour at 80°C for 1,5-dimethoxypentane and 2.5 hours at 80°C for diglyme, when using a catalyst loading of 5 mol%. Unlike in the case of $[\text{Si}(\text{cat}^{\text{Cl}})_2]_n$ no deactivation was observed for reactions with 1,5-dimeth-

Table 1. Ring closing metathesis experiments of 1,5-dimethoxypentane (1,5-DMP), diglyme, poly(ethyleneglycol)dimethylether (PEG-DME) and 18-crown-6 at 80°C using 1·MeCN as reaction catalyst.

Entry	Substrate	cat. (mol%)	Time [h]	Yield [%] ^[a]	TON ^[b]
1	1,5-DMP	1	20	97	97.0
2	1,5-DMP	5	1	96	19.2
3	Diglyme	1	20	96	96.0
4	Diglyme	5	2.5	96	19.2
6	Diglyme	10	96	99	9.9
7	18-crown-6	30	30	88	8.8
8	PEG-DME	225	18	87	8.7

1,5-DMP: X = CH₂, n = 1 Diglyme: X = O, n = 1
PEG-DME: X = O, n = 22.5 18-crown-6: X = O, n = 3, no Me₂O

[a] Yield determination of reaction products tetrahydropyran and 1,4-dioxane was conducted by ¹H NMR via integration against internal standard mesitylene. [b] Calculation: TON = n(cyclic product)/n(catalyst).

6. Catalytic Degradation of Aliphatic Ethers using the Lewis Superacidic Bis(perfluoropinacolato)silane – Dissertation Florian Tschernuth

oxypentane and diglyme, even allowing quantitative conversions with catalyst loadings of only 1 mol%.^[12]

Both reactions also proceeded at room temperature but required significantly elongated reaction periods for full conversion (see SI Table S1 and S2). Further screenings of 1-MeCN for the degradation of 18-crown-6 and poly(ethyleneglycol)-dimethylether ($M_w = \sim 2000 \text{ g mol}^{-1}$) revealed that significantly higher catalyst amounts were required for those substrates. In case of 18-crown-6, 30 mol% of the catalyst were used to ensure quantitative conversion. This correlates to the 21 mol% of catalyst $[\text{Si}(\text{cat}^{\text{Cl}})]$ that were applied in the literature.^[12,16] A similar result was observed for PEG-DME where 225 mol% of 1-MeCN were necessary for full conversion.^[12,17] The decreased turn over number (TON) in the case of 18-crown-6 and PEG-DME indicates a catalyst deactivation, that is more pronounced for substrates with more than one internal C–O metathesis cycle per molecule. To verify this hypothesis, fragmentation experiments with tetra(ethyleneglycol)dimethyl ether (TEG-DME) were conducted. In that case full conversion was not reached with catalyst loadings of 5–10 mol% and reaction times up to 6 days (Table 2).

However, quantitative conversion was reached with 20 mol% of the catalyst. Even though the number of metathesis cycles per catalyst molecule is the same as for experiments with diglyme when 10 mol% of 1-MeCN were used, significantly decreased turnover rates were observed. As outlined in Figure 2 most catalytic activity for those reactions was lost already during the first 20 h. Experiments with 5 mol% at 80 °C and at room temperature even demonstrated a faster catalyst deactivation at elevated temperatures (see SI Figure S5). This effect, however, was canceled out at higher catalyst loadings, due to solubility influences.

The observed deactivation can be explained by a mechanistic investigation of this reaction. According to literature findings, the reaction initiates *via* the mono-coordination of the ether substrate, followed by an intramolecular $\text{S}_{\text{N}}2$ attack forming an O-substituted dioxane cation as well as a pentavalent silicate anion (Figure 3).^[12] A subsequent $\text{S}_{\text{N}}2$ attack of the methoxy group on the methyl moiety of the cation releases 1,4-dioxane while forming Me_2O in case of diglyme. When substrates with more than one internal dioxane unit are

Table 2. Ring closing metathesis experiments of TEG-DME at various conditions using 1-MeCN as reaction catalyst.

Entry	cat. (mol%)	Temp. [°C]	Time [h]	Yield [%] ^[a]	TON ^[b]
1	5	80	120	26	10.4
2	5	25	144	34	13.4
3	10	80	120	58	11.6
4	10	25	144	39	7.8
5	20	80	48	75	15.0

[a] Yield determination of reaction product 1,4-dioxane was conducted by ¹H NMR *via* integration against internal standard mesitylene. [b] Calculation: $\text{TON} = n(1,4\text{-dioxane})/n(\text{catalyst})$.

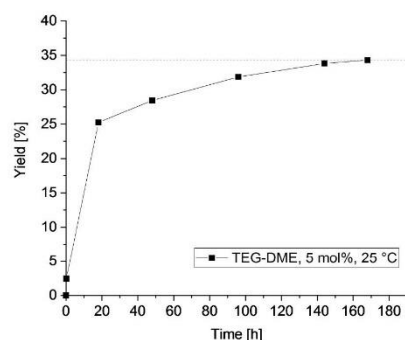


Figure 2. Yield of 1,4-dioxane during a degradation experiment of TEG-DME with 5 mol% of catalyst 1 at 25 °C over the course of 7 days.

degraded, the second $\text{S}_{\text{N}}2$ reaction encounters a kinetically less favored secondary carbon center, thus lowering the overall reaction speed.^[18] In that case the extended population of the highly electrophilic oxonium species caused by the less favored $\text{S}_{\text{N}}2$ reaction facilitates the likelihood for side-reactions. As oxonium species are prone for nucleophilic substitution an attack could also occur on one of the other secondary carbon atoms, leading to the irreversible deactivation of the catalyst.^[19]

The tremendous oxophilicity of 1-MeCN and reactivity for oxygen containing substrates was ultimately demonstrated by the cleavage of Et_2O . In this experiment 1-MeCN was

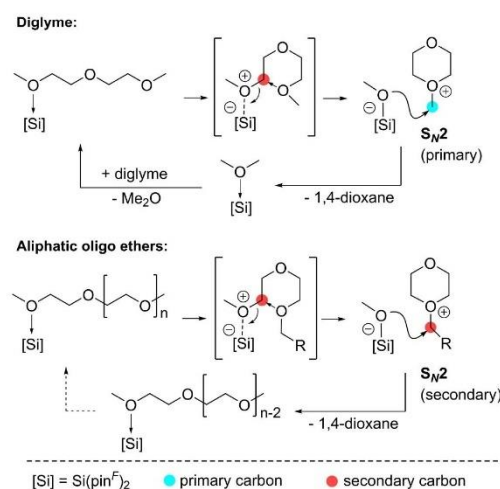


Figure 3. Potential reaction pathway of the ring-closing metathesis of diglyme and longer oligo(ethyleneglycol) catalyzed by *in situ* liberated 1 ($[\text{Si}]$) starting from the terminal ether bonds. The reaction determining $\text{S}_{\text{N}}2$ reaction are highlighted in red for secondary carbons and blue for primary carbons.

precipitated from a saturated diethylether solution at room temperature, yielding the salt of the ethoxy substituted silicate species with the respective triethyl oxonium counterion $[\text{Et}_3\text{O}][1\text{-OEt}]$ (Figure 4). The NMR analysis of the product in acetonitrile- d_3 showed the presence of the characteristic species $[\text{Et}_3\text{O}]^+$ when measured 10 min after solvent addition (see SI Figure S1). Another ^1H NMR spectrum of the same sample obtained 3 hours later, however, revealed the presence of Et_2O and another species that was attributed to the deuterated *N*-ethylacetoni-trium cation $[\text{MeCN-Et}]^+$. Despite this conversion, the characteristic ^1H -, ^{19}F - and ^{29}Si ($\delta = -106.6$ ppm) NMR signals of the silicate species $[1\text{-OEt}]^-$ were not affected (see SI for details). Interestingly, this characteristic ^{29}Si NMR signal at around $\delta = -106.6$ ppm was also observed during reactions of 1,5-dimethoxypentane and diglyme with 1·MeCN. This evidently demonstrated the presence of alkoxy-substituted penta-coordinate silicate anions as intermediates during ether degradation reactions (see SI chapter 3.3).

Single crystals suitable for SC-XRD analysis of $[\text{MeCN-Et}][1\text{-OEt}]$ were obtained from a saturated solution of $[\text{Et}_3\text{O}][1\text{-OEt}]$ in MeCN/ Et_2O . As can be seen in Figure 4 the silicon is penta-coordinate with two perfluoropinacolato groups and one ethoxy substituent attached. The Si–O(pin^f) bond lengths range from 1.7070(19) Å to 1.7613(19) Å and align well with the bond lengths already observed for the chloro-, fluoro and hydrido-substituted perfluoropinacolato silicates, published by our group.^[13] The Si1–O5 length of 1.6210(19) Å is slightly shorter as for comparable non-fluorinated bis(pinacolato)silicates holding MeO-, EtO-, *i*PrO- and *t*BuO-substituents (Si–O: 1.661(4)–1.670(3) Å).^[20] The perfluoropinacolato groups of $[1\text{-OEt}]^-$ arrange in a distorted see-saw geometry with bond angles of 124.54(9)° for O1–Si1–O4 and 170.95(9)° for the O2–Si1–O3 axis. A similar geometry was observed for previously reported

silicate anions with two perfluorinated pinacolato groups and a hydride, fluoride or chloride substituent.^[13] Related geometries were also found in the case bis(catecholato)silicates with different sterically demanding substituents attached to the silicon center.^[21]

Conclusion

In conclusion we demonstrated that the neutral Lewis superacid 1·MeCN efficiently catalyzed the degradation of oligo- and polyethers *via* C–O metathesis. The unmatched reactivity of 1·MeCN was explained by the sterically predefined mono-coordination of the corresponding adduct that is formed between the Lewis acid 1 and the employed etheric substrate, under the displacement of acetonitrile. The obtained reactivity aligned well with calculation on the reaction mechanism for related catecholato silanes that were given in the literature.^[12] With the isolation of an anionic ethoxy substituted silicate anion, we further presented a potential reaction intermediate derivative that supports the published mechanistic investigation. Additional degradation studies with TEG-DME revealed a gradual deactivation of catalytic activity which could be explained by an overall deceleration of the metathesis reaction caused by the slower substitution reactions on secondary carbon atoms for substrates holding more than one cyclic product unit. The striking oxophilicity of 1·MeCN was ultimately demonstrated by the cleavage of Et_2O , yielding the respective penta-oxo-coordinate silicate species, which was fully characterized including SC-XRD analysis.

Experimental Section

General Information. All reaction were performed under argon atmosphere in heat-dried reaction vessels. Reactants for catalytic experiments 1,5-dimethoxypentane, diglyme, tetra- and poly(ethylene-glycol) dimethyleher (TEG-DME, PEG-DME) were degassed and stored over molecular sieves (4 Å). 18-Crown-6 was dried in DCM-solution over molecular sieves (4 Å) prior to use. Solvents were distilled over elemental sodium/benzophenone (Et_2O) or calcium hydride (acetonitrile, chloroform) and stored over molecular sieves. The used $\text{Si}(\text{pin}^f)_2$ ·MeCN (1·MeCN) was synthesized according the literature.^[13]

Synthesis of $[\text{Et}_3\text{O}][1\text{-OEt}]$. In a screwcap reaction vessel 80.0 mg 1·MeCN (109 μmol, 1.00 equiv.) were dissolved in 1.3 ml Et_2O (1.25 μmol, 11.5 equiv.). The reaction mixture was kept at room temperature for 24 h and afterwards stored at -30°C for 5 days. A colorless precipitate was formed that was collected by filtration, washed three times with 1.0 ml hexane and dried in vacuum. A colorless solid was obtained in 44% yield.. **$^1\text{H-NMR}$** (500 MHz, acetonitrile- d_3) δ (ppm) = 4.65 (q, $^3J_{\text{C-H}} = 7.1$ Hz, 6H, $\text{O}(\text{CH}_2\text{CH}_3)_3$), 3.71 (q, $^3J_{\text{C-H}} = 7.0$ Hz, 2H, $\text{SiOCH}_2\text{CH}_3$), 1.51 (t, $^3J_{\text{C-H}} = 7.1$ Hz, 9H, $\text{O}(\text{CH}_2\text{CH}_3)_3$), 1.05 (t, $^3J_{\text{C-H}} = 7.0$ Hz, 3H, $\text{SiOCH}_2\text{CH}_3$). **^{13}C NMR** (126 MHz, acetonitrile- d_3) δ (ppm) = 122.82 (qm, $^1J_{\text{C-F}} = 293.1$ Hz), 84.81 (s, $\text{O}(\text{CH}_2\text{CH}_3)_3$), 83.77 (br, $\text{OC}(\text{CF}_3)_2$), 59.64 (s, $\text{SiOCH}_2\text{CH}_3$), 17.92 (s, $\text{SiOCH}_2\text{CH}_3$), 12.56 (s, $\text{O}(\text{CH}_2\text{CH}_3)_3$). **^{19}F NMR** (471 MHz, acetonitrile- d_3) δ (ppm) = -69.69 – -70.02 (m, 12F, CF_3), -70.18 – -70.37 (m, 12F, CF_3). **^{29}Si NMR** (99 MHz, acetonitrile- d_3) δ (ppm) = -106.61 (Si). **Elemental Analysis** calcd. [%] for $\text{C}_{20}\text{H}_{20}\text{F}_{24}\text{O}_4\text{Si}$: C

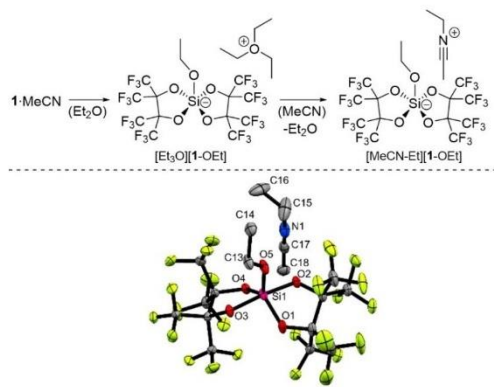


Figure 4. Top: Degradation experiment of diethyl ether in the presence of 1·MeCN, yielding the ethoxy substituted perfluoropinacolato silicate with respective triethyl oxonium or *N*-ethylacetoni-trium cation; Bottom: Molecular structure of $[\text{MeCN-Et}][1\text{-OEt}]$ obtained by SC-XRD analysis (ellipsoids at 50% probability level). Selected bond lengths (Å): Si1–O5 1.6210(19), Si1–O1 1.7165(19), Si1–O2 1.7613(19), Si1–O3 1.7529(19), Si1–O4 1.7070(19); N1–C15 1.446(4), N1–C17 1.124(4).^[22]

6. Catalytic Degradation of Aliphatic Ethers using the Lewis Superacidic Bis(perfluoropinacolato)silane – Dissertation Florian Tschernuth

(28.58), H (2.40), N (–), S (–); found (%): C (28.90), H (2.20), N (0.50), S (–). m.p.: 97.5–110.2 °C.

General procedure catalysis experiments. All C–O metathesis reactions were carried out in PTFE-sealed J-Young NMR tubes. The respective amount of reactant was dissolved in 0.4 ml CDCl₃ and 3.0 μl of mesitylene were added as an internal standard. A ¹H NMR analysis of that solution was performed as a zero-point measurement for yield determination. The reactions were started by the addition of the given amount of catalyst 1·MeCN. The samples were then stored at various temperatures using an oil-bath. Reaction progress was monitored via ¹H NMR spectroscopy by the integration of the product signals with respect to the internal standard.

Acknowledgements

We want to thank Dr. Franziska Hanusch for the SC-XRD measurement and refinement and Ivan Antsiurov M.Sc. for ESI MS measurements. Furthermore, we thank the WACKER Chemie AG for the unrestrained support that enabled us to carry out this research project. Open Access funding enabled and organized by Projekt DEAL.

Conflict of Interests

The authors declare no conflict of interest.

Data Availability Statement

The data that support the findings of this study are available in the supplementary material of this article.

Keywords: C–O bond metathesis · Et₂O cleavage · Lewis acidic silanes · poly(ether) degradation · silicon catalysis

- [1] United Nations Development Program, Green economy and green jobs: Challenges and opportunities, can be found under <https://www.undp.org/eurasia/publications/green-economy-and-green-jobs-challenges-and-opportunities>, 2019, (accessed 16 January 2023).
- [2] a) Plastics Europe, Plastics-the Facts 2022, can be found under https://plasticseurope.org/de/wp-content/uploads/sites/3/2022/10/PE-PLAS-TICS-THE-FACTS_20221017.pdf, 2022, (accessed 16 January 2023); b) Statista, Distribution of plastic waste treatment worldwide in 2018 by method (Basel Convention 24 February 2020), can be found under <https://www.statista.com/statistics/1271029/global-plastic-waste-treatment-by-sector/>, 2020, (accessed 17 January 2023).
- [3] a) A. Rahimi, J. M. García, *Nat. Chem. Rev.* **2017**, *1*, 0046; b) M. Hong, E. Y. X. Chen, *Green Chem.* **2017**, *19*, 3692–3706.
- [4] R. Klein, F. R. Wurm, *Macromol. Rapid Commun.* **2015**, *36*, 1147–1165.
- [5] A.-L. Brocas, C. Mantzaridis, D. Tunc, S. Carlotti, *Prog. Polym. Sci.* **2013**, *38*, 845–873.
- [6] a) S. Enthaler, *Catal. Lett.* **2014**, *144*, 850–859; b) S. Enthaler, M. Weidauer, *ChemSusChem* **2012**, *5*, 1195–1198; c) S. Enthaler, M. Weidauer, *Chem. Eur. J.* **2012**, *18*, 1910–1913.
- [7] a) Y. Wang, Y. Hou, H. Song, *Polym. Degrad. Stab.* **2017**, *144*, 17–23; b) S. Enthaler, *J. Appl. Polym. Sci.* **2014**, *131*; c) S. Enthaler, A. Trautner, *ChemSusChem* **2013**, *6*, 1334–1336.
- [8] T. Biberger, S. Makai, Z. Lian, B. Morandi, *Angew. Chem. Int. Ed.* **2018**, *57*, 6940–6944; *Angew. Chem.* **2018**, *130*, 7057–7061.
- [9] H. Wang, Y. Zhao, F. Zhang, Y. Wu, R. Li, J. Xiang, Z. Wang, B. Han, Z. Liu, *Angew. Chem. Int. Ed.* **2020**, *59*, 11850–11855; *Angew. Chem.* **2020**, *132*, 11948–11953.
- [10] a) L. Monsigny, J.-C. Berthet, T. Cantat, *ACS Sustainable Chem. Eng.* **2018**, *6*, 10481–10488; b) E. Feghalli, T. Cantat, *ChemSusChem* **2015**, *8*, 980–984.
- [11] K. Leszczyńska, A. Mix, R. J. F. Berger, B. Rummel, B. Neumann, H.-G. Stammer, P. Jutz, *Angew. Chem. Int. Ed.* **2011**, *50*, 6843–6846; *Angew. Chem.* **2011**, *123*, 6975–6978.
- [12] N. Ansmann, T. Thorwart, L. Greb, *Angew. Chem. Int. Ed.* **2022**, *61*, e202210132.
- [13] F. S. Tschernuth, T. Thorwart, L. Greb, F. Hanusch, S. Inoue, *Angew. Chem. Int. Ed.* **2021**, *60*, 25799–25803; *Angew. Chem.* **2021**, *133*, 26003–26007.
- [14] a) T. Thorwart, D. Roth, L. Greb, *Chem. Eur. J.* **2021**, *27*, 10422–10427; b) A. Hermannsdorfer, M. Driess, *Angew. Chem. Int. Ed.* **2021**, *60*, 13656–13660; *Angew. Chem.* **2021**, *133*, 13769–13773; c) D. Roth, H. Wadehoff, L. Greb, *Angew. Chem. Int. Ed.* **2020**, *59*, 20930–20934; *Angew. Chem.* **2020**, *132*, 21116–21120; d) D. Hartmann, M. Schädler, L. Greb, *Chem. Sci.* **2019**, *10*, 7379–7388; e) R. Maskey, M. Schädler, C. Legler, L. Greb, *Angew. Chem. Int. Ed.* **2018**, *57*, 1717–1720; *Angew. Chem.* **2018**, *130*, 1733–1736.
- [15] T. Thorwart, D. Hartmann, L. Greb, *Chem. Eur. J.* **2022**, *28*, e202202273.
- [16] *7 mol% when referenced to the reaction product 1,4-dioxane..
- [17] *10 mol% when referenced to the amount of reaction product.
- [18] a) R. J. Ouellette, J. D. Rawn, *Organic Chemistry*, Elsevier, Boston, **2014**, pp. 333–356; b) E. Uggerud, *J. Phys. Org. Chem.* **2006**, *19*, 461–466.
- [19] C. J. Forsyth, T. J. Murray, *Science of Synthesis, Category 5, Compounds with One Saturated Carbon Heteroatom Bond*, Vol. 37, 1st ed., Thieme Stuttgart, **2008**.
- [20] a) K. C. Kumara Swamy, V. Chandrasekhar, J. J. Harland, J. M. Holmes, R. O. Day, R. R. Holmes, *Phosphorus Sulfur Silicon Relat. Elem.* **1995**, *99*, 239–256; b) R. R. Holmes, R. O. Day, J. S. Payne, *Phosphorus Sulfur Silicon Relat. Elem.* **1989**, *42*, 1–13.
- [21] a) D. Hartmann, T. Thorwart, R. Müller, J. Thusek, J. Schwabedissen, A. Mix, J.-H. Lamm, B. Neumann, N. W. Mitzel, L. Greb, *J. Am. Chem. Soc.* **2021**, *143*, 18784–18793; b) D. Hartmann, S. Braner, L. Greb, *Chem. Commun.* **2021**, *57*, 8572–8575.
- [22] Deposition Number 2241855 [MeCN Et][1-OEt] contains the supplementary crystallographic data for this paper. These data are provided free of charge by the joint Cambridge Crystallographic Data Centre and Fachinformationszentrum Karlsruhe Access Structures service.

Manuscript received: February 14, 2023

Revised manuscript received: March 19, 2023

Accepted manuscript online: March 21, 2023

Version of record online: May 2, 2023

7 Tuning the Lewis Acidity of neutral Silanes using perfluorinated Aryl- and Alkyl Substituents

Journal: *European Journal of Inorganic Chemistry (EurJIC)*^[130]
Publisher: Wiley-VCH GmbH
Authors: Florian S. Tschernuth, Lukas Bichlmaier, and Shigeyoshi Inoue*
Status: Research Article, published 24. July 2023
DOI: 10.1002/ejic.202300388

Reproduced with open access permission.

Content: This research article issues the synthesis and characterization of novel Lewis acidic silanes by the installation of electron-withdrawing perfluorotolyl ($\text{ToI}^F = p\text{-C}_6\text{F}_4\text{CF}_3$) and perfluorocresolato ($\text{OToI}^F = p\text{-OC}_6\text{F}_4\text{CF}_3$) groups onto neutral Si(IV) centers. First, the tetrasubstituted $\text{Si}(\text{ToI}^F)_4$ was synthesized from SiCl_4 and $\text{BrC}_6\text{F}_4\text{CF}_3$ by lithiation with *n*BuLi. The obtained silane was fully characterized, including crystal structure analysis, illustrating a slightly distorted tetrahedral geometry. Lewis acidity assessment with the Gutmann-Beckett and Childs methods revealed no significant Lewis acidity, which was in stark contrast when compared to the trivalent boron analog ($\text{B}(\text{ToI}^F)_3$), which is outlined in the literature.^[131] The respective threefold-substituted hydrosilane derivative $\text{HSi}(\text{ToI}^F)_3$ was synthesized starting from HSiCl_3 using a similar synthetic strategy to rule out a potential negative influence of steric repulsion. The silane was obtained in a yield of 26 % and thoroughly analyzed. Crystal structure analysis revealed the successful formation $\text{HSi}(\text{ToI}^F)_3$, showing a slightly distorted tetrahedral geometry. Again, no Lewis acidity could be observed with the Gutmann-Beckett and Childs NMR methods. To boost the electrophilicity of the Si atom, additional oxygen bridges were installed, leading to the synthesis of $\text{Si}(\text{OToI}^F)_4$ from SiCl_4 and $\text{LiOC}_6\text{F}_4\text{CF}_3$ in acetonitrile. In this case, the Gutmann-Beckett analysis gave a $\Delta\delta(^{31}\text{P})$ shift of 29.2 ppm, revealing strong Lewis acidity. No Childs shift could be observed, however.

Furthermore, a heteroleptic silane was synthesized using one perfluoropinacol (pin^F) and two perfluorophenyl (Ph^F) substituents. The respective target compound $\text{Si}(\text{Ph}^F)_2\text{pin}^F$ was synthesized from $\text{Si}(\text{Ph}^F)_2\text{Cl}_2$ and Li_2pin^F in 66 % yield and comprehensively analyzed. A subsequent Gutmann-Beckett assessment revealed a significantly increased Lewis acidity compared to heteroleptic $\text{Si}(\text{Ph}^F)_4$. Again, no Childs shift was obtained, questioning the overall suitability of this method for silane-based Lewis acids.

*Florian S. Tschernuth planned and prepared synthesis experiments for this publication and wrote the manuscript as well as Supporting Information. Lukas Bichlmaier planned and designed syntheses during his master's thesis. Sebastian Stigler performed the SC-XRD measurement and refinement of the crystal data. Prof. Shigeyoshi Inoue directly supervised the research.



Tuning the Lewis Acidity of Neutral Silanes Using Perfluorinated Aryl- and Alkoxy Substituents

Florian S. Tschernuth,^[a] Lukas Bichlmaier,^[a] Sebastian Stigler,^[a] and Shigeyoshi Inoue^{*[a]}

The emerging field of Lewis acidic silanes demonstrates the versatility of molecular silicon compounds for catalytic applications. Nevertheless, when compared to the multifunctional boron Lewis acid $B(C_6F_5)_3$, silicon derivatives still lack in terms of reactivity. In this regard, we demonstrate the installation of perfluorotolyl groups (Tol^f) on neutral silicon atoms to obtain the respective tetra- and trisubstituted silanes $Si(Tol^f)_4$ and $HSi(Tol^f)_3$. These compounds were fully characterized including SC-XRD analysis but unexpectedly showed no significant Lewis

acidity. By using strongly electron-withdrawing perfluorocresolato groups ($OTol^f$) the tetrasubstituted silane $Si(OTol^f)_4$ was obtained, bearing an 8% increased $\Delta\delta(^{31}P)$ shift when applying the Gutmann-Beckett method, compared to literature-known $Si(OPh^f)_4$. Ultimately the heteroleptic $Si(Ph^f)_2pin^f$ was successfully synthesized and fully characterized including SC-XRD analysis, introducing a highly Lewis acidic silicon atom holding two silicon-carbon bonds.

Introduction

Main-group element-based Lewis acids for catalytic applications have been intensively researched in the past decades.^[1] Especially tris(pentafluorophenyl)borane and its structural derivatives like the Piers borane (bis(pentafluorophenyl)borane) have demonstrated outstanding catalytic potential for a variety of organic transformations.^[2] Moving to group-14 elements, highly Lewis acidic Si(IV)- and Si(II) cations were investigated to efficiently catalyze reactions including Diels-Alder additions, C–F hydrodefluorinations, sila-Friedel-Crafts reactions, carbonyl- and olefin hydrosilylation.^[1b,3] The utilization of silicon as a potential catalyst is most favorable, regarding its earth abundance and easy accessibility.^[4] By the implementation of perfluorinated aryl- and alkyl substituents, the groups of Tilley, Bergman and Hoge synthesized highly Lewis acidic but neutral silanes that were efficiently used for reactions including the catalytic hydrosilylation of electron-deficient carbonyls or transfer hydrogenation of 1,3,5-trimethylcyclohexa-2,4-diene.^[5] By the use of less π -back-donating perchloro-catecholato substituents,^[6] the Greb group furnished the synthesis of the first stable Lewis superacidic silane.^[7] According to the

definition given by Krossing such Lewis superacids possess a higher fluoride ion affinity (FIA) than isolated SbF_5 .^[8] Following this finding further Si-based Lewis superacids were developed, based on perhalogenated catecholato substituents, and investigated for catalytic applications in carbonyl hydrosilylation, ketone defunctionalization, and depolymerization reactions, among others.^[9] Our group reported the Lewis superacidic (perfluoropinacolato)silane, which showed outstanding catalytic activity for the fragmentation of oligo ethers and activated hard substrates such as Et_3SiF .^[10] Since Lewis acidity is a complex interplay of substrate-specific attractive and repulsive interactions during adduct formation, Greb additionally gave a definition for soft Lewis superacids, referring to Pearson's HSAB principle.^[11]

Attempts to fine-tune the Lewis acidity of benchmark soft Lewis superacid $B(C_6F_5)_3$ by the Mitzel group outlined a significant impact on the Lewis acidity of the boron atom by exchanging *para*-F moieties with CF_3 -groups. The resulting $B(Tol^f)_3$ showed a 9% increased Lewis acidity by Gutmann-Beckett measurement and a 10% higher FIA value than $B(C_6F_5)_3$.^[12a] Additional investigations by the White group demonstrated a significant Lewis acidity change upon the installation of oxygen bridges onto $B(C_6F_5)_3$ derivatives. The obtained $B(OC_6F_5)_x(C_6F_5)_{3-x}$ compounds were stronger and harder Lewis acids the more polarizing oxygen bridges were installed.^[13] The respective silicon analogues of $B(C_6F_5)_3$ and $B(OC_6F_5)_3$ were already synthesized in the mid-20th century, but unlike for their boron counterparts, no catalytic applications were reported.^[12c,d] In this context, we investigated the suitability of perfluorotolyl (Tol^f) and perfluorocresolato ($OTol^f$) substituents for fine-tuning the Lewis acidity of tetra- and trisubstituted silanes. Additionally, a heteroleptic approach with one perfluoropinacolato- (pin^f) and two perfluorophenyl (Ph^f) groups was examined (Figure 1).

[a] F. S. Tschernuth, L. Bichlmaier, S. Stigler, Prof. Dr. S. Inoue
TUM School of Natural Sciences, Department of Chemistry
WACKER-Institute of Silicon Chemistry
and Catalysis Research Center
Technical University of Munich
Lichtenbergstraße 4
85748 Garching (Germany)
E-mail: s.inoue@tum.de
Homepage: <http://www.ch.nat.tum.de/si/home/>

Supporting information for this article is available on the WWW under <https://doi.org/10.1002/ejic.202300388>

© 2023 The Authors. European Journal of Inorganic Chemistry published by Wiley-VCH GmbH. This is an open access article under the terms of the Creative Commons Attribution Non-Commercial License, which permits use, distribution and reproduction in any medium, provided the original work is properly cited and is not used for commercial purposes.

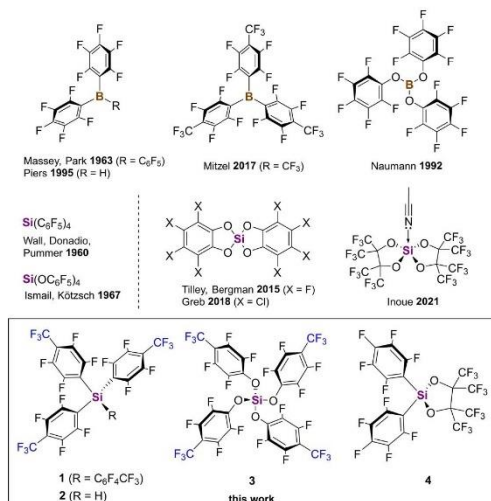
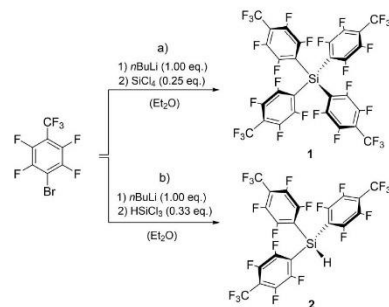


Figure 1. Boron Lewis acids holding C_6F_5 , $p-C_6F_4CF_3$ (Tol') and $p-OC_6F_4CF_3$ (OTol') substituents as well as related silicon-centered Lewis acids presented in the literature.^[26,5a,7,10a,12] Bottom: Neutral silicon-based Lewis acids 1, 2, and 3 with OTol' substituents and heteroleptic silane 4 presented in this work.

Results and Discussion

Tilley and Bergman *et al.* demonstrated that unlike $B(C_6F_5)_3$, $Si(C_6F_5)_4$ does not catalyze the hydrosilylation of electron-deficient carbonyls with Et_3SiH .^[5a] The reduced activity can be explained by the insufficient Lewis acidity of the tetravalent silane, compared to the electron-deficient, trivalent, boron compound.^[14] This is supported by the Gutmann-Beckett assessment of $Si(C_6F_5)_4$ where only a chemical shift of $\Delta\delta(^{31}P) = 15.2$ ppm is measured, which is significantly lower than that of $B(C_6F_5)_3$ ($\Delta\delta(^{31}P) = 30.1$ ppm).^[13] In analogy to the recently reported boron derivative, we synthesized $Si(Tol')_4$ to increase the Lewis acidity of the silicon atom by exploiting the inductive effect of the additional $p-CF_3$ groups.^[12a] According to the Hammett theory this should yield a more pronounced electron withdrawal on the silicon atom, thus resulting a stronger Lewis acid.^[15] Consequently, we synthesized **1** from $SiCl_4$ and perfluorotoluene in an adapted procedure given for the boron derivative.^[12a] In the case of silicon, however, no transmetalation with copper was required and compound **1** was directly synthesized in 77% yield using $p-BrC_6F_4CF_3$ via lithiation with $nBuLi$ (Scheme 1, a).

The same synthetic procedure was applied starting from $HSiCl_3$ to synthesize the sterically less congested silane **2** in 26% yield (Scheme 1, b). Both compounds were fully characterized using multi-nuclear NMR spectroscopy, EA, melting point and SC-XRD. The Lewis acidity assessment of **1** using the Gutmann-Beckett method revealed no interaction of the silane with Et_3PO . Also, no interaction was observed with the softer Lewis base *trans*-crotonaldehyde by conducting the Childs



Scheme 1. Syntheses of $Si(Tol')_4$ (**1**) and $HSi(Tol')_3$ (**2**) starting from $p-BrC_6F_4CF_3$ and $SiCl_4$ (path a) or $HSiCl_3$ (path b). Both reactions were conducted at $-78^\circ C$ to minimize the risk of explosive LiF elimination.

method. The ^{29}Si NMR signal of **1** in $THF-d_8$ was found at $\delta = -40.7$ ppm, which is in the same region as for the $Si(C_6F_5)_4$ derivative ($\delta(^{29}Si) = -41.1$ ppm). This result was unexpected as the Hammett constant of CF_3 ($\sigma_p = 0.54$) should result in more electron withdrawal when compared to F ($\sigma_p = 0.06$).^[15a] SC-XRD structure analysis of **1** crystallized from saturated THF solution ultimately demonstrated the untypically low Lewis acidity of **1** (Figure 2). The perfluorotolyl substituents arrange in a slightly distorted tetrahedral coordination with bond angles between $103.5(1)^\circ$ and $113.7(1)^\circ$. The unit cell additionally contains two THF molecules, that are not coordinating the silicon atom, displayed by Si–O distances of 4.247(2) Å (Si1–O1) and 4.249(2) Å (Si1–O2).

In contrast to the boron analogue, the introduction of Tol' groups quenched the Lewis acidity of the obtained silane completely. A potential explanation for this observation could be given by the enhanced steric bulk of the additional $p-CF_3$ groups. Consequently, less bulky silane **2** should show enhanced Lewis acidity due to the more accessible silicon site. The ^{29}Si NMR analysis of **2** revealed a singlet at $\delta = -54.3$ ppm, which is slightly shifted, but still in the same range as for **1**

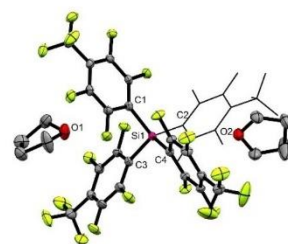


Figure 2. SC-XRD structure of $Si(Tol')_4$, **1** with thermal vibration ellipsoids plotted at 50% probability level. The structure additionally contains two non-coordinating THF molecules. For clarity reasons, hydrogens are omitted and one Tol' group is depicted in wireframe model. Selected bond lengths (Å) and angles ($^\circ$): Si1–C1 1.878(2), Si1–C2 1.879(2), Si1–C3 1.879(2), Si1–C4 1.880(2); C2–Si1–C1 113.2(1), C2–Si1–C3 111.0(1), C2–Si1–C4 103.5(1), C1–Si1–C3 104.4(1), C1–Si1–C4 111.4(1), C3–Si1–C4 113.7(1).^[16]

holding four perfluorotolyl substituents. The Gutmann-Beckett analysis with one equivalent of Et_3PO revealed a slight shift of $\Delta(\delta^{31}\text{P})=0.60$ ppm with respect to free Et_3PO . Only a chemical shift of $\Delta(\delta^1\text{H}^3)=0.01$ ppm was observed in case of the Childs method when *trans*-crotonaldehyde was applied in dichloromethane- d_2 solution. The observed low Lewis acidity remained unexpected as the silicon atom of **2** is easily accessible, which was validated by SC-XRD (Figure 3). A potential explanation could be intermolecular coordination of the CF_3 groups to the neighboring silicon site in solution. Nonetheless, no intermolecular adduct formation is seen in solid state.

Instead, compound **2** shows a slightly distorted tetrahedral geometry with a sum of angles of $330.2(6)^\circ$. The silicon-carbon distances are 1.879(5) Å for Si1–C1, 1.892(6) Å for Si1–C2, and 1.878(5) Å for Si1–C3. As demonstrated in case of boron, the installation of oxygen bridges heavily affects the Lewis acidity of the central boron atom.^[13] The strong polarization leads to “harder” and strongly Lewis acidic boron sites with respect to the HSAB theory.^[17] This effect is also true for $\text{Si}(\text{OC}_6\text{F}_5)_4$ where an increased Gutmann-Beckett shift of $\Delta\delta(\delta^{31}\text{P})=26.9$ ppm was observed. Consequently, the respective perfluorotolyl substituted orthosilicate **3** was synthesized. The synthetic strategy started from perfluorinated cresol, which was lithiated using *n*BuLi. The subsequent conversion with SiCl_4 furnished the desired product **3** in 72% yield (Scheme 2). Due to the enhanced Lewis acidity of the obtained silane, residual acetonitrile could not be completely removed by multiple washing attempts in hexanes.

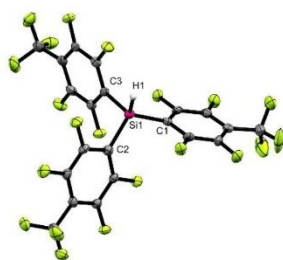
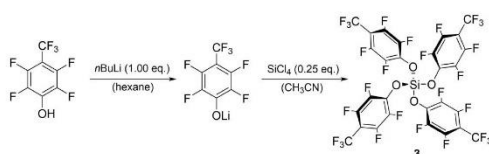


Figure 3. SC-XRD structure of $\text{HSi}(\text{ToI}^{\text{F}})_3$ (**2**) with thermal vibration ellipsoids plotted at 50% probability level. The unit cell contains a second molecule **3**, which is omitted for clarity. Selected bond lengths (Å) and angles ($^\circ$): Si1–H1 1.31(5), Si1–C1 1.879(5), Si1–C2 1.892(6), Si1–C3 1.878(5); C1–Si1–H1 119(2), C1–Si1–C2 112.4(2), C2–Si1–H1 113(2), C3–Si1–H1 105(2), C3–Si1–C1 111.3(2), C3–Si1–C2 105.8(2).^[16]



Scheme 2. Syntheses of $\text{Si}(\text{OTol}^{\text{F}})_4$ (**3**) starting with the lithiation of perfluorocresolato using *n*BuLi and subsequent reaction with SiCl_4 .

Moreover, ^{19}F NMR analysis revealed the presence of little amounts of unidentified side-products that could not be avoided by improved reaction parameters. For this reason, no elemental analysis and melting point measurement were performed for compound **3**. Nevertheless, successful product formation was proven by LIFDI-MS analysis (see SI). The ^{29}Si NMR signal was observed at $\delta=-153.4$ in $\text{THF}-d_3$ and $\delta=-153.2$ in acetonitrile- d_3 solution which corresponds to octahedral coordinated silicon species reported in the literature.^[18] A similar shift was obtained for oxygen-bridged $\text{Si}(\text{OC}_6\text{F}_5)_4$ (Table 1). The strong coordination of acetonitrile indicates an enhanced Lewis acidity, as it was already reported for the donor-coordinated Lewis superacid $\text{Si}(\text{pin}^{\text{F}})_2\text{MeCN}$.^[10a] The Gutmann-Beckett analysis revealed a change in the ^{31}P NMR shifts of $\Delta\delta(\delta^{31}\text{P})=29.2$ ppm and $\Delta\delta(\delta^{31}\text{P})=8.8$ ppm for the mono- and double-coordinated silane **3**. Double coordination was also observed in the case of $\text{Si}(\text{OC}_6\text{F}_5)_4$ ($\Delta\delta(\delta^{31}\text{P})=6.9$ ppm for twofold-coordinated product) with excess of Et_3PO present. The obtained shifts are in the range of strong Lewis acids and the increased electrophilicity of **3** matches the results reported for the boron derivative.^[12a] In the case of **3**, the installation of *p*- CF_3 groups leads to an 8% increase of the Gutmann-Beckett shift, when referenced to $\text{Si}(\text{OC}_6\text{F}_5)_4$ (for mono-coordinated products).

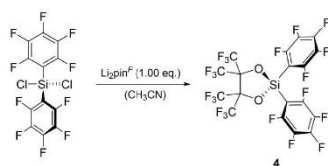
An additional strategy to synthesize a strongly Lewis acidic silane with a less polarized silicon atom is the installation of heteroleptic systems with the strongly electron-withdrawing perfluoropinacolato group (pin^{F}). A direct synthesis of such a species starting from SiCl_4 was not possible, due to inevitable tetrasubstitution with one substituent type. Consequently, a synthetic approach was adapted from the literature, using $\text{Si}(\text{C}_6\text{F}_5)_2\text{Cl}_2$ as a reaction intermediate, that is synthesized from Ph_2SiCl_2 .^[19] The subsequent conversion with $\text{Li}_2\text{pin}^{\text{F}}$ in acetonitrile solution yielded the desired heteroleptic product **4** in 66% yield. (Scheme 3).

Even though this compound was synthesized in acetonitrile solution, no remaining solvent coordination was observed in the ^1H NMR spectrum. The ^{29}Si NMR analysis in benzene- d_6 revealed a signal at $\delta=-5.25$ ppm. Interestingly, in more polar $\text{THF}-d_6$ the ^{29}Si signal was found at $\delta=-19.5$ ppm, indicating a geometry change, most likely caused by THF coordination. The

Table 1. Collected Lewis acidity data, obtained from ^{29}Si NMR, Gutmann-Beckett, and Childs method.

Compound	^{29}Si NMR signal [ppm] ^[a]	Gutmann-Beckett $\Delta\delta(\delta^{31}\text{P})$ [ppm] ^[b]	Childs $\Delta\delta(\delta^1\text{H}^3)$ [ppm] ^[c]
1	−40.7	0.0	0.00
2	−54.3	0.6	0.01
3	−153.2	29.2	0.04
4	−19.5	27.2	0.01
$\text{Si}(\text{OPh}^{\text{F}})_4$	−152.1	26.9	0.04
$\text{Si}(\text{Ph}^{\text{F}})_4$	−41.1	15.2	0.00

[a] ^{29}Si NMR measured in $\text{THF}-d_6$, [b] Et_3PO mono-coordination in CD_2Cl_2 , [c] shift of H^3 -proton of *trans*-crotonaldehyde in CD_2Cl_2 .



Scheme 3. Syntheses of $\text{Si}(\text{Ph}^f)_2\text{pin}^f$ (**4**) starting from preformed $\text{Si}(\text{C}_6\text{F}_5)_2\text{Cl}_2$ and Li_2pin^f in acetonitrile.

Gutmann-Beckett assessment of **4** revealed a change in ^{31}P NMR shift of $\Delta\delta = 27.2$ ppm, which is slightly smaller than that for compound **3**, but lies in the same range as for the perfluorophenyl substituted $\text{Si}(\text{OC}_6\text{F}_5)_4$. This high observed Lewis acidity renders remarking, as compound **4** holds two silicon-carbon bonds and only two directly bound oxygen atoms (Figure 4). According to the results obtained for boron by Britovsek *et al.* this should lead to a less hard Lewis acid. However, subsequent acidity determination by the Childs method did not show any coordination of *trans*-crotonaldehyde. This reflects the results obtained from all investigated Lewis acids in this study (Table 1). Single crystals suitable for XRD analysis were obtained from a saturated MeCN/DCM solution. The unit cell does not contain any MeCN molecules. Instead, a slightly distorted tetrahedral silicon central element was observed that is coordinated by one perfluoropinacolato group and two perfluorophenyl groups. The Si1–O1 and Si1–O2 bond lengths of 1.648(3) Å and 1.654(3) Å are in the same range as for $\text{Si}(\text{pin}^f)_2\text{MeCN}$ (Si–O bond lengths: 1.675(1)–1.723(1) Å).^[10a] With Si1–C1 and Si1–C7 bond lengths of 1.859(4) and 1.857(4) Å reflect the results obtained for homoleptic $\text{Si}(\text{C}_6\text{F}_5)_4$ (Si–O bond length: 1.886(1) Å).^[20]

The GB and Childs shifts, as well as the ^{29}Si NMR signals obtained in this study are summarized in Table 1.

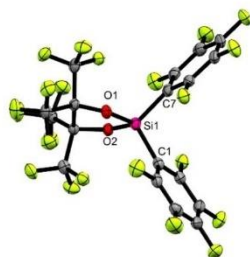


Figure 4. SC-XRD structure of $\text{Si}(\text{Ph}^f)_2\text{pin}^f$ (**4**) with thermal vibration ellipsoids plotted at 50% probability level. The unit cell additionally contains a second molecule **4**, which is omitted for clarity. Selected bond lengths (Å) and angles (°): Si1–O1 1.648(3), Si1–O2 1.654(3), Si1–C1 1.857(4), Si1–C7 1.859(4); O1–Si1–O2 95.5(1), C1–Si1–C7 108.0(2), O1–Si1–C1 113.5(2), O1–Si1–C7 113.2(2), O2–Si1–C1 113.1(2), O2–Si1–C7 113.1(2).^[16]

Conclusions

In this work we demonstrate the use of perfluorotolyl (To^f) and perfluorocresolato (OTo^f) substitutes for the synthesis of Lewis acidic silanes. It was shown that a direct bound oxygen bridge is essential to form strongly Lewis acidic silicon atoms as compounds **1** and **2** did not show considerable coordination by donor molecules. By the installation of (OTo^f) groups the Gutmann-Beckett shift of the respective silane **3** was 8% increased, when compared to $\text{Si}(\text{Ph}^f)_4$. Additionally, a heteroleptic silane was synthesized by employing one perfluoropinacolato and two perfluorophenyl groups. The Gutmann-Beckett shift of obtained compound **4** was in the same range as for tetra-oxo substituted $\text{Si}(\text{OPh}^f)_4$ and $\text{Si}(\text{OTo}^f)_4$ (**3**). In stark contrast to boron species, the additional $p\text{-CF}_3$ group had only a minor beneficial effect on the overall Lewis acidity but caused significant steric bulk. While the Childs method proved to be an effective tool for the assessment of boron Lewis acids, no reliable results were obtained in case of the portrayed silanes.

Experimental Section

Materials and Chemicals: All mentioned reactions were performed under argon 4.6 atmosphere. For sealing of glass connections *Triboflon III* grease from *Freudenberg* was used. Plastic materials like syringes or cannulas were flushed with argon before use. All chemicals for this project were purchased from commercial distributors: *Sigma-Aldrich*, *ABCR*, and *TCl*. *p*-Heptafluorocresol was dried over molecular sieves (4 Å) prior to use. Synthetic precursors Li_2pin^f ,^[10a] $p\text{-Br}(\text{C}_6\text{F}_4)\text{CF}_3$,^[12a] and $\text{Si}(\text{C}_6\text{F}_5)_2\text{Cl}_2$ were synthesized according to literature procedures. Solvents were distilled from mixtures with elemental sodium/benzophenone (Et_2O) or calcium hydride (acetonitrile, chloroform) and stored over molecular sieves (4 Å).

Synthesis and characterization of $p\text{-LiOTo}^f$: The title compound was synthesized according to an adapted procedure for LiOPh^f given in the literature.^[21] In this case 3.00 g *p*-heptafluorocresol (12.82 mmol, 1.00 equiv.) were dissolved in 50 ml hexane and 5.13 ml 2.5 M *n*BuLi solution in hexane (12.82 mmol, 1.00 equiv.) were added dropwise while stirring vigorously. After addition, the reaction mixture was stirred for 30 more minutes at 25 °C. After filtration, the obtained off-white residue was washed two times with 5 ml hexane. After drying in vacuum, the colorless product was obtained in 94% yield. ^{13}C NMR (126 MHz, acetonitrile- d_3 , 298 K) δ (ppm) = 153.55–150.71 (m, 1 C, C^1), 145.10 (dm, $^1J_{\text{C-F}}$ = 246.7 Hz, 2 C, ArC), 141.07 (dm, $^1J_{\text{C-F}}$ = 247.6 Hz, 2 C, ArC), 123.15 (q, $^1J_{\text{C-F}}$ = 269.8 Hz, 1 C, CF_3), 88.66–87.40 (m, 1 C, C^1). ^{19}F NMR (471 MHz, acetonitrile- d_3 , 298 K) δ (ppm) = –54.13 (t, $^4J_{\text{F-F}}$ = 20.9 Hz, 3F, CF_3), –151.03––151.40 (m, 2F, ArF), –167.45––167.66 (m, 2F, ArF).

Synthesis and characterization of $\text{Si}(\text{To}^f)_4$ (1**):** To 100 ml Et_2O were added 7.30 g of *p*-bromoheptafluorotoluene (24.58 mmol, 1.00 equiv.). The solution was cooled to –78 °C and 9.8 ml of 2.5 M *n*-BuLi solution in hexane (24.58 mmol, 1.00 equiv.) were added drop by drop. After complete addition 14.1 ml (1.04 g, 6.15 mmol, 0.25 equiv.) of a 0.436 M SiCl_4 solution in Et_2O were added. The obtained solution was stirred overnight whilst warming up to room temperature. After removal of the solvents in vacuum, a sublimation was carried out at 190 °C and 0.03 mbar. Compound **1** was obtained as a slightly off-white solid in a 77% yield. Single crystals suitable for SC-XRD analysis were obtained from a saturated THF solution at –30 °C. The obtained unit cell additionally contains two

non-attached solvent molecules (Figure S5, SI). **m.p.:** 232.0–234.2 °C. ¹³C NMR (126 MHz, THF-*d*₆, 298 K) δ (ppm) = 150.38 (dm, ¹J_{C-F} = 247.6 Hz, 6 C, C^{3,5}), 145.33 (dd, ¹J_{C-F} = 263.0, ¹J_{C-F} = 18.2 Hz, 8 C, C^{2,6}), 121.79 (q, ¹J_{F-C} = 275.3 Hz, 4 C, CF₃), 115.48–114.30 (m, 8 C, C⁴), 112.62 (t, ¹J_{C-F} = 27.0 Hz, 4 C, C¹). ¹⁹F NMR (471 MHz, THF-*d*₆, 298 K) δ (ppm) = –57.88 (t, ⁴J_{F-F} = 21.6 Hz, 12F, CF₃), –125.86–126.0 (m, 8F, ArF), –139.43–139.71 (m, 8F, ArF). ²⁹Si NMR (99 MHz, THF-*d*₆, 298 K) δ (ppm) = –40.68 (s). **Elemental analysis:** calculated (%): C (37.52), H (0.00), N(0.00), S(0.00); found (%): C (37.50) H (0.00), N(0.00), S(0.00).

Synthesis and characterization of HSi(Tol^f)₃ (2): To suspension of 0.165 g (6.73 mmol, 3.00 equiv.) magnesium turnings in 10 ml Et₂O were added 2.00 g (6.73 mmol, 3.00 equiv.) *p*-bromoheptafluorotoluene at room temperature until the start of the exothermic reaction was noticed by slight color change. Subsequently an ice bath was used to cool the reaction mixture to 0 °C. After complete reaction, the Grignard reagent was filtered into a solution of 0.23 ml (2.24 mmol, 1.00 equiv.) HSiCl₃ in 8 ml Et₂O. The resulting reaction mixture was stirred for 16 h and afterwards filtrated. The obtained solid was recrystallized from hexane solution, giving compound **2** as an off-white solid in 26% yield. Single crystals suitable for SC-XRD analysis were obtained from a saturated DCM solution at –30 °C (Figure S6, SI). **m.p.:** 97.2–101.2 °C. ¹H NMR (500 MHz, chloroform-*d*, 298 K) δ (ppm) = 6.00 (h, *J*_{H-F} = 3.9 Hz, 1H, Si-H). ¹³C NMR (126 MHz, chloroform-*d*, 298 K) δ (ppm) = 149.41 (dm, ¹J_{C-F} = 249.0 Hz, 6 C, C^{3,5}), 144.12 (dd, ¹J_{C-F} = 265.2, ²J_{C-F} = 18.3 Hz, 6 C, C^{2,6}), 120.45 (q, ¹J_{C-F} = 275.0 Hz, 3 C, CF₃), 114.70–113.68 (m, 3 C, C⁴), 110.79 (t, ¹J_{H-C} = 27.9 Hz, 3 C, C¹). ¹⁹F NMR (471 MHz, chloroform-*d*, 298 K) δ (ppm) = –56.87 (t, ⁴J_{F-F} = 21.8 Hz, 9F, CF₃), –122.85–125.19 (m, 8F, ArF), –135.60–138.81 (m, 8F, ArF). ²⁹Si NMR (99 MHz, chloroform-*d*, 298 K) δ (ppm) = –53.78 (s). ²⁹Si NMR (99 MHz, THF-*d*₆, 298 K) δ (ppm) = –153.43 (s). **Elemental analysis:** calculated (%): C (37.08), H (0.15), N(0.00), S(0.00); found (%): C (37.31) H (0.18), N(0.00), S(0.00).

Synthesis and characterization of Si(OTol^f)₄ (3): To a solution of 200 mg *p*-LiOTol^f (0.83 mmol, 4.00 equiv.) in 20 ml of acetonitrile were added 0.48 ml (0.21 mmol, 1.00 eq.) of a 0.456 M SiCl₄ solution. The reaction was stirred at room temperature for four days and afterwards filtered. The crude product was then washed with hexane and the volatiles were removed under vacuum. Product **3** was obtained as an oily, off-white solid in a 72% yield. ¹³C NMR (126 MHz, acetonitrile-*d*₃, 298 K) δ (ppm) = 145.61 (dm, ¹J_{C-F} = 251.3 Hz, 8 C, C^{3,5}), 142.02 (dm, ¹J_{C-F} = 248.3 Hz, ²J_{C-F} = 14.5 Hz, 8 C, C^{2,6}), 140.92–140.66 (m, 4 C, C¹), 122.58 (q, ²J_{C-F} = 272.0 Hz, 4 C, CF₃), 100.7 (qt, ²J_{C-F} = 34.4, 13.1 Hz, 4 C, C⁴). ¹⁹F NMR (471 MHz, acetonitrile-*d*₃, 298 K) δ (ppm) = –56.17 (t, ⁴J_{F-F} = 21.5 Hz, 12F, CF₃), –146.55–146.78 (m, 8F, *m*-ArF), –157.63 (d, ³J_{F-F} = 11.5 Hz, 8F, *o*-ArF). ²⁹Si NMR (99 MHz, acetonitrile-*d*₃, 298 K) δ (ppm) = –153.24 (s). ²⁹Si NMR (99 MHz, THF-*d*₆, 298 K) δ (ppm) = –153.43 (s). The obtained LIFDI-MS pattern for compound **3** can be found in the SI (Figure S1).

Synthesis and characterization of Si(Ph^f)₂pin^f (4): To a solution of 0.80 g Li₂pin^f (2.31 mmol, 1.00 equiv.) in 12 ml acetonitrile was dropwise added a solution of 1.00 g Si(C₆F₅)₂Cl₂ (2.31 mmol, 1.00 equiv.) in 6 ml acetonitrile while stirring vigorously. An off-white precipitate was formed, and the resulting mixture was heated 80 °C for 2.5 h. Afterwards the mixture was filtered, and all volatiles were removed in vacuum. The obtained off-white crude product was further purified by sublimation at 150 °C and 0.02 mbar to give product **4** as a colorless solid in 66% yield. Single crystals suitable for SC-XRD analysis were obtained from a saturated MeCN/DCM solution at –30 °C (Figure S7). **m.p.:** 95.3–104.7 °C. ¹³C-NMR (126 MHz, benzene-*d*₆, 298 K) δ (ppm) = 148.17 (dm, ¹J_{C-F} = 249.7 Hz, 4 C, ArC^{2,6}), 145.36 (dm, ¹J_{C-F} = 262.6 Hz, 2 C, ArC⁴), 137.37 (dm, ¹J_{C-F} = 258.2 Hz, 4 C, ArC^{3,5}), 121.01 (q, ¹J_{C-F} = 292.6 Hz, 4 C, CF₃), 101.00 (t,

²J_{C-F} = 28.6 Hz, 2 C, ArC¹), 85.66 (br, 2 C, OC(CF₃)₂). ¹⁹F-NMR (471 MHz, benzene-*d*₆, 298 K) δ (ppm) = –69.12 (s, 12F, CF₃), –126.9 (dm, 4F, *o*-ArF), –141.06 (tt, ³J_{F-F} = 21.2, ⁴J_{F-F} = 6.1 Hz, 2F, *p*-ArF), –157.14–157.38 (m, 4F, *m*-ArF). ²⁹Si-NMR (99 MHz, benzene-*d*₆, 298 K) δ (ppm) = –5.25 (s). ²⁹Si NMR (99 MHz, THF-*d*₆, 298 K) δ (ppm) = –19.47 (s). **Elemental analysis:** calculated (%): C (31.14), H (0.00), N(0.00), S(0.00); found (%): C (31.53) H (0.20), N(0.00), S(0.00).

Lewis acidity assessments by Gutmann-Beckett and Childs method: For the Lewis acidity assessment with the Gutmann-Beckett method, 12.0 μmol of the investigated Lewis acid **1**, **2**, **3**, **4**, or Si(Ph^f)₄ were placed together with 1.61 mg Et₃PO (12.0 μmol, 1.00 equiv.) in a *J*-Young-valved NMR tube and dissolved in 0.5 ml of dichloromethane-*d*₂. For compound Si(OPh^f)₄ the procedure was conducted using 36 μmol of the Lewis acid and Et₃PO. The obtained solution was then analyzed by ³¹P NMR spectroscopy, and the obtained ³¹P NMR shift was referenced to pure Et₃PO in dichloromethane-*d*₂ (Table S1, SI) Only in the case of compound **3** and Si(OPh^f)₄ double-coordination was observed when using 2.0 equiv. of Et₃PO (Figure S3, SI).

For the Childs assessment 6.00 mmol the respective Lewis acid **1**, **2**, **3**, **4**, Si(Ph^f)₄ or Si(OPh^f)₄ were first suspended in 0.5 ml of dichloromethane-*d*₂. Subsequently 0.5 μl *trans*-crotonaldehyde (0.42 mg, 6.00 mmol, 1.00 equiv.) were added with a precision pipette. The obtained mixture was shaken until complete dissolution and afterwards analyzed by ¹H NMR spectroscopy. The obtained signals of the H¹ proton are summarized in the Table S1 (see SI). No significant change in the chemical shift was observed for the presented silanes.

Supporting Information

Supplementary information to this article is available in a separate file. The authors have cited additional references within the Supporting Information.^[22]

Acknowledgements

We are exceptionally grateful to the WACKER Chemie AG for continuous financial and scientific support. We also want to thank Dr. John Kelly for conducting the XRD measurement of **4** and Anna Zehrer for invaluable contribution during her Bachelor's thesis. Open Access funding enabled and organized by Projekt DEAL.

Conflict of Interests

The authors declare no conflict of interest.

Data Availability Statement

The data that support the findings of this study are available in the supplementary material of this article.

Keywords: Childs method · Gutmann-Beckett method · Lewis acids · perfluorotolyl ligands · silanes

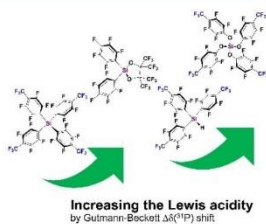
7. Tuning the Lewis Acidity of neutral Silanes using perfluorinated Aryl- and Alkyl Substituents – Dissertation Florian Tschernuth

- [1] a) P. Sarkar, S. Das, S. K. Pati, *Chem. Asian J.* **2022**, *17*, e202200148; b) J. C. L. Walker, H. F. T. Klare, M. Oestreich, *Nat. Chem. Rev.* **2020**, *4*, 54–62; c) J. Lam, K. M. Szkop, E. Mosafari, D. W. Stephan, *Chem. Soc. Rev.* **2019**, *48*, 3592–3612; d) J. R. Lawson, R. L. Melen, *Inorg. Chem.* **2017**, *56*, 8627–8643; e) J. M. Bayne, D. W. Stephan, *Chem. Soc. Rev.* **2016**, *45*, 765–774.
- [2] a) G. Kumar, S. Roy, I. Chatterjee, *Org. Biomol. Chem.* **2021**, *19*, 1230–1267; b) E. A. Patrick, W. E. Piers, *Chem. Commun.* **2020**, 56, 841–853; c) D. J. Parks, R. E. von H. Spence, W. E. Piers, *Angew. Chem. Int. Ed.* **1995**, *34*, 809–811; d) T. Hackel, N. A. McGrath, *Molecules* **2019**, *24*, 432; e) Q. Yin, Y. Soltani, R. L. Melen, M. Oestreich, *Organometallics* **2017**, *36*, 2381–2384; f) I. Chatterjee, M. Oestreich, *Angew. Chem. Int. Ed.* **2015**, *54*, 1965–1968; g) G. Erker, *Dalton Trans.* **2005**, 1883–1890.
- [3] a) H. F. T. Klare, L. Albers, L. Süsse, S. Keess, T. Müller, M. Oestreich, *Chem. Rev.* **2021**, *121*, 5889–5985; b) E. Fritz-Langhals, *Org. Process Res. Dev.* **2019**, *23*, 2369–2377.
- [4] A. F. Holleman, N. Wiberg, *Anorganische Chemie*, De Gruyter, Berlin, Boston, **2017**, 1062–1158.
- [5] a) A. L. Liberman-Martin, R. G. Bergman, T. D. Tilley, *J. Am. Chem. Soc.* **2015**, *137*, 5328–5331; b) J. Bader, A. F. G. Maier, J. Paradies, B. Hoge, *Eur. J. Inorg. Chem.* **2017**, 2017, 3053–3056.
- [6] D. H. McDaniel, H. C. Brown, *J. Org. Chem.* **1958**, *23*, 420–427.
- [7] R. Maskey, M. Schädler, C. Legler, L. Greb, *Angew. Chem. Int. Ed.* **2018**, *57*, 1717–1720.
- [8] L. O. Müller, D. Himmel, J. Stauffer, G. Steinfeld, J. Slattery, G. Santiso-Quiñones, V. Brecht, I. Krossing, *Angew. Chem. Int. Ed.* **2008**, *47*, 7659–7663.
- [9] a) T. Thorwart, D. Hartmann, L. Greb, *Chem. Eur. J.* **2022**, *28*, e202202273; b) N. Ansmann, T. Thorwart, L. Greb, *Angew. Chem. Int. Ed.* **2022**, *61*, e202210132; c) T. Thorwart, D. Roth, L. Greb, *Chem. Eur. J.* **2021**, *27*, 10422–10427; d) D. Hartmann, M. Schädler, L. Greb, *Chem. Sci.* **2019**, *10*, 7379–7388.
- [10] a) F. S. Tschernuth, T. Thorwart, L. Greb, F. Hanusch, S. Inoue, *Angew. Chem. Int. Ed.* **2021**, *60*, 25799–25803; b) F. S. Tschernuth, L. Bichlmaier, S. Inoue, *ChemCatChem* e202300281.
- [11] L. Greb, *Chem. Eur. J.* **2018**, *24*, 17881–17896.
- [12] a) L. A. Körte, J. Schwabedissen, M. Soffner, S. Blomeyer, C. G. Reuter, Y. V. Vishnevskiy, B. Neumann, H.-G. Stammer, N. W. Mitzel, *Angew. Chem. Int. Ed.* **2017**, *56*, 8578–8582; b) D. Naumann, H. Butler, R. Gnann, *Z. Anorg. Allg. Chem.* **1992**, *618*, 74–76; c) R. M. Ismail, H. J. Koetzsch, *J. Organomet. Chem.* **1967**, *10*, 421–426; d) A. G. Massey, A. J. Park, F. G. A. Stone, *Proceedings of the Chemical Society* **1963**, 212; e) L. A. Wall, R. E. Donadio, W. J. Pummer, *J. Am. Chem. Soc.* **1960**, *82*, 4846–4848.
- [13] G. J. P. Britovsek, J. Ugoletti, A. J. P. White, *Organometallics* **2005**, *24*, 1685–1691.
- [14] H. DeFrancesco, J. Dudley, A. Coca, *Boron Reagents in Synthesis*, Vol. 1236, American Chemical Society, **2016**, pp. 1–25.
- [15] a) C. Hansch, A. Leo, R. W. Taft, *Chem. Rev.* **1991**, *91*, 165–195; b) L. P. Hammett, *J. Am. Chem. Soc.* **1937**, *59*, 96–103.
- [16] Deposition Number a) 2269478 (Si(Tol)₄ (1)), 2269479 (HSi(Tol)₃ (2)), and 2269480 (Si(Ph)₃pin^f (4)) contain; b) the supplementary crystallographic data for this paper. These data are provided free of charge by the joint Cambridge Crystallographic Data Centre and Fachinformationszentrum Karlsruhe Access Structures service.
- [17] R. G. Pearson, *J. Chem. Educ.* **1968**, *45*, 581.
- [18] a) G. González-García, A. Pérez, J. A. López, E. Puello-Polo, A. González-García, *Main Group Met. Chem.* **2018**, *41*, 135–141; b) A. Doddi, J. V. Kingston, V. Ramkumar, M. Suzuki, M. Hojo, M. N. S. Rao, *Phosphorus Sulfur Silicon Relat. Elem.* **2012**, *187*, 343–356.
- [19] H. J. Frohn, A. Lewin, V. V. Bardin, *J. Organomet. Chem.* **1998**, *568*, 233–240.
- [20] A. Karipides, B. Foerst, *Acta Crystallogr. Sect. B* **1978**, *34*, 3494–3496.
- [21] K. M. Marczenko, C.-L. Johnson, S. S. Chitnis, *Chem. Eur. J.* **2019**, *25*, 8865–8874.
- [22] a) C. F. Macrae, I. Sovago, S. J. Cottrell, P. T. A. Galek, P. McCabe, E. Pidcock, M. Platings, G. P. Shields, J. S. Stevens, M. Towler, P. A. Wood, *J. Appl. Crystallogr.* **2020**, *53*, 226–235; b) G. Sheldrick, *Acta Crystallogr. Sect. C* **2015**, *71*, 3–8; c) L. J. Bourhis, O. V. Dolomanov, R. J. Gildea, J. A. K. Howard, H. Puschmann, *Acta Crystallogr. Sect. A* **2015**, *71*, 59–75; d) C. B. Hubschle, G. M. Sheldrick, B. Dittrich, *J. Appl. Crystallogr.* **2011**, *44*, 1281–1284; e) G. R. Fulmer, A. J. M. Miller, N. H. Sherden, H. E. Gottlieb, A. Nudelman, B. M. Stoltz, J. E. Bercaw, K. I. Goldberg, *Organometallics* **2010**, *29*, 2176–2179; f) O. V. Dolomanov, L. J. Bourhis, R. J. Gildea, J. A. K. Howard, H. Puschmann, *J. Appl. Crystallogr.* **2009**, *42*, 339–341; g) A. J. C. Wilson, *International Tables for Crystallography*, Vol. C, Kluwer Academic Publishers, Dordrecht, Netherlands **1992**.

Manuscript received: June 19, 2023
Revised manuscript received: July 18, 2023
Accepted manuscript online: July 24, 2023
Version of record online: ■■, ■■

RESEARCH ARTICLE

A set of Lewis acids was synthesized by installing perfluorotolyl- and perfluorocresolato ligands on neutral Si(IV) atoms. Additionally, a heteroleptic silane was synthesized using perfluoropinacolato and perfluorophenyl substituents. The obtained silanes were fully characterized and a Lewis acidity assessment was conducted by the Gutmann-Beckett and Childs method.



F. S. Tschernuth, L. Bichlmaier, S. Stigler,
Prof. Dr. S. Inoue*

1 – 7

Tuning the Lewis Acidity of Neutral
Silanes Using Perfluorinated Aryl-
and Alkoxy Substituents



8 A Neutral Germanium-centered Hard and Soft Lewis Superacid and its Unique Reactivity towards Hydrosilanes

Journal: *Dalton Transactions*

Publisher: Royal Society of Chemistry (RSC)^[132]

Authors: Florian S. Tschernuth, Arseni Kostenko, Sebastian Stigler, Anna Gradenegger and Shigeyoshi Inoue*

Status: Research Article, *accepted on the 14. November 2023*

DOI: DOI: 10.1039/D3DT03626J

Reproduced from Ref. 132 with permission from the Royal Society of Chemistry.

Content: The presented article draft displays the synthesis of a hard and soft Lewis superacidic germane holding two pin^F groups. The respective germane was synthesized from GeCl₄ using a similar strategy to the previously published silane derivative and obtained as the acetonitrile mono-adduct Ge(pin^F)₂·MeCN. Structural analysis revealed a similarly penta-coordinated germanium center holding two pin^F groups and one acetonitrile molecule. The strong solvent coordination was initially suggested by ATR-IR analysis outlining a distinct blueshift of the C≡N stretching vibration. The pronounced Lewis acidity of the germanium center was further proven by the Gutmann Beckett method displaying a Δδ(³¹P) shift of 38.8 ppm and calculated affinity values of 491 kJ mol⁻¹ (FIA) and 536 kJ mol⁻¹ (HIA), qualifying Ge(pin^F)₂ as a soft Lewis superacid. Consecutive fluoride and hydride abstraction experiments from Ag[SbF₆] and [HP(Mes)₃][HB(C₆F₅)₃] successfully yielded the respective pentavalent fluoro- and hydro-germanate species, thus proving hard and soft Lewis superacidity in experiment. The intensely bound acetonitrile was removed with surplus B(C₆F₅)₃ and subsequent sublimation giving access to the liberated germane Ge(pin^F)₂ and also silane Si(pin^F)₂ species. The obtained Lewis acids were comprehensively analyzed in both cases revealing a tetrahedral tetrrel center with no additional donor coordination. In contrast to Si(pin^F)₂, the softer Ge(pin^F)₂ was able to activate Et₃SiH to yield the germylene Ge(pin^F) and a mono-silylated pinacol side product or the pentavalent hydro germanate anion next to a MeCN-coordinated silyl cation, depending on the employed solvent. Hydrosilylation experiments with α-methylstyrene and Et₃SiH revealed an inversed temperature depending catalytic activity of the formed self-coordinated germylene unit. In-depth DFT calculations for various temperatures additionally supported the mechanism.

*Florian S. Tschernuth planned and prepared all experiments for this publication and wrote the manuscript as well as Supporting Information. Arseni Kostenko performed all DFT calculations and wrote parts of the manuscript and SI regarding calculations. Sebastian Stigler measured SC-XRD and refined the crystal data. Anna Gradenegger contributed with experiments within her mater's project and Prof. Shigeyoshi Inoue directly supervised the research.



Cite this: DOI: 10.1039/d3dt03626j

A neutral germanium-centred hard and soft lewis superacid and its unique reactivity towards hydrosilanes†

Florian S. Tschernuth,¹ Arseni Kostenko,¹ Sebastian Stigler,¹ Anna Gradenegger and Shigeyoshi Inoue^{1*}

The germanium-centred Lewis superacid $\text{Ge}(\text{pin})_2$ (**1**) was isolated as acetonitrile mono-adduct **1**·MeCN and thoroughly characterized by NMR spectroscopy, X-ray crystallography and quantum chemical calculations. Ion abstraction and NMR experiments revealed the hard as well as soft Lewis superacidic nature of **1**·MeCN. The title compound readily activates hydrosilanes such as Et_3SiH , which is not feasible for its harder silicon homologue **2**·MeCN, and even reacts with Et_3SiF . The strongly coordinating acetonitrile could be abstracted by $\text{B}(\text{C}_6\text{F}_5)_3$, giving the donor-free $\text{Ge}(\text{pin})_2$ (**1**) and $\text{Si}(\text{pin})_2$ (**2**) which are Lewis superacids. Unlike **1**·MeCN, the donor-free **1** efficiently catalyses hydrosilylation of α -methylstyrene by Et_3SiH . For this process, an inverse temperature dependence was observed, *i.e.* a complete conversion was achieved rapidly when the reaction was cooled to -35 °C, but the reaction stopped at elevated temperatures. Mechanistic investigations, including stoichiometric experiments and quantum chemical calculations, outlined the formation of germylene $\text{Ge}(\text{pin})$ (**3**), which acts as the active catalyst. The germylene is formed by reductive elimination of the silylated pinacol from the hydrogermane intermediate, which is obtained by the initial reaction of **1** with Et_3SiH . The inverse temperature dependence of the catalytic reaction could be explained by low entropy associated with the complexation of two cooperating germynes and the substrates. With this example we introduce an *in situ* generated Lewis acidic germylene complex for catalytic hydrosilylation of olefins and again exemplify the great potential of main-group-element-based complexes in catalysis.

Received 30th October 2023,
Accepted 14th November 2023
DOI: 10.1039/d3dt03626j

rsc.li/dalton

Introduction

The concept of Lewis acid (LA) mediated catalysis is broadly established in both laboratory and industrial-scale organic syntheses.^{1–3} In particular, cationic Lewis acids based on Earth-abundant and nontoxic main-group elements like silicon have drawn much attention as they demonstrated catalytic activities comparable to transition-metal catalysts.^{4–7} To compensate for the inherent drawbacks of ionic systems, such as low solubility and anion interactions, neutral Lewis acids have been extensively investigated.^{8–15} In the case of silicon, the isolation of the first Lewis superacidic silanes with perhalogenated catecholate-based substituents was accomplished. These species showed noticeable catalytic capabilities, *e.g.* in

hydrodefluorination, carbonyl reduction, and even dihydrogen activation.^{16–20} However, the research on neutral Ge-centred Lewis superacids and their catalytic potential is still in its infancy, and only a limited number of such compounds has been documented in the literature (Fig. 1).^{21–29}

In 2020, the first Ge-centred Lewis superacid $\text{Ge}(\text{cat}^{\text{Cl}})_2$ (**1**) was reported and additionally confirmed as a soft Lewis superacid by HIA calculations.³⁰ According to Crossing *et al.*, a Lewis superacid (LSA) possesses a higher fluoride anion affinity (FIAs) than molecular SbF_5 in the gas phase.³¹ To further consider the influence of the HSAB concept, an additional definition by Greb includes soft Lewis superacids (sLSA) which are compounds with a higher hydride ion affinity (HIA) than molecular $\text{B}(\text{C}_6\text{F}_5)_3$ in the gas phase.³²

Recently, differently substituted bis(catecholato)germanes have been successfully employed in the catalytic Friedel–Crafts dimerization³³ and alkylation³⁴ as well as carbonyl hydrosilylation and alkyne hydroboration.³⁵ In 2021, our group reported a stable Lewis superacidic silane **2**·MeCN with perfluorinated pinacolato substituents that demonstrated a formidable FIA (474 kJ mol^{-1}), even activating fluorosilanes, but lacked in

TUM School of Natural Sciences, Wacker-Institute of Silicon Chemistry and Catalysis Research Center, Technische Universität München, Lichtenbergstraße 4, 85748 Garching, Germany. E-mail: s.inoue@tum.de

† Electronic supplementary information (ESI) available. CCDC 2286080–2286083 and 2286830. For ESI and crystallographic data in CIF or other electronic format see DOI: <https://doi.org/10.1039/d3dt03626j>

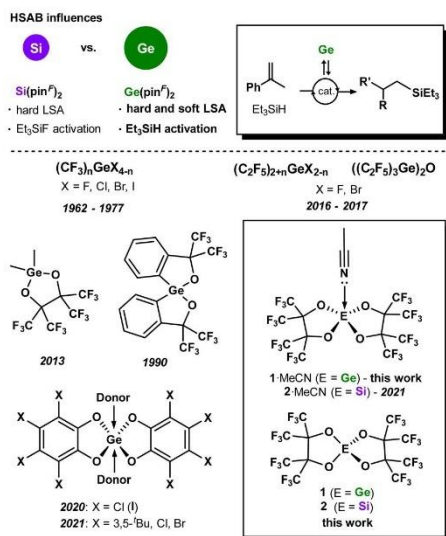


Fig. 1 Selected examples of literature-known Ge-centered, neutral Lewis acids and novel Lewis superacids **1** and **1-MeCN** presented in this work, and the scope of the article concerning the recently published silane derivative $\text{Si}(\text{pinF})_2\text{-MeCN}$.

terms of HIA (444 kJ mol^{-1}).³⁶ Since hydride abstraction is a crucial step in LA-mediated catalytic reactions, such as olefin hydrosilylation, suitable catalysts should ideally meet both definitions for a hard and soft Lewis superacid.^{37,38}

Herein, we report the preparation of the acetonitrile-coordinated bis(perfluoropinacolato)germane **1-MeCN**, which is the structural equivalent of our previously reported Si-based Lewis superacid **2-MeCN**, but features a germanium centre. The compound was consecutively analysed, revealing the hard and soft Lewis superacidic nature and the ability to activate hydrosilanes. Acetonitrile abstraction using $\text{B}(\text{C}_6\text{F}_5)_3$ furnished the synthesis of donor-free germane **1** and silane **2**. Reactivity investigations outlined a significant impact of the donor-substituent for hydrosilane activation in the case of the germane species. We additionally demonstrate the applicability of **1** as a pre-catalyst, which yields germylene **3** upon a reaction with a hydrosilane. **3** efficiently catalyses the hydrosilylation of α -methylstyrene with Et_3SiH at low temperatures. The mechanism of this unprecedented reactivity was further investigated by stoichiometric reaction experiments and quantum chemical calculations.

Results and discussion

The preparation of **1-MeCN** was accomplished by the reaction of lithium perfluoropincolate ($\text{Li}_2\text{pin}^{\text{F}}$) with GeCl_4 in acetonitrile, followed by heating the reaction mixture to reflux to

ensure the formation of the tetrasubstituted product. After 3 hours, the solvent was removed, yielding an off-white crude product that was heated to 150°C to release the neutral germane as acetonitrile mono-adduct **1-MeCN** by sublimation in 60% yield (Fig. 2).

NMR analysis of the obtained product was carried out in deuterated acetonitrile. Whereas the ^1H spectrum only showed the presence of non-deuterated CH_3CN at $\delta = 1.96 \text{ ppm}$, the ^{19}F NMR analysis presented a broad malformed multiplet at $\delta = -69.11$ to -70.77 ppm that distinctly differed in shape, but was still within the same range in case of the silicon derivative **2-MeCN**.³⁶ The ^{13}C NMR spectrum clearly demonstrated the presence of one single product. This was additionally confirmed by elemental analysis and single-crystal X-ray diffraction (SC-XRD). The X-ray structure of **1-MeCN** revealed a geometry similar to that of **2-MeCN**.³⁶ The germanium centre exhibited a pentacoordinate square-pyramidal geometry with two pinacolato groups slightly bent towards each other and one nitrogen-bound acetonitrile molecule at the tip of the pyramid. Although Lewis acidic germanium complexes usually show octahedral geometry with two neutral donor molecules, in this case, the acetonitrile mono-adduct was the predominant form.^{40–42} The Ge–O bonds arrange in a see-saw geometry with linearly aligned Ge1–O1 and Ge1–O4 bonds of $1.827(3) \text{ \AA}$ and $1.833(3) \text{ \AA}$ and slightly bent Ge1–O2 and Ge1–O3 bonds of $1.794(3) \text{ \AA}$ and $1.782(3) \text{ \AA}$ forming an O2–Ge1–O3 bond angle of $136.47(13)^\circ$. The averaged Ge–O bond length of 1.809 \AA is slightly shorter than that for **1** (1.845 \AA) or a germanate complex containing non-fluorinated pinacolato groups (1.835 \AA , averaged for pinacol groups).^{30,43} The Ge–N bond length of $1.933(4) \text{ \AA}$ is elongated compared to silicon-centred **2-MeCN** (Si–N $1.8412(16) \text{ \AA}$) but is still distinctly shorter, when compared to halo-acetonitrile coordinated GeF_3 (2.054 \AA , averaged Ge–N bond lengths) and the acetonitrile mono-adduct of a germanyl cation (Ge–N $2.0199(17) \text{ \AA}$).^{36,44,45}

To investigate the Lewis acidity by the Gutmann-Beckett method ≤ 1.0 equiv. of Et_3PO were carefully added to a solution of **1-MeCN** in dichloromethane- d_2 , giving a ^{31}P NMR shift of $\Delta\delta = 38.8 \text{ ppm}$ ($\delta = 89.1 \text{ ppm}$), thus demonstrating an excellent Lewis acidity even exceeding **2-MeCN** ($\Delta\delta = 35.8$).³⁶ The

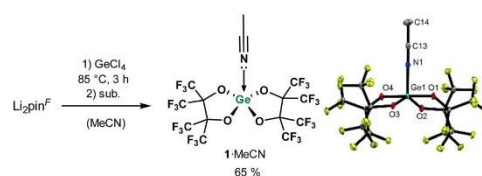


Fig. 2 Left panel: Synthesis scheme of bis(perfluoropinacolato)germane **1-MeCN** as the acetonitrile mono-adduct compared to recently published silicon derivative $\text{Si}(\text{pinF})_2\text{-MeCN}$. Right panel: Molecular SC-XRD structure of **1-MeCN** with ellipsoids plotted at the 50% probability level. Selected bond lengths (\AA) and angles (deg): Ge1–N1 $1.933(4)$, Ge1–O1 $1.827(3)$, Ge1–O2 $1.794(3)$, Ge1–O3 $1.782(3)$, Ge1–O4 $1.833(3)$; O1–Ge1–O2 $88.39(12)$, O1–Ge1–O4 $179.20(13)$, O3–Ge1–O4 $88.12(12)$, and O2–Ge1–O3 $136.47(13)$.³⁹

obtained shift aligns well with results reported for mono- Et_3PO adducts of bis(perhalocatecholato) germanes ($\text{X} = \text{Cl}, \text{Br}$) in the presence of MeCN ($\delta = 88.2\text{--}88.4$ ppm).³³ In the case of $1\text{-Et}_3\text{PO}$, however, no additional MeCN -coordination is expected as the same Gutmann–Beckett shift was obtained for MeCN -free **1**. Interestingly, by adding a slight surplus of Et_3PO , the sharp signal at $\delta = 89.1$ ppm utterly disappeared, and only a broad and hardly noticeable signal at $\delta = 51.4$ ppm (free Et_3PO : $\delta(^{31}\text{P}) = 50.4$ ppm) appeared. The chemical shift of only $\Delta\delta = 1.0$ ppm might be explained by the fast association/dissociation process of surplus Et_3PO molecules weakly coordinating to the Ge center. In contrast, related bis(catecholato) germanes distinctly favour the formation of bis- Et_3PO adducts, with defined signals for the *cis*- and *trans*-configuration ($\delta = 75.1$ ppm (*cis*) and $\delta = 70.6$ ppm (*trans*)).³⁰ The different reactivity of **1** is most likely explained by the pronounced steric repulsion that arises from the bulky perfluoropinacolato substituents.

To further compare the Lewis acidity of **1-MeCN** with the Si-analogue **2-MeCN**, NMR-scale abstraction experiments with AgSbF_6 , $[\text{HPMe}_3][\text{HB}(\text{C}_6\text{F}_5)_3]$, Et_3SiF and Et_3SiH were carried out (Scheme 1). Interestingly, when reacted with AgSbF_6 , no conversion could be observed at room temperature. However, by gently heating the reaction mixture to 60°C for 1 h, complete fluoride abstraction was detected in the ^{19}F NMR spectrum (Scheme 1, path a). The resulting fluoro germanate species ($[\text{F-1}]^-$) gave two multiplets in the characteristic range for the pin^f substituents at $\delta = -69.9$ to -70.1 ppm and $\delta = -70.7$ to -71.0 ppm as well as a small multiplet at $\delta = 144.9$ to -145.4 ppm that was attributed to the fluoride substituent directly attached to the Ge centre. In addition, **1-MeCN** was reacted with KF yielding the same ^{19}F pattern, thus verifying the formation of the anionic fluoride abstraction product $[\text{F-1}]^-$, which was validated by SC-XRD analysis (see the ESI†). Even though germanium was expected to be a softer Lewis acid than silicon, experimental results established that **1-MeCN** acts as a Lewis superacid (LSA).

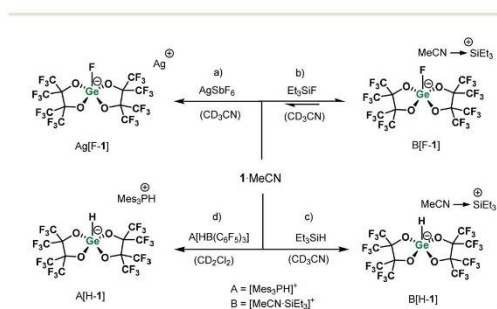
Since fluoride abstraction from Et_3SiF was easily achieved by **2-MeCN**, the same reactivity was tested for **1-MeCN**

(Scheme 1, path b). In this case, however, only partial conversion could be detected even after several hours at 80°C . When a surplus of Et_3SiF (5 equiv.) was introduced, an increased formation of the pentavalent fluorogermanate anion was detected in the ^{19}F NMR spectrum. Also, the ^{29}Si NMR gave the characteristic signal of the acetonitrile-coordinated silyl cation, which has already been described in the literature.³⁶ This experiment outlined an exceptional Lewis acidity for the germanium Lewis superacid **1-MeCN**, which is, however, slightly diminished when compared to its “harder” silane analogue **2-MeCN** (Scheme 1, path b).

According to the HSAB concept, germanium-centred Lewis acids are generally considered softer than their respective silicon counterparts, which is explained by a larger atomic radius.⁴⁶ The successful activation of hydrosilanes reflected this trend, as hydride is a softer Lewis base than fluoride.⁴⁷ Interestingly, Lewis superacid **2-MeCN** showed no reactivity towards hydrosilanes such as Et_3SiH , iPr_3SiH , or PhSiH_3 at all. In stark contrast, **1-MeCN** readily reacted with Et_3SiH in acetonitrile solution under the abstraction of the hydride (Scheme 1, path c), forming the MeCN stabilized silyl cation B^+ and the hydride substituted pentavalent germanate anion $[\text{H-1}]^-$. Complete conversion was detected after 10 minutes at room temperature by means of NMR spectroscopy.

The remarkable differences in reactivity of **1-MeCN** and **2-MeCN** can be explained by the HSAB concept as it was further demonstrated by the calculated gas phase FIA (492 kJ mol^{-1}) and HIA (536 kJ mol^{-1}) of **1**. While the FIA has a similar magnitude to $\text{Si}(\text{pin}^f)_2$ (FIA: 474 kJ mol^{-1}), the HIA of the softer Ge-centre is distinctly increased (HIA of $\text{Si}(\text{pin}^f)_2$: 444 kJ mol^{-1}), thus qualifying **1** as a soft Lewis superacid (sLSA) according to Greb's definition.³² Motivated by the successful hydrosilane activation and computational results, **1-MeCN** was experimentally tested for soft Lewis superacidity by direct comparison with $\text{B}(\text{C}_6\text{F}_5)_3$. For that experiment, **1-MeCN** was reacted with the H_2 -activation product $[\text{HPMe}_3][\text{HB}(\text{C}_6\text{F}_5)_3]$ in CD_2Cl_2 solution (Scheme 1, path d). Complete hydride abstraction from the $[\text{HB}(\text{C}_6\text{F}_5)_3]^-$ anion was observed by ^1H , ^{11}B , and ^{19}F NMR spectroscopy, resulting in the quantitative formation of the hydride substituted germanate species and neutral $\text{B}(\text{C}_6\text{F}_5)_3$. Consequently, **1-MeCN** can be considered a hard and soft Lewis superacid, whereas structurally identical silane **2-MeCN** only is a sole hard Lewis superacid.

As solvent coordination can disrupt specific reaction pathways in Lewis acid catalysis, isolation of donor-free Lewis acid **1** was of significant interest.⁴⁸ Unfortunately, attempts to synthesise **1** without using acetonitrile as a solvent were unsuccessful. For this reason, the abstraction of MeCN from **1-MeCN** was investigated, and $\text{B}(\text{C}_6\text{F}_5)_3$ proved to be a suitable reactant. This initially seemed counter-intuitive, considering the pronounced Lewis acidity of both compounds, compared to $\text{B}(\text{C}_6\text{F}_5)_3$ (HIA: 484 kJ mol^{-1} and FIA: 452 kJ mol^{-1}).⁴⁸ However, Lewis acidity is a complex interplay of attractive and repulsive interactions between the Lewis acid–base pair and strongly depends on the nature of the participating molecules.



Scheme 1 Reactivity experiments of **1-MeCN** for fluoride and hydride abstraction, revealing hard and soft Lewis superacidity (left arrows) and the activation of hydro and fluorosilanes (right hand side).

Therefore, it is not easy, or not even possible, to give a general measure for Lewis acidity itself, and a Lewis acid like $B(C_6F_5)_3$ can abstract MeCN even though it is considered weaker in terms of FIA, HIA, or the Gutmann Beckett characterization ($\Delta\delta(^{31}P) = 30.2$ ppm).⁴⁹

As outlined in Fig. 3, solvent-free Lewis superacids **1** and **2** were successfully obtained by acetonitrile abstraction using a slight surplus of $B(C_6F_5)_3$ in benzene solution. The calculated free energies for these reactions are -0.8 and -6.5 kcal mol⁻¹, respectively. The calculated affinity of **1** toward MeCN in benzene (6.5 kcal mol⁻¹) is by 5.5 kcal mol⁻¹ higher than that of **2** (1.0 kcal mol⁻¹) again demonstrating its superiority as a Lewis acid. The donor-free Lewis acids could be obtained by further sublimation of the reaction mixture in yields of 65% (**1**) and 54% (**2**). Multinuclear NMR analysis was carried out in CD_3CN (for better solubility), giving the same pattern as for the acetonitrile precursor, but with no signal of the liberated CH_3CN in the ¹H spectrum (see the ESI†).³⁶ To investigate the abstraction of MeCN, FT-ATR-IR spectra were recorded for **1** and **1**-MeCN, clearly showing the characteristic C≡N stretching and C-H deformation vibrations at 2342 cm⁻¹ and 2315 cm⁻¹ for the acetonitrile adduct **1**-MeCN, while these vibrations are absent in case of solvent-free **1** (see Fig. S1 and S2 in the ESI†). Similar results were obtained for the silicon derivative. The formation of the donor-free Lewis acids was further confirmed by SC-XRD analysis (Fig. 3). Suitable single crystals were obtained by slow sublimation at 40 °C. In the case of **1**, the tetracoordinate Ge centre exhibits a slightly distorted tetrahedral geometry. Due to insufficient data quality caused by a strong disorder of the CF₃ groups, no detailed bonding situation can be discussed. Nevertheless, the presence of acetonitrile can be distinctly excluded.

While Gutmann–Beckett analysis of the donor-free Lewis acids **1** and **2** only yielded ³¹P shifts identical to the respective

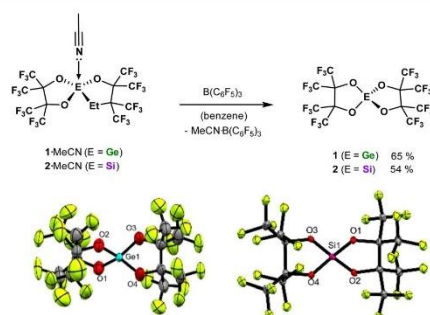
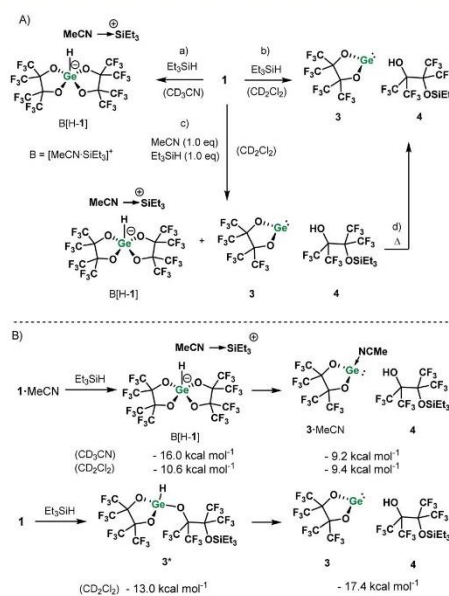


Fig. 3 Top panel: The reaction scheme for the acetonitrile abstraction experiment using $B(C_6F_5)_3$. Bottom panel: SC-XRD structures of acetonitrile-free germane **1** and silane **2**. Thermal ellipsoids are plotted at a 50% probability level. Selected bond lengths (Å) and angles (°) of **2**: Si1–O1 1.622(7), Si1–O2 1.644(7), Si1–O3 1.636(5), Si1–O4 1.635(5); O1–Si1–O2 97.5(3), O1–Si1–O4 116.5(3), O3–Si1–O4 97.4(2), and O2–Si1–O3 115.8(3).³⁹

acetonitrile adducts, the reaction of donor-free **1** with Et_3SiH furnished unexpected activation products (Scheme 2, A). In acetonitrile solution the hydride abstraction of Et_3SiH to form an acetonitrile coordinated silyl cation **B**⁺ (Scheme 2, path a) and pentavalent hydro germanate $[H-1]^-$ was observed. Calculations show that in acetonitrile the reaction of **1**-MeCN in the presence of silane to form the corresponding products is exergonic by 16.0 kcal mol⁻¹ (Scheme 2, B). When the same reaction was repeated in dichloromethane, using one added equivalent of MeCN, a mixture of the aforementioned acetonitrile coordinated silyl cation species $B[H-1]$, in addition to the perfluoropinacol-substituted germylene **3** (see below) and silylated pinacol **4** was observed in a ratio of 1.0:0.6 (Scheme 2, path c). Heating up the reaction mixture to 80 °C for 30 min resulted in the quantitative formation of **3** and **4**. Calculations show that in dichloromethane the reaction of **1**-MeCN with a silane to form the corresponding products $B[H-1]$ is exergonic by only 10.6 kcal mol⁻¹, while further reaction to form the **3** and **4** is almost ergoneutral (Scheme 2, B). This is in stark contrast to acetonitrile solution, in which the formation of the germylene and **4** is energetically disfavoured by 6.8 kcal mol⁻¹. This can be explained by the relative polarity of the solvents, as the more polar acetonitrile stabilizes the charged species more effectively than DCM. Consequently, in dichloromethane solution (in the absence of acetonitrile), **1**



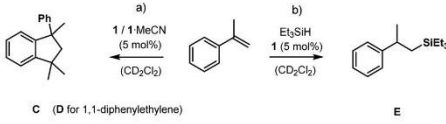
Scheme 2 (A) Hydrosilane activation furnishes different products depending on the applied conditions. (a) **1** h at 80 °C in CD_3CN ; (b) dissolving in CD_2Cl_2 at 25 °C; (c) dissolving in CD_2Cl_2 at 25 °C; and (d) 30 min at 80 °C. (B) Calculated reaction free energies in the respective solvents at the PBE0-D4(CPCM)/def2-TZVP level of theory.

selectively reacts with Et_3SiH to form the perfluoropinacol-substituted germylene **3** (Scheme 2, path b). The molecular germylene species was independently synthesized as the 1,4-dioxane-bridged adduct. (please see Fig. S41† for the SC-XRD structure). Calculations suggest that this process proceeds *via* an initial coordination of Et_3SiH to the Ge centre followed by a metathesis reaction of the Ge–O and Si–H bonds (Fig. S33†), which results in a hydrogermane intermediate **3***. This reaction can be explained by the weaker Ge–O bond in the presence of strongly electron-withdrawing substituents, when compared to the silicon derivative and the general increased stability of low-valent germanium species.⁵⁰ The formation of **3*** is exergonic by 13.0 kcal mol⁻¹, and it immediately decomposes to the germylene **3** and the corresponding alcohol with an additional energy gain of 4.4 kcal mol⁻¹ (Scheme 2, B and Fig. S33†). The product formation was identified by multinuclear NMR spectroscopy in CD_2Cl_2 , giving the OH signal at $\delta = 3.94$ ppm in the ¹H NMR spectrum. The ¹⁹F spectrum gave two septets at $\delta = -69.1$ ppm and $\delta = -70.0$ ppm, which is attributed to the silylated alcohol, and a broad singlet at $\delta = -70.9$ ppm that corresponds to symmetric germylene **3**. The ²⁹Si signal was found at $\delta = 31.7$ ppm, which was slightly shifted as for the MeCN coordinated silyl cation in B[H-1] ($\delta = 36.4$ ppm in CD_3CN). As mentioned above, this rearrangement was not observed in the CD_3CN solution, where the surplus of coordinating solvent sufficiently stabilizes the ionic reaction product B[H-1].

In the case of the harder silicon derivative **2**, no reaction with Et_3SiH was observed, as the formation of a hydrosilane similar to the hydrogermane **3*** is predicted to be endergonic by 7.8 kcal mol⁻¹. Moreover, the barrier for this transformation is 30.5 kcal mol⁻¹, which is unachievable under ambient conditions (Fig. S33†).

According to Lambert and Gevorgyan, the initial step for the Lewis acid-catalyzed hydrosilylation of olefins is the activation of the hydrosilane by partial or complete abstraction of the hydride, forming a silyl cation intermediate.^{37,38} Consequently, **1**-MeCN and **1** were investigated for the hydrosilylation of α -methylstyrene in a model reaction set-up to examine the catalytic activity. Interestingly, even though **1**-MeCN forms a silyl cation when reacted with Et_3SiH , no conversion of α -methylstyrene could be detected at various temperatures and reaction periods of up to 4 days (Table 1, entry 3). This was attributed to the deactivating effect of MeCN on Lewis acidic reaction centres, inhibiting the catalyst activity, as already observed in the literature.^{48,51} Without Et_3SiH present, a rapid dimerization of α -methylstyrene and 1,1-diphenylethylene was detected for both catalysts **1**-MeCN and **1**, yielding **C** and **D** (see the ESI†) as the main reaction products (Table 1, figure path a). The catalytic Friedel–Crafts dimerization of α -methylstyrene is well known for Lewis acidic catalysts,^{30,52–54} and was studied in detail by the Baines group for related catecholato germanes.³³ In our case, however, an exceptionally high conversion rate for **1** and **1**-MeCN was observed for the dimerization, quantitatively converting α -methylstyrene within 10 min at room temperature and catalyst loadings of 5 mol%,

Table 1 Catalytic reactivity of **1**-MeCN and **1** for the hydrosilylation and dimerization of α -methylstyrene



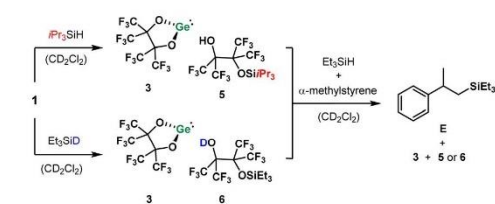
Entry	Path	Cat. 5 [mol%]	Temp. [°C]	Time [h]	Conv. [%]	Yield ^a [%]
1	a	1 -MeCN	25	0.17	99	83
2	a	1	25	0.17	99	65
3	b	1 -MeCN	25	96	0	0
4	b	1	25	24	28	26
5	b	1	-35	18	98	96

^a Olefin conversion and product yield was determined by ¹H NMR *via* integration against internal standard mesitylene.

thus outperforming literature-known catalyst systems based on Ge Lewis acids and even Ru complexes with ease.^{33,55}

In contrast, the same reaction set-up with an additional 1.0 eq. of Et_3SiH using 5 mol% acetonitrile-free **1** as the pre-catalyst, led to slow formation of the hydrosilylation product **E**. No hydrosilylation occurred in the case of bis(catecholato)germanes, when reacted with α -methylstyrene in the presence of Et_3SiH .³³ However, in our case only low conversion of 28% was achieved after 24 hours at room temperature. When the reaction mixture was heated to 80 °C, the conversion stopped. The process could be resumed when the same reaction mixture was cooled back to room temperature, implying that the annulment of the catalytic activity at the higher temperature was not due to catalyst degradation or destruction. To further investigate this inverted temperature dependence, another reaction set-up was cooled to -35 °C, which led to complete conversion, quantitatively forming the anti-Markovnikov hydrosilylation product already after 18 hours. To our knowledge this is the first testimonial of a neutral tetrel Lewis acid, which can be successfully applied in the challenging olefin hydrosilylation catalysis.

To investigate the underlying mechanism of the catalytic hydrosilylation reaction, stoichiometric reactions with alternating additions of two distinguishable hydrosilanes were carried out (Scheme 3). In the first experiment, **1** was reacted with $i\text{Pr}_3\text{SiH}$ to selectively form germylene **3** and the respective silylated pinacol derivative **5**. The subsequent addition of Et_3SiH and α -methylstyrene led to the selective formation of hydrosilylation product **E**, ruling out the transfer of the initially added $i\text{Pr}_3\text{SiH}$ species. The analogues experiment, this time with isotopically labelled Et_3SiD instead of $i\text{Pr}_3\text{SiH}$, again demonstrated the selective transfer of the secondary employed Et_3SiH species as no deuterated hydrosilylation product was obtained. The results consequently dismiss a potential silyl cation-mediated mechanism as proposed for trityl species or BCF by Lambert and Gevorgyan.^{37,38} In such a case, the primarily employed hydrosilane (marked with $i\text{Pr}$ or D) should be



Scheme 3 Stoichiometric hydrosilylation experiments of α -methylstyrene with **1** using initial $i\text{Pr}_3\text{SiH}$ and Et_3SiD demonstrating the transfer after the addition of a second hydrosilane unit.

converted to the respective hydrosilylation product. Also, no further reaction with additional Et_3SiH , possibly generating a silyl cation, is observed once the germylene-alcohol mixture has formed. In addition, the calculated energy barriers of classical Lewis acid mediated reaction cycles appear to be too high to explain the observed reactivity (see the ESI†). In accordance with the collected experimental data and DFT investigations, we therefore suggest a germylene-mediated catalytic cycle. When dioxane-bridged germylene **3** was used in this reaction, however, no selective product formation could be observed. This can be attributed to the negative impact of the dioxane molecule acting as a Lewis base, which might disrupt the formation of intermediate **INT1** that is a crucial component in the proposed mechanism of the catalytic reaction (see below). Successful olefin hydrosilylation with a low-valent germylumylidene cation was recently reported by Fritz-Langhals showing full hydrosilylation of α -methylstyrene with PMDS with catalyst loadings of only 0.1 mol% in 3 h at room temperature.⁵⁶ Other examples of reported catalytic systems include germylene ligated metal catalysts,^{57–59} NHC-coordinated germanium cations,⁶⁰ germa-acylium ions,⁶¹ and even neutral germylenes.^{62–64}

Upon formation, germylene **3**, bearing the strongly electron-withdrawing pin^F substituent, does not dimerize to the corresponding digermene $[(\text{pin}^F)\text{Ge}]_2$. However, according to calculations, in the presence of α -methylstyrene, **3** can form a homo-bimetallic Ge complex in which α -methylstyrene is coordinated to a Ge centre that donates its lone pair to the second germylene. The calculated ΔH for the formation of **INT1** in DCM at 298.15 K is $-22.4 \text{ kcal mol}^{-1}$, but it is entropically disfavoured, and the reaction is expected to be endergonic by $2.1 \text{ kcal mol}^{-1}$. The activated α -methylstyrene in complex **INT1** can undergo a reaction with triethylsilane, in two steps *via* a hydride abstraction from a silane **TS1**, forming **INT2** at $\Delta G = 14.2 \text{ kcal mol}^{-1}$, followed by the addition of SiEt_3 to the β -carbon *via* **TS2**. The **TS2** in which the silylium adds to the olefin carbon is expected to be the rate-determining step (Fig. 4, **TS2**). The overall calculated free energy gain of a catalytic cycle at rt is $11.1 \text{ kcal mol}^{-1}$.

In order to understand the observed temperature dependence, we carried out a thermochemistry analysis of the calculated reaction pathway at three different temperatures that correspond to the experiment (Fig. 4). The observation that the reaction proceeds faster at lower temperatures implies that the

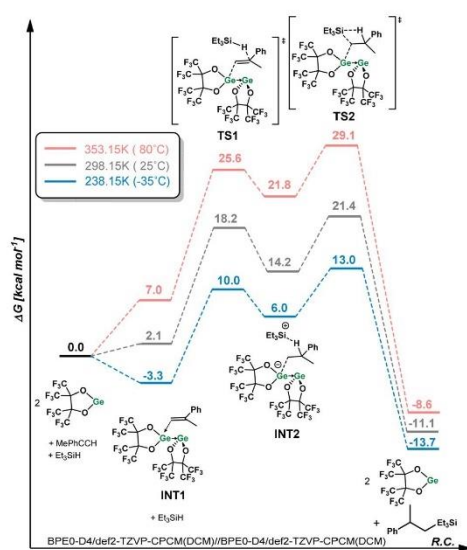


Fig. 4 Reaction mechanism for the hydrosilylation of α -methylstyrene and Et_3SiH with the *in situ* generated germylene **3** as the reaction catalyst, calculated at the BPE0-D4/def2-TZVP-CPCM(DCM)//BPE0-D4/def2-TZVP-CPCM(DCM) level of theory.

rate-determining step of the process is associated with low entropy. The activation barriers for the reaction at 25 °C and 80 °C, corresponding to the energy difference between the reactants and **TS2**, are 21.4 and 29.1 kcal mol^{-1} , respectively. The activation barrier for the reaction at -35 °C is 16.3 kcal mol^{-1} , corresponding to the energy difference between the **INT1** + Et_3SiH and **TS2**. To get an estimation for the relative reaction rates at different temperatures, we used the Eyring equation and computationally obtained barriers at the respective temperatures. Thus, the reaction rate at -35 °C is expected to be 4.3 times higher than the rate at 25 °C, and 757 times higher than the rate at 80 °C. These results are in line with the experimental observations. Without the internal adduct formation of two cooperating germylenes, leading to an increased Lewis electrophilicity of the donating germylene centre, the energy barrier of the transition state is increased (see the ESI†). The formation of a bis-germylene adduct is also observed using low-temperature NMR investigations of the reaction mixture containing **3** and **4** (see the ESI, Fig. S13†). Thus, the proposed mechanisms might be a plausible explanation for an increased reaction rate at lower temperatures.

Conclusions

Similar to the previously reported silane $\text{Si}(\text{pin}^F)_2\text{-MeCN}$ (2-MeCN), the installation of two perfluoropinacolato groups onto a germanium centre yielded bis(perfluoropinacolato)-

germane **1**-MeCN as the acetonitrile mono-adduct. Lewis acidity investigations by the Gutmann–Beckett method, abstraction experiments, and quantum chemical calculations demonstrated a Lewis superacidic nature. Due to the influence of the HSAB concept, **1**-MeCN possessed a considerably higher HIA than its silicon predecessor and could be confirmed as a hard and soft Lewis superacid that even activates hydrosilanes. Acetonitrile abstraction with $B(C_6F_5)_3$ yielded the solvent-free germane **1** and silane **2**, which were comprehensively characterized by methods, including SC-XRD analysis. While no significant differences in Lewis acidity were observed with the Gutmann–Beckett method, the reaction with Et_3SiH furnished different activation products for **1**-MeCN and **1**. In acetonitrile solution, the formation of an acetonitrile-coordinated silyl cation with a hydridogermane counteranion ($[B(H-1)]$) was observed. Without the presence of stabilizing acetonitrile, a neutral silyl substituted hydrogermane **3*** was formed that immediately decomposed, releasing perfluoropinacolato gerylene **3** and triethylsilyl perfluoropinacol **4**. While **1** and **1**-MeCN prove to be effective catalysts for the Friedel–Crafts dimerization of α -methylstyrene and 1,1-diphenylethylene, the gerylene species **3** was successfully introduced as a catalyst for the hydrosilylation of α -methylstyrene with Et_3SiH , showing a reversed temperature-controlled activity. This phenomenon was explained by unfavourable entropic effects resulting from the association of many components in the rate-determining transition state, which was demonstrated by quantum chemical calculations.

Conflicts of interest

The authors declare no conflict of interest.

Acknowledgements

We thank the Wacker Chemie AG for the scientific and financial support and all contributions in guidance and discussions, without which this project would not have been possible. We additionally thank Dr Alexander Pöthig, Dr Franziska Hanusch, Dr Andreas Saurwein and Jinyu Liu for the invaluable contribution to SC-XRD measurement and refinement. We further thank Karina Hemmer and Kathrin Kollmannsberger (Prof. R. A. Fischer) for conducting IR measurements. The authors gratefully acknowledge the computational and data resources provided by the Leibniz Supercomputing Centre.

References

- 1 A. Corma and H. García, *Chem. Rev.*, 2003, **103**, 4307–4366.
- 2 H. Yamamoto, *Lewis Acids in Organic Chemistry*, Wiley-VCH, Weinheim, 2000.
- 3 H. Yamamoto, *Lewis Acids in Organic Synthesis*, Wiley-VCH, Weinheim, 2000.
- 4 S. Rej, H. F. T. Klare and M. Oestreich, *Org. Lett.*, 2022, **24**, 1346–1350.
- 5 H. F. T. Klare, L. Albers, L. Süsse, S. Keess, T. Müller and M. Oestreich, *Chem. Rev.*, 2021, **121**, 5889–5985.
- 6 J. C. L. Walker, H. F. T. Klare and M. Oestreich, *Nat. Rev. Chem.*, 2020, **4**, 54–62.
- 7 T. Stahl, H. F. T. Klare and M. Oestreich, *ACS Catal.*, 2013, **3**, 1578–1587.
- 8 M. Yang, D. Tofan, C.-H. Chen, K. M. Jack and F. P. Gabbaï, *Angew. Chem., Int. Ed.*, 2018, **57**, 13868–13872.
- 9 M. Wiesemann and B. Hoge, *Chem. – Eur. J.*, 2018, **24**, 16457–16471.
- 10 J. F. Kögel, A. Y. Timoshkin, A. Schröder, E. Lork and J. Beckmann, *Chem. Sci.*, 2018, **9**, 8178–8183.
- 11 A. Wiesner, T. W. Gries, S. Steinhauer, H. Beckers and S. Riedel, *Angew. Chem., Int. Ed.*, 2017, **56**, 8263–8266.
- 12 L. A. Körte, J. Schwabedissen, M. Soffner, S. Blomeyer, C. G. Reuter, Y. V. Vishnevskiy, B. Neumann, H.-G. Stämmler and N. W. Mitzel, *Angew. Chem., Int. Ed.*, 2017, **56**, 8578–8582.
- 13 J. Bader, A. F. G. Maier, J. Paradies and B. Hoge, *Eur. J. Inorg. Chem.*, 2017, **2017**, 3053–3056.
- 14 N. Schwarze, B. Kurscheid, S. Steinhauer, B. Neumann, H.-G. Stämmler, N. Ignat'ev and B. Hoge, *Chem. – Eur. J.*, 2016, **22**, 17460–17467.
- 15 S. Steinhauer, J. Bader, H.-G. Stämmler, N. Ignat'ev and B. Hoge, *Angew. Chem. Int. Ed.*, 2014, **53**, 5206–5209.
- 16 T. Thorwart, D. Roth and L. Greb, *Chem. – Eur. J.*, 2021, **27**, 10422–10427.
- 17 D. Hartmann, M. Schädler and L. Greb, *Chem. Sci.*, 2019, **10**, 7379–7388.
- 18 R. Maskey, M. Schädler, C. Legler and L. Greb, *Angew. Chem., Int. Ed.*, 2018, **57**, 1717–1720.
- 19 T. Thorwart, D. Hartmann and L. Greb, *Chem. – Eur. J.*, 2022, e202202273.
- 20 A. L. Liberman-Martin, R. G. Bergman and T. D. Tilley, *J. Am. Chem. Soc.*, 2015, **137**, 5328–5331.
- 21 S. Pelzer, B. Neumann, H.-G. Stämmler, N. Ignat'ev, R. Eujen and B. Hoge, *Synthesis*, 2017, 2389–2393.
- 22 S. Pelzer, B. Neumann, H.-G. Stämmler, N. Ignat'ev and B. Hoge, *Chem. – Eur. J.*, 2017, **23**, 12233–12242.
- 23 S. Pelzer, B. Neumann, H.-G. Stämmler, N. Ignat'ev and B. Hoge, *Chem. – Eur. J.*, 2016, **22**, 4758–4763.
- 24 S. Pelzer, B. Neumann, H.-G. Stämmler, N. Ignat'ev and B. Hoge, *Chem. – Eur. J.*, 2016, **22**, 3327–3332.
- 25 L. Tahsini, S. E. Specht, J. S. Lum, J. J. M. Nelson, A. F. Long, J. A. Golen, A. L. Rheingold and L. H. Doerrer, *Inorg. Chem.*, 2013, **52**, 14050–14063.
- 26 S. E. Denmark, R. T. Jacobs, G. Dai-Ho and S. Wilson, *Organometallics*, 1990, **9**, 3015–3019.
- 27 J. A. Morrison, L. L. Gerchman, R. Eujen and R. J. Lagow, *J. Fluorine Chem.*, 1977, **10**, 333–339.
- 28 R. J. Lagow, L. L. Gerchman, R. A. Jacob and J. A. Morrison, *J. Am. Chem. Soc.*, 1975, **97**, 518–522.
- 29 H. C. Clark and C. J. Willis, *J. Am. Chem. Soc.*, 1962, **84**, 898–900.

8. A Neutral Germanium-centered Hard and Soft Lewis Superacid and its Unique Reactivity towards Hydrosilanes – Dissertation Florian Tschernuth

View Article Online

Paper

Dalton Transactions

- 30 D. Roth, H. Wadepohl and L. Greb, *Angew. Chem., Int. Ed.*, 2020, **59**, 20930–20934.
- 31 L. O. Müller, D. Himmel, J. Stauffer, G. Steinfeld, J. Slattery, G. Santiso-Quiñones, V. Brecht and I. Krossing, *Angew. Chem., Int. Ed.*, 2008, **47**, 7659–7663.
- 32 L. Greb, *Chem. – Eur. J.*, 2018, **24**, 17881–17896.
- 33 A. T. Henry, T. P. L. Cosby, P. D. Boyle and K. M. Baines, *Dalton Trans.*, 2021, **50**, 15906–15913.
- 34 D. Basu and H. P. Nayek, *Dalton Trans.*, 2022, **51**, 10587–10594.
- 35 A. T. Henry, D. A. R. Nanan and K. M. Baines, *Dalton Trans.*, 2023, **52**, 10363–10371.
- 36 F. S. Tschernuth, T. Thorwart, L. Greb, F. Hanusch and S. Inoue, *Angew. Chem., Int. Ed.*, 2021, **60**, 25799–25803.
- 37 M. Rubin, T. Schwier and V. Gevorgyan, *J. Org. Chem.*, 2002, **67**, 1936–1940.
- 38 J. B. Lambert, Y. Zhao and H. Wu, *J. Org. Chem.*, 1999, **64**, 2729–2736.
- 39 CCDC 2286080 (1)·(MeCN), 2286083 [K-(18-c-6)][F-1], 2286081 (2), 2286082 (3)₂·C₄H₈O₂ and 2286830 (1).†
- 40 F. Cheng, M. F. Davis, A. L. Hector, W. Levason, G. Reid, M. Webster and W. Zhang, *Eur. J. Inorg. Chem.*, 2007, **2007**, 2488–2495.
- 41 F. Cheng, M. F. Davis, A. L. Hector, W. Levason, G. Reid, M. Webster and W. Zhang, *Eur. J. Inorg. Chem.*, 2007, **2007**, 4897–4905.
- 42 E. L. Muetterties, *J. Am. Chem. Soc.*, 1960, **82**, 1082–1087.
- 43 H.-C. Chiang, S.-F. Hwang and C.-H. Ueng, *Acta Crystallogr., Sect. C: Cryst. Struct. Commun.*, 1995, **51**, 1258–1260.
- 44 A. W. Waller, N. M. Weiss, D. A. Decato and J. A. Phillips, *J. Mol. Struct.*, 2017, **1130**, 984–993.
- 45 A. Sekiguchi, T. Fukawa, V. Y. Lee, M. Nakamoto and M. Ichinohe, *Angew. Chem., Int. Ed.*, 2003, **42**, 1143–1145.
- 46 R. G. Pearson, *J. Am. Chem. Soc.*, 1963, **85**, 3533–3539.
- 47 R. G. Pearson, *J. Chem. Educ.*, 1968, **45**, 581.
- 48 H. Böhrer, N. Trapp, D. Himmel, M. Schleep and I. Krossing, *Dalton Trans.*, 2015, **44**, 7489–7499.
- 49 G. J. P. Britovsek, J. Ugoletti and A. J. P. White, *Organometallics*, 2005, **24**, 1685–1691.
- 50 N. Tokitoh and R. Okazaki, *Coord. Chem. Rev.*, 2000, **210**, 251–277.
- 51 C. A. Reed, *Acc. Chem. Res.*, 1998, **31**, 325–332.
- 52 M. Mehta and J. M. Goicoechea, *Angew. Chem., Int. Ed.*, 2020, **59**, 2715–2719.
- 53 H. Ma, Q. Sun, W. Li, J. Wang, Z. Zhang, Y. Yang and Z. Lei, *Tetrahedron Lett.*, 2011, **52**, 1569–1573.
- 54 H. Mitsuteru, I. Keita, Y. Yukiko and S. Tsutomu, *Chem. Lett.*, 2004, **33**, 728–729.
- 55 Y. Miyake, T. Moriyama, Y. Tanabe, G. Onodera and Y. Nishibayashi, *Organometallics*, 2011, **30**, 5972–5977.
- 56 E. Fritz-Langhals, *ChemCatChem*, 2023, **15**, e202300442.
- 57 P. M. Keil and T. J. Hadlington, *Angew. Chem., Int. Ed.*, 2022, **61**, e202114143.
- 58 M. L. Buil, J. A. Cabeza, M. A. Esteruelas, S. Izquierdo, C. J. Laglera-Gándara, A. I. Nicasio and E. Oñate, *Inorg. Chem.*, 2021, **60**, 16860–16870.
- 59 P. M. Keil, T. Szilvási and T. J. Hadlington, *Chem. Sci.*, 2021, **12**, 5582–5590.
- 60 D. Sarkar, S. Dutta, C. Weetman, E. Schubert, D. Koley and S. Inoue, *Chem. – Eur. J.*, 2021, **27**, 13072–13078.
- 61 D. Sarkar, C. Weetman, S. Dutta, E. Schubert, C. Jandl, D. Koley and S. Inoue, *J. Am. Chem. Soc.*, 2020, **142**, 15403–15411.
- 62 R. Dasgupta, S. Das, S. Hiwase, S. K. Pati and S. Khan, *Organometallics*, 2019, **38**, 1429–1435.
- 63 Y. Wu, C. Shan, Y. Sun, P. Chen, J. Ying, J. Zhu, L. L. Liu and Y. Zhao, *Chem. Commun.*, 2016, **52**, 13799–13802.
- 64 N. Del Rio, M. Lopez-Reyes, A. Baceiredo, N. Saffon-Merceron, D. Lutters, T. Müller and T. Kato, *Angew. Chem., Int. Ed.*, 2017, **56**, 1365–1370.

9 Summary and Outlook

The main objective of this Ph.D. project was dedicated to the utilization of the bidentate perfluorinated pinacolato substituents to form neutral but strongly electrophilic silicon- and germanium-centered molecules. The corresponding tetrasubstituted Lewis acids could be exclusively synthesized in acetonitrile solution starting from lithiated perfluoropinacol Li_2pin^F . In the case of silicon, a solid residue was collected after the solvent was stripped off which was identified as $\text{Li}[\text{Si}(\text{pin}^F)_2\text{Cl}]$ (**1**), the formal LiCl addition product to $\text{Si}(\text{pin}^F)_2$ with residual coordinating acetonitrile. Several analytical tools, including SC-XRD analysis, confirmed the formation of the pentavalent silicate anion. When using HSiCl_3 instead of SiCl_4 , a similar reaction occurred, selectively yielding $\text{Li}[\text{HSi}(\text{pin}^F)_2]$ (**2**) as the main reaction product with additional solvent coordination. Compound $\mathbf{2}\cdot(\text{MeCN})_2$ was crystallized from a saturated chloroform solution, proving the formation of a pentavalent hydrosilicate anion with a twofold acetonitrile-coordinated lithium counterion.

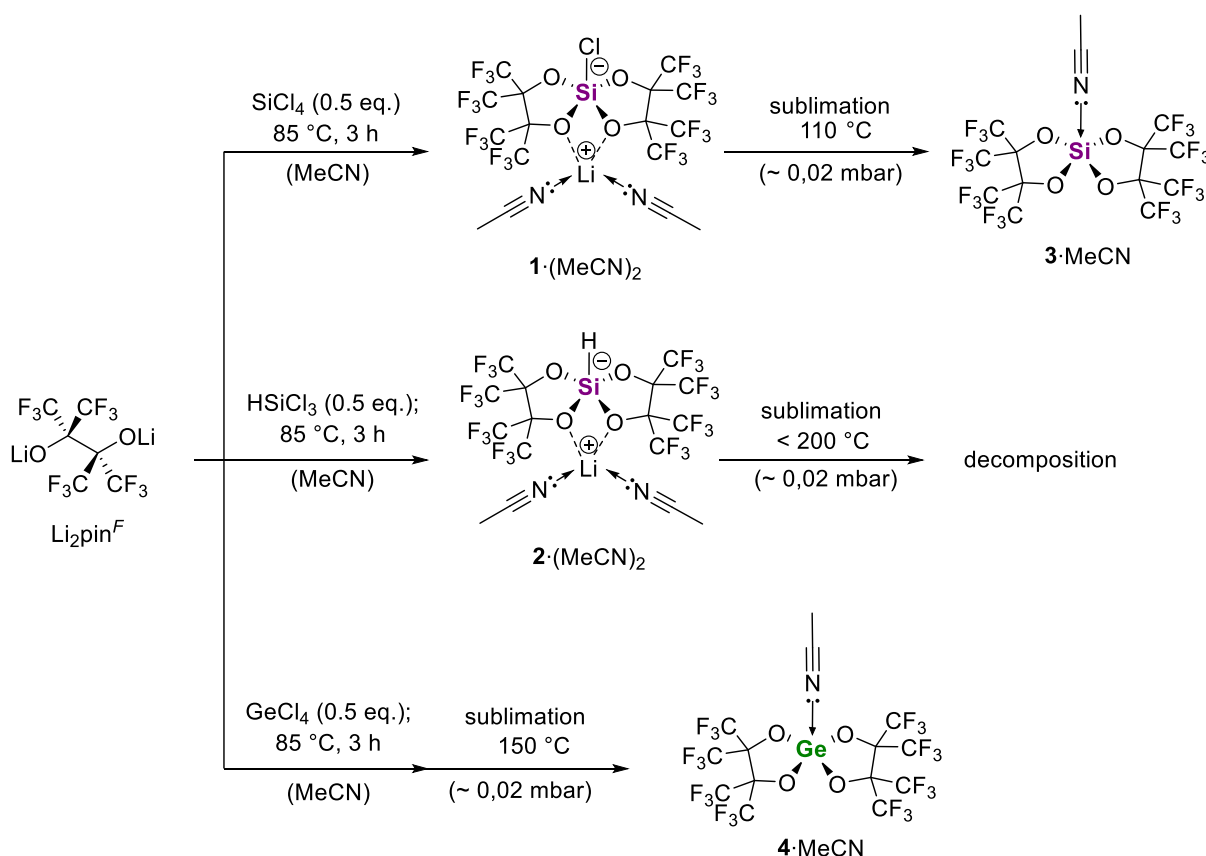
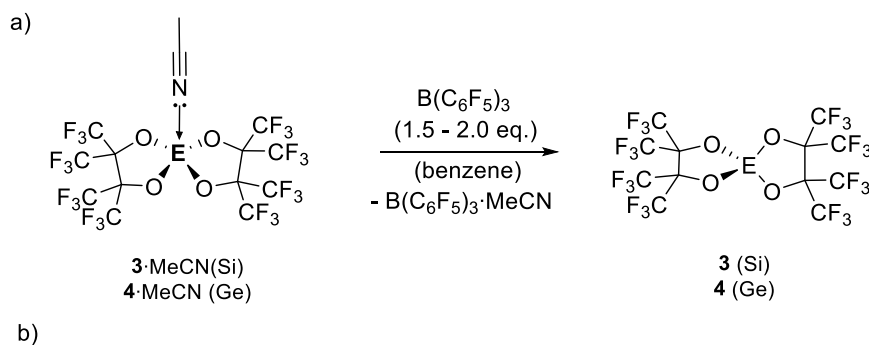


Figure 36: Synthetic strategies for obtaining Lewis acidic silane **3**·MeCN and germane **4**·MeCN, both obtained as the acetonitrile mono-adduct by thermolysis from preformed lithium chlorosilicate **1**·(MeCN)₂ and chlorogermanate species.

Heating compound **1**·(MeCN)₂ to $110\text{ }^\circ\text{C}$ at 0.02 mbar led to LiCl elimination, releasing the neutral silane as the acetonitrile mono-adduct **3**·MeCN, which was collected as a colorless solid. No LiH elimination was observed in the case of **2**·(MeCN)₂.

When applying the synthetic strategy to GeCl_4 , a complex product mixture was obtained that could not be fully structurally analyzed. Nevertheless, the presence of pentavalent chlorogermanate species was expected. Heating the obtained mixture to $150\text{ }^\circ\text{C}$ in vacuum again led to the liberation of the acetonitrile mono-coordinated germane $4\cdot\text{MeCN}$ which was collected by sublimation. Both treltel compounds were fully characterized by NMR, IR, and SC-XRD analysis, revealing strong coordination of the remaining acetonitrile molecule. In both cases, a distinct blueshift of the $\text{C}\equiv\text{N}$ vibrations could be observed with respect to free acetonitrile. Initial attempts to remove the donor molecule remained unsuccessful. Consequently, the solvent adducts ($3\cdot\text{MeCN}$ and $4\cdot\text{MeCN}$) were analyzed regarding their Lewis acidity by several literature methods. The Gutmann-Beckett assessment for $3\cdot\text{MeCN}$ revealed the substitution of MeCN by Et_3PO , yielding product $3\cdot\text{OPEt}_3$ with a $\Delta\delta(^{31}\text{P})$ shift of 35.8 ppm. No double coordination was observed. In the case of the bigger germanium derivative $4\cdot\text{MeCN}$, however, twofold substituted $4\cdot(\text{OPEt}_3)_2$ was predominantly formed. By employing substoichiometric Et_3PO amounts, the mono-coordinated adduct $4\cdot\text{OPEt}_3$ was obtained, showing a $\Delta\delta(^{31}\text{P})$ shift of 38.8 ppm. Both compounds displayed a tremendously high Lewis acidity compared to the perhalocatecholato-substituted silanes and germanes investigated by the Greb and Baines groups.

The strongly coordinating acetonitrile could be removed with a slight excess of $\text{B}(\text{C}_6\text{F}_5)_3$ in saturated benzene solution yielding the donor-free compounds **3** and **4** by crystallization (Figure 37, a). The pure Lewis acids were then obtained by slowly sublimating the crystalline precipitate in vacuum. Consecutive analysis by NMR and elemental analysis confirmed the quantitative removal of acetonitrile and $\text{B}(\text{C}_6\text{F}_5)_3$. In both cases, single crystals suitable for structural analysis were obtained by slow sublimation at $40\text{ }^\circ\text{C}$ in an argon atmosphere. The donor-free Lewis acids displayed a slightly distorted tetrahedral geometry of the central treltel element, substituted with two pin^F groups (Figure 37, b). No remaining donor coordination nor ring opening to form oligomeric species was observed.



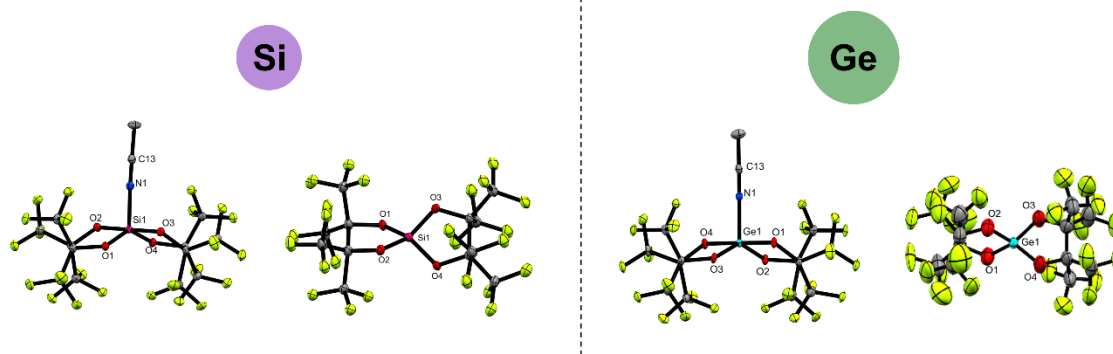


Figure 37: Crystal structures of acetonitrile-coordinated and donor-free Lewis superacids **3** and **4** with ellipsoids plotted at a 50% probability level.

Further Lewis acidity investigation by quantum chemical calculations revealed a similar hard Lewis acidity according to the FIA values of 474 kJ mol^{-1} for **3** and 492 kJ mol^{-1} for **4**. In the case of soft Lewis acidity, compound **4** displayed a significantly enhanced HIA of 536 kJ mol^{-1} , officially qualifying the germane a soft Lewis superacid by Greb's definition.^[19] In the case of the harder silane **3**, a decreased HIA value of 444 kJ mol^{-1} was obtained, which perfectly aligns with the HSAB principle.

Both compounds were analyzed for Lewis superacidity by abstraction experiments in solution. For this purpose, **3**·MeCN and **4**·MeCN were separately reacted with $\text{Ag}[\text{SbF}_6]$ in acetonitrile solution, quantitatively forming the pentavalent fluorosilicate and fluorogermanate anions. The corresponding fluoride-substituted anions were independently synthesized by the reaction of the Lewis acids with KF and fully characterized. Consequently, **3**·MeCN and **4**·MeCN were considered experimentally confirmed Lewis superacids in solution.

Hydride abstraction experiments from $[\text{HPMe}_3][\text{HB}(\text{C}_6\text{F}_5)_3]$ showed no reaction for **3**·MeCN, which aligns with the previously calculated decreased HIA value. In stark contrast, the soft Lewis superacid **4**·MeCN readily reacted with $[\text{HPMe}_3][\text{HB}(\text{C}_6\text{F}_5)_3]$ to release neutral $\text{B}(\text{C}_6\text{F}_5)_3$ by hydride abstraction. Consequently, silane **3** could be considered an exclusively hard Lewis acid, whereas germane **4** is a hard and soft Lewis superacid.

The investigated differences in ion affinities directly translate to the reactivity of the Lewis acids for activating fluoro- and hydrosilanes. The hard Lewis superacid **3**·MeCN readily reacted with Et_3SiF *via* fluoride abstraction, forming a MeCN-coordinated silyl cation with a fluorosilicate counterion (**5**). However, no reaction with Et_3SiH was observed, even at elevated temperatures. In the case of **4**·MeCN, a surplus of Et_3SiF was required to obtain sufficient fluoride abstraction due to an unfavorable reaction equilibrium. With softer Et_3SiH , in contrast, rapid hydride abstraction was observed, yielding a MeCN-stabilized silyl cation with a hydrogermane counterion (**6**) in acetonitrile solution, or a ring-opened hydrogermane species

that immediately decomposed to give a pinacol substituted germylene (**7**) and mono-silylated perfluoropinacol (**8**) in dichloromethane.

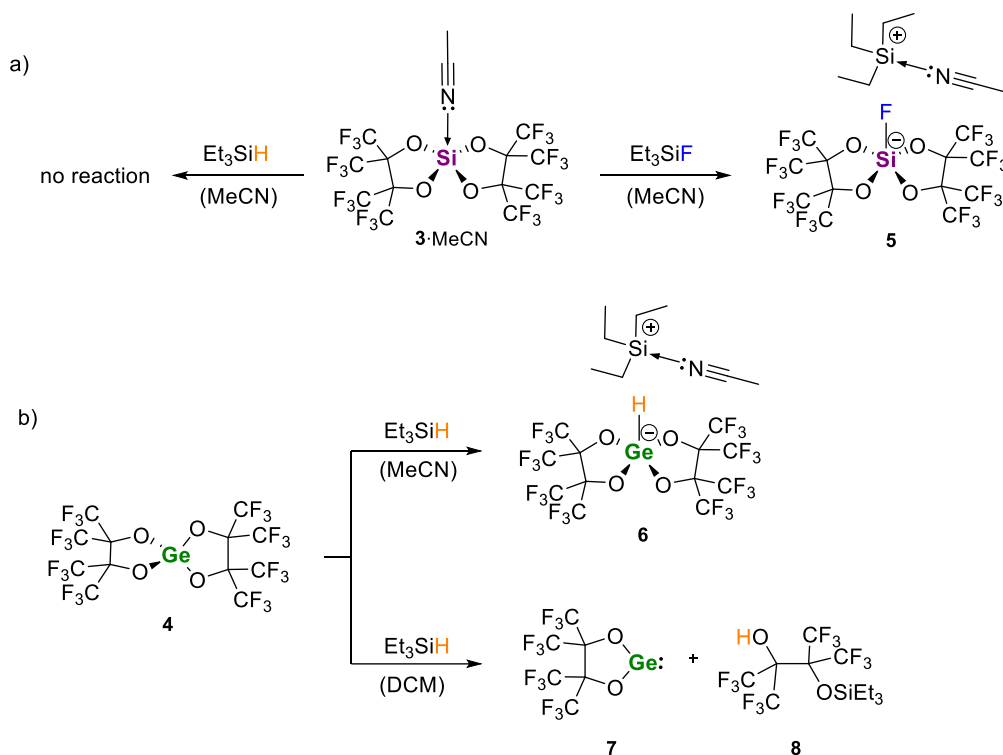


Figure 38: Reaction of Lewis superacid **3**·MeCN with Et_3SiF , selectively yielding ionic fluorosilicate species **5** while no reaction with Et_3SiH was observed (a) and the reaction of soft Lewis superacid **4** with Et_3SiH to form an ionic hydrosilicate species **6** in acetonitrile or germylene **7** in DCM (b).

As activation of hydrosilanes is a crucial step for olefin hydrosilylation, donor-free **4** was tested for the catalytic conversion of α -methylstyrene with Et_3SiH and displayed tremendous activity, quantitatively yielding the anti-Markovnikov hydrosilylation product after 18 h at -35°C with a catalyst loading of only 5 mol% (Figure 39, a). Consecutive mechanistic investigations by stoichiometric reaction experiments and high-level quantum chemical computations suggested germylene **7** to be the active catalyst, which forms a highly active dimeric push-pull complex at low temperatures. Therefore, Lewis superacid **4** can be considered a pre-catalyst. Only neglectable conversion was obtained for this reaction in the case of hard Lewis superacid **3**. No conversion could be observed in the presence of acetonitrile. Without the hydrosilane, however, both Lewis superacids rapidly catalyzed the Friedel-Crafts dimerization of α -methylstyrene (Figure 39, b). The hard Lewis superacid **3**·MeCN on the other hand, qualified as an efficient catalyst for the $\text{C}(\text{sp}^3)\text{-F}$ hydrodefluorination reaction, which was demonstrated by the conversion of 1-fluoroadamantane with Et_3SiH . Quantitative conversion selectively yielding adamantane and Et_3SiF was observed already with only 1 mol% of **3**·MeCN (Figure 39, c). Further catalytic reactions included the successful hydrosilylation of electron-deficient *p*- and *o*-nitrobenzaldehydes (Figure 39, d), the reductive ether formation of benzaldehyde and

methylated benzaldehyde (Figure 39, e), and the dihydrodeoxygenation of aceto- and benzophenone with Et_3SiH using 5 mol% of **3**·MeCN.

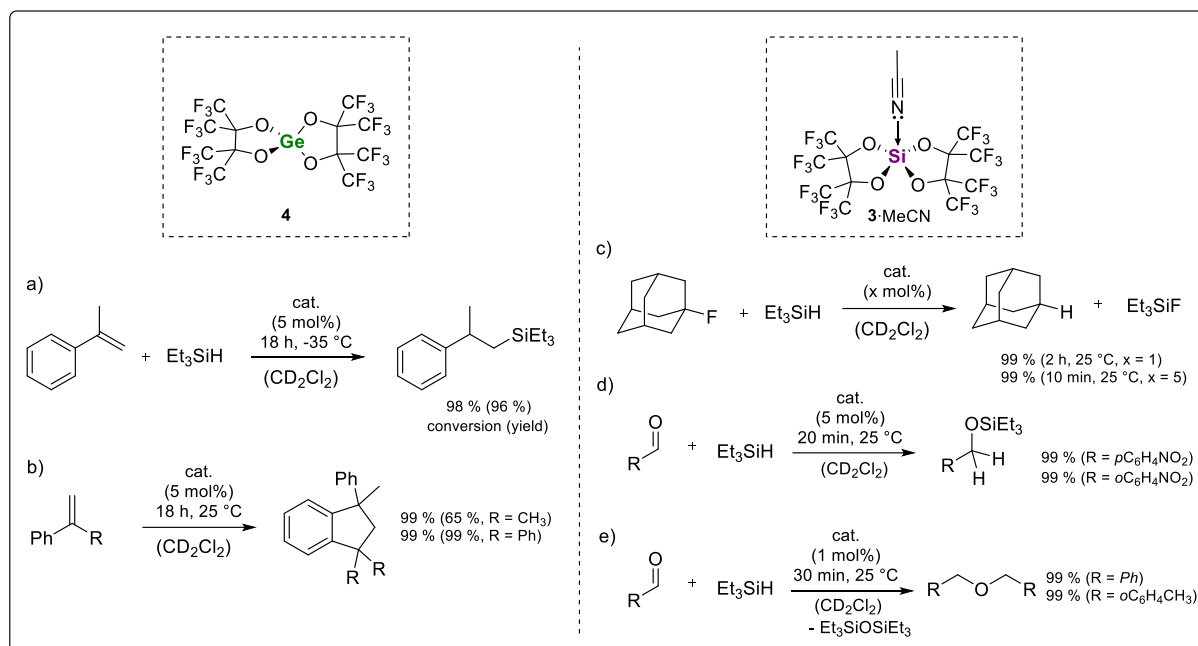


Figure 39: Selected catalytic reactions of Lewis superacids **3** and **4** derived from the tremendous fluoride and hydride affinities. The experiments include successful olefin hydrosilylation (a), Friedel-Crafts dimerization (b), hydrodefluorination (c), carbonyl hydrosilylation (d), and carbonyl reduction with hydrosilanes (e).

A further testimonial of the bright potential for the application of silicon-based catalysts is the degradation of oligomeric and polymeric ethylene glycol diethers. As outlined by a recent study from the Greb group, Lewis superacids such as **L-7*** and **L-16** efficiently catalyze the degradation of oligoethylenglycol derivatives by strong coordination of the ether bond to the Lewis acidic center triggering C-O bond cleavage.^[116] In fact, Lewis superacid **3**·MeCN was even more potent for this transformation as the sterically shielding pin^F substituents block catalyst deactivation by substrate chelation. For this reason, **3**·MeCN is the most efficient catalyst for the C-O ring-closing metathesis of 1,1-dimethoxypentane and diglyme known to the literature, quantitatively yielding cyclic reaction products tetrahydropyran and 1,4-dioxane after 20 h at 80 °C with a catalyst loading of only 1 mol% (Figure 40, a). Additional experiments with tetraethyleneglycol dimethylether (TEG-DME) and polyethyleneglycol diethers (PEG-DME) displayed quantitative fragmentation, yielding 1,4-dioxane. However, decreased turnover numbers were observed in the case of longer chained substrates because of successive catalyst deactivation. This effect could be explained based on Greb's previous mechanistic investigations suggesting a nucleophilic attack of a generated alcoholate on a secondary carbon atom after forming the pentaosilicate intermediate. The attack targets a primary carbon atom in the case of diglyme and 1,5-dimethoxypentane. In contrast, in the case

of longer chained substrates, this carbon is sterically less accessible because of an additional substituent. For this reason, the probability of side reactions that irreversibly lead to catalyst deactivation is more pronounced. The suggested formation of a pentaosilicate intermediate was additionally supported by the SC-XRD structure obtained from the reaction of **3**·MeCN with Et₂O, leading to ether cleavage. The obtained triethyloxonium pentaosilicate species was thoroughly analyzed by multinuclear NMR spectroscopy. In acetonitrile solution, the triethyloxonium decomposes by forming an *N*-ethyl acetonitrilium cation and Et₂O (Figure 40, a). This did not affect the corresponding ethoxy bis(perfluoro-pinacolato) silicate species.

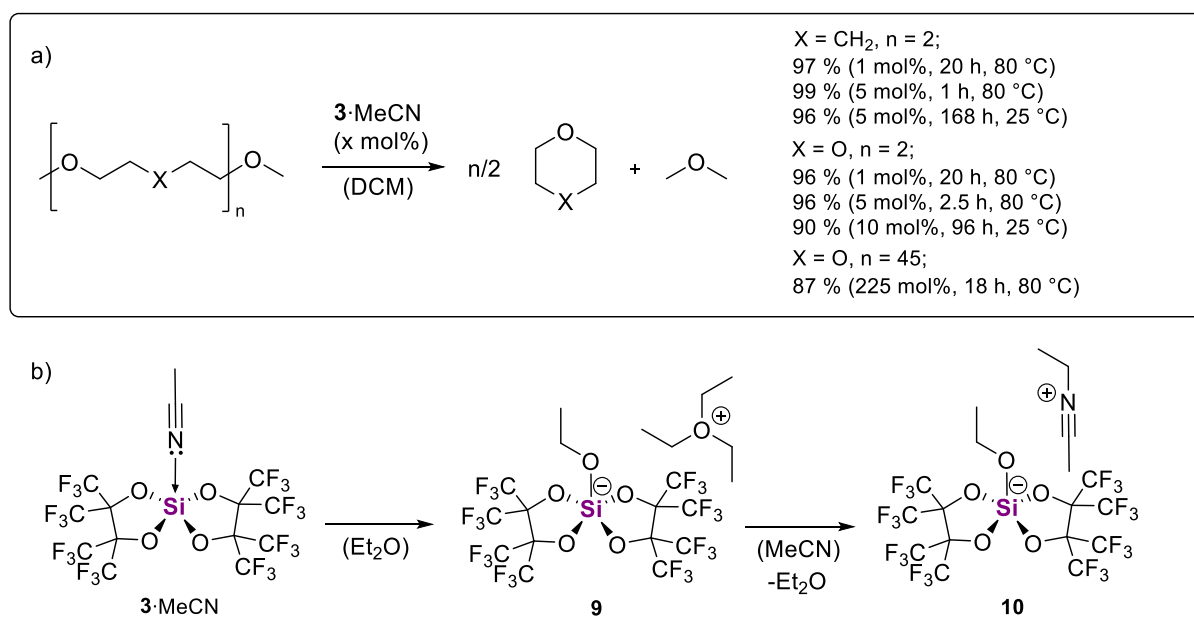


Figure 40: Successful application of **3**·MeCN in the C-O ring-closing metathesis of 1,1-dimethoxypentane, diglyme, and PEG-DME (a) and the cleavage of Et₂O (b) yielding the fully characterized potential pentaosilicate reaction intermediate holding either a triethyloxonium (**9**) or an *N*-ethyl acetonitrilium counterion (**10**).

After the significant success of bisperfluoropinacolato substituents for the synthesis of highly Lewis acidic complexes, the ligand scope was further extended by investigating *p*-perfluorotolyl (Tol^F) and perfluorocresolato (OTol^F) groups for the synthesis of Lewis acidic silanes. In the case of tetrasubstituted Si(Tol^F)₄ (**11**), no considerable Lewis acidity was found using the Gutmann-Beckett method, even though the successful synthesis was proven by crystal structure analysis. The same result was observed for less sterically congested HSi(Tol^F)₃ (**12**), displaying a slightly distorted tetrahedral geometry. The contrary was observed when adding four additional oxygen bridges. Consequently, in the case of Si(OTol^F)₄ (**13**), a Gutmann-Beckett shift of $\Delta\delta(^{31}\text{P}) = 29.2$ ppm was observed, qualifying compound **13** as a strong Lewis acid. No change could be detected by employing the Childs method. An additional silane (**14**) holding one perfluoropinacolato substituent and two perfluorophenyl (Ph^F) groups was synthesized and comprehensively characterized. In this case, a slightly diminished but

comparable Gutmann-Beckett shift of $\Delta\delta(^{31}\text{P}) = 27.2$ ppm was obtained, demonstrating the ability to tailor the Lewis acidity of silanes by employing heteroleptic substituents.

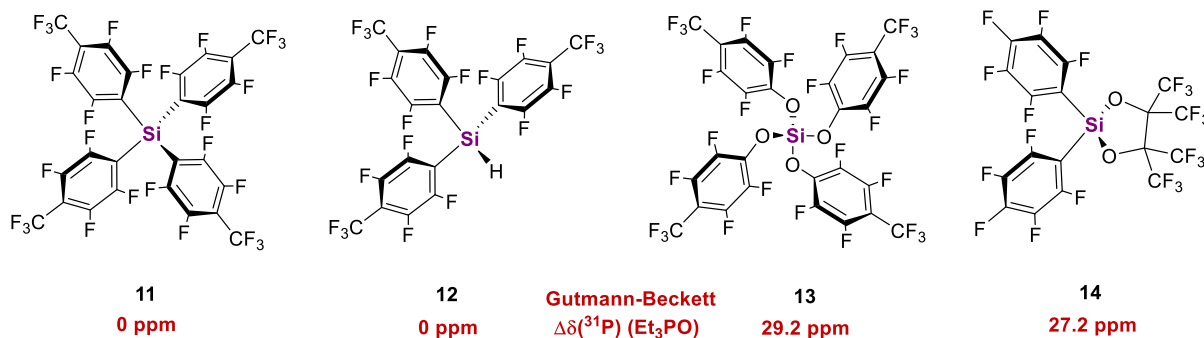


Figure 41: Additional Lewis acidic silanes **11-14** were synthesized by installing Tol^F, pOTol^F, and pin^F groups with the obtained Gutmann-Beckett ³¹P NMR shifts obtained by Et₃PO mono-coordination.

The striking catalytic activity of perfluoropinacolato-substituted silane **3** and germane **4** demonstrated the formidable potential of neutral main group element-based Lewis superacids for a broad range of chemical transformations, including olefin hydrosilylation and polymer degradation reactions. The conducted fundamental research contributes to the field of neutral silicon- and germanium-based homogenous catalysts and may enable the development of eco-friendly and industrially relevant catalysts for a more sustainable and eco-friendly chemical industry in the future.

10 Bibliography

- [1] (a) International Panel on Climate Change (IPCC), *Global Warming of 1.5°C - IPCC Special Report* can be found under https://www.ipcc.ch/site/assets/uploads/sites/2/2022/06/SR15_Full_Report_LR.pdf, **2022**, (accessed 26.04.2023); (b) R. J. Salawitch, T. P. Canty, A. P. Hope, W. R. Tribett, B. F. Bennett, *Paris Climate Agreement: Beacon of Hope*, 1st ed., Springer International Publishing, Cham, **2017**; (c) UNFCCC, *The Paris Agreement - Publication, Paris Climate Change Conference (COP21)*, United Nations **2015**.
- [2] (a) European Environment Agency (EEA), *Transport and environment report 2021, Decarbonising road transport — the role of vehicles, fuels and transport demand*, Luxembourg, can be found under <https://www.eea.europa.eu/publications/transport-and-environment-report-2021>, **2022**, (accessed 26.04.2023); (b) W. F. Lamb, M. Grubb, F. Diluiso, J. C. Minx, *Climate Policy* **2022**, *22*, 1-17; (c) International Energy Agency (IEA), *Renewable Energy Market Update - May 2022*, can be found under <https://www.iea.org/reports/renewable-energy-market-update-may-2022>, **2022**, (accessed 26.04.2022).
- [3] OurWorldInData.org, *CO₂ and Greenhouse Gas Emissions - Emissions by Sector*, can be found under <https://ourworldindata.org/co2-and-greenhouse-gas-emissions>, **2020**, (accessed 26.04.2023).
- [4] (a) A. Kätelhön, R. Meys, S. Deutz, S. Suh, A. Bardow, *Proceedings of the National Academy of Sciences* **2019**, *116*, 11187-11194; (b) Deutsche Gesellschaft für Internationale Zusammenarbeit (GIZ), *Climate Action Programme for the Chemical Industry - CAPCI*, can be found under <https://icca-chem.org/wp-content/uploads/2021/08/CAPCI-FactSheet.pdf>, **2021**, (accessed 27.04.2023); (c) R. C. Valencia, *The Future of the Chemical Industry by 2050*, **2013**, pp. 221-306.
- [5] International Energy Agency (IEA), *Chemicals - Tracking Report September 2022*, can be found under <https://www.iea.org/reports/chemicals>, **2022**, (accessed 26.04.2023).
- [6] World Economic Forum, Low Carbon Emitting Technologies Initiative, *Towards Net-Zero Emissions - Policy priorities for deployment of low-carbon emitting technologies in the chemical industry*, can be found under https://www3.weforum.org/docs/WEF_LCET_Policy_Priorities_2021.pdf, **2021**, (accessed 27.04.2023).
- [7] (a) C. R. Catlow, M. Davidson, C. Hardacre, G. J. Hutchings, *Philos. Trans. Royal Soc. A* **2016**, *374*, 20150089; (b) International Energy Agency (IEA), *Technology Roadmap - Energy and GHG Reductions in the Chemical Industry via Catalytic Processes*, can be found under <https://www.iea.org/reports/technology-roadmap-energy-and-ghg-reductions-in-the-chemical-industry-via-catalytic-processes>, **2013**, (accessed 27.04.2023).
- [8] J. Hagen, *Industrial Catalysis*, Wiley-VCH, Weinheim, **2015**, pp. 47-80.
- [9] J. Hagen, *Industrial Catalysis*, Wiley-VCH, Weinheim, **2015**, pp. 239-260.
- [10] W. A. Herrmann, B. Cornils, *Angew. Chem. Int. Ed.* **1997**, *36*, 1048-1067.
- [11] Arno Behr, P. Neubert, *Applied Homogeneous Catalysis* Wiley-VCH, Weinheim, **2012**, pp. 27 - 35.
- [12] D. R. Bryant, *Catalyst Separation, Recovery and Recycling: Chemistry and Process Design* (Eds.: D. J. Cole-Hamilton, R. P. Tooze), Springer Netherlands, Dordrecht, **2006**, pp. 9-37.
- [13] I. Vural Gürsel, T. Noël, Q. Wang, V. Hessel, *Green Chemistry* **2015**, *17*, 2012-2026.
- [14] Y. Nakajima, S. Shimada, *RSC Adv.* **2015**, *5*, 20603-20616.
- [15] (a) V. Nori, F. Pescioli, A. Sinibaldi, G. Giorgianni, A. Carlone, *Catalysts* **2022**, *12*, 5; (b) J. R. Lawson, R. L. Melen, *Inorg. Chem.* **2017**, *56*, 8627-8643; (c) P. P. Power, *Nature* **2010**, *463*, 171-177.
- [16] (a) J. C. L. Walker, H. F. T. Klare, M. Oestreich, *Nat. Rev. Chem.* **2020**, *4*, 54-62; (b) E. Fritz-Langhals, *Org. Process Res. Dev.* **2019**, *23*, 2369-2377.

- [17] K.-C. Kim, C. A. Reed, D. W. Elliott, L. J. Mueller, F. Tham, L. Lin, J. B. Lambert, *Science* **2002**, *297*, 825-827.
- [18] G. N. Lewis, *Valency Structure of Atoms and Molecules*, Wiley, New York, **1923**.
- [19] L. Greb, *Chem. Eur. J.* **2018**, *24*, 17881-17896.
- [20] R. G. Pearson, *J. Chem. Educ.* **1968**, *45*, 581.
- [21] R. S. Drago, *Coord. Chem. Rev.* **1980**, *33*, 251-277.
- [22] R. G. Pearson, *J. Am. Chem. Soc.* **1963**, *85*, 3533-3539.
- [23] R. G. Pearson, J. Songstad, *J. Am. Chem. Soc.* **1967**, *89*, 1827-1836.
- [24] S. Woodward, *Tetrahedron* **2002**, *58*, 1017-1050.
- [25] H. Mayr, M. Breugst, A. R. Ofial, *Angew. Chem. Int. Ed.* **2011**, *50*, 6470-6505.
- [26] R. G. Pearson, *Inorg. Chim. Acta* **1995**, *240*, 93-98.
- [27] R. J. Gillespie, T. E. Peel, *Adv. Phys. Org. Chem.*, Vol. 9 (Ed.: V. Gold), Academic Press, **1971**, pp. 1-24.
- [28] G. A. Olah, G. K. S. Prakash, J. Sommer, *Science* **1979**, *206*, 13-20.
- [29] F. Grandinetti, G. Occhiucci, O. Ursini, G. de Petris, M. Speranza, *Int. J. Mass Spectrom. Ion Processes* **1993**, *124*, 21-36.
- [30] A. Hasegawa, K. Ishihara, H. Yamamoto, *Angew. Chem. Int. Ed.* **2003**, *42*, 5731-5733.
- [31] S. Antoniotti, V. Dalla, E. Duñach, *Angew. Chem. Int. Ed.* **2010**, *49*, 7860-7888.
- [32] L. O. Müller, D. Himmel, J. Stauffer, G. Steinfeld, J. Slattery, G. Santiso-Quiñones, V. Brecht, I. Krossing, *Angew. Chem. Int. Ed.* **2008**, *47*, 7659-7663.
- [33] (a) G. C. Welch, R. R. S. Juan, J. D. Masuda, D. W. Stephan, *Science* **2006**, *314*, 1124-1126; (b) D. W. Stephan, *Science* **2016**, *354*, aaf7229.
- [34] J. A. Plumley, J. D. Evanseck, *J. Phys. Chem. A* **2009**, *113*, 5985-5992.
- [35] P. Erdmann, L. Greb, *Angew. Chem. Int. Ed.* **2022**, *61*, e202114550.
- [36] (a) T. E. Mallouk, G. L. Rosenthal, G. Mueller, R. Brusasco, N. Bartlett, *Inorg. Chem.* **1984**, *23*, 3167-3173; (b) K. O. Christe, D. A. Dixon, D. McLemore, W. W. Wilson, J. A. Sheehy, J. A. Boatz, *J. Fluorine Chem.* **2000**, *101*, 151-153; (c) I. Krossing, I. Raabe, *Chem. Eur. J.* **2004**, *10*, 5017-5030.
- [37] J. Klosin, G. R. Roof, E. Y. X. Chen, K. A. Abboud, *Organometallics* **2000**, *19*, 4684-4686.
- [38] H. Böhrer, N. Trapp, D. Himmel, M. Schleep, I. Krossing, *Dalton Trans.* **2015**, *44*, 7489-7499.
- [39] M. T. Mock, R. G. Potter, D. M. Camaioni, J. Li, W. G. Dougherty, W. S. Kassel, B. Twamley, D. L. DuBois, *J. Am. Chem. Soc.* **2009**, *131*, 14454-14465.
- [40] (a) S. Fukuzumi, K. Ohkubo, *J. Am. Chem. Soc.* **2002**, *124*, 10270-10271; (b) B. v. Ahsen, B. Bley, S. Proemmel, R. Wartchow, H. Willner, F. Aubke, *Z. Anorg. Allg. Chem.* **1998**, *624*, 1225-1234; (c) A. Wiesner, T. W. Gries, S. Steinhauer, H. Beckers, S. Riedel, *Angew. Chem. Int. Ed.* **2017**, *56*, 8263-8266; (d) J. R. Gaffen, J. N. Bentley, L. C. Torres, C. Chu, T. Baumgartner, C. B. Caputo, *Chem* **2019**, *5*, 1567-1583; (e) M. Ravi, V. L. Sushkevich, J. A. van Bokhoven, *Nat. Mater.* **2020**, *19*, 1047-1056.
- [41] I. B. Sivaev, V. I. Bregadze, *Coord. Chem. Rev.* **2014**, *270-271*, 75-88.
- [42] S. Künzler, S. Rathjen, A. Merk, M. Schmidtman, T. Müller, *Chem. Eur. J.* **2019**, *25*, 15123-15130.
- [43] V. Gutmann, *Coord. Chem. Rev.* **1976**, *18*, 225-255.
- [44] U. Mayer, V. Gutmann, W. Gerger, *Monatsh. Chem.* **1975**, *106*, 1235-1257.
- [45] M. A. Beckett, G. C. Strickland, J. R. Holland, K. Sukumar Varma, *Polymer* **1996**, *37*, 4629-4631.
- [46] (a) F. A. Tsao, A. E. Waked, L. Cao, J. Hofmann, L. Liu, S. Grimme, D. W. Stephan, *Chem. Commun.* **2016**, *52*, 12418-12421; (b) A. R. Jupp, T. C. Johnstone, D. W. Stephan, *Dalton Trans.* **2018**, *47*, 7029-7035.
- [47] J. Ramler, C. Lichtenberg, *Chem. Eur. J.* **2020**, *26*, 10250-10258.
- [48] R. F. Childs, D. L. Mulholland, A. Nixon, *Can. J. Chem.* **1982**, *60*, 809-812.
- [49] L. Luo, T. J. Marks, *Top. Catal.* **1999**, *7*, 97-106.
- [50] P. V. Bonnesen, C. L. Puckett, R. V. Honeychuck, W. H. Hersh, *J. Am. Chem. Soc.* **1989**, *111*, 6070-6081.

- [51] (a) P. Laszlo, M. Teston, *J. Am. Chem. Soc.* **1990**, *112*, 8750-8754; (b) R. J. Mayer, N. Hampel, A. R. Ofial, *Chem. Eur. J.* **2021**, *27*, 4070-4080.
- [52] G. J. P. Britovsek, J. Ugolotti, A. J. P. White, *Organometallics* **2005**, *24*, 1685-1691.
- [53] H. Großekappenberg, M. Reißmann, M. Schmidtman, T. Müller, *Organometallics* **2015**, *34*, 4952-4958.
- [54] (a) H. F. T. Klare, L. Albers, L. Süsse, S. Keess, T. Müller, M. Oestreich, *Chem. Rev.* **2021**, *121*, 5889-5985; (b) H. Yamamoto, *Lewis Acids in Organic Synthesis, Vol. 1*, Wiley-VCH, Weinheim, **2000**.
- [55] B. Zaidi, S. Belghit, *Silicon Materials*, IntechOpen, Rijeka, **2019**.
- [56] (a) R. Noyori, S. Murata, M. Suzuki, *Tetrahedron* **1981**, *37*, 3899-3910; (b) A. D. Dilman, S. L. Ioffe, *Chem. Rev.* **2003**, *103*, 733-772; (c) S. Steinhauer, J. Bader, H.-G. Stammer, N. Ignat'ev, B. Hoge, *Angew. Chem. Int. Ed.* **2014**, *53*, 5206-5209; (d) B. Waerder, M. Pieper, L. A. Körte, T. A. Kinder, A. Mix, B. Neumann, H.-G. Stammer, N. W. Mitzel, *Angew. Chem. Int. Ed.* **2015**, *54*, 13416-13419; (e) N. Schwarze, B. Kurscheid, S. Steinhauer, B. Neumann, H.-G. Stammer, N. Ignat'ev, B. Hoge, *Chem. Eur. J.* **2016**, *22*, 17460-17467.
- [57] P. Jutzi, A. Mix, B. Rummel, W. W. Schoeller, B. Neumann, H.-G. Stammer, *Science* **2004**, *305*, 849-851.
- [58] (a) D. Wendel, D. Reiter, A. Porzelt, P. J. Altmann, S. Inoue, B. Rieger, *J. Am. Chem. Soc.* **2017**, *139*, 17193-17198; (b) C. Shan, S. Yao, M. Driess, *Chem. Soc. Rev.* **2020**, *49*, 6733-6754; (c) D. Wendel, W. Eisenreich, C. Jandl, A. Pöthig, B. Rieger, *Organometallics* **2016**, *35*, 1-4; (d) A. V. Protchenko, K. H. Birjkumar, D. Dange, A. D. Schwarz, D. Vidovic, C. Jones, N. Kaltsoyannis, P. Mountford, S. Aldridge, *J. Am. Chem. Soc.* **2012**, *134*, 6500-6503.
- [59] V. Y. Lee, A. Sekiguchi, *Organosilicon Compounds* (Ed.: V. Y. Lee), Academic Press, **2017**, pp. 197-230.
- [60] A. F. Holleman, N. Wiberg, *Anorganische Chemie*, De Gruyter, Berlin, Boston, **2017**.
- [61] (a) M. Talavera, G. Meißner, S. G. Rachor, T. Braun, *Chem. Commun.* **2020**, *56*, 4452-4455; (b) A. Hayatifar, A. Borrego, D. Bosek, M. Czarnecki, G. Derocher, A. Kuplicki, E. Lytle, J. Padilla, C. Paroly, G. Tubay, J. Vyletel, C. S. Weinert, *Chem. Commun.* **2019**, *55*, 10852-10855; (c) N. Kordts, C. Borner, R. Panisch, W. Saak, T. Müller, *Organometallics* **2014**, *33*, 1492-1498.
- [62] (a) E. Fritz-Langhals, *ChemCatChem* **2023**, *15*, e202300442; (b) D. Sarkar, S. Dutta, C. Weetman, E. Schubert, D. Koley, S. Inoue, *Chem. Eur. J.* **2021**, *27*, 13072-13078.
- [63] (a) R. Dasgupta, S. Das, S. Hiwase, S. K. Pati, S. Khan, *Organometallics* **2019**, *38*, 1429-1435; (b) R. K. Siwatch, S. Nagendran, *Chem. Eur. J.* **2014**, *20*, 13551-13556.
- [64] (a) A. T. Henry, T. P. L. Cosby, P. D. Boyle, K. M. Baines, *Dalton Trans.* **2021**, *50*, 15906-15913; (b) D. Roth, H. Wadehohl, L. Greb, *Angew. Chem. Int. Ed.* **2020**, *59*, 20930-20934.
- [65] (a) J. W. Linnett, *J. Am. Chem. Soc.* **1961**, *83*, 2643-2653; (b) I. Langmuir, *J. Am. Chem. Soc.* **1919**, *41*, 868-934.
- [66] (a) C. Chuit, R. J. P. Corriu, C. Reye, *Chemistry of Hypervalent Compounds* (Ed.: K.-y. Akiba), Wiley-VCH, Weinheim, **1998**, pp. 81 - 147; (b) M. Kaftory, M. Kapon, M. Botoshansky, *The Chemistry of Organic Silicon Compounds* (Ed.: Y. Apeloig), Wiley-VCH, Weinheim, **1998**, pp. 181-265.
- [67] (a) Joseph L. Gay-Lussac, Louis J. Thenard, *Mémoires de physique et de chimie, de la Société d'Arcueil* **1809**, *2*, 317; (b) C. Chuit, R. J. P. Corriu, C. Reye, J. C. Young, *Chem. Rev.* **1993**, *93*, 1371-1448; (c) J. Davy, H. Davy, *Philos. Trans. Royal Soc. A* **1812**, *102*, 352-369.
- [68] H. Kwart, K. King, *D-orbitals in the chemistry of silicon, phosphorus and sulfur* Springer, Berlin, **1977**.
- [69] S. N. Tandura, M. G. Voronkov, N. V. Alekseev, *Structural Chemistry of Boron and Silicon*, Springer Berlin Heidelberg, Berlin, Heidelberg, **1986**, pp. 99-189.
- [70] S. E. Denmark, G. L. Beutner, *Angew. Chem. Int. Ed.* **2008**, *47*, 1560-1638.
- [71] S. Rossi, S. E. Denmark, *Organosilicon Chemistry: Novel Approaches and Reactions* (Eds.: T. Hiyama, M. Oestreich), Wiley-VCH, Weinheim, **2019**, pp. 333-415.

- [72] (a) R. J. Gillespie, B. Silvi, *Coord. Chem. Rev.* **2002**, 233-234, 53-62; (b) S. Noury, B. Silvi, R. J. Gillespie, *Inorg. Chem.* **2002**, 41, 2164-2172; (c) W. B. Jensen, *J. Chem. Educ.* **2006**, 83, 1751.
- [73] (a) A. Khan, D. Foucher, *Coord. Chem. Rev.* **2016**, 312, 41-66; (b) Y. I. Baukov, S. N. Tandura, *The Chemistry of Organic Germanium, Tin and Lead Compounds* (Ed.: Z. Rappoport), Wiley-VCH, Weinheim, **2002**, pp. 963-1239.
- [74] E. I. Davydova, A. Y. Timoshkin, T. N. Sevastianova, A. V. Suvorov, G. Frenking, *J. Mol. Struct.* **2006**, 767, 103-111.
- [75] (a) K. Shu, Y. Masaru, H. Iwao, *Chem. Lett.* **1996**, 25, 407-408; (b) F. Iwasaki, O. Onomura, K. Mishima, T. Kanematsu, T. Maki, Y. Matsumura, *Tetrahedron Lett.* **2001**, 42, 2525-2527.
- [76] S. E. Denmark, P. A. Barsanti, K.-T. Wong, R. A. Stavenger, *J. Org. Chem.* **1998**, 63, 2428-2429.
- [77] S. E. Denmark, T. Wynn, *J. Am. Chem. Soc.* **2001**, 123, 6199-6200.
- [78] (a) S. Murata, M. Suzuki, R. Noyori, *J. Am. Chem. Soc.* **1980**, 102, 3248-3249; (b) S. Murata, M. Suzuki, R. Noyori, *Tetrahedron Lett.* **1980**, 21, 2527-2528.
- [79] A. P. Davis, J. E. Muir, S. J. Plunkett, *Tetrahedron Lett.* **1996**, 37, 9401-9402.
- [80] A. P. Davis, S. J. Plunkett, *J. Chem. Soc., Chem. Commun.* **1995**, 2173-2174.
- [81] T. Tsunoda, M. Suzuki, R. Noyori, *Tetrahedron Lett.* **1980**, 21, 71-74.
- [82] (a) T. Tsunoda, M. Suzuki, R. Noyori, *Tetrahedron Lett.* **1979**, 20, 4679-4680; (b) M. Suzuki, H. Takada, R. Noyori, *J. Org. Chem.* **1982**, 47, 902-904.
- [83] N. Azizi, R. Baghi, H. Ghafari, M. Bolourtchian, M. Hashemi, *Synlett* **2010**, 2010, 379-382.
- [84] G. K. S. Prakash, A. K. Yudin, *Chem. Rev.* **1997**, 97, 757-786.
- [85] (a) K. G. Sharp, T. D. Coyle, *Inorg. Chem.* **1972**, 11, 1259-1264; (b) G. K. S. Prakash, P. V. Jog, P. T. D. Batamack, G. A. Olah, *Science* **2012**, 338, 1324-1327.
- [86] S. Steinhauer, T. Böttcher, N. Schwarze, B. Neumann, H.-G. Stammler, B. Hoge, *Angew. Chem. Int. Ed.* **2014**, 53, 13269-13272.
- [87] J. Bader, A. F. G. Maier, J. Paradies, B. Hoge, *Eur. J. Inorg. Chem.* **2017**, 2017, 3053-3056.
- [88] (a) I. Chatterjee, Z.-W. Qu, S. Grimme, M. Oestreich, *Angew. Chem. Int. Ed.* **2015**, 54, 12158-12162; (b) J. C. L. Walker, M. Oestreich, *Org. Lett.* **2018**, 20, 6411-6414.
- [89] D. W. Stephan, *J. Am. Chem. Soc.* **2015**, 137, 10018-10032.
- [90] J. B. Lambert, Y. Zhao, *Angew. Chem. Int. Ed.* **1997**, 36, 400-401.
- [91] K. Müther, P. Hrobárik, V. Hrobáriková, M. Kaupp, M. Oestreich, *Chem. Eur. J.* **2013**, 19, 16579-16594.
- [92] H. F. T. Klare, M. Oestreich, *Dalton Trans.* **2010**, 39, 9176-9184.
- [93] B. Mathieu, L. Ghosez, *Tetrahedron Lett.* **1997**, 38, 5497-5500.
- [94] (a) K. Hara, R. Akiyama, M. Sawamura, *Org. Lett.* **2005**, 7, 5621-5623; (b) H. F. T. Klare, K. Bergander, M. Oestreich, *Angew. Chem. Int. Ed.* **2009**, 48, 9077-9079.
- [95] V. J. Scott, R. Çelenligil-Çetin, O. V. Ozerov, *J. Am. Chem. Soc.* **2005**, 127, 2852-2853.
- [96] J. B. Lambert, Y. Zhao, H. Wu, *J. Org. Chem.* **1999**, 64, 2729-2736.
- [97] (a) K. Müther, M. Oestreich, *Chem. Commun.* **2011**, 47, 334-336; (b) K. Müther, J. Mohr, M. Oestreich, *Organometallics* **2013**, 32, 6643-6646.
- [98] (a) M. Mahlau, P. García-García, B. List, *Chem. Eur. J.* **2012**, 18, 16283-16287; (b) T. Gatzemeier, P. S. J. Kaib, J. B. Lingnau, R. Goddard, B. List, *Angew. Chem. Int. Ed.* **2018**, 57, 2464-2468.
- [99] O. Allemann, K. K. Baldridge, J. S. Siegel, *Org. Chem. Front.* **2015**, 2, 1018-1021.
- [100] (a) B. Shao, A. L. Bagdasarian, S. Popov, H. M. Nelson, *Science* **2017**, 355, 1403-1407; (b) S. Popov, B. Shao, A. L. Bagdasarian, T. R. Benton, L. Zou, Z. Yang, K. N. Houk, H. M. Nelson, *Science* **2018**, 361, 381-387.
- [101] Q. Wu, A. Roy, E. Irran, Z.-W. Qu, S. Grimme, H. F. T. Klare, M. Oestreich, *Angew. Chem. Int. Ed.* **2019**, 58, 17307-17311.
- [102] G. Bertrand, *Science* **2004**, 305, 783-785.
- [103] V. S. V. S. N. Swamy, S. Pal, S. Khan, S. S. Sen, *Dalton Trans.* **2015**, 44, 12903-12923.
- [104] P. Jutzi, F. Kohl, P. Hofmann, C. Krüger, Y.-H. Tsay, *Chem. Ber.* **1980**, 113, 757-769.

- [105] Y. Li, Y.-C. Chan, B.-X. Leong, Y. Li, E. Richards, I. Purushothaman, S. De, P. Parameswaran, C.-W. So, *Angew. Chem. Int. Ed.* **2017**, *56*, 7573-7578.
- [106] K. Leszczyńska, A. Mix, R. J. F. Berger, B. Rummel, B. Neumann, H.-G. Stammler, P. Jutzi, *Angew. Chem. Int. Ed.* **2011**, *50*, 6843-6846.
- [107] (a) E. Fritz-Langhals, S. Werge, S. Kneissl, P. Piroutek, *Org. Process Res. Dev.* **2020**, *24*, 1484-1495; (b) E. Fritz-Langhals, *Reactions* **2021**, *2*, 442-456.
- [108] B.-X. Leong, J. Lee, Y. Li, M.-C. Yang, C.-K. Siu, M.-D. Su, C.-W. So, *J. Am. Chem. Soc.* **2019**, *141*, 17629-17636.
- [109] A. L. Liberman-Martin, R. G. Bergman, T. D. Tilley, *J. Am. Chem. Soc.* **2015**, *137*, 5328-5331.
- [110] D. J. Parks, J. M. Blackwell, W. E. Piers, *J. Org. Chem.* **2000**, *65*, 3090-3098.
- [111] R. Maskey, M. Schädler, C. Legler, L. Greb, *Angew. Chem. Int. Ed.* **2018**, *57*, 1717-1720.
- [112] N. Ansmann, D. Hartmann, S. Sailer, P. Erdmann, R. Maskey, M. Schorpp, L. Greb, *Angew. Chem. Int. Ed.* **2022**, *61*, e202203947.
- [113] D. Hartmann, T. Thorwart, R. Müller, J. Thusek, J. Schwabedissen, A. Mix, J.-H. Lamm, B. Neumann, N. W. Mitzel, L. Greb, *J. Am. Chem. Soc.* **2021**, *143*, 18784-18793.
- [114] D. Hartmann, M. Schädler, L. Greb, *Chem. Sci.* **2019**, *10*, 7379-7388.
- [115] D. Hartmann, T. Strunden, L. Greb, *Inorg. Chem.* **2022**, *61*, 15693-15698.
- [116] N. Ansmann, T. Thorwart, L. Greb, *Angew. Chem. Int. Ed.* **2022**, *61*, e202210132.
- [117] T. Biberger, S. Makai, Z. Lian, B. Morandi, *Angew. Chem. Int. Ed.* **2018**, *57*, 6940-6944.
- [118] L. P. Hammett, *J. Am. Chem. Soc.* **1937**, *59*, 96-103.
- [119] H. C. Brown, Y. Okamoto, *J. Am. Chem. Soc.* **1958**, *80*, 4979-4987.
- [120] T. Thorwart, D. Roth, L. Greb, *Chem. Eur. J.* **2021**, *27*, 10422-10427.
- [121] T. Thorwart, D. Hartmann, L. Greb, *Chem. Eur. J.* **2022**, *28*, e202202273.
- [122] A. Hermannsdorfer, M. Driess, *Angew. Chem. Int. Ed.* **2021**, *60*, 13656-13660.
- [123] (a) P. M. Keil, T. J. Hadlington, *Angew. Chem. Int. Ed.* **2022**, *61*, e202114143; (b) P. M. Keil, T. Szilvási, T. J. Hadlington, *Chem. Sci.* **2021**, *12*, 5582-5590; (c) R. D. Rittinghaus, J. Tremmel, A. Růžička, C. Conrads, P. Albrecht, A. Hoffmann, A. N. Ksiazkiewicz, A. Pich, R. Jambor, S. Herres-Pawlis, *Chem. Eur. J.* **2020**, *26*, 212-221.
- [124] Y. Miyake, T. Moriyama, Y. Tanabe, G. Onodera, Y. Nishibayashi, *Organometallics* **2011**, *30*, 5972-5977.
- [125] K. Sakai, K. Oisaki, M. Kanai, *Org. Lett.* **2022**, *24*, 3325-3330.
- [126] W. J. Middleton, R. V. Lindsey, *J. Am. Chem. Soc.* **1964**, *86*, 4948-4952.
- [127] F. S. Tschernuth, T. Thorwart, L. Greb, F. Hanusch, S. Inoue, *Angew. Chem. Int. Ed.* **2021**, *60*, 25799-25803.
- [128] F. S. Tschernuth, T. Thorwart, L. Greb, F. Hanusch, S. Inoue, *Angew. Chem.* **2021**, *133*, 26003-26007.
- [129] F. S. Tschernuth, L. Bichlmaier, S. Inoue, *ChemCatChem* **2023**, *15*, e202300281.
- [130] F. S. Tschernuth, L. Bichlmaier, S. Stigler, S. Inoue, *Eur. J. Inorg. Chem.* **2023**, *26*, e202300388.
- [131] L. A. Körte, J. Schwabedissen, M. Soffner, S. Blomeyer, C. G. Reuter, Y. V. Vishnevskiy, B. Neumann, H.-G. Stammler, N. W. Mitzel, *Angew. Chem. Int. Ed.* **2017**, *56*, 8578-8582.
- [132] F. S. Tschernuth, A. Kostenko, S. Stigler, A. Gradenegger, S. Inoue, *Dalton Trans.* **2023**
Accepted Manuscript.

11 Appendix

11.1 Supporting Information Chapter 5



Supporting Information

Bis(perfluoropinacolato)silane: A Neutral Silane Lewis Superacid Activates Si–F Bonds

*Florian S. Tschernuth, Thaddäus Thorwart, Lutz Greb, Franziska Hanusch, and Shigeyoshi Inoue**

anie_202110980_sm_miscellaneous_information.pdf

Supporting Information

Table of Contents

1	Experimental Section.....	3
1.1	General methods and Instrumentation.....	3
1.2	Synthesis and Characterization.....	5
1.2.1	Synthesis and characterization of $\text{Li}_2\text{pin}^{\text{F}}$	5
1.2.2	Synthesis and characterization of $\text{Li}[1\text{-H}]\cdot(\text{MeCN})_2$	5
1.2.3	Synthesis and characterization of $\text{Li}[1\text{-Cl}]\cdot(\text{MeCN})_2$	6
1.2.4	Synthesis and characterization of $1\cdot\text{MeCN}$	6
1.2.5	Synthesis and characterization of $[\text{K}\cdot(18\text{-c-6})][1\text{-F}]$	8
1.2.6	Synthesis and characterization of $[\text{Et}_3\text{Si}\cdot\text{MeCN}][1\text{-F}]$	8
2	NMR experiments with $1\cdot\text{MeCN}$	9
2.1	Lewis acidity determination by <i>Gutmann-Beckett</i> method.....	9
2.2	Halide Abstraction Experiments.....	12
2.2.1	Reaction with Ph_3CCl	12
2.2.2	Reaction with AgSbF_6	15
2.3	Catalytic experiments.....	19
2.3.1	Hydrodefluorination of 1-fluoroadamantane.....	19
2.3.2	Hydrosilylation of <i>o</i> - and <i>p</i> -nitrobenzaldehyde.....	20
2.3.3	Reductive ether formation of benzaldehydes.....	23
2.3.4	Dihydrodeoxygenation of ketones.....	25
3	Computational Details.....	28
4	SC-XRD Analysis.....	31
4.1	Crystal Structure of $\text{Li}[1\text{-H}]\cdot(\text{MeCN})_2$	31
4.2	Crystal Structure of $[1\text{-Cl}]^-$	32
4.3	Crystal Structure of $1\cdot\text{MeCN}$	34
4.4	Crystal Structure of $[\text{K}\cdot(18\text{-c-6})][1\text{-F}]$	35
4.5	Crystal Structure of $[\text{Et}_3\text{Si}\cdot\text{MeCN}][1\text{-F}]$	37
5	NMR Spectra.....	39
5.1	NMR spectra of $\text{Li}_2\text{pin}^{\text{F}}$	39
5.2	NMR spectra of $\text{Li}[1\text{-H}]\cdot(\text{MeCN})_2$	40
5.3	NMR spectra of $\text{Li}[1\text{-Cl}]\cdot(\text{MeCN})_2$	42
5.4	NMR spectra of $1\cdot\text{MeCN}$	44

5.5	NMR spectra of [K·18-c-6][1-F]	46
5.6	NMR spectra of [Et ₃ Si·MeCN][1-F]	48
6	References	50

1 Experimental Section

1.1 General methods and Instrumentation

Materials

All presented reactions were carried out in heat dried borosilicate reaction vessels, filled with argon 4.6 ($\geq 99.996\%$; *Westfalen AG*) or in glovebox systems (*LABstar*) from *MBraun Inertgas-Systeme GmbH* with H_2O and O_2 levels not exceeding 0.5 ppm. In case of closed vessels, a small overpressure of argon atmosphere was used to prevent the intrusion of air. As a sealant PTFE/PEPE grease (*Triboflon III*) from *Freudenberg & Co. KG* was used. All heat-sensitive materials such as plastic syringes or cannulas were stored originally packed and flushed three times with argon directly prior to use.

Chemicals

Chemicals for the synthesis reactions were purchased from the commercial distributors: *Merck KGaA* (*Sigma-Aldrich*), *ABCR GmbH* and *TCl Co. Ltd.* The used hexafluoropinacol (H_2pin^F) was purchased from *Sigma-Aldrich* and *ABCR GmbH* and dried with molecular sieves (4 Å) in diluted Et_2O solution. After filtration and solvent removal in fine vacuo a mixture of 80 – 88 w% H_2pin^F in Et_2O was obtained. Liquid reactants for catalytic experiments were degassed and stored over molecular sieves. Solid reactants were dried in fine vacuo. The used solvents for applications on highly water and air sensitive reactions were distilled over elemental sodium/benzophenone (toluene, *n*-hexane, Et_2O), calcium hydride (acetonitrile, chloroform, acetonitrile- d_3 , chloroform- d and dichloromethane- d_2), additionally degassed and stored over molecular sieves. Solvents for other applications were purchased from the material administration of the chemistry faculty and purified by distillation.

NMR-spectroscopy

All NMR samples were prepared in an argon atmosphere using *J-Young* PTFE valve NMR tubes. All ^1H , ^{13}C , ^{19}F and ^{29}Si NMR spectra were recorded on a *Bruker Avance Neo* 400 MHz spectrometer a *Bruker AV500C* spectrometer at ambient temperatures (300 K). The obtained ^1H - and ^{13}C -NMR spectra were calibrated on the residual proton and natural abundance carbon signals of deuterated NMR solvents acetonitrile- d_3 , chloroform- d , and dichloromethane- d_2 . The obtained chemical shifts δ are reported in ppm values, relative to tetramethylsilane. The observed signals were abbreviated as following: s = singlet, br = broad signal and combinations, d = doublet, m = multiplet and qm = quartet of multiplets. The spectra were processed and analyzed using *MestReNova* software version 12.0.1-20560. Some NMR spectra include resonances of silicone grease (C_6D_6 : $\delta(^1\text{H}) = 0.29$ ppm, $\delta(^{13}\text{C}) = 1.4$ ppm and $\delta(^{29}\text{Si}) = -21.8$ ppm) from *B. Braun Melsungen AG Sterican®* cannulas.

IR spectra

Infrared (IR) spectra were recorded on a *Perkin Elmer FT-IR* spectrometer (*diamond ATR, Spectrum Two*) in the range of 400–4000 cm^{-1} at room temperature under an argon atmosphere. IR intensity bands are abbreviated as following: s = strong, m = medium, w = weak.

Elemental analysis

Compounds were analyzed by the central analytics laboratory of the *TUM Catalysis Research Center*. 0.5 – 1.0 mg of the investigated compounds were closely packed within two layers of tin foil under an argon atmosphere and subsequently handed to the elemental analysis team. The EA was carried out using a *EURO EA (HEKAtech)* instrument equipped with a CHNS combustion analyzer.

Melting Point

Melting Points (m.p.) were determined in sealed glass capillaries under inert gas using a *Büchi M-565* melting point apparatus.

Single crystal X-ray diffraction analysis

The X-ray intensity data were collected on an X-ray single crystal diffractometer equipped with a CMOS detector (*Bruker Photon-100*), a rotating anode (*Bruker TXS*) with $\text{MoK}\alpha$ radiation ($\lambda = 0.71073$ Å) and a Helios mirror optic by using the *APEX III* software package^[1] or an X-ray single crystal diffractometer equipped with a CMOS detector (*Bruker Photon-100*), an IMS microsource with $\text{MoK}\alpha$ radiation ($\lambda = 0.71073$ Å) and a Helios mirror optic by using the *APEX III* software package^[1] The measurement was performed on single crystals coated with perfluorinated ether. The crystal was fixed on the top of a

microsampler, transferred to the diffractometer and measured under a stream of cold nitrogen. A matrix scan was used to determine the initial lattice parameters. Reflections were merged and corrected for Lorenz and polarization effects, scan speed, and background using SAINT.^[2] Absorption corrections, including odd and even ordered spherical harmonics were performed using SADABS.^[2] Space group assignments were based upon systematic absences, E statistics, and successful refinement of the structures. Structures were solved by direct methods with the aid of successive difference Fourier maps, and were refined against all data using the APEX III software^[1] in conjunction with SHELXL-2014^[3] and SHELXLE.^[4] Methyl hydrogen atoms were refined as part of rigid rotating groups, with a C–H distance of 0.98 Å and $U_{iso}(H) = 1.5 \cdot U_{eq}(C)$. Other H atoms were placed in calculated positions and refined using a riding model, with methylene and aromatic C–H distances of 0.99 and 0.95 Å, respectively, and $U_{iso}(H) = 1.2 \cdot U_{eq}(C)$. If not mentioned otherwise, non-hydrogen atoms were refined with anisotropic displacement parameters. Full-matrix least-squares refinements were carried out by minimizing $\Delta w(F_o^2 - F_c^2)^2$ with SHELXL-97^[5] weighting scheme. Neutral atom scattering factors for all atoms and anomalous dispersion corrections for the non-hydrogen atoms were taken from International Tables for Crystallography.^[6] Images of the crystal structures were generated by PLATON and MERCURY.^[7] The CCDC numbers CCDC- (2102990 - 2102994) contain the supplementary crystallographic data for the structures 1MeCN, [1-Cl], Li[1-H](MeCN)2, [K(18c6)][1-F] and [Et3SiMeCN][1-F]. These data can be obtained free of charge from the Cambridge Crystallographic Data Centre via <https://www.ccdc.cam.ac.uk/structures/>.

Computational Details

All geometry optimizations and single point energies were calculated using the Orca 4.2.1 program package.^[8] As starting geometries, VSEPR structures preoptimized with UFF were used. Geometry optimizations for all compounds were performed with the PBE0 functional,^[9] utilizing *Grimme's* semi-empirical dispersion correction^[10] (D3), the *Becke-Johnson* damping function^[11] (BJ), and the def2-TZVPP basis set,^[12] using *grid5* settings. All calculated geometries have been confirmed as energetic minima on the potential energy surface by analytical calculation of harmonic frequencies at the level of optimization, revealing only positive Hessian eigenvalues. Enthalpies at 298.15 K have been calculated by using the rigid-rotor harmonic oscillator (RRHO) approximation,^[13] as implemented in ORCA.

For the final anion affinities, single point energies were calculated at the DLPNO-CCSD(T)/aug-cc-pVQZ level of theory.^[14] Using the protocol proposed by *Krossing*,^[15] anion affinities were determined by an isodesmic reaction scheme using CCSD(T)/CBS anchor points,^[16] thus by subtraction of the anchor enthalpies for the reaction $\text{Me}_3\text{Si}^+ + \text{X}^- \rightarrow \text{Me}_3\text{SiX}$ from the column [(B) – (A)] in Table S5.

Final single point energies for the structures were obtained with double-hybrid DSD-BLYP,^[17] including *Grimme's* semi-empirical dispersion correction^[10] with *Becke-Johnson* damping function^[11] (D3(BJ)) and the def2-QZVPP^[12] basis set.

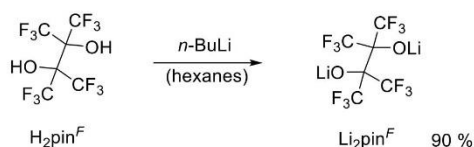
In all computations, the resolution-of-identity^[18] and “chain of spheres”^[19] approximation in the form of RIJCOSX was used in combination with matching auxiliary basis sets.^[20]

Solvation free energies were obtained by COSMO-RS in dichloromethane or acetonitrile as implemented in ADF^[21] based on BP86/TZP^[22] single point energy calculations for the electrostatic solute-solvent interaction on the PBE0/def2-TZVPP gas-phase structures.^[23] COSMO-RS correction for enthalpies was achieved by calculating ΔG -corrections at five different temperatures (278.15, 288.15, 298.15, 308.15, 318.15 K). Satisfying $\Delta G = \Delta H - T\Delta S$, the plot of the obtained Gibbs free energy corrections against the temperature allows to fit a straight line from which the corrections for ΔH were extracted.

Calculation of ²⁹Si NMR resonances (Table S8) was conducted with the PBE0 functional,^[9] utilizing *Grimme's* semi-empirical dispersion correction^[10] (D3), the *Becke-Johnson* damping function^[11] (BJ), and the def2-TZVPP basis set, as this combination was shown to be a reliable method in a recent benchmark.^[24] Additionally, the auxiliary basis set def2/JK and *grid4* settings were applied.^[25] Solvation effects were considered implicitly, using the *Universal Solvent Model* (SMD),^[26] as implemented in the Orca program package. Resonances were referenced against tetramethylsilane, for which optimization and chemical shielding were calculated in the same manner.

1.2 Synthesis and Characterization

1.2.1 Synthesis and characterization of Li_2pin^F



To a solution of 2.4 g H_2pin^F (80 w%, 7.18 mmol, 1.0 eq.) in 50 ml hexane were dropwise added 5.75 ml (14.37 mmol, 2.0 eq.) of a 2.5 M *n*-BuLi solution in hexane at room temperature over the course of 10 min. The resulting gelatinous reaction mixture was heated to 70 °C and stirred for 30 min. Afterwards all volatile components were removed in fine vacuo and the obtained solid was washed twice with 5 ml of toluene. After removal of the residual solvent in vacuo Li_2pin^F was obtained as a colorless powdery solid in quantitative yield.

Note: Attention! H_2pin^F is extremely toxic.

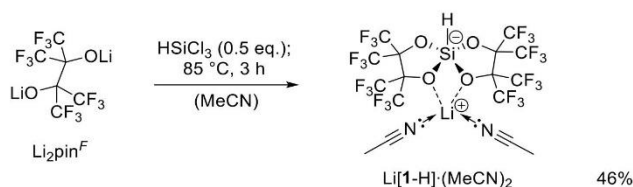
m.p.: 225 °C (decomposition).

^{13}C NMR (126 MHz, acetonitrile- d_3) δ (ppm) = 125.9 (q, $^1J_{\text{C-F}}$ = 296 Hz, CF_3), 88.6 (br, $\text{OC}(\text{CF}_3)_2$)

^{19}F NMR (149 MHz, acetonitrile- d_3) δ (ppm) = -72.5 (s, CF_3).

Elemental Analysis calcd. [%] for $\text{C}_6\text{F}_{12}\text{Li}_2\text{O}_2$: C (20.83), H (-), N (-), S (-); found (%): C (21.97), H (0.21), N (-), S (-). (Affected by little amounts of persistent residual solvents Et_2O and hexane.)

1.2.2 Synthesis and characterization of $\text{Li}[\text{1-H}]\cdot(\text{MeCN})_2$



To a solution of 500 mg (1.45 mmol, 2.0 eq.) Li_2pin^F in 12 ml MeCN were added 1.46 ml (0.73 mmol, 1.0 eq.) of a 0.49 M HSiCl_3 solution in MeCN (0.25 ml HSiCl_3 diluted in 4.75 ml MeCN) at room temperature. The obtained cloudy reaction mixture was heated to 85 °C and stirred for 3 h. A precipitation was formed, which was filtered-off. The filtrate was separated from the solvent in fine vacuo and the obtained sticky solid was crushed mechanically and residual solvent afterwards removed at 25 °C in fine vacuo. The obtained powder was then washed three times with 2 ml toluene and afterwards completely dried to give a colorless powdery solid in 46 % yield.

Crystals suitable for SC-XRD analysis were obtained from a saturated chloroform solution at -30 °C (Figure S18).

m.p.: 130 – 150 °C (decomposition).

^1H NMR (400 MHz, acetonitrile- d_3) δ (ppm) = 4.52 – 4.45 (m, $^1J_{\text{Si-H}}$ = 169 Hz, 1H, Si-H), 1.96 (s, 6H, NCC_2H_5).

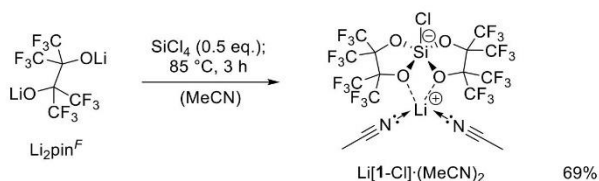
^{13}C NMR (126 MHz, acetonitrile- d_3) δ (ppm) = 122.9 (qm, $^1J_{\text{C-F}}$ = 291 Hz, CF_3), 83.4 (br, $\text{OC}(\text{CF}_3)_2$).

^{19}F NMR (149 MHz, acetonitrile- d_3) δ (ppm) = -69.86 – -70.17 (m, 12F, CF_3), -70.67 – -70.93 (m, 12F, CF_3).

^{29}Si NMR (80 MHz, acetonitrile- d_3) δ (ppm) = -90.19 (*Si*-H). (hydrogen decoupled spectrum)

Elemental Analysis calcd. [%] for $\text{C}_{16}\text{H}_7\text{F}_{24}\text{LiN}_2\text{O}_4\text{Si}$: C (24.57), H (0.90), N (3.58), S (-); found (%): C (23.98), H (0.90), N (3.55), S (-).

1.2.3 Synthesis and characterization of $\text{Li}[\text{1-Cl}](\text{MeCN})_2$



To a solution of 1.5 g (4.34 mmol, 2.0 eq.) $\text{Li}_2\text{pin}^{\text{F}}$ in 40 ml MeCN were added 4.98 ml (2.17 mmol, 1.0 eq.) of a 0.44 M SiCl_4 solution in MeCN (0.5 ml SiCl_4 diluted in 9.5 ml MeCN) at room temperature. The obtained slightly yellow and cloudy reaction mixture was heated to 85 °C and stirred for 3 h. The precipitation was filtered-off and the filtrate was treated in fine vacuo to give an off-white solid in 69 % yield.

Crystals suitable for SC-XRD analysis were obtained from a co-crystallization experiment with 1.0 eq. Et_3PO in dichloromethane (Figure S19).

m.p.: 110 °C (decomposition).

^1H -NMR (400 MHz, acetonitrile- d_3) δ (ppm) = 1.96 (s, 6H, NCCH_3).

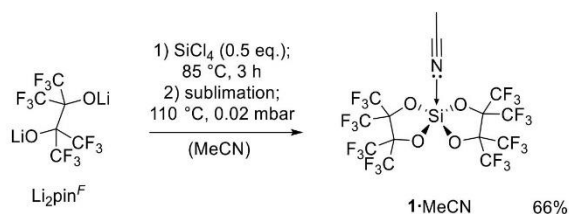
^{13}C NMR (126 MHz, acetonitrile- d_3) δ (ppm) = 122.6 (qm, $^1J_{\text{C-F}} = 291$ Hz, CF_3), 83.9 (br, $\text{OC}(\text{CF}_3)_2$).

^{19}F NMR (149 MHz, acetonitrile- d_3) δ (ppm) = -69.01 – -69.19 (m, 12F, CF_3), -69.94 – -70.18 (m, 12F, CF_3).

^{29}Si NMR (80 MHz, acetonitrile- d_3) δ (ppm) = -93.26 (*Si*-Cl).

Elemental Analysis calcd. [%] for $\text{C}_{16}\text{H}_6\text{ClF}_{24}\text{LiN}_2\text{O}_4\text{Si}$: C (23.53), H (0.74), N (3.43), S (-); found (%): C (23.70), H (0.66), N (3.43), S (-).

1.2.4 Synthesis and characterization of $\text{1}\cdot\text{MeCN}$



To a solution of 1.5 g (4.34 mmol, 2.0 eq.) Li_2pin^F in 40 ml MeCN were added 4.98 ml (2.17 mmol, 1.0 eq.) of a 0.44 M SiCl_4 solution in MeCN (0.5 ml SiCl_4 diluted in 9.5 ml MeCN) at room temperature. The obtained slightly yellow and cloudy reaction mixture was heated to 85 °C and stirred for 3 h. Afterwards, the cloudy suspension was reduced to dryness under fine vacuo and the obtained off-white solid was crushed mechanically to obtain a powder (mixture of $\text{Li}[\mathbf{1}\text{-Cl}](\text{MeCN})_2$ and LiCl). This mixture was then sublimated under a 0.02 mbar argon atmosphere (fine vacuo) at 110 °C to give a colorless solid in 66 % yield.

Crystals suitable for SC-XRD analysis were obtained from a saturated toluene solution at room temperature. For crystal structure please see Figure S20.

Note: $\mathbf{1}\cdot\text{MeCN}$ is also obtained by sublimation of purified $\text{Li}[\mathbf{1}\text{-Cl}](\text{MeCN})_2$, however, lower yields were obtained.

m.p.: 113 °C (decomposition).

$^1\text{H-NMR}$ (400 MHz, acetonitrile- d_3) δ (ppm) = 1.96 (s, 6H, NCCCH_3).

$^{13}\text{C NMR}$ (126 MHz, acetonitrile- d_3) δ (ppm) = 122.1 (qm, $^1J_{\text{C-F}} = 291$ Hz, CF_3), 83.3 (br, $\text{OC}(\text{CF}_3)_2$).

$^{19}\text{F NMR}$ (149 MHz, acetonitrile- d_3) δ (ppm) = -69.50 – -70.10 (m, 12F, CF_3), -70.10 – -70.60 (m, 12F, CF_3).

$^{29}\text{Si NMR}$ (80 MHz, acetonitrile- d_3) δ (ppm) = -110.34 (Si).

Elemental Analysis calcd. [%] for $\text{C}_{14}\text{H}_3\text{F}_{24}\text{NO}_4\text{Si}$: C (22.93), H (0.41), N (1.91), S (-); found (%): C (23.36), H (0.36), N (1.96), S (-).

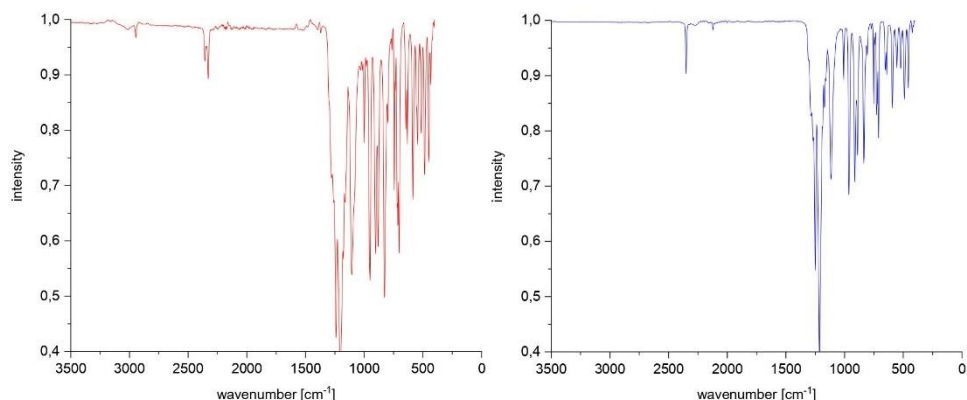
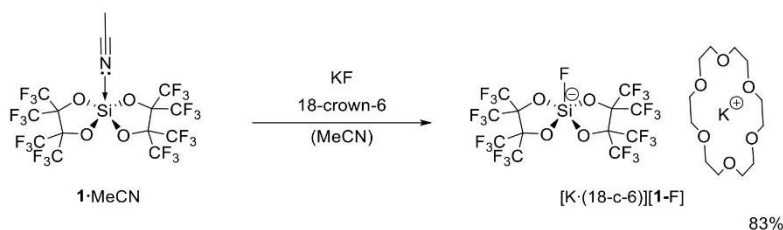


Figure S 1: Left: IR-spectrum of $\mathbf{1}\cdot\text{CH}_3\text{CN}$ showing two superimposed frequencies of blue-shifted $\text{C}\equiv\text{N}$ and C-H vibrations originating from the coordinated acetonitrile. Right: IR-spectrum of deuterated $\mathbf{1}\cdot\text{CD}_3\text{CN}$ showing only one strongly blue-shifted frequency at 2352 cm^{-1} that can be assigned to the $\text{C}\equiv\text{N}$ stretching vibration of the coordinating solvent (free $\text{MeCN-}d_3$: 2258 cm^{-1}).

1.2.5 Synthesis and characterization of $[\text{K} \cdot (18\text{-c-}6)][1\text{-F}]$ 

For the synthesis of the pentavalent fluorosilicate $[1\text{-F}]^-$ species, 100 mg **1**·MeCN (136 μmol , 1.0 eq.), 7.90 mg KF (136 μmol , 1.0 eq.) and 36.1 mg 18-crown-6 (136 μmol , 1.0 eq.) were dissolved in 2.0 ml acetonitrile and stirred for 2 h at room temperature. Afterwards, all volatile components were removed in fine vacuo to give a colorless crystalline solid in 83 % yield.

Crystals suitable for SC-XRD analysis were obtained from a saturated dichloromethane solution at $-30\text{ }^\circ\text{C}$. For crystal structure please see Figure S21.

m.p.: 150 – 217 $^\circ\text{C}$ (decomposition).

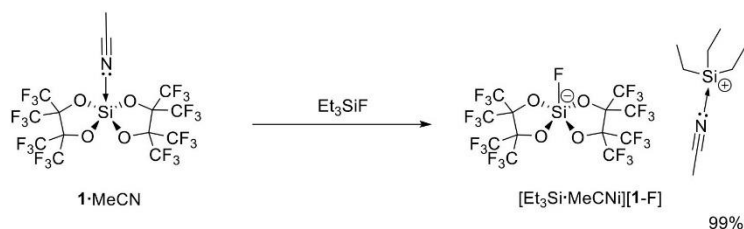
^1H NMR (400 MHz, acetonitrile- d_3) δ (ppm) = 3.57 (s, 24H, O- CH_2 - CH_2 -O).

^{13}C NMR (126 MHz, acetonitrile- d_3) δ (ppm) = 122.7 (qm, $^1J_{\text{C-F}} = 291$ Hz, CF_3), 70.8 (s, 12C, OCH₂), 83.4 (br, OC(CF₃)₂).

^{19}F NMR (149 MHz, acetonitrile- d_3) δ (ppm) = -69.75 – -70.10 (m, 12F, CF_3), -70.81 – -71.11 (m, 12F, CF_3), -138.75 (h, $J = 8.7$ Hz, 1F, Si-F).

^{29}Si NMR (99 MHz, acetonitrile- d_3) δ (ppm) = -108.37 (d, $J_{\text{Si-F}} = 179.8$ Hz; Si-F).

Elemental Analysis calcd. [%] for $\text{C}_{24}\text{H}_{24}\text{F}_{25}\text{KO}_{10}\text{Si}$: C (28.41), H (2.38), N (-), S (-); found (%): C (28.69), H (2.32), N (-), S (-).

1.2.6 Synthesis and characterization of $[\text{Et}_3\text{Si} \cdot \text{MeCN}][1\text{-F}]$ 

To 50 mg **1**·MeCN (68.2 μmol , 1.0 eq.) were added 46 mg Et_3SiF (341 μmol , 5.0 eq.) at room temperature. The gelatinous reaction mixture was stirred for 10 min at room temperature and afterwards stripped from all volatiles in fine vacuo. A colorless solid was obtained in quantitative yield.

Crystals suitable for SC-XRD analysis were obtained from a saturated dichloromethane solution at $-30\text{ }^\circ\text{C}$. For crystal structure please see Figure S22.

m.p.: 121 $^\circ\text{C}$ (decomposition).

^1H -NMR (400 MHz, acetonitrile- d_3) δ (ppm) = 1.96 (s, 3H, NCCCH_3), 1.08 (m, 9H, CH_3), 1.03 (m, 6H, CH_2).

^{13}C NMR (126 MHz, acetonitrile- d_3) δ (ppm) = 122.6 (qm, $^1J_{\text{C-F}} = 291$ Hz, CF_3), 83.2 (br, OC(CF₃)₂), 6.11 (s, 3C, CH_2), 4.11 (s, 3C, CH_3).

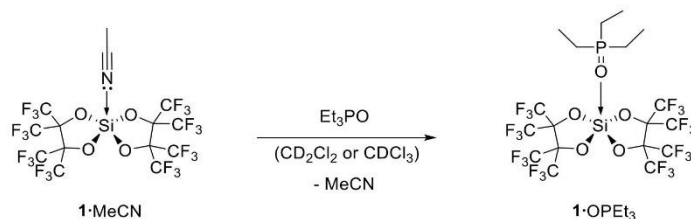
^{19}F -NMR (149 MHz, acetonitrile- d_3) δ (ppm) = -69.90 – -70.08 (m, 12F, CF_3), -70.82 – -71.14 (m, 12F, CF_3), -138.61 – -138.86 (m, 1F, Si-F).

^{29}Si NMR (99 MHz, acetonitrile- d_3) δ (ppm) = 36.63 (s, Et_3Si^+), -108.37 (d, $^1J_{\text{Si-F}} = 179.8$ Hz, Si-F).

Elemental Analysis calcd. [%] for $\text{C}_{18}\text{H}_{15}\text{F}_{25}\text{O}_4\text{Si}_2$: C (27.69), H (2.09), N (1.61), S (-); found (%): C (27.47), H (1.69), N (1.53), S (-).

2 NMR experiments with 1·MeCN

2.1 Lewis acidity determination by Gutmann-Beckett method



To examine the Lewis acidity of the obtained silane, 11.0 mg **1·MeCN** (14.9 μmol , 1.0 eq.) were dissolved in 0.4 ml dichloromethane- d_2 and reacted with 2.0 mg Et_3PO (14.9 μmol , 1.0 eq.) in a PTFE-sealed J-Young NMR tube. A clear solution was obtained which was analyzed by ^1H , ^{19}F and ^{31}P NMR spectroscopy.

^1H NMR (400 MHz, CD_2Cl_2) δ (ppm) = 2.11 (dq, $^2J_{\text{P-H}}$, $^3J_{\text{H-H}} = 12.2, 7.7$ Hz, 6H), 1.27 (dt, $^3J_{\text{P-H}}$, $^3J_{\text{H-H}} = 19.4, 7.7$ Hz, 9H).

^{13}C NMR (126 MHz, CD_2Cl_2) δ (ppm) = 17.37 (d, $^1J_{\text{P-C}} = 64.0$ Hz, PCH_2), 5.13 (d, $^3J_{\text{P-C}} = 4.7$ Hz, PCH_2CH_3).

^{19}F -NMR (149 MHz, CD_2Cl_2) δ (ppm) = -69.23 – -69.44 (m, 12F, CF_3), -69.67 – -69.87 (m, 12F, CF_3).

^{31}P NMR (162 MHz, CD_2Cl_2) δ (ppm) = 86.21 (s).

^{29}Si NMR (99 MHz, CD_2Cl_2) δ (ppm) = -110.86 (s).

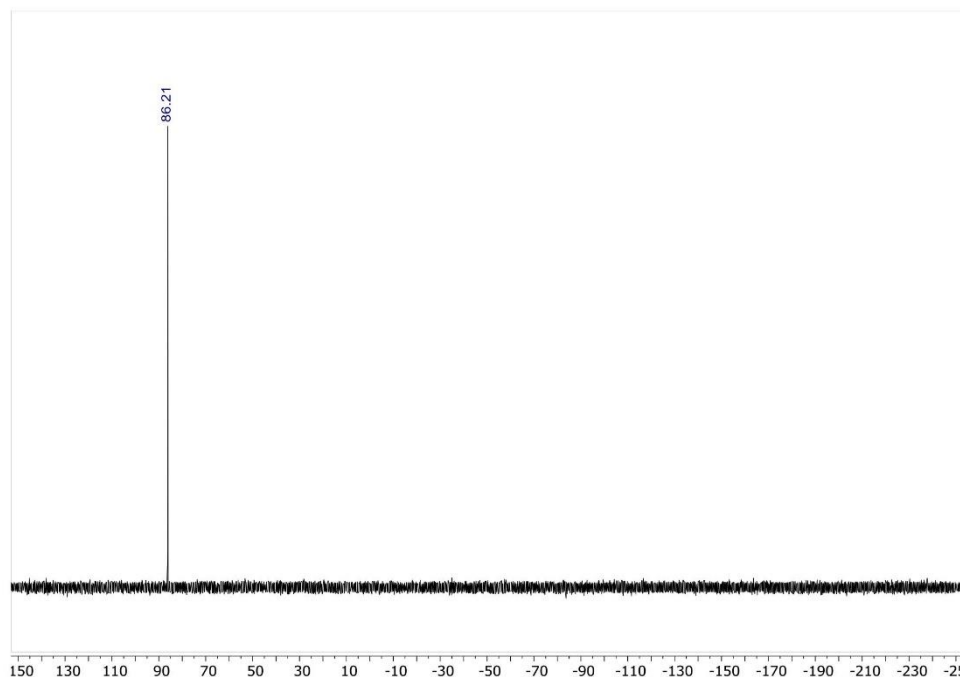


Figure S 2: ^{31}P NMR spectrum of 1-OPEt_3 obtained by the reaction of 1-MeCN with Et_3PO in dichloromethane- d_2 .

To further analyze the adduct formation 11.0 mg 1-MeCN (14.9 μmol , 1.0 eq.) were reacted with 0.5, 1.0, 2.0 and 3.0 eq. of Et_3PO in chloroform- d solution. To ensure complete solution, the NMR samples were heated to 60 $^\circ\text{C}$ for 1 h. Afterwards ^{31}P NMR spectra were recorded, showing the favored formation of the mono-adduct. No bis-adduct formation was observed.

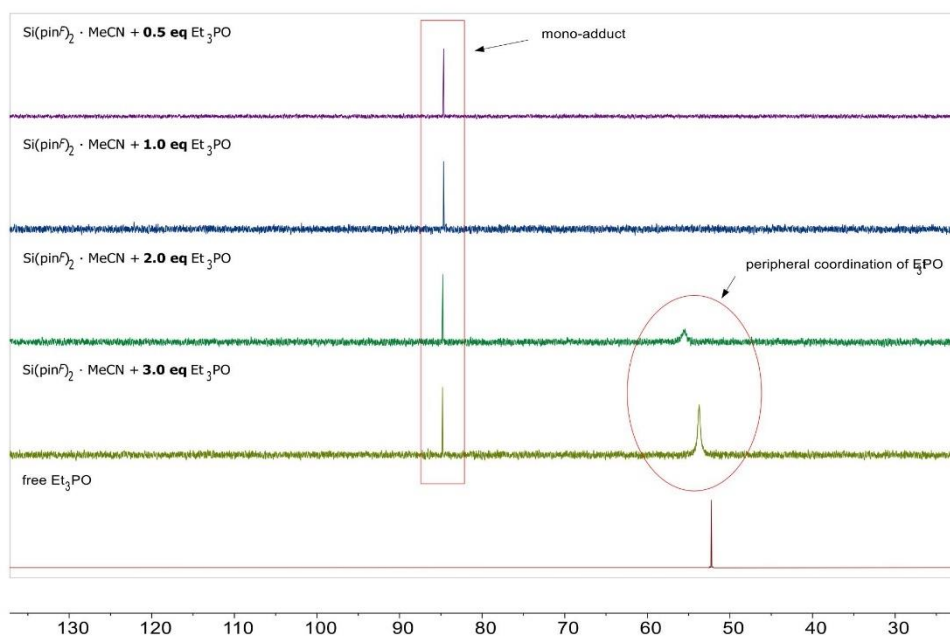
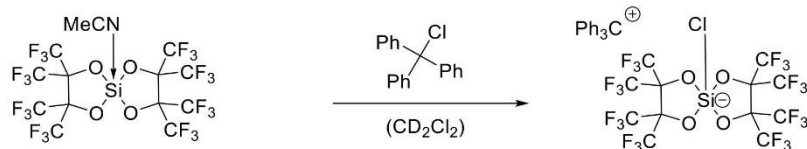


Figure S 3: Stacked ^{31}P NMR spectra of the reaction of $1\cdot\text{MeCN}$ with 0.5, 1.0, 2.0 and 3.0 eq. of Et_3PO in chloroform- d at 300 K. Even when surplus amounts of the phosphine oxide were used, no formation of the bis-adduct was observed.

2.2 Halide Abstraction Experiments

2.2.1 Reaction with Ph₃CCl



A mixture of 10.0 mg **1**·MeCN (13.6 μmol, 1.0 eq.) and 3.80 mg triphenylmethyl chloride (13.6 μmol, 1.0 eq.) was dissolved in 0.4 ml dichloromethane-*d*₂ and transferred into a PTFE-sealed J-Young NMR tube. The reaction mixture was analyzed by ¹H, ¹³C, ¹⁹F and ²⁹Si NMR spectroscopy after 24 h at room temperature showing quantitative consumption of the Lewis acid **1**·MeCN.

Note: Whereas the ¹⁹F and ²⁹Si NMR show complete consumption of **1**·MeCN and the predominant formation of the pentavalent chlorosilicate species Ph₃C[**1**-Cl], the ¹H NMR spectrum still showed partly unreacted trityl chloride. This might be caused by a side reaction consuming **1**·MeCN. In the ¹⁹F NMR spectrum a minor amount of an unidentified side product was found, giving a singlet at δ = -69.8 ppm. Nevertheless, Ph₃C[**1**-Cl] is the main reaction product and no equilibrium adjustment between **1**·MeCN and Ph₃C[**1**-Cl] was observed in the ¹⁹F NMR spectrum.

¹H NMR (400 MHz, CD₂Cl₂) δ (ppm) = 8.29 (t, ³J_{H-H} = 7.5 Hz, 3H, *p*-CH), 7.90 (t, ³J_{H-H} = 7.5 Hz, 6H, *o*-CH), 7.70 – 7.65 (m, , 6H, *m*-CH).

¹³C NMR (126 MHz, CD₂Cl₂) δ (ppm) = 211.3 (s, Et₃C), 144.1 (s, Ar-C), 143.1 (s, Ar-C), 140.3 (s, Ar-C), 131.1 (s),m 121.7 (qm, ¹J_{C-F} = 291 Hz, CF₃), 82.9 (br, OC(CF₃)₂).

¹⁹F-NMR (149 MHz, CD₂Cl₂) δ (ppm) = -68.60 – -68.86 (m, 12F, CF₃), -69.63 – -69.81 (m, 12F, CF₃).

²⁹Si NMR (99 MHz, CD₂Cl₂) δ (ppm) = -93.28 (s).

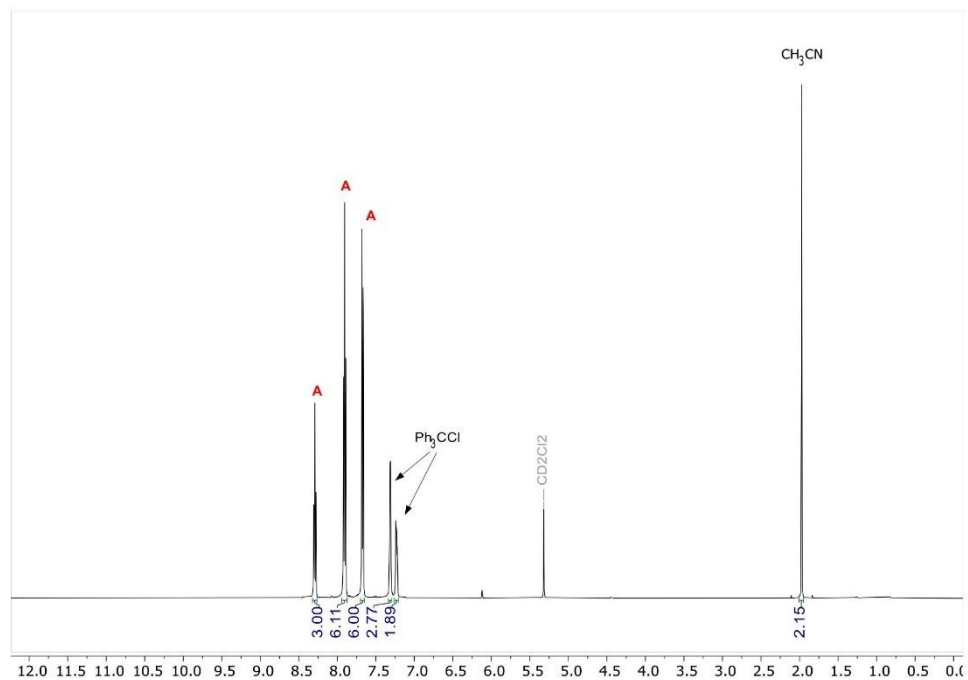


Figure S 4: ^1H NMR spectrum in CD_2Cl_2 of the reaction of Ph_3CCl and $\mathbf{1}\cdot\text{MeCN}$ after 24 h at r.t. showing the formation of the trityl cation (**A**) as the main reaction product.

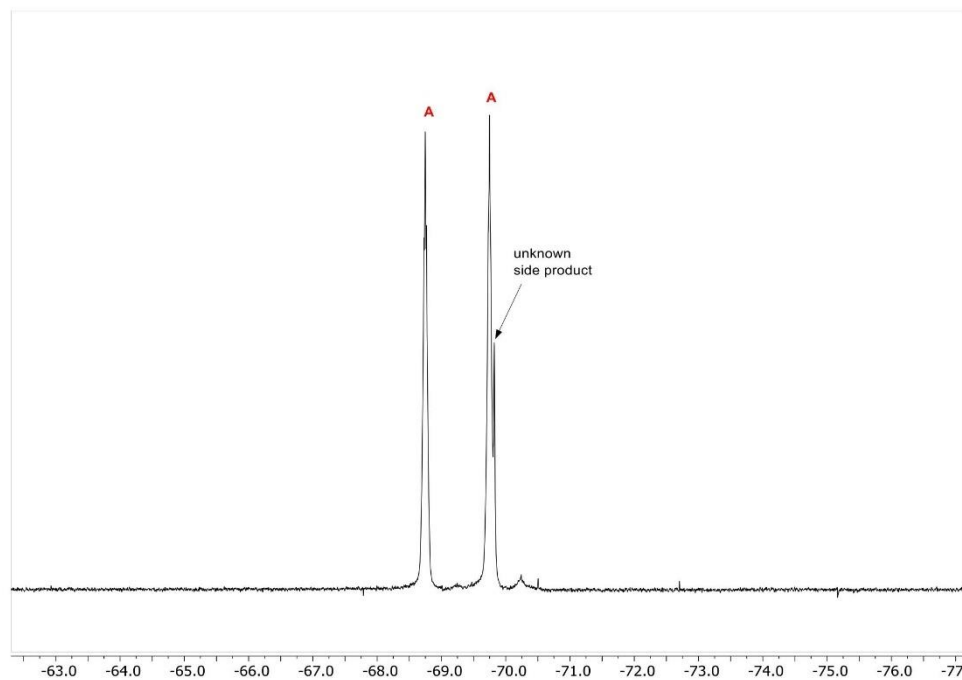


Figure S 5: ^{19}F NMR spectrum in CD_2Cl_2 of the reaction of Ph_3CCl and $\mathbf{1}\cdot\text{MeCN}$ after 24 h at r.t. showing nearly quantitative formation of the silicate anion $[\mathbf{1}\text{-Cl}]^-$ (**A**) as the main reaction product and an undefined side product.

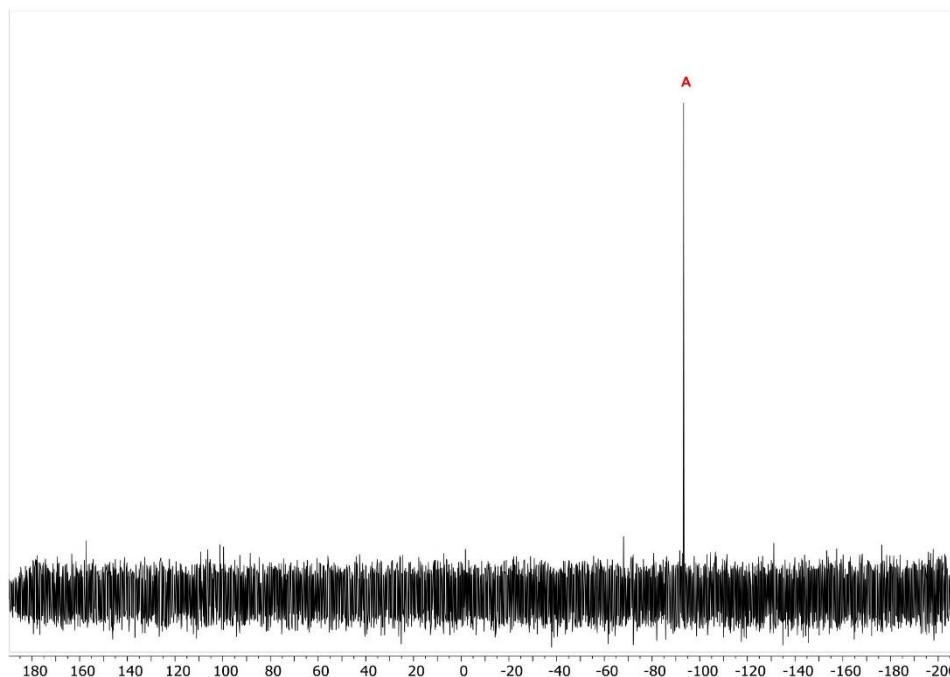
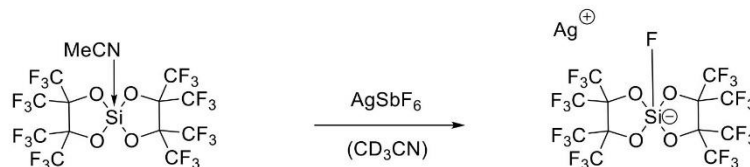


Figure S 6: ^{29}Si NMR spectrum in CD_2Cl_2 of the reaction of Ph_3CCl and $\mathbf{1}\cdot\text{MeCN}$ after 24 h at r.t. showing the quantitative formation of the silicate anion $[\mathbf{1}\text{-Cl}]^-$ (A).

2.2.2 Reaction with AgSbF_6



A mixture of 15.0 mg $\mathbf{1}\cdot\text{MeCN}$ (20.5 μmol , 1.0 eq.) and 7.0 mg AgSbF_6 (20.5 μmol , 1.0 eq.) was dissolved in 0.5 ml acetonitrile- d_3 and stirred for 10 minutes yielding a clear solution. The reaction mixture was transferred into PTFE-sealed J-Young NMR tube and analyzed by ^{13}C , ^{19}F and ^{29}Si NMR spectroscopy after 10 min and 24 h at room temperature showing quantitative fluoride abstraction by the Lewis acid $\mathbf{1}\cdot\text{MeCN}$.

^{13}C NMR (126 MHz, acetonitrile- d_3) δ (ppm) = 122.6 (qm, $^1J_{\text{C-F}} = 292$ Hz, CF_3), 83.3 (br, $\text{OC}(\text{CF}_3)_2$).

^{19}F -NMR (149 MHz, acetonitrile- d_3) δ (ppm) = -69.88 – -70.09 (m, 12F, CF_3), -70.84 – -71.04 (m, 12F, CF_3), -138.51 – -138.91 (m, 1F, Si-F).

^{29}Si NMR (99 MHz, CD_3CN) δ (ppm) = -108.37 (d, $^1J_{\text{Si-F}} = 179.8$ Hz).

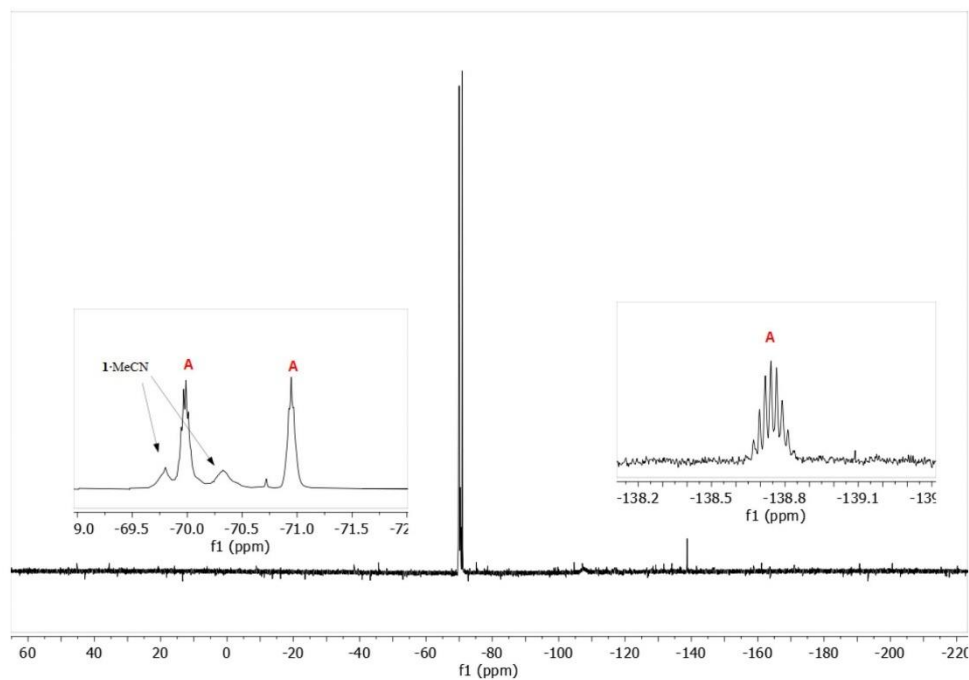


Figure S 7: ^{19}F NMR spectrum in CD_2Cl_2 of the reaction of AgSbF_6 and $\mathbf{1}\cdot\text{MeCN}$ after 10 min at r.t. showing the nearly quantitative formation of the silicate anion $[\mathbf{1}\text{-F}]^-$ (A).

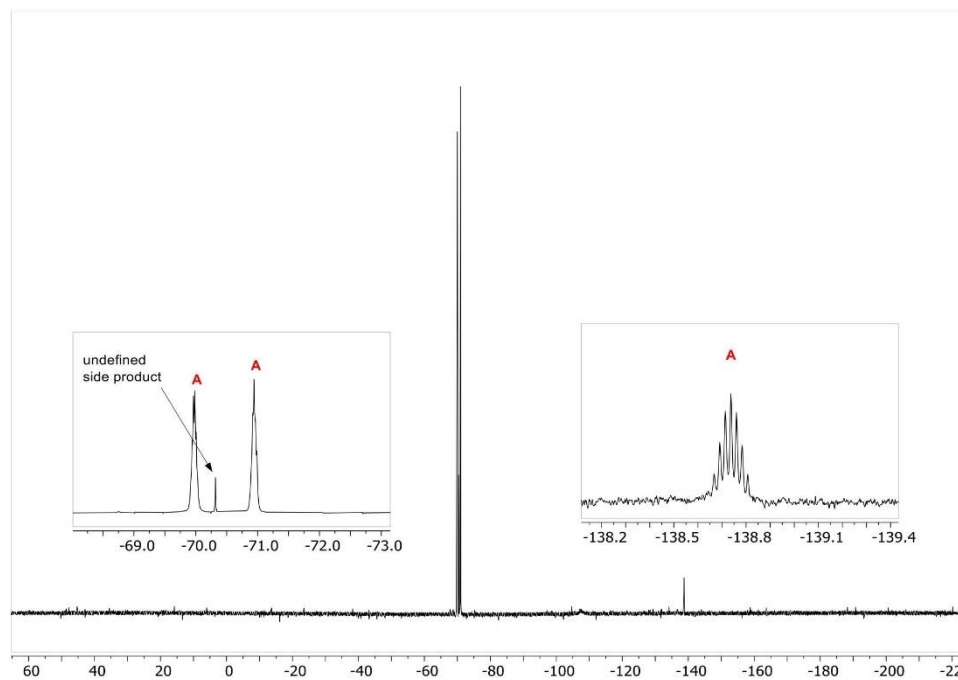


Figure S 8: ^{19}F NMR spectrum in CD_2Cl_2 of the reaction of AgSbF_6 and $1\cdot\text{MeCN}$ after 18 h at r.t. showing quantitative formation of the silicate anion $[\text{1-F}]^-$ (A) and trace amounts of an undefined side product.

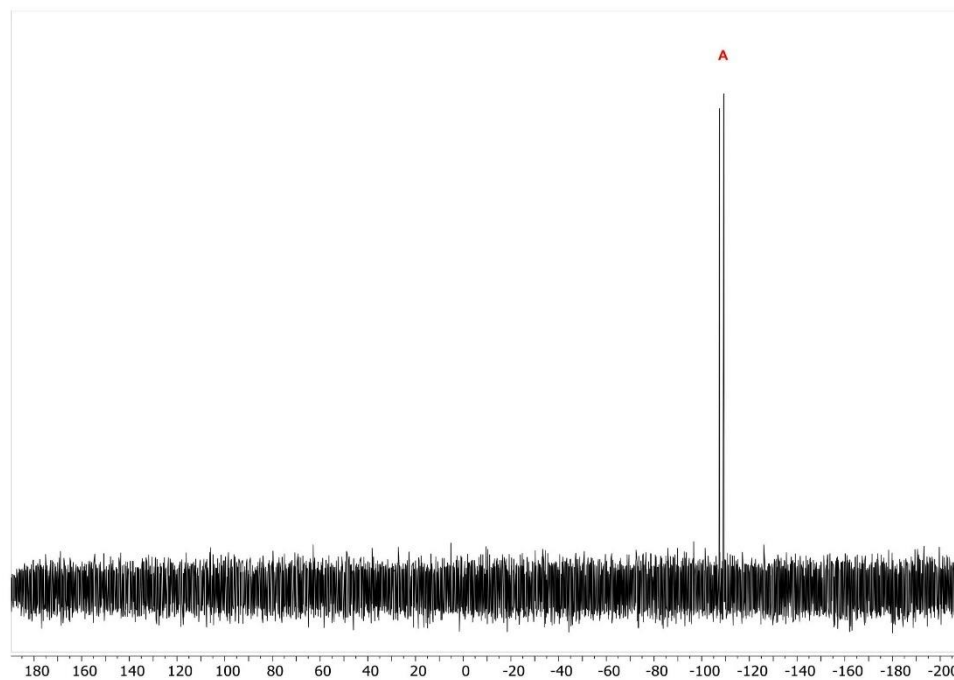
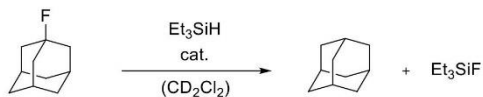


Figure S 9: ^{29}Si NMR spectrum in CD_2Cl_2 of the reaction of AgSbF_6 and $1\cdot\text{MeCN}$ after 18 h at r.t. showing quantitative formation of the silicate anion $[\mathbf{1}\text{-F}]^-$.

2.3 Catalytic experiments

2.3.1 Hydrodefluorination of 1-fluoroadamantane



To a solution of 21 mg 1-fluoroadamantane (138 μmol , 1.0 eq.) and 5 mg **1**·MeCN (6.89 μmol , 0.05 eq.) in 0.4 ml CD_2Cl_2 were added 22 μl Et_3SiH (138 μmol , 1.0 eq.) at room temperature. The reaction mixture was immediately transferred into a PTFE-sealed J-Young NMR tube and analyzed by ^1H and ^{19}F NMR spectroscopy after several periods. To monitor the reaction conversion, 10 μl mesitylene (71.9 μmol) were additionally added as an internal standard.

The experiment was also conducted using only 1 mol% of the catalyst (1.38 μmol , 0.01 eq.).

Adamantane: ^1H NMR (400 MHz, CD_2Cl_2 δ (ppm) = 1.88 (br, 3H, R_3CH), 1.79 (br, 12H, R_2CH_2).

Et_3SiF : ^1H NMR (400 MHz, CD_2Cl_2 δ (ppm) = 1.01 (t, 9H, CH_3), 0.76 – 0.64 (m, 6H, SiCH_2CH_3); ^{19}F NMR (377 MHz, CD_2Cl_2) δ (ppm) = -175.94.

Product identification corresponds with literature values for adamantane^[27] and separately synthesized Et_3SiF .

Table S 1: Reaction conditions and yield of hydrodefluorination experiments after several minutes.

Sample	Et_3SiH eq.	Cat. [mol%]	Temp. [$^\circ\text{C}$]	Time [min]	Yield [%]
A	1.0	1	25	10	61
A	1.0	1	25	30	94
A	1.0	1	25	120	99
B	1.0	5	25	10	99

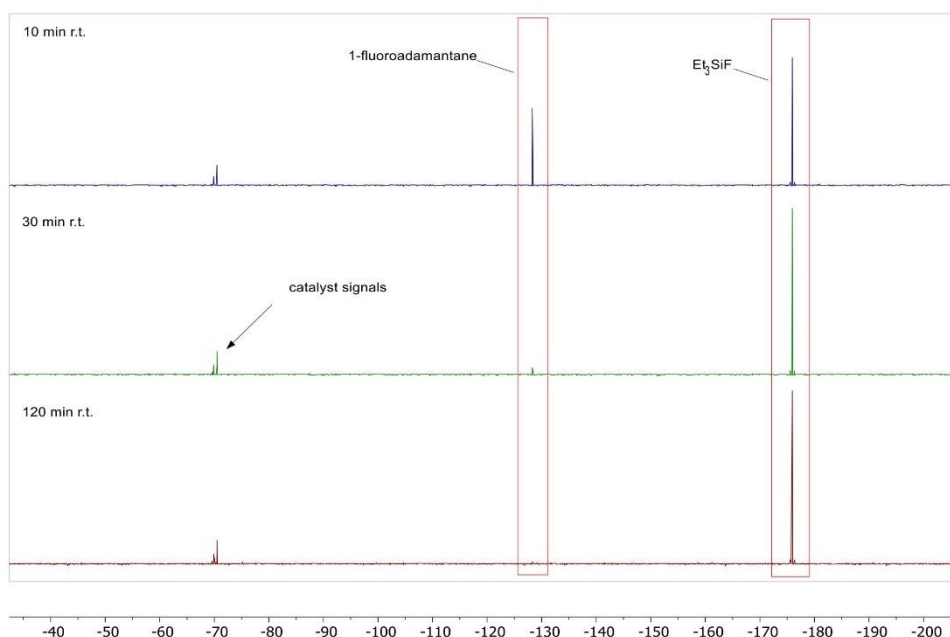
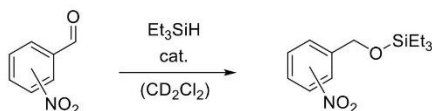


Figure S 10: Stacked ^{19}F NMR spectra in CD_2Cl_2 of sample A after several minutes at room temperature, showing the fast defluorination of 1-fluoroadamantane and the formation of Et_3SiF as the side-product. Complete conversion was observed within 2 hours.

2.3.2 Hydrosilylation of *o*- and *p*-nitrobenzaldehyde



To a solution of 20 mg *p*- or *o*-nitrobenzaldehyde (125 μmol , 1.0 eq.) and 5 mg **1**·MeCN (6.26 mmol, 0.05 eq.) in 0.4 ml dichloromethane- d_2 were added 20 μl Et_3SiH (125 μmol , 1.0 eq.). The obtained solution was immediately transferred into a PTFE-sealed J-Young NMR tube and analyzed by the means of ^1H NMR spectroscopy. For the determination of the reaction conversion 10 ml mesitylene (71.9 mmol) were additionally added as an internal standard.

Full conversion yielding the respective silyl-ethers were observed already after 20 minutes. Interestingly after 2 hours in both cases the beginning of a slow conversion of the silylethers into the di(nitrobenzyl)ethers and $(\text{Et}_3\text{Si})_2\text{O}$ ^[28] was observed. Also, a not further investigated conversion of the mesitylene appeared after longer periods. These reactions, however, were not completed within 24 h at room temperature.

p-Nitrobenzylox-triethylsilane: (R = H): ^1H -NMR (400 MHz, CD_2Cl_2 δ (ppm) = 8.19 (d, $^3J = 8.8$ Hz, 2H, *m*-Ar-H), 7.53 (d, $^3J = 8.4$ Hz, 2H, *m*-Ar-H), 4.85 (s, 2H, CH_2O), 1.01 (t, $^3J = 8.0$ Hz, 9H, Si- CH_2CH_3), 0.70 (q, $^3J = 8.0$ Hz, 6H, Si- CH_2).

o-Nitrobenzylox-triethylsilane: (R = *o*- $\text{C}_6\text{H}_4\text{CH}_3$): ^1H -NMR (400 MHz, CD_2Cl_2 δ (ppm) = 8.12 (d, $^3J = 9.6$ Hz, 1H, Ar-H), 8.00 (d, $^3J = 7.8$ Hz, 1H, Ar-H), 7.73 (t, $^3J = 7.6$ Hz, 1H, Ar-H), 7.49 (t, $^3J = 7.8$ Hz, 1H, Ar-H), 5.16 (s, 2H, CH_2O), 1.06 (t, $J = 7.9$ Hz, 9H, Si- CH_2CH_3), 0.76 (q, $J = 8.0$ Hz, 6H, Si- CH_2).

Observed signals of respective silylethers were consistent with literature values for *p*-nitrobenzylox-triethylsilane^[29] and *o*-nitrobenzylox-triethylsilane.^[30]

Table S 2: Reaction conditions and yield of hydrodefluorination experiments after several minutes.

Reactant	Et ₃ SiH eq.	Cat. [mol%]	Temp. [°C]	Time [min]	Yield [%]
<i>p</i> -nitrobenzaldehyde	1.0	5	25	20	99 ^[a]
<i>o</i> -nitrobenzaldehyde	1.0	5	25	20	99 ^[b]

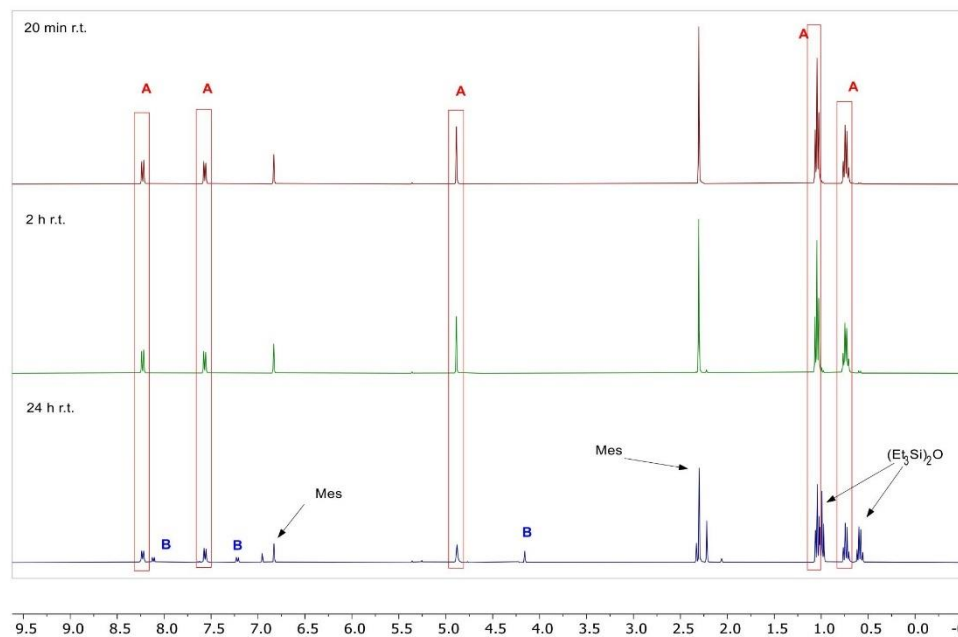


Figure S 11: Exemplary stacked ¹H NMR spectra in CD₂Cl₂ of the hydrosilylation experiment of *p*-nitrobenzaldehyde after several minutes at room temperature. Already after 20 min quantitative formation of the *p*-nitrobenzylox-triethylsilane (**A**) was observed. After 24 h further conversion was detected yielding di(*p*-nitrobenzyl)ether (**B**), (Et₃Si)₂O and slowly decomposing the mesitylene.

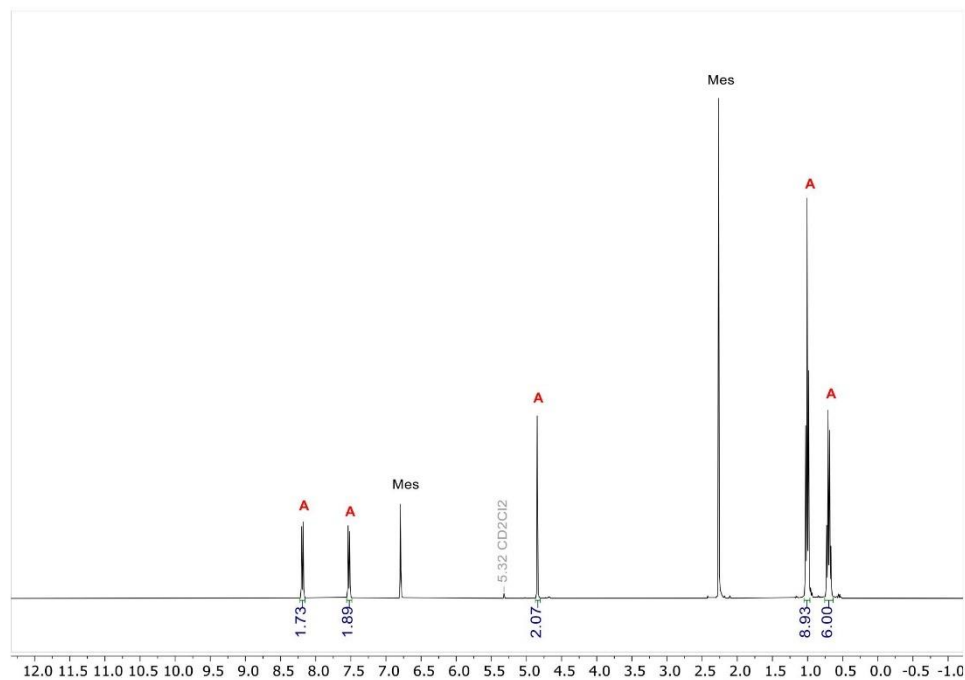


Figure S 12: ^1H NMR spectrum in CD_2Cl_2 of the reduction of *p*-nitrobenzaldehyde with Et_3SiH after 20 min at r.t. showing quantitative and selective formation of hydrosilylation product (A).

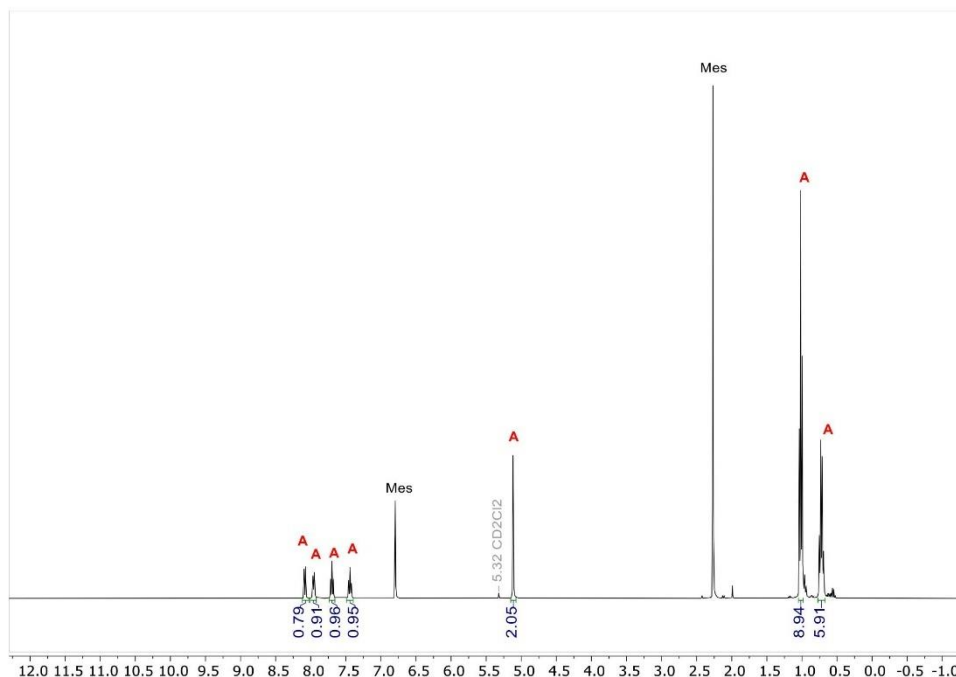
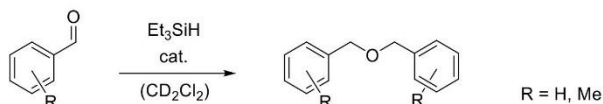


Figure S 13: ^1H NMR spectrum in CD_2Cl_2 of the reduction of *o*-nitrobenzaldehyde with Et_3SiH after 20 min at r.t. showing quantitative and selective formation of hydrosilylation product (**A**).

2.3.3 Reductive ether formation of benzaldehydes



To a solution of 13 μl benzaldehyde (125 μmol , 1.0 eq.) or 15 μl *o*-methylbenzaldehyde (130 μmol , 1.0 eq.) and 5 mg **1**·MeCN (6.26 mmol, 0.05 eq.) in 0.4 ml dichloromethane- d_2 were added 30 μl Et_3SiH (188 μmol , 1.5 eq.). The obtained solutions were immediately transferred into a PTFE-scaled J-Young NMR tube and analyzed by the means of ^1H NMR spectroscopy. For the determination of the reaction conversion 10 ml mesitylene (71.9 mmol) were additionally added as an internal standard.

Dibenzylether (R = H): ^1H -NMR (400 MHz, CD_2Cl_2 δ (ppm) = 7.43 – 7.28 (m, 4H, Ph-*H*), 4.58 (s, 2H, PhCH₂O).

Di(*o*-methylbenzyl)ether: (R = *o*-C₆H₅CH₃): ^1H -NMR (400 MHz, CD_2Cl_2 δ (ppm) = 7.43 – 7.33 (m, 1H, Ar-*H*), 7.25 – 7.16 (m, 3H, Ar-*H*), 4.59 (s, 2H, ArCH₂O), 2.35 (s, 3H, CH₃).

Product identification corresponds with literature values for dibenzylether^[31] and di(*o*-methylbenzyl)-ether.^[32]

Table S 3: Reaction conditions and yield of hydrodefluorination experiments after several minutes.

Reactant	Et_3SiH eq.	Cat. [mol%]	Temp. [°C]	Time [min]	Yield [%]
benzaldehyde	1.5	1	25	30	99 ^[a]

S23

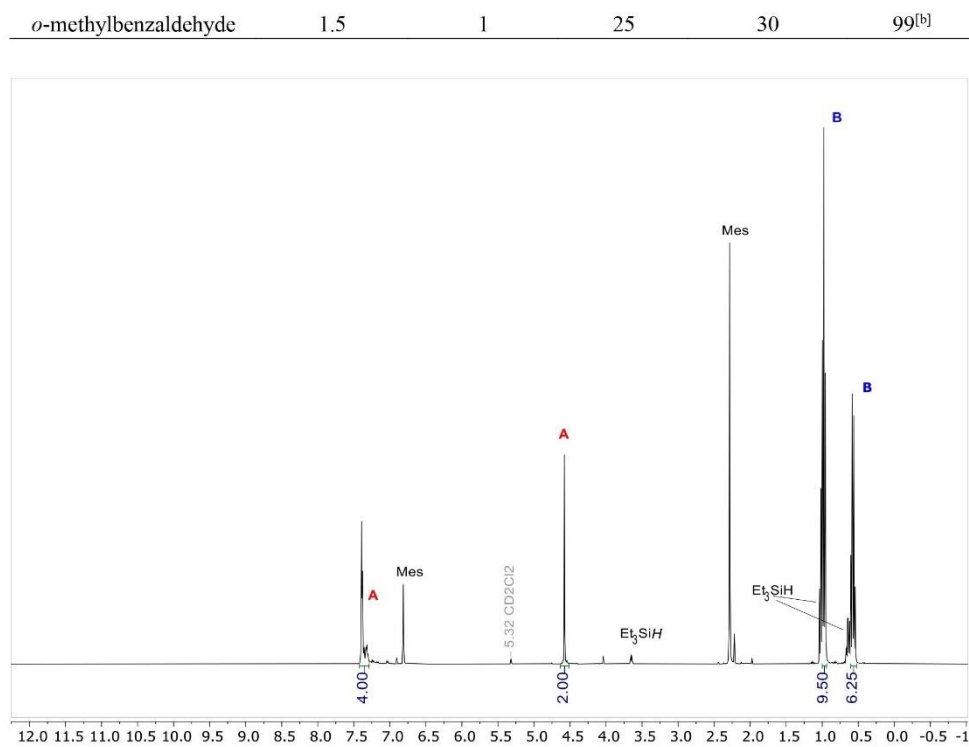


Figure S 14: ¹H NMR spectrum in CD₂Cl₂ of the reduction of benzaldehyde with Et₃SiH after 30 min at r.t. showing quantitative formation of dibenzylether (**A**) and (Et₃Si)₂O (**B**).

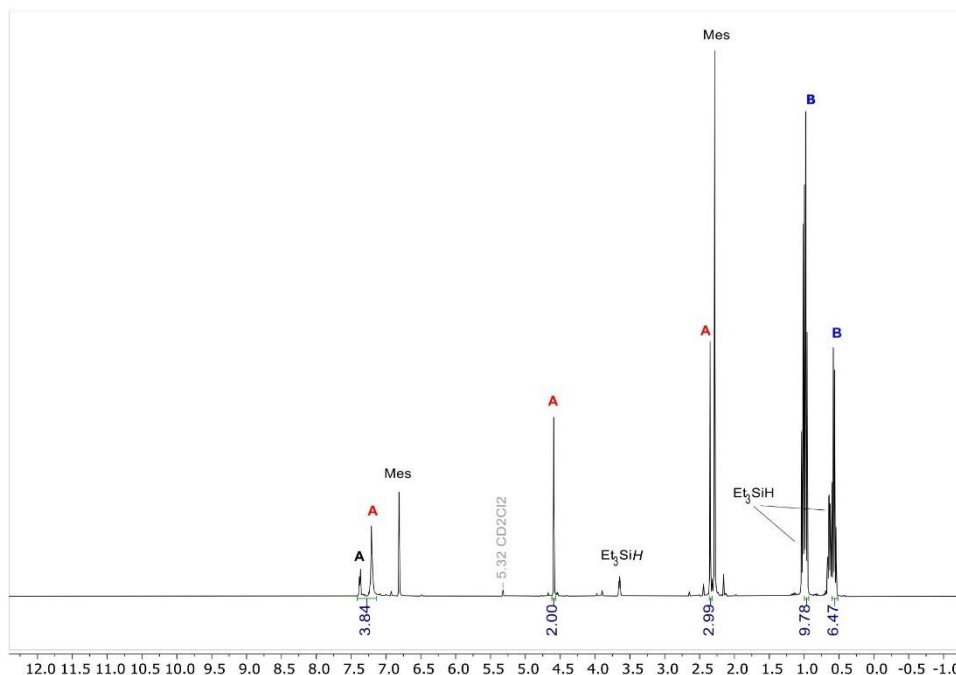
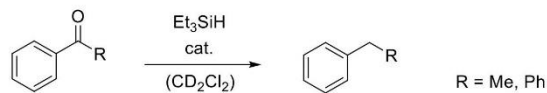


Figure S 15: ^1H NMR spectrum in CD_2Cl_2 of the reduction of *o*-methylbenzaldehyde with Et_3SiH after 30 min at r.t. showing quantitative formation of the hydrosilylation product di(*o*-methylbenzyl)ether (**A**) and $(\text{Et}_3\text{Si})_2\text{O}$ (**B**).

2.3.4 Dihydrodeoxygenation of ketones



To a solution of 25 mg benzophenone (137 μmol , 1.0 eq.) and 1 mg **1-MeCN** (1.37 μmol , 0.01 eq.) in 0.4 ml dichloromethane- d_2 were added 42 μl Et_3SiH (288 μmol , 2.1 eq.) and 10 μl (71.9 mmol) mesitylene as an internal standard. The reaction mixture was immediately transferred into a PTFE-sealed J-Young NMR tube and analyzed by the means of ^1H NMR spectroscopy. The reaction was repeated using 5 mol% of the catalyst.

In case of acetophenone, 10 μl (85.7 μmol , 1.0 eq.), 3.1 mg **1-MeCN** (4.29 μmol , 0.05 eq.) and 41 μl Et_3SiH (257 μmol , 3 eq.) were used. Also, additional mesitylene appeared to hamper the reaction progress and for this reason it was suspended for this experiment. Instead, the intrinsically present of MeCN was used as the internal standard.

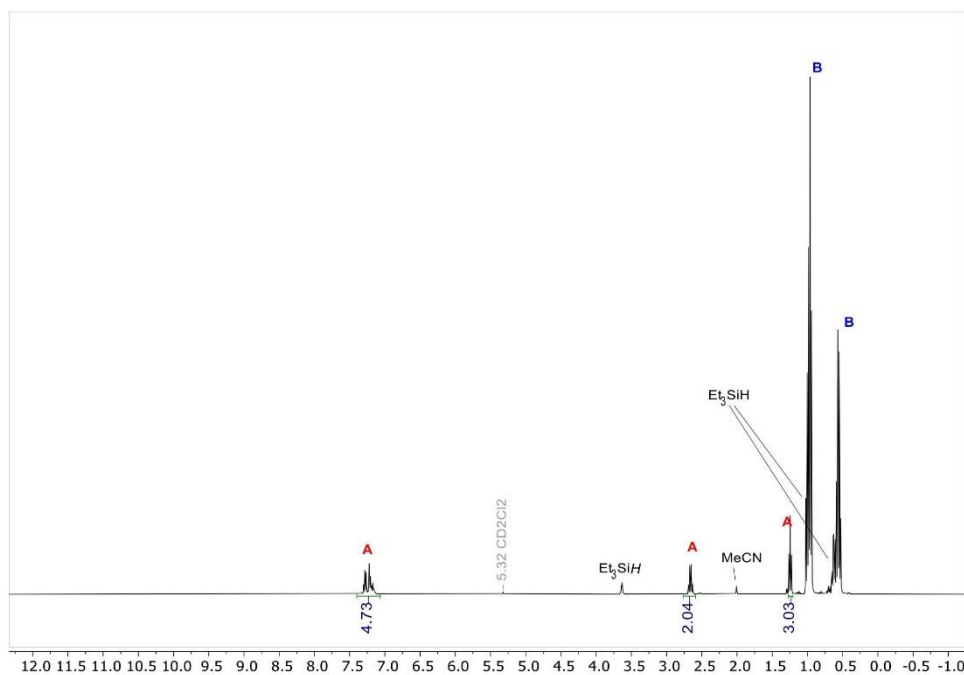
Ethylbenzene (R = CH_3): $^1\text{H-NMR}$ (400 MHz, CD_2Cl_2 δ (ppm) = 7.35 – 7.13 (m, 5H, Ph-*H*), 2.66 (q, $^3J = 7.6$ Hz, 3H), 1.25 (t, $^3J = 7.6$ Hz, 2H).

Benzylbenzene (R = Ph): $^1\text{H-NMR}$ (400 MHz, CD_2Cl_2 δ (ppm) = 7.36 – 7.28 (m, 4H, Ph-*H*), 7.27 – 7.19 (m, 6H, Ph-*H*), 4.01 (s, 2H, CH_2).

Product identification corresponds with literature values for ethylbenzene^[33] and benzylbenzene.^[31]

Table S 4: Reaction conditions and yield of hydrodefluorination experiments after several minutes.

Reactant	Et ₃ SiH eq.	Cat. [mol%]	Temp. [°C]	Time [min]	Yield [%]
benzophenone	2.1	1	25	120	79
benzophenone	2.1	1	25	720	99
benzophenone	2.1	5	25	15	99
acetophenone	3.0	5	25	60	99

**Figure S 16:** ¹H NMR spectrum in CD₂Cl₂ of the reduction of acetophenone with Et₃SiH after 12 h at r.t. showing quantitative formation of the hydrosilylation product ethylbenzene (A) and (Et₃Si)₂O (B).

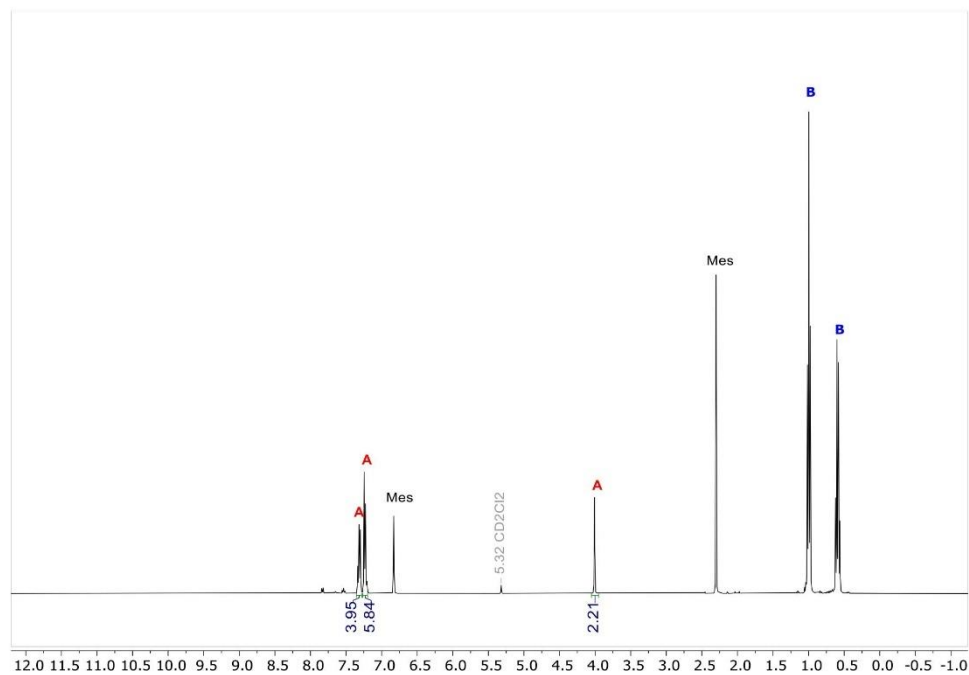


Figure S 17: ^1H NMR spectrum in CD_2Cl_2 of the reduction of benzophenone with Et_3SiH after 12 h at r.t. showing quantitative formation of the hydrosilylation product benzylbenzene (A) and $(\text{Et}_3\text{Si})_2\text{O}$ (B).

3 Computational Details

Table S 5: Computed energies for the calculation of vacuum anion affinities.

PBE0-D3/def2-TZVPP level of theory							
Compound	E [a.u.]	in kJ mol ⁻¹	Total therm. Correction [kJ mol ⁻¹]	Enthalpy [kJ mol ⁻¹]	LA + Me ₃ SiY (A)	Me ₃ Si ⁺ + A-Y (B)	(B) - (A) FIA / HIA
1	-3442.3244	-9037822.8	540.6				
[1-H] ⁻	-3443.0226	-9039655.9	559.7	-9039096.2	-10112487.3	-10112014.8	472.5 451 (HIA)
[1-F] ⁻	-3542.2998	-9300308.1	547.0	-9299761.2	-10373141.7	-10372679.8	461.9 491 (FIA)
trans-[1-F ₂] ²⁻	-3642.0768	-9562272.7	549.7	-9561723.0	-10635620.6	-10634641.7	979.0 -27 (2nd FIA)
cis-[1-F ₂] ²⁻	-3642.0847	-9562293.3	549.7	-9561743.6	-10635620.6	-10634662.2	958.4 -6 (2nd FIA)
DLPNO-CCSD(T)/aug-cc-pVQZ level of theory							
Compound	E [a.u.]	in kJ mol ⁻¹		Enthalpy [kJ mol ⁻¹]	LA + Me ₃ SiY (A)	Me ₃ Si ⁺ + A-Y (B)	(B) - (A) FIA / HIA
1	-3440.9852	-9034306.8		-9033766.2			
[1-H] ⁻	-3441.6886	-9036153.4		-9035593.7	-10107929.06	-10107449.1	480.0 444 (HIA)
[1-F] ⁻	-3540.9469	-9296756.0		-9296209.0	-10368543.21	-10368064.4	478.8 474 (FIA)
trans-[1-F ₂] ²⁻	-3640.7106	-9558136.0		-9557586.4	-10630438.99	-10629441.8	997.2 -45 (2nd FIA)
cis-[1-F ₂] ²⁻	-3640.7189	-9558157.9		-9557608.2	-10630438.99	-10629463.6	975.4 -23 (2nd FIA)
Ion affinities (<i>vacuum</i>) of reference compounds SbF ₅ and Si(CH ₃) ₃ ⁺ .							
Compound	FIA	HIA	level of theory	reference			
SbF ₅	496	535	DLPNO-CCSD(T)/aug-cc-pVQZ//PBEh-3c-def2-mSVP	[16]			
Si(CH ₃) ₃ ⁺	953	924	CCSD(T)/CBS (serve as anchor points)	[16]			

Table S 6: Solvation corrected ion affinities at the DLPNO-CCSD(T)/aug-cc-pVQZ/PBE0-D3/def2-TZVPP level of theory, solvation correction via COSMO-RS using dichloromethane as solvent.

System	FIA / HIA
	(solvent corrected)
	[kJ mol ⁻¹]
1 / [1-H] ⁻	373 (HIA)
1 / [1-F] ⁻	268 (FIA)
1 / trans-[1-F ₂] ²⁻	49 (2 nd FIA)
1 / cis-[1-F ₂] ²⁻	69 (2 nd FIA)

Table S 7: Computed energies and thermodynamics for the reactivity of **1** with acetonitrile and triethylsilyl fluoride.

PBE0-D3/def2-TZVPP level of theory (level of optimization)				
Compound	E [a.u.]	Total therm. correction [a.u.]	Enthalpy [kJ mol ⁻¹]	Gibbs free energy (298 K) [kJ mol ⁻¹]
1	-3442.3244	0.2061	-9037282.4	-9037538.4
1 -MeCN	-3574.9823	0.2579	-9385439.4	-9385720.8
trans- 1 -(MeCN) ₂	-3707.6354	0.3094	-9733585.1	-9733887.9
cis- 1 -(MeCN) ₂	-3707.6262	0.3094	-9733560.8	-9733866.5
MeCN	-132.6448	0.0500	-348127.9	-348202.8
Et ₃ SiF	-626.7543	0.2137	-1644982.6	-1645116.2
[1 -F] ⁻	-3542.2998	0.2085	-9299761.3	-9300022.9
[Et ₃ Si-MeCN] ⁻	-659.3376	0.2625	-1730401.7	-1730555.6

DSD-BLYP-D3/def2-QZVPP level of theory – single point energies (therm. correction from level of optimization)				
Compound	E [a.u.]		Enthalpy [kJ mol ⁻¹]	Gibbs free energy (298 K) [kJ mol ⁻¹]
1	-3442.9288		-9038869.1	-9039125.1
1 -MeCN	-3575.6009		-9387063.5	-9387344.9
trans- 1 -(MeCN) ₂	-3708.2696		-9735250.2	-9735553.0
cis- 1 -(MeCN) ₂	-3708.2609		-9735227.2	-9735532.9
MeCN	-132.6612		-348170.8	-348245.7
Et ₃ SiF	-626.6989		-1644837.0	-1644970.6
[1 -F] ⁻	-3542.9359		-9301431.3	-9301692.9
[Et ₃ Si-MeCN] ⁻	-659.2637		-1730207.7	-1730361.6

COSMO-RS for acetonitrile, BP86/TZP level of theory				
Compound		Solvation correction for Enthalpy [kJ mol ⁻¹]	Solvation correction for Gibbs free energy [kJ mol ⁻¹]	
1		-23.7	-16.3	
1 -MeCN		-90.1	-71.9	
trans- 1 -(MeCN) ₂		-102.0	-81.0	
cis- 1 -(MeCN) ₂		-114.8	-93.1	
MeCN		-30.6	-22.0	
Et ₃ SiF		-24.0	-17.2	
[1 -F] ⁻		-198.5	-172.0	
[Et ₃ Si-MeCN] ⁻		-200.9	-197.6	

Thermodynamic data – DSD-BLYP-D3/def2-QZVPP level of theory, therm. correction at PBE0-D3/def2-TZVPP level of theory (ΔH and ΔG values are not listed at the PBE0-D3/def2-TZVPP level), solvation correction via COSMO-RS for acetonitrile				
	ΔH_{vacuum} [kJ mol ⁻¹]	ΔG_{vacuum} [kJ mol ⁻¹]	ΔH_{MeCN} [kJ mol ⁻¹]	ΔG_{MeCN} [kJ mol ⁻¹]
1 + MeCN \rightarrow 1 -MeCN	-23.6	25.9	-59.5	-7.7
1 -MeCN + MeCN \rightarrow trans- 1 -(MeCN) ₂	-15.8	37.7	2.8	50.5
1 -MeCN + MeCN \rightarrow cis- 1 -(MeCN) ₂	7.1	57.8	13.0	58.5
1 -MeCN + Et ₃ SiF \rightarrow [Et ₃ Si-MeCN] ⁻ + [1 -F] ⁻	261.5	261.0	-23.9	-19.5

Table S 8: Computed ^{29}Si NMR resonances.

PBE0-D3/def2-TZVPP, SMD(Acetonitrile)			
Compound	Isotropic Shielding	Calculated Resonance δ [ppm]	Experimentally obtained Resonance δ [ppm]
$\text{Si}(\text{CH}_3)_4$	332.782	0.00	
$\text{I}-(\text{CH}_3\text{CN})$	443.081	-110.30	-110.35
$[\text{I-F}]^-$	440.513	-107.73	-108.37
$[\text{I-H}]^-$	422.220	-89.44	-90.22

4 SC-XRD Analysis

4.1 Crystal Structure of Li[1-H]·(MeCN)₂

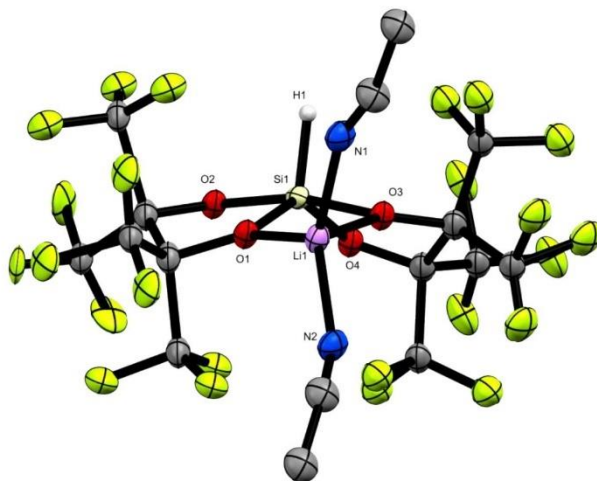


Figure S 18: Molecular structure of Li[1-H]·(MeCN)₂ with translational ellipsoids plotted at 50% probability level. Hydrogen atoms, except Si-H, are omitted for reasons of clarity. The structure contains a second, inversely overlaying disordered part, which is also omitted for clarity reasons. Selected bond lengths [Å] and angles [°]: Si1–O1 1.744(18), Si1–O2 1.754(17), Si1–O3 1.779(18), Si1–O4 1.684(18); O1–Si1–O4 131.7(8), O2–Si1–O3 166.0(8).

Table S 9: Crystal data and structure refinement for compound Li[1-H]·(MeCN)₂.

Chemical formula	C ₁₆ H ₇ F ₂₄ LiN ₂ O ₄ Si	
CCDC Database number	2102992	
Formula weight	782.27 g/mol	
Temperature	100(2) K	
Wavelength	0.71073 Å	
Crystal size	0.168 × 0.144 × 0.071 mm	
Crystal habit	clear colorless fragment	
Crystal system	monoclinic	
Space group	C-2yc	
Unit cell dimensions	a = 21.909(3) Å	α = 90°
	b = 8.3881(9) Å	β = 119.862(7)°
	c = 15.9995(19) Å	γ = 90°
Volume	2549.9(6) Å ³	
Z	4	
Density (calculated)	2.038 g/cm ³	
Absorption coefficient μ	0.299 mm ⁻¹	

F(000)	1528
Diffractometer	Bruker Photon CMOS
Radiation source	IMS microsource, MoK α
Theta range for data collection	2.14 to 25.35°
Index ranges	-26<=h<=26, -10<=k<=10, -19<=l<=19
Reflections collected	14389
Independent reflections	4516
Absorption correction	multi-scan
Max. and min. transmission	0.7452 and 0.6745
Refinement method	Full-matrix least-squares on F ²
Function minimized	$\Sigma w(F_o^2 - F_c^2)^2$
Data / restraints / parameters	4516 / 165 / 397
Goodness-of-fit on F²	0.994
Final R indices	I>2 σ (I) R1 = 0.0693, wR2 = 0.1704 all data R1 = 0.0939, wR2 = 0.1902
Largest diff. peak and hole	0.397 and -0.381 eÅ ⁻³
R.M.S. deviation	0.083 cÅ ⁻³

4.2 Crystal Structure of [1-Cl]⁻

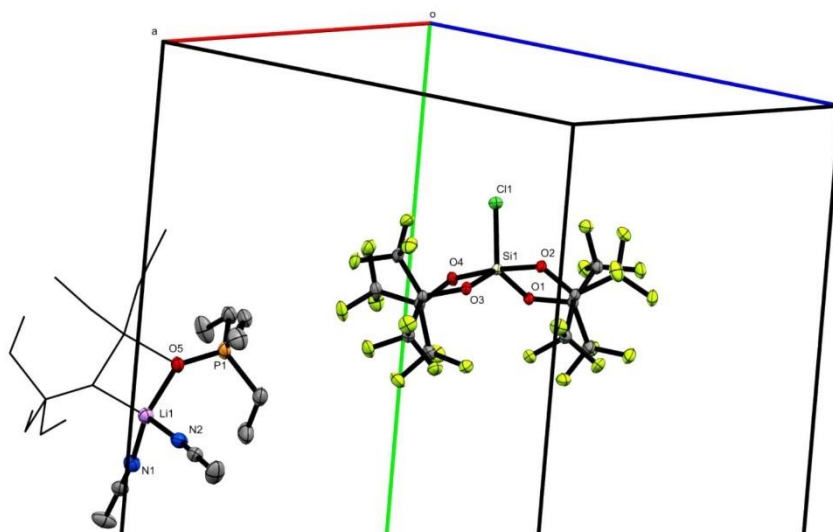


Figure S 19: Molecular structure of pentavalent [1-Cl]⁻ obtained from the reaction of Li[1-Cl]·(MeCN)₂ with 1.0 eq. of Et₃PO in dichloromethane. Translational ellipsoids plotted at 50% probability level. For reason of clarity hydrogens are omitted and the cell axes are highlighted. Selected bond lengths [Å] and angles [°]: Si1–Cl1 2.0694(8), Si1–O1 1.6980(16), Si1–O2 1.7497(15), Si1–O3 1.7032(16), Si1–O4 1.7521(15); O1–Si1–O3 127.61(8), O2–Si1–O4 173.36(8).

Table S 10: Crystal data and structure refinement for compound Et₃PO·Li[1-Cl](MeCN)₂.

Chemical formula	C ₂₂ H ₂₁ ClF ₂₄ LiN ₂ O ₅ PSi	
CCDC Database number	2102991	
Formula weight	950.86 g/mol	
Temperature	100(2) K	
Wavelength	0.71073 Å	
Crystal size	0.337 × 0.185 × 0.143 mm	
Crystal habit	clear colorless fragment	
Crystal system	monoclinic	
Space group	-P 2 ₁ /n	
Unit cell dimensions	a = 11.0219(7) Å	α = 90°
	b = 20.8841(13) Å	β = 103.358(2)°
	c = 15.4464(9) Å	γ = 90°
Volume	3459.3(4) Å ³	
Z	4	
Density (calculated)	1.826 g/cm ³	
Absorption coefficient μ	0.359 mm ⁻¹	
F(000)	1888	
Diffractometer	Bruker Photon CMOS	
Radiation source	TXS rotating anode, MoK α	
Theta range for data collection	2.13 to 25.35°	
Index ranges	-13 ≤ h ≤ 13, -25 ≤ k ≤ 25, -18 ≤ l ≤ 18	
Reflections collected	79210	
Independent reflections	6344	
Absorption correction	multi-scan	
Max. and min. transmission	0.7452 and 0.7153	
Refinement method	Full-matrix least-squares on F ²	
Function minimized	Σ w(F _o ² - F _c ²) ²	
Data / restraints / parameters	6344 / 0 / 519	
Goodness-of-fit on F²	1.037	
Final R indices	I > 2σ(I) R1 = 0.0334, wR2 = 0.0771	
	all data R1 = 0.0417, wR2 = 0.0812	
Largest diff. peak and hole	1.200 and -0.837 eÅ ⁻³	
R.M.S. deviation	0.057 eÅ ⁻³	

4.3 Crystal Structure of 1-MeCN

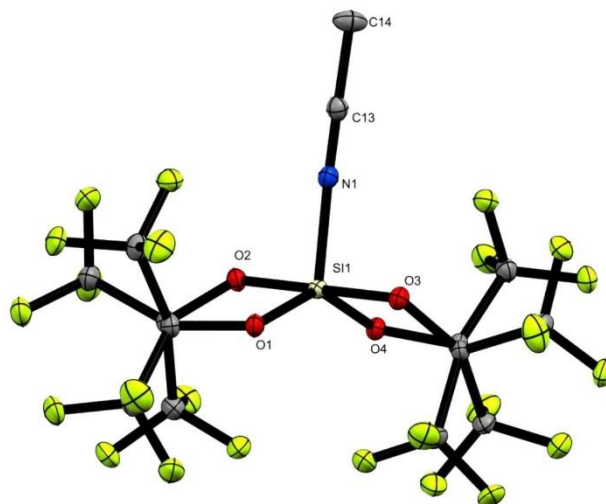


Figure S 20: Molecular structure of Lewis superacid 1-MeCN with translational ellipsoids plotted at 50% probability level. Hydrogen atoms are omitted for reasons of clarity. Selected bond lengths [Å] and angles [°]: Si1–N1 1.8412(16), Si1–O1 1.6745(14), Si1–O2 1.7223(14), Si1–O3 1.7234(14), Si1–O4 1.6886(14), N1–C13 1.135(2); O1–Si1–O4 136.31(7), O2–Si1–O3 179.60(7).

Table S 11: Crystal data and structure refinement for compound 1-MeCN.

Chemical formula	C ₁₄ H ₃ F ₂₄ NO ₄ Si	
CCDC Database number	2102990	
Formula weight	733.26 g/mol	
Temperature	100(2) K	
Wavelength	0.71073 Å	
Crystal size	0.557 × 0.316 × 0.254 mm	
Crystal habit	clear colorless fragment	
Crystal system	monoclinic	
Space group	-P 2ybc	
Unit cell dimensions	a = 8.6436(11) Å	α = 90°
	b = 21.248(2) Å	β = 90.190(4)°
	c = 11.9816(13) Å	γ = 90°
Volume	2200.5(4) Å ³	
Z	4	
Density (calculated)	2.213 g/cm ³	
Absorption coefficient μ	0.338 mm ⁻¹	
F(000)	1424	

Diffractometer	Bruker Photon CMOS
Radiation source	IMS microsource, MoK α
Theta range for data collection	1.95 to 25.35°
Index ranges	-10<math>\leq h \leq 10, -25 \leq k \leq 25, -14 \leq l \leq 14
Reflections collected	40295
Independent reflections	4033
Absorption correction	multi-scan
Max. and min. transmission	0.7452 and 0.6984
Refinement method	Full-matrix least-squares on F ²
Function minimized	$\Sigma w(F_o^2 - F_c^2)^2$
Data / restraints / parameters	4033 / 0 / 402
Goodness-of-fit on F ²	0.819
Final R indices	I>2 σ (I) R1 = 0.0246, wR2 = 0.0840 all data R1 = 0.0252, wR2 = 0.0855
Largest diff. peak and hole	0.334 and -0.245 e \AA^{-3}
R.M.S. deviation	0.063 e \AA^{-3}

4.4 Crystal Structure of [K-(18-c-6)][1-F]

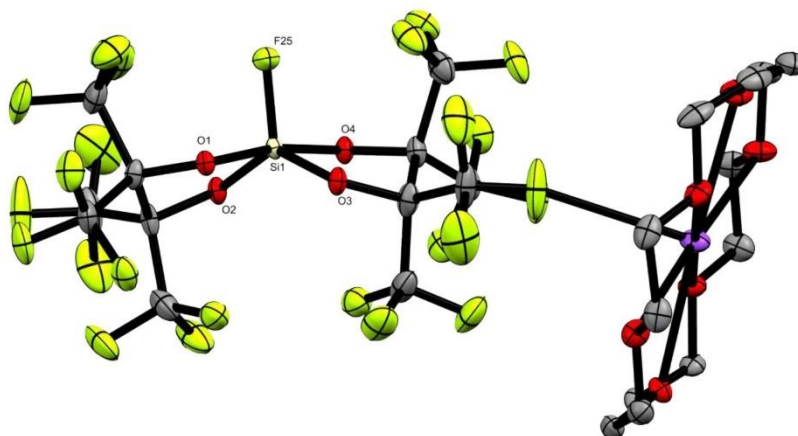


Figure S 21: Molecular structure of [K-(18-c-6)][1-F] with translational ellipsoids plotted at 50% probability level. Hydrogen atoms are omitted for reasons of clarity. Selected bond lengths [\AA] and angles [$^\circ$]: Si1–F25 1.592(2), Si1–O1 1.740(2), Si1–O2 1.698(2), Si1–O3 1.711(2), Si1–O4 1.739(2); O1–Si1–O4 169.82(11), O2–Si1–O3 133.11(11).

Table S 12: Crystal data and structure refinement for compound [K-(18-c-6)][1-F].

Chemical formula	C ₄₈ H ₄₈ F ₅₀ K ₂ O ₂₀ Si ₂
CCDC Database number	2102993

Formula weight	2029.25 g/mol		
Temperature	100(2) K		
Wavelength	0.71073 Å		
Crystal size	0.359 × 0.257 × 0.206 mm		
Crystal habit	clear colorless fragment		
Crystal system	triclinic		
Space group	-P 1		
Unit cell dimensions	a = 11.079(2) Å	$\alpha = 67.235(4)^\circ$	
	b = 17.128(3) Å	$\beta = 85.018(5)^\circ$	
	c = 20.912(4) Å	$\gamma = 79.721(4)^\circ$	
Volume	3599.7(11) Å ³		
Z	2		
Density (calculated)	1.872 g/cm ³		
Absorption coefficient μ	0.363 mm ⁻¹		
F(000)	2024		
Diffractometer	Bruker Photon CMOS		
Radiation source	IMS microsource, MoK α		
Theta range for data collection	1.87 to 25.35°		
Index ranges	-13 ≤ h ≤ 13, -20 ≤ k ≤ 20, -25 ≤ l ≤ 25		
Reflections collected	115649		
Independent reflections	13195		
Absorption correction	multi-scan		
Max. and min. transmission	0.7452 and 0.7048		
Refinement method	Full-matrix least-squares on F ²		
Function minimized	$\Sigma w(F_o^2 - F_c^2)^2$		
Data / restraints / parameters	13195 / 510 / 1209		
Goodness-of-fit on F²	1.040		
Final R indices	I > 2 σ (I) R1 = 0.0527, wR2 = 0.1397		
	all data R1 = 0.0593, wR2 = 0.1455		
Largest diff. peak and hole	0.978 and -0.392 eÅ ⁻³		
R.M.S. deviation	0.085 eÅ ⁻³		

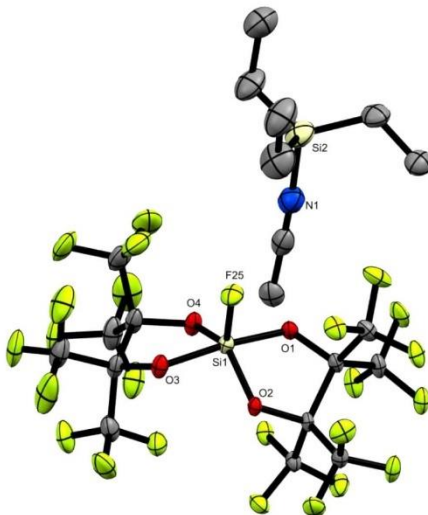
4.5 Crystal Structure of [Et₃Si-MeCN][1-F]

Figure S 22: Molecular structure of [Et₃Si-MeCN][1-F] with translational ellipsoids plotted at 50% probability level. Hydrogen atoms are omitted for reasons of clarity. Selected bond lengths [Å] and angles [°]: Si1–F25 1.5923(17), Si1–O1 1.7438(19), Si1–O2 1.6998(18), Si1–O3 1.7501(19), Si1–O4 1.6991(19), Si2–N1 1.826(3); O1–Si1–O3 169.63(9), O2–Si1–O4 133.98(9).

Table S 13: Crystal data and structure refinement for compound [Et₃Si-MeCN][1-F].

Chemical formula	C ₂₀ H ₁₈ F ₂₅ NO ₄ Si ₂	
CCDC Database number	2102994	
Formula weight	867.53 g/mol	
Temperature	100(2) K	
Wavelength	0.71073 Å	
Crystal size	0.480 × 0.260 × 0.196 mm	
Crystal habit	clear colorless fragment	
Crystal system	triclinic	
Space group	-P 1	
Unit cell dimensions	a = 8.3346(8) Å	α = 94.201(3)°
	b = 10.8369(10) Å	β = 96.396(3)°
	c = 16.9650(17) Å	γ = 94.015(3)°
Volume	1513.9(3) Å ³	
Z	2	
Density (calculated)	1.903 g/cm ³	
Absorption coefficient μ	0.304 mm ⁻¹	
F(000)	860	
Diffractometer	Bruker Photon CMOS	
Radiation source	TXS rotating anode, MoK α	

Theta range for data collection	2.47 to 25.35°
Index ranges	-10<=h<=10, -13<=k<=13, -20<=l<=20
Reflections collected	73589
Independent reflections	5515
Absorption correction	multi-scan
Max. and min. transmission	0.7452 and 0.6292
Refinement method	Full-matrix least-squares on F ²
Function minimized	$\Sigma w(F_o^2 - F_c^2)^2$
Data / restraints / parameters	5515 / 0 / 473
Goodness-of-fit on F²	0.990
Final R indices	I>2σ(I) R1 = 0.0497, wR2 = 0.1403 all data R1 = 0.0559, wR2 = 0.1472
Largest diff. peak and hole	0.897 and -0.847 eÅ ⁻³
R.M.S. deviation	0.080 eÅ ⁻³

5 NMR Spectra

5.1 NMR spectra of $\text{Li}_2\text{pin}^{\text{F}}$

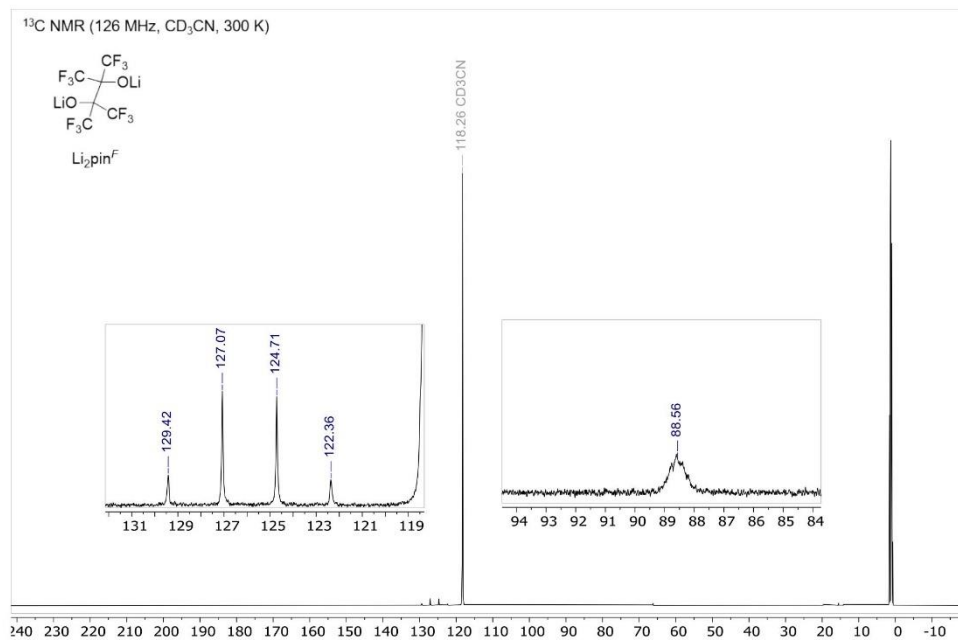


Figure S 23: ^{13}C NMR spectrum of $\text{Li}_2\text{pin}^{\text{F}}$ in CD_3CN at 300 K.

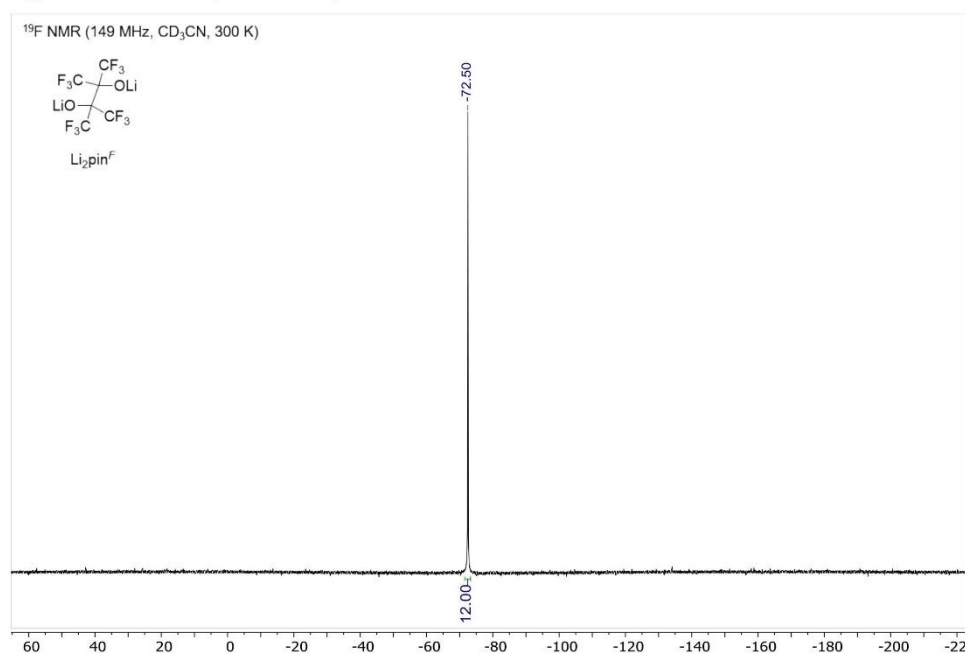
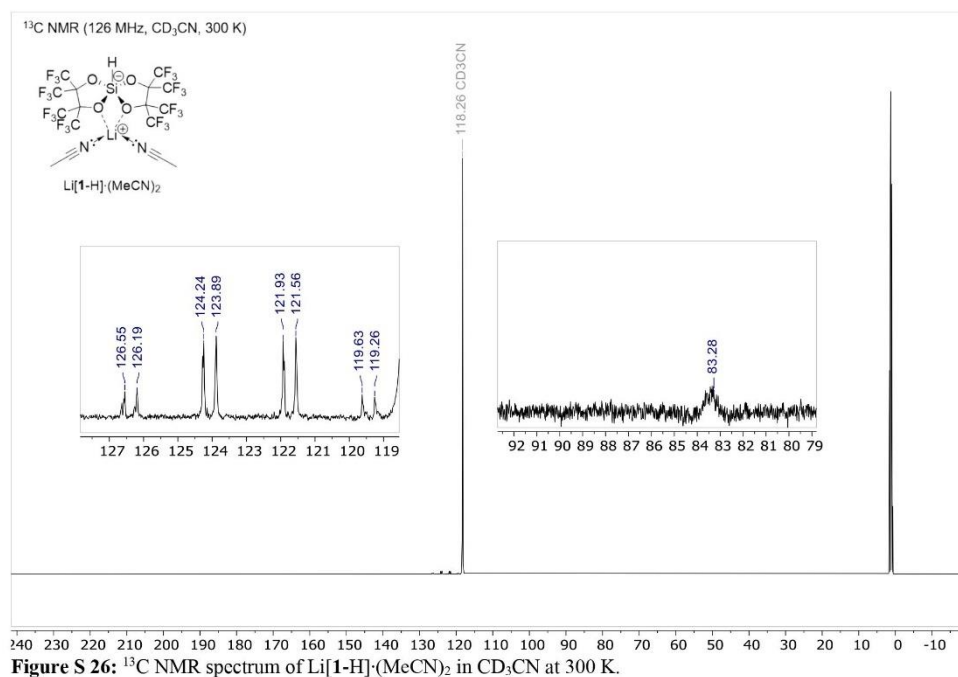
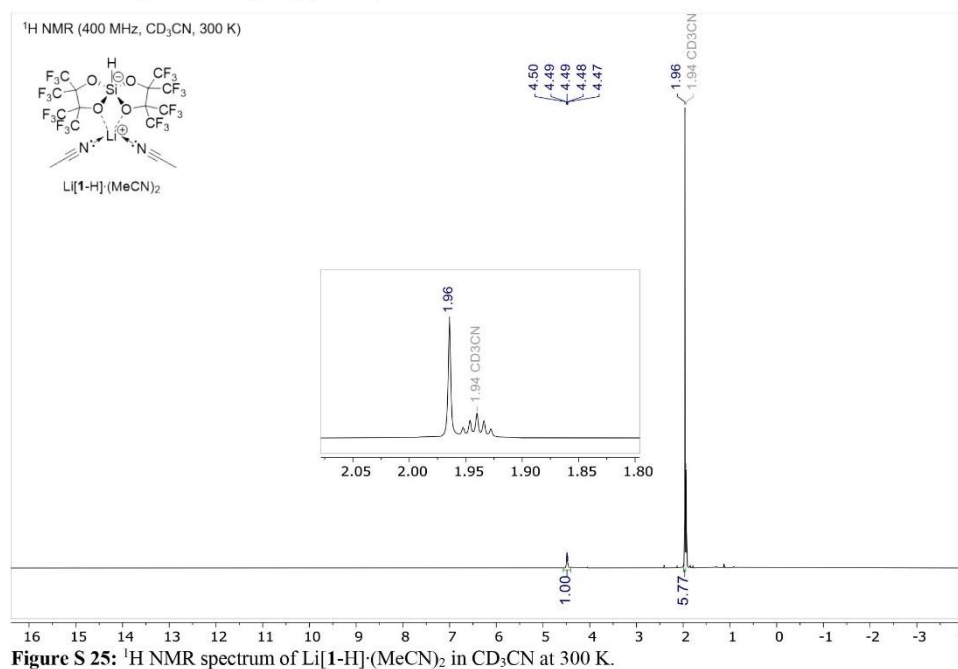


Figure S 24: ^{19}F NMR spectrum of $\text{Li}_2\text{pin}^{\text{F}}$ in CD_3CN at 300 K

5.2 NMR spectra of Li[1-H]·(MeCN)₂

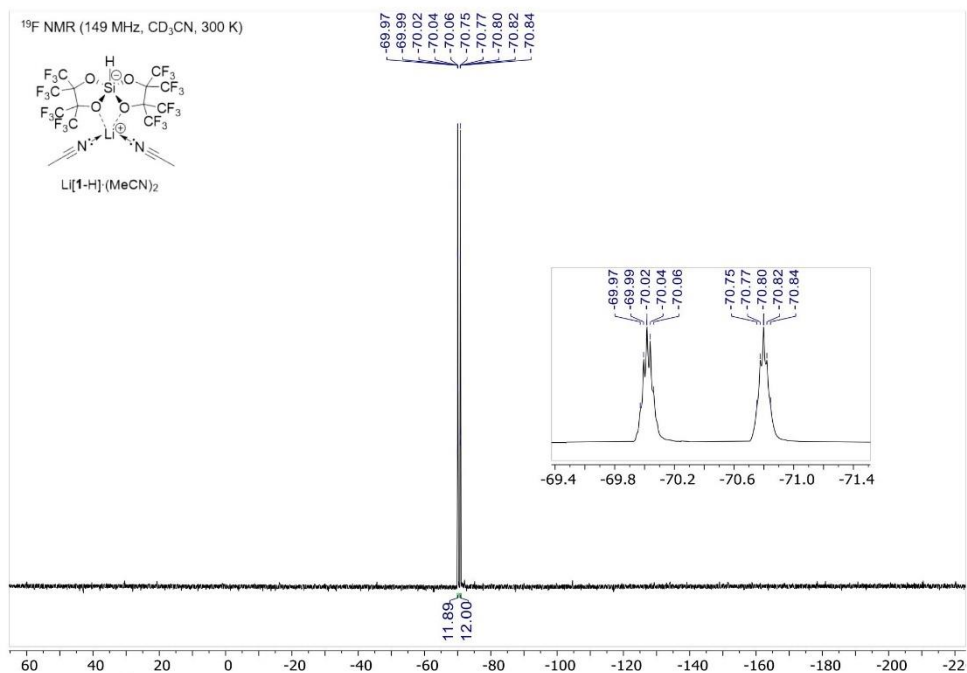


Figure S 27: ¹⁹F NMR spectrum of Li[1-H]·(MeCN)₂ in CD₃CN at 300 K.

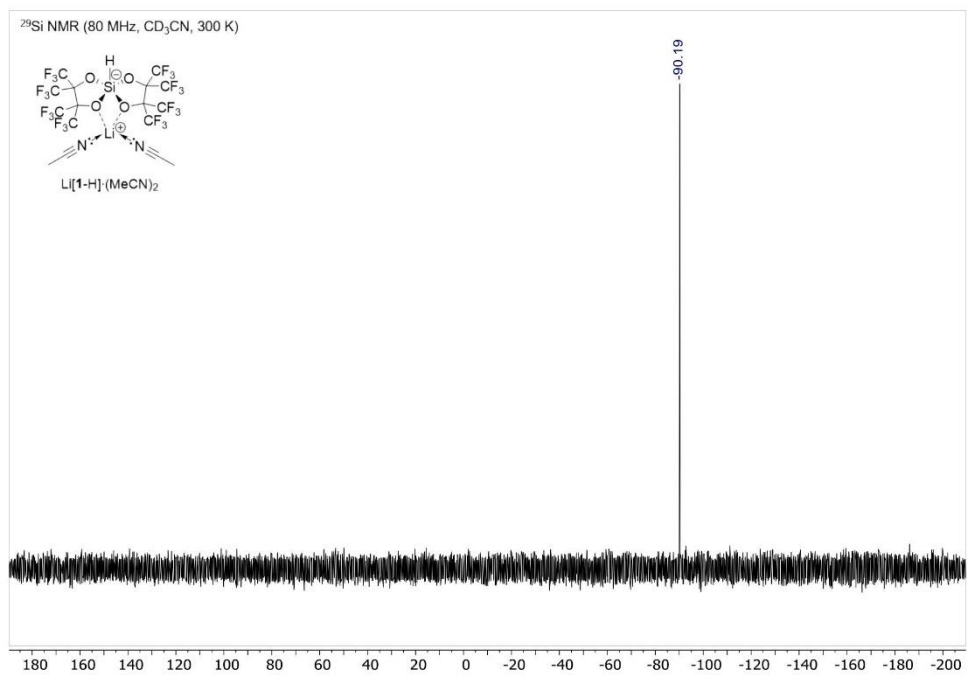
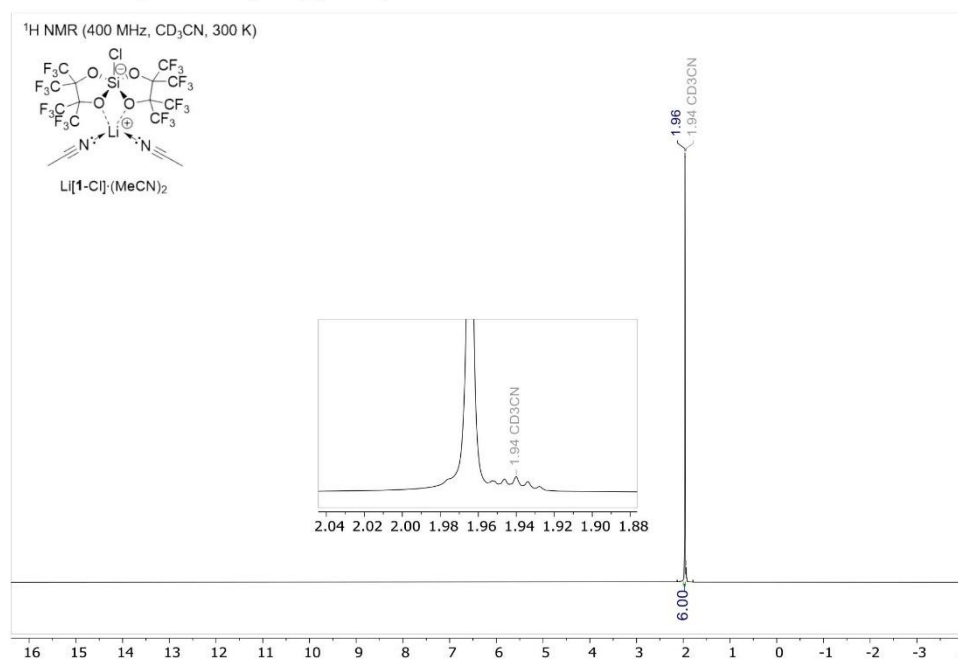
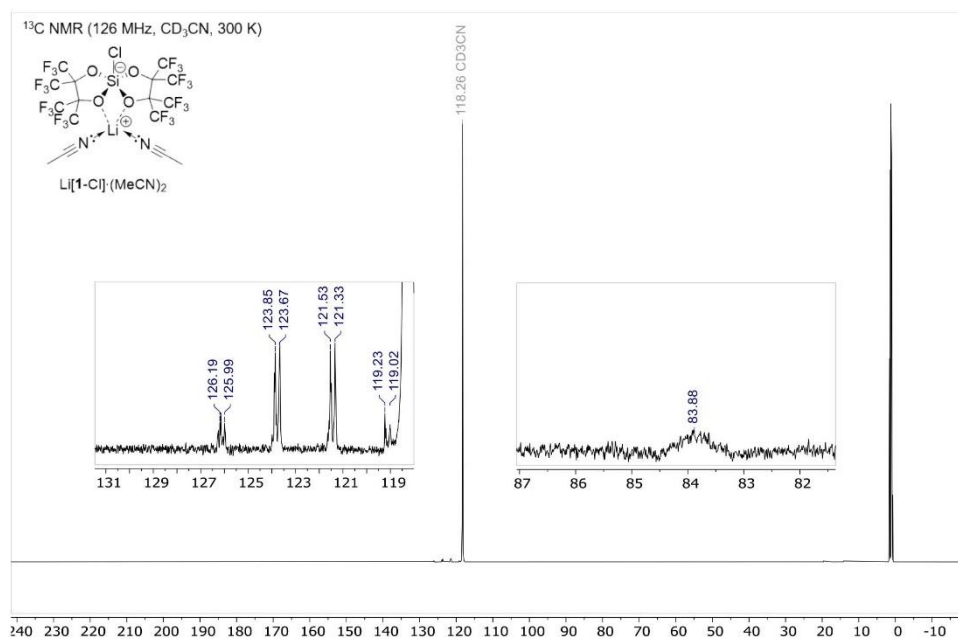


Figure S 28: ²⁹Si[¹H] NMR spectrum of Li[1-H]·(MeCN)₂ in CD₃CN at 300 K.

5.3 NMR spectra of Li[1-Cl]-(MeCN)₂Figure S 29: ¹H NMR spectrum of Li[1-Cl]-(MeCN)₂ in CD₃CN at 300 K.Figure S 30: ¹³C NMR spectrum of Li[1-Cl]-(MeCN)₂ in CD₃CN at 300 K.

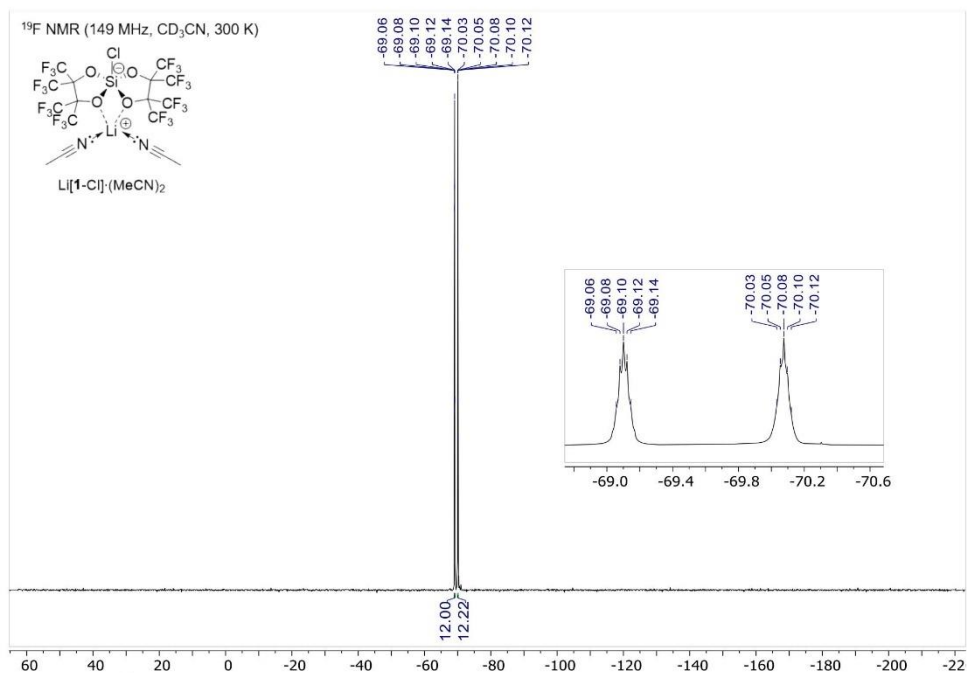


Figure S 31: ¹⁹F NMR spectrum of Li[1-Cl]·(MeCN)₂ in CD₃CN at 300 K.

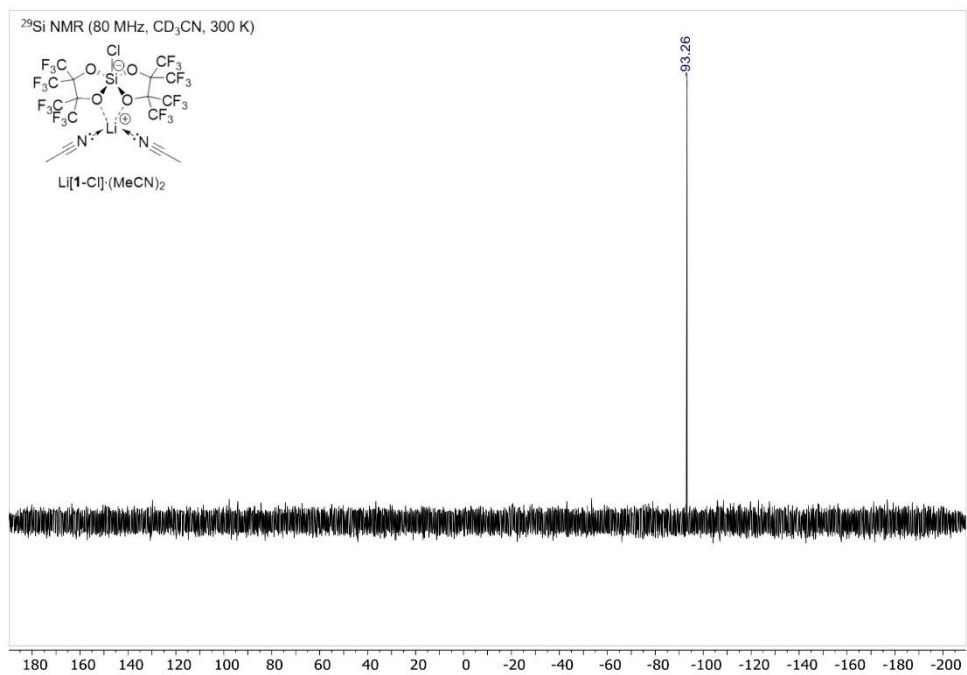
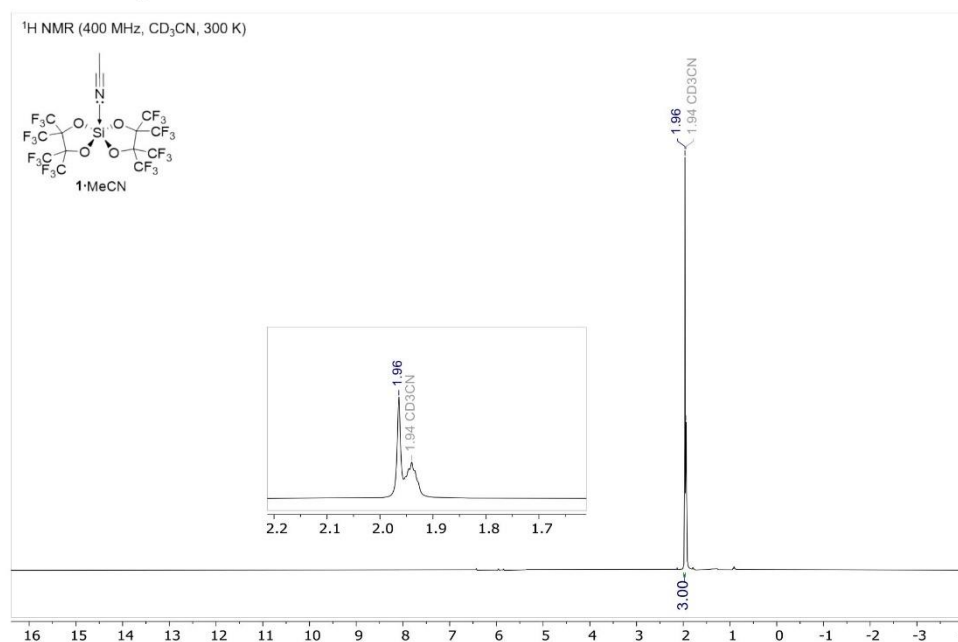
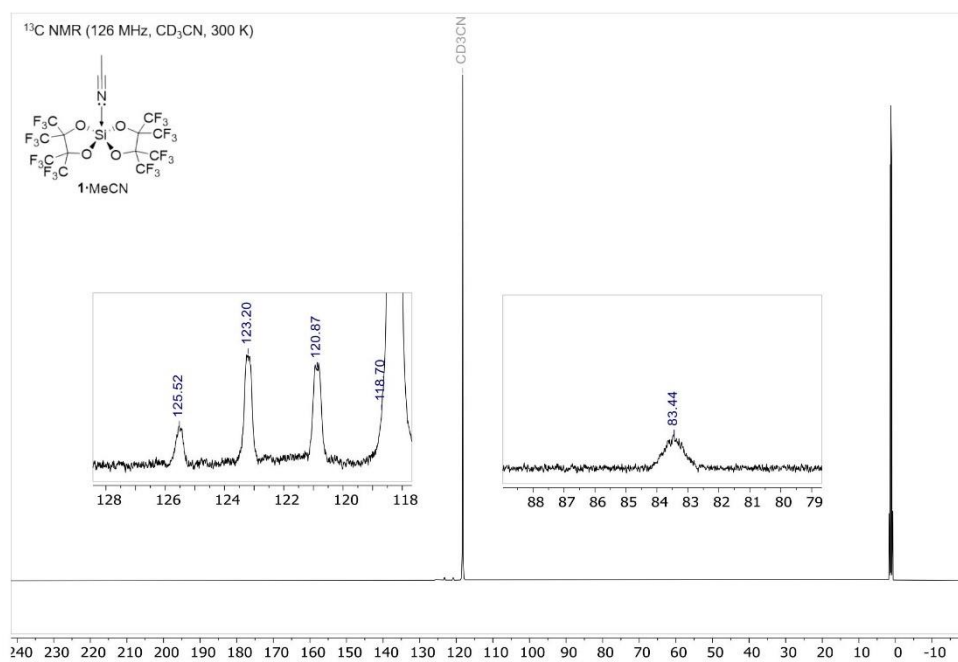
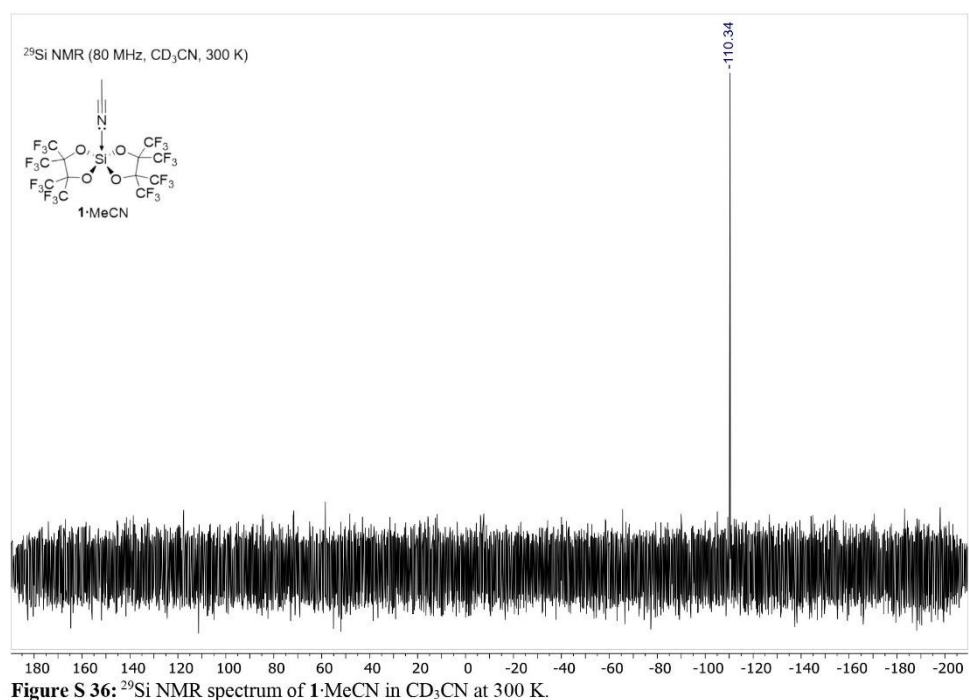
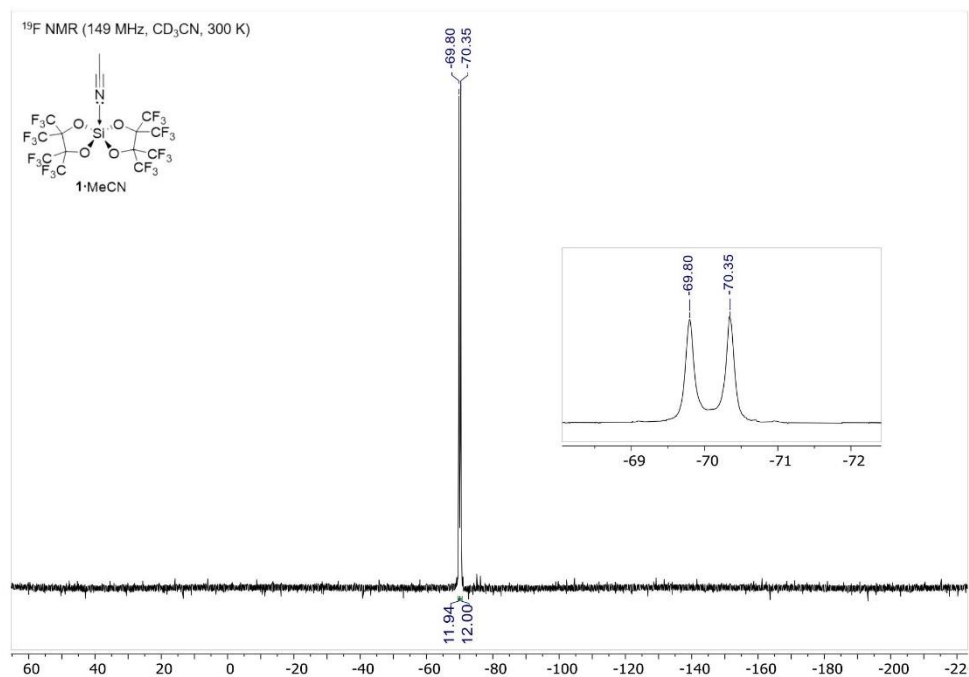
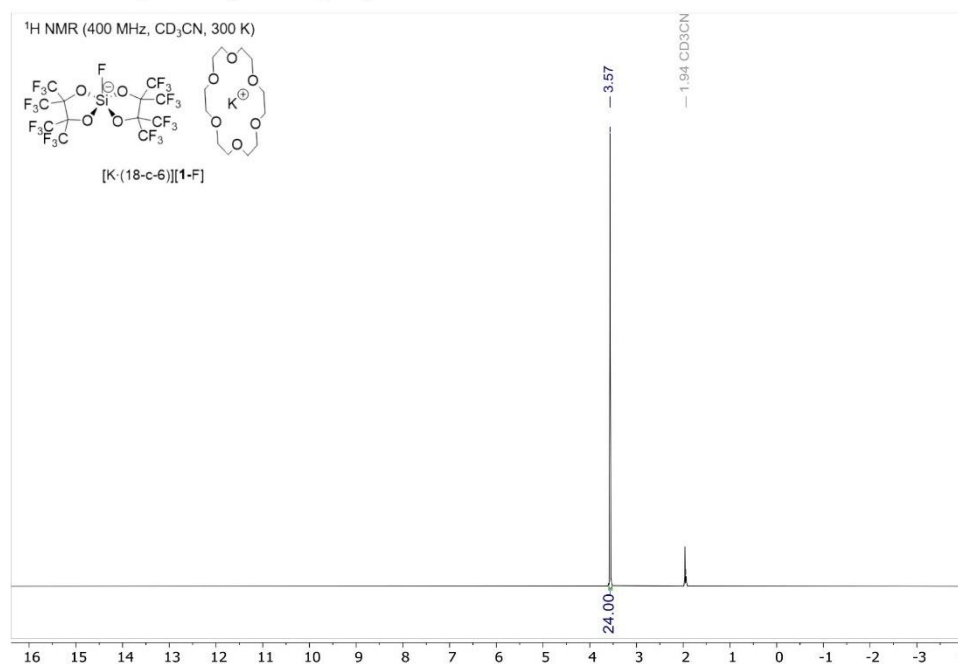
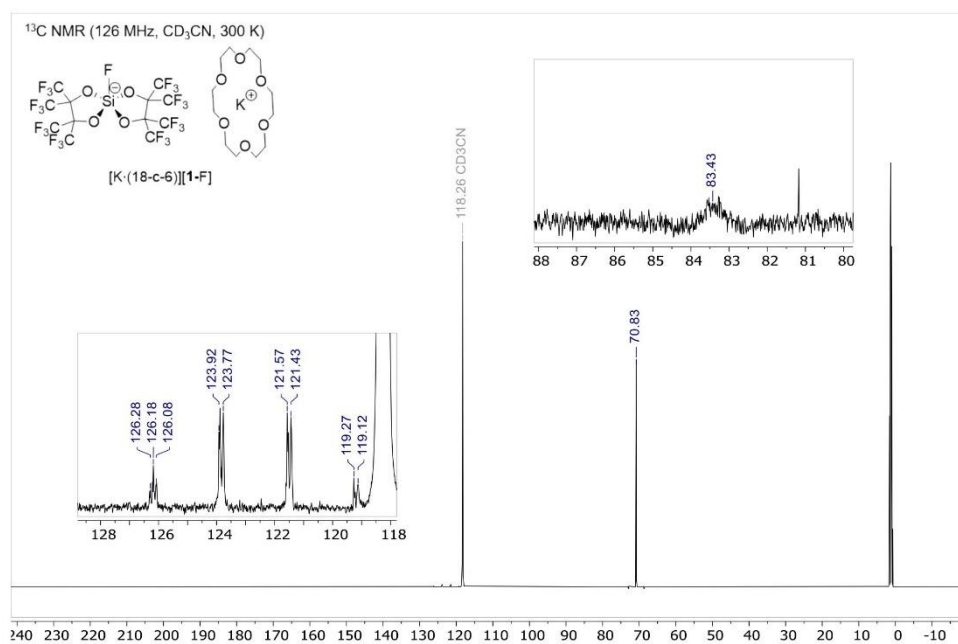


Figure S 32: ²⁹Si NMR spectrum of Li[1-Cl]·(MeCN)₂ in CD₃CN at 300 K.

5.4 NMR spectra of **1**·MeCNFigure S 33: ¹H NMR spectrum of **1**·MeCN in CD₃CN at 300 K.Figure S 34: ¹³C NMR spectrum of **1**·MeCN in CD₃CN at 300 K.



5.5 NMR spectra of [K·18-c-6][1-F]

Figure S 37: ¹H NMR spectrum of [K·(18-c-6)][1-F] in CD₃CN at 300 K.Figure S 38: ¹³C NMR spectrum of [K·(18-c-6)][1-F] in CD₃CN at 300 K.

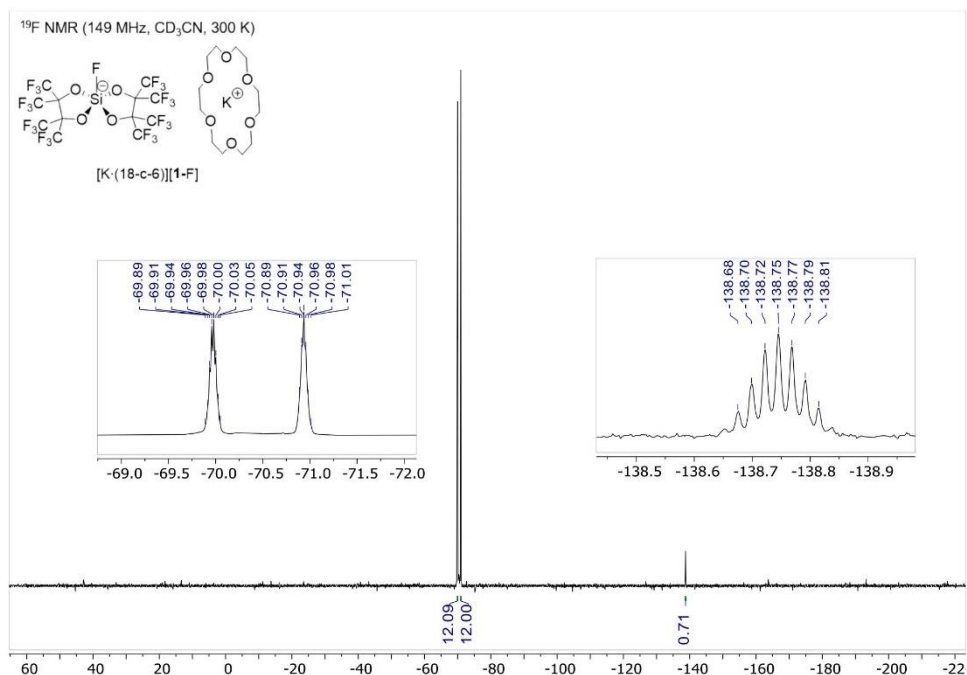


Figure S 39: ¹⁹F NMR spectrum of [K·(18-c-6)][1-F] in CD₃CN at 300 K.

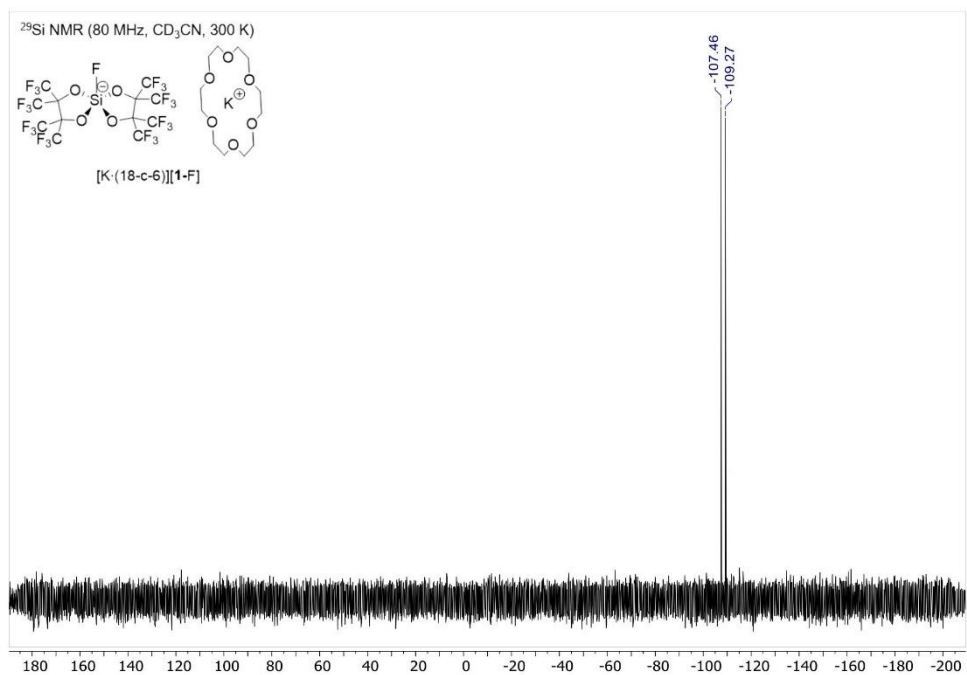
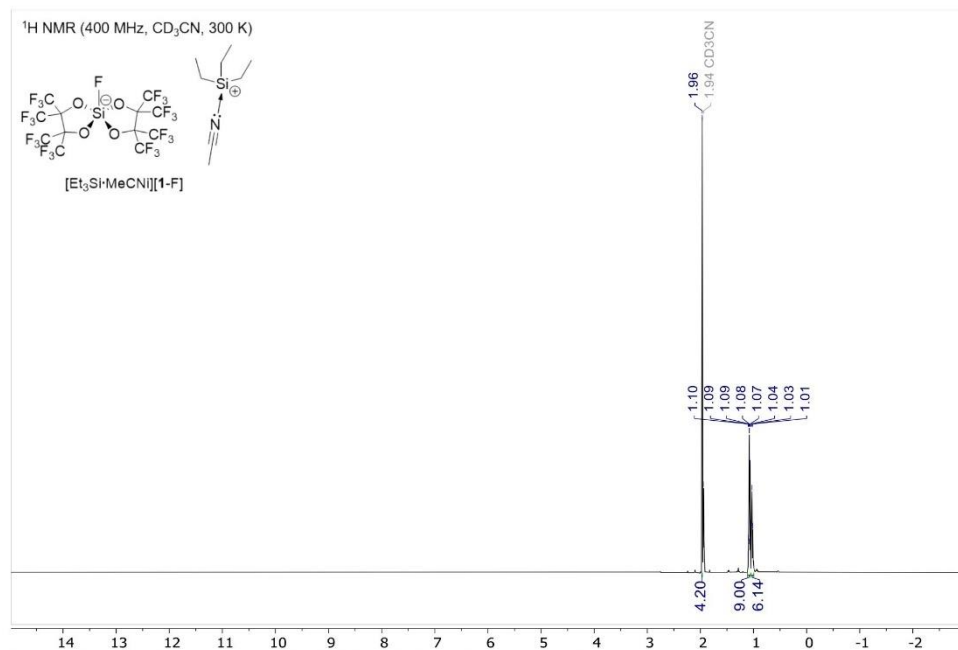
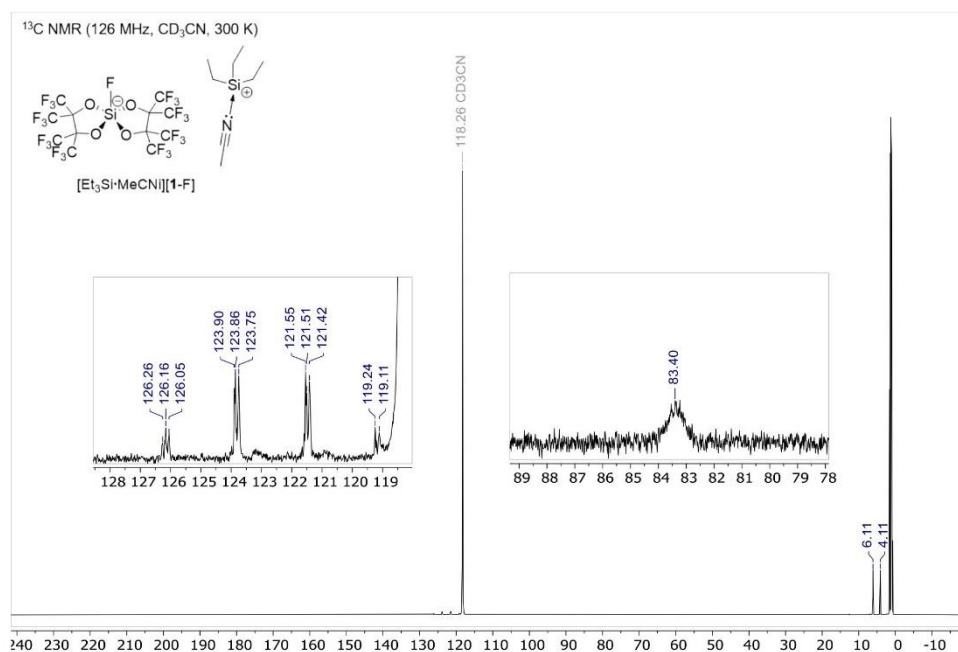
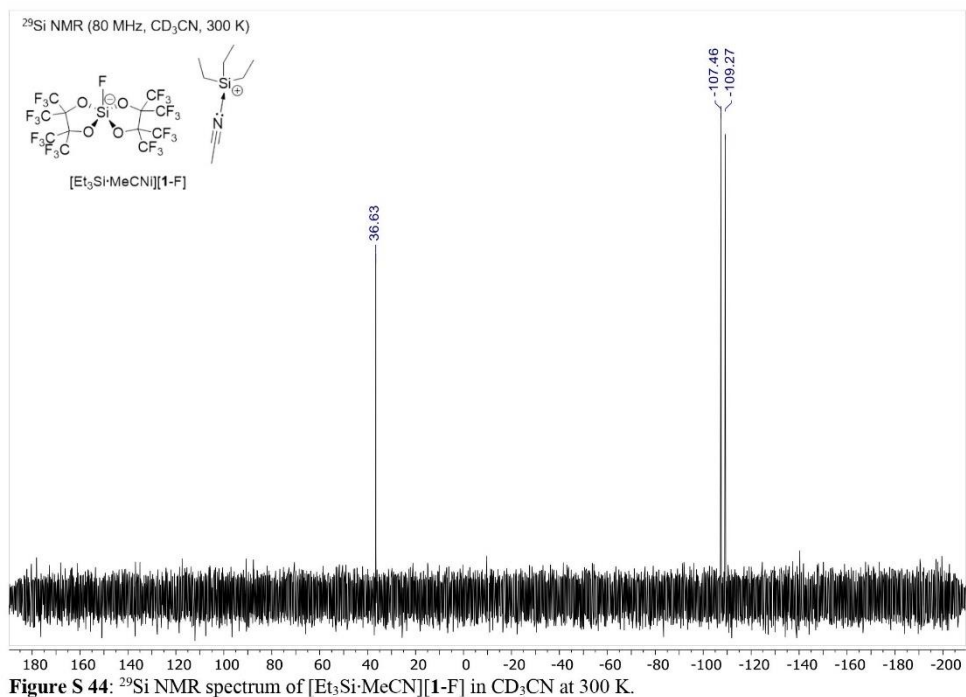
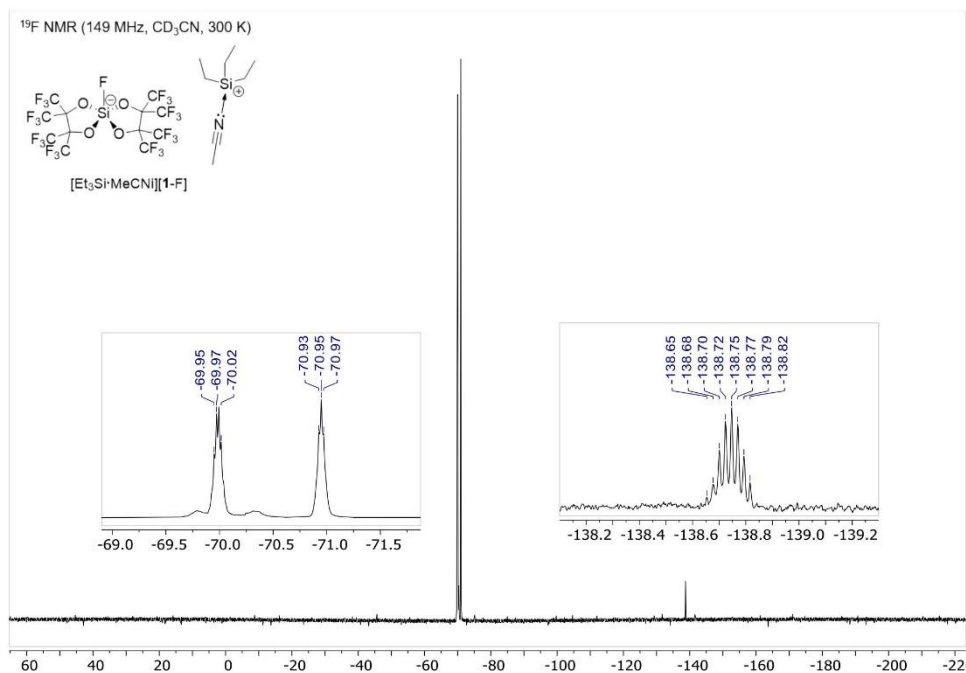


Figure S 40: ²⁹Si NMR spectrum of [K·(18-c-6)][1-F] in CD₃CN at 300 K.

5.6 NMR spectra of $[\text{Et}_3\text{Si-MeCN}][\text{1-F}]$ Figure S 41: ^1H NMR spectrum of $[\text{Et}_3\text{Si-MeCN}][\text{1-F}]$ in CD_3CN at 300 K.Figure S 42: ^{13}C NMR spectrum of $[\text{Et}_3\text{Si-MeCN}][\text{1-F}]$ in CD_3CN at 300 K.



6 References

- [1] Bruker AXS Inc., Madison, Wisconsin, USA, **2015**.
- [2] Bruker AXS Inc., Madison, Wisconsin, USA **2008**.
- [3] G. M. Sheldrick, University of Göttingen, Göttingen, Germany, **2014**.
- [4] C. B. Huebschle, G. M. Sheldrick, B. Dittrich, *J. Appl. Cryst.* **2011**, *44*, 1281.
- [5] G. M. Sheldrick, University of Göttingen, Göttingen, Germany, **1998**.
- [6] A. J. C. Wilson, *International Tables for Crystallography, Vol. C*, Kluwer Academic Publishers, Dordrecht, Netherlands **1992**.
- [7] A. L. Spek, Utrecht University, Utrecht, Netherlands **2010**.
- [8] (a) F. Neese, *Wiley Interdiscip. Rev. Comput. Mol. Sci.* **2012**, *2*, 73-78; (b) F. Neese, *WIREs Computational Molecular Science* **2018**, *8*, e1327.
- [9] (a) J. P. Perdew, K. Burke, M. Ernzerhof, *Phys. Rev. Lett.* **1996**, *77*, 3865-3868; (b) C. Adamo, V. Barone, *J. Chem. Phys.* **1999**, *110*, 6158-6170.
- [10] S. Grimme, J. Antony, S. Ehrlich, H. Krieg, *J. Chem. Phys.* **2010**, *132*, 1-19.
- [11] (a) S. Grimme, S. Ehrlich, L. Goerigk, *J. Comput. Chem.* **2011**, *32*, 1456-1465; (b) E. R. Johnson, A. D. Becke, *J. Chem. Phys.* **2005**, *123*; (c) A. D. Becke, E. R. Johnson, *J. Chem. Phys.* **2005**, *122*, 1-5.
- [12] A. Schafer, C. Huber, R. Ahlrichs, *J. Chem. Phys.* **1994**, *100*, 5829-5835.
- [13] S. Grimme, *Chem-Eur. J.* **2012**, *18*, 9955-9964.
- [14] (a) F. Neese, A. Hansen, D. G. Liakos, *J. Chem. Phys.* **2009**, *131*, 064103; (b) C. Riplinger, F. Neese, *J. Chem. Phys.* **2013**, *138*, 034106; (c) C. Riplinger, B. Sandhoefer, A. Hansen, F. Neese, *J. Chem. Phys.* **2013**, *139*, 134101.
- [15] (a) H. Böhrer, N. Trapp, D. Himmel, M. Schleep, I. Krossing, *Dalton Trans.* **2015**, *44*, 7489-7499; (b) L. O. Müller, D. Himmel, J. Stauffer, G. Steinfeld, J. Slattery, G. Santiso-Quiñones, V. Brecht, I. Krossing, *Angew. Chem. Int. Ed.* **2008**, *47*, 7659-7663.
- [16] (a) P. Erdmann, J. Leitner, J. Schwarz, L. Greb, *ChemPhysChem* **2020**, *21*, 987-994; (b) P. Erdmann, L. Greb, *ChemPhysChem* **2021**, *22*, 935-943.
- [17] S. Kozuch, D. Gruzman, J. M. L. Martin, *J. Phys. Chem. C* **2010**, *114*, 20801-20808.
- [18] K. Eichkorn, O. Treutler, H. Ohm, M. Haser, R. Ahlrichs, *Chem. Phys. Lett.* **1995**, *242*, 652-660.
- [19] F. Neese, F. Wennmohs, A. Hansen, U. Becker, *Chem. Phys.* **2009**, *356*, 98-109.
- [20] K. Eichkorn, F. Weigend, O. Treutler, R. Ahlrichs, *Theor. Chem. Acc.* **1997**, *97*, 119-124.
- [21] E. J. Baerends, T. Ziegler, A. J. Atkins, J. Autschbach, D. Bashford, O. Baseggio, A. Brces, F. M. Bickelhaupt, C. Bo, P. M. Boerritger, L. Cavallo, C. Daul, D. P. Chong, D. V. Chulhai, L. Deng, R. M. Dickson, J. M. Dieterich, D. E. Ellis, M. van Faassen, A. Ghysels, A. Giammona, S. J. A. van Gisbergen, A. Goetz, A. W. Gtz, S. Gusarov, F. E. Harris, P. van den Hoek, Z. Hu, C. R. Jacob, H. Jacobsen, L. Jensen, L. Joubert, J. W. Kaminski, G. van Kessel, C. Knig, F. Kootstra, A. Kovalenko, M. Krykunov, E. van Lenthe, D. A. McCormack, A. Michalak, M. Mitoraj, S. M. Morton, J. Neugebauer, V. P. Nicu, L. Noodleman, V. P. Osinga, S. Patchkovskii, M. Pavanello, C. A. Peeples, P. H. T. Philipsen, D. Post, C. C. Pye, H. Ramanantoanina, P. Ramos, W. Ravenek, J. I. Rodriguez, P. Ros, R. Rger, P. R. T. Schipper, D. Schlus, H. van Schoot, G. Schreckenbach, J. S. Seldenthuis, M. Seth, J. G. Snijders, Sol.
- [22] E. Van Lenthe, E. J. Baerends, *J. Comput. Chem.* **2003**, *24*, 1142-1156.
- [23] (a) F. Eckert, A. Klamt, *Aiche J* **2002**, *48*, 369-385; (b) A. Klamt, M. Diedenhofen, *Journal of Computer-Aided Molecular Design* **2010**, *24*, 357-360; (c) A. Klamt, *J. Phys. Chem.* **1995**, *99*, 2224-2235; (d) A. Klamt, B. Mennucci, J. Tomasi, V. Barone, C. Curutchet, M. Orozco, F. J. Luque, *Acc. Chem. Res.* **2009**, *42*, 489-492.
- [24] M. Bursch, T. Gasevic, J. B. Stückrath, S. Grimme, *Inorg. Chem.* **2021**, *60*, 272-285.

- [25] F. Weigend, *J. Comput. Chem.* **2008**, *29*, 167-175.
- [26] A. V. Marenich, C. J. Cramer, D. G. Truhlar, *J. Phys. Chem. B* **2009**, *113*, 6378-6396.
- [27] M. Mehta, J. M. Goicoechea, *Angew. Chem. Int. Ed.* **2020**, *59*, 2715-2719.
- [28] E. Fritz-Langhals, S. Werge, S. Kneissl, P. Piroutek, *Org. Process Res. Dev.* **2020**, *24*, 1484-1495.
- [29] A. L. Liberman-Martin, R. G. Bergman, T. D. Tilley, *J. Am. Chem. Soc.* **2015**, *137*, 5328-5331.
- [30] S. Rawat, M. Bhandari, V. K. Porwal, S. Singh, *Inorg. Chem.* **2020**, *59*, 7195-7203.
- [31] T. Thorwart, D. Roth, L. Greb, *Chem. Eur. J.*, **2021**, *27*, 10422-10427.
- [32] R. J. Andrews, S. S. Chitnis, D. W. Stephan, *Chem. Commun.* **2019**, *55*, 5599-5602.
- [33] L. Süssé, J. H. W. LaFortune, D. W. Stephan, M. Oestreich, *Organometallics* **2019**, *38*, 712-721.

11.2 Supporting Information Chapter 6

ChemCatChem

Supporting Information

Catalytic Degradation of Aliphatic Ethers using the Lewis Superacidic Bis(perfluoropinacolato)silane

Florian S. Tschernuth, Lukas Bichlmaier, and Shigeyoshi Inoue*

Table of Contents

1	General Methods and Instrumentation	2
2	Synthesis and Characterization.....	4
2.1	Synthesis and characterization of [Et ₃ O][1-OEt]	4
3	Catalytic experiments	9
3.1	NMR characterization of reaction products:	9
3.2	Catalytic degradation experiments	10
3.2.1	Degradation of 1,5-dimethoxypentane	10
3.2.2	Degradation of diglyme	10
3.2.3	Degradation of tetra(ethyleneglycol)dimethylether (TEG-DME)	11
3.2.4	Degradation of poly(ethyleneglycol)dimethylether (PEG-DEM)	18
3.2.5	Degradation of 18-crown-6.....	19
3.3	Investigation of reaction intermediates for 1,5-dimethoxypentane and diglyme degradation.....	21
4	NMR Spectra.....	25
4.1	NMR spectra of [Et ₃ O][1-OEt].....	25
4.2	NMR spectra of catalytic metathesis reactions.....	28
5	References	38

1 General Methods and Instrumentation

Materials and Chemicals

All mentioned reactions were carried out in heat-dried glassware in argon 4.6 atmosphere ($\geq 99.996\%$; Westfalen AG) or in LABstar gloveboxes from MBraun Inertgas-Systeme GmbH. For sealing glass valves Triboflon III PTFE/PEPE grease from Freudenberg & Co. KG was used. Plastic materials like syringes or cannulas were flushed three times with argon prior to use. All chemicals for this project were purchased from the commercial distributors: Merck KGaA (Sigma-Aldrich), ABCR GmbH. Hexafluoropinacol ($\text{H}_2\text{pin}^{\text{F}}$) was purchased from Sigma-Aldrich and ABCR GmbH and dried with molecular sieves (4 Å) in Et_2O , giving an etheric solution with 80 – 88 w% of $\text{H}_2\text{pin}^{\text{F}}$. $\text{Si}(\text{pin}^{\text{F}})_2 \cdot \text{MeCN}$ (1·MeCN) was synthesized according to literature procedures.^[1] Safety note: The use of directly dried, Et_2O -free $\text{H}_2\text{pin}^{\text{F}}$ in one lithiation experiment resulted in an explosion in the glovebox when the product was scraped from the glass wall with a spatula.

Analytcs

All NMR samples were prepared in J-Young PTFE valve NMR tubes in an argon (4.6) atmosphere. The recorded ^1H , ^{13}C , ^{19}F and ^{29}Si NMR spectra were obtained from a Bruker Avance Neo 400 MHz spectrometer and a Bruker AV500C spectrometer at ambient temperatures (300 K), unless otherwise stated. The obtained ^1H - and ^{13}C -NMR spectra were calibrated on the residual proton and natural abundance carbon signals of deuterated NMR solvents. The observed signals were abbreviated as following: s = singlet, br = broad signal and combinations, d = doublet, t = triplet, q = quartet, m = multiplet and qm = quartet of multiplets. The spectra were processed and analyzed with MestReNova software (version 12.0.1-20560).

Elemental Analysis (CHNS) was carried out by the central analytics laboratory of the TUM Catalysis Research Center. For the procedure 0.5 – 1.0 mg of the investigated compounds were closely packed within two layers of tin foil under an argon atmosphere and subsequently handed to the elemental analysis team. The Analysis was performed on a EURO EA (HEKAtech) instrument equipped with a CHNS combustion analyzer. Due to high F-content, the formation of CF_4 hampers an accurate detection of the N-content.

Melting Points (m.p.) were determined in wax-sealed capillaries under argon atmosphere with the Büchi B-540 apparatus. #

Electron Spray Ionization Mass Spectroscopy (ESI MS) was performed with an Exactive Plus Orbitrap system from Thermo Fisher Scientific equipped with an ESI source.

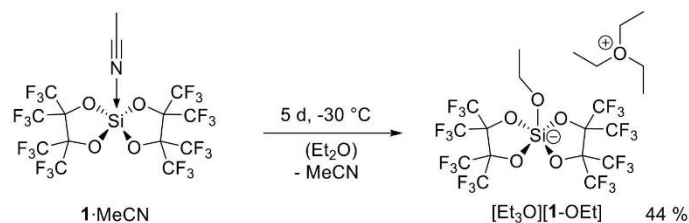
The X-ray intensity data were collected on an X-ray single crystal diffractometer equipped with a CMOS detector (Bruker Photon-100), a rotating anode (Bruker TXS) with MoK_α radiation ($\lambda = 0.71073 \text{ \AA}$) and a Helios mirror optic by using the APEX III software package^[2] or an X-ray single crystal diffractometer equipped with a CMOS detector (Bruker Photon-100), an IMS microsource with MoK_α radiation ($\lambda = 0.71073 \text{ \AA}$) and a Helios mirror optic by using the APEX III software package.^[2] The measurement was performed on single crystals coated with perfluorinated ether. The crystal was fixed on the top of a microsampler, transferred to the diffractometer and measured under a stream of cold nitrogen. A matrix scan was used to determine the initial lattice parameters. Reflections were merged and corrected for Lorentz and polarization effects, scan speed, and background using SAINT.^[3] Absorption corrections, including odd and even ordered spherical harmonics were performed using SADABS.^[3] Space group assignments were based upon systematic absences, E statistics, and successful refinement of the structures. Structures were solved by direct methods with the aid of successive difference Fourier maps, and were refined against all data using the APEX III software^[2] in conjunction with SHELXL-2014^[4] and SHELXL.^[5] Methyl hydrogen atoms were refined as part of rigid rotating groups, with a C–H distance of 0.98 \AA and $\text{Uiso}(\text{H}) = 1.5 \cdot \text{Ueq}(\text{C})$. Other H atoms were placed in calculated positions and refined using a riding model, with methylene and

S2

aromatic C–H distances of 0.99 and 0.95 Å, respectively, and $U_{iso}(H) = 1.2 \cdot U_{eq}(C)$. If not mentioned otherwise, non-hydrogen atoms were refined with anisotropic displacement parameters. Full-matrix least-squares refinements were carried out by minimizing $\Delta w(F_o^2 - F_c^2)^2$ with SHELXL-97^[6] weighting scheme. Neutral atom scattering factors for all atoms and anomalous dispersion corrections for the non-hydrogen atoms were taken from International Tables for Crystallography.^[7] Images of the crystal structures were generated by PLATON and MERCURY.^[8] The CCDC number 2241855 contains the supplementary crystallographic data for the structure [MeCN-Et][1-OEt]. These data can be obtained free of charge from the Cambridge Crystallographic Data Centre *via* <https://www.ccdc.cam.ac.uk/structures/>.

2 Synthesis and Characterization

2.1 Synthesis and characterization of [Et₃O][1-OEt]



In a screwcap reaction vessel 80.0 mg **1**-MeCN (109 μmol , 1.00 equiv.) were dissolved in 1.3 ml Et₂O (1.25 μmol , 11.5 equiv.). The reaction mixture was kept at room temperature for 24 h and afterwards stored at -30 °C for 5 days. A colorless precipitate was formed that was collected by filtration, washed three times with 1.0 ml hexane and dried in vacuum. A colorless solid was obtained in 44 % yield.

The subsequent ¹H NMR analysis showed the characteristic pattern of the triethyloxonium cation, that however changed to Et₂O and *N*-ethyl substituted acetonitrilium [CD₃CN-Et]⁺ species only 3 h at room temperature after the addition of NMR solvent CD₃CN. The pattern assigned to the respective pentavalent silicate anion [1-OEt]⁻ did not change during this reaction.

Crystallization from a saturated Et₂O/MeCN solution gave the structure of [MeCN-Et][1-OEt]. For SC-XRD structure see Figure S 3.

m.p.: 97.5 – 110.2 °C.

¹H-NMR (500 MHz, acetonitrile-*d*₃) δ (ppm) = 4.65 (q, ³*J*_{C-H} = 7.1 Hz, 6H, O(CH₂CH₃)₃), 3.71 (q, ³*J*_{C-H} = 7.0 Hz, 2H, SiOCH₂CH₃), 1.51 (t, ³*J*_{C-H} = 7.1 Hz, 9H, O(CH₂CH₃)₃), 1.05 (t, ³*J*_{C-H} = 7.0 Hz, 3H, SiOCH₂CH₃).

¹³C NMR (126 MHz, acetonitrile-*d*₃) δ (ppm) = 122.82 (qm, ¹*J*_{C-F} = 293.1 Hz), 84.81 (s, O(CH₂CH₃)₃), 83.77 (br, OC(CF₃)₂), 59.64 (s, SiOCH₂CH₃), 17.92 (s, SiOCH₂CH₃), 12.56 (s, O(CH₂CH₃)₃).

¹⁹F NMR (471 MHz, acetonitrile-*d*₃) δ (ppm) = -69.69 – -70.02 (m, 12F, CF₃), -70.18 – -70.37 (m, 12F, CF₃).

²⁹Si NMR (99 MHz, acetonitrile-*d*₃) δ (ppm) = -106.61(*Si*).

Elemental Analysis calcd. [%] for C₂₀H₂₀F₂₄O₄Si: C (28.58), H (2.40), N (-), S (-); found (%): C (28,90), H (2.20), N (0.50), S (-).

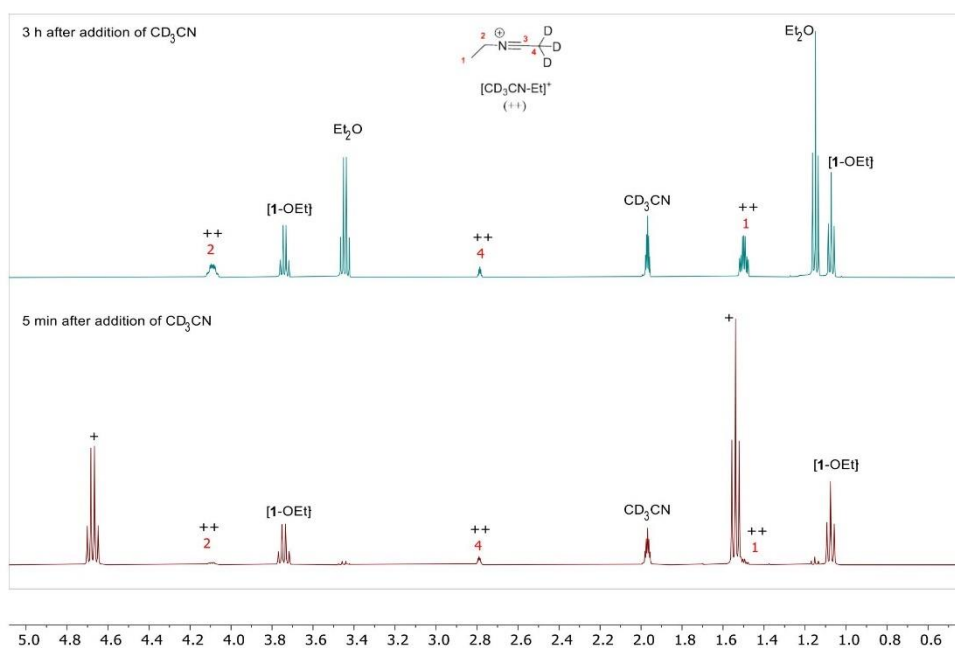


Figure S 1: Stacked ^1H NMR spectra of the reaction of the reaction product $[\text{Et}_3\text{O}][\mathbf{1-OEt}]$ in CD_3CN . After 5 min the triethyloxonium cation (+) is prevalent, whereas after 3 h the nearly quantitative formation of the *N*-ethyl acetonitrilium- d_3 ion (++) is observed. The signals for “+” and “++” align with pattern found in the literature.^[9]

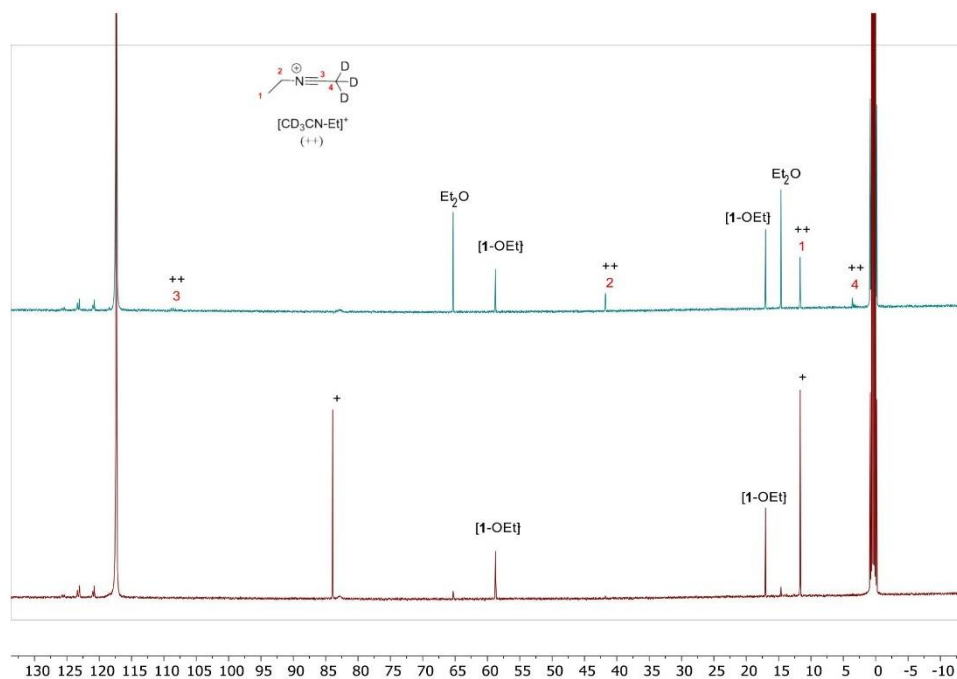


Figure S 2: Stacked ^{13}C NMR spectra of the reaction of the reaction product $[\text{Et}_3\text{O}][\text{1-OEt}]$ in CD_3CN . After 5 min the triethyloxonium cation (+) is prevalent, whereas after 3 h the nearly quantitative formation of the *N*-ethyl acetonitrilium- d_3 ion (++) is observed.

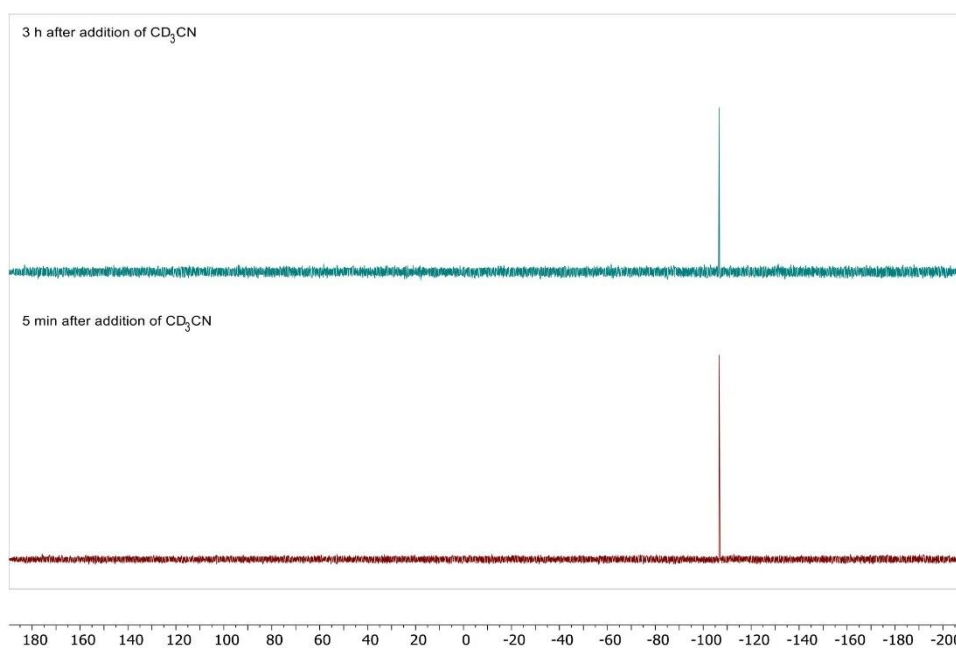


Figure S 3: Stacked ^{29}Si NMR spectra of the reaction of the reaction product $[\text{Et}_3\text{O}][\mathbf{1-OEt}]$ in CD_3CN after 5 min and 3 h at room temperature. The spectra show the unchanged presence of the ethoxy substituted silicate anion $[\mathbf{1-OEt}]^-$.

XRD-structure

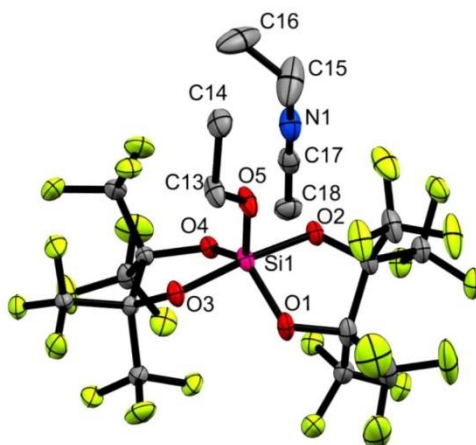


Figure S 4: Molecular structure of $[\text{MeCN-Et}][\mathbf{1-OEt}]$ with translational ellipsoids plotted at 50% probability level. Hydrogen atoms are omitted for clarity. Selected bond lengths [Å] and angles [deg]: Si1–O5 1.6210(19), Si1–O1

1.7165(19), Si1–O2 1.7613(19), Si1–O3 1.7529(19), Si1–O4 1.7070(19), O5–C13 1.429(4), N1–C15 1.446(4), N1–C17 1.124(4); O1–Si1–O4 124.54(9), O2–Si1–O3 170.95(9), C18–C17–N1 179.0(3).

Table S 1: Crystal data and structure refinement for compound [MeCN-Et][1-OEt].

Chemical formula	C ₁₈ H ₁₃ F ₂₄ N O ₅ Si		
CCDC Database number	2241855		
Formula weight	807.38 g/mol		
Temperature	100(2) K		
Wavelength	0.71073 Å		
Crystal size	0.256 × 0.202 × 0.117 mm		
Crystal habit	clear colorless fragment		
Crystal system	monoclinic		
Space group	P 21/n		
Unit cell dimensions	a = 8.4656(6) Å	α = 90°	
	b = 33.566(2) Å	β = 110.070(2)°	
	c = 9.7724(7) Å	γ = 90°	
Volume	2549.9(6) Å ³		
Z	4		
Density (calculated)	2.056 g/cm ³		
Absorption coefficient μ	0.298 mm ⁻¹		
F(000)	1592		
Diffractometer	Bruker Photon CMOS		
Radiation source	IMS microsource, MoKα		
Theta range for data collection	2.30 to 25.34°		
Index ranges	-10 ≤ h ≤ 9, -40 ≤ k ≤ 40, -11 ≤ l ≤ 11		
Reflections collected	51444		
Independent reflections	4775		
Absorption correction	multi-scan		
Max. and min. transmission	0.7452 and 0.7100		
Refinement method	Full-matrix least-squares on F ²		
Function minimized	Σ w(F _o ² - F _c ²) ²		
Data / restraints / parameters	4775 / 0 / 445		
Goodness-of-fit on F²	1.009		
Final R indices	I > 2σ(I) R1 = 0.0389, wR2 = 0.0961		
	all data R1 = 0.0482, wR2 = 0.1025		
Largest diff. peak and hole	0.400 and -0.419 eÅ ⁻³		
R.M.S. deviation	0.059 eÅ ⁻³		

3 Catalytic experiments

3.1 NMR characterization of reaction products:

Dimethylether



$^1\text{H NMR}$ (400 MHz, CDCl_3) δ (ppm) = 3.31 (s, 6H, CH_3).

$^{13}\text{C NMR}$ (101 MHz, CDCl_3) δ (ppm) = 60.61 (CH_3).

The found NMR shifts are slightly shifted but still correspond to reported signals in dichloromethane- d_2 literature findings.^[10]

Tetrahydropyran



$^1\text{H NMR}$ (400 MHz, CDCl_3) δ (ppm) = 3.65 (t, $^3J = 5.2$ Hz, 4H, αCH_2), 1.69 – 1.60 (m, 2H, βCH_2), 1.60 – 1.53 (m, 4H, γCH_2).

$^{13}\text{C NMR}$ (101 MHz, CDCl_3) δ (ppm) = 68.86 (αCH_2), 26.69 (βCH_2), 23.55 (γCH_2).

The found NMR shifts are slightly shifted but still align with literature findings.^[11]

1,4-Dioxane



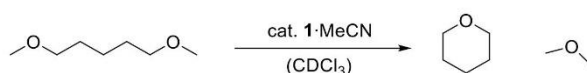
$^1\text{H NMR}$ (400 MHz, CDCl_3) δ (ppm) = 3.68 (s, 8H, OCH_2).

$^{13}\text{C NMR}$ (101 MHz, CDCl_3) δ (ppm) = 67.20 (OCH_2).

The found NMR shifts are slightly shifted but still align with literature findings.^[12]

3.2 Catalytic degradation experiments

3.2.1 Degradation of 1,5-dimethoxypentane

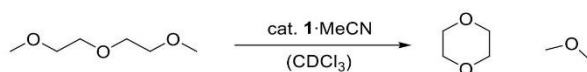


For reactions with 5 mol% of catalyst **1-MeCN** (2.50 mg, 3.20 μmol , 0.05 equiv.) 10.0 μl of 1,5-dimethoxypentane (8.42 mg, 63.7 μmol , 1.00 equiv.) were used; For reactions with 1 mol% of the catalyst (1.03 mg, 1.40 μmol , 0.01 equiv.) 22.0 μl of 1,5-dimethoxypentane (18.5 mg, 140 μmol , 1.00 equiv.) were used.

Table S 2: Conditions of the degradation experiments of 1,5-dimethoxypentane. Product yield was calculated by integration of the $^1\text{CH}_2$ -signal with respect to the initial reactant amount. The conversion was traced by the consumption of the MeO-singlet. Mesitylene was used as an internal standard.

Sample	Cat. [mol%]	Temp. [°C]	Time [h]	Conversion [%]	Yield [%]
blind	-	80	18	0	0
I	1	80	2	70	69
I	1	80	20	99	97
II	5	80	1	99	96
III	5	25	20	16	15
III	5	25	72	42	40
III	5	25	120	72	70
III	5	25	168	97	95

3.2.2 Degradation of diglyme

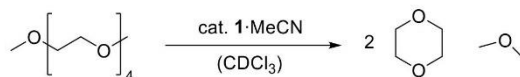


For the degradation experiments with 1 mol% (1.03 mg, 1.41 μmol , 0.01 equiv.) of catalyst **1-MeCN**, 20.0 μl (15.2 mg, 141 μmol , 1.00 equiv.) of diglyme were used. For catalyst loadings of 5 mol% (3.86 mg, 5.27 μmol , 0.05 equiv.) and 10 mol% (7.73 mg, 10.5 μmol , 0.10 equiv.) 15 μl (14.1 mg, 105 μmol , 1.00 equiv.) of diglyme were used.

Table S 3: Conditions of the degradation experiments of diglyme. Product yield was calculated by integration of the dioxane-singlet with respect to the initial reactant amount. The conversion was traced by the consumption of the CH_2 -multiplet at $\delta = 3.54$ ppm. Mesitylene was used as an internal standard.

Sample	Cat. [mol%]	Temp. [°C]	Time [h]	Conversion [%]	Yield [%]
blind	-	80	18	0	0
I	1	80	2	50	49
I	1	80	20	98	96
II	5	80	2.5	98	96
III	10	25	18	68	65
III	10	25	96	96	90

3.2.3 Degradation of tetra(ethyleneglycol)dimethylether (TEG-DME)



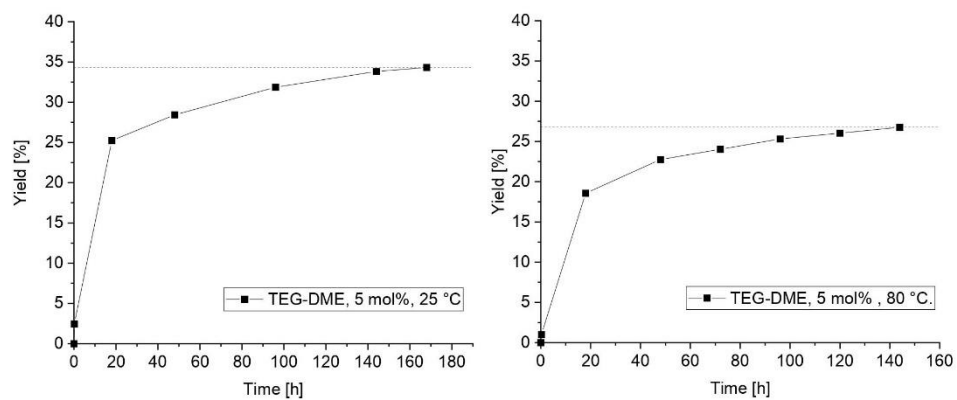
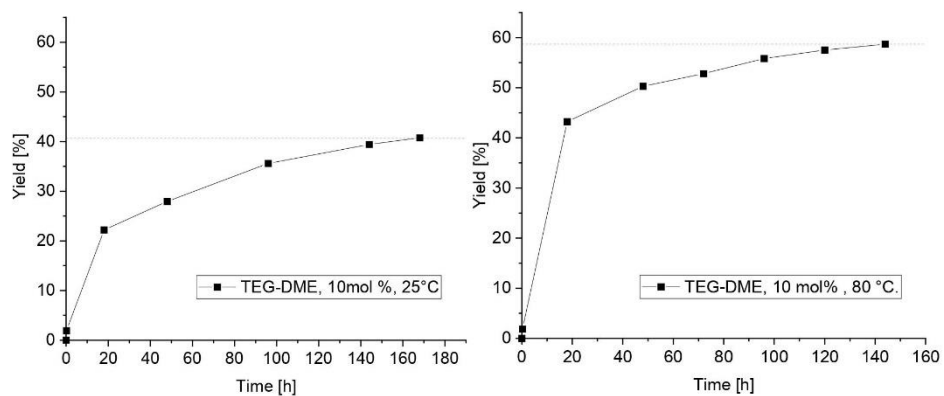
For the degradation experiments 15.0 μl (15.2 mg, 68.2 μmol , 1.00 equiv.) TEG-DME were reacted with 5 mol% (2.50 mg, 3.41 μmol , 0.05 equiv.), 10 mol% (5.00 mg, 6.82 μmol , 0.10 equiv.) and 20 mol% (7.50 mg, 13.6 μmol , 0.20 equiv.) of catalyst **1**·MeCN, respectively.

Table S 4: Conditions of TEG-DME degradation. Product yield was calculated by integration of the dioxane-singlet with respect to the initial reactant amount. The conversion was traced by the consumption of the signal at $\delta = 3.64$ ppm. Mesitylene was used as an internal standard.

Sample	Cat. [mol%]	Temp. [°C]	Time [h]	Conversion [%]	Yield [%]
blind	-	80	18	0	0
I	5	80	18	27	19
I	5	80	72	37	24
I	5	80	120	42	26
II	5	25	18	34	25
II	5	25	96	44	32
II	5	25	168	48	34
III	10	80	18	66	43
III	10	80	72	73	53
III	10	80	120	77	58
IV	10	25	18	33	22
IV	10	25	96	50	36
IV	10	25	168	57	41
V	20	80	18	91	70
V	20	80	48	98	75

To further trace the reaction progress two samples with 5 mol% and 10 mol% of **1**·MeCN were analyzed over the course of 6 days at 25 °C and 80 °C, respectively. The obtained yield-plots show a rapid deactivation of catalyst performance after the first hours of the reaction that is even more pronounced for at elevated temperatures.

Plots of the reaction yield:

**Figure S 5:** Reaction yields for the degradation of TEG-DME with 5 mol% of 1-McCN at room temperature and 80 °C.**Figure S 6:** Reaction yields for the degradation of TEG-DME with 10 mol% of 1-McCN at room temperature and 80 °C.

Stacks of corresponding ^1H NMR spectra:

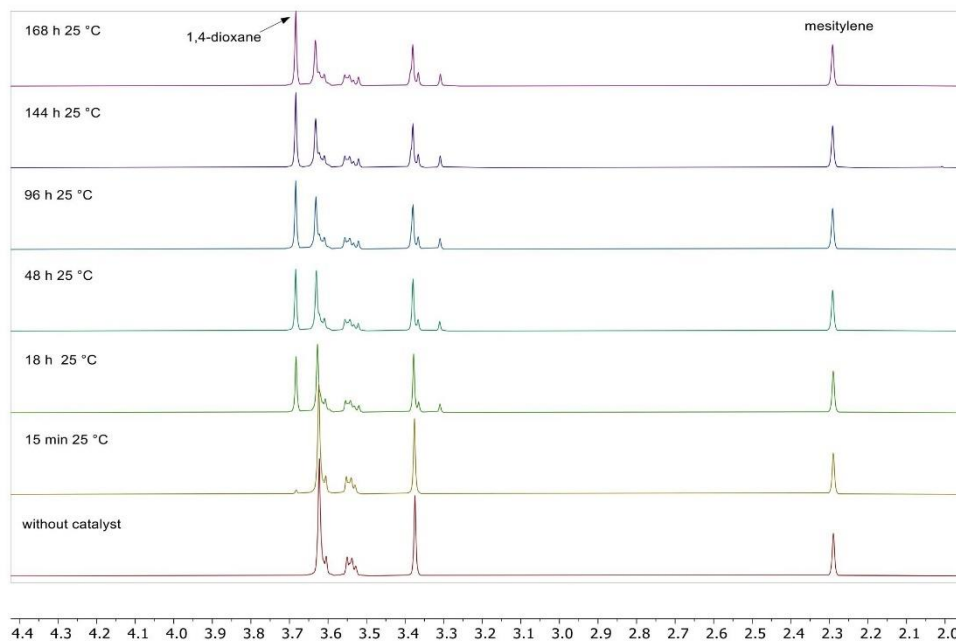


Figure S 7: Stacked ^1H NMR spectra for the degradation experiment of TEG-DME with 5 mol% of catalyst **1**·MeCN at 25 °C monitored over a period of 168 hours.

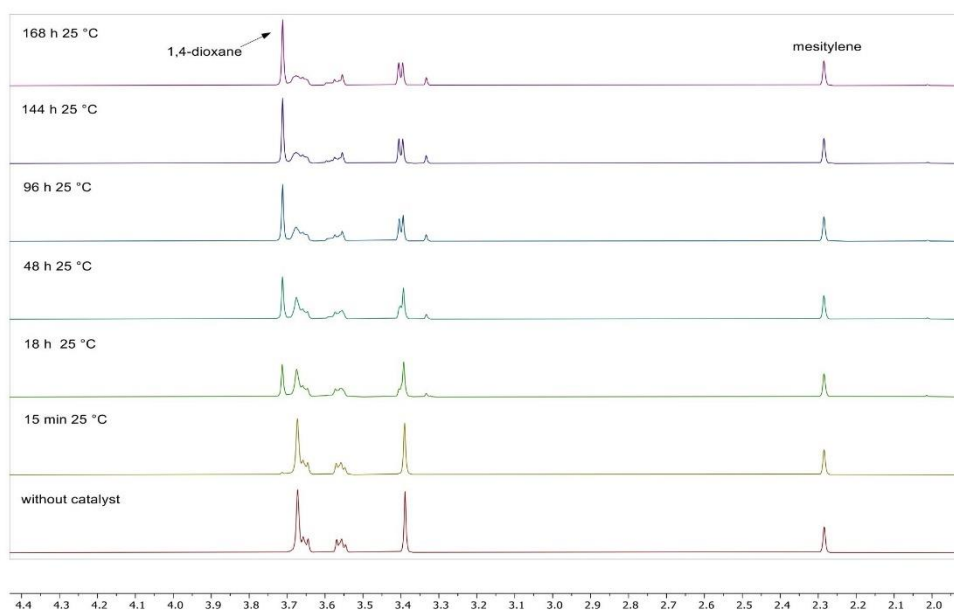


Figure S 8: Stacked ^1H NMR spectra for the degradation experiment of TEG-DME with 10 mol% of catalyst 1-McCN at 25 °C monitored over a period of 168 hours.

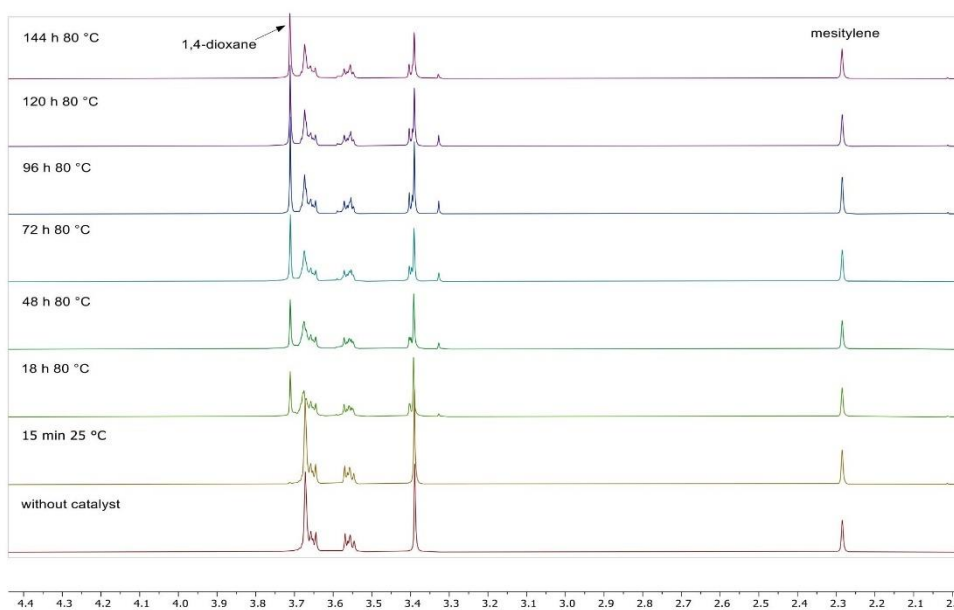


Figure S 9: Stacked ^1H NMR spectra for the degradation experiment of TEG-DME with 5 mol% of catalyst 1-McCN at 80 °C monitored over a period of 144 hours.

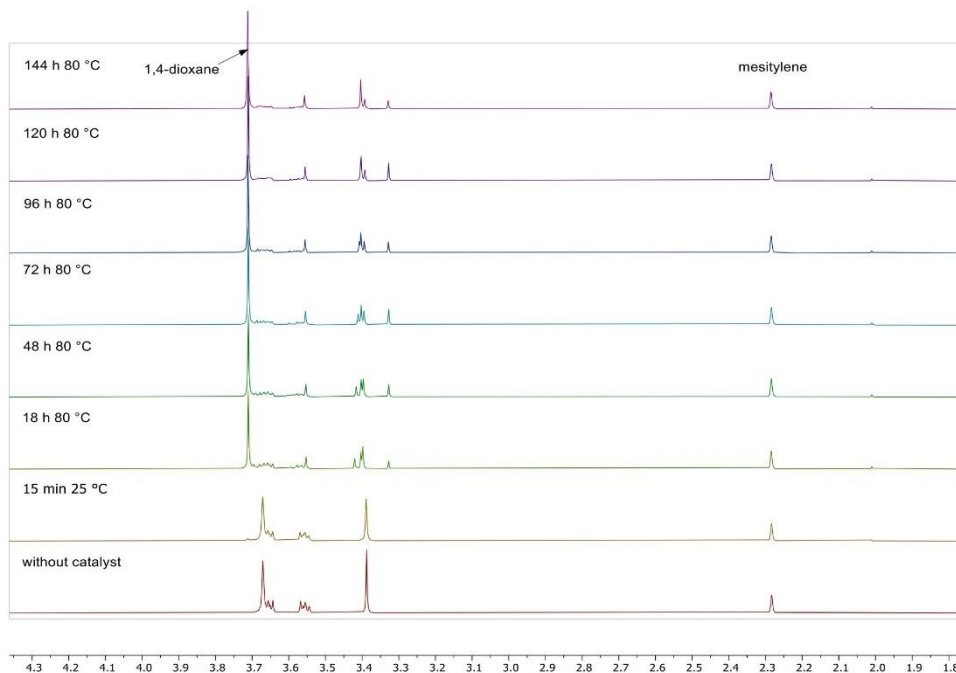


Figure S 10: Stacked ^1H NMR spectra for the degradation experiment of TEG-DME with 10 mol% of catalyst $1\cdot\text{MeCN}$ at $80\text{ }^\circ\text{C}$ monitored over a period of 144 hours.

Analysis of a potential reaction equilibrium:

To further investigate if the reaction progress could be affected by the adjustment of an equilibrium between the substrate and the reaction product 1,4-dioxane, an additional sample was prepared using $15.0\ \mu\text{l}$ TEG-DME ($15.0\ \text{mg}$, $68.2\ \mu\text{mol}$, $1.00\ \text{equiv.}$) and $5\ \text{mol\%}$ of $1\cdot\text{MeCN}$ ($2.50\ \text{mg}$, $3.41\ \mu\text{mol}$, $0.05\ \text{equiv.}$). Mesitylene was used as an internal standard. The sample was stored at $25\text{ }^\circ\text{C}$ and analyzed over the course of 4 days. After 96 h additional $11.7\ \mu\text{l}$ 1,4-dioxane ($12.0\ \text{mg}$, $136\ \mu\text{mol}$, $2.00\ \text{equiv.}$) were added to the reaction solution and the obtained sample was analyzed after 2 h, 24 h and 48 h at $25\text{ }^\circ\text{C}$. No significant difference could be observed, when compared to degradation experiments without the additional 1,4-dioxane. Consequently, the adjustment of a reaction equilibrium cannot explain the loss of catalytic activity for TEG-DME.

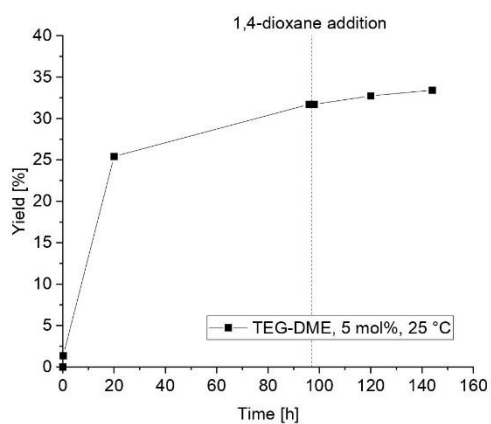


Figure S 11: Reaction yields for the degradation of TEG-DME with 5 mol% of 1-McCN at room temperature. Additional 1,4-dioxane was added after 96 h.

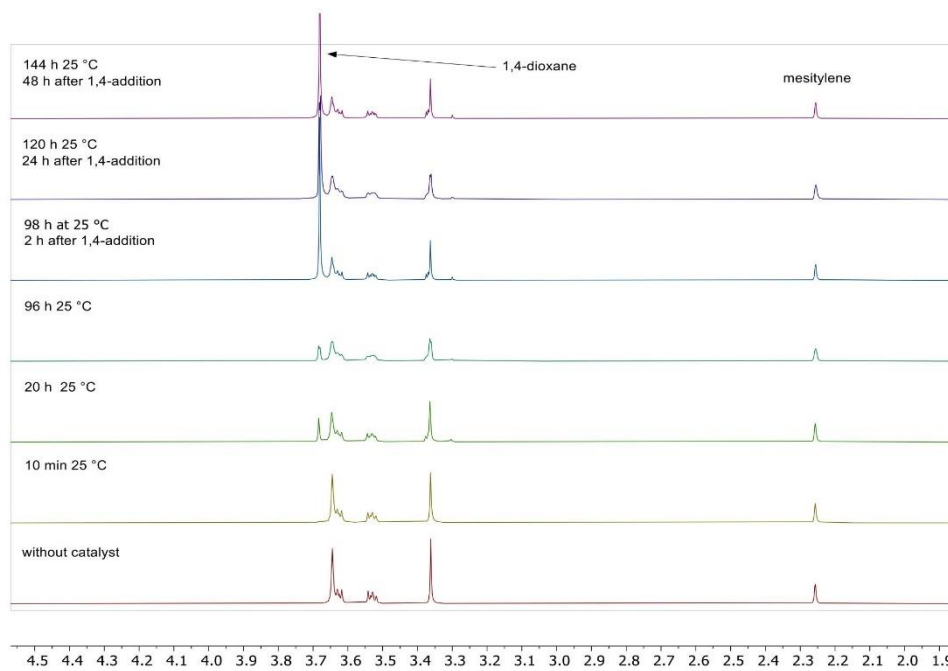


Figure S 12: Stacked ^1H NMR spectra for the degradation experiment of TEG-DME with 5 mol% of catalyst 1-McCN at 25 °C and additional 1,4-dioxane added after 96 h, monitored over a period of 144 hours.

ESI MS analysis of the reaction solution:

To further investigate the formation of side-products during TEG-DME degradation, the reaction solution of an experiment with 5 mol% catalyst loading was analyzed by ESI-MS after 168 h at 25 °C. The main reaction products 1,4-dioxane and Me₂O are not visible in this spectrum because their molecular masses of 88.11 g/mol and 46.07 g/mol were beyond the limits of the analyzer. The spectrum contained several peaks in the m/z range of 250 to 550 with predominant m/z differences of 44.03, which can be assigned to CH₂CH₂O units (half of 1,4-dioxane). No formation of higher molecular weight polymers could be observed.

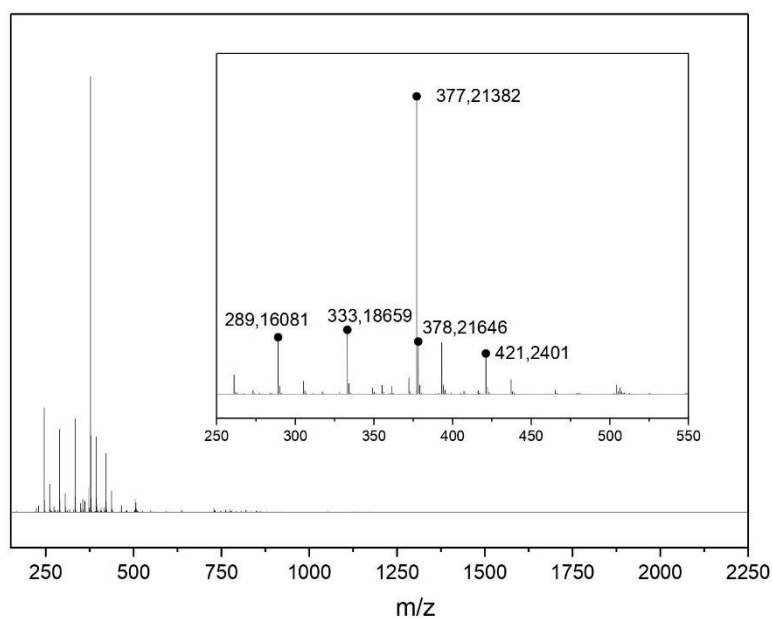
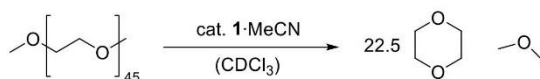


Figure S 13: ESI-MS spectrum of TEG-DME degradation with 5 mol% of 1-McCN after 168 h at 25 °C.

3.2.4 Degradation of poly(ethyleneglycol)dimethylether (PEG-DEM)



The polyether degradation experiments were performed with 15 mg (7.48 μmol , 1.00 equiv.) of PEG-DME and 60 mol% (3.29 mg, 4.49 μmol , 0.60 equiv.) or 225 mol% (12.3 mg, 16.8 μmol , 2.25 equiv.) of catalyst 1-MeCN. In both cases the formation of a dark precipitate was observed during the reaction which was more pronounced for higher catalyst loadings.

Table S 5: Conditions of the degradation PEG-DME. Product yield was calculated by integration of the dioxane-singlet with respect to the initial reactant amount. The conversion was traced by the consumption of the signal at $\delta = 3.64$ ppm. Mesitylene was used as an internal standard.

Sample	Cat. [mol%]	Temp. [°C]	Time [h]	Conversion [%]	Yield [%]
blind	-	80	18	0	0
I	60	80	18	38	30
II	225	80	18	95	87

ESI MS analysis of the reaction solution:

For investigation of potential polymeric side-products during PEG-DME degradation, the reaction solution of an experiment with 225 mol% catalyst loading was analyzed by ESI-MS after 18 h at 80 °C. Due to instrumental limitations the main reaction products 1,4-dioxane and Me_2O (88.11 g/mol and 46.07 g/mol) could not be observed. The reaction solution contained solid residues, which were attributed to catalyst decomposition and removed by filtration prior to measurement. The spectrum of the reaction solution obtained several oligomeric side-products in the m/z range of 250 to 1000 with predominant mass differences of 44.03 m/z that could be assigned to the expected $\text{CH}_2\text{CH}_2\text{O}$ units (half of a dioxane unit). No formation of higher molecular weight polymers could be observed.

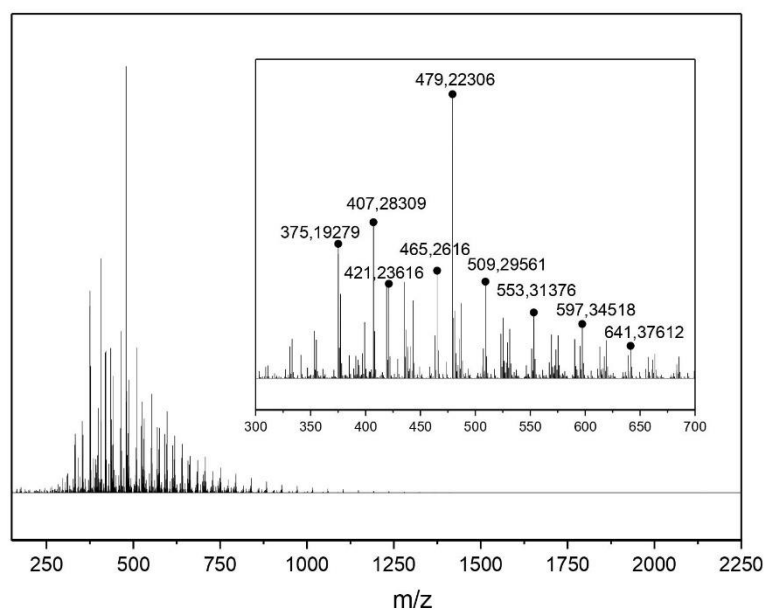
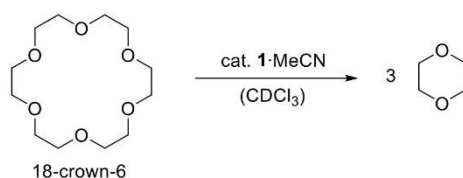


Figure S 14: ESI-MS spectrum of PEG-DME degradation with 225 mol% of **1**-MeCN after 18 h at 80 °C.

3.2.5 Degradation of 18-crown-6



Crown ether degradation experiments were performed with 15 mg 18-crown-6 (56.8 μmol , 1.00 equiv.) and 20 mol% (8.32 mg, 11.4 μmol , 0.20 equiv.), respectively, 30 mol% (12.5 mg, 17.0 μmol , 0.30 equiv.) of catalyst **1**-MeCN. In all cases the formation of a dark precipitation was observed during the reaction which was more pronounced for higher catalyst loadings.

Table S 6: Degradation of 18-crown-6. Product yield was calculated by integration of the dioxane-singlet with respect to the initial reactant amount. The conversion was traced by the consumption of the reactant signal. Mesitylene was used as an internal standard.

Sample	Cat. [mol%]	Temp. [°C]	Time [h]	Conversion [%]	Yield [%]
blind	-	80	18	0	0
I	20	80	3.5	40	34

I	20	80	18	45	39
I	20	80	42	47	40
II	30	80	6	99	93
III	30	25	2	40	35
III	30	25	6	44	38
III	30	25	22	73	64
III	30	25	30	97	88

3.3 Investigation of reaction intermediates for 1,5-dimethoxypentane and diglyme degradation

1,5-Dimethoxypentane

To further investigate the potential reaction intermediates a degradation experiment of 1,5-dimethoxypentane (30.0 μl , 191 μmol , 1.00 equiv.) with 10 mol% of catalyst **1**·MeCN (14.0 mg, 19.1 μmol , 0.10 equiv.) was performed in CD_3CN for reasons of better solubility. Mesitylene was used as internal standard. The sample was heated for 20 min at 80 °C and afterwards analyzed by ^1H and ^{29}Si NMR spectroscopy. No product formation was detected in the ^1H NMR spectrum. The ^{29}Si NMR spectrum gave a singlet at $\delta = -105.4$ ppm that would fit in the range of the expected pentavalent alkoxy silicate species. However, no substrate conversion was detected in the ^1H NMR spectrum, questioning the result. The same sample was then heated for 20 h at 80 °C and again analyzed, still showing no product formation. This indicated that in acetonitrile, no degradation of 1,5-dimethoxypentane occurred. Therefore, the observed signal is more likely to originate from a coordination complex formed between the Lewis acid and 1,5-dimethoxypentane.

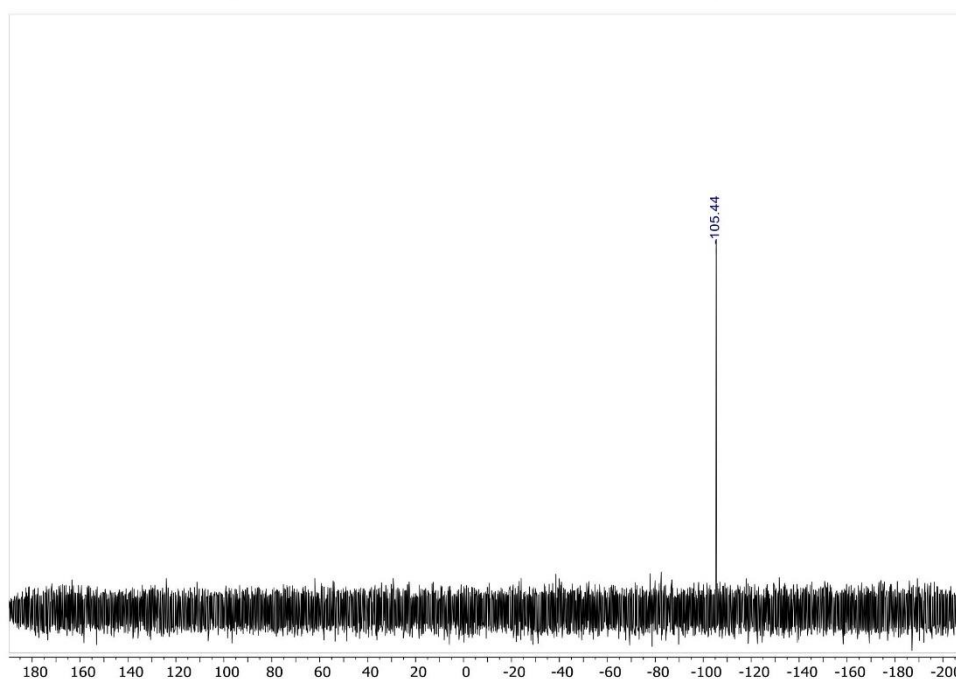


Figure S 15: ^{29}Si NMR spectrum of the degradation experiment of 1,5-dimethoxypentane and 10 mol% catalyst **1**·MeCN in CD_3CN after 20 min at 80 °C.

To gain further insights another attempt was made using a more diluted solution of 1,5-dimethoxypentane (15.0 μl , 95.5 μmol , 1.00 equiv.) and **1**·MeCN (7.00 mg, 9.55 μmol , 0.10 equiv.) in CDCl_3 . Because of the previously observed high reaction speed, this sample was only treated for 5 min at 80 °C and subsequently analyzed by ^{29}Si NMR with an increased number of scans. In this case the spectrum gave a singlet at $\delta = -106.2$ ppm which aligns well with the chemical shift of a pentavalent silicate anion.

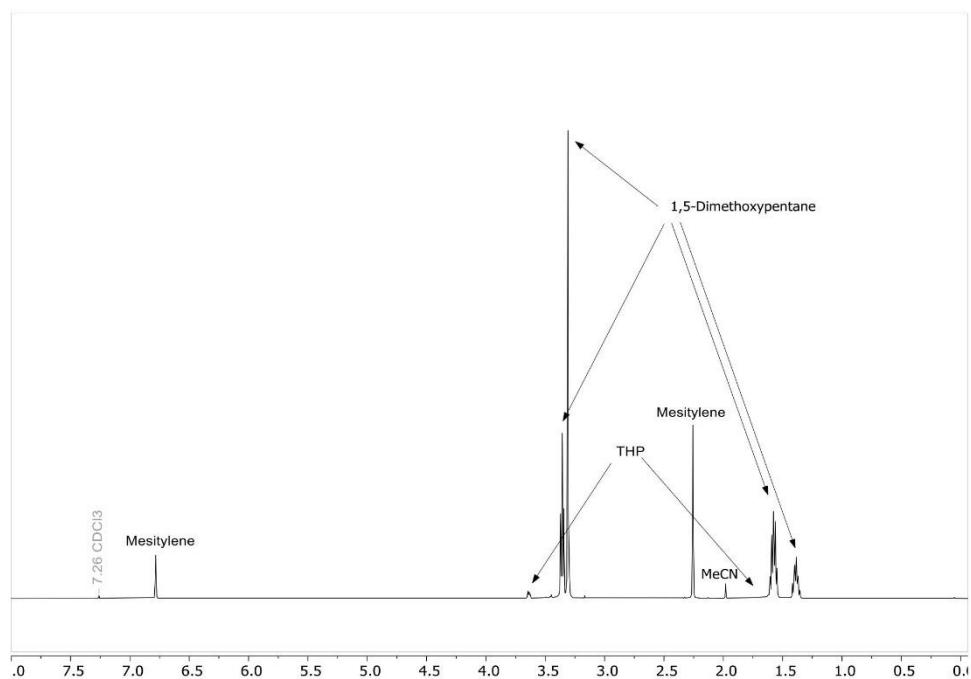


Figure S 16: ¹H NMR spectrum of the degradation experiment of 1,5-dimethoxypentane and 10 mol% of catalyst 1·MeCN in CDCl₃ after 5 min at 80 °C, showing the partial formation of tetrahydropyran (THP).

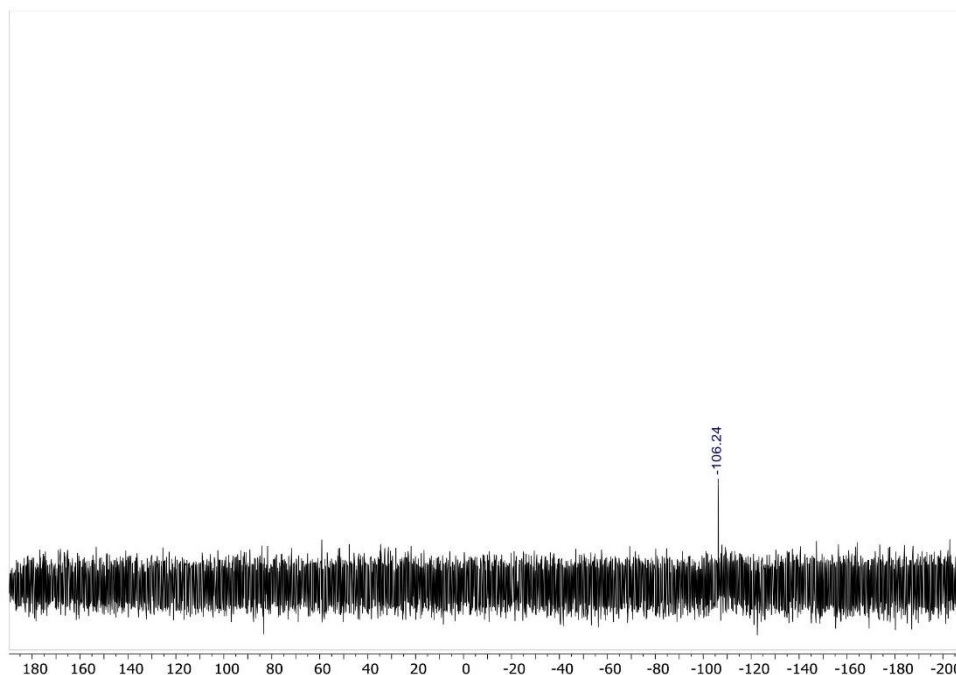


Figure S 17: ^{29}Si NMR spectrum of the degradation experiment of 1,5-dimethoxypentane and 10 mol% catalyst **1**·MeCN in CDCl_3 after 5 min at 80 °C.

Diglyme

Also in this case, a degradation reaction was performed by dissolving diglyme (30.0 μl , 211 μmol , 1.00 equiv.) and **1**·MeCN (15.5 mg, 21.1 mmol, 0.10 equiv.) in 0.4 ml of CD_3CN . Mesitylene was used as internal standard. The sample was heated for 20 min at 80 °C and afterwards analyzed by ^1H and ^{29}Si NMR spectroscopy. The ^1H NMR spectrum showed the partial formation of 1,4-dioxane.^[12] Interestingly in this case the ^{29}Si NMR spectrum gave two signals at $\delta = -105.4$ ppm and $\delta = -106.4$ ppm. The latter signal precisely met the chemical shift of $[\mathbf{1}\text{-OEt}]^-$ already characterized in this work, indicating that an alkoxy substituted pentavalent silicate anion is involved as an intermediate during the degradation reaction. The other signal at $\delta = -105.4$ ppm was also observed in the case of 1,5-dimethoxypentane, supporting the thesis of a coordination complex formed between the neutral Lewis acid and the etheric substrate prior to the C-O bond cleavage.

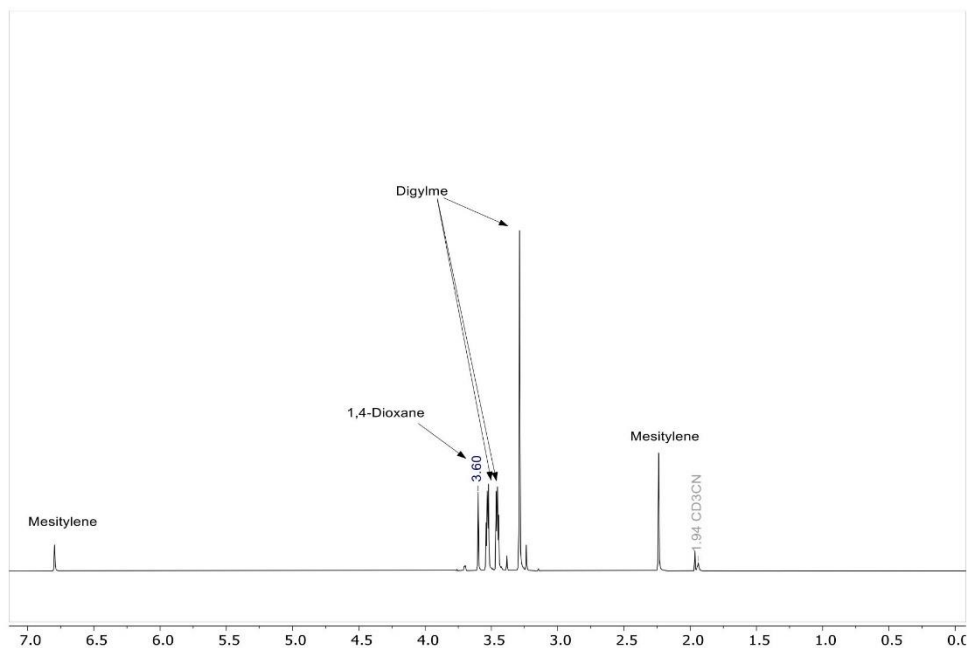


Figure S 18: ¹H NMR spectrum of the degradation experiment of diglyme and 10 mol% of catalyst 1-MeCN in CD₃CN after 20 min at 80 °C, showing the partial formation of 1,4-dioxane.

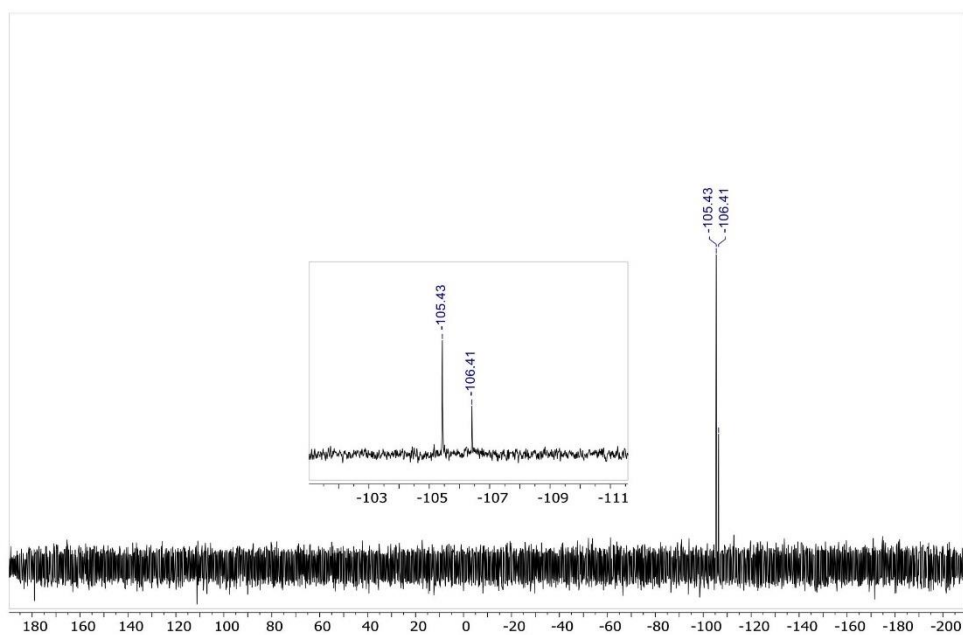


Figure S 19: ²⁹Si NMR spectrum of the degradation experiment of diglyme and 10 mol% catalyst 1-MeCN in CD₃CN after 20 min at 80 °C.

4 NMR Spectra

4.1 NMR spectra of $[\text{Et}_3\text{O}][1\text{-OEt}]$

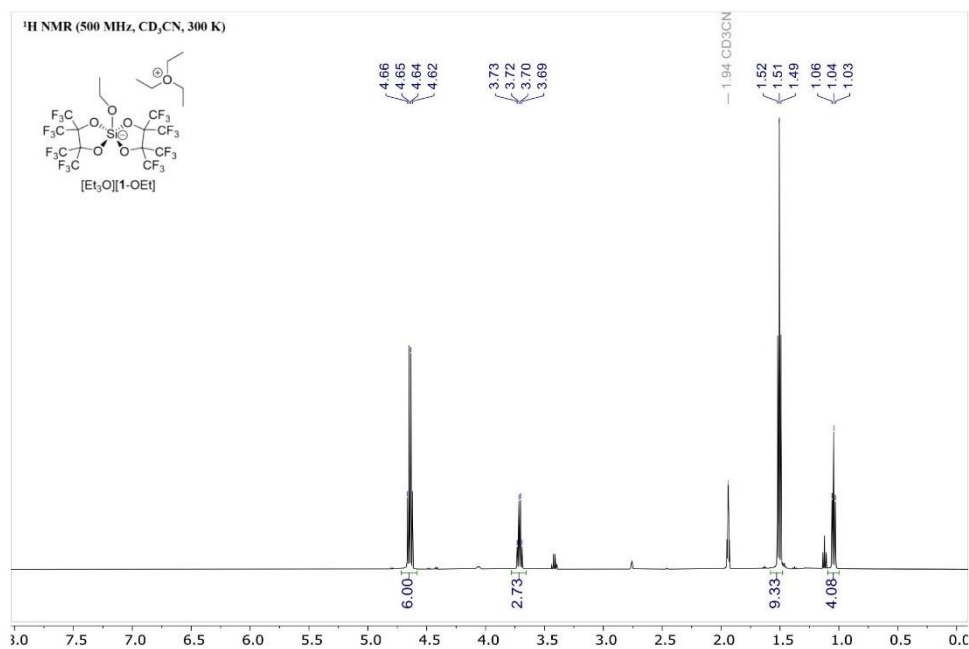


Figure S 20: ^1H NMR spectrum of $[\text{Et}_3\text{O}][1\text{-OEt}]$ in CD_3CN at 300 K.

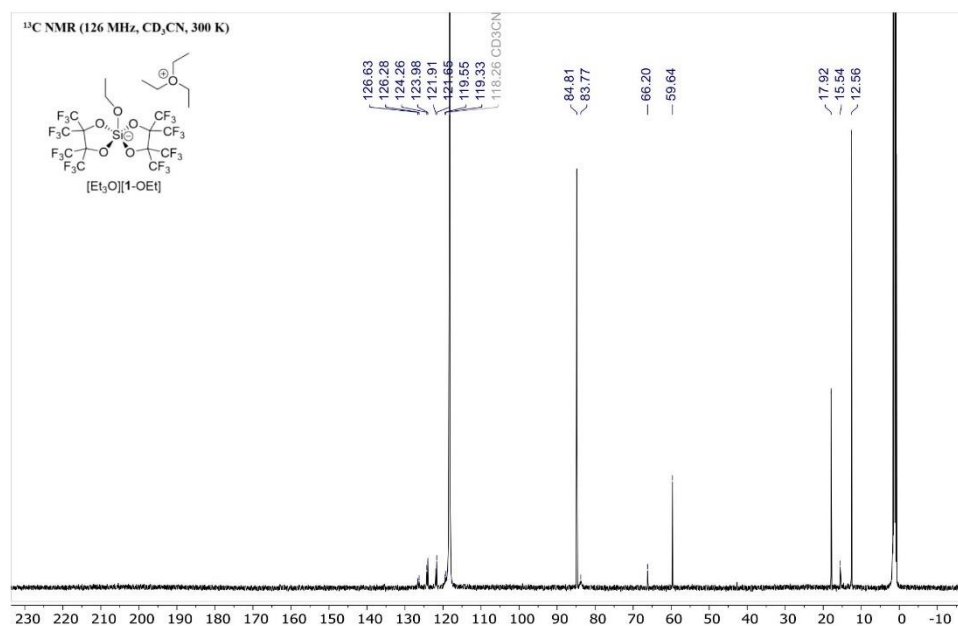


Figure S 21: ^{13}C NMR spectrum of $[\text{Et}_3\text{O}][1\text{-OEt}]$ in CD_3CN at 300 K.

S25

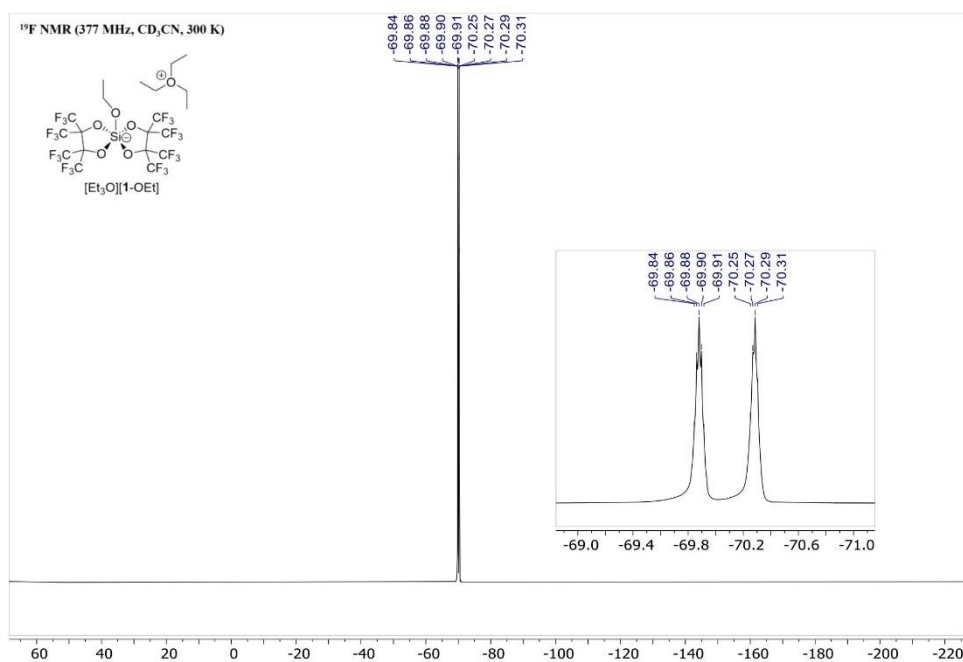


Figure S 22: ¹⁹F NMR spectrum of [Et₃O][1-OEt] in CD₃CN at 300 K.

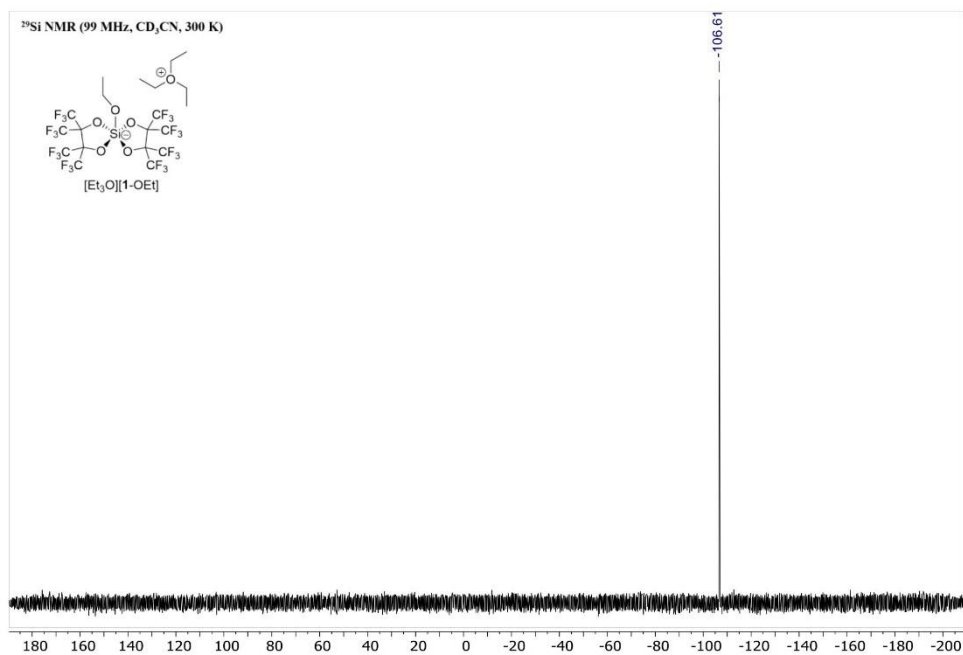


Figure S 23: ²⁹Si NMR spectrum of [Et₃O][1-OEt] in CD₃CN at 300 K.

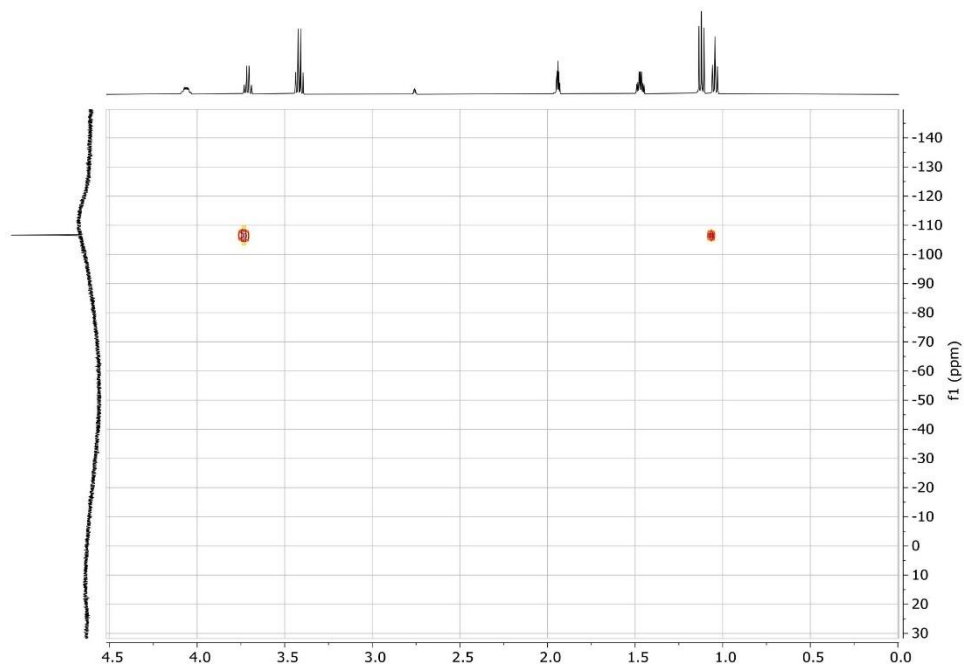


Figure S 24: $^1\text{H}/^{29}\text{Si}$ HMBC NMR spectrum of $[\text{Et}_3\text{O}][1\text{-OEt}]$ in CD_3CN at 300 K.

4.2 NMR spectra of catalytic metathesis reactions

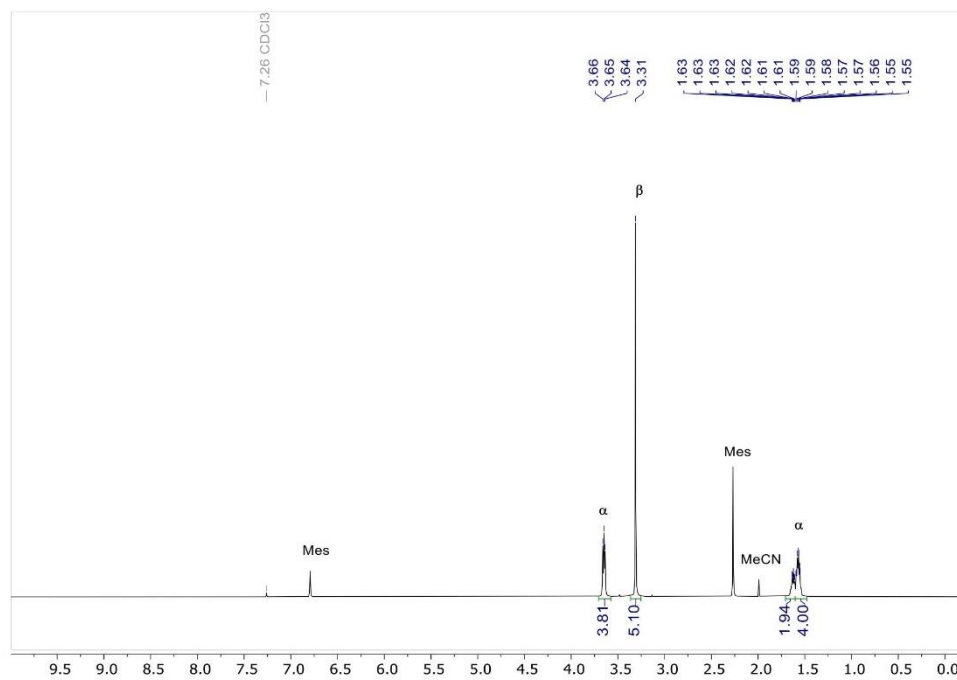


Figure S 25: ^1H NMR spectrum of the ring closing metathesis of 1,5-dimethoxypentane at 300 K using 5 mol% of catalyst **1**-MeCN after 1 h at 80 °C, showing the formation dimethylether (β) and tetrahydropyran (α). The spectrum additionally contains the internal standard mesitylene and acetonitrile.

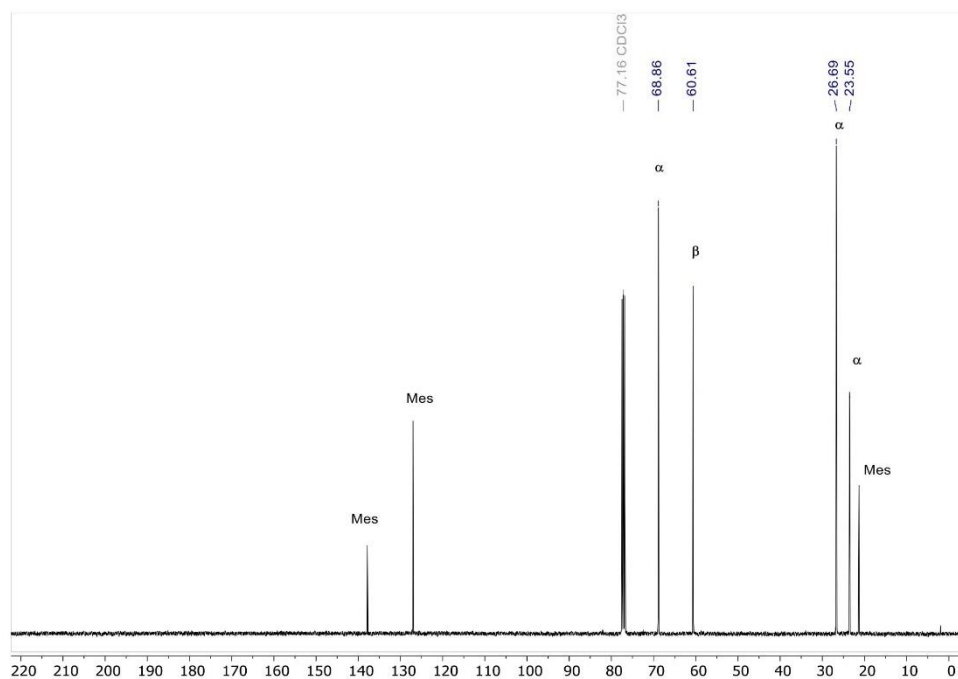


Figure S 26: ^{13}C NMR spectrum of the ring closing metathesis of 1,5-dimethoxy-pentane at 300 K using 5 mol% of catalyst **1**-MeCN after 1 h at 80 °C, showing the formation dimethylether (β) and tetrahydropyran (α). The spectrum additionally contains signals of internal standard mesitylene.

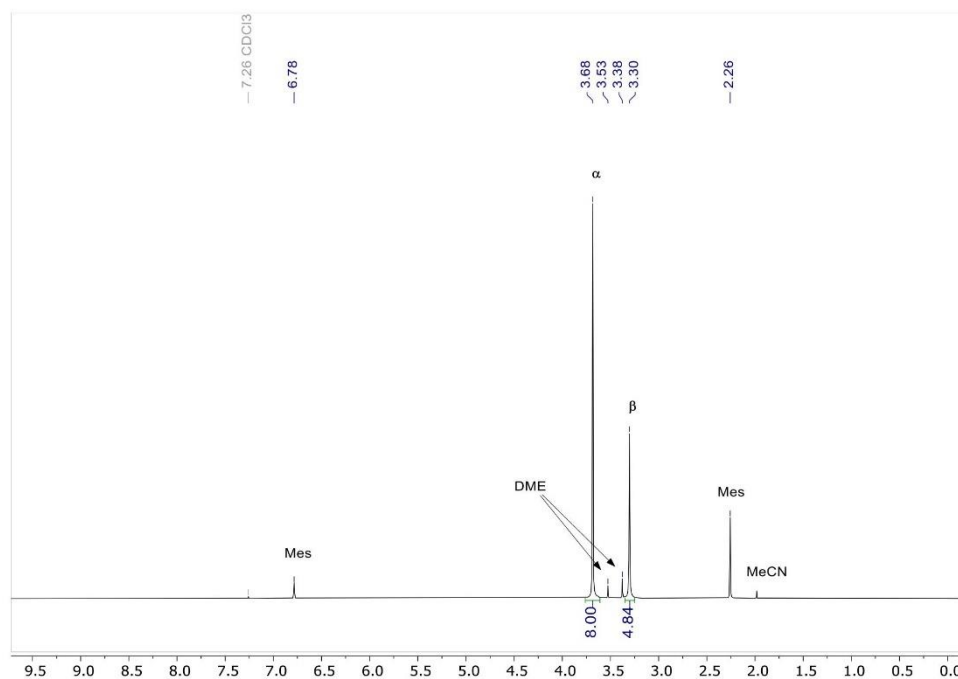


Figure S 27: ¹H NMR spectrum of the ring closing metathesis of diglyme at 300 K using 5 mol% of catalyst 1-MeCN after 3 h at 80 °C, showing the formation dimethylether (β) and 1,4-dioxane (α). The spectrum additionally shows internal standard mesitylene, acetonitrile and little amounts of side-product dimethoxyethane (DME).^[12]

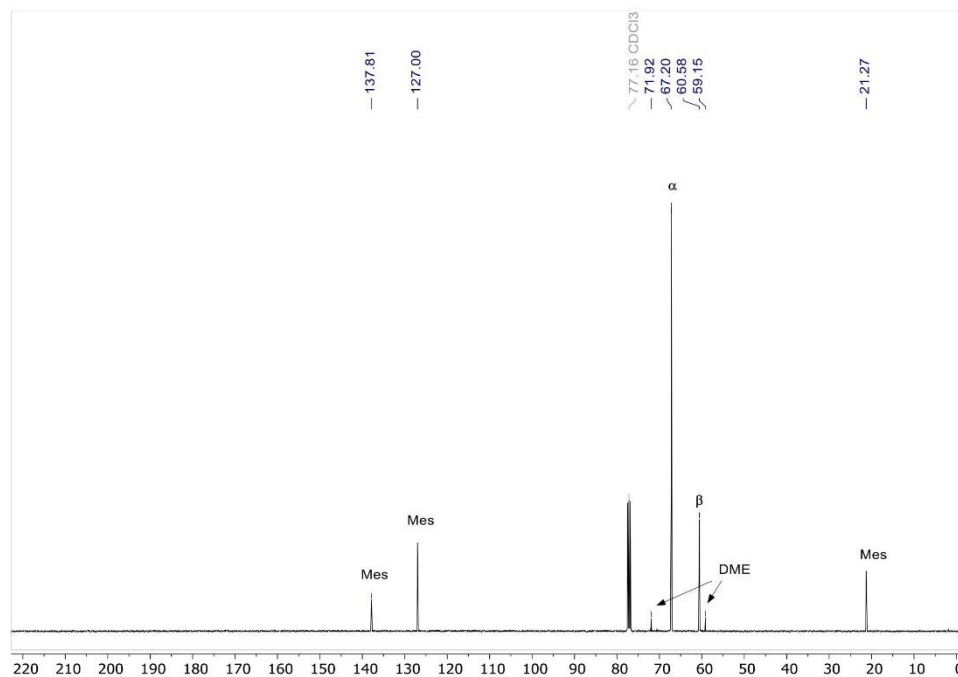


Figure S 28: ^{13}C NMR spectrum of the ring closing metathesis of diglyme at 300 K using 5 mol% of catalyst 1-MeCN after 3 h at 80 °C, showing the formation dimethylether (β) and 1,4-dioxane (α). The spectrum additionally shows internal standard mesitylene and little amounts of side-product dimethoxyethane (DME).^[12]

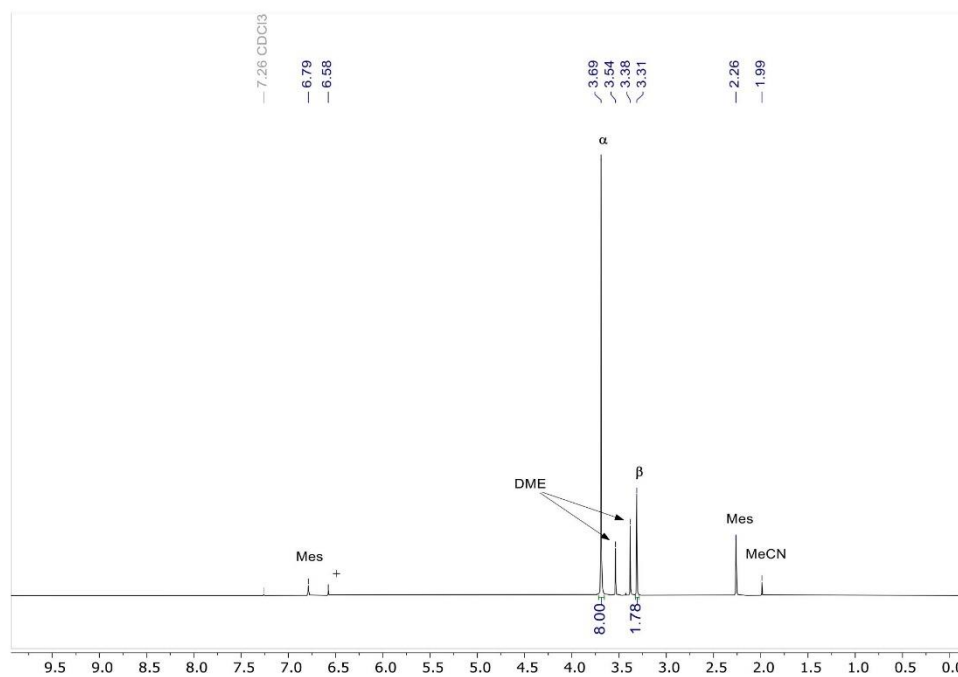


Figure S 29: ¹H NMR spectrum of the ring closing metathesis of tetra(ethyleneglycol)dimethylether (TEG-DME) at 300 K using 20 mol% of catalyst **1**-MeCN after 48 h at 80 °C, showing the formation dimethylether (β) and 1,4-dioxane (α). The spectrum additionally contains mesitylene, acetonitrile and side-product dimethoxyethane (DME) as well as little amounts of an undefined species (+).^[12]

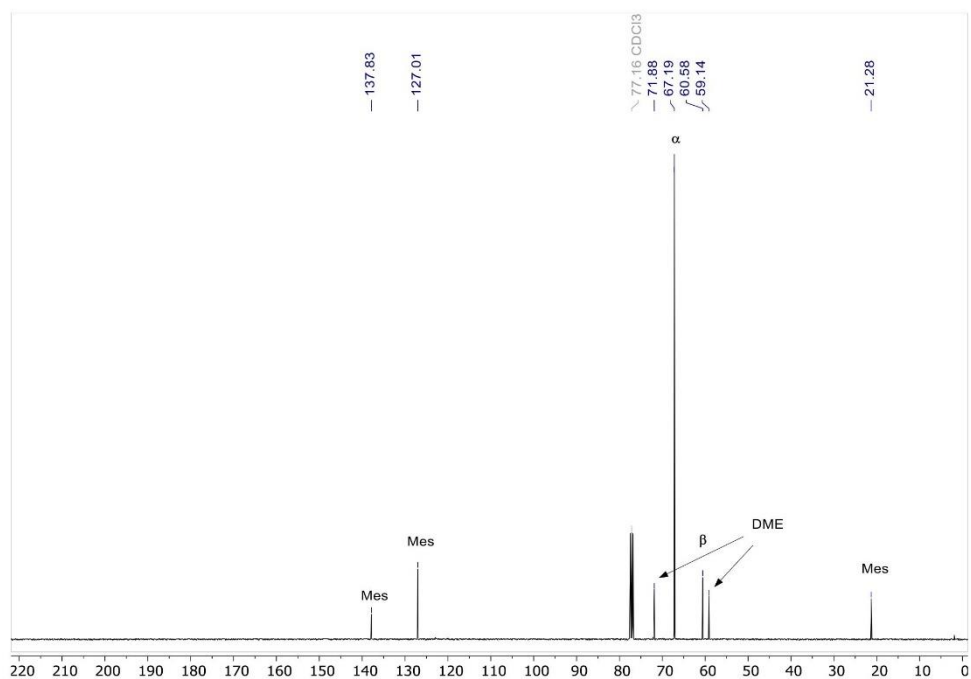


Figure S 30: ^{13}C NMR spectrum of the ring closing metathesis of tetra(ethyleneglycol)dimethylether (TEG-DME) at 300 K using 20 mol% of catalyst 1-McCN after 48 h at 80 °C, showing the formation dimethylether (β) and 1,4-dioxane (α). The spectrum additionally shows mesitylene, and dimethoxyethane (DME).^[12]

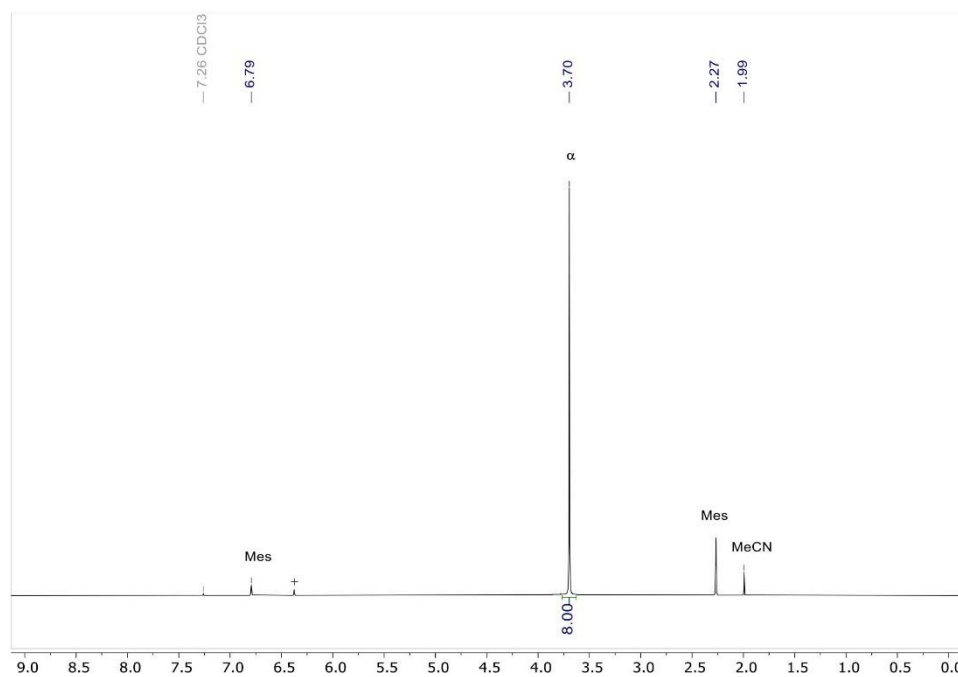


Figure S 31: ¹H NMR spectrum of the ring closing metathesis of 18-crown-6 using 30 mol% of catalyst **1**-McCN at 300 K after 18 h at 80 °C, showing the 1,4-dioxane (α). The spectrum additionally shows mesitylene and acetonitrile and an undefined side-product (+).

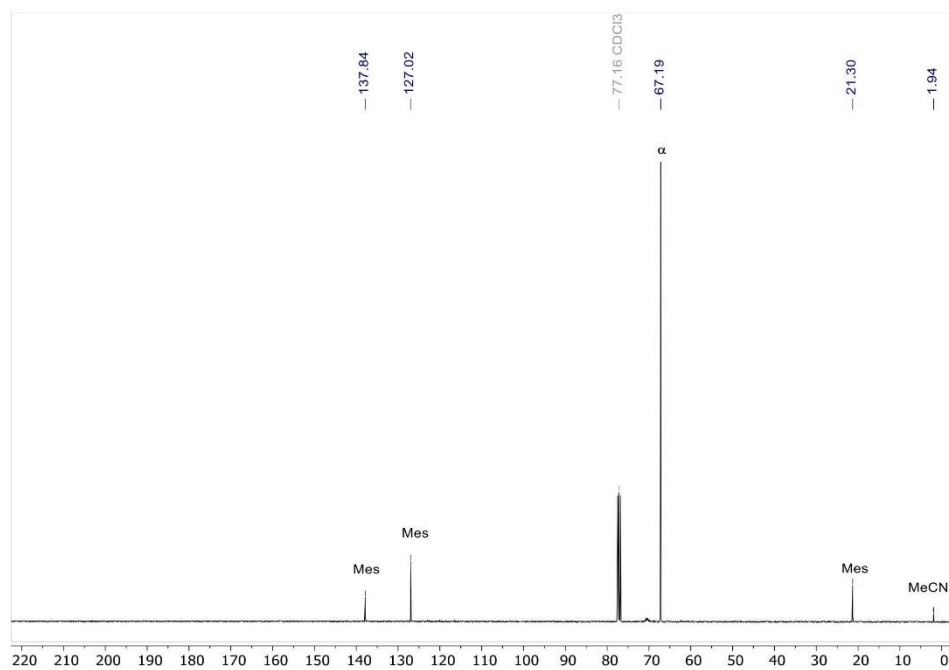


Figure S 32: ¹³C NMR spectrum of the ring closing metathesis of 18-crown-6 using 30 mol% of catalyst **1**·MeCN at 300 K after 18 h at 80 °C, showing the formation of 1,4-dioxane (α). The spectrum additionally shows mesitylene and acetonitrile.

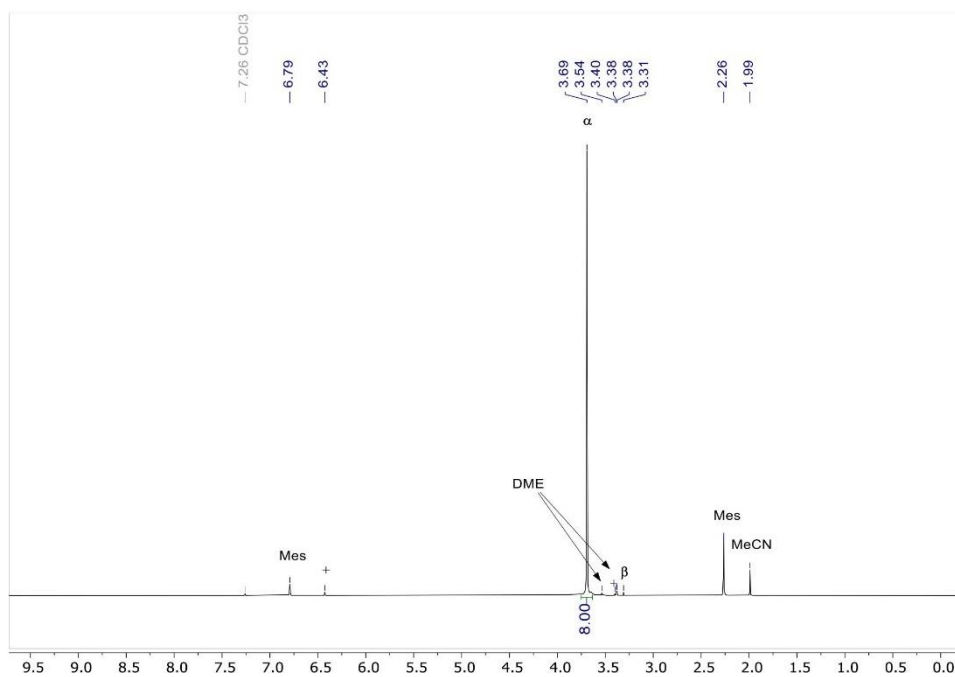


Figure S 33: ^1H NMR spectrum of the ring closing metathesis of poly(ethylene glycol)dimethylether (PEG-DME, $M_w \approx 2000 \text{ g mol}^{-1}$) using 225 mol% of catalyst **1**·MeCN at 300 K, showing the formation dimethylether (β) and 1,4-dioxane (α). The spectrum additionally shows mesitylene, acetonitrile and minor side-products (+) including dimethoxyethane (DME) and undefined species (+).^[12]

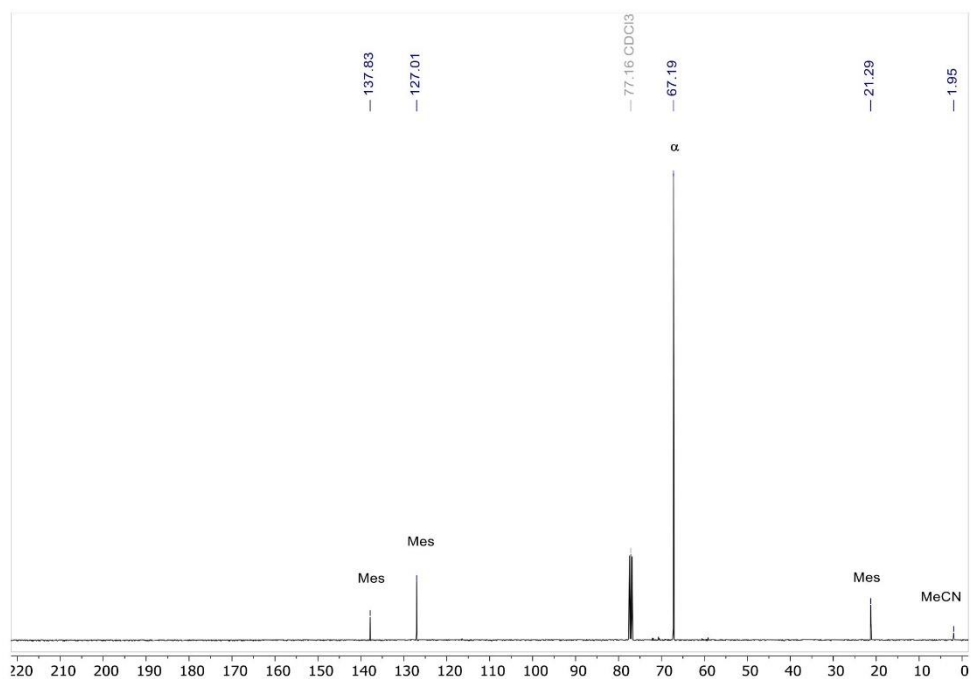


Figure S 34: ^{13}C NMR spectrum of the ring closing metathesis of poly(ethyleneglycol)dimethylether (PEG-DME, $M_w \approx 2000 \text{ g mol}^{-1}$) using 225 mol% of catalyst **1**-MeCN at 300 K after 18 h at 80 °C, showing the formation dimethylether (β) and 1,4-dioxane (α). The spectrum additionally contains mesitylene and acetonitrile signals.

5 References

- [1] F. S. Tschernuth, T. Thorwart, L. Greb, F. Hanusch, S. Inoue, *Angew. Chem. Int. Ed.* **2021**, *60*, 25799-25803.
- [2] Bruker AXS Inc., Madison, Wisconsin, USA, **2015**.
- [3] Bruker AXS Inc., Madison, Wisconsin, USA **2008**.
- [4] G. M. Sheldrick, University of Göttingen, Göttingen, Germany, **2014**.
- [5] C. B. Huebschle, G. M. Sheldrick, B. Dittrich, *J. Appl. Cryst.* **2011**, *44*, 1281.
- [6] G. M. Sheldrick, University of Göttingen, Göttingen, Germany, **1998**.
- [7] A. J. C. Wilson, *International Tables for Crystallography, Vol. C*, Kluwer Academic Publishers, Dordrecht, Netherlands **1992**.
- [8] A. L. Spek, Utrecht University, Utrecht, Netherlands **2010**.
- [9] (a) R. G. Giles, H. Heaney, M. J. Plater, *Tetrahedron* **2015**, *71*, 7367-7385; (b) D. Tsiourvas, A. Tsetsekou, A. Papavasiliou, M. Arkas, N. Boukos, *Microporous Mesoporous Mater.* **2013**, *175*, 59-66.
- [10] K. Leszczyńska, A. Mix, R. J. F. Berger, B. Rummel, B. Neumann, H.-G. Stammer, P. Jutzi, *Angew. Chem. Int. Ed.* **2011**, *50*, 6843-6846.
- [11] T. Liang, G. Dong, C. Li, X. Xu, Z. Xu, *Org. Lett.* **2022**, *24*, 1817-1821.
- [12] G. R. Fulmer, A. J. M. Miller, N. H. Sherden, H. E. Gottlieb, A. Nudelman, B. M. Stoltz, J. E. Bercaw, K. I. Goldberg, *Organometallics* **2010**, *29*, 2176-2179.

11.3 Supporting Information Chapter 7

European Journal of Inorganic Chemistry

Supporting Information

Tuning the Lewis Acidity of Neutral Silanes Using Perfluorinated Aryl- and Alkoxy Substituents

Florian S. Tschernuth, Lukas Bichlmaier, Sebastian Stigler, and Shigeyoshi Inoue*

Supporting Information

Table of Contents

1	General Methods and Instrumentation.....	2
2	Characterization.....	3
2.1	LIFDI-MS analysis of compound 3.....	3
2.2	Lewis acidity assessments by Gutmann-Beckett and Childs method.....	3
3	Single-Crystal X-ray Diffraction Analysis.....	6
3.1	ORTEP depiction of Si(Tol ^F) ₄ (1).....	6
3.2	ORTEP depiction of HSi(Tol ^F) ₃ (2).....	6
3.3	ORTEP depiction of Si(Ph ^F) ₂ pin ^F (4).....	7
4	NMR spectra of title compounds.....	10
4.1	NMR spectra of compound <i>p</i> -LiOTol ^F	10
4.2	NMR spectra of compound Si(Tol ^F) ₄ (1).....	11
4.3	NMR spectra of compound HSi(Tol ^F) ₃ (2).....	13
4.4	NMR spectra of compound Si(OTol ^F) ₄ (3).....	15
4.5	NMR spectra of compound Si(Ph ^F) ₂ pin ^F (4).....	17
5	References.....	19

1 General Methods and Instrumentation

Analytics

All NMR samples were prepared in PTFE valve *J-Young* NMR tubes in an argon atmosphere. The recorded ^1H , ^{13}C , ^{19}F and ^{29}Si NMR spectra were recorded on a *Bruker Avance Neo* 400 MHz spectrometer and a *Bruker AV500C* spectrometer at 300 K. The obtained ^1H - and ^{13}C -NMR spectra were referenced to the residual proton and natural abundance carbon signals of deuterated NMR solvents. The observed signals were abbreviated as following: s = singlet, br = broad signal and combinations, d = doublet, t = triplet, q = quartet, h = septet, m = multiplet and qm = quartet of multiplets. The spectra were processed and analyzed with the *Mestrenova* software.

Elemental Analysis (CHNS) was carried out by the central analytics laboratory of the *TUM Catalysis Research Center* on a *EURO EA (HEKAtech)* instrument equipped with a CHNS combustion analyzer. Due to high F-content, the formation of CF_4 hampers an accurate measurement.

Melting Points (m.p.) were measured in wax-sealed capillaries under argon atmosphere on a *Büchi B-540*.

Liquid Injection Field Desorption Ionization Mass Spectrometry (LIFDI-MS) was measured directly from glovebox filled with argon, with a *Thermo Fisher Scientific Exactive Plus Orbitrap* and a *Linden CMS* ion source.^[1]

Single crystal diffraction data were recorded on diffractometers equipped with a CMOS detector (*Bruker Photon-100*) and an IMS microsource and MoK_α radiation ($\lambda = 0.71073 \text{ \AA}$) was used. The crystals were placed in perfluorinated ether and stored at 100 K in a nitrogen stream for measurement. Reflections were merged and corrected for Lorenz and polarization effects, scan speed, and background using the *Bruker SAINT* software package.^[2] Absorption corrections, including odd and even-ordered spherical harmonics were performed using *SADABS*.^[3] Space group assignments were based upon systematic absences, E statistics, and successful refinement of the structures. Structures were solved using the *APEX4*^[4] and *OLEX2*^[5] software in conjunction with *SHELXL-2014*^[6] and *SHELXLE*.^[7] The hydrogen atoms in (**2**) were found in the difference Fourier map and were allowed to refine freely. Hydrogen atoms of the solvent were placed in calculated position and refined using a riding model, with a C–H distance of 0.99 Å and $U_{\text{iso}}(\text{H}) = 1.2 \cdot U_{\text{eq}}(\text{C})$. If not mentioned otherwise, non-hydrogen atoms were refined with anisotropic displacement parameters. Full-matrix least-squares refinements were carried out by minimizing $\Delta w(\text{Fo}^2 - \text{Fc}^2)^2$ with *SHELXL* weighting scheme.^[8] Neutral atom scattering factors for all atoms and anomalous dispersion corrections for the non-hydrogen atoms were taken from International Tables for Crystallography.^[9] Images of the crystal structures were generated by *MERCURY*.^[10] Supplementary crystallographic data for this paper are contained in CCDC 2269478 ($\text{Si}(\text{Tol}^F)_4$ (**1**)), CCDC 2269479 ($\text{HSi}(\text{Tol}^F)_3$ (**2**)), and CCDC 2269480 ($\text{Si}(\text{Ph}^F)_2\text{pin}^F$ (**4**)). These data can be obtained free of charge from the Cambridge Crystallographic Data Centre via <https://www.ccdc.cam.ac.uk/structures/>.

2 Characterization

2.1 LIFDI-MS analysis of compound 3

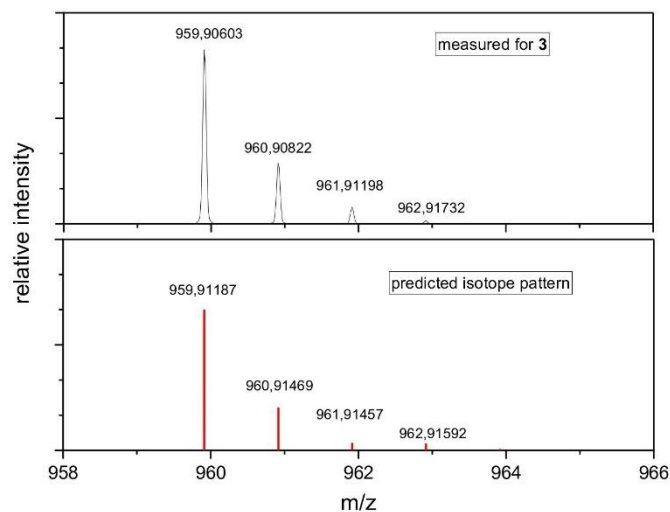


Figure S 1: Top: LIFDI MS spectrum for compound **3** (detailed view for isotope pattern in the range of 958 – 966 m/z) measured from toluene solution; Bottom: Predicted isotope pattern of compound **3** ($\text{SiO}_4\text{C}_{28}\text{F}_{28}$).

2.2 Lewis acidity assessments by Gutmann-Beckett and Childs method

Table S 1: Summary of ^{31}P and ^1H NMR shifts for Lewis acids **1**, **2**, **3**, **4**, $\text{Si}(\text{Ph}^F)_4$, and $\text{Si}(\text{OPh}^F)_4$ obtained from Lewis acid assessment with the Gutmann-Beckett and Childs method.

Lewis Acid	Gutmann-Beckett method		Childs method	
	^{31}P of Et_3PO adduct	$\Delta\delta(^{31}\text{P})^{[\text{a}]}$	$^1\text{H}^3$ of <i>tr</i> -CA adduct	$\Delta\delta(^1\text{H}^3)^{[\text{b}]}$
$\text{Si}(\text{C}_6\text{F}_5)_4$	65.56	15.17	6.87	0.00
$\text{Si}(\text{OC}_6\text{F}_5)_4$	77.32 (57.28)*	26.93 (6.89)*	6.91	0.04
1	50.39	0.00	6.87	0.00
2	50.99	0.60	6.88	0.01
3	79.61 (59.16)*	29.22 (8.77)*	6.91	0.04
4	77.55	27.16	6.87	0.00

[a] referenced to free Et_3PO in CD_2Cl_2 ($\delta(^{31}\text{P}) = 50.39$ ppm); referenced to free *trans*-CA in CD_2Cl_2 ($\delta(^1\text{H}^3) = 6.87$ ppm); * double coordinated product in brackets.

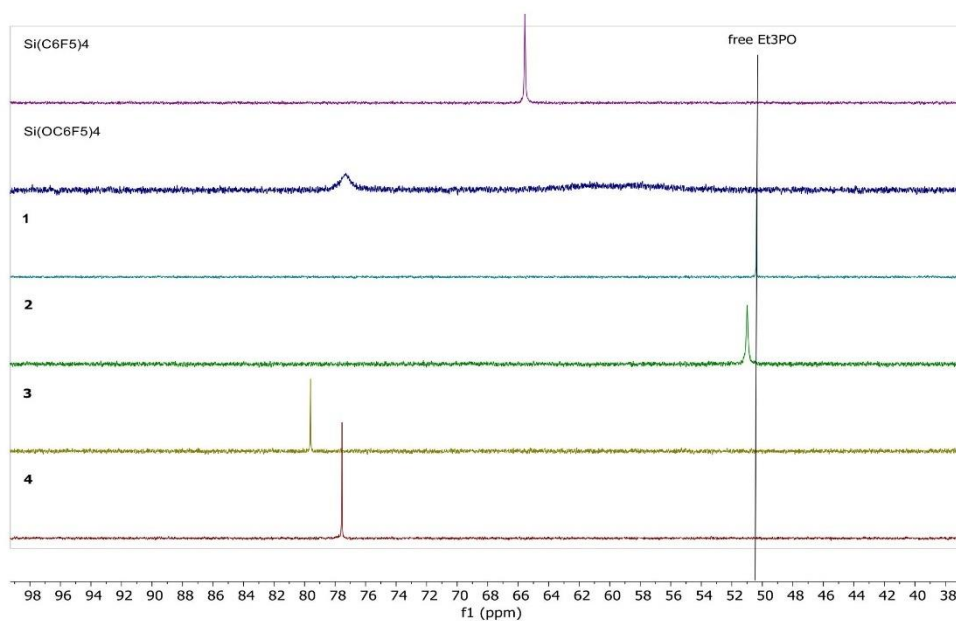


Figure S 2: Stacked $^{31}\text{P}\{^1\text{H}\}$ NMR spectra of **1**, **2**, **3**, **4**, $\text{Si}(\text{Ph}^F)_4$, and $\text{Si}(\text{OPh}^F)_4$ with 1.00 equiv. of Et_3PO in dichloromethane- d_2 solution at 298 K.

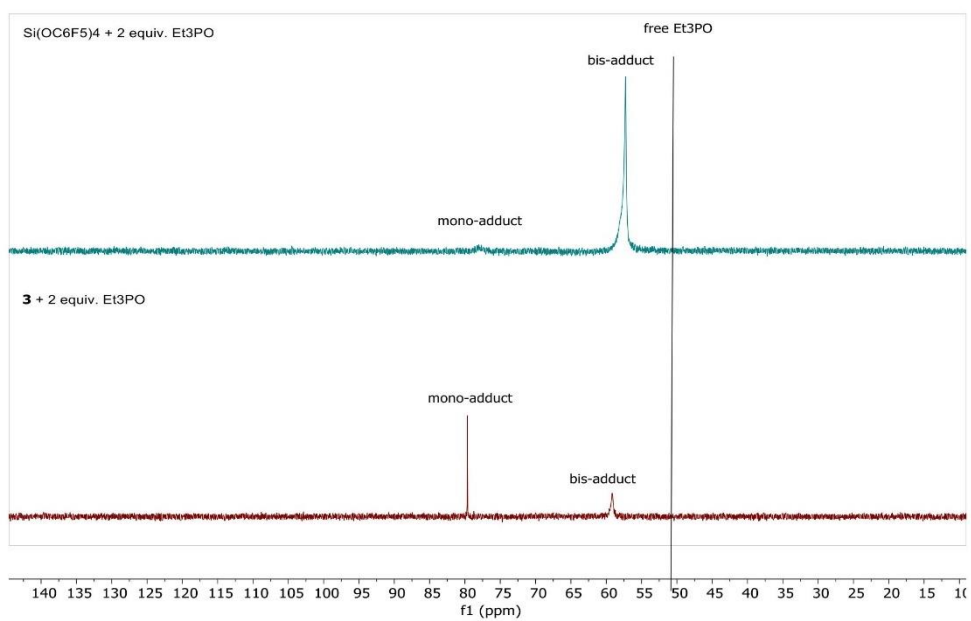


Figure S 3: Stacked $^{31}\text{P}\{^1\text{H}\}$ NMR spectra of **3** and $\text{Si}(\text{OPh}^F)_4$ with 2.00 equiv. of Et_3PO in dichloromethane- d_2 solution at 298 K showing twofold-coordination.

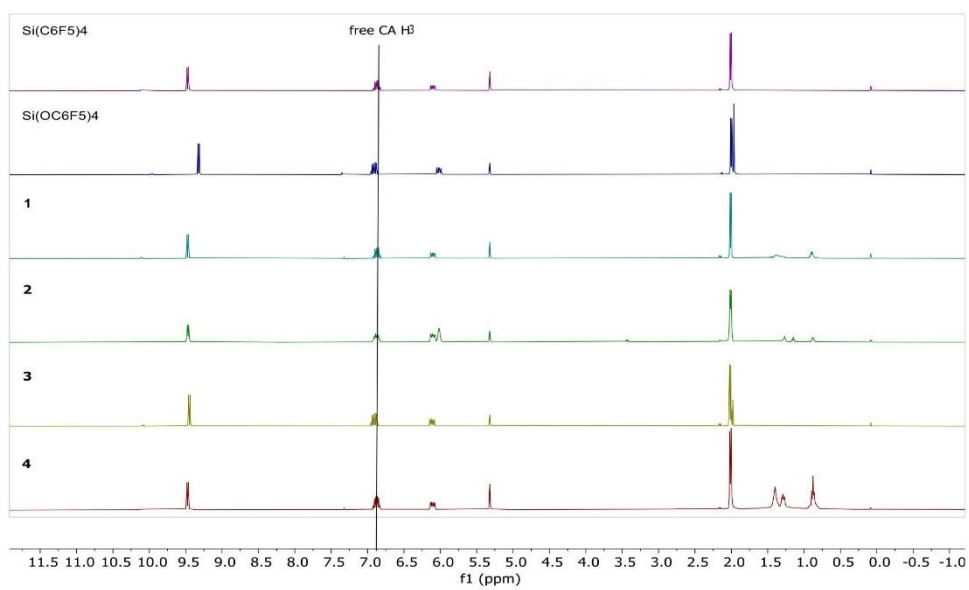


Figure S 4: Stacked ¹H NMR spectra of **1**, **2**, **3**, **4**, Si(Ph^F)₄, and Si(OPh^F)₄ with 1.00 equiv. of *trans*-crotonaldehyde in dichloromethane-*d*₂ solution at 298 K, showing neglectable changes in the chemical shift of the H^β proton.

3 Single-Crystal X-ray Diffraction Analysis

3.1 ORTEP depiction of $\text{Si}(\text{Tol}^f)_4$ (1)

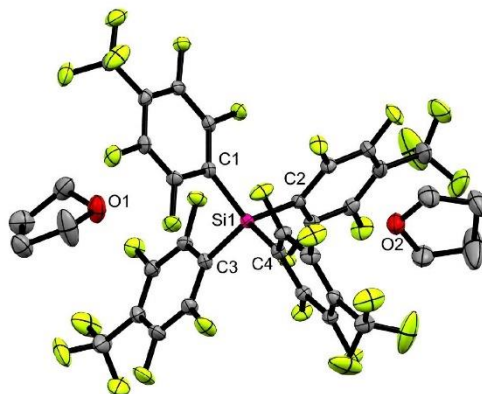


Figure S 5: Molecular structure of $\text{Si}(\text{Tol}^f)_4$ (1) with translational ellipsoids plotted at 50 % probability level. Hydrogen atoms are omitted for clarity. Selected bond lengths [Å] and angles [deg]: Si1–C1 1.8784(19), Si1–C2 1.8786(19), Si1–C3 1.8789(19), Si1–C4 1.8800(19); C2–Si1–C1 113.18(8), C2–Si1–C3 110.97(8), C2–Si1–C4 103.51(8), C1–Si1–C3 104.43(8), C1–Si1–C4 111.36(8), C3–Si1–C4 113.67(8).

3.2 ORTEP depiction of $\text{HSi}(\text{Tol}^f)_3$ (2)

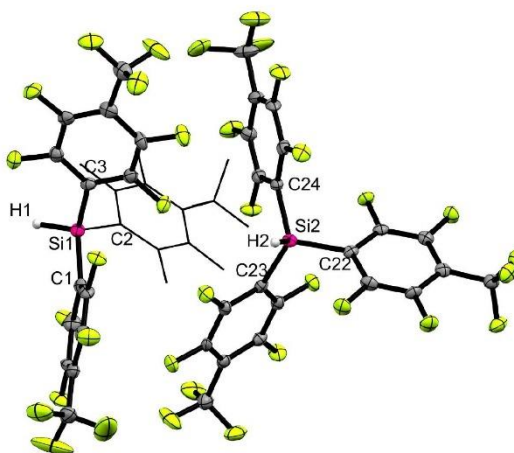


Figure S 6: Molecular structure of $\text{HSi}(\text{Tol}^f)_3$ (2) with translational ellipsoids plotted at 50 % probability level. For reasons of clarity, one Ph^f group is depicted in wireframe model. Selected bond lengths [Å] and angles [deg]: Si1–H1

1.31(5), Si2-H2 1.37(6), Si1-C1 1.879(5), Si1-C2 1.892(6), Si1-C3 1.878(5); C1-Si1-H1 119(2), C1-Si1-C2 112.4(2), C2-Si1-H1 113(2), C3-Si1-H1 105(2), C3-Si1-C1 111.3(2), C3-Si1-C2 105.8(2).

3.3 ORTEP depiction of $\text{Si}(\text{Ph}^F)_2\text{pin}^F$ (**4**)

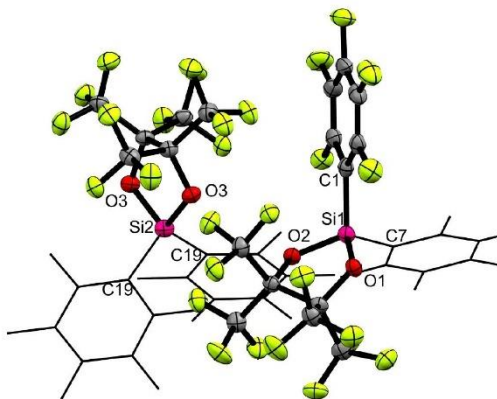


Figure S 7: Molecular structure of $\text{Si}(\text{Ph}^F)_2\text{pin}^F$ (**4**) with translational ellipsoids plotted at 50 % probability level. For reasons of clarity, three Ph^F groups are depicted in wireframe model. Selected bond lengths [Å] and angles [deg]: Si1-O1 1.648(3), Si1-O2 1.654(3), Si1-C1 1.857(4), Si1-C7 1.859(4); O1-Si1-O2 95.53(13), C1-Si1-C7 107.98(17), O1-Si1-C1 113.48(16), O1-Si1-C7 113.22(16), O2-Si1-C1 113.06(16), O2-Si1-C7 113.06(16).

Table S 2: Crystallographic Details.

	Si(Tol ^F) ₄ (1)	HSi(Tol ^F) ₃ (2)	Si(Ph ^F) ₂ pin ^F (4)
CCDC-Number	2269478	2269479	2269480
Crystal Data			
Chemical formula	C ₂₈ F ₂₈ Si · 2(C ₈ H ₁₆ O)	C ₂₁ HF ₂₁ Si	C ₁₈ F ₂₂ O ₂ Si
<i>M_r</i>	1040.58	680.31	694.27
Crystal system, space group	Triclinic, <i>P</i> ̄1	Triclinic, <i>P</i> ̄1	Monoclinic, <i>C2/c</i>
Temperature (K)	100	100	100
<i>a</i> , <i>b</i> , <i>c</i> (Å)	13.0359 (9), 13.6454 (9), 13.8048 (9)	10.0583 (14), 14.765 (2), 15.852 (2)	19.293(12), 23.252(12), 15.123(8)
α, β, γ (°)	63.646 (2), 62.845 (2), 69.576 (2)	89.118 (5), 76.593 (5), 80.910 (5)	90, 106.71(2), 90
<i>V</i> (Å ³)	1924.6 (2)	2260.7 (5)	6498(6)
<i>Z</i>	2	4	12
Radiation type	Mo <i>K</i> α	Mo <i>K</i> α	Mo <i>K</i> α
μ (mm ⁻¹)	0.233	0.289	0.317
Crystal size (mm)	0.66 × 0.59 × 0.52	0.41 × 0.31 × 0.12	0.07 × 0.01 × 0.01
Crystal shape	Block	Block	Needle
Color	Clear colorless	Clear colorless	Clear colorless
Data Collection			
Diffractometer	Bruker Photon CMOS	Bruker Photon CMOS	Bruker Photon CMOS
Absorption correction	Multi-scan	Multi-scan	Multi-scan
<i>T</i> _{min} , <i>T</i> _{max}	0.7452, 0.6811	0.7452, 0.6269	0.7452, 0.6010
No. of measured, independent, and observed [<i>I</i> > 2σ(<i>I</i>)] reflections	82100, 7079, 6658	59692, 8240, 6942	63457, 5745, 3994
<i>R</i> _{int}	0.0283	0.0679	0.1400
θ range (°) for cell measurement	1.94-25.40	1.90-25.35	2.81-23.28
Data completeness	0.999	0.997	0.994
Refinement			
<i>R</i> [<i>F</i> ² > 2σ(<i>F</i> ²)], <i>R</i> (<i>F</i> ²), <i>S</i>	0.040, 0.101, 1.03	0.075, 0.232, 1.10	0.052, 0.131, 1.04
No. of reflections	7079	8240	5745
No. of parameters	660	803	582
No. of restraints	174	3	0
Δρ _{max} , Δρ _{min} (e Å ⁻³)	0.82, -0.82	0.71, -0.63	0.30, -0.34

The data have been assigned the following deposition numbers which can either be quoted as CCDC Numbers or CSD Numbers. A CCDC Number is usually quoted for an organic or metal-organic structure, whereas a CSD Number is usually quoted for an inorganic structure.

CCDC XXXXXXXX-YYYYYYYY (generally used for organic and metal-organic structures)

CSD XXXXXXXX-YYYYYYYY (generally used for inorganic structures)

Deposition Number 2269478-2269480

Summary of Data - Deposition Number 2269478

Compound Name:

Data Block Name: data_mo_biclu1_0m

Unit Cell Parameters: a 13.0359(9) b 13.6454(9) c 13.8048(9) P-1

Summary of Data - Deposition Number 2269479

Compound Name:

Data Block Name: data_mo_biclu3_0m

Unit Cell Parameters: a 10.0583(14) b 14.765(2) c 15.852(2) P-1

Summary of Data - Deposition Number 2269480

Compound Name:

Data Block Name: data_mo_ft_jk1_0ma

Unit Cell Parameters: a 19.293(12) b 23.252(12) c 15.123(8) C2/c

4 NMR spectra of title compounds

4.1 NMR spectra of compound $p\text{-LiOTol}^F$

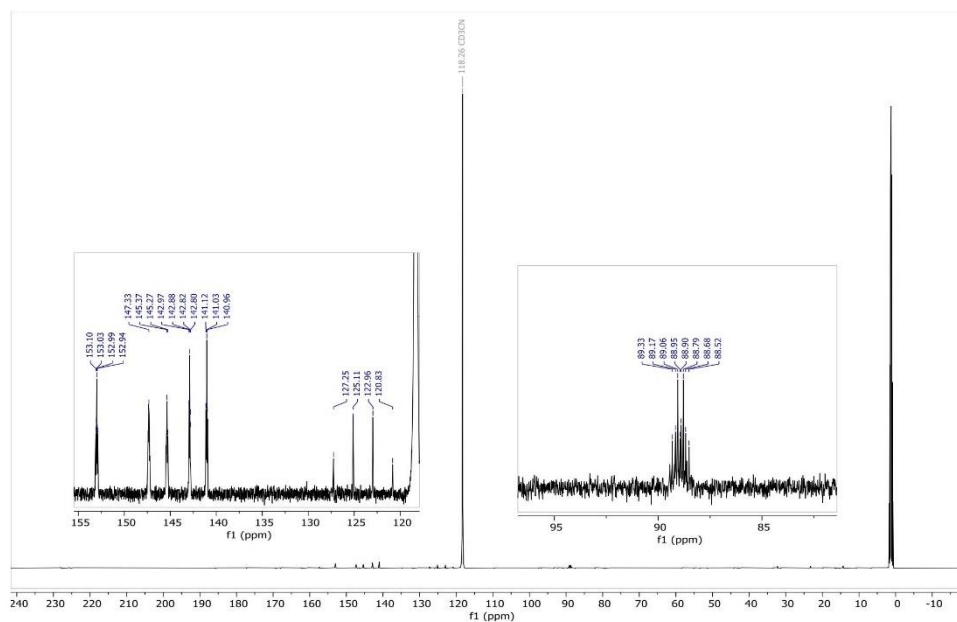


Figure S 8: ^{13}C NMR spectrum of $p\text{-LiOTol}^F$ in acetonitrile- d_3 solution at 298 K.

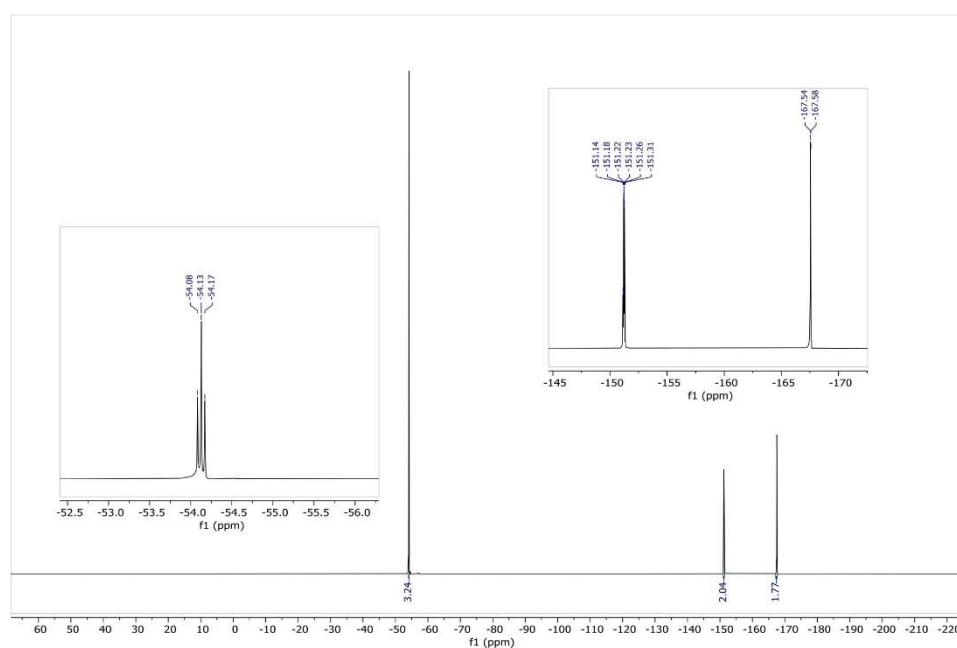
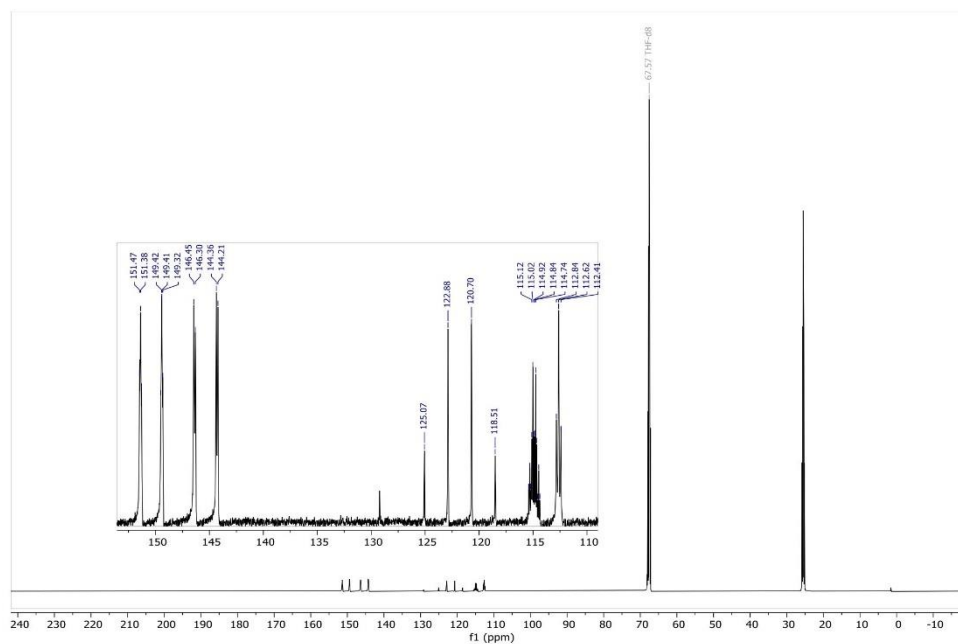
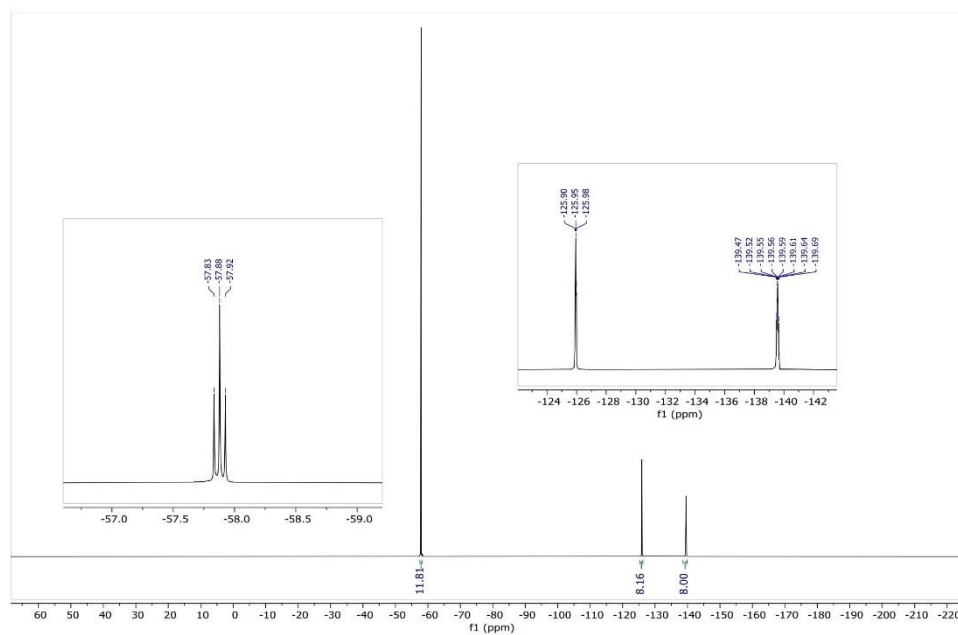


Figure S 9: ^{19}F NMR spectrum of $p\text{-LiOTol}^F$ in acetonitrile- d_3 solution at 298 K.

S10

4.2 NMR spectra of compound $\text{Si}(\text{Tol}^F)_4$ (**1**)**Figure S 10:** ^{13}C NMR spectrum of **1** in $\text{THF-}d_8$ solution at 298 K.**Figure S 11:** ^{19}F NMR spectrum of **1** in $\text{THF-}d_8$ solution at 298 K.

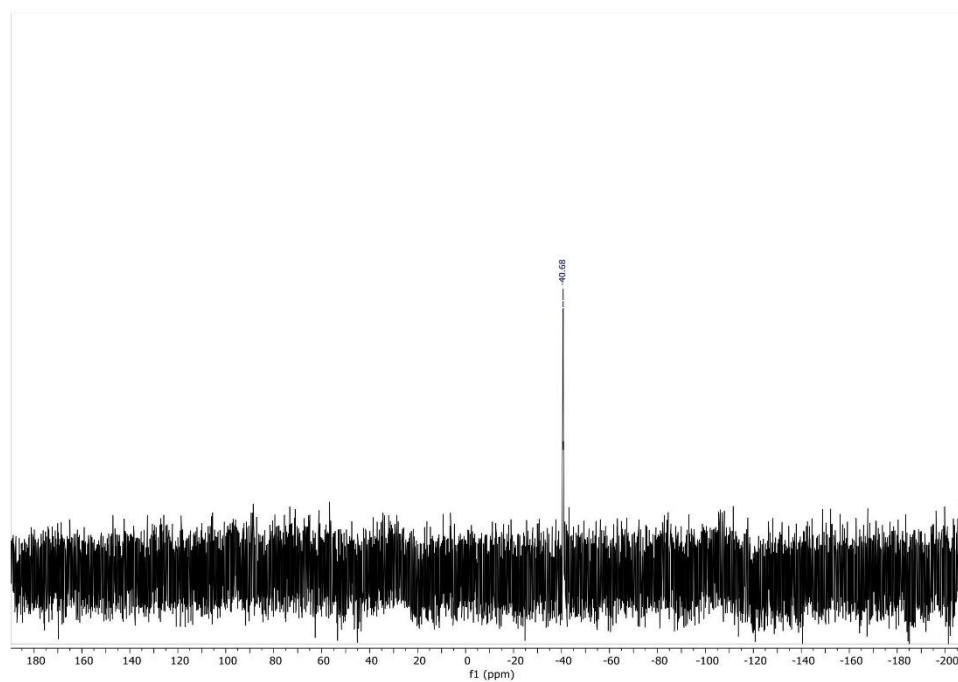


Figure S 12: ^{29}Si NMR spectrum of **1** in $\text{THF-}d_8$ solution at 298 K.

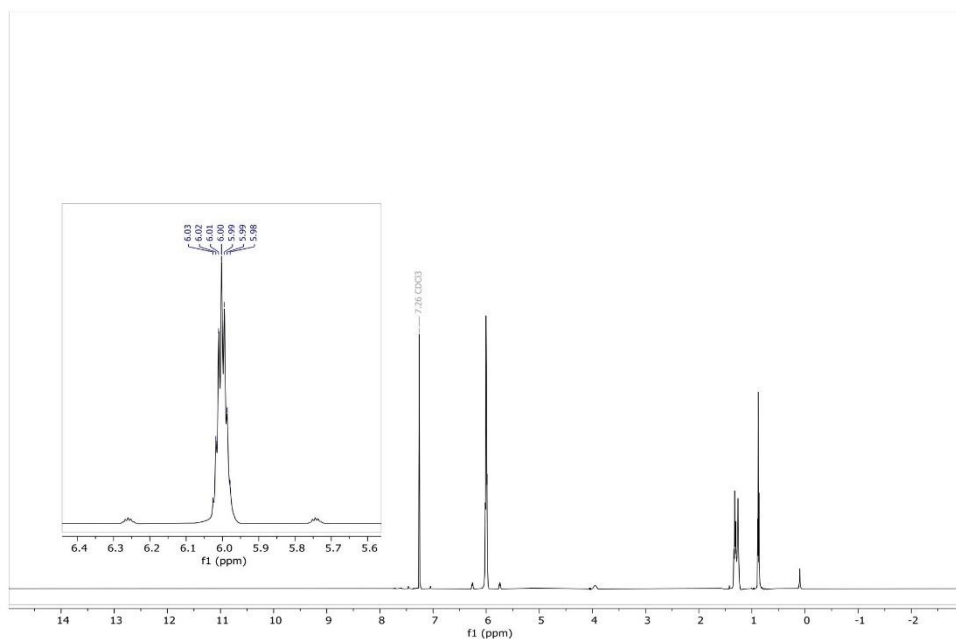
4.3 NMR spectra of compound $\text{HSi}(\text{Tol}^F)_3$ (**2**)

Figure S 13: ^1H NMR spectrum of **2** in chloroform-*d* at 298 K. The spectrum contains hexane and minor undefined impurities.^[11]

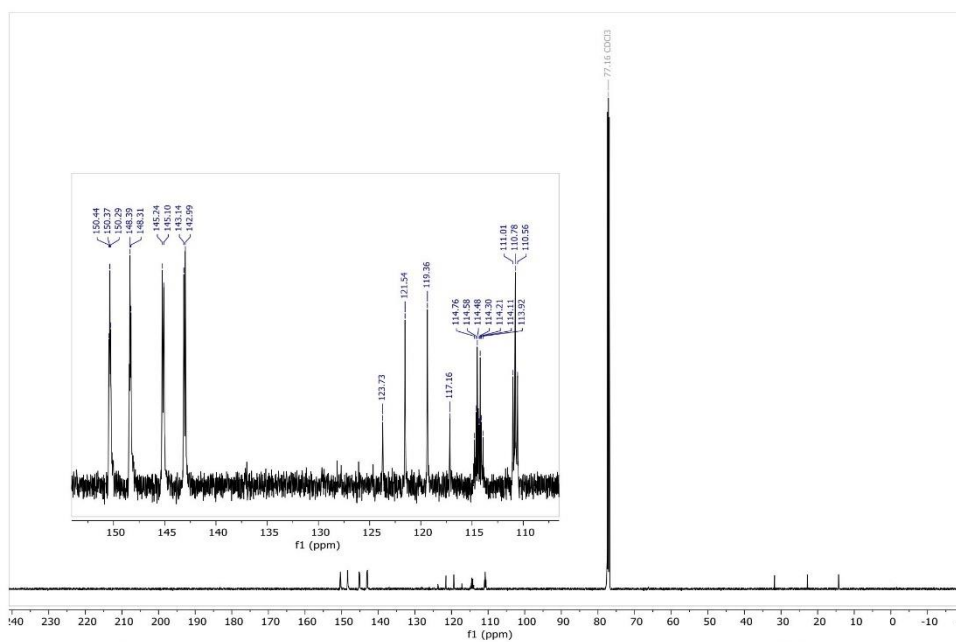


Figure S 14: ^{13}C NMR spectrum of **2** in chloroform-*d* at 298 K. The spectrum contains hexane.^[11]

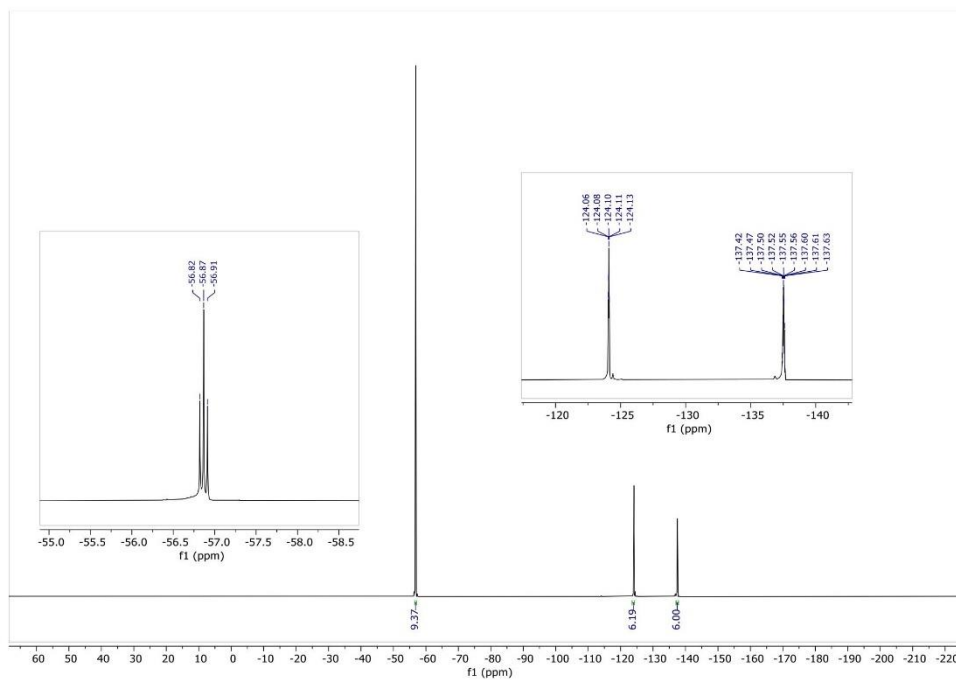
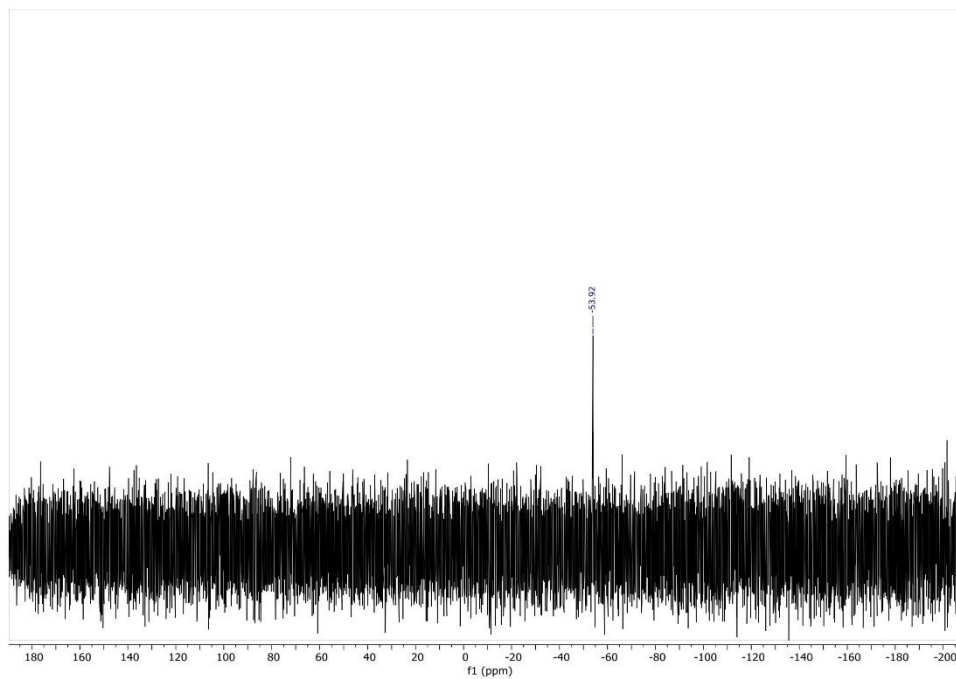
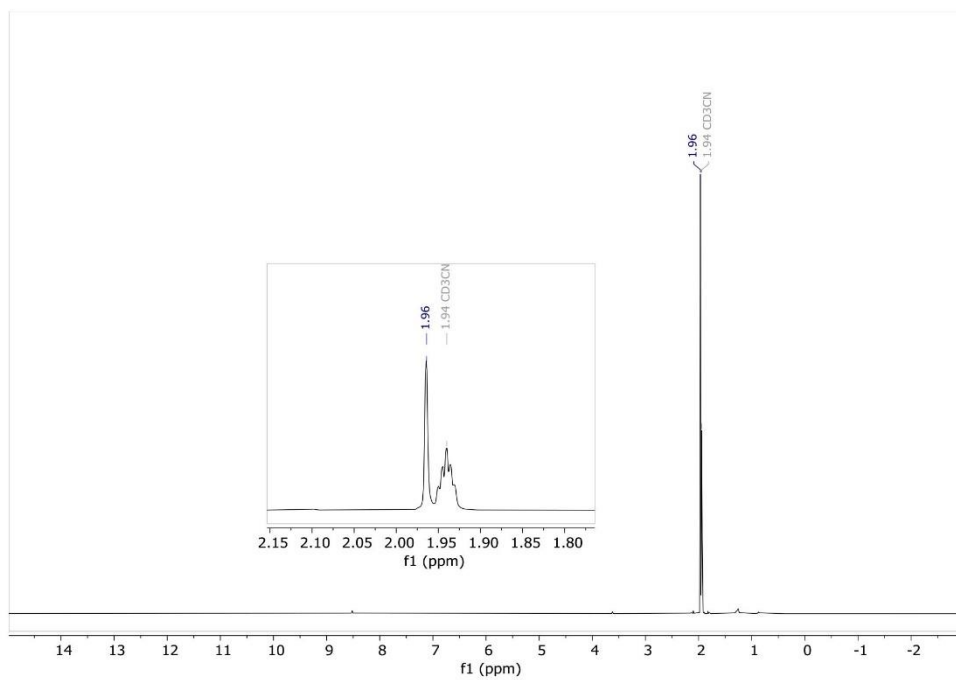
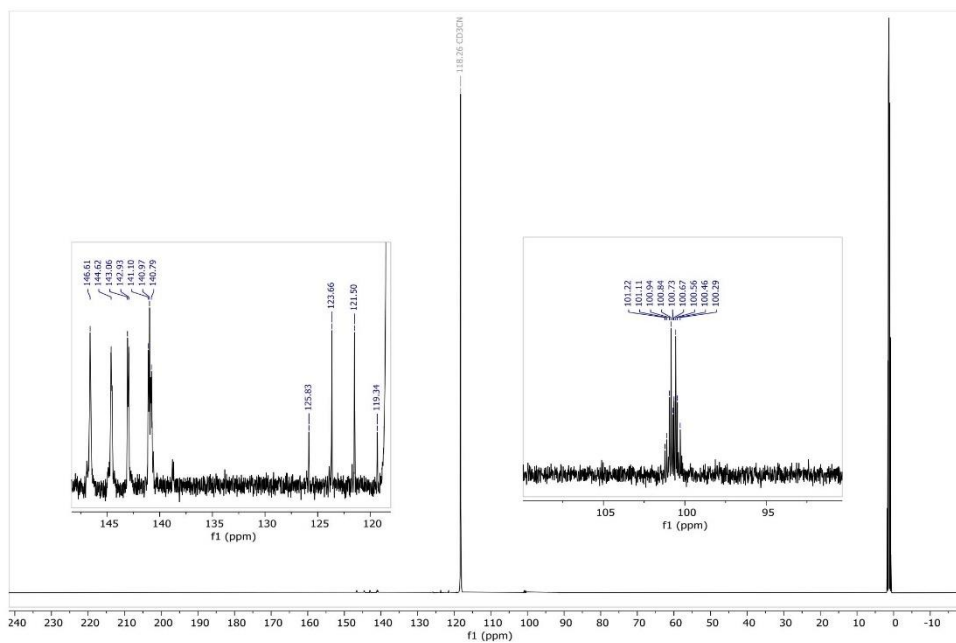


Figure S 15: ^{19}F NMR spectrum of **2** in chloroform-*d* solution at 298 K.



$^{29}\text{Si}\{^1\text{H}\}$ NMR spectrum of **2** in chloroform-*d* solution at 298 K.

4.4 NMR spectra of compound $\text{Si}(\text{OTol}^F)_4$ (**3**)Figure S 16: ^1H NMR spectrum of **3** in acetonitrile- d_3 at 298 K.Figure S 17: ^{13}C NMR spectrum of **3** in acetonitrile- d_3 at 298 K.

S15

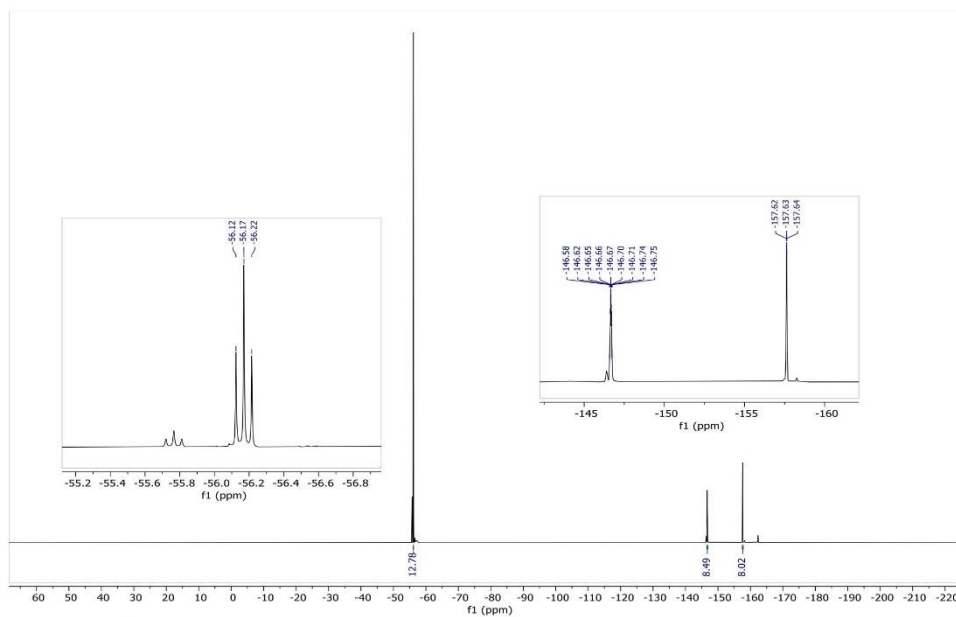


Figure S 18: ^{19}F NMR spectrum of **3** in acetonitrile- d_3 solution at 298 K. The spectrum additionally contains minor signals of an unidentified side-product.

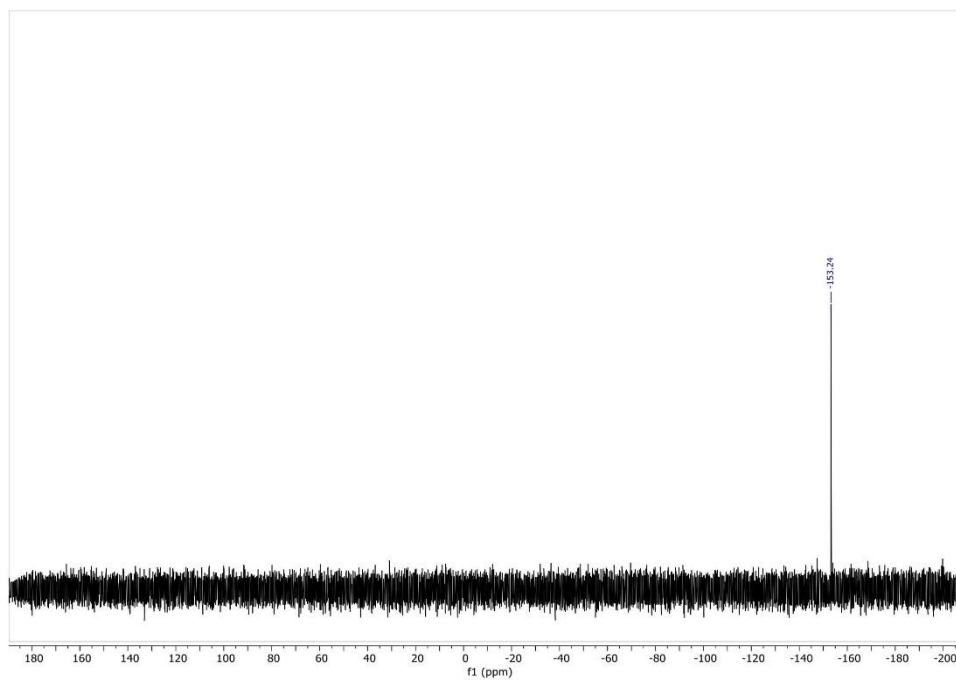


Figure S 19: ^{29}Si NMR spectrum of **3** in acetonitrile- d_3 solution at 298 K.

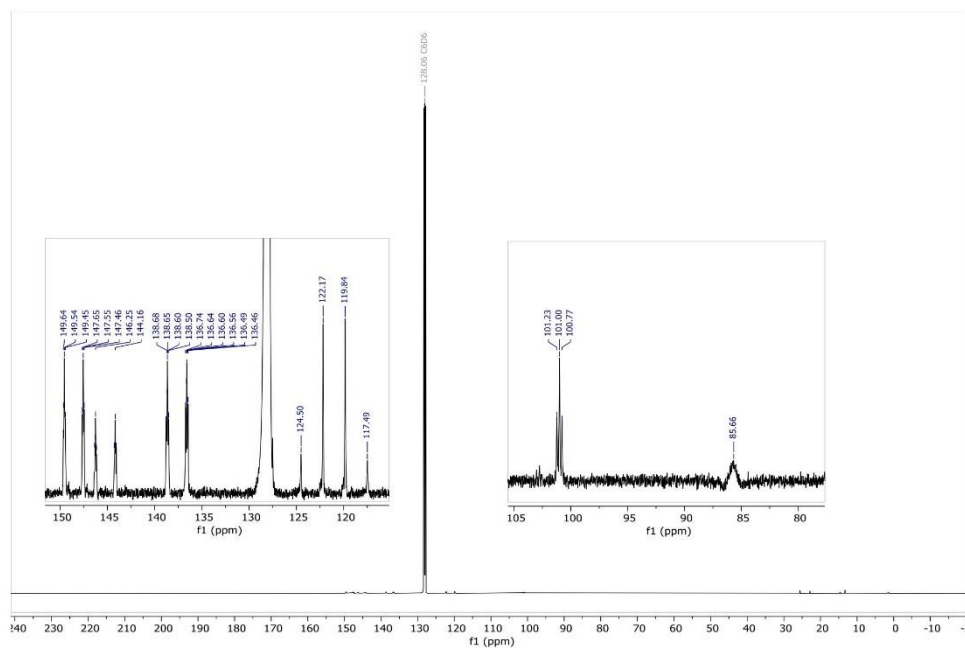
4.5 NMR spectra of compound $\text{Si}(\text{Ph}^F)_2\text{pin}^F$ (**4**)

Figure S 20: ^{13}C NMR spectrum of **4** in benzene- d_6 solution at 298 K.

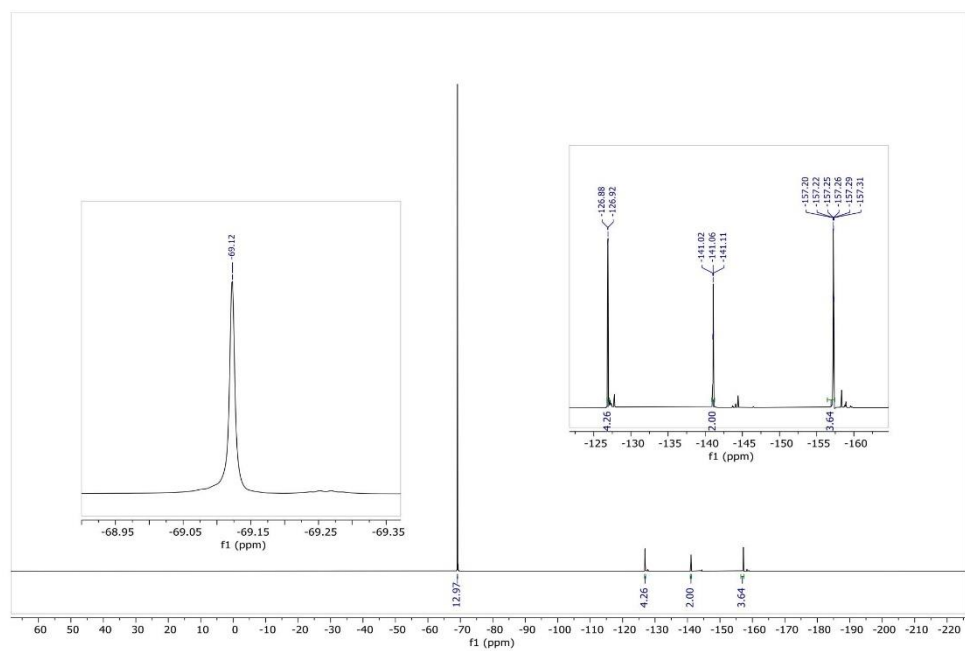


Figure S 21: ^{19}F NMR spectrum of **4** in benzene- d_6 solution at 298 K. The spectrum additional contains minor signals of an unidentified side-product.

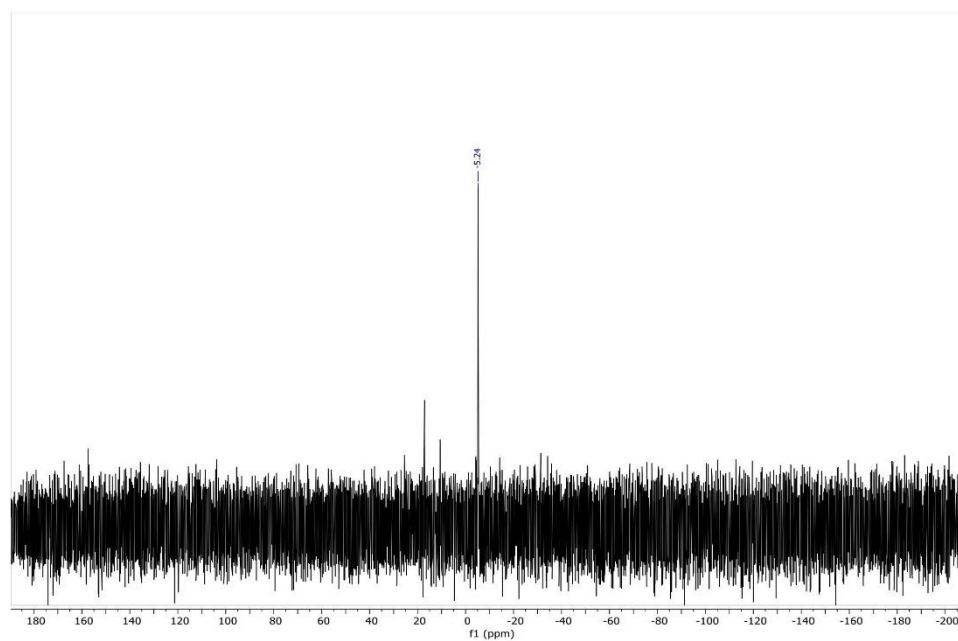


Figure S 22: ^{29}Si NMR spectrum of **4** in benzene- d_6 solution at 298 K.

5 References

- [1] M. Muhr, P. Heiß, M. Schütz, R. Bühler, C. Gemel, M. H. Linden, H. B. Linden, R. A. Fischer, *Dalton Trans.* **2021**, 50, 9031-9036.
- [2] SAINT, Version 8.40A ed., Bruker AXS Inc., Madison, Wisconsin, USA, **2016**.
- [3] SADABS, Version 2016/2, ed., Bruker AXS Inc., Madison, Wisconsin, USA, **2016**.
- [4] Bruker AXS Inc., Madison, Wisconsin, USA, **2015**.
- [5] (a) L. J. Bourhis, O. V. Dolomanov, R. J. Gildea, J. A. K. Howard, H. Puschmann, *Acta Crystallogr., Sect. A* **2015**, 71, 59-75; (b) O. V. Dolomanov, L. J. Bourhis, R. J. Gildea, J. A. K. Howard, H. Puschmann, *J. Appl. Crystallogr.* **2009**, 42, 339-341; (c) G. M. Sheldrick, *Acta Crystallogr., Sect. C* **2015**, 71, 3-8.
- [6] G. M. Sheldrick, University of Göttingen, Göttingen, Germany, **2014**.
- [7] C. B. Huebschle, G. M. Sheldrick, B. Dittrich, *J. Appl. Cryst.* **2011**, 44, 1281.
- [8] G. M. Sheldrick, *Acta Crystallogr., Sect. A* **2015**, 71, 3-8.
- [9] A. J. C. Wilson, *International Tables for Crystallography, Vol. C*, Kluwer Academic Publishers, Dordrecht, Netherlands **1992**.
- [10] C. F. Macrae, I. Sovago, S. J. Cottrell, P. T. A. Galek, P. McCabe, E. Pidcock, M. Platings, G. P. Shields, J. S. Stevens, M. Towler, P. A. Wood, *J. Appl. Crystallogr.* **2020**, 53, 226-235.
- [11] G. R. Fulmer, A. J. M. Miller, N. H. Sherden, H. E. Gottlieb, A. Nudelman, B. M. Stoltz, J. E. Bercaw, K. I. Goldberg, *Organometallics* **2010**, 29, 2176-2179.

11.4 Supporting Information Chapter 8

Supporting Information

Table of Contents

1	Experimental Section.....	3
1.1	General methods and Instrumentation.....	3
1.2	Synthesis and Characterization.....	5
1.2.1	Synthesis and characterization of 1·MeCN.....	5
1.2.2	Synthesis and characterization of acetonitrile-free germane 1	6
1.2.3	Synthesis and characterization of acetonitrile-free silane 2.....	7
1.2.4	Synthesis of and characterization of [K·(18-c-6)] [1-F]	8
1.2.5	Synthesis of and characterization of [MeCN·SiEt ₃] [H-1].....	8
1.2.6	Synthesis of and characterization of dioxane-bridged germylene 3	9
2	NMR experiments with 1·MeCN	10
2.1	Lewis acidity determination by <i>Gutmann-Beckett</i> method	10
2.2	NMR-Scale Abstraction Experiments	12
2.2.1	Reaction of 1·MeCN with AgSbF ₆	12
2.2.2	Reaction of 1·MeCN with [Mes ₃ PH][HB(C ₆ F ₅) ₃]	13
2.2.3	Reaction of 1·MeCN with Et ₃ SiF	15
2.2.4	Reaction of acetonitrile-free 1 with Et ₃ SiH	16
2.2.5	Reaction of 1 with Et ₃ SiH in presence of acetonitrile	19
2.3	Catalytic experiments	23
2.3.1	Dimerization of α -methylstyrene and 1,1-diphenylethylene.....	23
2.3.2	Hydrosilylation of α -methylstyrene	26
2.3.3	Stoichiometric hydrosilylation of methylstyrene with Et ₃ SiH.....	28
2.3.4	Hydrosilylation of α -methylstyrene with mixed silanes (iPr ₃ SiH vs Et ₃ SiH)	30
2.3.5	Hydrosilylation of α -methylstyrene with isotopically marked Et ₃ SiD	32
3	Computational Section	37
3.1	General Information	37
3.2	Hydrosilane activation mechanism.....	37

3.3	Thermochemistry analysis of the hydrosilylation catalytic cycle.....	39
3.4	Alternative mechanisms for the catalytic hydrosilylation	39
3.5	Calculated energies for compounds in Figure 3 and Scheme 2B.....	41
3.6	Calculation of ion affinities	42
4	Single-Crystal X-ray Diffraction Analysis	43
4.1	Crystal Structure of 1·MeCN.....	43
4.2	Crystal Structure of [K·(18-c-6)][F-1].....	43
4.3	Crystal Structure of donor-free silane 2	44
4.4	Crystal Structure of dioxane-coordinated germylene 3	44
4.5	Preliminary crystal structure of donor-free 1	45
5	NMR Spectra.....	49
5.1	NMR spectra of 1·MeCN	49
5.2	NMR spectra of 1	51
5.3	NMR spectra of 2	53
5.4	NMR spectra of [K·18-c-6][1-F]	55
5.5	NMR spectra of [Et ₃ Si·MeCN][H-1].....	57
5.6	NMR spectra of compound mixture 3 and 4	59
5.7	NMR spectra of 1,4-dioxane-coordinated germylene 3	61
6	References	63
7	Appendix A	64

1 Experimental Section

1.1 General methods and Instrumentation

Materials

All mentioned reactions were carried out in properly dried borosilicate glassware, filled with argon 4.6 ($\geq 99.996\%$; *Westfalen AG*) or in *LABstar* gloveboxes from *MBraun Inertgas-Systeme GmbH* with H_2O and O_2 levels not exceeding 5 ppm. In each reaction small overpressure of argon atmosphere was used to additionally prevent the intrusion of air. For sealing glass apparatuses *Triboflon III* PTFE/PEPE grease from *Freudenberg & Co. KG* was used. All heat-sensitive plastic materials such as syringes or cannulas were stored originally packed and flushed three times with argon.

Chemicals

The Chemicals for this project were purchased from the commercial distributors: *Merck KGaA (Sigma-Aldrich)*, *ABCR GmbH and TCI Co. Ltd.* The used hexafluoropinacol (H_2pin^F) was purchased from *Sigma-Aldrich* and *ABCR GmbH* and dried with molecular sieves (4 Å) in diluted Et_2O solution. After filtration and solvent removal in fine vacuo a mixture of 80 – 88 w% H_2pin^F in Et_2O was obtained. Li_2pin^F ,^[1] $[\text{Mes}_3\text{PH}][\text{HB}(\text{C}_6\text{F}_5)_3]^{[2]}$ and $\text{B}(\text{C}_6\text{F}_5)_3$ ^[3] were synthesized according to literature procedures. Safety note: The use of directly dried, Et_2O -free H_2pin^F in one lithiation experiment resulted in an explosion in the glovebox when the product was scraped from the glass wall with a spatula. Reactants for catalytic experiments were degassed and stored over molecular sieves. The used solvents for applications were distilled over elemental sodium/benzophenone (toluene, *n*-hexane, Et_2O), calcium hydride (acetonitrile, chloroform, acetonitrile-*d*₃, chloroform-*d* and dichloromethane-*d*₂), additionally degassed and stored over molecular sieves.

NMR-spectroscopy

All NMR samples were prepared in an argon (4.6) atmosphere using *J-Young* PTFE valve NMR tubes. The recorded ^1H , ^{13}C , ^{19}F and ^{29}Si NMR spectra were obtained from a *Bruker Avance Neo 400 MHz* spectrometer and a *Bruker AV500C* spectrometer at ambient temperatures (300 K), unless otherwise stated. The VT-NMR experiments were carried out the *Bruker Avance Neo 400 MHz* spectrometer at the given temperature. The obtained ^1H - and ^{13}C -NMR spectra were calibrated on the residual proton and natural abundance carbon signals of deuterated NMR solvents acetonitrile-*d*₃ and dichloromethane-*d*₂. The obtained chemical shifts δ are reported in ppm values, calibrated on tetramethylsilane. The observed signals were abbreviated as following: s = singlet, br = broad signal and combinations, d = doublet, t = triplet, q = quartet, p = quintet, h = septet, m = multiplet and qm = quartet of multiplets. The spectra were processed and analyzed on the software *MestReNova* (version 12.0.1-20560).

FT-ATR-IR spectra

The attenuated total reflection infrared ATR-IR spectra were recorded on a *Perkin Elmer* spectrometer (*diamond ATR, Spectrum Two*) in the range of 400 – 4000 cm^{-1} at room temperature under an argon atmosphere.

Elemental analysis

The analysis was carried out by the central analytics laboratory of the *TUM Catalysis Research Center*. For the procedure 0.5 – 1.0 mg of the investigated compounds were closely packed within two layers of tin foil under an argon atmosphere and subsequently handed to the elemental analysis team. The Analysis was performed on a *EURO EA (HEKAtech)* instrument equipped with a CHNS combustion analyzer.

LIFDI

Liquid Injection Field Desorption Ionization Mass Spectrometry (LIFDI-MS) was measured directly from an argon-filled glovebox with a *Thermo Fisher Scientific Exactive Plus Orbitrap* equipped with a *Linden CMS* ion source.^[4]

Melting Point

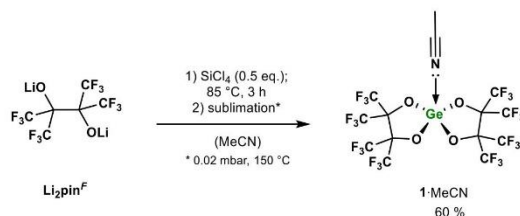
The Melting Points (m.p.) were determined in sealed glass capillaries under argon atmosphere using a *Büchi B-540* melting point apparatus.

Single crystal X-ray diffraction analysis

The X-ray intensity data were collected on an X-ray single crystal diffractometer equipped with a CMOS detector (Bruker Photon-100), a rotating anode (Bruker TXS) with MoK α radiation ($\lambda = 0.71073 \text{ \AA}$) and a Helios mirror optic by using the APEX4 software package^[5] or an X-ray single crystal diffractometer equipped with a CMOS detector (Bruker Photon-100), an IMS microsource with MoK α radiation ($\lambda = 0.71073 \text{ \AA}$) and a Helios mirror optic by using the APEX III software package.^[5] The measurement was performed on single crystals coated with perfluorinated ether. The crystal was fixed on the top of a micro-sampler, transferred to the diffractometer and measured under a stream of cold nitrogen. A matrix scan was used to determine the initial lattice parameters. Reflections were merged and corrected for Lorentz and polarization effects, scan speed, and background using SAINT.^[6] Absorption corrections, including odd and even ordered spherical harmonics were performed using SADABS.^[7] Space group assignments were based upon systematic absences, E statistics, and successful refinement of the structures. Structures were solved by direct methods with the aid of successive difference Fourier maps, and were refined against all data using the APEX4^[5] and OLEX2^[8] in conjunction with SHELXL-2014^[9] and SHELXLE.^[10] Methyl hydrogen atoms were refined as part of rigid rotating groups, with a C–H distance of 0.98 \AA and $U_{iso}(H) = 1.5 \cdot U_{eq}(C)$. Other H atoms were placed in calculated positions and refined using a riding model, with methylene and aromatic C–H distances of 0.99 and 0.95 \AA , respectively, and $U_{iso}(H) = 1.2 \cdot U_{eq}(C)$. If not mentioned otherwise, non-hydrogen atoms were refined with anisotropic displacement parameters. Full-matrix least-squares refinements were carried out by minimizing $\Delta w(F_o^2 - F_c^2)^2$ with SHELXL-97^[11] weighting scheme. Neutral atom scattering factors for all atoms and anomalous dispersion corrections for the non-hydrogen atoms were taken from International Tables for Crystallography.^[12] Images of the crystal structures were generated by PLATON and MERCURY.^[13] The CCDC numbers CCDC- (2286080-2286083, 2286830) contain the supplementary crystallographic data for the structures **1MeCN**, [K(18c6)][**1-F**], **2**, **3** and **1**. These data can be obtained free of charge from the Cambridge Crystallographic Data Centre via <https://www.ccdc.cam.ac.uk/structures/>.

1.2 Synthesis and Characterization

1.2.1 Synthesis and characterization of 1·MeCN



To a solution of 3.0 g (8.67 mmol, 2.0 equiv.) $\text{Li}_2\text{pin}^{\text{F}}$ in 40 ml MeCN were added 0.49 ml (4.30 mmol, 1.0 equiv.) GeCl_4 at room temperature. The obtained solution slowly turned cloudy, and the reaction mixture was heated to 85 °C and stirred for 3 h. Afterwards, all volatiles were stripped off in vacuum and the obtained off-white solid was slowly heated to 150 °C and sublimated at a pressure of 0.02 mbar to give a colorless solid in 60 % yield.

Crystals suitable for SC-XRD analysis were obtained from a DCM solution at room temperature. For crystal structure please see Figure S 38.

m.p.: 142 -179 °C (sublimation and molten parts).

$^1\text{H-NMR}$ (400 MHz, acetonitrile- d_3) δ (ppm) = 1.96 (s, 3H, $\text{NCC}H_3$).

$^{13}\text{C NMR}$ (126 MHz, acetonitrile- d_3) δ (ppm) = 122.2 (q, $^1J_{\text{C-F}} = 293 \text{ Hz}$, CF_3), 81.5 (br, $\text{OC}(\text{CF}_3)_2$).

$^{19}\text{F NMR}$ (377 MHz, acetonitrile- d_3) δ (ppm) = -69.04 – -70.93 (m, 24F, CF_3).

Elemental Analysis calcd. [%] for $\text{C}_{14}\text{H}_3\text{F}_{24}\text{NO}_4\text{Ge}$: C (21.62), H (0.39), N (1.80), S (-); **found (%)**: C (21.15), H (0.30), N (1.17), S (-).

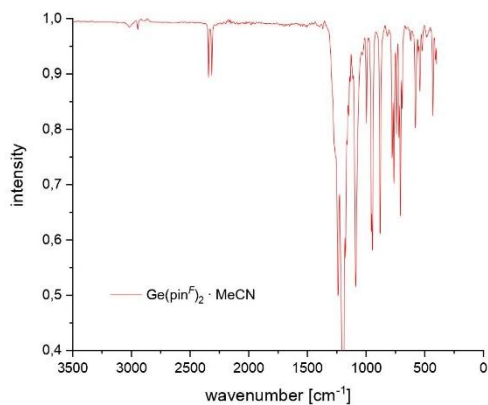
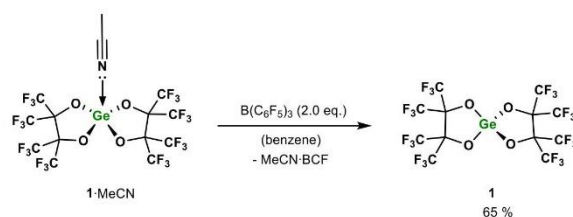


Figure S 1: FT-IR-spectrum of 1·CH₃CN showing two superimposed frequencies of blue-shifted C≡N and C–H vibrations originating from the coordinated acetonitrile.

1.2.2 Synthesis and characterization of acetonitrile-free germane **1**

A mixture of 800 mg (1.03 mmol, 1.0 equiv.) **1**-MeCN and 1.05 g (2.06 mmol, 2.0 equiv.) $\text{B(C}_6\text{F}_5)_3$ were dissolved in 4 mL of benzene and heated to 80 °C. For ensuring a complete dissolution and thus mixture of the reactants, the walls of the glass vessel were additionally gently heated with a heat gun. Afterwards, the obtained clear solution was slowly cooled to 0 °C. The formed precipitation was collected by filtration dried under reduced pressure. For a complete product separation, the crude-product was sublimated at 60 °C and a pressure of 0.02 mbar. Compound **1** was then collected as a crystalline, colorless solid in 65 % yield.

Crystals suitable for SC-XRD analysis were obtained from a slow sublimation at 40 °C temperature and 1 bar of argon atmosphere. For crystal structure please see S 42.

m.p.: 67.1 – 71.9 °C (partially sublimated).

^{13}C NMR (126 MHz, acetonitrile- d_3) δ (ppm) = 122.2 (q, $^1J_{\text{C-F}} = 293$ Hz, CF_3), 81.5 (br, $\text{OC(CF}_3)_2$).

^{19}F NMR (377 MHz, acetonitrile- d_3) δ (ppm) = -68.93 – -71.19 (m, 24F, CF_3).

Elemental Analysis calcd. [%] for $\text{C}_{12}\text{F}_{24}\text{O}_4\text{Ge}$: C (19.56), H (-), N (-), S (-); found (%): C (20.02), H (0.06), N (-), S (-).

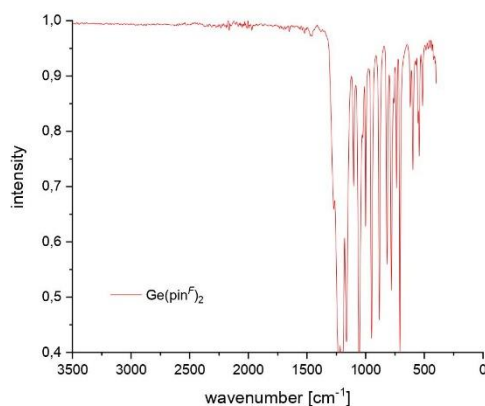
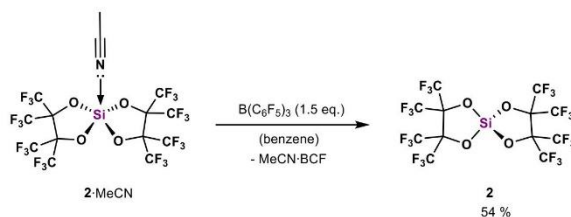


Figure S 2: FT-IR-spectrum of **1** showing the absence of the characteristic acetonitrile vibrations in the region of 2000 – 2500 cm^{-1} .

1.2.3 Synthesis and characterization of acetonitrile-free silane **2**

A mixture of 500 mg (682 μmol , 1.0 equiv.) **2**·MeCN and 524 mg (614 μmol , 1.5 equiv.) $\text{B(C}_6\text{F}_5)_3$ were dissolved in 6 mL of benzene and heated to 80 °C. Complete dissolution was obtained by gently heating the glass walls with a heat gun. The obtained clear solution was slowly cooled to 0 °C and the formed precipitation was filtered off and washed with 1 ml benzene in the cold. After drying under reduced pressure, the solvent-free product **2** was obtained as a colorless solid in 54 % yield. Alternatively, the crude product can be purified by sublimation (60 °C, 0.04 mbar).

Crystals suitable for SC-XRD analysis were obtained from a slow sublimation at 40 °C temperature under 1 bar of argon atmosphere in a screw-cap glass vessel. For crystal structure please see Figure S 40.

m.p.: 66 – 68 °C.

^{13}C NMR (126 MHz, acetonitrile- d_3) δ (ppm) = 122.0 (qm, $^1J_{\text{C-F}} = 293$ Hz, CF_3), 83.5 (br, $\text{OC(CF}_3)_2$).

^{19}F NMR (377 MHz, acetonitrile- d_3) δ (ppm) = -69.48 – -70.05 (m, 12F, CF_3), -70.05 – -70.55 (m, 12F, CF_3).

^{29}Si NMR (99 MHz, acetonitrile- d_3) δ (ppm) = -110.33 (*Si*).

Elemental Analysis calcd. [%] for $\text{C}_{12}\text{F}_{24}\text{O}_4\text{Si}$: C (20.82), H (-), N (-), S (-); found (%): C (21.19), H (0.09), N (-), S (-).

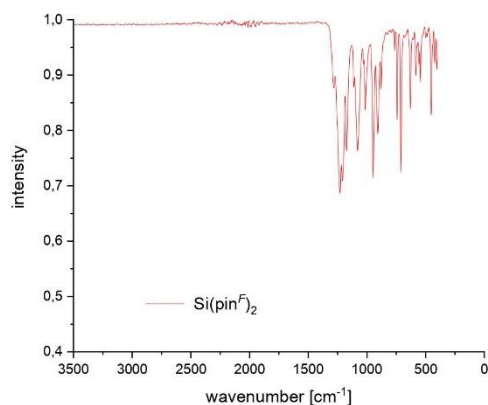
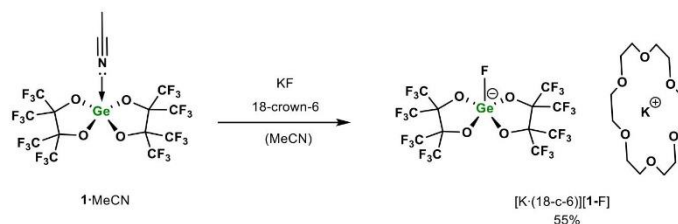


Figure S 3: FT-IR-spectrum of **2** showing the absence of the characteristic acetonitrile vibrations in the region of 2000 – 2500 cm^{-1} .

1.2.4 Synthesis of and characterization of [K·(18-c-6)][1-F]



To synthesize the pentavalent fluorogermanate species [1-F]⁻, 100 mg 1·MeCN (129 μmol, 1.0 equiv.), 7.50 mg KF (129 μmol, 1.0 equiv.) were dissolved in 1.0 ml acetonitrile. To this solution and 34.0 mg (129 μmol, 1.0 equiv.) 18-crown-6 dissolved in another 2.0 ml acetonitrile were added and the obtained solution was stirred for 230 minutes at room temperature. Afterwards, all volatile components were removed under reduced pressure. The obtained crude product was dissolved in 2.0 ml dichloromethane and precipitated by the addition of 10 ml hexane. The supernatant liquid phase was filtered off and the step was repeated once again. The obtained precipitation was then dried under reduced pressure to give a off-white solid in 55 % yield.

Crystals suitable for SC-XRD analysis were obtained from a saturated dichloromethane solution at -30 °C. For crystal structure please see Figure S 39.

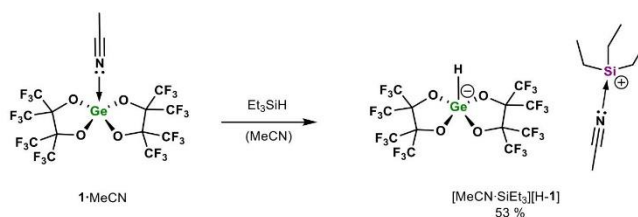
m.p.: 204 -225 °C (decomposition).

¹H NMR (400 MHz, acetonitrile-*d*₃) δ (ppm) = 3.57 (s, 24H, O-CH₂-CH₂-O).

¹³C NMR (126 MHz, acetonitrile-*d*₃) δ (ppm) = 122.8 (qm, ¹J_{C-F} = 293 Hz, CF₃), 81.6 (br, OC(CF₃)₂), 70.8 (s, 12C, OCH₂).

¹⁹F NMR (377 MHz, acetonitrile-*d*₃) δ (ppm) = -69.79 – -70.14(m, 12F, CF₃), -70.76 – -70.97 (m, 12F, CF₃), -145.04 – -145.25 (h, *J* = 8.3 Hz, 1F, Si-F).

Elemental Analysis calcd. [%] for C₂₄H₂₄F₂₅GeKO₁₀: C (27.22), H (2.28), N (-), S (-); found (%): C (27.36), H (1.95), N (-), S (-).

1.2.5 Synthesis of and characterization of [MeCN·SiEt₃][H-1]

To a solution of 100 mg (129 μmol, 1.0 equiv.) 1·MeCN diluted in 2.0 ml acetonitrile were added 15 mg (129 μmol, 5.0 equiv.) Et₃SiH at room temperature. The obtained solution was heated to 80 °C for 30 minutes. Afterwards all volatiles were removed under reduced pressure to give the product as a colorless solid in 53 % yield.

m.p.: 81-86 °C.

$^1\text{H NMR}$ (400 MHz, acetonitrile- d_3) δ (ppm) = 6.44 – 6.38 (m, 1H, GeH), 1.96 (s, 3H, NCCH_3), 1.10 – 0.99 (m, 15H, CH_2CH_3).

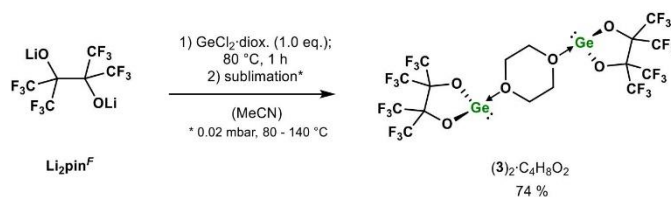
$^{13}\text{C NMR}$ (126 MHz, acetonitrile- d_3) δ (ppm) = 123.5 (q, $^1J_{\text{C-F}} = 293$ Hz, CF_3), 123.1 (q, $^1J_{\text{C-F}} = 293$ Hz, CF_3), 82.2 (br, $\text{OC}(\text{CF}_3)_2$), 6.13 (s, 3C, CH_2), 4.11 (s, 3C, CH_3).

$^{19}\text{F-NMR}$ (377 MHz, acetonitrile- d_3) δ (ppm) = -70.18 – -70.35 (m, 12F, CF_3), -70.63 – -70.82 (m, 12F, CF_3).

$^{29}\text{Si NMR}$ (99 MHz, acetonitrile- d_3) δ (ppm) = 36.38 (s, Et_3Si^+).

Elemental Analysis calcd. [%] for $\text{C}_{20}\text{H}_{19}\text{F}_{24}\text{GeNO}_4\text{Si}$: C (26.87), H (2.44), N (1.57), S (-); **found (%)**: C (26.58), H (1.63), N (1.67), S (-).

1.2.6 Synthesis of and characterization of dioxane-bridged germylene 3



A mixture of 600 mg (1.73 mmol, 1.0 equiv.) $\text{Li}_2\text{pin}^{\text{F}}$ and 402 mg (1.73 mmol, 1.0 equiv.) $\text{GeCl}_2 \cdot 1,4\text{-dioxane}$ was dissolved in 5 ml acetonitrile. The solution immediately turned opaque because of LiCl precipitation and was further heated to 80 °C for 1 hour to ensure complete conversion. Afterwards all volatiles were removed under reduced pressure at 0 °C to give the crude product. The title compound was isolated by twofold sublimation at 0.02 mbar while slowly heating from 80 °C to 140 °C over a 2-hour period.

Dioxane could not be removed under reduced pressure. The product additionally contains impurities of acetonitrile, which could not be removed. Single crystals suitable for XRD analysis were obtained from saturated DCM solution at -30 °C (Figure S 41).

m.p.: 72 – 75 °C.

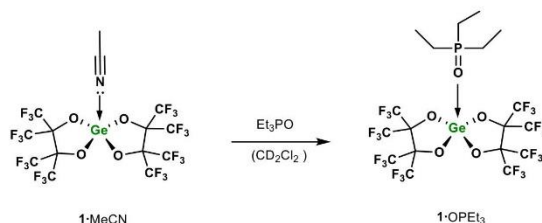
$^1\text{H NMR}$ (500 MHz, dichloromethane- d_2) δ (ppm) = 3.89 (s, 8H, CH_2).

$^{13}\text{C NMR}$ (126 MHz, dichloromethane- d_2) δ (ppm) = 122.2 (q, $^1J_{\text{C-F}} = 294$ Hz), 88.4 (br, $\text{OC}(\text{CF}_3)_2$), 67.1 (s, 4C, CH_2).

$^{19}\text{F-NMR}$ (377 MHz, dichloromethane- d_2) δ (ppm) = -70.6 (s, 12F, CF_3).

2 NMR experiments with 1·MeCN

2.1 Lewis acidity determination by Gutmann-Beckett method



For the Lewis acidity assessment of the obtained compounds the by Gutmann-Beckett was applied. In case of **1·MeCN**, 6.00 mg (7.71 μmol , 1.0 equiv.) of the Lewis acid were dissolved in 0.4 ml dichloromethane- d_2 and reacted with 1.03 mg Et_3PO (7.71 μmol , 1.0 equiv.) in a gas-tight J-Young NMR tube. The obtained clear solution was analyzed by ^1H , ^{19}F and ^{31}P NMR spectroscopy.

^1H NMR (400 MHz, CD_2Cl_2) δ (ppm) = 2.11 (dq, $^2J_{\text{P-H}} = 12.4$ Hz, $^3J_{\text{H-H}} = 7.7$ Hz, 6H, PCH_2), 1.26 (dt, $^2J_{\text{P-H}} = 12.4$ Hz, $^3J_{\text{H-H}} = 7.7$ Hz, 9H, PCH_2CH_3).

^{13}C NMR (126 MHz, CD_2Cl_2) δ (ppm) = 17.37 (d, $^1J_{\text{P-C}} = 64.0$ Hz, PCH_2), 5.13 (d, $^3J_{\text{P-C}} = 4.7$ Hz, PCH_2CH_3).

^{19}F -NMR (149 MHz, CD_2Cl_2) δ (ppm) = -69.19 – -69.99 (m, 24F, CF_3).

^{31}P NMR (162 MHz, CD_2Cl_2) δ (ppm) = 89.13 (s).

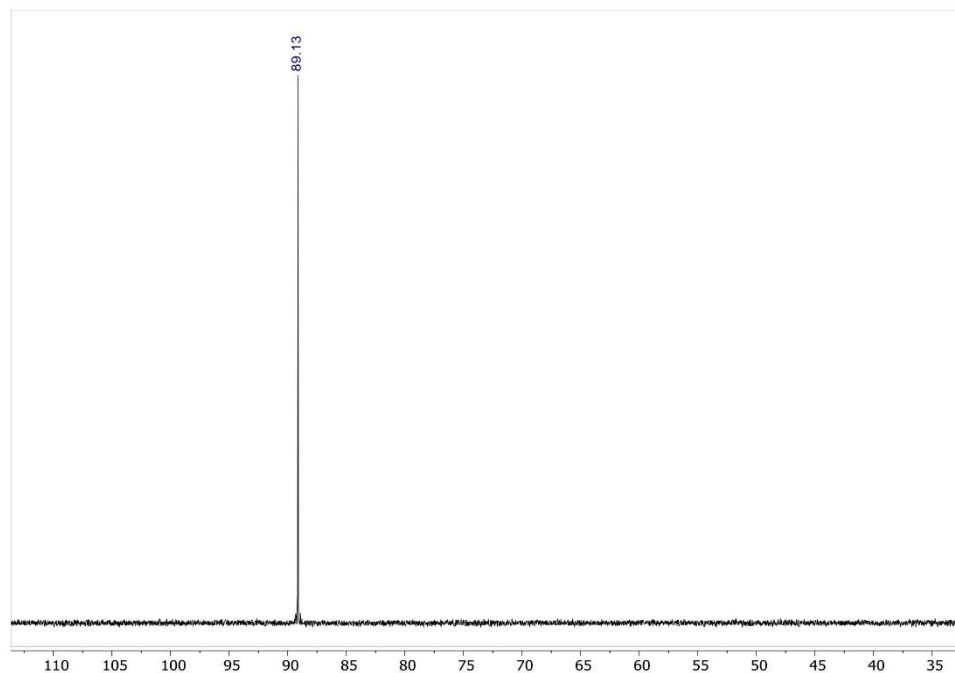


Figure S 4: ^{31}P NMR spectrum of **1·OPEt₃** obtained by the reaction of **1·MeCN** with Et_3PO in dichloromethane- d_2 .

The same sample was additionally treated with another equivalent of Et_3PO (total of 2.0 equiv.) and again analyzed by ^{31}P NMR spectroscopy. Figure S 5 shows a stack of free Et_3PO and the obtained coordination products.

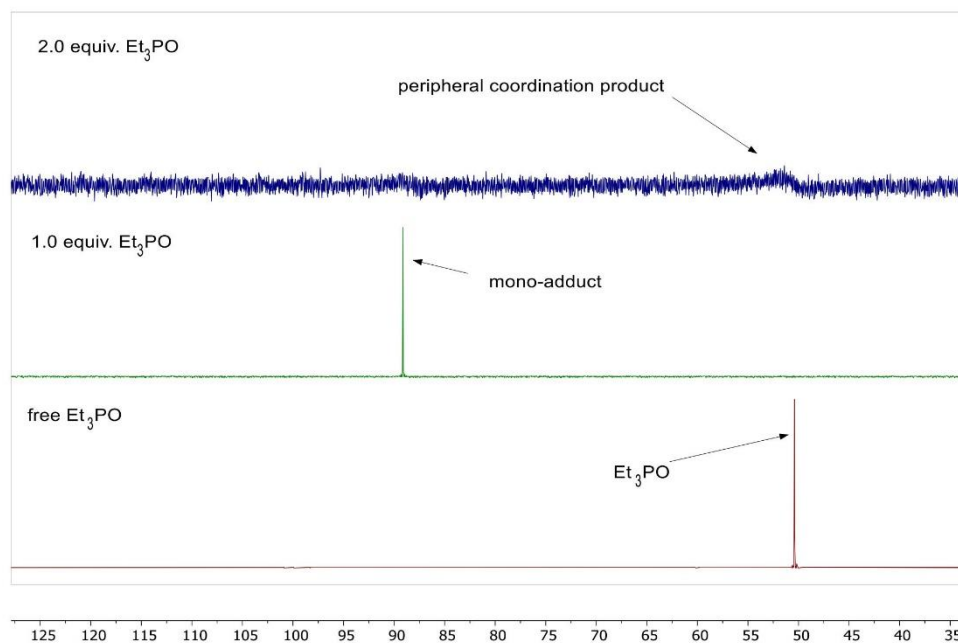
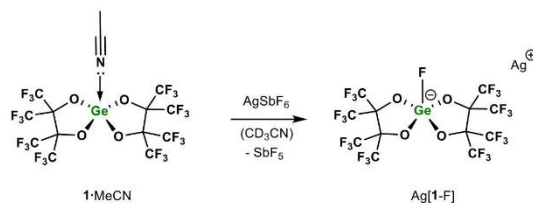


Figure S 5: Stacked ^{31}P NMR spectra of the reaction of **1-MeCN** with 1.0 and 2.0 equiv. of Et_3PO in dichloromethane- d_2 at 300 K.

2.2 NMR-Scale Abstraction Experiments

2.2.1 Reaction of 1·MeCN with AgSbF₆

A mixture of 16.0 mg (20.6 μmol , 1.0 equiv.) 1·MeCN and 7.10 (20.7 μmol , 1.0 equiv.) AgSbF₆ was placed in a PTFE-valved J-Young NMR tube and dissolved in 0.4 ml of acetonitrile-*d*₃. The obtained solution was heated to 60 °C for one hour and afterwards analyzed by multinuclear NMR spectroscopy.

¹³C NMR (126 MHz, acetonitrile-*d*₃) δ (ppm) = 122.7 (qm, ¹J_{C-F} = 295 Hz, CF₃), 81.6 (br, OC(CF₃)₂).

¹⁹F-NMR (149 MHz, acetonitrile-*d*₃) δ (ppm) = -69.83 – -70.12 (m, 12F, CF₃), -70.67 – -71.02 (m, 12F, CF₃), -145.00 – -145.24 (m, 1F, Si-F).

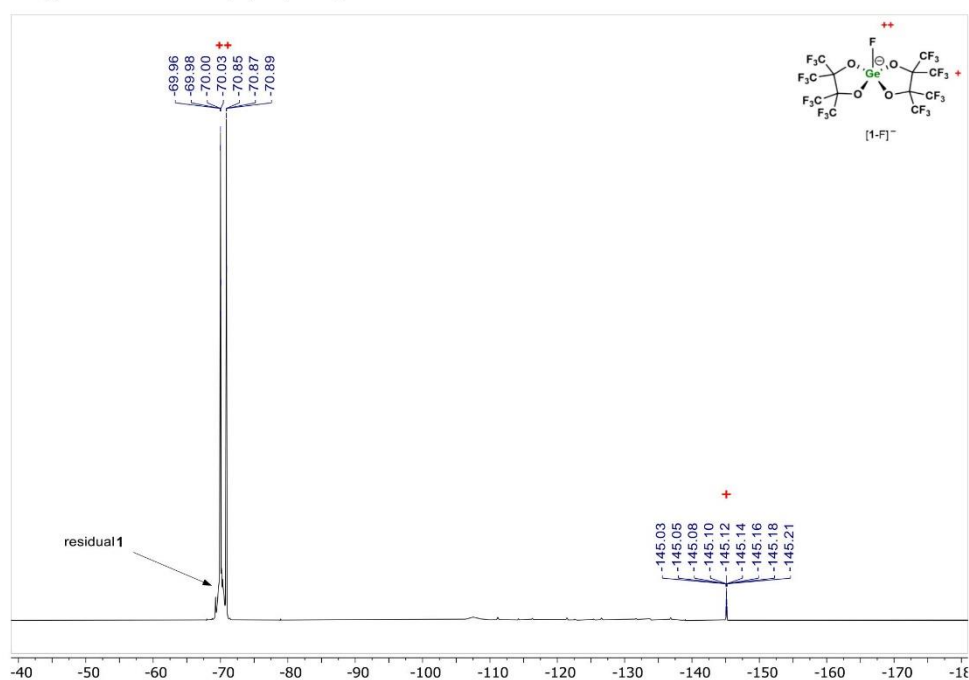
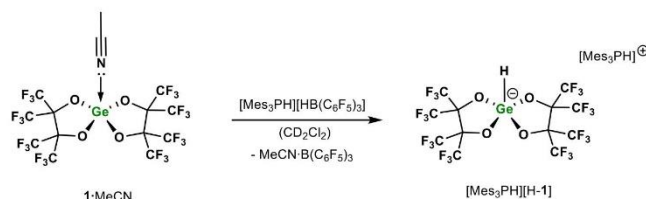


Figure S 6: ¹⁹F NMR of the reaction mixture after 1h at 60 °C showing the formation of the fluorogermanate anion [1-F]⁻, thus confirming a successful fluoride abstraction.

2.2.2 Reaction of 1·MeCN with [Mes₃PH][HB(C₆F₅)₃]

To a solution of [Mes₃PH][HB(C₆F₅)₃] in 0.4 ml CD₂Cl₂ was added 1·MeCN. The reaction mixture was transferred into a J-Young NMR tube and shaken until a clear solution was obtained. Reaction progress was traced by ¹H, ¹¹B and ¹⁹F NMR spectroscopy.

For further verifying the hydride abstraction from [HB(C₆F₅)₃]⁻ the obtained reaction mixture was compared to separately synthesized MeCN·B(C₆F₅)₃.

¹H NMR (400 MHz, CD₂Cl₂) δ (ppm) = δ 8.25 (d, ¹J_{p-H} = 478.1 Hz, 1H, PH), 7.13 (d, ⁴J_{p-H} = 36.1 Hz, 6H, *m*-ArH), 6.47 – 6.41 (m, 1H, GeH), 2.39 (s, 9H, *p*-Ar-CH₃), 2.30 (s, 9H, *o*-Ar-CH₃), 2.02 (s, 9H, *o*-Ar-CH₃).

¹¹B NMR (128 MHz, CD₂Cl₂) δ (ppm) = -10.68 (s, B(C₆F₅)₃).

¹⁹F NMR (377 MHz, CD₂Cl₂) δ (ppm) = -69.80 – -69.98 (m, 12F, CF₃), -70.36 – -70.53 (m, 12F, CF₃).

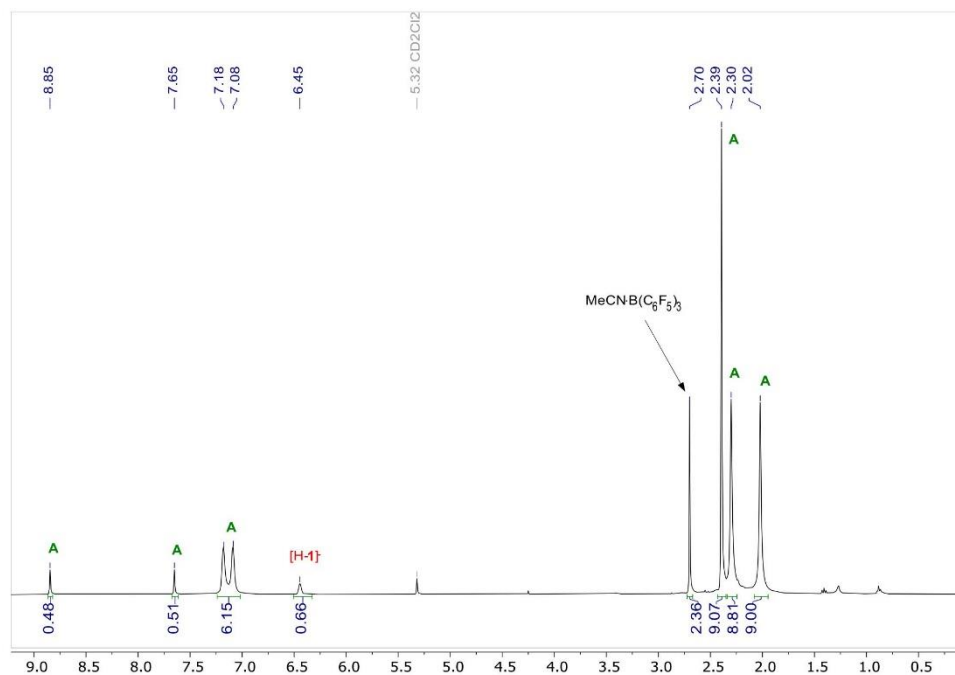


Figure S 7: ¹H NMR of the reaction mixture after complete dissolution of the reactants in CD₂Cl₂ showing the formation of the hydrido germanate anion [H-1]⁻ with the [Mes₃PH]⁺ (A) counter cation. No [HB(C₆F₅)₃]⁻ signal could be observed.

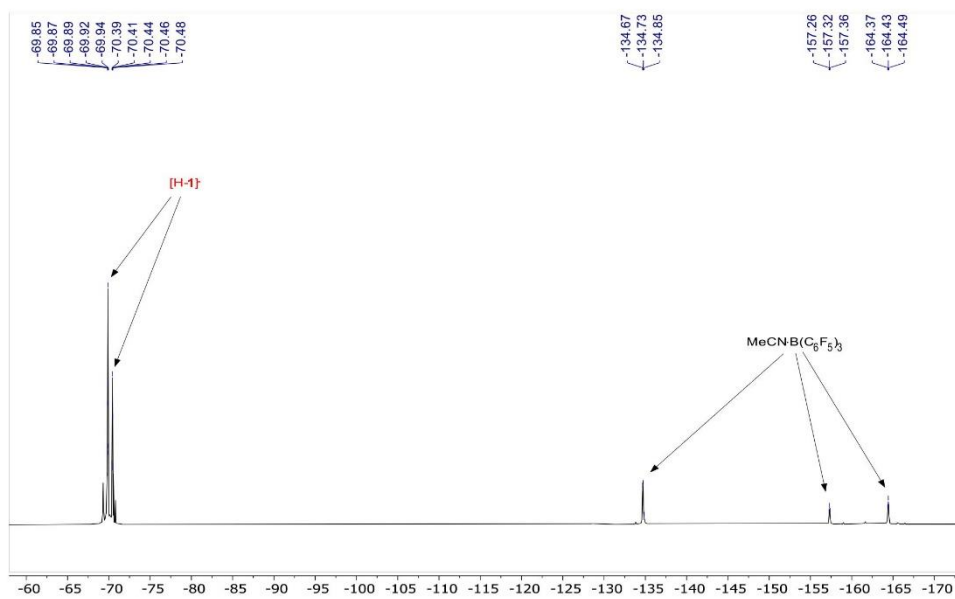


Figure S 8: ^{19}F NMR of the reaction mixture showing the presence of hydrido germanate anion $[\text{H-1}]^-$ and MeCN-coordinated BCF. No $[\text{HB}(\text{C}_6\text{F}_5)_3]$ signals are present.

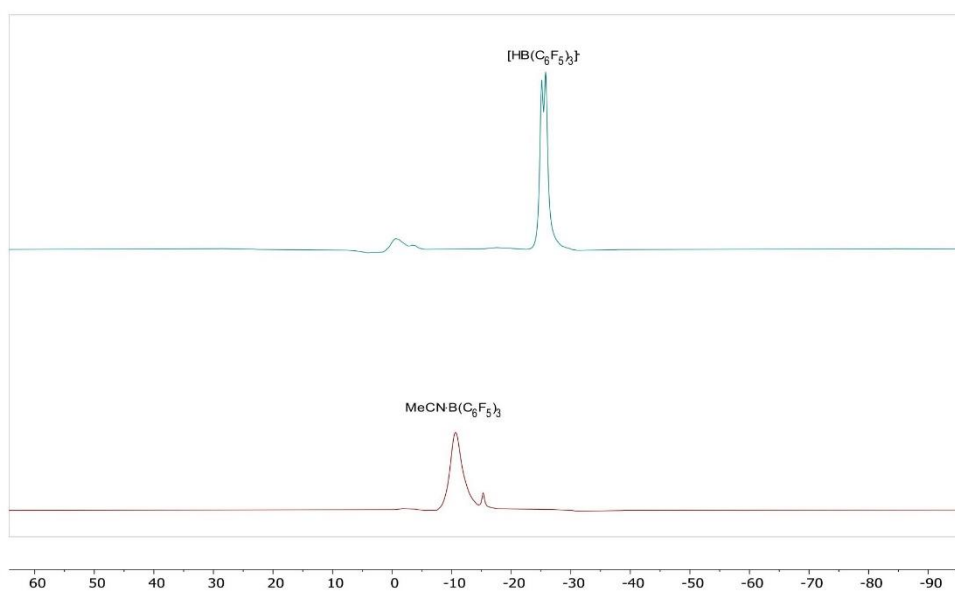
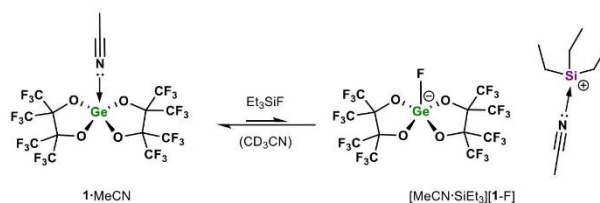


Figure S 9: Stacked ^{11}B NMR showing the characteristic doublet of $[\text{HB}(\text{C}_6\text{F}_5)_3]$ before $1 \cdot \text{MeCN}$ was added to the reaction mixture (top) and the signal of MeCN-coordinated BCF after addition of $1 \cdot \text{MeCN}$ (bottom).

2.2.3 Reaction of 1·MeCN with Et₃SiF

To 10 mg (12.9 μmol , 1.0 equiv.) of **1**·MeCN in 0.4 ml acetonitrile-*d*₃ were added 17.3 mg (129 μmol , 10.0 equiv.) Et₃SiF in a PTFE-valved J-Young NMR tube. The obtained solution was analyzed by multinuclear NMR spectroscopy. No difference in reaction conversion was observed at longer periods at room temperature or upon heating to 80 °C for several hours. The conversion progress correlated with the amount of added Et₃SiF. When fewer equivalents Et₃SiF were used, significantly lower conversion was observed.

¹H-NMR (500 MHz, acetonitrile-*d*₃) δ (ppm) = 1.96 (s, 3H, NCC*H*₃), 1.11 – 1.02 (m, 15H, *CH*₃).

¹³C NMR (126 MHz, acetonitrile-*d*₃) δ (ppm) = 122.8 (qm, ¹*J*_{C-F} = 295 Hz, *CF*₃), 81.5 (br, OC(*CF*₃)₂), 6.18 (s, 3C, *CH*₂), 4.16 (s, 3C, *CH*₃).

¹⁹F-NMR (377 MHz, acetonitrile-*d*₃) δ (ppm) = -69.88 – -70.11 (m, 12F, *CF*₃), -70.76 – -70.99 (m, 12F, *CF*₃), -145.05 – -145.31 (m, 1F, Ge-*F*).

²⁹Si NMR (99 MHz, acetonitrile-*d*₃) δ (ppm) = 36.60 (s, Et₃Si⁺).

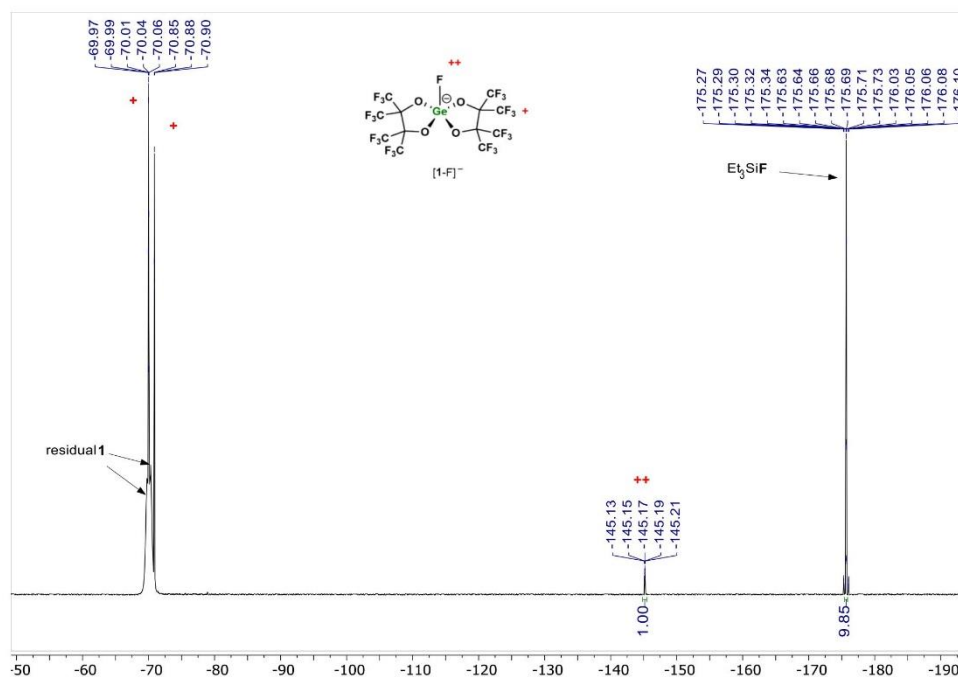


Figure S 10: ^{19}F NMR of the reaction mixture showing the partial formation of the fluorogermanate anion $[\mathbf{1}\text{-F}]^-$ in an reaction equilibrium, thus confirming a successful fluoride abstraction when a surplus of Et_3SiF is present. No further reaction progress was observed after various periods or upon heating.

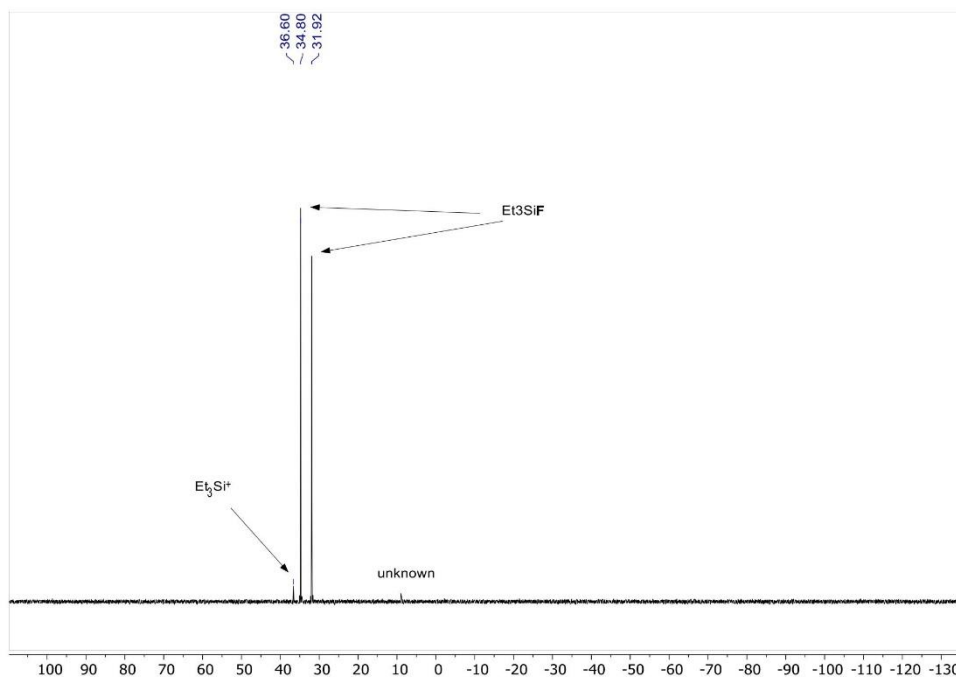
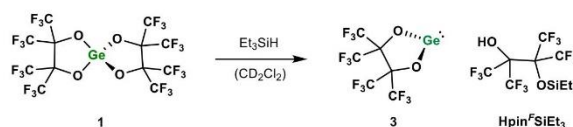


Figure S 11: $^{29}\text{Si}\{^1\text{H}\}$ NMR of the reaction mixture showing the partial formation of the MeCN-coordinated silyl cation (Et_3Si^+) next to the characteristic doublet ($^1J_{\text{Si-F}} = 286$ Hz) of Et_3SiF .

2.2.4 Reaction of acetonitrile-free **1** with Et_3SiH



To a suspension of 30 mg (40.7 mmol, 1.0 equiv.) of **1** in 0.4 ml of dichloromethane- d_2 were added 6.50 μl (40.7 mmol, 1.0 equiv.) Et_3SiH in a PTFE-sealed J-Young NMR tube. The obtained solution was analyzed by multi nuclear NMR spectroscopy. Product separation and isolation failed in multiple attempts.

^1H -NMR (400 MHz, dichloromethane- d_2) δ (ppm) = 3.94(s, 1H, OH), 0.98 (t, $^3J_{\text{H-H}} = 7.9$ Hz, 9H, CH_3), 0.80 (q, $^3J_{\text{H-H}} = 8.0$ Hz, 6H, CH_2).

^{13}C NMR (126 MHz, dichloromethane- d_2) δ (ppm) = 121.5 (qm, $^1J_{\text{C-F}} = 293$ Hz, CF_3), 121.9 (q, $^1J_{\text{C-F}} = 293$ Hz, CF_3), 88.8 (br, $\text{GeOC}(\text{CF}_3)_2$), 82.9 (p, $^2J_{\text{C-F}} = 31.2$ Hz, 1C, $\text{HO}(\text{C}(\text{CF}_3)_2)\text{OSi}$), 81.4(p, $^2J_{\text{C-F}} = 30.4$ Hz, 1C, $\text{HO}(\text{C}(\text{CF}_3)_2)\text{OSi}$), 6.41 (s, 3C, CH_2), 5.76 (s, 3C, CH_3).

^{19}F -NMR (377 MHz, dichloromethane- d_2) δ (ppm) = -68.97 – -69.26 (m, 6F, HO- CCF_3), -69.90 – -70.14 (m, 6F, SiO- CCF_3), -70.91 (s, 12F, Ge($\text{OC}(\text{CF}_3)_2$) $_2$).

^{29}Si NMR (99 MHz, dichloromethane- d_2) δ (ppm) = 31.69 (s, Si Et $_3$).

LIFDI-MS

For further investigation a high resolution LIFDI-MS analysis of the reaction mixture was performed, revealing the cleavage of the Si-O bond and consecutive hydride abstraction, by selectively giving the mass pattern for the hydrido germanate anion $[\text{H-1}]^-$ in negative mode:

calculated for $[\text{C}_{12}\text{HF}_{24}\text{GeO}_4]^-$: 738.87056

observed: 738.87157

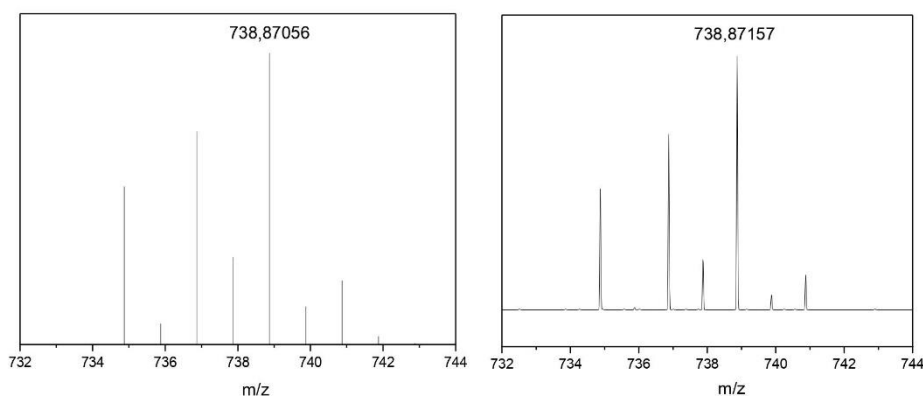
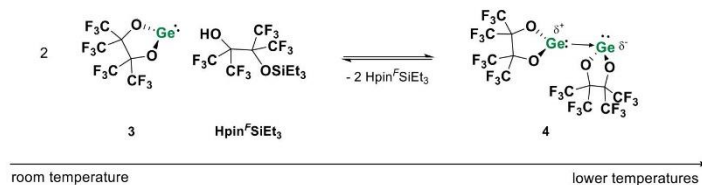


Figure S12: LIFDI-MS spectrometry (detail view with isotope pattern) of **3** obtained in negative mode. Measured (right; $m/z = 738.87157$) and simulated (left; $m/z = 738.87056$) mass spectrum.

Low Temperature NMR

At lower temperatures the thermodynamically favored dimerization of the perfluoropinacolato germylene is observed, leading to the formation of complex **4**. As a result of decreasing symmetry upon dimerization the sharp singlet at $\delta = -70.91$ ppm completely disappears at -80 °C due to heavy broadening. A related trend is also seen in the ^{29}Si NMR spectra where the silicon signal of the silylated alcohol shifts from $\delta = -31.69$ ppm (25 °C) to $\delta = -33.65$ ppm (-80 °C). This could be an effect of weak coordination at room temperature that decreases in favor of the germylene dimerization at low temperatures.



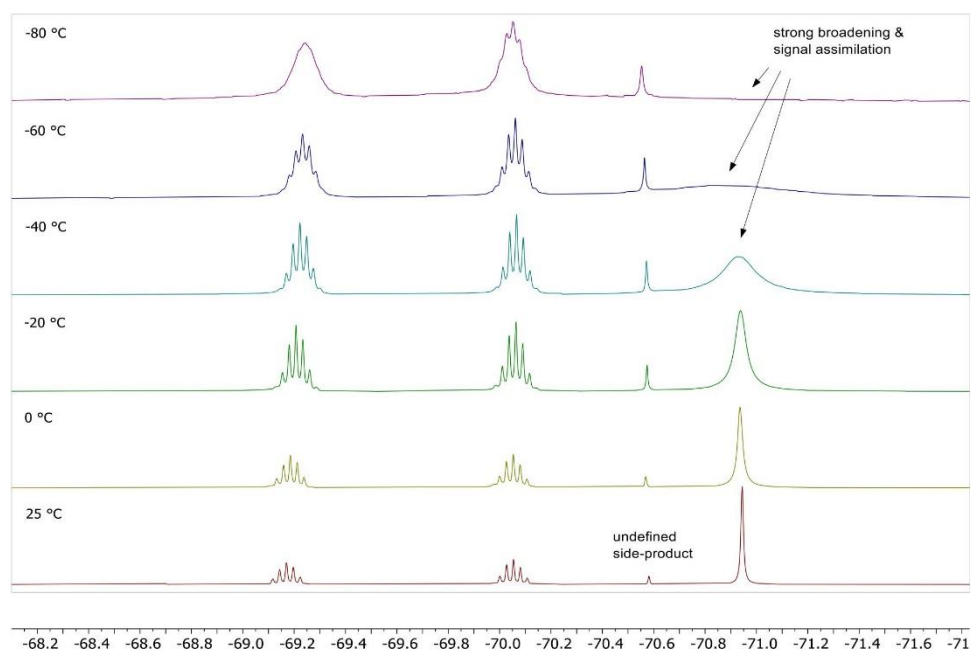


Figure S 13: Stacked ^{19}F NMR spectra in CD_2Cl_2 of a freshly prepared mixture of **3** and $\text{Hpin}^{\text{F}}\text{SiEt}_3$ at a temperature range from -80 °C to 25 °C.

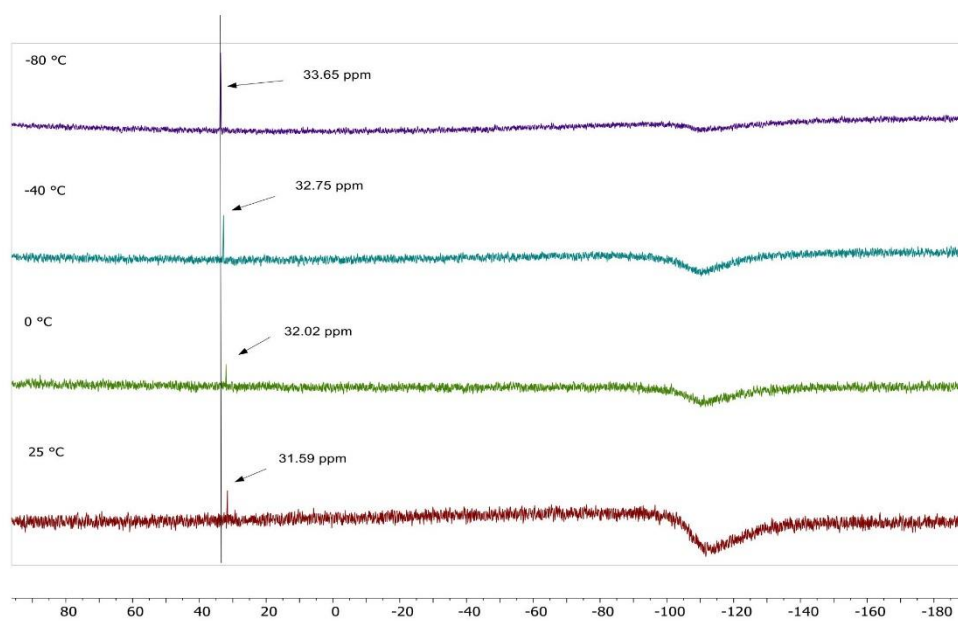
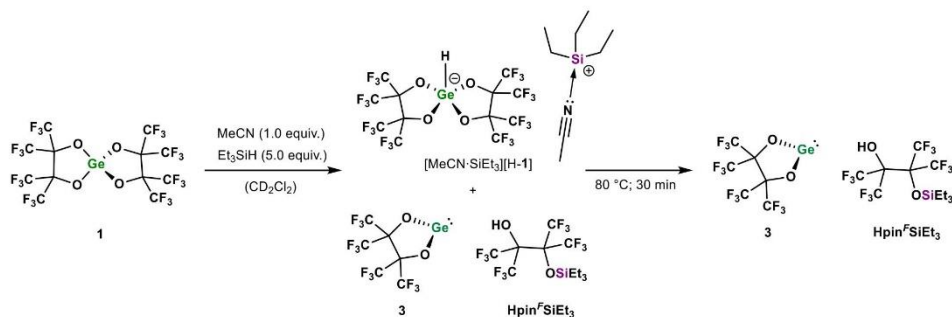


Figure S 14: Stacked $^{29}\text{Si}\{^1\text{H}\}$ NMR spectra in CD_2Cl_2 of freshly prepared **3** and $\text{Hpin}^{\text{F}}\text{SiEt}_3$ at a temperature range from $-80\text{ }^\circ\text{C}$ to $25\text{ }^\circ\text{C}$.

2.2.5 Reaction of **1** with Et_3SiH in presence of acetonitrile



In a PTFE-sealed J-Young NMR tube was dissolved 15 mg (20.4 μmol , 1.0 equiv.) **1** in 0.4 ml CD_2Cl_2 . To the mixture were subsequently added 1.2 μl (22.4 μmol , 1.0 equiv.) MeCN and 3.6 μl Et_3SiH . The NMR tube was shaken vigorously and analyzed by multinuclear NMR spectroscopy. Afterwards, the product mixture was heated to $80\text{ }^\circ\text{C}$ for 30 min and again analyzed.

The first NMR outlined the presence of the two main reaction products **3** (with by-product $\text{Hpin}^{\text{F}}\text{SiEt}_3$) and $[\text{MeCN}\cdot\text{SiEt}_3][\text{H-1}]$ in a molar ratio of 0.58/1.00 (referenced by integration of the Ge-H and OH signals). The second NMR (after heating) showed the selective formation of reaction product mixture **3** and $\text{Hpin}^{\text{F}}\text{SiEt}_3$. No residual traces of ionic $[\text{MeCN}\cdot\text{SiEt}_3][\text{H-1}]$ could be observed.

Note: The same results were obtained when **1**-MeCN was used instead of **1** and additional MeCN.

Observed product signals for **3** and $\text{Hpin}^{\text{F}}\text{SiEt}_3$:

$^1\text{H-NMR}$ (400 MHz, dichloromethane- d_2) δ (ppm) = 4.04/4.07 (s, 1H, OH), 0.97 (t, $^3J_{\text{H-H}} = 7.9\text{ Hz}$, 9H, CH_3), 0.80 (q, $^3J_{\text{H-H}} = 8.0\text{ Hz}$, 6H, CH_2).

$^{19}\text{F-NMR}$ (377 MHz, dichloromethane- d_2) δ (ppm) = -69.06 – -69.20/-69.03 – -69.25 (m, 6F, HO- CCF_3), -69.92 – -70.07/-69.90 – -70.11 (m, 6F, SiO- CCF_3), -70.61/-70.55 (s, 12F, $\text{Ge}(\text{OC}(\text{CF}_3)_2)_2$).

$^{29}\text{Si NMR}$ (99 MHz, dichloromethane- d_2) δ (ppm) = 31.61/31.53 (s, Si Et_3).

Observed product signals of $[\text{MeCN}\cdot\text{SiEt}_3][\text{H-1}]$:

$^1\text{H-NMR}$ (400 MHz, dichloromethane- d_2) δ (ppm) = 6.50 (s, 1H, GeH), 2.28 (s, 3H, CH_3CN), 1.14 – 1.02 (m, 15H, CH_2CH_3).

$^{19}\text{F-NMR}$ (377 MHz, dichloromethane- d_2) δ (ppm) = -69.66 – -69.88 (m, 12F, CF_3), -70.25 – -70.43 (m, 12F, CF_3).

$^{29}\text{Si NMR}$ (99 MHz, dichloromethane- d_2) δ (ppm) = 40.38 (s, Si Et_3).

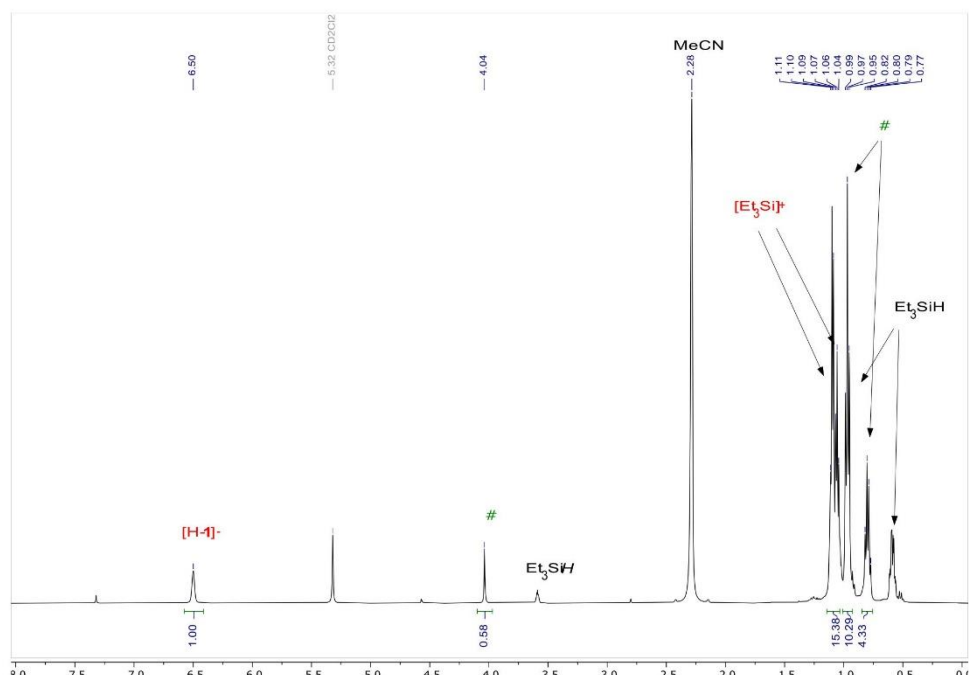
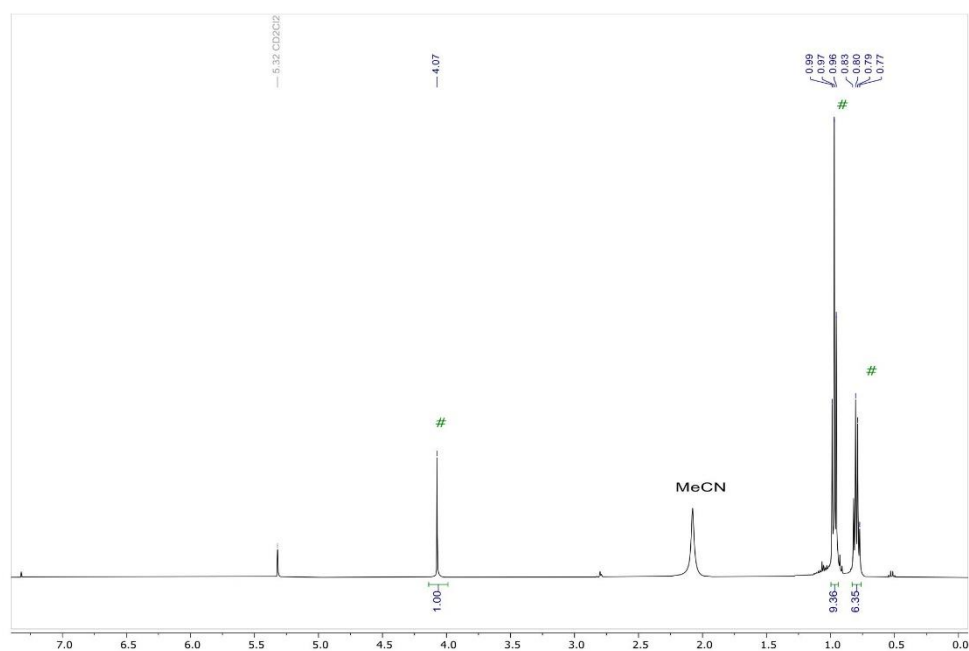


Figure S 15: ^1H NMR spectrum of the reaction mixture after 10 minutes at room temperature in CD_2Cl_2 , showing the formation of two main reaction products $\text{Hpin}^f\text{SiEt}_3$ (#) and $[\text{MeCN}\cdot\text{SiEt}_3][\text{H-1}]$ with an integral ratio of 0.58/1.00 and residual/unreacted Et_3SiH .



S20

Figure S 16: ^1H NMR spectrum of the reaction mixture after 30 minutes at 80 °C in CD_2Cl_2 , showing the selective formation of $\text{Hpin}^F\text{SiEt}_3$ (#) as the main reaction product. No more $[\text{MeCN}\cdot\text{SiEt}_3][\text{H-1}]$ can be observed.

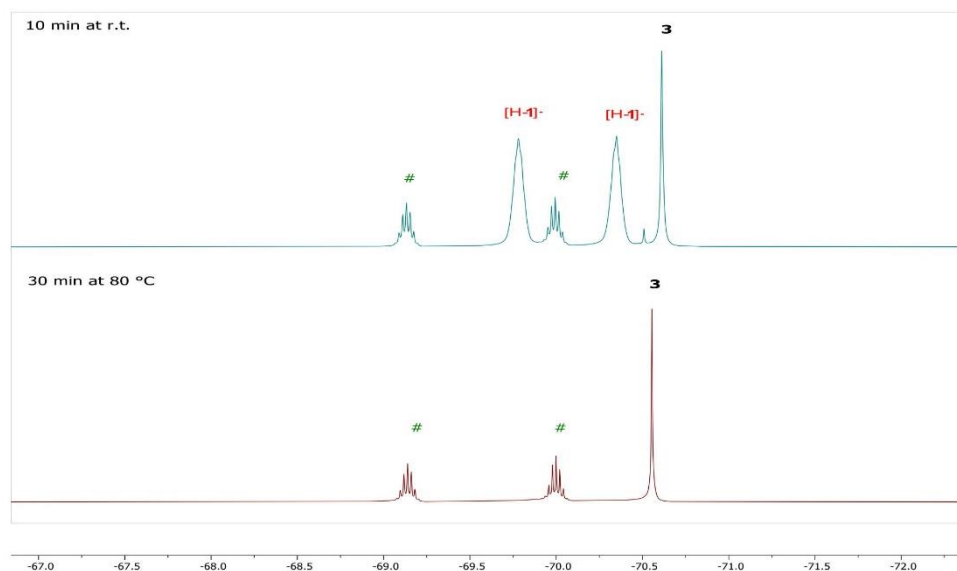


Figure S 17: Stacked ^{19}F NMR spectra of the reaction mixture after 10 minutes at room temperature in CD_2Cl_2 , showing the formation of two main reaction products **3**, $\text{Hpin}^F\text{SiEt}_3$ (#) and $[\text{MeCN}\cdot\text{SiEt}_3][\text{H-1}]$ (top) and the selective conversion to towards **3** and $\text{Hpin}^F\text{SiEt}_3$ (#) after 30 min at 80 °C (bottom).

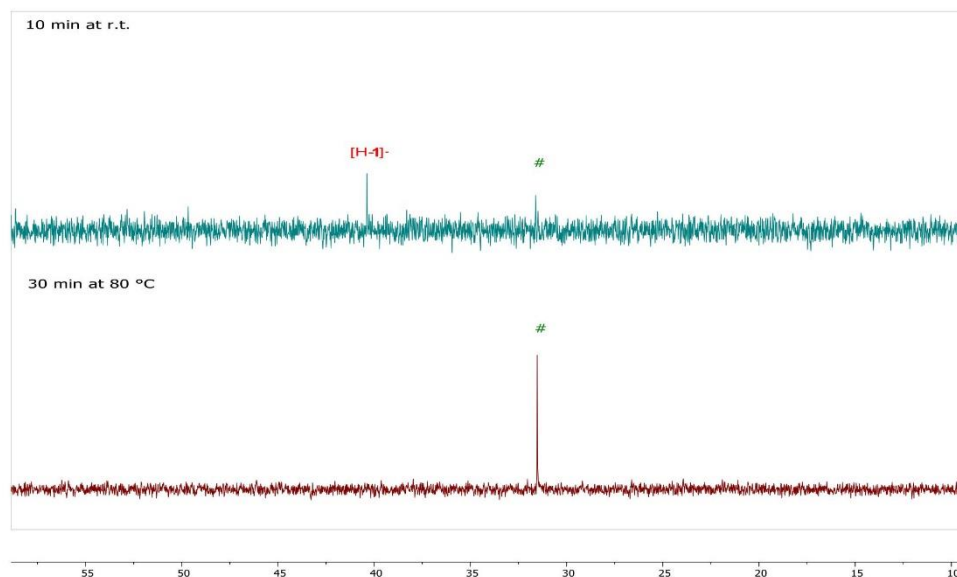
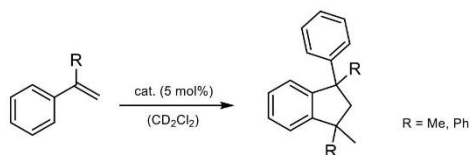


Figure S 18: Stacked $^{29}\text{Si}\{^1\text{H}\}$ NMR spectra of the reaction mixture after 10 minutes at room temperature in CD_2Cl_2 ,

showing the formation of two main reaction products $\text{Hpin}^f\text{SiEt}_3$ (#) and $[\text{MeCN}\cdot\text{SiEt}_3][\text{H-1}]$ (top) and the selective conversion to **3** and $\text{Hpin}^f\text{SiEt}_3$ (#) after 30 min at 80 °C (bottom).

2.3.1 Dimerization of α -methylstyrene and 1,1-diphenylethylene

In a PTFE-sealed J-Young NMR tube was dissolved 15 μ l α -methyl styrene or 15 μ l 1,1-diphenylethylene as well as 3 μ L of the internal standard mesitylene in 0.4 mL CD_2Cl_2 . After zero-point measurements, 0.05 mol% of the respective catalyst were added and the NMR tube was vigorously shaken. The mixture was then analyzed by ^1H NMR spectroscopy after 10 minutes at r.t. and several more intervals if necessary.

1,1,3-Trimethyl-3-phenyl-2,3-dihydro-1H-indene (R = Me)

^1H NMR (400 MHz, CD_2Cl_2) δ (ppm) = 7.34 – 7.07 (m, 9H, ArH), 2.44(d, $^2J_{\text{H-H}} = 13.1$ Hz, 1H, CHH), 2.22 (d, $^1J_{\text{H-H}} = 13.1$ Hz, 1H, CHH), 1.69 (s, 3H, CH_3), 1.36 (s, 3H, CH_3), 1.05 (s, 3H, CH_3).

^{13}C NMR (101 MHz, CD_2Cl_2) δ (ppm) = 152.69, 151.53, 149.24(ArC), 128.35, 127.09, 125.35, 122.96 (PhC), 59.54(CH_2), 51.19 (CMePh), 43.21 (CMe₂), 31.17 (CH_3), 30.89 (CH_3), 30.50 (CH_3).

1-Methyl-1,3,3-triphenyl-2,3-dihydro-1H-indene (R = Ph)

^1H NMR (400 MHz, CD_2Cl_2) δ (ppm) = 7.36 – 7.01 (m, 19H, ArH), 3.41 (d, $^2J_{\text{H-H}} = 13.5$ Hz, 1H, CHH), 3.14(d, $^2J_{\text{H-H}} = 13.5$ Hz, 1H, CHH), 1.57 (s, 3H, CH_3).

^{13}C NMR (101 MHz, CD_2Cl_2) δ (ppm) = 150.97, 149.81, 149.21, 149.08, 148.07 (ArC), 129.11, 129.07, 128.36, 128.23, 127.98, 127.86, 127.22, 126.40, 126.06, 125.95, 125.49 (PhC), 61.49 (CH_2), 61.33 (CPh₂), 51.57 (CMePh), 29.28 (CH_3).

Product signals correspond with pattern given in the literature.^[14]

Table S 1: Reaction conditions and conversion and yield of dimerization experiments after several hours at room temperature. Product yield and conversion of reactants were calculated by integration with respect to the internal standard.

Sample	Reagent	Catalyst	Temp. [°C]	Time	Conversion [%]	Yield [%]
I	α -methyl styrene	1	25	10 min	99	65
II	α -methyl styrene	1 ·MeCN	25	10 min	99	83
III	1,1-diphenylethylene	1	25	1 h	99	99
IV	1,1-diphenylethylene	1 ·MeCN	25	10 min	75	70
IV	1,1-diphenylethylene	1 ·MeCN	25	5 h	94	88
IV	1,1-diphenylethylene	1 ·MeCN	25	48 h	99	98

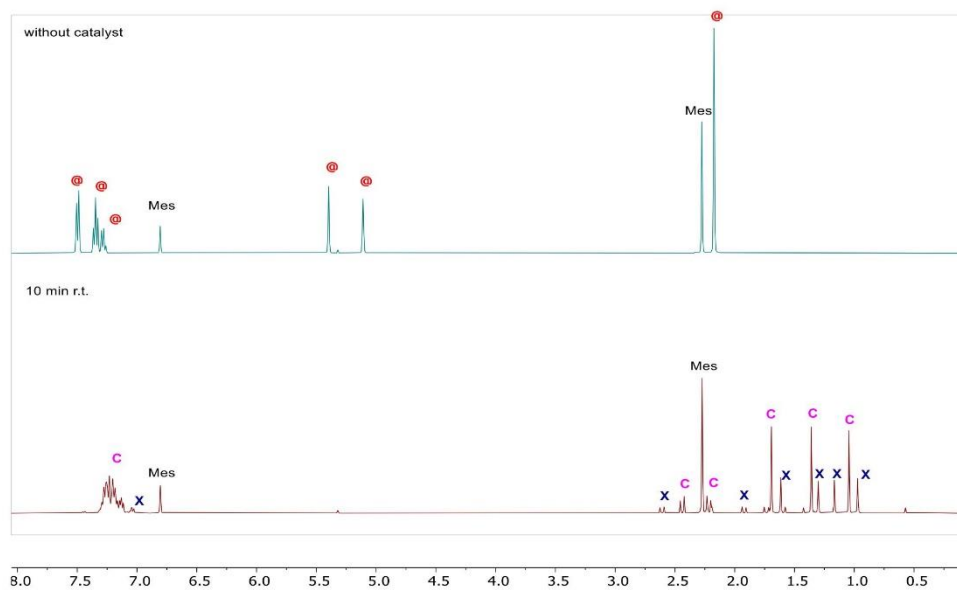


Figure S 19: Stacked ¹H NMR spectra in CD₂Cl₂ of the dimerization experiment of α-methyl styrene (A) using **1** as catalyst. After 10 min full conversion was obtained showing giving the dimer (C) as the main reaction product as well as minor amounts of undefined side products (X).

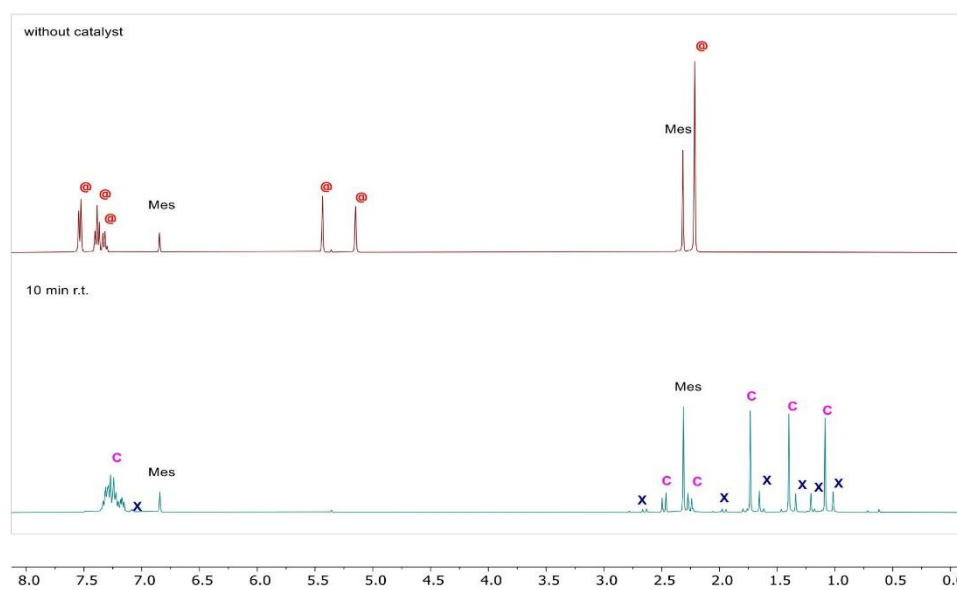


Figure S 20: Stacked ¹H NMR spectra in CD₂Cl₂ of the dimerization experiment of α-methyl styrene (A) using **1-MeCN** as catalyst. After 10 min full conversion was obtained showing giving the dimer (C) as the main reaction product as well as minor amounts of undefined side products (X).

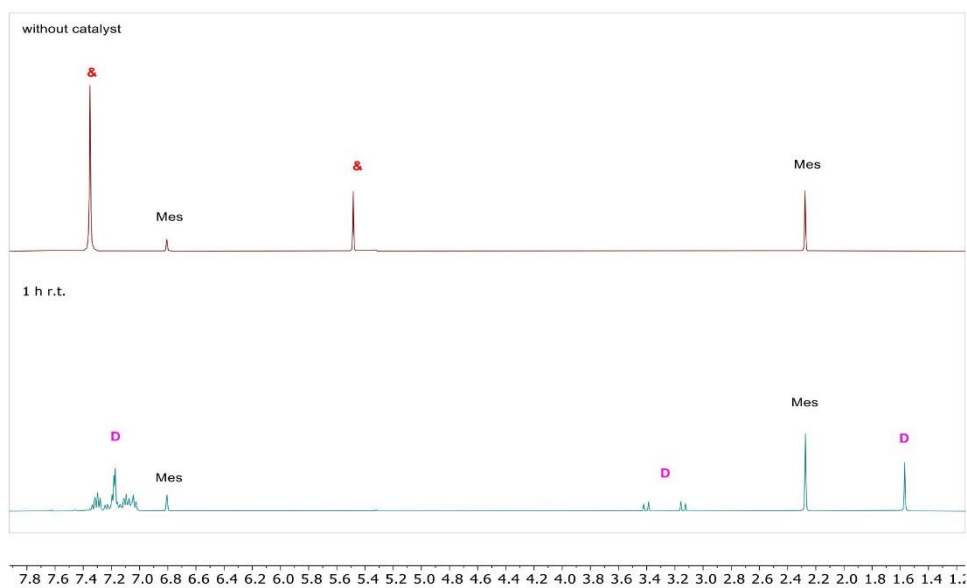


Figure S 21: Stacked ¹H NMR spectra in CD₂Cl₂ of the dimerization experiment of 1,1-diphenylethylene (A) using 1 as catalyst. After 10 min full conversion was obtained selectively yielding the dimerization product (B).

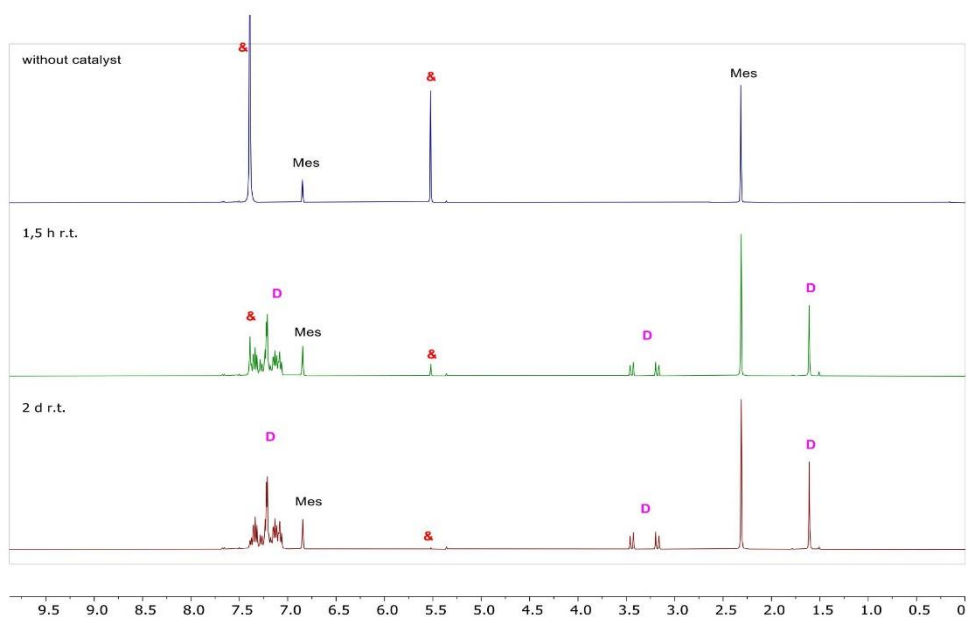
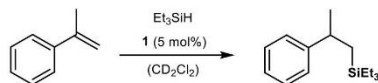


Figure S 22: Stacked ¹H NMR spectra in CD₂Cl₂ of the dimerization experiment of 1,1-diphenylethylene (&) using 1·MeCN as catalyst. After 2 days at room temperature nearly quantitative conversion was obtained selectively yielding the dimerization product (D).

2.3.2 Hydrosilylation of α -methylstyrene

To a solution 3.70 mg (500 μ mol, 0.05 equiv.) **1** in 0.4 ml CD_2Cl_2 were added 16 μ l (100 mmol, 1.00 equiv.) Et_3SiH in a PTFE-sealed J-Young NMR tube. After complete dissolution 13.0 μ l (100 mmol, 1.00 equiv.) α -methylstyrene and the internal standard mesitylene (3.00 μ l) was added. The reaction mixture was analyzed by ^1H NMR spectroscopy after several periods at defined temperatures.

Triethyl(2-phenylpropyl)silane:

^1H NMR (400 MHz, CD_2Cl_2) δ (ppm) = 7.32 – 7.21 (m, 4H, *o,m-CH*), 7.20 – 7.10 (m, 1H, *p-CH*), 2.96 – 2.83 (m, 1H, PhCHCH_3), 1.29 (d, $^3J_{\text{H-H}} = 6.9$ Hz, 3H, PhCHCH_3), 0.97 (dd, $^1J_{\text{H-H}} = 17.2$, $^3J_{\text{H-H}} = 7.5$ Hz, 2H, $\text{CH}(\text{CH}_3)\text{CH}_2$), 0.90 (t, $^3J_{\text{H-H}} = 7.9$ Hz, 9H, SiCH_2CH_3), 0.54 – 0.35 (m, 6H, SiCH_2CH_3).

^{13}C NMR (101 MHz, CD_2Cl_2) δ (ppm) = 150.75 (C), 128.64(*o,m-CH*), 127.04(*o,m-CH*), 126.09 (*p-CH*), 36.60 (CH), 26.82 (CH_3), 21.92 (CH_2), 7.62 (SiCH_2CH_3), 4.09 (SiCH_2CH_3).

Product signals corresponds to separately synthesized triethyl(2-phenylpropyl)silane and NMR signals given in the literature.^[15]

Table S 2: Reaction conditions and yield hydrosilylation experiments several hours at various temperatures. Product yield was calculated by integration of the PhCHCH_3 -Signal with respect to the internal standard.

Sample	Temp. [°C]	Time [h]	Conversion [%]	Yield [%]
I	25	24	28	26
I	25	72	33	31
I	25	216	69	65
I	25	336	95	89
II	-35	18	98	96

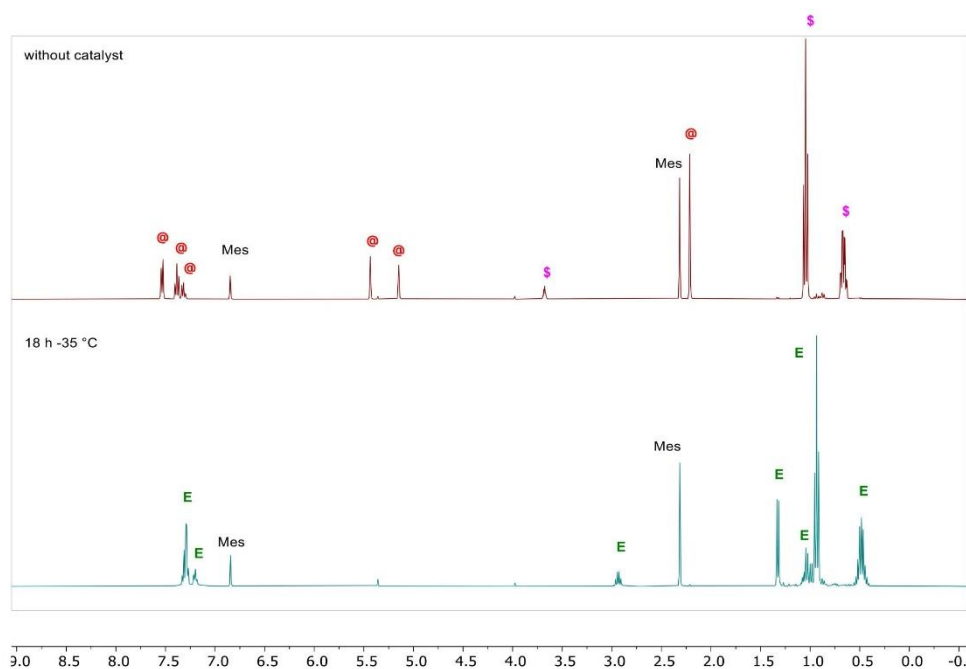


Figure S 23: Stacked ^1H NMR spectra in CD_2Cl_2 of sample **II** after 18 hours at $-35\text{ }^\circ\text{C}$, showing complete conversion, selectively forming the hydrosilylation product (**E**) from α -methylstyrene (**@**) and Et_3SiH (**\$**).

Tracing the reaction progress

To additionally monitor the reaction progress, an equal NMR sample as described above was placed in a cooled NMR probe head at $-44.3\text{ }^\circ\text{C}$ (displayed value: $-50\text{ }^\circ\text{C}$) and measured over the course of 12 hours. The obtained reaction progress is displayed in Table S 3.

Table S 3: Reaction progress of a freshly prepared sample at $-44.3\text{ }^\circ\text{C}$. Conversion and product yield was calculated by integration of the Et_3SiH - and PhCHCH_3 signals with respect to the internal standard.

Time [min]	Conversion [%]	Yield [%]
1	19	17
2	30	29
3	41	39
4	49	47
6	59	59
9	72	71
12	78	77

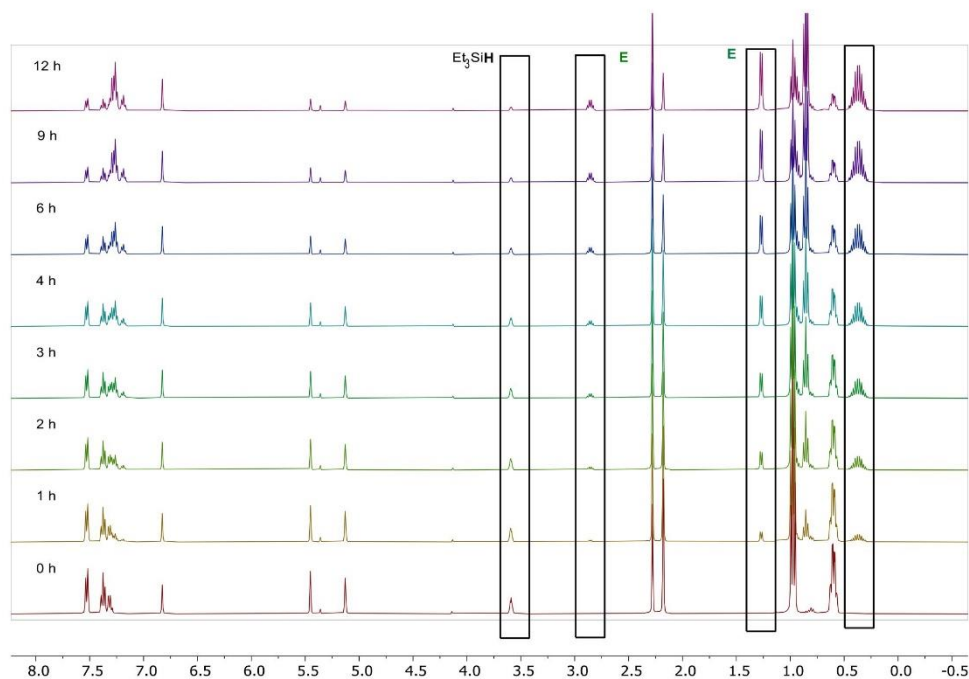
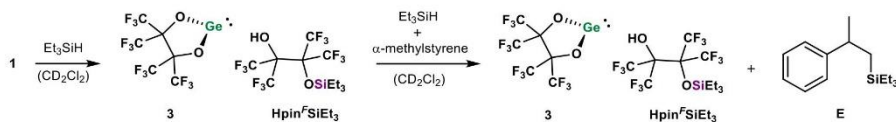


Figure S 24: Stacked ^1H NMR spectra in CD_2Cl_2 of a freshly prepared hydrosilylation experiment after several hours at -44.3°C . Selected reactant (Et_3SiH) and product (**E**) signals are highlighted by dashed frames.

2.3.3 Stoichiometric hydrosilylation of methylstyrene with Et_3SiH



In this stoichiometric experiment compound **1** (6.00 mg, 8.14 μmol , 1.00 equiv.) was reacted with Et_3SiH (1.30 μl , 8.14 μmol , 1.00 equiv.) in 0.4 ml CD_2Cl_2 to selectively form hydrosilane activation products **3** and $\text{Hpin}^F\text{SiEt}_3$. Afterwards another equivalent of Et_3SiH (1.30 μl , 8.14 μmol , 1.00 equiv.) and one equivalent of α -methylstyrene (1.06 ml, 8.14 μmol , 1.00 equiv.) were added. The mixture was analysed after 15 min at room temperature and then stored for 18 h at -36°C . Multinuclear NMR analysis revealed the quantitative formation of hydrosilylation product **E**. The initially formed germylene species **3** as well as the silylated alcohol $\text{Hpin}^F\text{SiEt}_3$ stayed intact during this experiment, which could be observed by ^{19}F NMR spectroscopy.

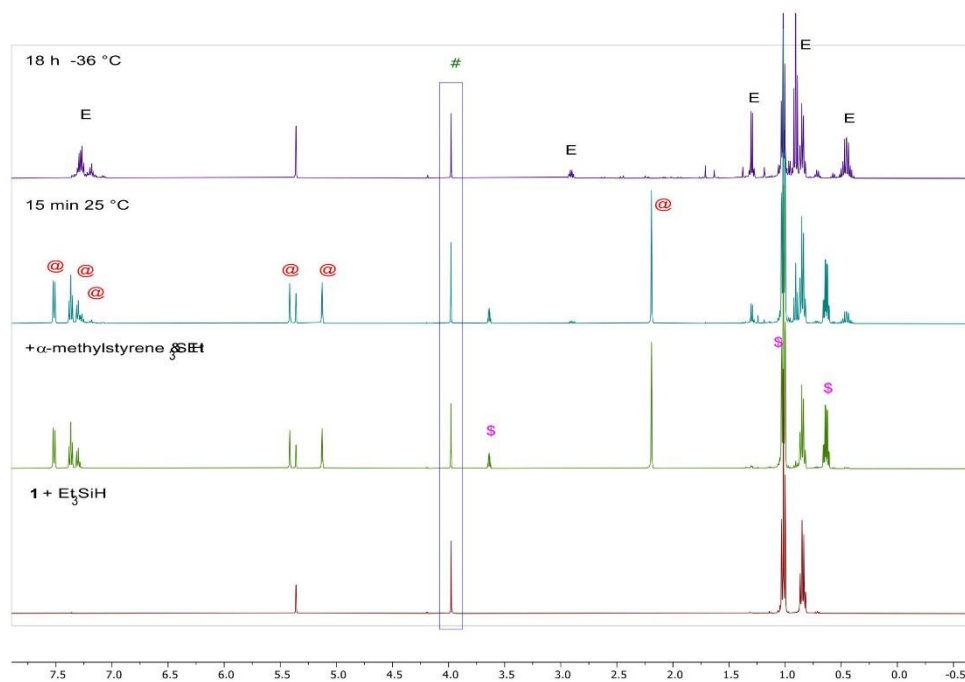


Figure S 25: Stacked ¹H NMR spectra of stepwise hydrosilylation experiment in CD₂Cl₂. The experiments showed the selective formation of the product mixture containing Hpin^FSiEt₃ (#), which stayed intact over the course the catalytic reaction. Et₃SiH (S) and α-methylstyrene (@) were fully converted to hydrosilylation product E.

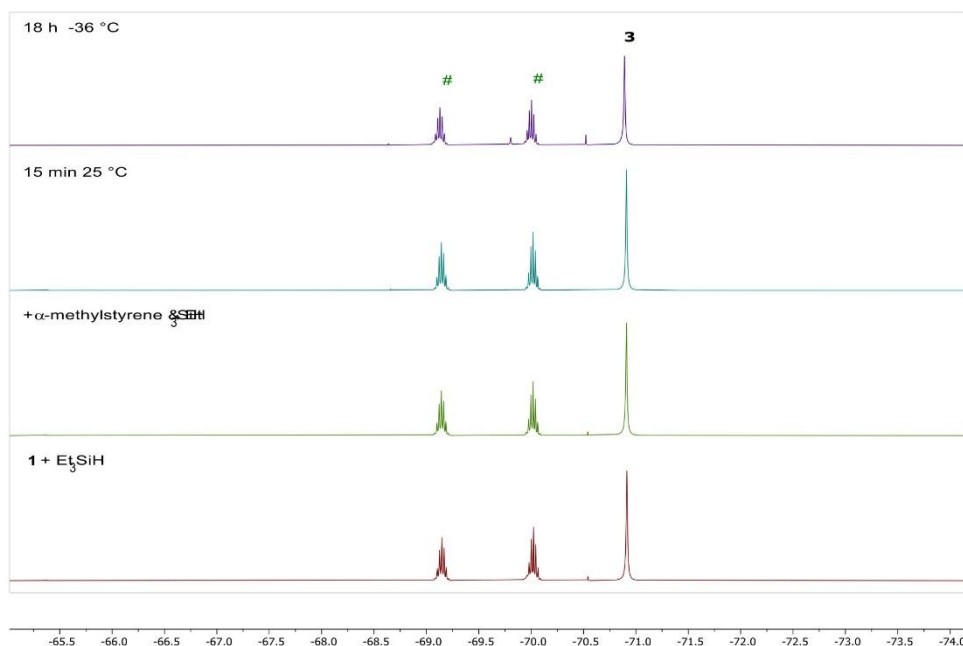
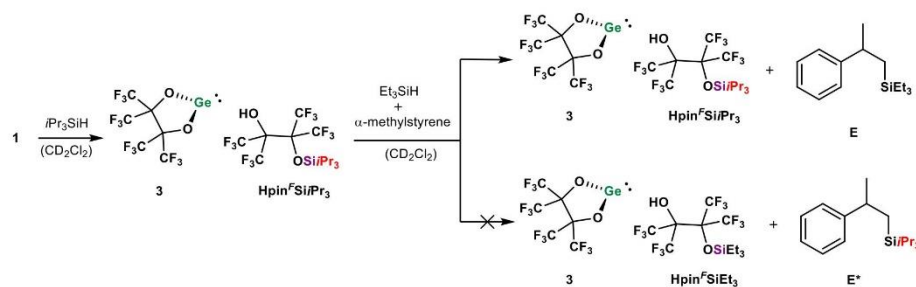


Figure S 26: Stacked ^{19}F NMR spectra of stepwise hydrosilylation experiment in CD_2Cl_2 . No change of the germylene species **3** and triethylsilyl perfluoropinacol $\text{Hpin}^{\text{F}}\text{SiEt}_3$ (**#**) is observed over the course of the reaction.

2.3.4 Hydrosilylation of α -methylstyrene with mixed silanes ($i\text{Pr}_3\text{SiH}$ vs Et_3SiH)

Initiation with $i\text{Pr}_3\text{SiH}$



In a first experiment **1** (6.00 mg, 8.14 μmol , 1.00 equiv.) was reacted with $i\text{Pr}_3\text{SiH}$ (1.67 μl , 8.14 μmol , 1.00 equiv.) in 0.4 ml CD_2Cl_2 to generate the hydrosilane activation products **3** and $\text{Hpin}^{\text{F}}\text{SiPr}_3$. Full conversion but less selective product formation, when compared to Et_3SiH , was confirmed by NMR analysis. Afterwards Et_3SiH (1.30 μl , 8.14 μmol , 1.00 equiv.) and α -methylstyrene (1.06 ml, 8.14 μmol , 1.00 equiv.) were added and the mixture was stored for 18 h at -36 °C. Subsequent multinuclear NMR analysis revealed the quantitative formation of hydrosilylationproduct **E**. The formation of **E*** was not observed. The catalyst mixture stayed intact as no change could be observed within the ^{19}F NMR spectrum.

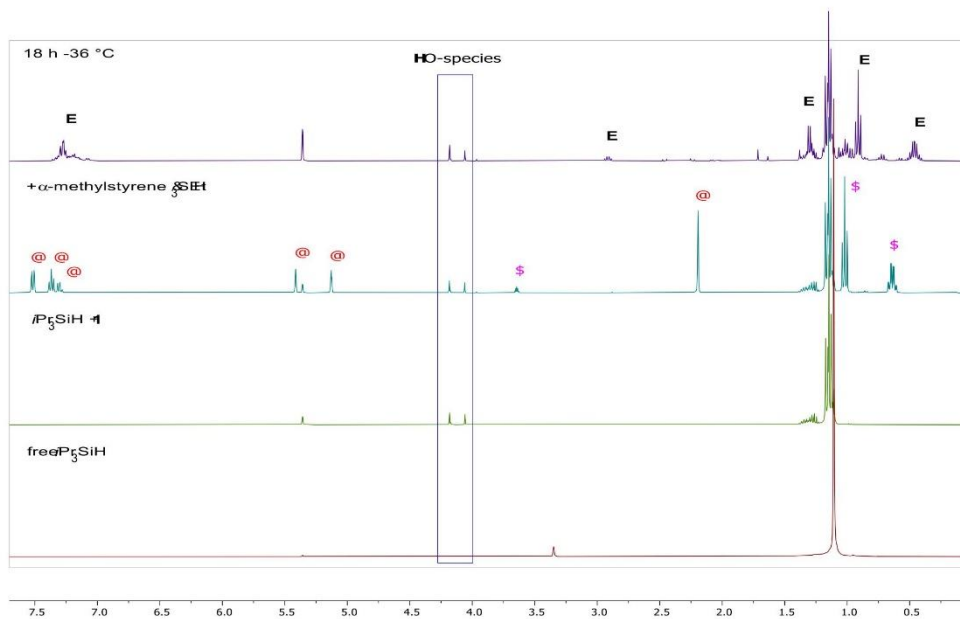


Figure S 27: Stacked ^1H NMR spectra of stepwise hydrosilylation experiment in CD_2Cl_2 selectively forming product **E**. The experiments initiated with the addition of $i\text{Pr}_3\text{SiH}$, followed by Et_3SiH (\$) and α -methylstyrene (@). The formation of two alcohol species is observed after $i\text{Pr}_3\text{SiH}$ addition.

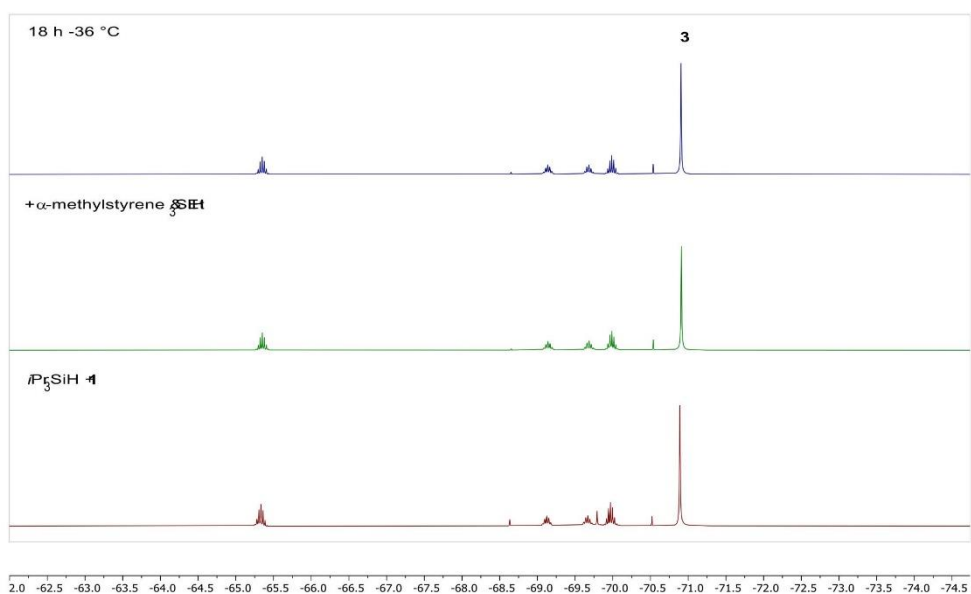
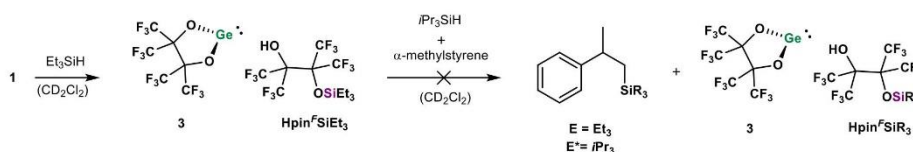
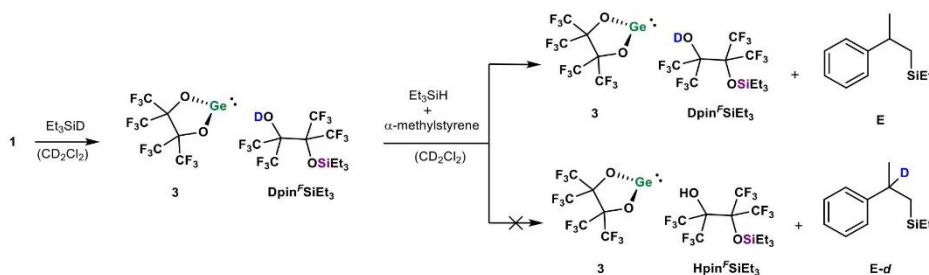


Figure S 28: Stacked ^{19}F NMR spectra of stepwise hydrosilylation experiment in CD_2Cl_2 . No change of the germylene species **3** is observed after reactant addition and after full conversion.

Initiation with Et₃SiH

In this experiment **1** (6.00 mg, 8.14 μmol , 1.00 equiv.) was reacted with Et₃SiH (1.30 μl , 8.14 μmol , 1.00 equiv.) in 0.4 ml CD₂Cl₂ to generate the hydrosilane activation product **3** and Hpin^FSiEt₃. Afterwards *i*Pr₃SiH (1.67 μl , 8.14 μmol , 1.00 equiv.) and α -methylstyrene (1.06 ml, 8.14 μmol , 1.00 equiv.) were added and the mixture was stored for 18 h at -36 °C. Subsequent multinuclear NMR analysis revealed the quantitative conversion of α -methylstyrene but no hydrosilylation product could be identified. An ill-defined product mixture containing various dimerization products was obtained.

2.3.5 Hydrosilylation of α -methylstyrene with isotopically marked Et₃SiDInitiation with Et₃SiD

Here **1** (6.00 mg, 8.14 μmol , 1.00 equiv.) was reacted with Et₃SiD (1.67 μl , 8.14 μmol , 1.00 equiv.) in 0.4 ml CD₂Cl₂ to generate **3** and deuterated Dpin^FSiEt₃. Full conversion was confirmed by NMR analysis. Afterwards Et₃SiH (1.30 μl , 8.14 μmol , 1.00 equiv.) and α -methylstyrene (1.06 ml, 8.14 μmol , 1.00 equiv.) were added and the mixture was stored for 18 h at -36 °C. NMR analysis revealed the quantitative formation of hydrosilylation product **E** while both **3** and Hpin^FSiEt₃ stayed intact. The formation of deuterated **E-d** was not observed.

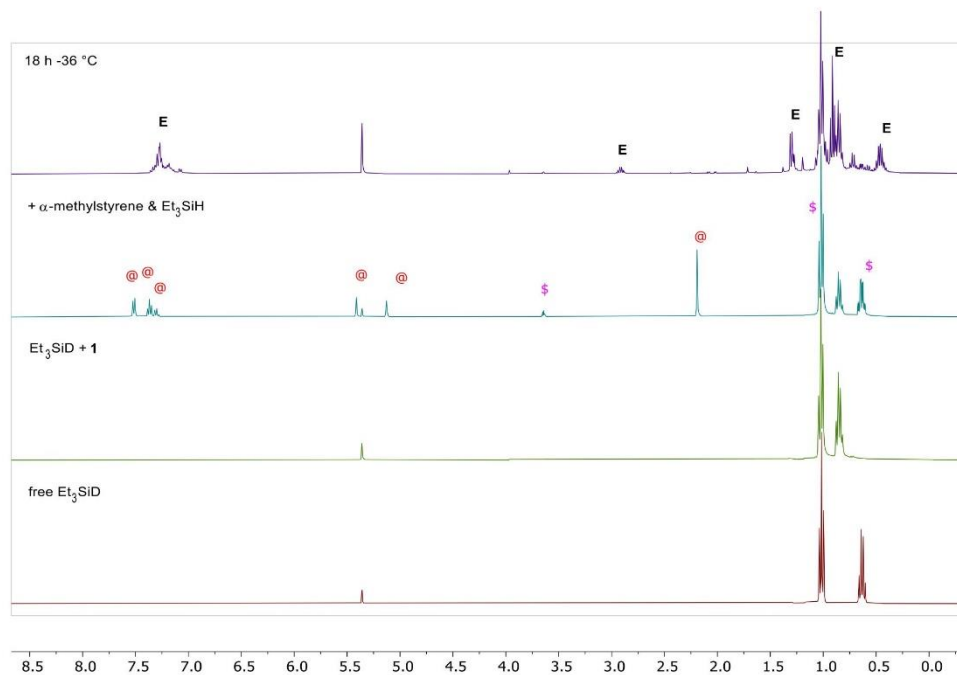


Figure S 29: Stacked ^1H NMR spectra of stoichiometric hydrosilylation experiment with isotopically marked Et_3SiD in CD_2Cl_2 selectively forming product **E**. The spectra show additionally show reactants Et_3SiH (**S**) and α -methylstyrene (**@**) directly after the addition. No formation of the Ge-H species or potential reaction product **E-d** was observed.

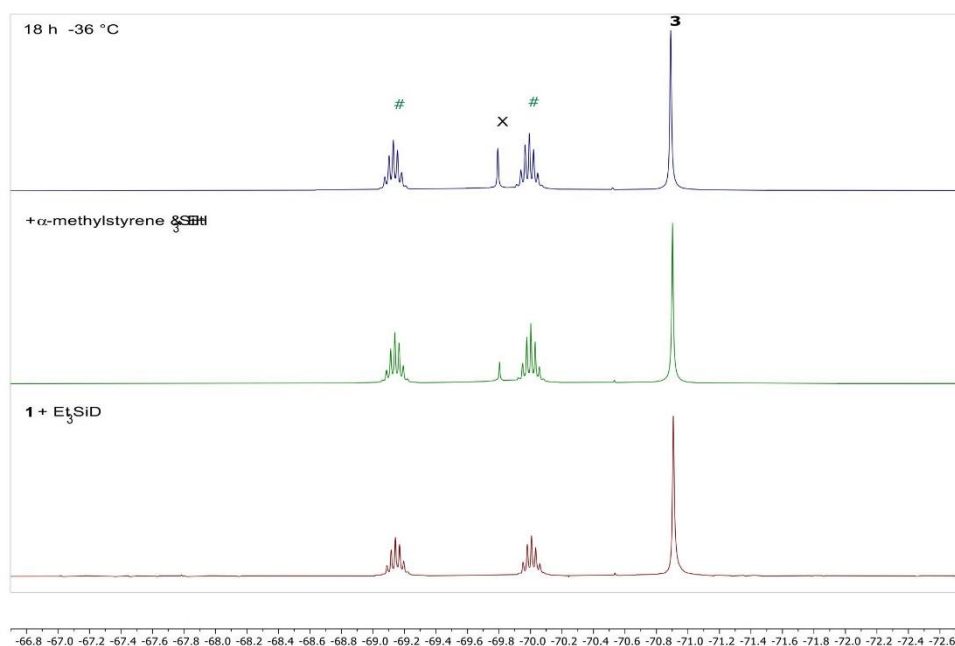
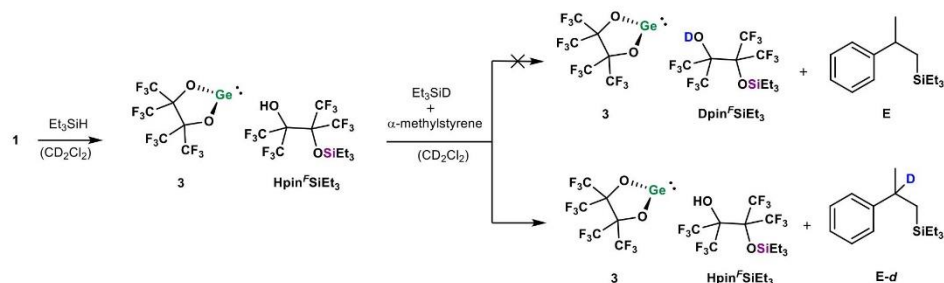


Figure S 30: Stacked ^{19}F NMR spectra of stoichiometric hydrosilylation experiment with Et_3SiD in CD_2Cl_2 . The formation of an undefined side product **X** is observed while the germylene species **3** and $\text{Dpin}^{\text{F}}\text{SiEt}_3$ (**#**) stayed intact.

Initiation with Et_3SiH



To double check the obtained results **1** (6.00 mg, 8.14 μmol , 1.00 equiv.) was reacted with non-deuterated Et_3SiH (1.67 μl , 8.14 μmol , 1.00 equiv.) in 0.4 ml CD_2Cl_2 to generate perfluoropinacolatermylene **3** and triethylsilyl perfluoropinacol $\text{Hpin}^{\text{F}}\text{SiEt}_3$. Full conversion was confirmed by NMR analysis. Afterwards deuterated Et_3SiD (1.30 μl , 8.14 μmol , 1.00 equiv.) and α -methylstyrene (1.06 ml, 8.14 μmol , 1.00 equiv.) were added and the mixture was stored for 18 h at -36°C . NMR analysis revealed the quantitative formation of hydrosilylationproduct **E-d** while catalyst **3** and $\text{Hpin}^{\text{F}}\text{SiEt}_3$ stayed intact. This time, no formation of non-deuterated **E** was observed.

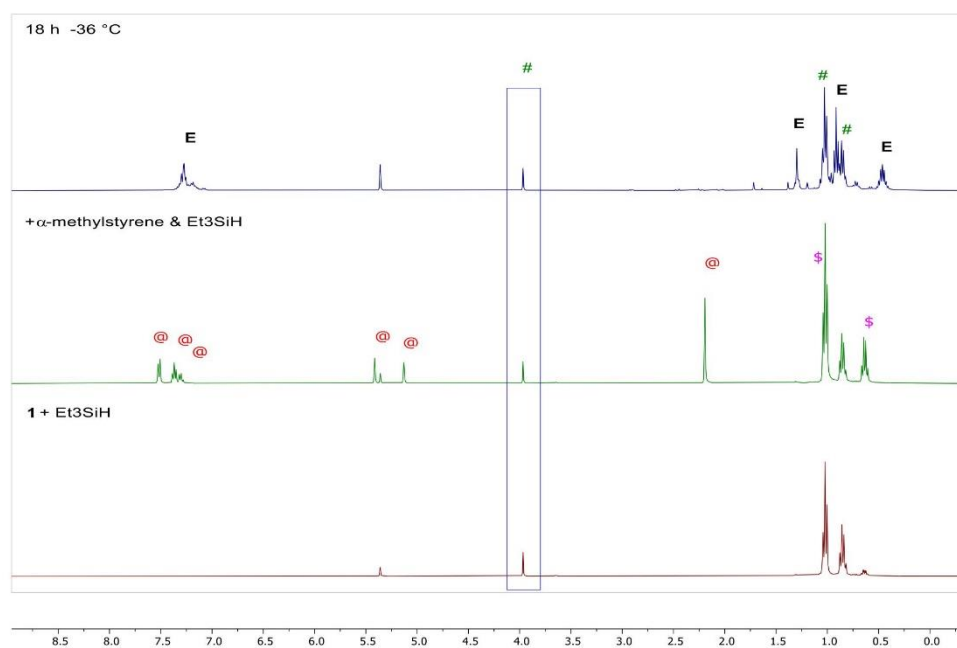


Figure S 31: Stacked ^1H NMR spectra of stoichiometric hydrosilylation experiment with Et_3SiD (initiating with Et_3SiH addition) in CD_2Cl_2 selectively forming hydrosilylation product **E-d**. The spectra additionally contain reactants isotopically marked Et_3SiD (\$) and α -methylstyrene (@) directly after the addition. No conversion of $\text{Hpin}^t\text{SiEt}_3$ (#) species or formation of reaction product **E** was observed in this case.

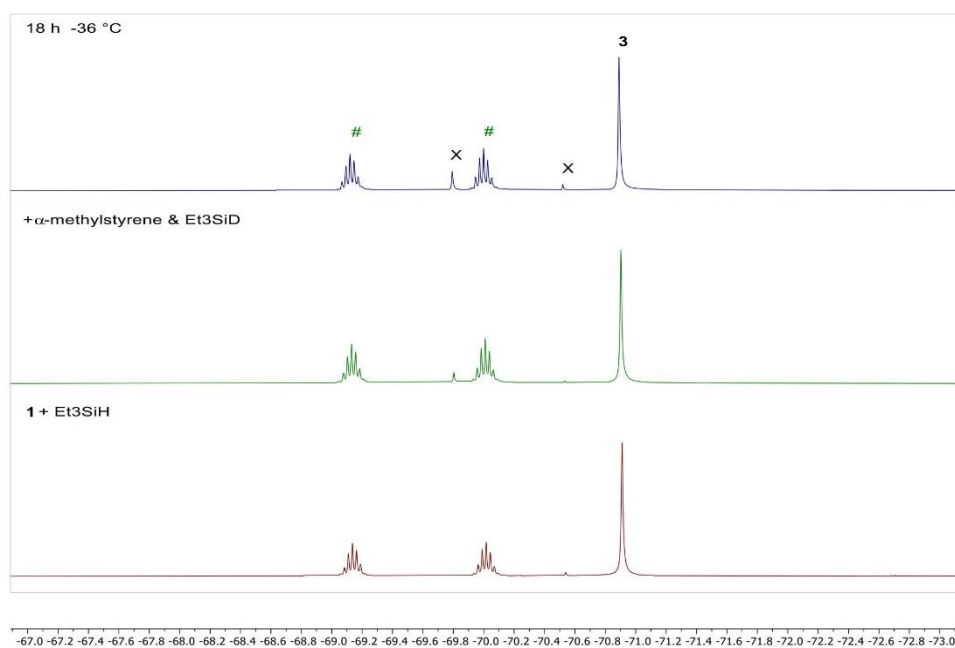


Figure S 32: Stacked ¹⁹F NMR spectra of stoichiometric hydrosilylation experiment with Et₃SiD (initiating with Et₃SiH addition) in CD₂Cl₂. The formation of an undefined side product **X** was observed while the germylene species **3** and Hpin^δSiEt₃ (#) stayed untouched.

3 Computational Section

Calculations were carried out using ORCA 5.0.4.^[16]

Geometry optimizations for the mechanistic investigations were carried out at the PBE0^[17] level of theory. The calculations utilized the atom-pairwise dispersion correction based on tight binding partial charges (D4),^[18] the def2-TZVP basis set,^[19] CPCM solvation model with the corresponding parameters for dichloromethane, benzene, and acetonitrile. The method is denoted as PBE0-D4(CPCM)/def2-TZVP. The calculations were accelerated by resolution-of-identity (RI) approximation with def2/J auxiliary basis set.^[20] The optimized geometries were verified as minima or transition states by analytical frequency calculations. The transition states were verified by IRC calculations. Cartesian coordinates of the optimized geometries are given in Appendix A.

For details regarding the ion affinities calculations see section 3.6 Calculation of ion affinities.

3.2 Hydrosilane activation mechanism

The activation of HSiEt₃ with donor-free germane **1** and silane **2** was calculated on the BPE0-D4(CPCM=DCM)/BPE0-D4(CPCM=DCM) level of theory (Figure S 33). The reactions are predicted to proceed in two steps. First, the silane coordinates to the Lewis acidic center to form the intermediate **INT_A**. The second step involves the formal metathesis reaction of Si-H E-O bond to form the ring-opening product **3***. With a barrier of 12.8 kcal mol⁻¹ (TS(1_INT_A_Ge)) the hydride abstraction and the ring opening are easily accessible in the case of germane **1**. In the silicon case, the barrier (TS(INT_A_Si_3*)) is significantly higher in energy (28.8 kcal mol⁻¹). Furthermore, the overall process is endergonic by 5.9 kcal mol⁻¹. In contrast, for germane **1** the reaction is exergonic by 13.0 kcal mol⁻¹. The calculations align well with the experimentally observed reactivity, as no interaction between silane **2** and hydrosilanes was monitored. Germylene **1** on the other hand readily activates Et₃SiH forming compound **3*** that decomposes to release the germylene **3** and mono-silylated perfluoropinacol **4**.

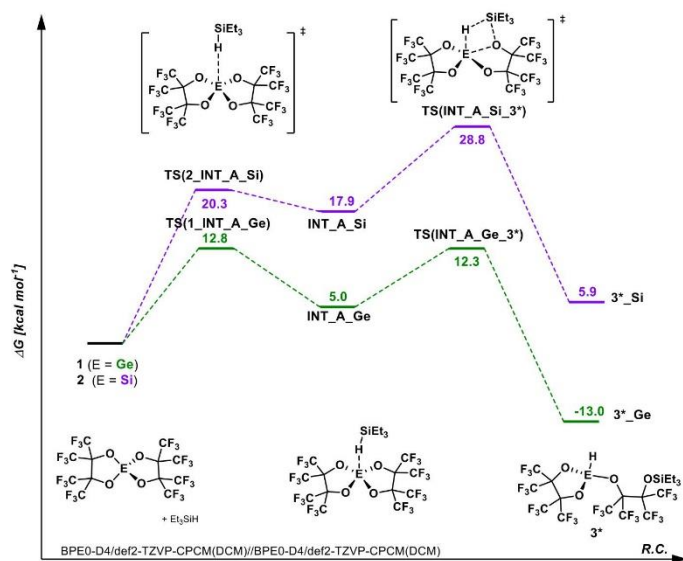


Figure S 33: Reaction mechanism for the activation Et_3SiH with **1** and **2**.

Table S 4: PBE0-D4(CPCM=DCM)/def2-TZVP//PBE0-D4(CPCM=DCM)/def2-TZVP calculated energies (E_h) (E – electronic energy; H – total enthalpy; G – Gibbs energy; $G_S = G + G_{\text{corr}}$) of the compounds in Figure S33. Thermochemistry at 298.15 K.

Compound	E	H	G	G_S
HSiEt_3	-527.47794089	-527.26095375	-527.30955265	-527.3065325
1	-5229.60383427	-5229.40102877	-5229.50026724	-5229.497247
TS(1_INT_A_Ge)	-5757.08372525	-5756.66273811	-5756.78633436	-5756.783314
INT_A_Ge	-5757.09570753	-5756.67461003	-5756.79886433	-5756.795844
TS(INT_A_3*_Ge)	-5757.08459280	-5756.66407390	-5756.78714612	-5756.784126
3*_Ge	-5757.12723823	-5756.70436594	-5756.82749411	-5756.784126
2	-3442.33762144	-3442.13280403	-3442.23043761	-3442.227417
TS(1_INT_A_Si)	-3969.80591658	-3969.38299325	-3969.50463621	-3969.501616
INT_A_Si	-3969.80988667	-3969.38569342	-3969.50849320	-3969.505473
TS(INT_A_3*_Si)	-3969.79415802	-3969.37080317	-3969.49109157	-3969.488071
3*_Si	-3969.83058328	-3969.40556420	-3969.52758424	-3969.524564

3.3 Thermochemistry analysis of the hydrosilylation catalytic cycle

The reported energy differences for reaction components are at the PBE0-D4(CPCM)/def2-TZVP//PBE0-D4(CPCM)/def2-TZVP level of theory with the gas to liquid phase correction term, i.e. concentration-induced free-energy shift $G_{\text{conc}} = RT \ln(24.5)$ (1.51, 1.90 and 2.24 kcal mol⁻¹ at 238.15, 298.15 and 298.15K, respectively) is included in the free energy G_{s} of each compound.

Table S 5: Thermochemistry analysis at 238.15, 298.15 and 353.15 K for the components of the reaction mechanism in Figure 4, calculated at the PBE0-D4(CPCM=DCM)/def2-TZVP level of theory. E – Electronic energy (E_{el}); $(G-E)_{\text{T}}$ – Gibbs energy minus the electronic energy at the different temperatures (E_{el}); $G_{\text{T}} = E + (G-E)_{\text{T}} + G_{\text{conc T}}$.

Compound	E	$(G-E)_{238.15\text{K}}$	$(G-E)_{298.15\text{K}}$	$(G-E)_{353.15\text{K}}$	$G_{\text{s},238.15\text{K}}$	$G_{\text{s},298.15\text{K}}$	$G_{\text{s},353.15\text{K}}$
HSiEt ₃	-527.47794	0.17746	0.16839	0.15941	-527.29806	-527.30653	-527.31495
C ₆ H ₅ C(CH ₃)=CH ₂	-348.67931	0.13738	0.12950	0.12174	-348.53952	-348.54679	-348.55399
PhC(H)(CH ₃)-CH ₂ SiEt ₃	-876.20164	0.33974	0.32769	0.31545	-875.85948	-875.87093	-875.88261
(pin) ^F Ge: (3)	-3653.18557	0.04907	0.03726	0.02535	-3653.13409	-3653.14529	-3653.15664
INT1	-7655.09020	0.27477	0.25312	0.23058	-7654.81303	-7654.83406	-7654.85605
TS1	-7655.08522	0.27506	0.25363	0.23130	-7654.80775	-7654.82857	-7654.85034
INT2	-8182.57273	0.47418	0.44852	0.42165	-8182.09614	-8182.12119	-8182.14750
TS2	-8182.56381	0.47632	0.45096	0.42439	-8182.08508	-8182.10984	-8182.13585

3.4 Alternative mechanisms for the catalytic hydrosilylation

Initially we considered a few proposed mechanisms for catalytic hydrosilylation of the α -methylstyrene mediated by the germylene **3**, which involved one molecule of the germylene.

In the mechanism shown in Figure S34, α -methylstyrene coordinates to the germylene to form the coordination intermediate INT1'. The concerted addition of the silane across the C-C bond is exergonic by 12.3 kcal mol⁻¹, however it need to overcome a very high lying transition state **TS3** at 37.0 kcal mol⁻¹, making this reaction pathway infeasible under the experimental conditions.

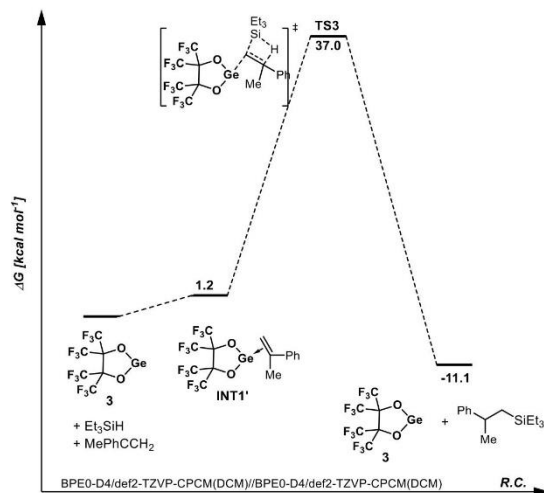


Figure S 34: Alternative mechanism for hydrosilylation by **3**, via olefin activation.

In an additional mechanism that was considered by us, the silane and the olefin are activated in a concerted fashion via a 5-membered transition state **TS4** at 23.8 kcal mol⁻¹ to form the Ge(IV) intermediate **INT3**. However, **TS4** is by 2.0 kcal mol⁻¹ higher in energy than the rate determining transition state **TS2**. Additionally, the intermediate **INT3** is a very deep minimum. The reductive elimination of the silylated product from **INT3** is endergonic by 8.8 kcal mol⁻¹ and would need to overcome a barrier of 54.6 kcal mol⁻¹, which is unfeasible. Since **INT3** is not observed in the catalytic reaction mixtures we also rule out this scenario.

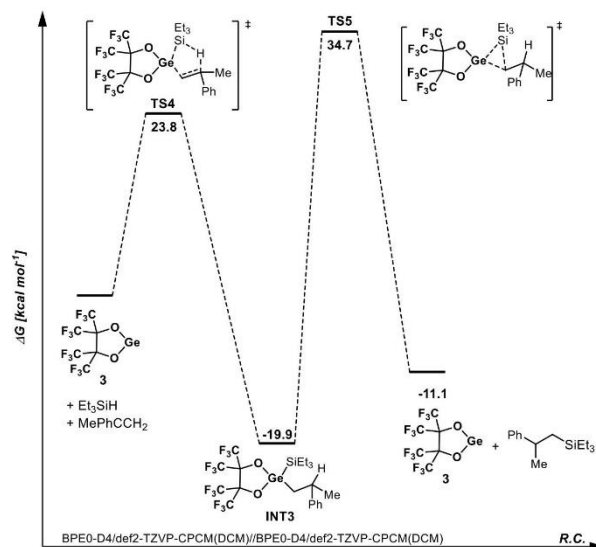


Figure S 35: Alternative mechanism for hydro-silylation by **3**, via concerted activation of the silane and the olefin.

We also considered a possibility in which the germylene activates the silane at the first step of the catalytic cycle. Thus, we calculated the transition states and the products of the oxidation addition of the germanium center across the Si-H bond to form the corresponding germane **5** (Figure 36, purple), as well the addition across the Ge-O bond to form the silyl ether **6** (Figure 36, orange). In the former case, the reaction is exergonic by 2.5 kcal mol⁻¹, however the barrier, **TS6** at 34.5 kcal mol⁻¹ is too high to overcome at rt. The formation of **6**, is both endergonic and requires a very high barrier, **TS7** at 36.0 kcal mol⁻¹. Thus, we had to rule out the mechanism of the catalytic hydro-silylation that involve initial activation of the silane by **3**.

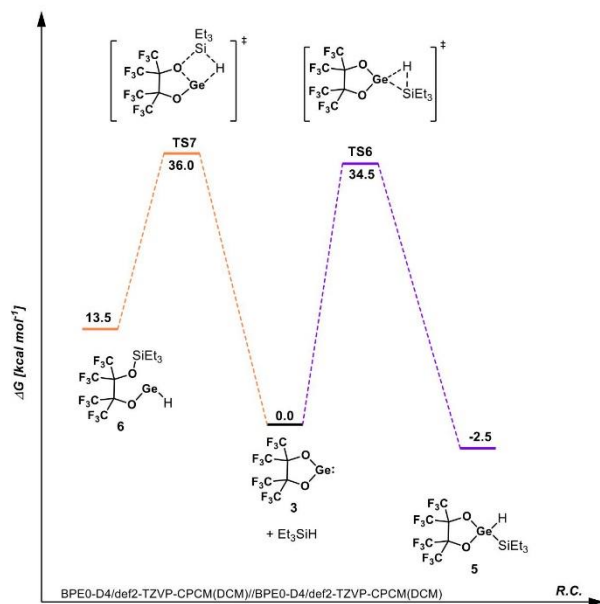


Figure S 36. Activation of Et_3SiH by **3**.

Table S 6: PBE0-D4(CPCM=DCM)/def2-TZVP//PBE0-D4(CPCM=DCM)/def2-TZVP calculated energies (E_e) (E – electronic energy; H – total enthalpy; G – Gibbs energy; $G_S = G + G_{\text{conc}}$) of the compounds in Figures S34, S35, S36. Thermochemistry at 298.15 K.

Compound	E	H	G	G_S
Et_3SiH	-527.47794089	-527.26095375	-527.30955265	-527.3065325
$\text{C}_6\text{H}_5\text{C}(\text{CH}_3)=\text{CH}_2$	-348.67930941	-348.50860159	-348.54980691	-348.5467868
$\text{PhC}(\text{H})(\text{CH}_3)-\text{CH}_2\text{SiEt}_3$	-876.20163736	-875.80789303	-875.87394682	-875.8709267
$(\text{pin})^2\text{Ge}$: (3)	-3653.18556968	-3653.08432860	-3653.14830528	-3653.145285
INT1'	-4001.88343534	-4001.60950462	-4001.69322602	-4001.690206
INT3	-4529.42479979	-4528.92716084	-4529.03327144	-4529.030251
5	-4180.68961685	-4180.36895133	-4180.45874709	-4180.455727
6	4180.66063500	-4180.34073622	-4180.43037547	-4180.427355
TS3	-4529.33050459	-4528.83632640	-4528.94268493	-4528.939665
TS4	-4529.34815297	-4528.85730789	-4528.96362146	-4528.960601
TS5	-4529.33432713	-4528.83959212	-4528.94643774	-4528.943418
TS6	-4180.62860727	-4180.31071973	-4180.39985862	-4180.396838
TS7	-4180.62859703	-4180.31011627	-4180.39745030	-4180.394430

3.5 Calculated energies for compounds in Figure 3 and Scheme 2B.

Table S 7: PBE0-D4(CPCM=Benzene)/def2-TZVP//PBE0-D4(CPCM=Benzene)/def2-TZVP calculated energies (E_e) (E – electronic energy; H – total enthalpy; G – Gibbs energy; $G_S = G + G_{\text{conc}}$) of the compounds in Figure 3. Thermochemistry at 298.15 K.

Compound	E	H	G	G_S
1 -MeCN	-5362.27989486	-5362.02487581	-5362.13407019	-5362.13105
2 -MeCN	-3575.00611941	-3574.74907229	-3574.85531876	-3574.852299
$\text{B}(\text{C}_6\text{F}_5)_3$	-2207.04435998	-2206.85835763	-2206.94390926	-2206.940889
$\text{MeCN-B}(\text{C}_6\text{F}_5)_3$	-2339.72502805	-2339.48685703	-2339.58041533	-2339.577602
1	-5229.60274820	-5229.39943902	-5229.49860457	-5229.495584
2	-3442.33672263	-3442.13138544	-3442.22895812	-3442.225938

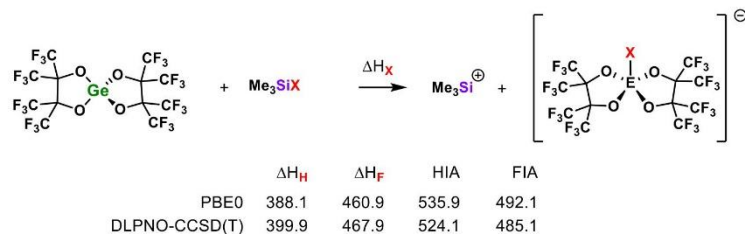
Table S 8: PBE0-D4(CPCM=**DCM**)/def2-TZVP//PBE0-D4(CPCM=**DCM**)/def2-TZVP calculated energies (E_h) (E – electronic energy; H – total enthalpy; G – Gibbs energy; $G_s = G + G_{\text{corr}}$) of the compounds in Scheme 2B. Thermochemistry at 298.15 K.

Compound	E	H	G	G_s
Et ₃ SiH	-527.47794089	-527.26095375	-527.30955265	-527.3065325
1	-5229.60383427	-5229.40102877	-5229.50026724	-5229.497247
1 -MeCN	-5362.28957277	-5362.03518325	-5362.14349099	-5362.140471
B[H-1]	-5230.38307456	-5230.17303971	-5230.27259092	-5230.269571
[MeCN→Et ₃ Si] ⁺	-659.40109109	-659.13947027	-659.19731608	-659.1942959
3	-3653.18556968	-3653.08432860	-3653.14830528	-3653.145285
3 -MeCN	-3785.85639647	-3785.70362806	-3785.77885706	-3785.775837
3 * _{Ge}	-5757.12723823	-5756.70436594	-5756.82749411	-5756.784126
4	-2103.92509554	-2103.60313079	-2103.68923676	-2103.686217

Table S 9: PBE0-D4(CPCM=**acetonitrile**)/def2-TZVP//PBE0-D4(CPCM=**acetonitrile**)/def2-TZVP calculated energies (E_h) (E – electronic energy; H – total enthalpy; G – Gibbs energy; $G_s = G + G_{\text{corr}}$) of the compounds in Scheme 2B. Thermochemistry at 298.15 K.

Compound	E	H	G	G_s
Et ₃ SiH	-527.47814599	-527.26125033	-527.30985532	-527.3068352
1	-5229.60411347	-5229.40144558	-5229.50070480	-5229.497685
1 -MeCN	-5362.29230028	-5362.03809409	-5362.14640094	-5362.143381
B[H-1]	-5230.38799575	-5230.17806933	-5230.27760702	-5230.274587
[MeCN→Et ₃ Si] ⁺	-659.40790905	-659.14636791	-659.20410583	-659.2010857
3 -MeCN	-3785.85836779	-3785.70572528	-3785.78067625	-3785.777656
4	-2103.92589053	-2103.60407120	-2103.69020638	-2103.687186

For comparison with the previously published results,^[1] the gas phase ion affinities of **1** were calculated at the same level of theory, i.e. PBE0-D3BJ^[21]/def2-TZVPP//DLPNO-CCSD(T)/aug-cc-pVQZ.^[22] The ion affinity values of the reference compound Me₃Si⁺ (FIA = 953 kJ, HIA = 924 kJ) calculated at the CCSD(T)/CBS level of theory are taken from literature (Figure S 37).^[23] The calculated energies are given in Table 1.

**Figure S 37.** Hydride and fluoride ion affinities of **1**, relative to the reference compound Me₃Si⁺.**Table 1.** Calculated $E_{\text{PBE0-D3}}$ (electronic energy, (E_h)) and $H_{\text{PBE0-D3}}$ (enthalpy, (E_h)) at the PBE0-D3/def2-TZVPP//PBE0-D3/def2-TZVPP level of theory. $E_{\text{(DLPNO-CCSD(T))}}$ – electronic energy at the DLPNO-CCSD(T)/aug-cc-pVQZ//PBE0-D3/def2-TZVPP level of theory.

Compound	$E_{\text{PBE0-D3}}$	$H_{\text{PBE0-D3}}$	$E_{\text{(DLPNO-CCSD(T))}}$
(pin ^F) ₂ Ge	-5229.589261	-5229.385278	-5227.503704
[(pin ^F) ₂ GeH] (B[H-1])	-5230.319351	-5230.108305	-5228.237155
[(pin ^F) ₂ GeF] (B[F-1])	-5329.565126	-5329.358558	-5327.464448
Me ₃ SiH	-409.6509397	-409.5238372	-409.254734
Me ₃ SiF	-508.9243983	-508.8018046	-508.5078966
Me ₃ Si ⁺	-408.7706389	-408.6529826	-408.3665695

4 Single-Crystal X-ray Diffraction Analysis

4.1 Crystal Structure of 1·MeCN

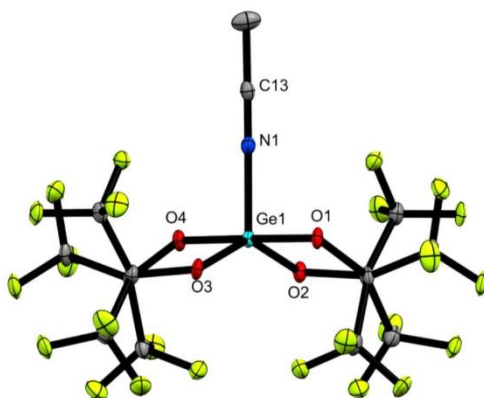


Figure S 38: Molecular structure of 1·MeCN with translational ellipsoids plotted at 50% probability level. Hydrogen atoms are omitted for clarity. Selected bond lengths [Å] and angles [deg]: Ge1–N1 1.933(4), Ge1–O1 1.827(3), Ge1–O2 1.794(3), Ge1–O3 1.782(3), Ge1–O4 1.833(3); O1–Ge1–O2 88.39(12), O1–Ge1–O4 179.20(13), O3–Ge1–O4 88.12(12), O2–Ge1–O3 136.47(13).

4.2 Crystal Structure of [K·(18-c-6)][F-1]

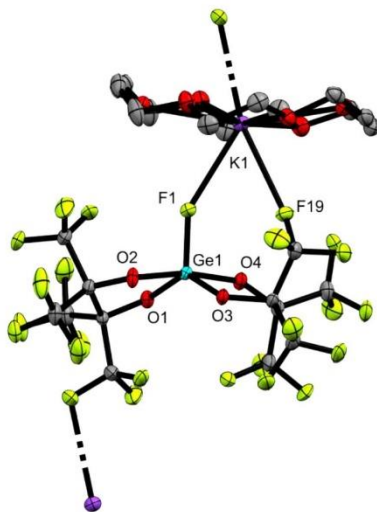


Figure S 39: Molecular structure of [K·(18-c-6)][F-1] with translational ellipsoids plotted at 50% probability level. Hydrogen atoms are omitted for clarity. Selected bond lengths [Å] and angles [deg]: Ge1–F1 1.7274(16), Ge1–O1 1.8122(19), Ge1–O2 1.841(2), Ge1–O3 1.8100(19), Ge1–O4 1.8467(19), F1–K1 2.8189(18); O1–Ge1–O4 90.60(9), O2–Ge1–O3 87.58(8), O1–Ge1–O2 86.70(9), O3–Ge1–O4 86.88(8).

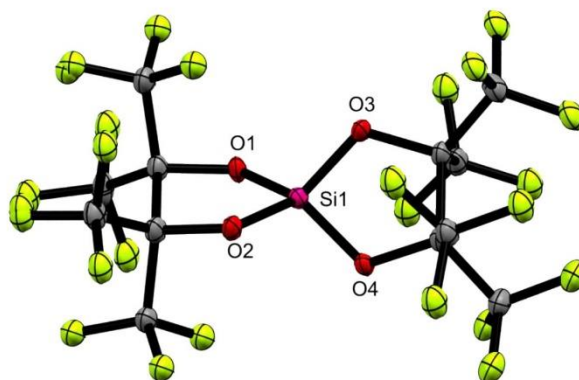
4.3 Crystal Structure of donor-free silane **2**

Figure S 40: Molecular structure of MeCN-free **2** with translational ellipsoids plotted at 50% probability level. Hydrogen atoms are omitted for clarity. The structure contains a second, twisted overlaying disordered, that is also omitted for clarity reasons. Selected bond lengths [Å] and angles [°]: Si1–O1 1.744(18), Si1–O2 1.754(17), Si1–O3 1.779(18), Si1–O4 1.684(18); O1–Si1–O4 131.7(8), O2–Si1–O3 166.0(8).

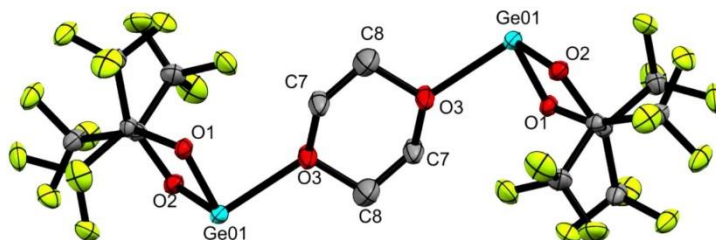
4.4 Crystal Structure of dioxane-coordinated germylene **3**

Figure S 41: Molecular structure of 1,4-dioxane-coordinated germylene **3** with translational ellipsoids plotted at 50% probability. Hydrogen atoms are omitted for clarity. The figure contains two symmetry-generated unit cells. Selected bond lengths [Å] and angles [°]: Ge011–O1 1.853(2), Ge01–O2 1.853(2), Ge01–O3 2.241(3); O1–Ge01–O2 85.60(10), O1–Ge01–O3 84.71(10), O2–Ge01–O3 106.29(11).

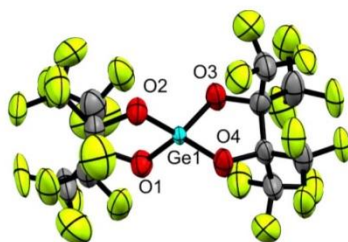
4.5 Preliminary crystal structure of donor-free **1**

Figure S 42: Preliminary molecular structure of **1** with translational ellipsoids plotted at 50% probability. Because of heavy disorder only insufficient data refinement was possible. The depicted structure demonstrates a similar connectivity as for compound **2**. However, no bond lengths and angles can be discussed. This depiction is no structure evidence due to lacking data quality.

Table S 10: Crystallographic Details.

	1·MeCN	[K·(18-c-6)][F-1]	2
CCDC-Number	2286080	2286083	2286081
Crystal Data			
Chemical formula	C ₁₄ H ₃ F ₂₄ GeNO ₄	C ₄₈ H ₄₇ F ₅₀ Ge ₂ K ₂ O ₂₀	C ₁₂ F ₂₄ O ₄ Si
<i>M_r</i>	777.78	2116.91	692.21
Crystal system, space group	Orthorhombic, <i>Pbcn</i>	Triclinic, <i>-P1</i>	Orthorhombic, <i>P2₁2₁2</i>
Temperature (K)	100	100	100
<i>a, b, c</i> (Å)	23.5238(15), 8.6067(5), 21.8982(13)	11.2001(10), 15.7831(14), 22.3057(19)	8.3174(7), 10.3383(8), 11.4253(8)
<i>α, β, γ</i> (°)	90, 90, 90	107.062(3), 102.834(3), 95.235(3)	90, 90, 90
<i>V</i> (Å ³)	4433.6(5)	3623.2(6)	982.44(13)
<i>Z</i>	8	2	2
Radiation type	Mo <i>Kα</i>	Mo <i>Kα</i>	Mo <i>Kα</i>
<i>μ</i> (mm ⁻¹)	1.611	1.141	0.369
Crystal size (mm)	0.174 × 0.112 × 0.068	0.58 × 0.318 × 0.279	0.255 × 0.207 × 0.160
Crystal shape	Fragment	Block	Fragment
Color	Clear colorless	Clear colorless	Clear colorless
Data Collection			
Diffractometer	Bruker Photon CMOS	Bruker Photon CMOS	Bruker Photon CMOS
Absorption correction	Multi-scan	Multi-scan	Multi-scan
<i>T_{min}, T_{max}</i>	0.7453, 0.6764	0.7453, 0.6350	0.7452, 0.5419
No. of measured, independent, and observed [<i>I</i> > 2σ(<i>I</i>)] reflections	117042, 4064, 3029	133009, 13270, 11373	6489, 1797, 1437
<i>R_{int}</i>	0.0960	0.0472	0.0820
<i>θ</i> range (°) for cell measurement	2.52–25.35	2.33–25.72	2.66–25.34
Data completeness	0.999	1.000	0.998
Refinement			
<i>R</i> [<i>F</i> ² > 2σ(<i>F</i> ²), <i>R</i> (<i>F</i> ²), <i>S</i>]	0.0458, 0.1171, 1.017	0.0348, 0.0717, 1.087	0.0619, 0.1409, 1.047
No. of reflections	4046	13270	1797
No. of parameters	270	1277	177
No. of restraints	398	56	523
Δρ _{max} , Δρ _{min} (e Å ⁻³)	2.38, -2.38	0.55, -0.48	0.47, -0.49

	1	(3):C₄H₈O₂
CCDC-Number	2286830	2286082
Crystal Data		
Chemical formula	C ₁₂ F ₂₄ GeO ₄₇	C ₁₆ H ₃₂ F ₂₄ Ge ₂ O ₆
<i>M_r</i>	736.73	897.40
Crystal system, space group	Orthorhombic, <i>P</i> 2 ₁ 2 ₁ 2	Monoclinic, <i>P</i> 2 ₁ / <i>n</i>
Temperature (K)	100	100
<i>a</i> , <i>b</i> , <i>c</i> (Å)	18.5204(10), 18.7351(9), 11.6382(6)	11.8448(8), 7.7953(5), 14.4848(9)
α , β , γ (°)	90, 90, 90	90, 93.398(2), 90
<i>V</i> (Å ³)	4038.2(4)	1335.08(15)
<i>Z</i>	8	2
Radiation type	Mo <i>K</i> α	Mo <i>K</i> α
μ (mm ⁻¹)	1.760	2.454
Crystal size (mm)	0.258 × 0.245 × 0.201	0.298 × 0.25 × 0.154
Crystal shape	Fragment	Block
Color	Clear colorless	Clear colorless
Data Collection		
Diffractometer	Bruker Photon CMOS	Bruker Photon CMOS
Absorption correction	Multi-scan	Multi-scan
<i>T</i> _{min} , <i>T</i> _{max}	0.7453, 0.5705	0.7453, 0.5707
No. of measured, independent, and observed [<i>I</i> > 2 σ (<i>I</i>)] reflections	154374, 8248, 7776	54591, 2443, 2328
<i>R</i> _{int}	0.0486	0.0412
θ range (°) for cell measurement	2.20–26.67	2.16–25.35
Data completeness	0.999	1.000
Refinement		
<i>R</i> [<i>F</i> ² > 2 σ (<i>F</i> ²)], <i>R</i> (<i>F</i> ²), <i>S</i>	0.1054, 0.3131, 1.618	0.0374, 0.0891, 1.157
No. of reflections	8248	2443
No. of parameters	720	217
No. of restraints	2945	0
$\Delta\rho_{\max}$, $\Delta\rho_{\min}$ (e Å ⁻³)	1.93, -1.34	1.59, -0.62

The data have been assigned the following deposition numbers which can either be quoted as CCDC Numbers or CSD Numbers. A CCDC Number is usually quoted for an organic or metal-organic structure, whereas a CSD Number is usually quoted for an inorganic structure.

CCDC XXXXXXXX-YYYYYYYY (generally used for organic and metal-organic structures)

CSD XXXXXXXX-YYYYYYYY (generally used for inorganic structures)

Deposition Number 2286080-2286083, 2286830

Summary of Data - Deposition Number 2286080

Compound Name:
Data Block Name: data_GraAn1_fine
Unit Cell Parameters: a 23.5238(15) b 8.6067(5) c 21.8982(13) Pbcn

Summary of Data - Deposition Number 2286081

Compound Name:
Data Block Name: data_TscFl23_fine
Unit Cell Parameters: a 8.3174(7) b 10.3383(8) c 11.4253(8) P21212

Summary of Data - Deposition Number 2286082

Compound Name:
Data Block Name: data_mo_tscfl32_0ma_a
Unit Cell Parameters: a 11.8448(8) b 7.7953(5) c 14.4848(9) P21/n

Summary of Data - Deposition Number 2286083

Compound Name:
Data Block Name: data_mo_tscfl29_0m
Unit Cell Parameters: a 11.2001(10) b 15.7831(14) c 22.3057(19) P-1

Summary of Data - Deposition Number 2286830

Compound Name:
Data Block Name: data_TscFl26_fine2
Unit Cell Parameters: a 18.5204(10) b 18.7351(9) c 11.6382(6) P21212

5 NMR Spectra

5.1 NMR spectra of 1·MeCN

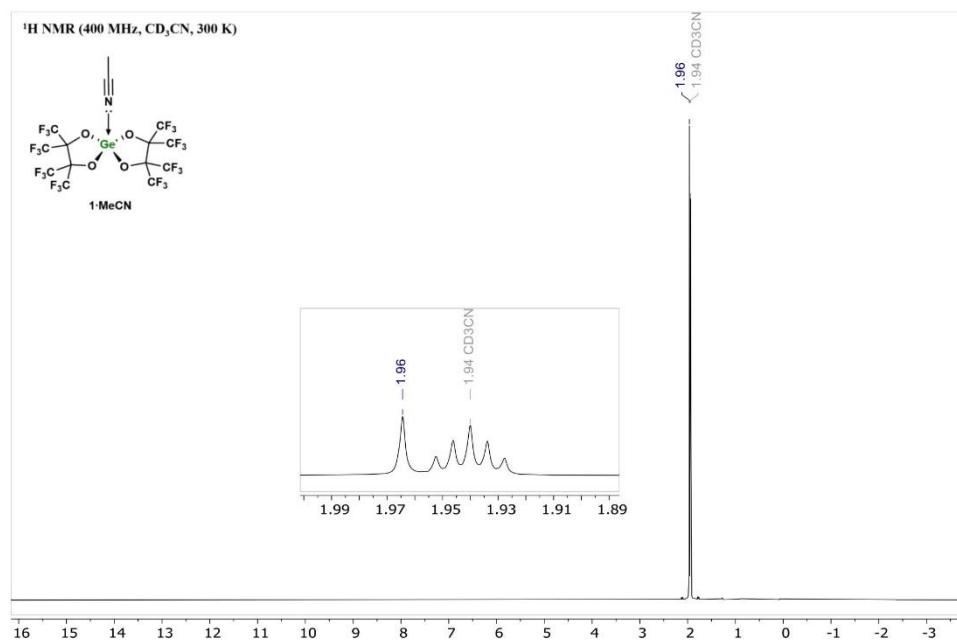


Figure S 43: ¹H NMR spectrum of 1·MeCN in CD₃CN at 300 K.

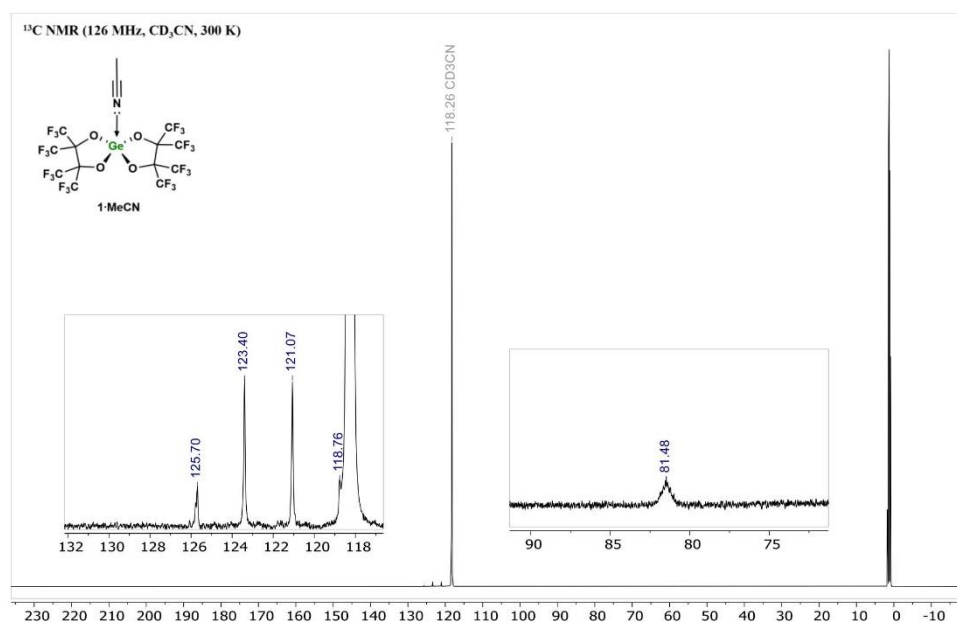


Figure S 44: ¹³C NMR spectrum of 1·MeCN in CD₃CN at 300 K.

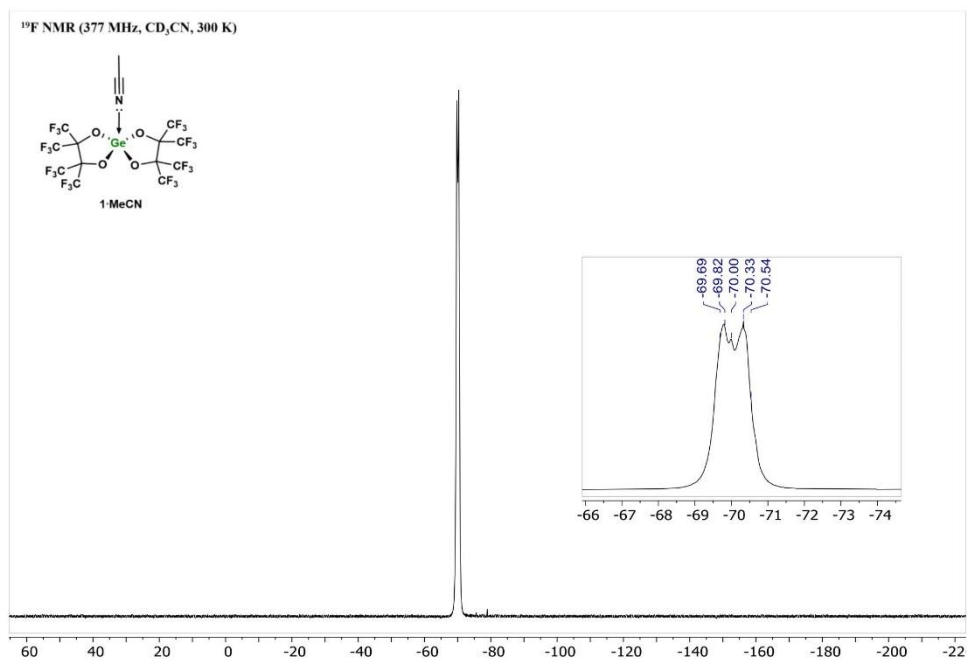
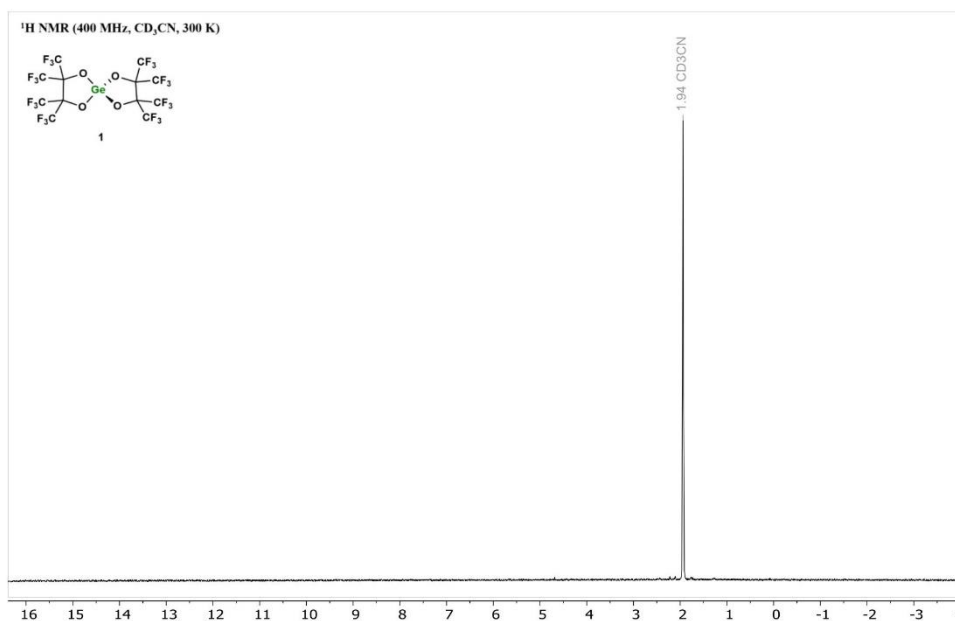
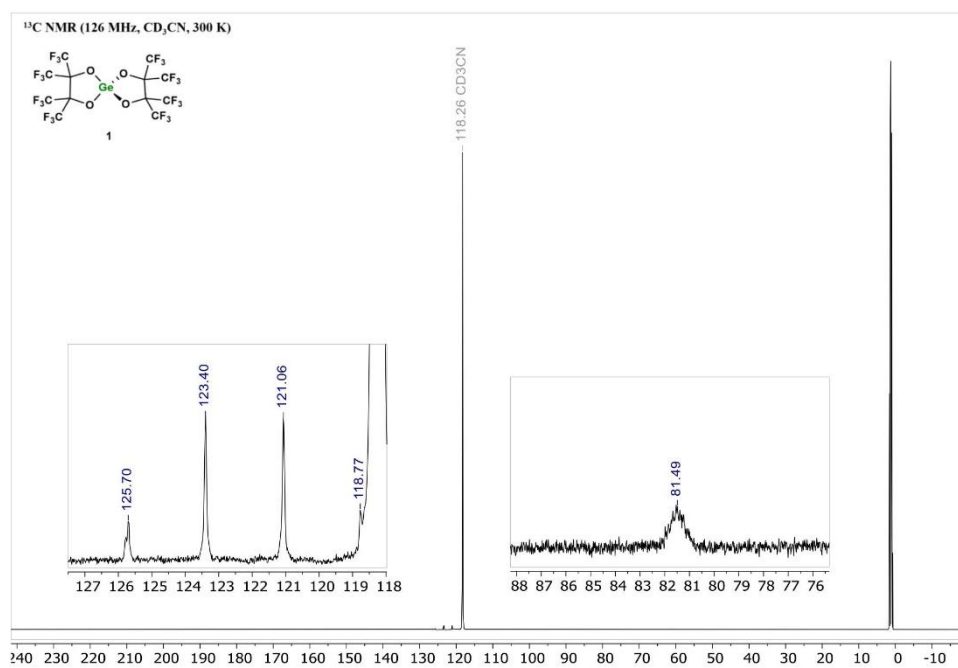


Figure S 45: ¹⁹F NMR spectrum of 1-MeCN in CD₃CN at 300 K.

5.2 NMR spectra of **1**Figure S 46: ¹H NMR spectrum of **1** in CD₃CN at 300 K.Figure S 47: ¹³C NMR spectrum of **1** in CD₃CN at 300 K.

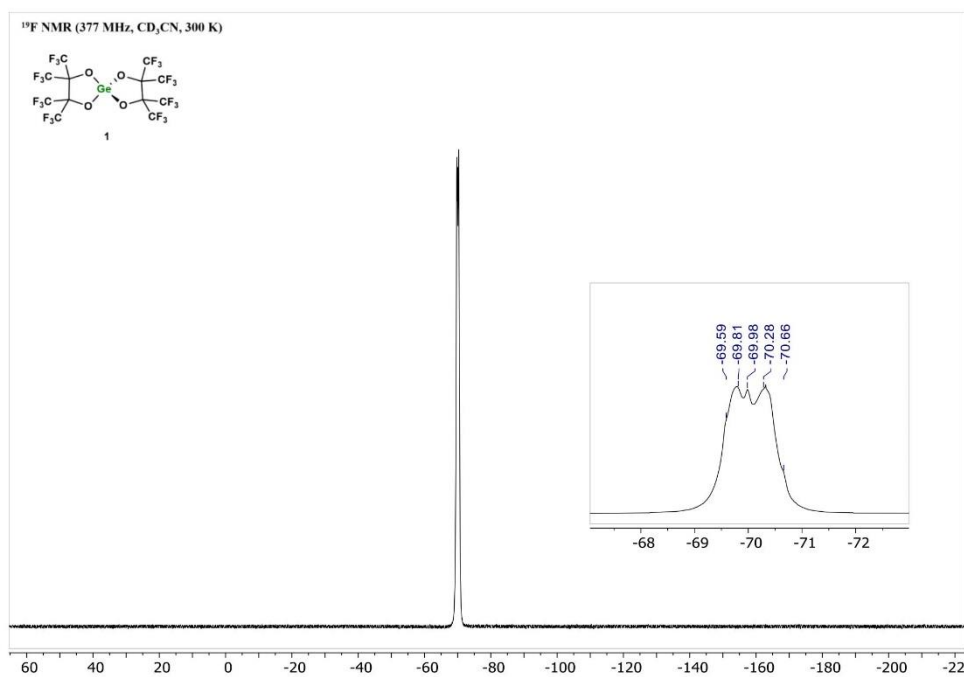
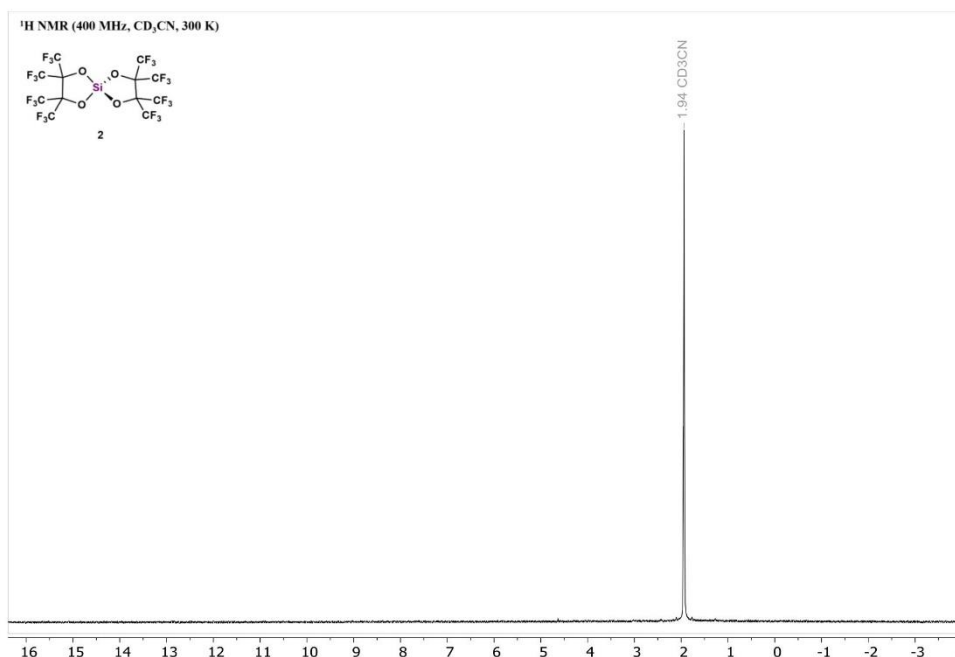
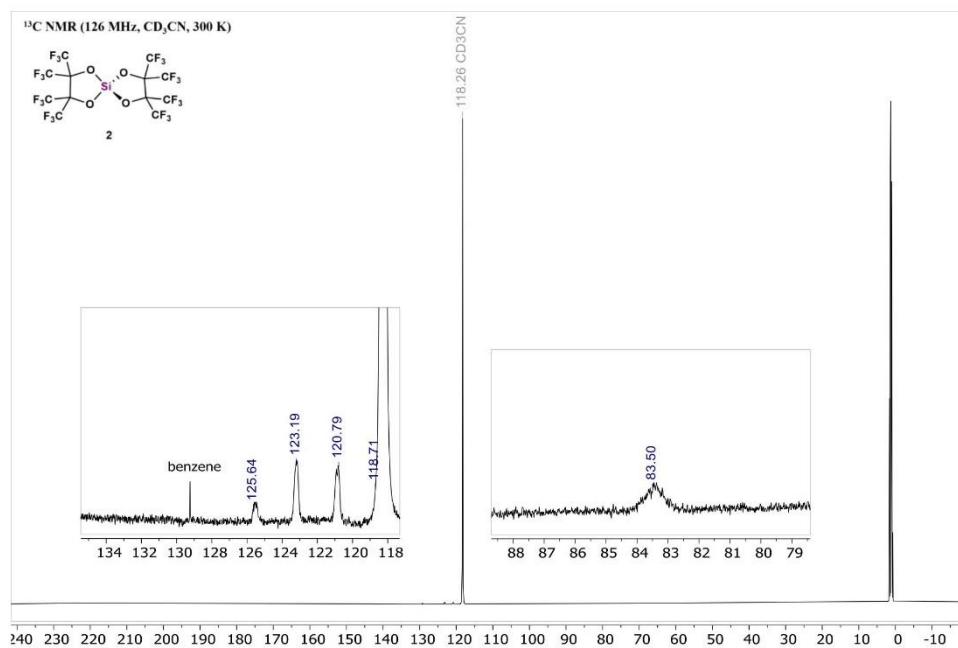


Figure S 48: ¹⁹F NMR spectrum of **1** in CD₃CN at 300 K.

5.3 NMR spectra of **2**Figure S 49: ¹H NMR spectrum of **2** in CD₃CN at 300 K.Figure S 50: ¹³C NMR spectrum of **2** in CD₃CN at 300 K.

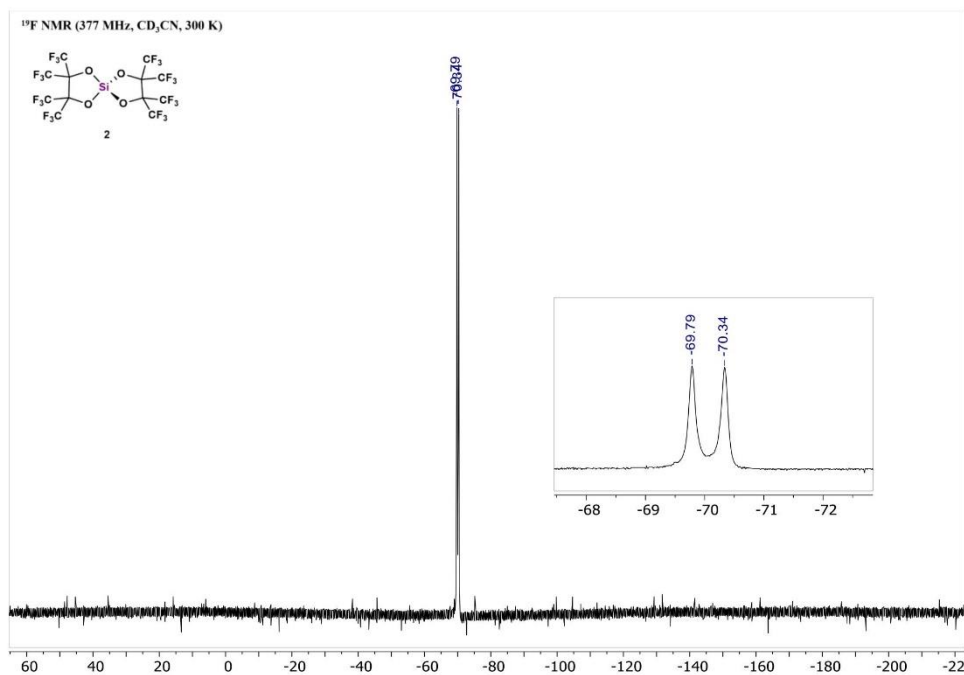


Figure S 51: ¹⁹F NMR spectrum of **2** in CD₃CN at 300 K.

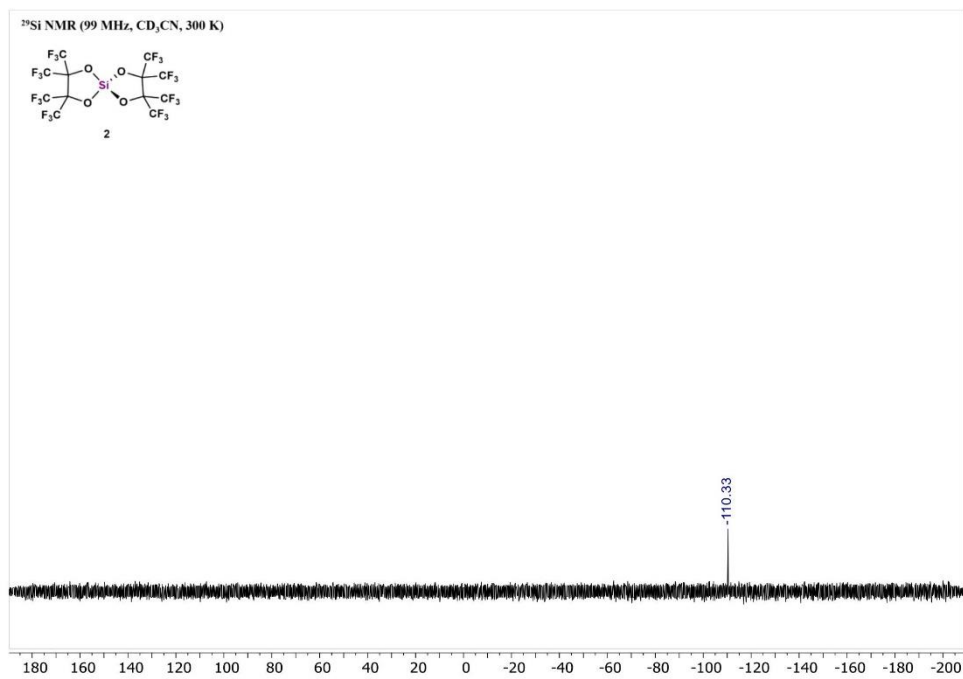
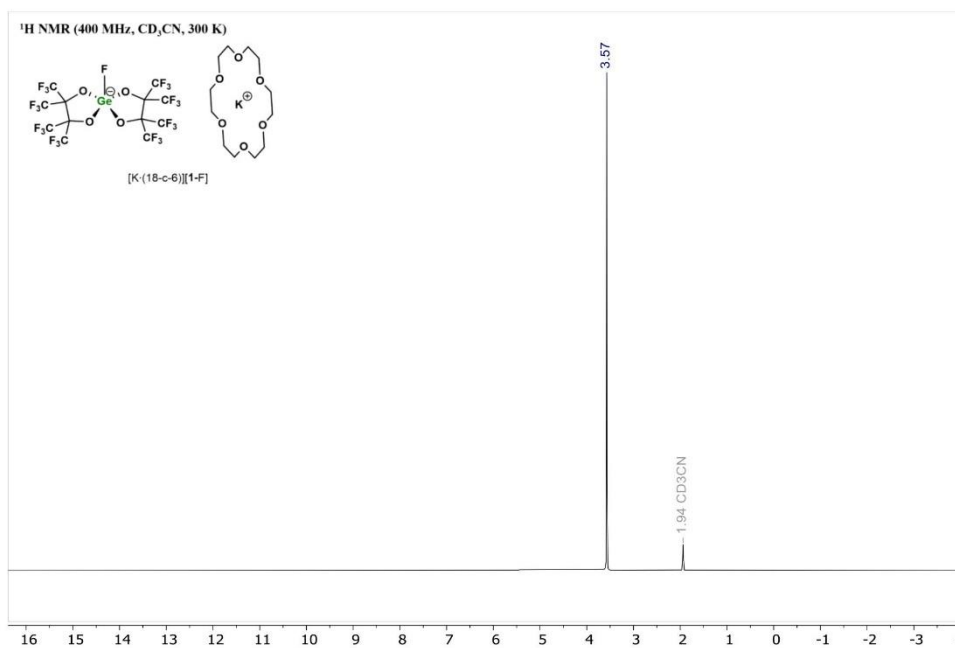
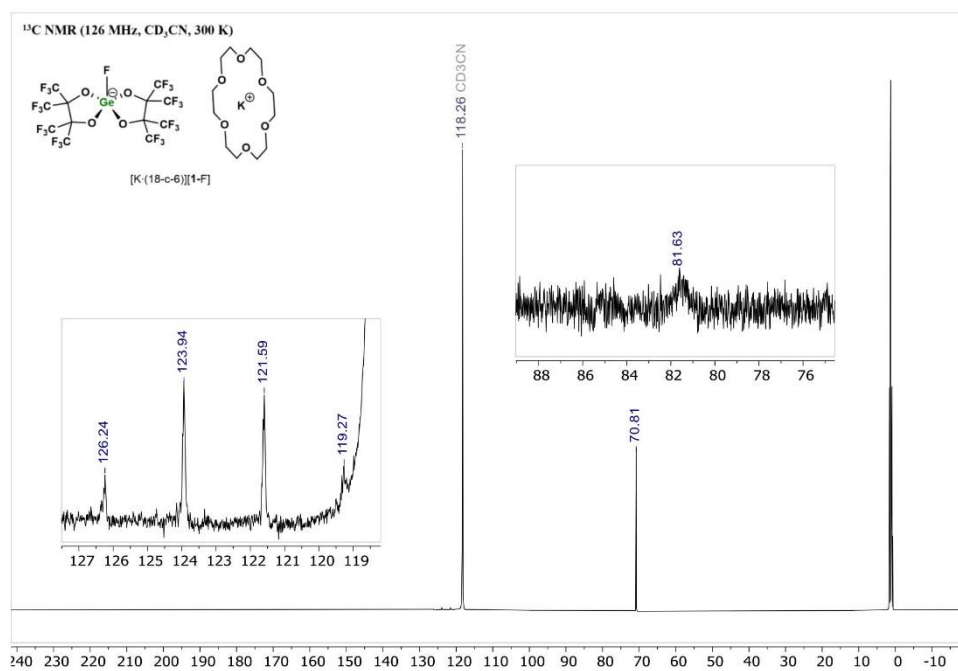


Figure S 52: ²⁹Si{¹H} NMR spectrum of **2** in CD₃CN at 300 K.

5.4 NMR spectra of [K·18-c-6][1-F]

Figure S 53: ¹H NMR spectrum of [K·(18-c-6)][1-F] in CD₃CN at 300 K.Figure S 54: ¹³C NMR spectrum of [K·(18-c-6)][1-F] in CD₃CN at 300 K.

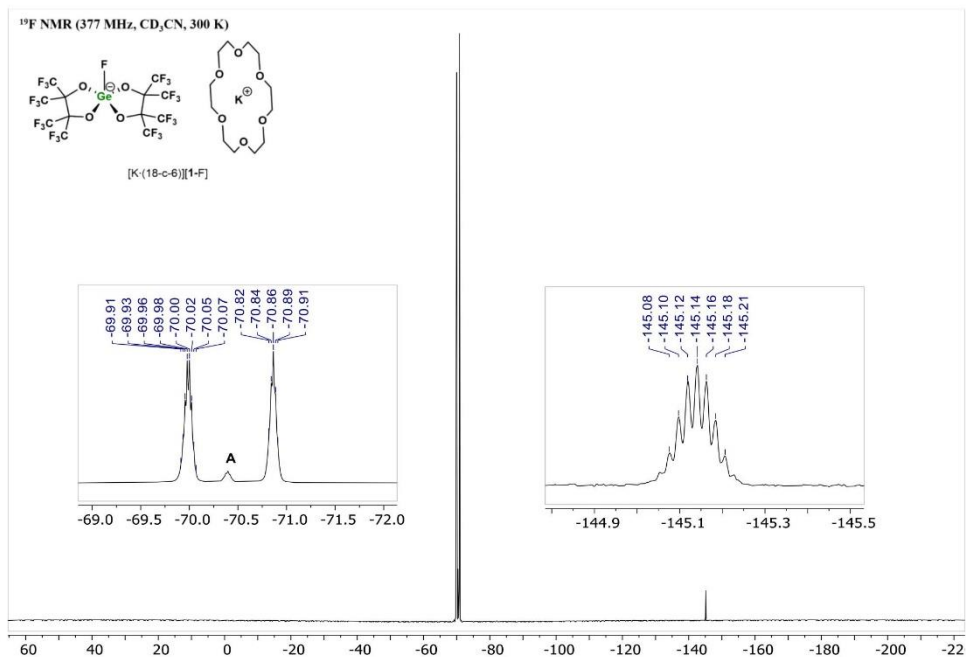
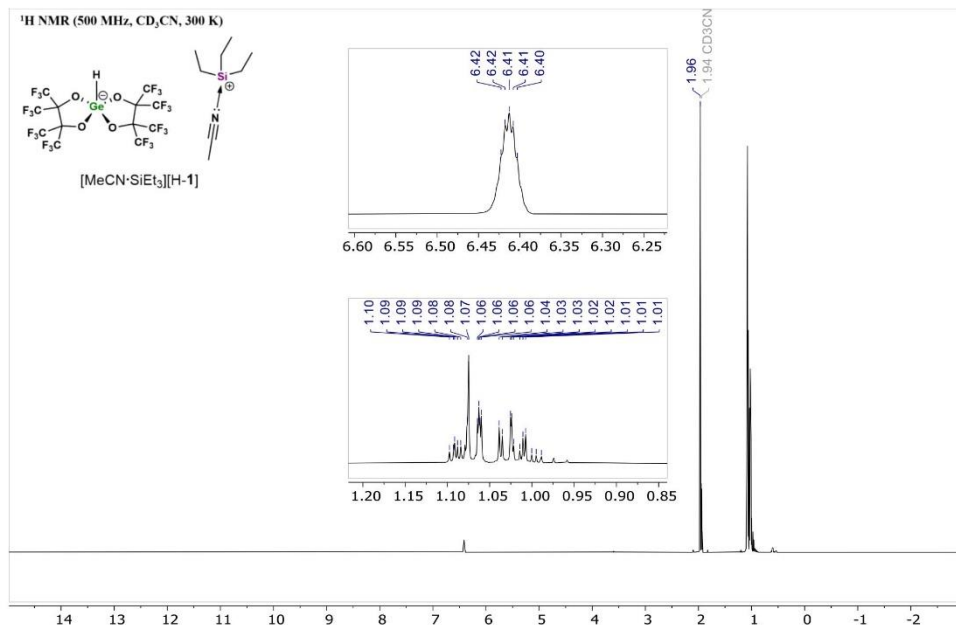
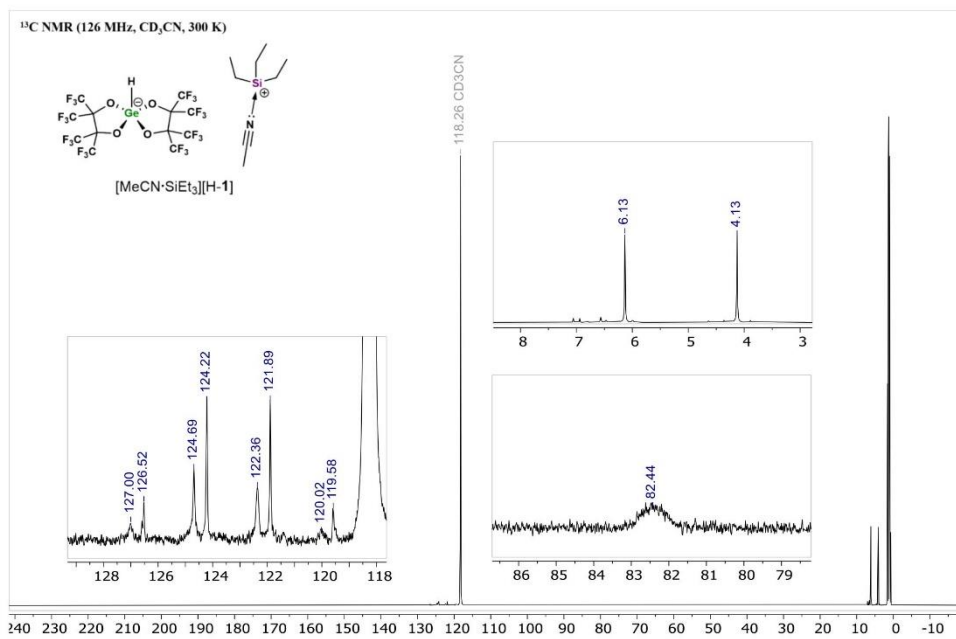


Figure S 55: ¹⁹F NMR spectrum of [K-(18-c-6)][1-F] in CD₃CN at 300 K. The spectrum additionally contains little amounts of an impurity (A) which could be identified as unreacted 1-McCN.

5.5 NMR spectra of $[\text{Et}_3\text{Si}\cdot\text{MeCN}][\text{H-1}]$ Figure S 56: ^1H NMR spectrum of $[\text{Et}_3\text{Si}\cdot\text{MeCN}][\text{H-1}]$ in CD_3CN at 300 K.Figure S 57: ^{13}C NMR spectrum of $[\text{Et}_3\text{Si}\cdot\text{MeCN}][\text{H-1}]$ in CD_3CN at 300 K.

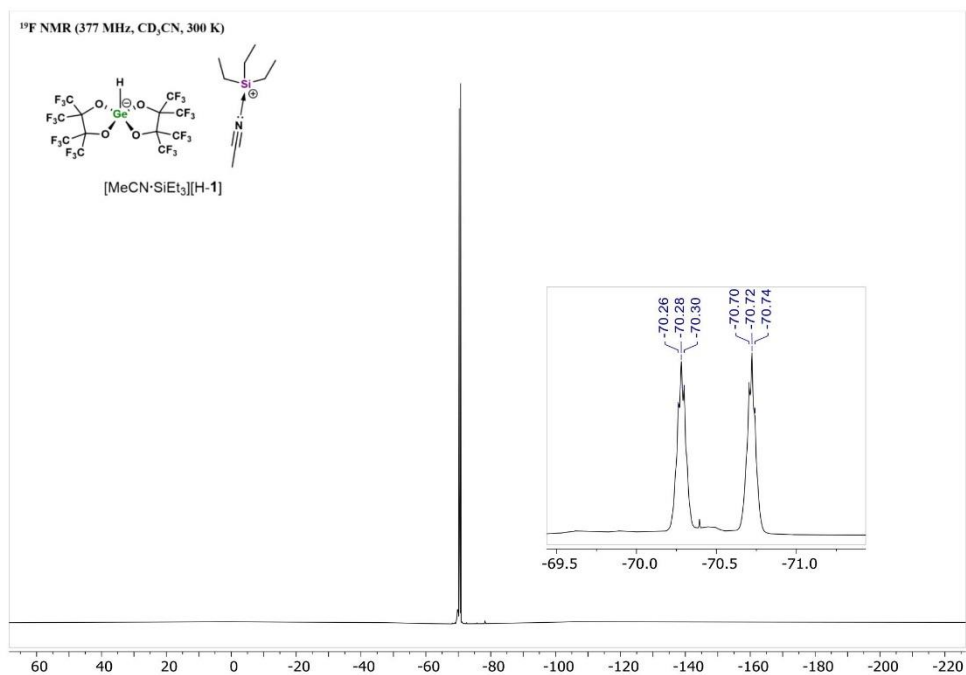


Figure S 58: ¹⁹F NMR spectrum of [Et₃Si·MeCN][1-F] in CD₃CN at 300 K.

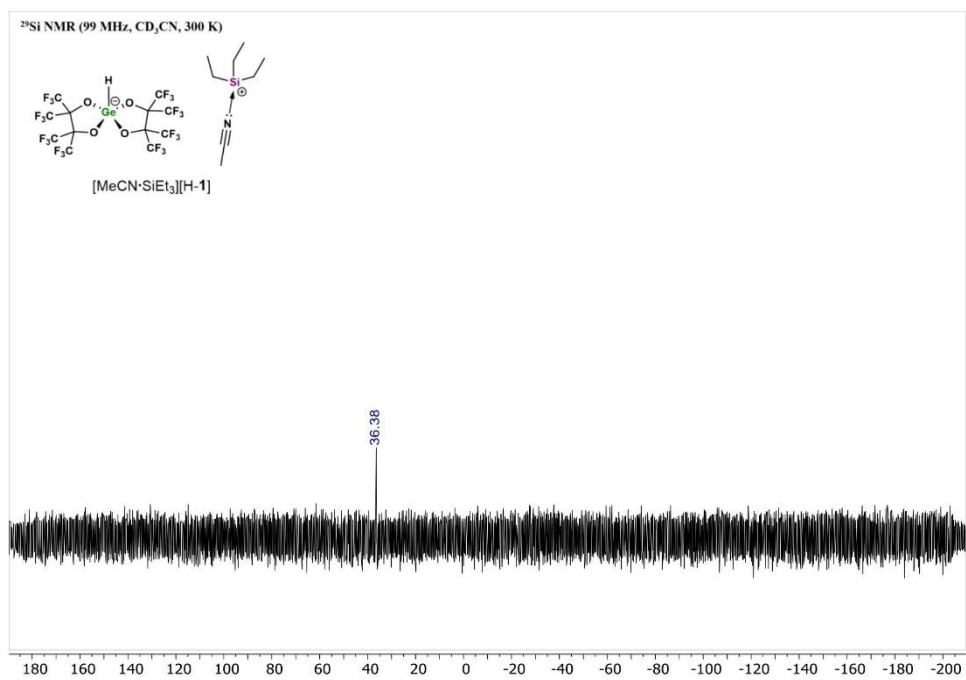
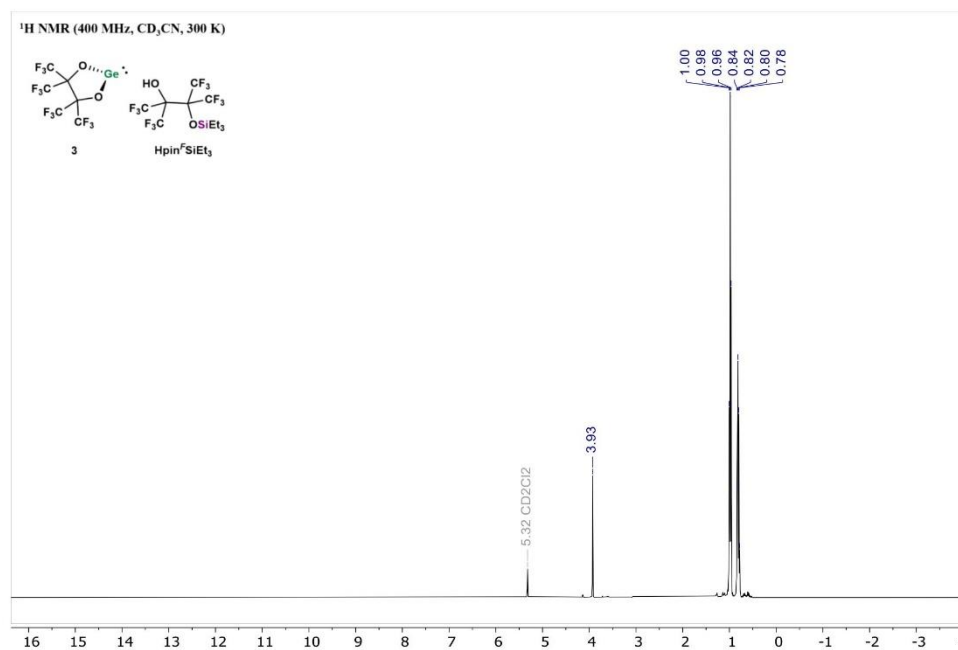
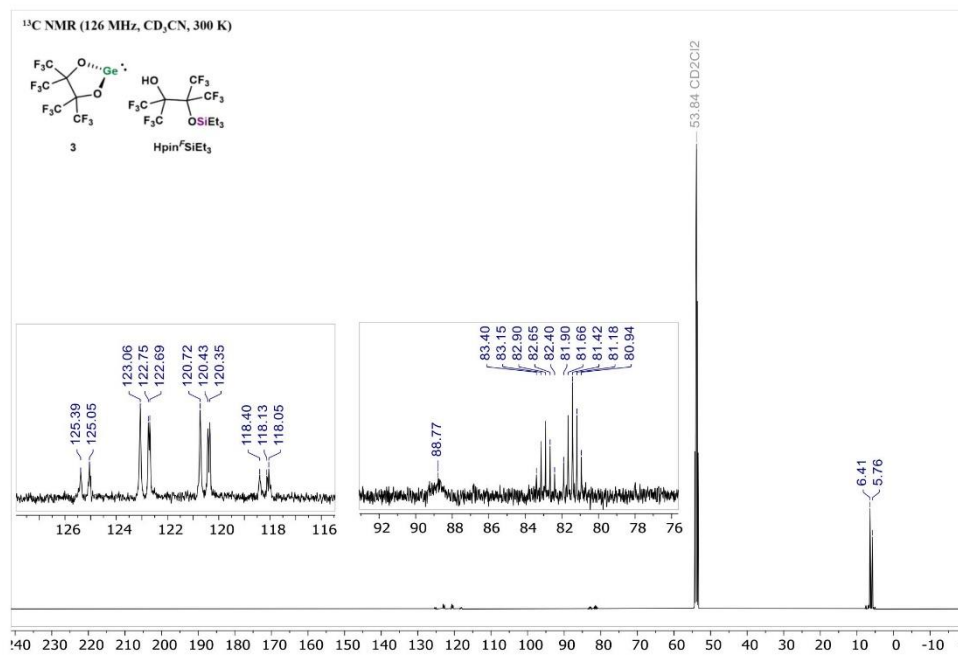


Figure S 59: ²⁹Si{¹H} NMR spectrum of [Et₃Si·MeCN][1-F] in CD₃CN at 300 K.

5.6 NMR spectra of compound mixture 3 and 4

Figure S 60: ¹H NMR spectrum of **3** and **4** in CD₂Cl₂ at 300 K.Figure S 61: ¹³C NMR spectrum of **3** and **4** in CD₂Cl₂ at 300 K.

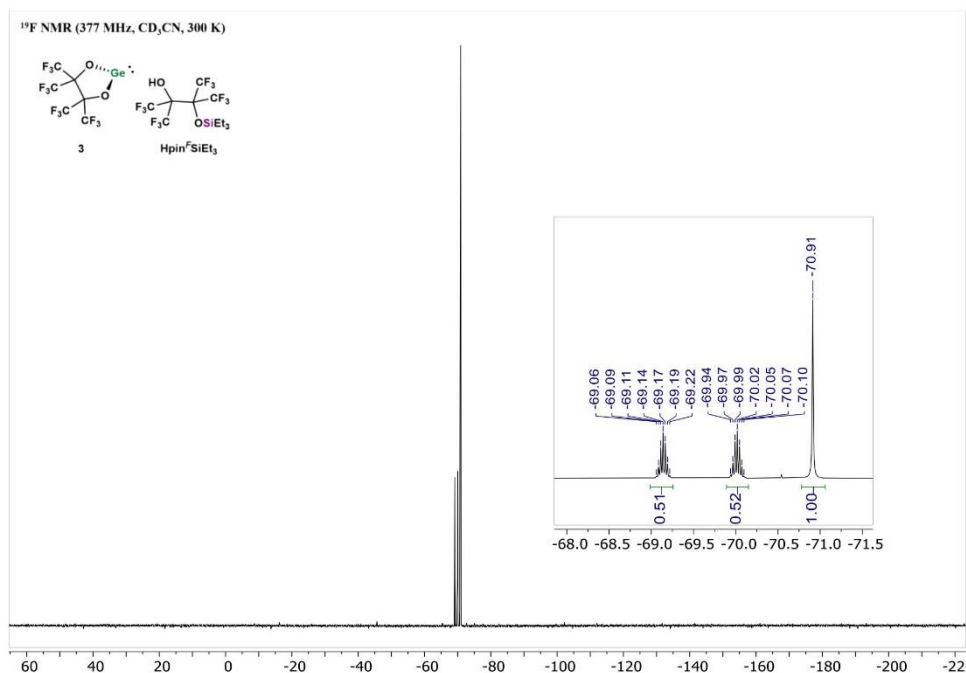


Figure S 62: ¹⁹F NMR spectrum of **3** and **4** in CD₂Cl₂ at 300 K.

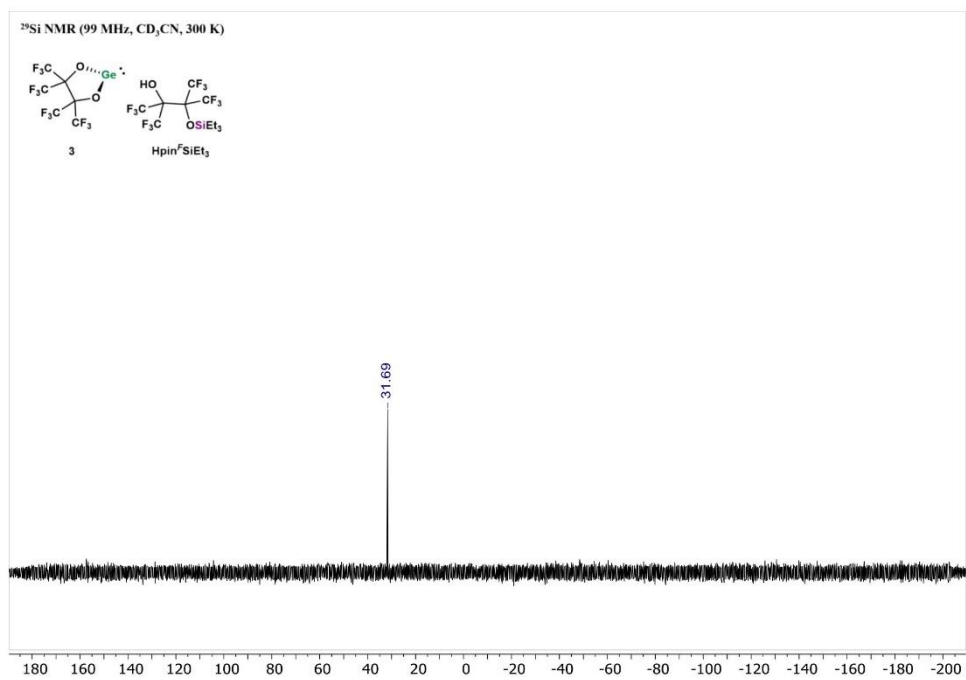
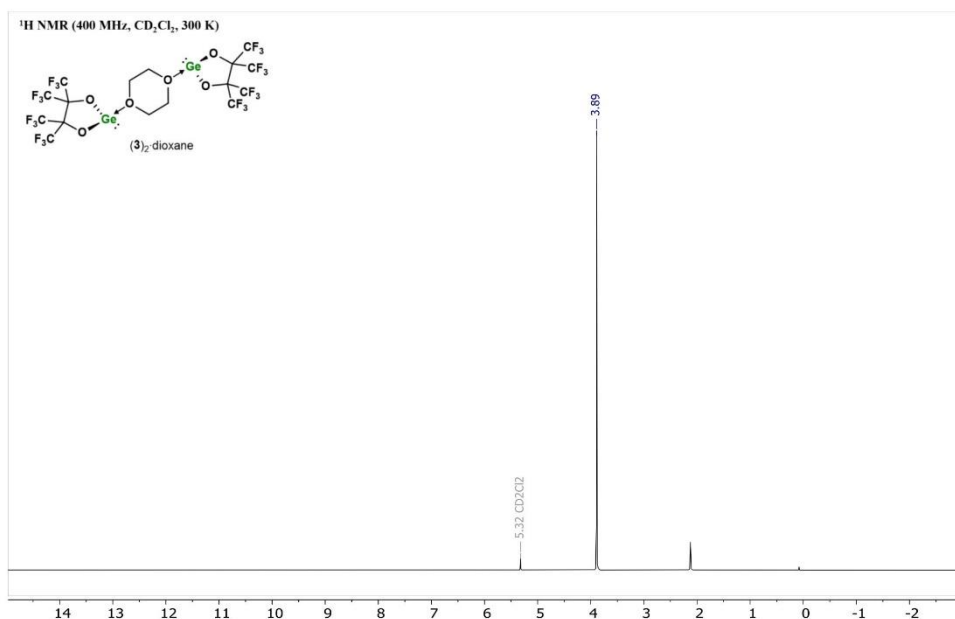
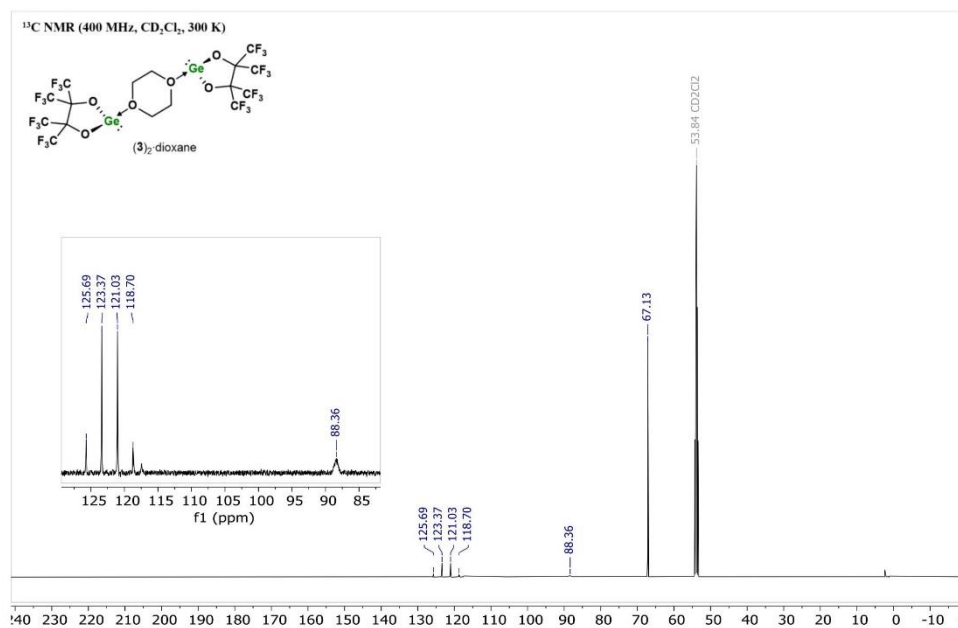


Figure S 63: ²⁹Si{¹H} NMR spectrum of **3** and **4** in CD₂Cl₂ at 300 K.

5.7 NMR spectra of 1,4-dioxane-coordinated germylene 3

Figure S 64: ¹H NMR spectrum of (3)₂·dioxane in CD₂Cl₂ at 300 K.Figure S 65: ¹³C NMR spectrum of (3)₂·dioxane in CD₂Cl₂ at 300 K.

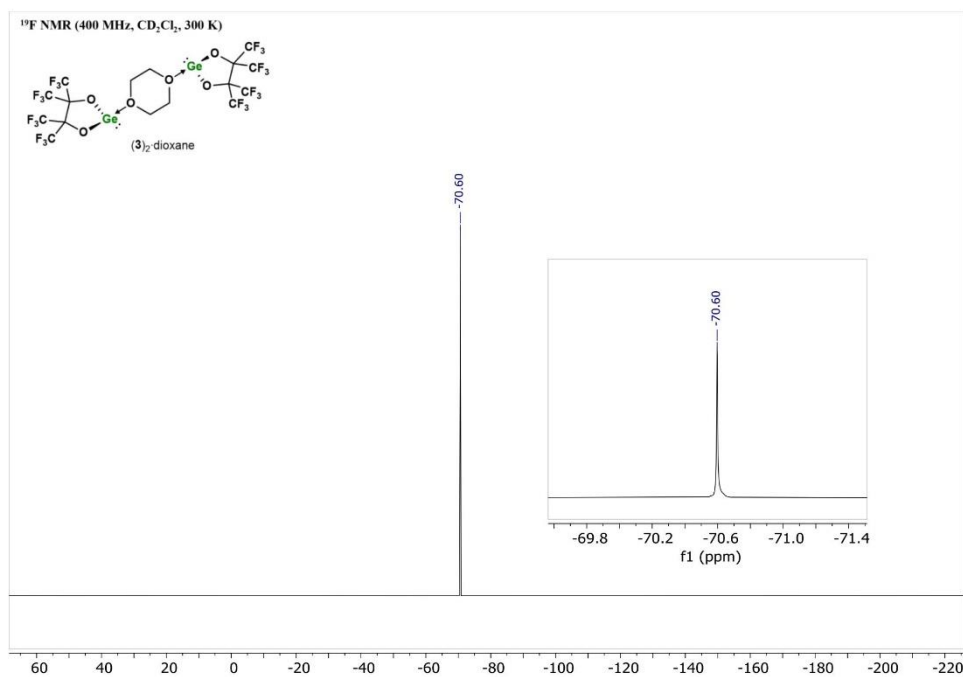


Figure S 66: ¹⁹F NMR spectrum of (3)₂-dioxane in CD₂Cl₂ at 300 K.

6 References

- [1] F. S. Tschernuth, T. Thorwart, L. Greb, F. Hanusch, S. Inoue, *Angew. Chem. Int. Ed.* **2021**, *60*, 25799-25803.
- [2] G. C. Welch, D. W. Stephan, *J. Am. Chem. Soc.* **2007**, *129*, 1880-1881.
- [3] Y. Soltani, L. C. Wilkins, R. L. Melen, *Angew. Chem. Int. Ed.* **2017**, *56*, 11995-11999.
- [4] M. Muhr, P. Heiß, M. Schütz, R. Bühler, C. Gemel, M. H. Linden, H. B. Linden, R. A. Fischer, *Dalton Trans.* **2021**, *50*, 9031-9036.
- [5] Bruker AXS Inc., Madison, Wisconsin, USA, **2015**.
- [6] SAINT, Version 8.40A ed., Bruker AXS Inc., Madison, Wisconsin, USA, **2016**.
- [7] SADABS, Version 2016/2, ed., Bruker AXS Inc., Madison, Wisconsin, USA, **2016**.
- [8] (a) L. J. Bourhis, O. V. Dolomanov, R. J. Gildea, J. A. K. Howard, H. Puschmann, *Acta Crystallogr., Sect. A* **2015**, *71*, 59-75; (b) O. V. Dolomanov, L. J. Bourhis, R. J. Gildea, J. A. K. Howard, H. Puschmann, *J. Appl. Crystallogr.* **2009**, *42*, 339-341; (c) G. M. Sheldrick, *Acta Crystallogr., Sect. C* **2015**, *71*, 3-8.
- [9] G. M. Sheldrick, University of Göttingen, Göttingen, Germany, **2014**.
- [10] C. B. Huebschle, G. M. Sheldrick, B. Dittrich, *J. Appl. Cryst.* **2011**, *44*, 1281.
- [11] G. M. Sheldrick, University of Göttingen, Göttingen, Germany, **1998**.
- [12] A. J. C. Wilson, *International Tables for Crystallography, Vol. C*, Kluwer Academic Publishers, Dordrecht, Netherlands **1992**.
- [13] (a) A. L. Spek, Utrecht University, Utrecht, Netherlands **2010**; (b) C. F. Macrae, I. Sovago, S. J. Cottrell, P. T. A. Galek, P. McCabe, E. Pidcock, M. Platings, G. P. Shields, J. S. Stevens, M. Towler, P. A. Wood, *J. Appl. Crystallogr.* **2020**, *53*, 226-235.
- [14] (a) X. Yuan, Y. Wang, *Angew. Chem. Int. Ed.* **2022**, *61*, e202203671; (b) N. Bartalucci, M. Bortoluzzi, S. Zacchini, G. Pampaloni, F. Marchetti, *Dalton Trans.* **2019**, *48*, 1574-1577.
- [15] R. J. Andrews, S. S. Chitnis, D. W. Stephan, *Chemical Communications* **2019**, *55*, 5599-5602.
- [16] F. Neese, *WIREs Comput. Mol. Sci.* **2022**, *12*, e1606.
- [17] C. Adamo, V. Barone, *The Journal of Chemical Physics* **1999**, *110*, 6158-6170.
- [18] (a) E. Caldeweyher, J.-M. Mewes, S. Ehlert, S. Grimme, *Physical Chemistry Chemical Physics* **2020**, *22*, 8499-8512; (b) E. Caldeweyher, S. Ehlert, A. Hansen, H. Neugebauer, S. Spicher, C. Bannwarth, S. Grimme, *The Journal of Chemical Physics* **2019**, *150*; (c) E. Caldeweyher, C. Bannwarth, S. Grimme, *The Journal of Chemical Physics* **2017**, *147*.
- [19] F. Weigend, R. Ahlrichs, *Physical Chemistry Chemical Physics* **2005**, *7*, 3297-3305.
- [20] F. Weigend, *Physical Chemistry Chemical Physics* **2006**, *8*, 1057-1065.
- [21] (a) S. Grimme, S. Ehrlich, L. Goerigk, *J. Comput. Chem.* **2011**, *32*, 1456-1465; (b) S. Grimme, J. Antony, S. Ehrlich, H. Krieg, *The Journal of Chemical Physics* **2010**, *132*.
- [22] (a) A. K. Wilson, D. E. Woon, K. A. Peterson, T. H. Dunning, Jr., *The Journal of Chemical Physics* **1999**, *110*, 7667-7676; (b) R. A. Kendall, T. H. Dunning, Jr., R. J. Harrison, *The Journal of Chemical Physics* **1992**, *96*, 6796-6806.
- [23] (a) P. Erdmann, L. Greb, *ChemPhysChem* **2021**, *22*, 935-943; (b) P. Erdmann, J. Leitner, J. Schwarz, L. Greb, *ChemPhysChem* **2020**, *21*, 987-994.

7 Appendix A

 Calculated energies and coordinates of **1** at PBE0-D4(CPCM-DCM)/def2-TZVP

Electronic energy ... -5229.60383427 Eh
 Total Enthalpy ... -5229.40102877 Eh
 Final Gibbs free energy ... -5229.50026724 Eh

CARTESIAN COORDINATES (ANGSTROEM)

Ge 4.685199 14.396301 8.765874
 O 3.400303 14.407805 7.561079
 O 5.968291 14.387158 7.558922
 O 4.503637 13.123260 9.970294
 O 4.867964 15.666865 9.972762
 C 3.918783 14.673253 6.291482
 C 5.447681 14.122588 6.289949
 C 2.933721 14.010537 5.270178
 F 2.726050 12.736069 5.563454
 F 3.400052 14.098629 4.031885
 F 1.750827 14.612131 5.307761
 C 3.834705 16.236199 6.149355
 F 4.150103 16.662887 4.937730
 F 4.654749 16.797439 7.045402
 F 2.617044 16.666525 6.437658
 C 5.531834 12.559691 6.146527
 F 6.750730 12.129629 6.429950
 F 5.211964 12.133313 4.936010
 F 4.715328 11.997694 7.045382
 C 6.430489 14.786252 5.267081
 F 7.614271 14.186346 5.303116
 F 6.636861 16.061142 5.559341
 F 5.962245 14.696999 4.029548
 C 4.844835 13.598852 11.239649
 C 4.527968 15.188572 11.241476
 C 4.045778 12.726153 12.265204
 F 2.756748 12.695973 11.965633
 F 4.188409 13.182577 13.502119
 F 4.481358 11.473039 12.238279
 C 6.377693 13.284298 11.385876
 F 6.832931 13.511492 12.607785
 F 7.064497 14.028300 10.512440
 F 6.625161 12.022199 11.075366
 C 2.995291 15.502877 11.390005
 F 2.307268 14.760211 10.516445
 F 2.747454 16.765457 11.081687
 F 2.541760 15.273873 12.612236
 C 5.327789 16.058812 12.268524
 F 4.890622 17.311460 12.247018
 F 6.616231 16.091654 11.966783
 F 5.187776 15.597790 13.504033

 Calculated energies and coordinates of **1** at PBE0-D4(CPCM=acetonitrile)/def2-TZVP level of theory

Electronic energy ... -5229.60411347 Eh
 Total Enthalpy ... -5229.40144558 Eh
 Final Gibbs free energy ... -5229.50070480 Eh

CARTESIAN COORDINATES (ANGSTROEM)

Ge 4.685208 14.396305 8.765831
 O 3.400375 14.407608 7.560853
 O 5.968231 14.387365 7.558691
 O 4.503546 13.123351 9.970455
 O 4.868078 15.666779 9.972926
 C 3.918751 14.673209 6.291305
 C 5.447717 14.122640 6.289769
 C 2.933685 14.010358 5.270076
 F 2.726365 12.735773 5.563236
 F 3.399694 14.098727 4.031695
 F 1.750524 14.611511 5.308049
 C 3.834579 16.236193 6.149051
 F 4.150346 16.662657 4.937426
 F 4.654262 16.797565 7.045179

F 2.616702 16.666361 6.436814
 C 5.531953 12.559704 6.146226
 F 6.751059 12.129792 6.429107
 F 5.211703 12.133548 4.935714
 F 4.715805 11.997585 7.045166
 C 6.430526 14.786426 5.266964
 F 7.614566 14.186940 5.303368
 F 6.636575 16.061428 5.559107
 F 5.962584 14.696905 4.029350
 C 4.844797 13.598832 11.239770
 C 4.528018 15.188596 11.241595
 C 4.045565 12.726174 12.265220
 F 2.756451 12.696478 11.965869
 F 4.188539 13.182175 13.502250
 F 4.480579 11.472822 12.237822
 C 6.377681 13.284214 11.386250
 F 6.832579 13.511656 12.608282
 F 7.064600 14.027991 10.512912
 F 6.625052 12.021961 11.076178
 C 2.995313 15.502957 11.390361
 F 2.307189 14.760504 10.516897
 F 2.747567 16.765685 11.082467
 F 2.542109 15.273711 12.612708
 C 5.327996 16.058793 12.268554
 F 4.891368 17.311672 12.246598
 F 6.616521 16.091182 11.967037
 F 5.187644 15.598168 13.504173

 Calculated energies and coordinates of **1** at PBE0-D4(CPCM=benzene)/def2-TZVP level of theory

Electronic energy ... -5229.60274820 Eh
 Total Enthalpy ... -5229.39943902 Eh
 Final Gibbs free energy ... -5229.49860457 Eh

CARTESIAN COORDINATES (ANGSTROEM)

Ge 4.685159 14.396278 8.766037
 O 3.400027 14.408503 7.561928
 O 5.968514 14.386406 7.559797
 O 4.503965 13.122915 9.969689
 O 4.867537 15.667182 9.972142
 C 3.918895 14.673396 6.292163
 C 5.447549 14.122414 6.290641
 C 2.933897 14.011170 5.270558
 F 2.724846 12.737162 5.564280
 F 3.401474 14.098159 4.032600
 F 1.752007 14.614445 5.306566
 C 3.835142 16.236194 6.150513
 F 4.149021 16.663698 4.938822
 F 4.656629 16.796962 7.046130
 F 2.618322 16.667110 6.440935
 C 5.531425 12.559665 6.147664
 F 6.749502 12.129044 6.433206
 F 5.213111 12.132489 4.937059
 F 4.713488 11.998092 7.046072
 C 6.430309 14.785644 5.267529
 F 7.613125 14.184130 5.302067
 F 6.637957 16.060091 5.560250
 F 5.969093 14.697465 4.030303
 C 4.844963 13.598921 11.239188
 C 4.527789 15.188490 11.241016
 C 4.046565 12.726069 12.265129
 F 2.757850 12.694010 11.964770
 F 4.187900 13.184070 13.501630
 F 4.484300 11.473848 12.240018
 C 6.377710 13.284568 11.384469
 F 6.834191 13.510772 12.605975
 F 7.064131 14.029418 10.510749
 F 6.625511 12.023050 11.072317
 C 2.995232 15.502637 11.388668
 F 2.307528 14.759179 10.514830
 F 2.747098 16.764657 11.078757
 F 2.540502 15.274615 12.610514
 C 5.327033 16.058878 12.268384
 F 4.887846 17.310671 12.248584

F 6.615158 16.093442 11.965846
F 5.188286 15.596394 13.503507

Calculated energies and coordinates of **1** at PBE0-D3/def2-TZVPP

Electronic energy ... -5229.58926089 Eh
Total Enthalpy ... -5229.38527772 Eh
Final Gibbs free energy ... -5229.48435440 Eh

CARTESIAN COORDINATES (ANGSTROEM)

Ge 4.684919 14.396541 8.766367
O 3.399086 14.412018 7.562320
O 5.969183 14.382601 7.560445
O 4.506453 13.121920 9.969751
O 4.864792 15.668539 9.972346
C 3.918862 14.674686 6.291791
C 5.447532 14.121081 6.290399
C 2.933239 14.012655 5.269991
F 2.722095 12.739530 5.565186
F 3.402303 14.097044 4.032190
F 1.752695 14.618443 5.303234
C 3.836937 16.237708 6.149144
F 4.149339 16.664890 4.936867
F 4.661179 16.798339 7.043268
F 2.621726 16.671221 6.441714
C 5.528933 12.558146 6.146174
F 6.745049 12.124259 6.434428
F 5.212506 12.131806 4.934668
F 4.707386 11.996959 7.042419
C 6.431544 14.783798 5.267429
F 7.612518 14.178800 5.299191
F 6.642368 16.057085 5.562082
F 5.960840 14.699001 4.030238
C 4.846105 13.598709 11.240026
C 4.526538 15.188882 11.241986
C 4.048964 12.723829 12.266021
F 2.760739 12.687565 11.964553
F 4.187659 13.183269 13.502525
F 4.491165 11.473290 12.242906
C 6.379292 13.285847 11.385148
F 6.836488 13.510751 12.606599
F 7.065632 14.032787 10.512081
F 6.629081 12.025397 11.070870
C 2.993620 15.501896 11.389709
F 2.305667 14.756853 10.516345
F 2.743842 16.763008 11.078032
F 2.538224 15.275022 12.611489
C 5.324900 16.060913 12.269420
F 4.881691 17.311181 12.251892
F 6.612498 16.099226 11.965588
F 5.188811 15.596806 13.504466

Calculated energies and coordinates of **1**:MeCN at PBE0-D4(CPCM=DCM)/def2-TZVP level of theory

Electronic energy ... -5362.28957277 Eh
Total Enthalpy ... -5362.03518325 Eh
Final Gibbs free energy ... -5362.14349099 Eh

CARTESIAN COORDINATES (ANGSTROEM)

Ge 7.941027 6.425840 12.129435
F 10.650589 5.585874 13.222187
F 10.003093 3.775457 14.131377
F 10.993176 5.254610 15.333120
F 8.275080 3.786967 15.924550
F 8.797273 5.563325 17.009722
F 6.861235 5.370436 16.083213
F 11.097633 7.784765 14.388082
F 10.253484 7.702834 16.369903
F 9.880015 9.383743 15.089405
F 7.501127 7.967676 16.520499
F 7.406383 9.306875 14.843194
F 6.366733 7.456059 14.750052

F 9.838419 3.420537 9.189356
F 11.086210 4.991779 9.900026
F 10.261287 5.091347 7.910933
F 6.366974 5.426940 9.495620
F 7.505170 4.888682 7.735565
F 7.366022 3.553359 9.412842
F 11.046699 7.522922 8.947431
F 10.681527 7.203471 11.056494
F 10.081800 9.026340 10.139616
F 8.858120 7.263922 7.255576
F 6.919424 7.499549 8.166545
F 8.365936 9.052019 8.335627
O 7.912244 5.318295 13.587399
O 8.672917 7.679395 13.196825
O 8.652723 5.154543 11.069285
O 7.952680 7.532476 10.670618
N 6.014015 6.451158 12.121214
C 8.720782 5.731518 14.614932
C 8.746126 7.355197 14.536179
C 8.746106 5.475172 9.730490
C 8.758984 7.099198 9.649744
C 10.127604 5.081240 14.339260
C 8.154227 5.112732 15.936520
C 10.021270 8.059976 15.110325
C 7.486580 8.027801 15.192919
C 10.010057 4.740717 9.168702
C 7.477774 4.830068 9.062944
C 10.178203 7.717680 9.934794
C 8.216496 7.729188 8.323374
C 4.871807 6.456613 12.108538
C 3.444045 6.465372 12.092814
H 3.099708 6.220020 11.085471
H 3.095965 7.462334 12.373813
H 3.076746 5.725778 12.807771

Calculated energies and coordinates of **1**:MeCN at PBE0-D4(CPCM=acetonitrile)/def2-TZVP level of theory

Electronic energy ... -5362.29230028 Eh
Total Enthalpy ... -5362.03809409 Eh
Final Gibbs free energy ... -5362.14640094 Eh

CARTESIAN COORDINATES (ANGSTROEM)

Ge 7.930206 6.422622 12.129657
F 10.652518 5.589092 13.218577
F 10.010828 3.777110 14.128164
F 10.998191 5.259113 15.328957
F 8.286886 3.783436 15.924501
F 8.806611 5.561343 17.008514
F 6.868719 5.362555 16.087213
F 11.093057 7.789951 14.381337
F 10.253640 7.706748 16.364935
F 9.871969 9.385565 15.084002
F 7.502475 7.961833 16.522945
F 7.398174 9.300596 14.845654
F 6.364201 7.446211 14.756276
F 9.839248 3.419613 9.194039
F 11.085562 4.991525 9.905478
F 10.263986 5.089612 7.915064
F 6.367163 5.425837 9.491312
F 7.509609 4.888113 7.733932
F 7.366787 3.552282 9.410692
F 11.046778 7.523820 8.951148
F 10.680849 7.202661 11.059558
F 10.080360 9.025752 10.144221
F 8.863042 7.264189 7.257320
F 6.922181 7.498763 8.163889
F 8.367666 9.051632 8.337146
O 7.914313 5.313411 13.588064
O 8.665882 7.676754 13.195626
O 8.649985 5.153681 11.070542
O 7.950898 7.531590 10.670971
N 6.010001 6.444837 12.120900
C 8.723110 5.729491 14.613649
C 8.742881 7.353154 14.534762

C 8.745315 5.474331 9.731986
 C 8.758339 7.098337 9.651577
 C 10.131579 5.083612 14.336110
 C 8.161588 5.109088 15.936818
 C 10.016858 8.062091 15.105704
 C 7.482637 8.021439 15.195072
 C 10.010099 4.739996 9.172598
 C 7.478119 4.829513 9.061562
 C 10.177202 7.716942 9.938149
 C 8.218308 7.728491 8.324043
 C 4.867424 6.457451 12.108450
 C 3.440968 6.476778 12.091577
 H 3.096587 6.228996 11.084651
 H 3.101154 7.478342 12.366940
 H 3.067547 5.743499 12.810017

 Calculated energies and coordinates of 1-McCN at PBE0-D4(CPCM=benzene)/def2-TZVP level of theory

Electronic energy ... -5362.27989486 Eh
 Total Enthalpy ... -5362.02487581 Eh
 Final Gibbs free energy ... -5362.13407019 Eh

CARTESIAN COORDINATES (ANGSTROEM)

Ge 7.979426 6.424732 12.128480
 F 10.649927 5.576141 13.235244
 F 9.991239 3.767957 14.142598
 F 10.981727 5.242783 15.348469
 F 8.251139 3.788144 15.925208
 F 8.767469 5.563868 17.013445
 F 6.840568 5.376560 16.066835
 F 11.105869 7.771797 14.411163
 F 10.247176 7.687402 16.387079
 F 9.890646 9.374289 15.110198
 F 7.490642 7.974244 16.512473
 F 7.419747 9.312157 14.833506
 F 6.370072 7.468114 14.731497
 F 9.851700 3.429953 9.165345
 F 11.096649 5.004028 9.876352
 F 10.258730 5.108506 7.892552
 F 6.371651 5.413639 9.512165
 F 7.496644 4.884165 7.740782
 F 7.381825 3.547172 9.418031
 F 11.037518 7.536977 8.933571
 F 10.681411 7.211462 11.044070
 F 10.070029 9.033519 10.131563
 F 8.832608 7.264837 7.250374
 F 6.901702 7.493844 8.179523
 F 8.344869 9.051491 8.333943
 O 7.912341 5.321924 13.583823
 O 8.691794 7.679396 13.201197
 O 8.672826 5.153258 11.063041
 O 7.952376 7.527563 10.671940
 N 6.027545 6.449310 12.120395
 C 8.716637 5.729745 14.618866
 C 8.752658 7.353077 14.541323
 C 8.754503 5.476781 9.723523
 C 8.756331 7.100588 9.644481
 C 10.121394 5.071844 14.350489
 C 8.135509 5.113381 15.934614
 C 10.027490 8.050406 15.126988
 C 7.492160 8.034322 15.186062
 C 10.018890 4.750354 9.150381
 C 7.485297 4.823314 9.067058
 C 10.173144 7.727043 9.924616
 C 8.200778 7.729037 8.323417
 C 4.886662 6.455184 12.111010
 C 3.455042 6.465799 12.099322
 H 3.104217 6.112203 11.127500
 H 3.107792 7.487450 12.268202
 H 3.085131 5.812042 12.891586

 Calculated energies and coordinates of B[II-I] at PBE0-D4(CPCM=DCM)/def2-TZVP level of theory

Electronic energy ... -5230.38307456 Eh
 Total Enthalpy ... -5230.17303971 Eh
 Final Gibbs free energy ... -5230.27259092 Eh

CARTESIAN COORDINATES (ANGSTROEM)

Ge 1.084469 -2.222684 -0.633854
 O -0.173615 -1.450155 -1.721323
 O 1.787132 -2.932278 -2.238259
 O 0.881109 -3.926621 0.017242
 O 0.054349 -1.710609 0.866204
 C 0.116479 -1.430656 -3.059612
 C 1.030650 -2.750814 -3.350123
 C -1.245689 -1.337826 -3.822472
 F -2.090048 -2.290435 -3.448007
 F -1.087875 -1.416225 -5.143006
 F -1.858938 -0.180207 -3.568047
 C 0.895750 -0.088022 -3.308534
 F 1.095826 0.178226 -4.599145
 F 2.077912 -0.107666 -2.691840
 F 0.232100 0.943606 -2.789161
 C 0.175547 -4.058817 -3.522639
 F 0.959134 -5.135558 -3.471789
 F -0.490835 -4.110013 -4.680300
 F -0.694780 -4.190781 -2.527487
 C 1.990192 -2.652943 -4.584818
 F 2.606404 -3.815908 -4.805081
 F 2.953642 -1.758528 -4.394460
 F 1.346042 -2.334244 -5.708154
 C 0.455542 -4.023072 1.315870
 C -0.492793 -2.722688 1.584419
 C -0.217838 -5.423845 1.484724
 F -1.161974 -5.633840 0.576828
 F -0.763520 -5.572849 2.691166
 F 0.672265 -6.406868 1.331716
 C 1.760823 -4.013033 2.189944
 F 1.540355 -4.286306 3.475633
 F 2.374135 -2.832454 2.106037
 F 2.635344 -4.909845 1.735505
 C -1.957385 -2.913115 1.043074
 F -1.949962 -3.375131 -0.202061
 F -2.587737 -1.739599 0.996561
 F -2.700314 -3.732095 1.795037
 C -0.603390 -2.246875 3.072607
 F -1.478442 -1.244406 3.184550
 F 0.553938 -1.779391 3.527289
 F -1.010197 -3.211488 3.897797
 H 2.327244 -1.427602 -0.254208

 Calculated energies and coordinates of B[II-I] at PBE0-D4(CPCM=acetonitrile)/def2-TZVP level of theory

Electronic energy ... -5230.38799575 Eh
 Total Enthalpy ... -5230.17806933 Eh
 Final Gibbs free energy ... -5230.27760702 Eh

CARTESIAN COORDINATES (ANGSTROEM)

Ge 1.081630 -2.224234 -0.634726
 O -0.176247 -1.451850 -1.723010
 O 1.783342 -2.936136 -2.238893
 O 0.878953 -3.928015 0.017599
 O 0.049629 -1.711907 0.864466
 C 0.116819 -1.430205 -3.061097
 C 1.028507 -2.751378 -3.351873
 C -1.243440 -1.333125 -3.826880
 F -2.090118 -2.285684 -3.456565
 F -1.082697 -1.408385 -5.146803
 F -1.855248 -0.175448 -3.569830
 C 0.899155 -0.088518 -3.306124
 F 1.101498 0.179438 -4.595562
 F 2.080173 -0.111816 -2.687351
 F 0.236329 0.942878 -2.785202
 C 0.171015 -4.057419 -3.526999
 F 0.952410 -5.135950 -3.474755
 F -0.493209 -4.106629 -4.685322

11. Appendix – Dissertation Florian Tschernuth

```

F -0.701244 -4.188521 -2.532843
C 1.990159 -2.654207 -4.585057
F 2.604727 -3.818283 -4.803933
F 2.954644 -1.761547 -4.392174
F 1.348395 -2.334103 -5.708909
C 0.455820 -4.023063 1.317600
C -0.494430 -2.724464 1.585181
C -0.214676 -5.424853 1.490008
F -1.160572 -5.637335 0.584115
F -0.757241 -5.573100 2.697467
F 0.676940 -6.406056 1.335344
C 1.762569 -4.009209 2.189629
F 1.544318 -4.280642 3.475617
F 2.373521 -2.827632 2.102371
F 2.637701 -4.905167 1.734678
C -1.959085 -2.918459 1.045610
F -1.951595 -3.381205 -0.199685
F -2.591615 -1.745912 0.997884
F -2.699635 -3.737775 1.798477
C -0.604172 -2.246635 3.072846
F -1.480459 -1.245092 3.183494
F 0.553118 -1.776736 3.524977
F -1.008655 -3.210459 3.899487
H 2.324015 -1.428819 -0.255437

```

Calculated energies and coordinates of **B[H-1]** at PBE0-D3/def2-TZVPP

```

Electronic energy ... -5230.31935171 Eh
Total Enthalpy ... -5230.10830518 Eh
Final Gibbs free energy ... -5230.20821438 Eh

```

CARTESIAN COORDINATES (ANGSTROEM)

```

Ge 7.823400 6.436069 12.130075
F 10.826701 5.806517 13.319296
F 10.290230 3.915316 14.127873
F 11.080994 5.430654 15.432488
F 8.570607 3.749251 15.935007
F 8.864150 5.572819 17.023877
F 6.982468 5.161948 16.063516
F 10.991087 8.042926 14.474086
F 10.119053 7.832470 16.431051
F 9.595996 9.490088 15.177262
F 7.356366 7.846098 16.522433
F 7.145428 9.166852 14.842430
F 6.302419 7.219073 14.741018
F 9.518145 3.325227 9.090864
F 10.957480 4.719034 9.812361
F 10.109938 4.968063 7.849403
F 6.301136 5.702229 9.511787
F 7.344502 5.029538 7.740761
F 7.078729 3.727439 9.427965
F 11.140745 7.323893 8.856201
F 10.849100 6.969724 10.967928
F 10.386418 8.873311 10.141873
F 8.930690 7.255678 7.243526
F 7.052976 7.724820 8.185031
F 8.680792 9.089686 8.325762
O 8.064273 5.265838 13.584850
O 8.629398 7.681948 13.219083
O 8.602713 5.164900 11.050579
O 8.114790 7.596831 10.676345
C 8.810766 5.732181 14.612606
C 8.691221 7.362077 14.545357
C 8.682052 5.480072 9.724039
C 8.852156 7.104006 9.653999
C 10.280274 5.222723 14.376880
C 8.299589 5.057779 15.928970
C 9.870234 8.181552 15.166615
C 7.359218 7.897626 15.186627
C 9.838067 4.623027 9.109863
C 7.337195 4.985952 9.076960
C 10.335261 7.565462 9.900659
C 8.371561 7.790021 8.332018
H 6.299502 6.460467 12.122742

```

Calculated energies and coordinates of **B[F-1]** at PBE0-D3/def2-TZVPP

```

Electronic energy ... -5329.56512578 Eh
Total Enthalpy ... -5329.35855798 Eh
Final Gibbs free energy ... -5329.46017603 Eh

```

CARTESIAN COORDINATES (ANGSTROEM)

```

Ge 7.892306 6.433745 12.130303
F 10.806868 5.808770 13.312452
F 10.271362 3.921531 14.128929
F 11.071891 5.436697 15.425557
F 8.538057 3.752433 15.911734
F 8.853375 5.564069 17.014963
F 6.964327 5.177865 16.058274
F 10.989581 8.042717 14.459325
F 10.139066 7.819969 16.424582
F 9.612114 9.491760 15.190988
F 7.392955 7.874086 16.550071
F 7.159013 9.191349 14.868156
F 6.299891 7.249317 14.794033
F 9.533155 3.323402 9.071044
F 10.952511 4.717835 9.828689
F 10.132359 4.983608 7.856164
F 6.296275 5.672579 9.454613
F 7.380235 4.999294 7.710573
F 7.088924 3.702470 9.400021
F 11.130596 7.319276 8.868315
F 10.824107 6.966195 10.978722
F 10.363051 8.866748 10.146229
F 8.921817 7.268011 7.252852
F 7.034854 7.712349 8.188162
F 8.649258 9.088899 8.352408
O 8.060187 5.283612 13.570686
O 8.613160 7.704294 13.227711
O 8.583671 5.141420 11.039614
O 8.105064 7.576733 10.689274
C 8.799087 5.746172 14.611933
C 8.684757 7.375781 14.554962
C 8.673116 5.465890 9.712455
C 8.837602 7.089598 9.654567
C 10.266462 5.228164 14.376978
C 8.277442 5.062546 15.919803
C 9.877870 8.182836 15.167417
C 7.362939 7.920823 15.212569
C 9.844361 4.621837 9.107409
C 7.338616 4.962350 9.048342
C 10.318198 7.559807 9.904276
C 8.349491 7.787533 8.341436
F 6.167886 6.460910 12.124341

```

Calculated energies and coordinates of **2** at PBE0-D4(CPCM=DCM)/def2-TZVP level of theory

```

Electronic energy ... -3442.33762144 Eh
Total Enthalpy ... -3442.13280403 Eh
Final Gibbs free energy ... -3442.23043761 Eh

```

CARTESIAN COORDINATES (ANGSTROEM)

```

Si 6.241492 7.760971 4.237656
O 6.213586 6.537301 5.325411
O 6.278562 8.983590 5.326575
O 5.012339 7.710685 3.156829
O 7.457513 7.812316 3.141670
C 6.492106 6.989285 6.619950
C 6.003057 8.530428 6.621419
C 5.452926 7.997748 1.860262
C 6.999952 7.530484 1.849380
C 5.789244 6.017728 7.624251
C 6.707763 9.501203 7.625183
C 4.484088 7.283945 0.861241
C 7.953533 8.248474 0.838467
C 5.280406 9.553708 1.716583

```

11. Appendix – Dissertation Florian Tschernuth

```

C 7.170630 5.975172 1.696457
C 4.445381 8.680576 6.772567
C 8.049986 6.838437 6.766452
F 6.344312 4.813274 7.574040
F 4.507221 5.864056 7.333336
F 5.898196 6.472486 8.865994
F 6.601174 9.045054 8.866632
F 6.152235 10.705548 7.577313
F 7.989169 9.655713 7.332150
F 4.025210 8.407999 7.997428
F 4.064525 9.908784 6.461843
F 3.839062 7.867741 5.904342
F 8.473701 7.109437 7.990489
F 8.429381 5.610388 6.453344
F 8.654122 7.651716 5.897118
F 9.165063 7.707985 0.875357
F 8.094115 9.531455 1.131345
F 7.488181 8.137500 -0.399250
F 4.928434 7.398783 -0.383651
F 3.273814 7.825358 0.920563
F 4.347798 6.000023 1.152363
F 5.532276 9.980930 0.489516
F 4.051309 9.916814 2.043992
F 6.095137 10.168572 2.576960
F 6.897793 5.552831 0.472274
F 8.405519 5.611406 2.000780
F 6.370692 5.356095 2.567471

```

Calculated energies and coordinates of **2** at PBE0-D4(CPCM=benzene)/def2-TZVP level of theory

```

Electronic energy ... -3442.33672263 Eh
Total Enthalpy ... -3442.13138544 Eh
Final Gibbs free energy ... -3442.22895812 Eh

```

CARTESIAN COORDINATES (ANGSTROEM)

```

Si 6.241477 7.760966 4.237644
O 6.213627 6.537278 5.325321
O 6.278502 8.983605 5.326480
O 5.012309 7.710710 3.156898
O 7.457520 7.812266 3.141744
C 6.492019 6.989255 6.619875
C 6.003131 8.530460 6.621340
C 5.452882 7.997668 1.860322
C 6.999971 7.530564 1.849439
C 5.789252 6.017675 7.624073
C 6.707750 9.501273 7.624982
C 4.484025 7.283959 0.861382
C 7.953604 8.248448 0.838635
C 5.279901 9.553507 1.716809
C 7.171131 5.975382 1.696645
C 4.445577 8.681086 6.772399
C 8.049776 6.837924 6.766269
F 6.344982 4.813595 7.574377
F 4.507378 5.863349 7.333005
F 5.897808 6.472635 8.865798
F 6.601577 9.044940 8.866420
F 6.151562 10.705243 7.577617
F 7.989005 9.656436 7.331780
F 4.025086 8.410615 7.997683
F 4.064829 9.908811 6.459952
F 3.838814 7.867298 5.905322
F 8.473843 7.106867 7.990702
F 8.429052 5.610347 6.451478
F 8.654351 7.652112 5.898027
F 9.164764 7.707297 0.875060
F 8.094845 9.531295 1.131642
F 7.488088 8.137856 -0.399073
F 4.928528 7.398510 -0.383503
F 3.274066 7.825926 0.920261
F 4.347188 6.000145 1.152578
F 5.529694 9.981097 0.489382
F 4.051323 9.916514 2.045960
F 6.095558 10.168783 2.576074
F 6.900359 5.552705 0.472058

```

```

F 8.405560 5.611742 2.002674
F 6.370288 5.355857 2.566567

```

Calculated energies and coordinates of **2-McCN** at PBE0-D4(CPCM=benzene)/def2-TZVP level of theory

```

Electronic energy ... -3575.00611941 Eh
Total Enthalpy ... -3574.74907229 Eh
Final Gibbs free energy ... -3574.85531876 Eh

```

CARTESIAN COORDINATES (ANGSTROEM)

```

Si 7.968816 6.417901 12.130199
F 10.651801 5.509481 13.194334
F 9.930128 3.725002 14.096314
F 10.935683 5.182846 15.313637
F 8.172199 3.781415 15.847277
F 8.716822 5.551328 16.934100
F 6.794146 5.397694 15.971660
F 11.107344 7.711511 14.284951
F 10.267011 7.679465 16.270438
F 9.929488 9.348265 14.962164
F 7.532046 8.000424 16.442965
F 7.464743 9.321677 14.749159
F 6.369517 7.504567 14.688391
F 9.905416 3.457569 9.311339
F 11.103727 5.074148 10.001026
F 10.281031 5.122613 8.008659
F 6.372956 5.356143 9.557116
F 7.543105 4.842289 7.812956
F 7.440428 3.522333 9.506160
F 10.979314 7.608347 8.970343
F 10.674777 7.283601 11.086887
F 9.986732 9.079889 10.182044
F 8.767833 7.273399 7.332301
F 6.840574 7.457850 8.280064
F 8.243666 9.051591 8.415520
O 7.907768 5.357852 13.483132
O 8.642800 7.601097 13.110591
O 8.631488 5.224299 11.154689
O 7.934709 7.478595 10.776713
N 6.129225 6.433397 12.122930
C 8.695209 5.716926 14.546516
C 8.748114 7.329780 14.460986
C 8.752207 5.494120 9.805300
C 8.725190 7.107614 9.719744
C 10.090159 5.027144 14.299203
C 8.084708 5.108386 15.851161
C 10.041795 8.023259 15.005027
C 7.512160 8.046756 15.116437
C 10.039412 4.780672 9.271518
C 7.510834 4.796315 9.139275
C 10.128636 7.775732 9.978597
C 8.134761 7.726203 8.410535
C 4.988988 6.442476 12.110941
C 3.558060 6.456184 12.097399
H 3.210047 6.721974 11.097333
H 3.206781 7.194111 12.822347
H 3.189331 5.465863 12.372601

```

Calculated energies and coordinates of **Compound 3** at PBE0-D4(CPCM=DCM)/def2-TZVP level of theory

```

Electronic energy ... -3653.18556968 Eh
Total Enthalpy ... -3653.08432860 Eh
Final Gibbs free energy ... -3653.14830528 Eh

```

CARTESIAN COORDINATES (ANGSTROEM)

```

Ge -0.000129 2.529572 0.000093
O -0.971458 1.204605 0.792892
O 0.971511 1.204906 -0.792825
C -0.757176 -0.063161 0.285918
C 0.757212 -0.063020 -0.286240
C -1.069636 -1.081325 1.430953
F -0.412555 -0.770233 2.540674

```

F -0.753468 -2.324591 1.085207
 F -2.363709 -1.067533 1.739124
 C -1.838791 -0.236670 -0.843042
 F -1.867504 -1.463007 -1.350781
 F -1.613590 0.635383 -1.830044
 F -3.050957 0.040123 -0.378364
 C 1.838341 -0.236669 0.843143
 F 3.050625 0.041169 0.379393
 F 1.867438 -1.463323 1.350087
 F 1.611950 0.634530 1.830632
 C 1.070264 -1.081046 -1.431311
 F 0.413712 -0.769984 -2.541345
 F 0.754119 -2.324391 -1.085823
 F 2.364466 -1.067105 -1.738918

 Calculated energies and coordinates of 3-McCN at PBE0-D4(CPCM=DCM)/def2-TZVP level of theory

Electronic energy ... -3785.85639647 Eh
 Total Enthalpy ... -3785.70362806 Eh
 Final Gibbs free energy ... -3785.77885706 Eh

CARTESIAN COORDINATES (ANGSTROEM)

Ge 1.510846 1.421875 -0.648441
 O 0.478545 0.012467 -1.307624
 O 0.520514 1.179007 0.926000
 C -0.442759 -0.535898 -0.451338
 C -0.687297 0.566834 0.721116
 C -1.702441 -0.922584 -1.298596
 F -1.435224 -1.943718 -2.114505
 F -2.095111 0.081299 -2.073364
 F -2.731468 -1.289764 -0.537877
 C 0.183620 -1.874802 0.076704
 F 1.208051 -1.652488 0.892324
 F 0.671504 -2.586203 -0.938314
 F -0.703372 -2.640972 0.715944
 C -1.668517 1.712061 0.269555
 F -1.635657 2.722809 1.132068
 F -2.936071 1.330381 0.149352
 F -1.264838 2.218480 -0.903346
 C -1.186457 0.030776 2.102693
 F -1.407109 1.039344 2.946428
 F -0.285211 -0.750367 2.684015
 F -2.322919 -0.655780 1.999215
 N 3.105356 0.172225 0.150571
 C 4.032149 -0.388554 0.523460
 C 5.171490 -1.120706 1.004298
 H 5.452141 -1.871363 0.263121
 H 4.908191 -1.613489 1.942202
 H 6.005035 -0.436090 1.168715

 Calculated energies and coordinates of 3-McCN at PBE0-D4(CPCM=acetonitrile)/def2-TZVP level of theory

Electronic energy ... -3785.85836779 Eh
 Total Enthalpy ... -3785.70572528 Eh
 Final Gibbs free energy ... -3785.78067625 Eh

CARTESIAN COORDINATES (ANGSTROEM)

Ge 1.558017 1.267225 -0.631483
 O 0.423254 -0.014588 -1.376760
 O 0.585183 0.959432 0.941971
 C -0.517117 -0.570638 -0.547590
 C -0.661737 0.440346 0.724630
 C -1.816198 -0.792939 -1.394325
 F -1.632816 -1.739015 -2.317254
 F -2.161261 0.307121 -2.053850
 F -2.850526 -1.171611 -0.645980
 C 0.028944 -1.987052 -0.149900
 F 1.099920 -1.895652 0.629975
 F 0.418763 -2.654813 -1.234911
 F -0.883761 -2.735834 0.473839
 C -1.583222 1.677205 0.409260
 F -1.451895 2.611622 1.346661

F -2.876630 1.381695 0.316982
 F -1.195893 2.253959 -0.735044
 C -1.152269 -0.192194 2.068615
 F -1.322913 0.747144 3.000442
 F -0.267110 -1.049194 2.562493
 F -2.313599 -0.828959 1.932223
 N 3.096472 -0.058874 0.092034
 C 4.078768 -0.369973 0.596241
 C 5.304427 -0.771137 1.227595
 H 5.105099 -1.596483 1.913445
 H 5.714282 0.076146 1.781147
 H 6.016809 -1.088160 0.463920

 Calculated energies and coordinates of Compound 3*_Ge at PBE0-D4(CPCM=DCM)/def2-TZVP level of theory

Electronic energy ... -5757.12723823 Eh
 Total Enthalpy ... -5756.70436594 Eh
 Final Gibbs free energy ... -5756.82749411 Eh

CARTESIAN COORDINATES (ANGSTROEM)

Ge 0.682796 -1.060073 -0.827283
 O -0.855276 -0.498433 -1.554416
 O 0.930780 -2.184535 -2.210720
 O 0.315017 -2.159560 0.498172
 O 0.174515 0.305897 1.399935
 C -0.961172 -0.857607 -2.890068
 C -0.157555 -2.261202 -3.056956
 C -2.488959 -0.876560 -3.230158
 F -3.166101 -1.668659 -2.412868
 F -2.699455 -1.277609 -4.479919
 F -3.013082 0.338883 -3.100138
 C -0.291383 0.315358 -3.699085
 F -0.415598 0.188315 -5.011959
 F 1.009135 0.383384 -3.390516
 F -0.812899 1.485802 -3.356487
 C -0.990372 -3.507727 -2.585160
 F -0.201612 -4.566956 -2.443376
 F -1.951154 -3.826962 -3.448785
 F -1.534009 -3.286389 -1.392591
 C 0.403297 -2.568317 -4.488303
 F 0.917303 -3.794518 -4.540497
 F 1.382400 -1.733191 -4.807199
 F -0.540953 -2.490776 -5.420166
 C 0.474763 -2.025990 1.855641
 C -0.201864 -0.632442 2.338060
 C -0.162634 -3.367129 2.399487
 F -1.379888 -3.539778 1.903824
 F -0.238397 -3.432971 3.719375
 F 0.572462 -4.399049 1.991194
 C 2.021687 -2.066446 2.146881
 F 2.300671 -2.298497 3.422585
 F 2.593586 -0.916071 1.790851
 F 2.603975 -3.013061 1.420971
 C -1.768810 -0.703561 2.280750
 F -2.190580 -1.206289 1.128916
 F -2.287592 0.517154 2.372960
 F -2.261714 -1.431745 3.281024
 C 0.206893 -0.195274 3.798451
 F -0.651752 0.689765 4.295303
 F 1.408054 0.378645 3.776280
 F 0.247071 -1.201380 4.655820
 Si 0.491637 2.022801 1.309402
 C -0.236790 3.021070 2.712629
 C -0.307242 2.521215 -0.294966
 C 2.349384 2.285251 1.272556
 H -1.266675 2.728384 2.921317
 C -0.183517 4.511683 2.359917
 H 0.335869 2.845551 3.626035
 H -0.832120 4.750568 1.514604
 H 0.827876 4.838249 2.101974
 H -0.512423 5.116572 3.208109
 C -1.828056 2.415984 -0.335222
 H 0.141650 1.971622 -1.125038
 H 0.005443 3.561449 -0.451541

11. Appendix – Dissertation Florian Tschernuth

H -2.157149 1.381095 -0.238938
H -2.223464 2.798263 -1.278956
H -2.290041 2.988081 0.473073
H 2.843736 1.449174 1.771607
H 2.524761 3.151226 1.921914
C 2.985115 2.546712 -0.091054
H 2.872732 1.701166 -0.773925
H 4.056531 2.737592 0.008543
H 2.540097 3.415379 -0.581315
H 1.867915 -0.138768 -0.685677

Calculated energies and coordinates of Compound 3*_Si at PBE0-D4(CPCM=DCM)/def2-TZVP level of theory

Electronic energy ... -3969.83058328 Eh
Total Enthalpy ... -3969.40556420 Eh
Final Gibbs free energy ... -3969.52758424 Eh

CARTESIAN COORDINATES (ANGSTROEM)

Si 0.590319 -1.126301 -0.923720
O -0.804881 -0.508939 -1.578391
O 0.871172 -2.176068 -2.186058
O 0.260584 -2.006267 0.396751
O 0.179193 0.386232 1.431928
C -0.970318 -0.852257 -2.915380
C -0.188266 -2.264650 -3.077317
C -2.502869 -0.856565 -3.224495
F -3.170183 -1.639658 -2.391507
F -2.729300 -1.266053 -4.468606
F -3.015384 0.362062 -3.093862
C -0.300809 0.319703 -3.725769
F -0.446488 0.194094 -5.036358
F 1.000649 0.377520 -3.433734
F -0.813619 1.489139 -3.368748
C -1.028196 -3.508809 -2.610539
F -0.244945 -4.572559 -2.482658
F -1.997331 -3.810205 -3.467503
F -1.557160 -3.289276 -1.410935
C 0.399660 -2.573833 -4.494648
F 0.915556 -3.797556 -4.540907
F 1.379098 -1.736516 -4.801708
F -0.540207 -2.494761 -5.430616
C 0.492135 -1.956418 1.749633
C -0.168231 -0.592223 2.324099
C -0.101702 -3.334968 2.248464
F -1.341083 -3.495203 1.806174
F -0.107920 -3.478531 3.563065
F 0.622549 -4.330092 1.739251
C 2.052341 -1.996863 1.955082
F 2.381509 -2.371594 3.184442
F 2.607347 -0.815219 1.711607
F 2.598213 -2.854453 1.098403
C -1.737207 -0.677894 2.309413
F -2.189200 -1.135849 1.149598
F -2.266243 0.530233 2.469778
F -2.193651 -1.457344 3.288697
C 0.280791 -0.229422 3.791637
F -0.556481 0.646044 4.340353
F 1.486562 0.331864 3.775563
F 0.326506 -1.276103 4.600102
Si 0.492679 2.084644 1.346970
C -0.265300 3.060438 2.753285
C -0.291861 2.572295 -0.268812
C 2.333319 2.412291 1.341549
H -1.275894 2.710276 2.969403
C -0.301715 4.554537 2.417645
H 0.321361 2.904655 3.662538
H -0.949209 4.760692 1.562582
H 0.689976 4.947886 2.179878
H -0.684320 5.130339 3.263943
C -1.811126 2.444736 -0.314763
H 0.166697 2.005207 -1.082045
H 0.009456 3.613191 -0.441285
H -2.126797 1.407936 -0.191140
H -2.209444 2.794819 -1.269903

H -2.287202 3.030426 0.475571
H 2.787750 1.923557 2.208259
H 2.389094 3.487739 1.558281
C 3.132831 2.119678 0.075895
H 3.251709 1.048350 -0.092168
H 4.136747 2.547087 0.141356
H 2.655590 2.541335 -0.812118
H 1.711674 -0.214318 -0.774573

Calculated energies and coordinates of 4 at PBE0-D4(CPCM=DCM)/def2-TZVP level of theory

Electronic energy ... -2103.92509554 Eh
Total Enthalpy ... -2103.60313079 Eh
Final Gibbs free energy ... -2103.68923676 Eh

CARTESIAN COORDINATES (ANGSTROEM)

O -2.560390 -0.458770 1.112834
O 0.647962 0.190914 -0.165216
C -1.672346 0.212335 0.295832
C -0.337001 -0.634404 0.267369
C -2.350036 0.413034 -1.110235
F -3.356866 1.287768 -0.978701
F -2.890610 -0.715778 -1.549394
F -1.530505 0.874562 -2.043661
C -1.404458 1.682165 0.841922
F -2.539242 2.121024 1.400099
F -1.081662 2.529044 -0.131753
F -0.462927 1.779139 1.765708
C -0.042929 -1.252232 1.703124
F 1.262161 -1.522015 1.785476
F -0.703774 -2.391102 1.894740
F -0.335661 -0.457347 2.720409
C -0.395732 -1.879078 -0.701662
F -1.483756 -2.625004 -0.555823
F 0.661085 -2.664522 -0.481657
F -0.323749 -1.486187 -1.968396
Si 2.319227 0.468045 -0.250706
C 2.939990 1.034089 1.426504
C 2.393450 1.843176 -1.511840
C 3.223068 -1.047817 -0.867634
H 2.088033 1.434617 1.984655
C 4.054746 2.079146 1.371523
H 3.278207 0.154180 1.983000
H 3.720607 2.994428 0.877770
H 4.928799 1.714913 0.825909
H 4.387974 2.350585 2.376657
C 1.942111 1.439713 -2.913162
H 3.424390 2.213851 -1.539777
H 1.787112 2.675159 -1.135591
H 1.975556 2.286457 -3.603796
H 0.919282 1.057499 -2.909239
H 2.581950 0.655487 -3.326263
H 2.720180 -1.416442 -1.767611
H 3.143388 -1.844121 -0.122361
C 4.694648 -0.761978 -1.172921
H 4.805104 0.012605 -1.936453
H 5.202291 -1.657549 -1.540181
H 5.233727 -0.424326 -0.284126
H -3.371183 0.049921 1.243635

Calculated energies and coordinates of 4 at PBE0-D4(CPCM=acetonitrile)/def2-TZVP level of theory

Electronic energy ... -2103.92589053 Eh
Total Enthalpy ... -2103.60407120 Eh
Final Gibbs free energy ... -2103.69020638 Eh

CARTESIAN COORDINATES (ANGSTROEM)

O -2.560156 -0.463934 1.111694
O 0.647741 0.193354 -0.162901
C -1.673303 0.212735 0.298573
C -0.337182 -0.633169 0.266436
C -2.349040 0.420726 -1.107500

F -3.353448 1.297625 -0.975730
 F -2.891512 -0.705491 -1.551655
 F -1.526410 0.883135 -2.038224
 C -1.406093 1.680069 0.851680
 F -2.540899 2.116876 1.410343
 F -1.081824 2.531157 -0.118335
 F -0.465050 1.772839 1.776476
 C -0.043064 -1.256557 1.700008
 F 1.262245 -1.523998 1.782753
 F -0.701690 -2.398222 1.885905
 F -0.339028 -0.467477 2.720882
 C -0.396065 -1.874658 -0.706890
 F -1.485031 -2.620620 -0.564994
 F 0.659651 -2.662029 -0.488615
 F -0.322828 -1.477971 -1.972337
 Si 2.319994 0.469097 -0.250574
 C 2.939561 1.039163 1.425514
 C 2.394175 1.840134 -1.515999
 C 3.223390 -1.048685 -0.863370
 H 2.086954 1.440046 1.982450
 C 4.053298 2.085269 1.368382
 H 3.278757 0.160581 1.983582
 H 3.718232 2.998819 0.872005
 H 4.927806 1.720299 0.824020
 H 4.385665 2.359525 2.373077
 C 1.944120 1.431514 -2.916292
 H 3.425332 2.210127 -1.544519
 H 1.787940 2.673583 -1.142843
 H 1.977804 2.275858 -3.609911
 H 0.921435 1.048736 -2.912041
 H 2.584799 0.646092 -3.325812
 H 2.720735 -1.419815 -1.762443
 H 3.144399 -1.842721 -0.115585
 C 4.694874 -0.762957 -1.169692
 H 4.804553 0.009278 -1.935700
 H 5.202695 -1.659623 -1.534145
 H 5.233723 -0.422120 -0.281983
 H -3.375034 0.038594 1.243322

 Calculated Energies and Coordinates of **5** at PBE0-
 D4(CPCM=DCM)/def2-TZVP level of theory

Electronic energy ... -4180.68961685 Eh
 Total Enthalpy ... -4180.36895133 Eh
 Final Gibbs free energy ... -4180.45874709 Eh

CARTESIAN COORDINATES (ANGSTROM)

Ge 1.250435 -0.269376 0.955904
 O -0.004367 1.072603 0.962854
 O 0.052254 -1.304277 0.031089
 C -1.050391 0.836954 0.104142
 C -1.219019 -0.779462 0.014031
 C -2.278435 1.635384 0.655360
 C -0.638624 1.476997 -1.272337
 C -1.960365 -1.379304 1.263426
 C -1.916866 -1.335062 -1.272224
 F -2.511637 1.356248 1.930709
 F -3.387347 1.387120 -0.036165
 F -2.052259 2.947503 0.591777
 F -1.628786 1.510956 -2.159396
 F 0.386896 0.810203 -1.808271
 F -0.213016 2.724662 -1.096536
 F -1.801695 -2.699199 1.305430
 F -3.268710 -1.129579 1.264553
 F -1.435812 -0.908240 2.393506
 F -2.084711 -2.654074 -1.185708
 F -1.182303 -1.120016 -2.356518
 F -3.115924 -0.794002 -1.466835
 Si 3.306104 0.156925 -0.249563
 C 3.345839 1.989893 -0.644177
 C 3.294853 -0.879333 -1.814596
 C 4.649436 -0.281254 0.985527
 H 2.561261 2.205110 -1.374600
 H 4.296803 2.157562 -1.166202
 C 3.232519 2.924664 0.556229

H 4.499483 0.354018 1.865919
 H 5.596109 0.049513 0.539980
 C 4.746891 -1.745757 1.401877
 H 4.313599 -0.812461 -2.217974
 H 2.655783 -0.357784 -2.534575
 C 2.867884 -2.340704 -1.698576
 H 3.311775 3.970379 0.248785
 H 4.019527 2.737619 1.290421
 H 2.271819 2.810168 1.065931
 H 5.502335 -1.883117 2.179544
 H 5.023201 -2.382855 0.559914
 H 3.799967 -2.122828 1.799993
 H 1.839653 -2.430272 -1.342101
 H 3.505765 -2.899342 -1.011620
 H 2.919797 -2.837959 -2.670539
 H 1.256443 -0.755094 2.419695

 Calculated energies and coordinates of **6** at PBE0-
 D4(CPCM=DCM)/def2-TZVP level of theory

Electronic energy ... -4180.66063500 Eh
 Total Enthalpy ... -4180.34073622 Eh
 Final Gibbs free energy ... -4180.43037547 Eh

CARTESIAN COORDINATES (ANGSTROM)

Ge 0.093836 2.665039 0.723946
 O -1.149136 1.310592 0.845998
 O 0.914745 -0.110126 0.058480
 C -1.423598 0.284039 -0.010243
 C -0.241077 -0.824563 0.134235
 C -2.873382 -0.154941 0.425558
 C -1.511500 0.826943 -1.486672
 C -0.278441 -1.533846 1.534979
 C -0.244358 -1.949578 -0.968190
 F -3.347972 -1.225439 -0.197875
 F -3.720903 0.848128 0.189611
 F -2.916888 -0.394866 1.731354
 F -2.185151 1.976958 -1.511809
 F -2.132455 -0.024253 -2.301112
 F -0.312835 1.085873 -2.000295
 F 0.884355 -2.145547 1.764290
 F -1.238475 -2.457013 1.595347
 F -0.447127 -0.676927 2.531926
 F 0.235942 -1.473029 -2.112566
 F -1.444659 -2.459217 -1.203160
 F 0.541007 -2.965234 -0.609687
 Si 2.610240 -0.166514 -0.068592
 C 3.280370 -1.840617 -0.555227
 C 3.235508 0.321003 1.624746
 C 2.968609 1.137090 -1.364621
 H 2.827818 -2.156610 -1.499209
 H 2.984571 -2.577966 0.195862
 C 4.804958 -1.826173 -0.698205
 H 2.171355 1.884940 -1.313188
 H 2.864410 0.659604 -2.346164
 C 4.326013 1.828035 -1.246078
 H 4.309340 0.519246 1.534004
 H 3.141920 -0.547219 2.285436
 C 2.535340 1.523336 2.243375
 H 5.182638 -2.827936 -0.917189
 H 5.297853 -1.483378 0.215101
 H 5.127564 -1.172679 -1.511744
 H 5.156220 1.120300 -1.296408
 H 4.415163 2.366502 -0.299308
 H 4.467478 2.554728 -2.050265
 H 2.946330 1.789184 3.220687
 H 1.472804 1.309877 2.419467
 H 2.633718 2.414851 1.611989
 H -0.262165 3.065610 2.231063

 Calculated energies and coordinates of **INT1** at PBE0-
 D4(CPCM=DCM)/def2-TZVP level of theory

Electronic energy ... -7655.09020443 Eh

Total Enthalpy ... -7654.71296486 Eh
Final Gibbs free energy ... -7654.83708072 Eh

CARTESIAN COORDINATES (ANGSTROEM)

O 1.587694 -0.731176 -1.302240
O 2.553278 1.257381 -0.104446
C 2.711852 -1.082982 -0.594523
C 3.515059 0.299550 -0.309282
C 2.204068 -1.773814 0.720084
F 1.619421 -0.888265 1.531094
F 3.181626 -2.378242 1.393612
F 1.276511 -2.683884 0.445220
C 3.478644 -2.164590 -1.428778
F 2.803796 -3.314272 -1.452167
F 4.684769 -2.425901 -0.930631
F 3.623499 -1.784549 -2.692347
C 4.476138 0.324416 0.923943
F 5.112513 1.493367 1.000486
F 5.401611 -0.629406 0.858091
F 3.815510 0.185128 2.065780
C 4.327301 0.790068 -1.565049
F 4.729032 2.046999 -1.402508
F 3.533172 0.798018 -2.643210
F 5.399356 0.054726 -1.836401
Ge 1.045510 1.047539 -1.183120
Ge -0.908522 0.666631 0.920318
O -2.630242 0.985017 0.323847
O -1.551639 -0.918575 1.593355
C -3.371649 -0.165625 0.196187
C -2.895842 -1.147959 1.407803
C -4.881201 0.252583 0.179812
C -3.013318 -0.737810 -1.225206
C -3.574404 -0.801165 2.778877
C -3.063516 -2.685418 1.158592
F -5.689114 -0.803094 0.159395
F -5.156263 0.987977 -0.896758
F -5.196158 0.998390 1.230992
F -3.745875 -1.785986 -1.577921
F -1.720128 -1.086488 -1.260829
F -3.161673 0.195515 -2.158197
F -2.943813 -1.408287 3.779398
F -4.854797 -1.160542 2.827995
F -3.489000 0.505306 3.027863
F -4.305351 -3.002732 0.804273
F -2.772798 -3.379347 2.258092
F -2.235073 -3.113831 0.215025
C -0.769169 2.113534 2.707297
C -1.320508 3.164392 2.005018
H 0.307949 1.973603 2.733814
H -1.327462 1.667275 3.522485
C -0.560414 3.803912 0.936895
C -2.741257 3.541152 2.213830
H -3.119421 3.146369 3.154296
H -3.359728 3.138786 1.404312
H -2.853319 4.626840 2.199929
C -1.232744 4.364231 -0.158013
C -0.526392 4.844088 -1.245259
C 0.861883 4.801077 -1.248300
C 1.544229 4.282295 -0.153963
C 0.841749 3.779652 0.924626
H -2.314771 4.390469 -0.173817
H -1.059833 5.250495 -2.096071
H 1.414626 5.181655 -2.099343
H 2.626904 4.262350 -0.145270
H 1.389166 3.388710 1.772748

Calculated energies and coordinates of INT1' at PBE0-D4(CPCM=DCM)/def2-TZVP level of theory

Electronic energy ... -4001.88343534 Eh
Total Enthalpy ... -4001.60950462 Eh
Final Gibbs free energy ... -4001.69322602 Eh

CARTESIAN COORDINATES (ANGSTROEM)

Ge -0.353138 -2.112188 0.243427

O 1.068321 -1.536388 -0.804147
O -0.433026 -0.345211 0.818608
C 1.418539 -0.210968 -0.705165
C 0.749520 0.334717 0.675295
C 2.979487 -0.132427 -0.791674
F 3.554571 -0.941019 0.089995
F 3.436348 1.101752 -0.588921
F 3.408971 -0.521582 -1.992115
C 0.837042 0.481552 -1.987072
F 1.266197 1.733677 -2.144014
F -0.493214 0.491146 -1.957818
F 1.176046 -0.199532 -3.079158
C 1.594781 -0.033910 1.950323
F 0.892044 0.187297 3.056519
F 2.733319 0.642018 2.054771
F 1.871925 -1.344688 1.951177
C 0.440010 1.867372 0.742516
F 1.533125 2.600923 0.536209
F -0.043577 2.199852 1.939653
F -0.475477 2.230812 -0.143836
C -2.376485 -1.987688 -1.374523
C -3.181155 -1.574517 -0.364674
H -1.977906 -1.298875 -2.108151
H -2.267111 -3.047606 -1.578788
C -3.704699 -2.569019 0.616297
C -3.493630 -0.156817 -0.150257
H -3.196776 -2.457927 1.582885
H -3.541143 -3.588000 0.267948
H -4.769127 -2.413480 0.803669
C -3.754323 0.323793 1.135818
C -4.012808 1.667163 1.349797
C -4.038923 2.550978 0.280148
C -3.805158 2.082022 -1.006706
C -3.532923 0.742281 -1.218765
H -3.369720 0.384383 -2.228222
H -3.730345 -0.351843 1.981762
H -4.195220 2.025280 2.356525
H -4.247175 3.601643 0.447311
H -3.838006 2.764142 -1.847820

Calculated energies and coordinates of TS1 at PBE0-D4(CPCM=DCM)/def2-TZVP level of theory

Electronic energy ... -8182.56427396 Eh
Total Enthalpy ... -8181.96958506 Eh
Final Gibbs free energy ... -8182.11783335 Eh

CARTESIAN COORDINATES (ANGSTROEM)

O 1.820067 -2.804771 -2.743941
O 2.325025 -0.580658 -1.662804
C 2.830037 -2.917169 -1.828886
C 3.405945 -1.411367 -1.593728
C 2.194913 -3.536662 -0.534566
F 1.378481 -2.662310 0.067959
F 3.099601 -3.932054 0.360912
F 1.442545 -4.586847 -0.839467
C 3.855017 -3.966508 -2.378276
F 3.323201 -5.190509 -2.390490
F 4.964157 -4.027799 -1.642618
F 4.204067 -3.696842 -3.629696
C 4.129966 -1.132235 -0.232391
F 4.602145 0.115413 -0.195915
F 5.160668 -1.948328 -0.024550
F 3.303748 -1.242434 0.802614
C 4.381366 -0.956076 -2.742996
F 4.593726 0.357148 -2.683473
F 3.827197 -1.180230 -3.937645
F 5.570769 -1.552963 -2.709993
Ge 1.039969 -1.100548 -2.964978
Ge -0.818254 -1.330274 -1.039221
O -2.609415 -0.971271 -1.369285
O -1.364314 -3.031409 -0.577138
C -3.353274 -2.105164 -1.575574

C	-2.717243	-3.250259	-0.603781
C	-4.852714	-1.731894	-1.321221
C	-3.204390	-2.446814	-3.102832
C	-3.198213	-3.125724	0.886003
C	-2.933625	-4.737308	-1.048586
F	-5.649696	-2.795309	-1.363123
F	-5.292485	-0.868808	-2.237190
F	-5.014352	-1.138876	-0.144440
F	-4.019239	-3.414344	-3.511182
F	-1.946266	-2.802073	-3.380317
F	-3.452053	-1.371566	-3.844855
F	-2.436223	-3.868296	1.684884
F	-4.462422	-3.506380	1.064236
F	-3.069871	-1.872184	1.319676
F	-4.220161	-5.025589	-1.233939
F	-2.466076	-5.580888	-0.128419
F	-2.279607	-5.009877	-2.170156
C	-0.448886	-0.255207	0.699135
C	-1.147052	0.983686	0.506776
H	0.633717	-0.196418	0.591548
H	-0.743820	-0.827367	1.574617
C	-0.800211	1.763813	-0.690598
C	-2.511491	1.127086	1.087285
H	-2.559930	0.669011	2.073381
H	-3.214625	0.600708	0.434394
H	-2.817685	2.169859	1.148690
C	-1.803081	2.385551	-1.437304
C	-1.498473	2.992406	-2.644280
C	-0.191612	3.005926	-3.109321
C	0.818604	2.413241	-2.360593
C	0.516366	1.796450	-1.161836
II	-2.830068	2.363197	-1.097694
H	-2.288370	3.450882	-3.227044
H	0.042894	3.482117	-4.054229
H	1.844026	2.433679	-2.710014
H	1.315703	1.354665	-0.582122
Si	0.338052	2.718900	2.713214
C	1.078793	1.335633	3.731889
C	-0.981960	3.738974	3.562237
C	1.613427	3.745009	1.810726
C	1.030098	4.831243	0.910853
C	2.034646	1.793903	4.834125
C	-0.444806	4.785494	4.539718
H	2.440160	0.939179	5.381307
II	1.535525	2.440117	5.559168
H	2.879396	2.352021	4.423845
H	1.599286	0.662337	3.041411
H	0.253369	0.755080	4.158134
H	-1.259411	5.376505	4.966009
H	0.240684	5.479526	4.046890
H	0.095720	4.325050	5.369597
H	-1.667000	3.051481	4.070153
H	-1.569961	4.227906	2.777296
H	2.243034	3.058744	1.233406
H	2.272776	4.189180	2.566587
II	0.382693	4.408092	0.139187
H	1.819656	5.392873	0.405230
H	0.432883	5.545945	1.482272
H	-0.428088	1.964330	1.597335

Calculated energies and coordinates of INT2 at PBE0-D4(CPCM=DCM)/def2-TZVP level of theory			
Electronic energy	...	-8182.57273282 Eh	
Total Enthalpy	...	-8181.97493985 Eh	
Final Gibbs free energy	...	-8182.12421382 Eh	
CARTESIAN COORDINATES (ANGSTROEM)			
O	1.840294	-2.913531	-2.533007
O	2.375046	-0.702835	-1.416829
C	2.824361	-3.049373	-1.598424
C	3.433789	-1.555722	-1.346544
C	2.148247	-3.649482	-0.316725
F	1.346502	-2.757510	0.276009
F	3.028170	-4.078318	0.591553
F	1.370239	-4.678557	-0.636901
C	3.835349	-4.120859	-2.128169
F	3.280646	-5.335950	-2.146033
F	4.934507	-4.205027	-1.378290
F	4.208739	-3.862079	-3.375831
C	4.151219	-1.300945	0.022560
F	4.632210	-0.055356	0.079461
F	5.176737	-2.124896	0.230834
F	3.319302	-1.417657	1.052662
C	4.434076	-1.118676	-2.483194
F	4.672344	0.191607	-2.415315
F	3.900362	-1.327813	-3.688262
F	5.614353	-1.736602	-2.434880
Ge	1.080323	-1.182479	-2.749550
Ge	-0.820219	-1.286533	-0.907366
O	-2.537328	-0.850733	-1.497801
O	-1.540981	-2.940286	-0.437808
C	-3.322905	-1.949152	-1.722282
C	-2.896718	-3.049865	-0.598465
C	-4.812165	-1.461622	-1.702145
C	-3.009681	-2.439442	-3.185762
C	-3.538042	-2.752742	0.803837
C	-3.199315	-4.548111	-0.939136
F	-5.682169	-2.466683	-1.760837
F	-5.061523	-0.665514	-2.743941
F	-5.082590	-0.748215	-0.614492
F	-3.858500	-3.369316	-3.621263
F	-1.768922	-2.926102	-3.271402
F	-3.058638	-1.422003	-4.041025
F	-2.919061	-3.446474	1.756712
F	-4.835563	-3.058455	0.860926
F	-3.397452	-1.471507	1.136833
F	-4.477642	-4.754373	-1.251798
F	-2.917017	-5.333185	0.102515
F	-2.453307	-4.981220	-1.946729
C	-0.565117	-0.240933	0.779552
C	-1.036309	1.189379	0.652668
H	0.520344	-0.284190	0.896344
H	-1.021110	-0.744376	1.631966
C	-0.662422	1.818744	-0.664267
C	-2.461439	1.415770	1.096461
II	-2.615478	1.006769	2.095071
H	-3.139407	0.901878	0.413907
H	-2.713818	2.476991	1.104394
C	-1.623968	2.366796	-1.507050
C	-1.262837	2.880198	-2.744962
C	0.061569	2.860546	-3.152694
C	1.029237	2.319158	-2.316467
C	0.667918	1.803516	-1.082594
H	-2.665083	2.381183	-1.213027
H	-2.026185	3.294662	-3.393344
H	0.340409	3.261207	-4.120333
H	2.068047	2.293158	-2.624320
H	1.432751	1.372801	-0.447315
Si	0.548698	2.784006	2.618696
C	1.894873	1.539617	2.873491
C	-0.760952	2.973870	3.911808
C	0.906797	4.245598	1.548459
C	-0.302141	5.094792	1.165118
C	2.900047	1.986725	3.946111
C	-0.353913	4.005798	4.975659
H	3.694080	1.242990	4.036620
II	2.427185	2.089302	4.924675
H	3.366239	2.941363	3.693488
H	2.402790	1.380158	1.917739
II	1.434565	0.588069	3.157621
H	-1.155425	4.115294	5.708690
H	-0.170210	4.987964	4.534573
H	0.547753	3.704237	5.512082
H	-0.952564	1.997410	4.365309
H	-1.685910	3.288748	3.418774
H	1.452399	3.895611	0.666759
H	1.632797	4.836267	2.127664
II	-1.011165	4.525793	0.560568
H	0.012373	5.961508	0.581006

11. Appendix – Dissertation Florian Tschernuth

H -0.832100 5.461584 2.046465
H -0.392692 1.776375 1.440934

Calculated energies and coordinates of Compound INT3 at PBE0-D4(CPCM=DCM)/def2-TZVP level of theory

Electronic energy ... -4529.42479979 Eh
Total Enthalpy ... -4528.92716084 Eh
Final Gibbs free energy ... -4529.03327144 Eh

CARTESIAN COORDINATES (ANGSTROEM)

II 3.280049 -0.788382 -2.281279
Ge 0.709949 -0.016175 -0.544009
O -0.276614 -0.835179 0.788039
O -0.897130 0.599280 -1.217935
C -1.594550 -0.458777 0.840390
C -2.011060 0.020723 -0.668707
C -2.400743 -1.670189 1.420129
C -1.674968 0.703546 1.893088
C -2.391896 -1.179233 -1.610273
C -3.164326 1.077357 -0.769488
F -3.712246 -1.436959 1.421318
F -2.041122 -1.925038 2.677962
F -2.175606 -2.785891 0.739568
F -2.919799 1.089577 2.164428
F -0.986931 1.759930 1.463844
F -1.112712 0.341128 3.043265
F -2.426934 -0.780922 -2.879084
F -3.578298 -1.715112 -1.326102
F -1.468847 -2.136692 -1.554807
F -3.475545 1.314254 -2.044347
F -2.803451 2.246129 -0.253282
F -4.277803 0.675372 -0.160822
C 1.378172 -1.511412 -1.620992
C 2.895811 -1.629544 -1.695122
H 0.962115 -1.394921 -2.625438
H 0.935651 -2.416738 -1.199578
C 3.574506 -1.573222 -0.347679
C 3.289106 -2.910173 -2.434026
II 2.846021 -2.928098 -3.432659
H 2.936916 -3.788403 -1.886029
II 4.374017 -2.984198 -2.537021
C 2.932476 -1.955815 0.827269
C 3.593632 -1.911066 2.049373
C 4.911348 -1.488948 2.115225
C 5.566218 -1.111230 0.948358
C 4.901911 -1.152460 -0.266127
H 1.908517 -2.312773 0.802664
H 3.071017 -2.208655 2.951483
H 5.426609 -1.448688 3.068046
H 6.596022 -0.773696 0.988080
H 5.416919 -0.847409 -1.172092
Si 2.080603 1.947441 -0.126084
C 0.970760 3.465866 -0.116936
C 3.224556 2.011490 -1.615287
C 3.036466 1.746984 1.470923
H 0.445258 3.504703 0.839626
H 0.199322 3.360759 -0.885584
C 1.760247 4.757666 -0.327787
H 3.614577 2.672168 1.592683
II 3.770837 0.948553 1.330729
C 2.193610 1.482116 2.713111
H 3.922226 1.171256 -1.567402
H 3.837163 2.912526 -1.489209
C 2.505967 2.053148 -2.960997
II 2.230326 4.788615 -1.313391
H 2.552424 4.874206 0.417143
H 1.107295 5.630920 -0.248931
H 2.820658 1.404230 3.605162
H 1.636954 0.546595 2.622747
H 1.467796 2.279821 2.888491
H 3.213113 2.131945 -3.790557
H 1.825072 2.905638 -3.026001
II 1.909725 1.151760 -3.135072

Calculated Energies and Coordinates TS2 at PBE0-D4(CPCM=DCM)/def2-TZVP level of theory

Electronic energy ... -8182.56381263 Eh
Total Enthalpy ... -8181.96541925 Eh
Final Gibbs free energy ... -8182.11285675 Eh

CARTESIAN COORDINATES (ANGSTROEM)

O -3.304682 -1.936539 1.401643
O -2.952351 -1.726895 -1.101508
C -3.524921 -3.125126 0.774640
C -2.793978 -3.016224 -0.683013
C -3.017225 -4.259238 1.727124
F -1.770991 -4.041196 2.131152
F -3.061317 -5.464686 1.159130
F -3.762012 -4.320188 2.832883
C -5.085538 -3.282689 0.647798
F -5.469186 -4.487266 0.223376
F -5.589413 -2.365298 -0.181899
F -5.673873 -3.068950 1.822717
C -1.249694 -3.283344 -0.596151
F -0.638396 -2.894670 -1.714722
F -0.941314 -4.566360 -0.403619
F -0.690013 -2.572454 0.386497
C -3.356613 -3.943673 -1.812925
F -2.608066 -3.854575 -2.916896
F -4.585388 -3.590493 -2.170565
F -3.382159 -5.229132 -1.463019
Ge -3.368196 -0.431312 0.237727
Ge -0.890351 0.275306 0.819401
O -0.750419 1.851698 1.809490
O -0.205951 -0.570226 2.336035
C -0.715891 1.640737 3.158991
C 0.114012 0.252291 3.380868
C -0.112041 2.928491 3.813221
C -2.211461 1.533708 3.636647
C 1.670114 0.460374 3.318290
C -0.194264 -0.532728 4.701844
F 1.040027 3.274909 3.251317
F 0.093030 2.785978 5.121204
F -0.932520 3.968667 3.653262
F -2.348670 1.530042 4.960945
F -2.783733 0.427220 3.153632
F -2.926969 2.549402 3.160821
F 2.290620 -0.709741 3.177564
F 2.165389 1.047710 4.408667
F 2.022953 1.187856 2.258741
F 0.631127 -1.573007 4.837885
F -1.424301 -1.029917 4.700422
F -0.053976 0.223126 5.790223
C 0.637525 0.424256 -0.453471
C 0.238693 1.132266 -1.756622
H 0.969282 -0.600673 -0.631205
II 1.405871 0.972648 0.090537
C -0.547632 2.384743 -1.431642
C -0.450398 0.193493 -2.729060
H 0.209297 -0.633627 -2.998816
II -0.743300 0.715833 -3.641413
H -1.340609 -0.258823 -2.288051
C 0.105935 3.500291 -0.913409
C -0.605628 4.617222 -0.510574
C -1.991282 4.635159 -0.611400
C -2.651870 3.535100 -1.133233
C -1.934148 2.420524 -1.549871
II 1.185932 3.489900 -0.811428
H -0.078333 5.475120 -0.108942
H -2.550648 5.505511 -0.288247
H -3.732153 3.538184 -1.224486
H -2.471268 1.582753 -1.979269
H 1.151301 1.519632 -2.269712
Si 3.093793 0.477255 -2.155347
C 2.889180 0.799925 -3.964291
C 3.274414 -1.287035 -1.659956
C 3.849173 1.786463 -1.107747

```

C 4.022102 0.169909 -4.788754
C 3.576262 -1.585071 -0.196946
C 5.352380 1.803576 -1.450562
H 3.883324 0.419345 -5.842326
H 4.023677 -0.917728 -4.701229
H 5.005565 0.536628 -4.488553
H 2.847315 1.883228 -4.111850
H 1.927234 0.392963 -4.289397
H 4.110856 -1.613774 -2.299968
H 2.409238 -1.846371 -2.033450
H 4.455844 -1.039591 0.150022
H 3.772022 -2.650680 -0.066162
H 2.741553 -1.319877 0.452589
H 5.856073 2.535441 -0.816458
H 5.529929 2.087458 -2.489769
H 5.826086 0.834574 -1.273466
H 3.699981 1.566787 -0.049140
H 3.396034 2.755474 -1.326766

```

Calculated energies and coordinates of **TS3** at PBE0-D4(CPCM=DCM)/def2-TZVP level of theory

```

Electronic energy ... -4529.33050459 Eh
Total Enthalpy ... -4528.83632640 Eh
Final Gibbs free energy ... -4528.94268493 Eh

```

CARTESIAN COORDINATES (ANGSTROEM)

```

Ge 1.387864 -1.270136 1.313157
O 2.715831 -1.552813 -0.063594
O 2.107709 0.517446 1.272523
C 3.536154 -0.511461 -0.360869
C 3.399626 0.568875 0.868225
C 4.971447 -1.090070 -0.610439
F 5.373129 -1.866823 0.390047
F 5.895793 -0.143260 -0.786666
F 4.994539 -1.859267 -1.705098
C 3.048274 0.082250 -1.731142
F 3.900796 0.965506 -2.264015
F 1.862392 0.678151 -1.620056
F 2.882085 -0.888901 -2.631226
C 4.294956 0.184710 2.107345
F 3.928325 0.887405 3.180643
F 5.599191 0.407834 1.917433
F 4.141071 -1.095490 2.446237
C 3.725837 2.061793 0.523624
F 4.934966 2.220780 -0.016887
F 3.688719 2.824497 1.621537
F 2.835910 2.586130 -0.313542
C -0.249056 -0.856667 0.109761
C -1.444225 -0.447167 0.972056
H 0.058440 -0.065001 -0.566267
H -0.435816 -1.781063 -0.448489
C -1.970857 -1.591269 1.819585
C -1.124876 0.819839 1.734713
H -1.195183 -1.948101 2.499819
H -2.255056 -2.433199 1.188124
H -2.838305 -1.287641 2.407761
C -0.966838 0.823076 3.116087
C -0.590872 1.984070 3.780684
C -0.382993 3.158485 3.075710
C -0.554269 3.168024 1.696877
C -0.918478 2.007796 1.036744
H -1.025366 2.027669 -0.043115
H -1.125173 -0.083288 3.686770
H -0.461672 1.964958 4.856997
H -0.089859 4.063464 3.595456
H -0.395698 4.080961 1.134134
H -2.350891 -0.124894 0.369224
Si -2.550530 -0.402103 -1.530964
C -1.327955 0.092787 -2.826783
C -3.782762 0.955186 -1.234430
C -3.267076 -2.101921 -1.439382
C -0.419021 -0.956896 -3.448626
C -4.750171 0.802044 -0.068506
C -2.419999 -3.352302 -1.634362

```

```

H 0.242685 -0.491638 -4.181454
H -0.996780 -1.725325 -3.964185
H 0.207898 -1.445468 -2.702960
H -0.762457 0.946394 -2.439386
H -1.995622 0.524752 -3.590298
H -4.330366 0.984791 -2.189670
H -3.240019 1.904372 -1.183179
H -5.307625 -0.134893 -0.124570
H -5.473508 1.619682 -0.063954
H -4.228236 0.824312 0.891414
H -4.009224 -2.022267 -2.253792
H -3.867563 -2.161272 -0.526464
H -1.842057 -3.313816 -2.557344
H -3.065222 -4.231816 -1.680993
H -1.721959 -3.501808 -0.809979

```

Calculated energies and coordinates of **TS4** at PBE0-D4(CPCM=DCM)/def2-TZVP level of theory

```

Electronic energy ... -4529.34815297 Eh
Total Enthalpy ... -4528.85730789 Eh
Final Gibbs free energy ... -4528.96362146 Eh

```

CARTESIAN COORDINATES (ANGSTROEM)

```

H 2.511085 0.285203 -0.728478
Ge 0.208824 0.210682 -1.189824
O -0.485539 -0.257040 0.495169
O -1.540584 -0.108511 -1.802187
C -1.848238 -0.185632 0.583362
C -2.429267 -0.597468 -0.883739
C -2.283752 -1.087524 1.785082
C -2.182236 1.303999 0.963703
C -2.475720 -2.151797 -1.108087
C -3.844210 -0.031462 -1.247562
F -3.607316 -1.170226 1.904089
F -1.812069 -0.603642 2.935551
F -1.801168 -2.319826 1.676710
F -3.465174 1.507382 1.257655
F -1.842355 2.128335 -0.029720
F -1.466379 1.688157 2.017953
F -2.638958 -2.432617 -2.399427
F -3.463474 -2.751402 -0.440386
F -1.324638 -2.721656 -0.755418
F -4.282687 -0.548702 -2.397133
F -3.812305 1.285035 -1.420586
F -4.761311 -0.305012 -0.321028
C 1.392231 -1.500908 -1.559417
C 2.721957 -1.174395 -1.137178
H 1.277425 -1.641464 -2.632436
H 0.882962 -2.258874 -0.975347
C 3.205701 -1.663611 0.173384
C 3.723632 -0.934498 -2.229174
H 3.247830 -0.429518 -3.070370
H 4.091647 -1.901582 -2.588650
H 4.581701 -0.346874 -1.904681
C 2.314938 -1.896656 1.226317
C 2.772525 -2.331385 2.456916
C 4.128714 -2.556180 2.662463
C 5.020604 -2.337859 1.623726
C 4.565142 -1.889950 0.392878
H 1.255072 -1.716196 1.094809
H 2.065608 -2.493790 3.262707
H 4.485721 -2.898489 3.627020
H 6.080468 -2.512265 1.770254
H 5.280246 -1.722283 -0.401983
Si 2.701698 1.909124 -0.602182
C 1.461756 2.957289 0.341642
C 3.050590 2.568028 -2.322192
C 4.303674 1.829404 0.383844
H 1.112951 2.401315 1.217539
H 0.585246 3.096518 -0.297185
C 2.031339 4.313143 0.757427
H 4.762175 2.822837 0.293264
H 4.994693 1.137371 -0.107708
C 4.136453 1.456913 1.854228

```

```

H 3.909796 2.024478 -2.727538
H 3.409438 3.591242 -2.144010
C 1.905551 2.590006 -3.325977
H 2.369083 4.888338 -0.108830
H 2.882603 4.208599 1.433734
H 1.274657 4.911142 1.272221
H 5.096149 1.469359 2.377840
H 3.713538 0.456957 1.968823
H 3.472808 2.153408 2.372460
H 2.191906 3.119436 -4.238982
H 1.020909 3.086799 -2.919344
H 1.607689 1.578498 -3.613006

```

Calculated energies and coordinates of **TS5** at PBE0-D4(CPCM=DCM)/def2-TZVP level of theory

```

Electronic energy ... -4529.33432713 Eh
Total Enthalpy ... -4528.83959212 Eh
Final Gibbs free energy ... -4528.94643774 Eh

```

CARTESIAN COORDINATES (ANGSTROEM)

```

H 3.885854 -0.297343 -0.828542
Ge 0.874910 0.641874 0.422674
O 0.077399 -0.890503 1.151901
O -0.840094 0.968708 -0.300883
C -1.265046 -0.725725 1.357280
C -1.823360 0.092791 0.056931
C -1.870435 -2.149170 1.608194
C -1.429907 0.090456 2.696315
C -2.072266 -0.835980 -1.186090
C -3.134726 0.927035 0.272675
F -3.201148 -2.126946 1.665148
F -1.433216 -2.652978 2.764057
F -1.514390 -3.016233 0.669392
F -2.689411 0.156722 3.124468
F -0.971791 1.337082 2.557420
F -0.704959 -0.455610 3.669881
F -2.169962 -0.106163 -2.296268
F -3.188483 -1.561302 -1.081007
F -1.057514 -1.673170 -1.391386
F -3.586256 1.408266 -0.888874
F -2.917248 1.980558 1.051506
F -4.125294 0.214968 0.807812
C 1.768047 -0.300568 -1.293365
C 3.093703 -1.025996 -1.034767
H 1.727900 0.168562 -2.279034
H 0.960736 -1.036807 -1.326221
C 2.971838 -1.871302 0.212924
C 3.525558 -1.821482 -2.262011
H 3.682340 -1.149788 -3.109422
H 2.760787 -2.544344 -2.554654
H 4.456599 -2.362674 -2.074274
C 2.355212 -3.120057 0.188447
C 2.197355 -3.857249 1.350937
C 2.647777 -3.356011 2.565819
C 3.263945 -2.114942 2.604609
C 3.426975 -1.383393 1.434855
H 1.985530 -3.521918 -0.748277
H 1.715802 -4.828142 1.310151
H 2.520858 -3.932666 3.475018
H 3.626234 -1.714374 3.544874
H 3.927015 -0.420940 1.473589
Si 2.506809 2.127985 -0.897191
C 1.111886 3.365918 -1.078539
C 3.446015 1.991526 -2.511912
C 3.774284 2.435001 0.437571
H 0.588907 3.485068 -0.128361
H 0.381310 2.986985 -1.798549
C 1.684859 4.711136 -1.541141
H 4.312793 3.296108 0.011957
H 4.499765 1.615391 0.422533
C 3.312913 2.750053 1.848894
H 4.170826 1.175074 -2.462789
H 4.051047 2.909636 -2.464645
C 2.671458 1.963532 -3.822673

```

```

H 2.168301 4.642261 -2.517336
H 2.416718 5.103847 -0.831063
H 0.879620 5.445088 -1.623233
H 4.153487 3.088085 2.460207
H 2.876349 1.871712 2.327528
H 2.553831 3.535775 1.857508
H 3.347887 2.099164 -4.669884
H 1.919545 2.753907 -3.871335
H 2.155886 1.013206 -3.976341

```

Calculated energies and coordinates of **TS6** at PBE0-D4(CPCM=DCM)/def2-TZVP level of theory

```

Electronic energy ... -4180.62860727 Eh
Total Enthalpy ... -4180.31071973 Eh
Final Gibbs free energy ... -4180.39985862 Eh

```

CARTESIAN COORDINATES (ANGSTROEM)

```

Ge -0.122363 0.655842 -0.399763
O -1.451412 0.880317 0.871655
O -1.253337 -0.511568 -1.268521
C -2.678390 0.466954 0.412201
C -2.400758 -0.802205 -0.570017
C -3.575869 0.194918 1.667455
C -3.293082 1.696341 -0.356160
C -2.125572 -2.129781 0.226382
C -3.497326 -1.107888 -1.645813
F -3.009230 -0.657118 2.510953
F -4.769499 -0.287892 1.329884
F -3.780227 1.319333 2.352869
F -4.562265 1.517273 -0.712734
F -2.576444 1.969115 -1.450464
F -3.238737 2.790162 0.397898
F -1.578471 -3.043389 -0.572050
F -3.235878 -2.661210 0.738935
F -1.257639 -1.933829 1.214863
F -3.199312 -2.224234 -2.312094
F -3.572530 -0.139871 -2.550893
F -4.704660 -1.273567 -1.113406
Si 2.366104 0.456902 -0.238710
C 2.965073 1.987297 -1.132346
C 2.739180 -1.056869 -1.263117
C 2.865584 0.532424 1.555224
H 2.599345 1.937268 -2.162545
H 4.057517 1.863120 -1.182696
C 2.609809 3.318143 -0.486850
H 2.273982 1.321957 2.032744
H 3.893096 0.921137 1.524258
C 2.799294 -0.758492 2.358543
H 3.828680 -1.153216 -1.137821
H 2.592572 -0.778780 -2.311828
C 2.049338 -2.375706 -0.947488
H 2.996496 4.155869 -1.071889
H 3.022019 3.400344 0.521490
H 1.524811 3.440307 -0.413768
H 3.122290 -0.590426 3.388624
H 3.442421 -1.530555 1.930507
H 1.781425 -1.154567 2.390184
H 0.979412 -2.321315 -1.156439
H 2.167068 -2.656826 0.100192
H 2.464229 -3.180727 -1.559086
H 0.743254 -0.494990 0.491639

```

Calculated energies and coordinates of Compound **TS7** at PBE0-D4(CPCM=DCM)/def2-TZVP level of theory

```

Electronic energy ... -4180.62859703 Eh
Total Enthalpy ... -4180.31011627 Eh
Final Gibbs free energy ... -4180.39745030 Eh

```

CARTESIAN COORDINATES (ANGSTROEM)

```

Ge 0.564790 1.816858 -0.702186
O -1.052986 1.443030 0.160461
O 0.693344 -0.201719 -0.718255

```

C	-1.627616	0.265784	-0.218156
C	-0.424390	-0.841220	-0.211522
C	-2.841215	0.023201	0.752423
C	-2.225224	0.480117	-1.660086
C	-0.131448	-1.292348	1.260820
C	-0.661205	-2.125355	-1.079289
F	-3.392994	-1.177338	0.607041
F	-3.798817	0.923925	0.526354
F	-2.484659	0.171575	2.022066
F	-2.933378	1.602803	-1.711141
F	-3.009381	-0.515350	-2.061170
F	-1.240985	0.629071	-2.555128
F	0.986955	-2.014616	1.333110
F	-1.107289	-2.039622	1.767025
F	0.060662	-0.237832	2.046975
F	-0.631196	-1.840688	-2.374642
F	-1.823395	-2.712085	-0.808683
F	0.294402	-3.031061	-0.868040
Si	2.769894	0.104701	0.022883
C	3.187087	-1.577825	-0.705700
C	3.384190	0.135249	1.798992
C	3.529807	1.325607	-1.189219
H	2.949866	-1.534103	-1.773771
H	2.573301	-2.369783	-0.283519
C	4.666499	-1.917765	-0.504681
H	2.910867	1.386627	-2.094250
H	4.435665	0.806450	-1.525707
C	3.875896	2.712348	-0.671301
H	4.472483	0.038963	1.677521
II	3.060874	-0.799039	2.267645
C	3.055079	1.327396	2.682252
II	4.924901	-2.835804	-1.039013
H	4.900777	-2.077931	0.549977
H	5.332425	-1.132769	-0.873597
H	4.592312	2.661777	0.151311
H	2.995212	3.246585	-0.301181
H	4.316507	3.326276	-1.460347
H	3.531872	1.228784	3.660983
H	1.978790	1.415249	2.844276
H	3.396155	2.265428	2.240318
H	1.645551	1.434656	0.567801

F	-0.018462	-0.547046	-4.996035
C	-0.024080	-2.316203	2.211892
C	-1.336794	-1.368343	2.367264
C	-0.125935	-3.745254	2.849795
F	-1.021559	-4.495322	2.228909
F	-0.445799	-3.672212	4.136271
F	1.036597	-4.380842	2.755690
C	1.294757	-1.642721	2.738615
F	1.326444	-1.551276	4.061114
F	1.416959	-0.425161	2.212488
F	2.360282	-2.325379	2.345478
C	-2.686968	-2.164123	2.206038
F	-2.634064	-2.920917	1.109659
F	-3.702097	-1.330245	2.033719
F	-2.956468	-2.931974	3.252465
C	-1.431495	-0.503302	3.670139
F	-2.583674	0.158449	3.698454
F	-0.467853	0.401840	3.726653
F	-1.369677	-1.261409	4.757475
Si	1.227036	2.219833	0.337895
C	1.009431	2.879192	2.080832
C	0.533085	3.414844	-0.928685
C	3.025881	1.799177	0.018874
H	-0.060668	2.936896	2.304568
C	1.668889	4.243458	2.283469
H	1.427666	2.151454	2.782293
H	1.250907	4.997710	1.611542
II	2.745093	4.201505	2.096455
H	1.529672	4.603659	3.306233
C	-0.859254	3.942502	-0.591386
H	0.533351	2.927764	-1.907696
II	1.243097	4.247251	-1.008964
H	-1.579838	3.130474	-0.467877
H	-1.238959	4.600469	-1.377600
H	-0.853564	4.514172	0.339847
H	3.339558	1.071010	0.774943
H	3.589018	2.715141	0.238829
C	3.373469	1.299071	-1.378800
H	2.886813	0.346501	-1.591954
H	4.450952	1.150693	-1.490793
H	3.059170	2.007232	-2.149742
H	0.405589	0.942889	0.234055

 Calculated Energies and Coordinates TS(1_INT_A_Ge) at PBE0-D4(CPCM=DCM)/def2-TZVP level of theory

Electronic energy ... -5757.08372525 Eh
 Total Enthalpy ... -5756.66273811 Eh
 Final Gibbs free energy ... -5756.78633436 Eh

CARTESIAN COORDINATES (ANGSTROEM)

Ge -0.535373 -1.190453 -0.126389
 O -1.822951 -1.727008 -1.232043
 O 0.512519 -0.756597 -1.495006
 O 0.180943 -2.490850 0.847071
 O -1.311169 -0.466543 1.302332
 C -1.596541 -1.322465 -2.537857
 C 0.009079 -1.238211 -2.706577
 C -2.350398 -2.337885 -3.461572
 F -1.994644 -3.586542 -3.203714
 F -2.123115 -2.086277 -4.744668
 F -3.660419 -2.262569 -3.254875
 C -2.301220 0.079494 -2.646686
 F -2.308151 0.572710 -3.874807
 F -1.683322 0.942933 -1.831826
 F -3.553032 0.003119 -2.222344
 C 0.682579 -2.644780 -2.896612
 F 1.991534 -2.557781 -2.708829
 F 0.469146 -3.148992 -4.104259
 F 0.227252 -3.495762 -1.976011
 C 0.536701 -0.274842 -3.822234
 F 1.851588 -0.390661 -3.961470
 F 0.287364 0.989445 -3.516241

 Calculated energies and coordinates of INT_A_Ge at PBE0-D4(CPCM=DCM)/def2-TZVP level of theory

Electronic energy ... -5757.09570753 Eh
 Total Enthalpy ... -5756.67461003 Eh
 Final Gibbs free energy ... -5756.79886433 Eh

CARTESIAN COORDINATES (ANGSTROEM)

Ge 0.015597 -0.722304 -0.120794
 O -1.398932 -0.591784 -1.236586
 O 0.992150 -1.313797 -1.572943
 O 0.435506 -2.208049 0.821362
 O -0.881873 -0.150836 1.388464
 C -1.133817 -0.850896 -2.567280
 C 0.201547 -1.771123 -2.597805
 C -2.435656 -1.462824 -3.184545
 F -2.861678 -2.516250 -2.504908
 F -2.257832 -1.825779 -4.451639
 F -3.421693 -0.567307 -3.157510
 C -0.908000 0.551005 -3.235284
 F -0.836315 0.494030 -4.560540
 F 0.214843 1.102301 -2.773441
 F -1.888706 1.388851 -2.917890
 C -0.100244 -3.290898 -2.304331
 F 1.021446 -3.934174 -1.999098
 F -0.660089 -3.911743 -3.342168
 F -0.902102 -3.422906 -1.253107
 C 1.054579 -1.719905 -3.911958
 F 2.034386 -2.620955 -3.863006
 F 1.634999 -0.539605 -4.078967
 F 0.325333 -1.983707 -4.992301
 C 0.089007 -2.209552 2.151924

C -1.123728 -1.134966 2.312945
 C -0.240514 -3.686801 2.552149
 F -1.159946 -4.219955 1.761244
 F -0.669812 -3.763592 3.809355
 F 0.838902 -4.458989 2.450054
 C 1.406515 -1.787273 2.893455
 F 1.321262 -1.858735 4.216723
 F 1.737390 -0.542088 2.543364
 F 2.422233 -2.553919 2.514036
 C -2.535497 -1.727517 1.941977
 F -2.483485 -2.331113 0.757603
 F -3.425688 -0.747307 1.819988
 F -3.003750 -2.588491 2.841968
 C -1.248282 -0.449745 3.714915
 F -2.280378 0.390332 3.733931
 F -0.176230 0.272925 4.015229
 F -1.431643 -1.340197 4.685551
 Si 1.204626 2.395770 0.280904
 C 1.195665 2.505449 2.128245
 C -0.211393 3.273932 -0.525560
 C 2.878649 2.508716 -0.502110
 H 0.273706 2.063394 2.505875
 C 1.293524 3.975865 2.562824
 H 2.026415 1.927345 2.537403
 H 0.440275 4.559275 2.209991
 H 2.203857 4.454342 2.194018
 H 1.306619 4.037495 3.652989
 C -1.600713 2.996212 0.041489
 H -0.176679 3.144937 -1.607248
 H 0.060544 4.327476 -0.349652
 H -1.920453 1.972162 -0.156193
 H -2.335329 3.664153 -0.412627
 H -1.633972 3.150272 1.122025
 H 3.524155 1.778853 -0.002759
 H 3.231660 3.493570 -0.157717
 C 2.982243 2.404950 -2.018187
 H 2.740156 1.399024 -2.362657
 H 3.998678 2.632915 -2.345474
 H 2.308078 3.102896 -2.518728
 H 0.909681 0.663844 -0.048971

 Calculated energies and coordinates of TS(INT_A_3*_{Ge}) at
 PBE0-D4(CPCM=DCM)/def2-TZVP level of theory

Electronic energy ... -5757.08459280 Eh
 Total Enthalpy ... -5756.66407390 Eh
 Final Gibbs free energy ... -5756.78714612 Eh

CARTESIAN COORDINATES (ANGSTROEM)

Ge 0.265890 -0.756781 -0.339418
 O -1.235576 -0.560912 -1.340652
 O 1.018782 -1.580589 -1.826779
 O 0.462542 -2.263455 0.640955
 O -0.487279 -0.020863 1.256706
 C -1.107212 -0.881543 -2.675411
 C 0.121138 -1.945845 -2.787803
 C -2.511172 -1.364632 -3.170540
 F -2.976477 -2.380548 -2.459740
 F -2.475054 -1.733341 -4.448898
 F -3.411113 -0.387605 -3.057971
 C -0.788653 0.471420 -3.406030
 F -0.779158 0.374684 -4.730379
 F 0.396169 0.939913 -3.005079
 F -1.680929 1.404272 -3.080820
 C -0.314889 -3.423424 -2.462981
 F 0.755957 -4.177252 -2.227850
 F -0.998824 -3.991265 -3.458712
 F -1.052057 -3.474272 -1.359440
 C 0.890470 -1.979548 -4.155193
 F 1.787089 -2.966183 -4.159688
 F 1.571808 -0.859892 -4.365894
 F 0.080996 -2.175825 -5.193622
 C 0.234202 -2.177195 1.990200
 C -0.816842 -0.954973 2.206924
 C -0.231846 -3.596096 2.458366

F -1.277477 -4.020838 1.763728
 F -0.551047 -3.617787 3.749495
 F 0.737249 -4.491334 2.272876
 C 1.648904 -1.899470 2.617680
 F 1.669373 -1.985273 3.943667
 F 2.084999 -0.687138 2.256421
 F 2.542976 -2.761034 2.144400
 C -2.310913 -1.360394 1.922291
 F -2.417712 -2.006373 0.768087
 F -3.064061 -0.267605 1.813385
 F -2.839771 -2.116304 2.883673
 C -0.786982 -0.297834 3.625986
 F -1.716264 0.653894 3.727230
 F 0.377875 0.283505 3.879098
 F -1.015220 -1.181926 4.591928
 Si 0.959383 2.367195 0.761840
 C 0.738699 2.832968 2.528199
 C -0.362605 2.923604 -0.387419
 C 2.720677 2.377399 0.200139
 H -0.245511 2.539716 2.889903
 C 0.881907 4.367123 2.579788
 H 1.493724 2.355697 3.153293
 H 0.121537 4.870243 1.978166
 H 1.863789 4.705288 2.241541
 H 0.757504 4.700572 3.611981
 C -1.801720 2.845643 0.106050
 H -0.233491 2.469751 -1.368326
 H -0.060638 3.977467 -0.526365
 H -2.127096 1.811037 0.211352
 H -2.467123 3.340955 -0.603245
 H -1.922045 3.335378 1.074447
 H 3.265186 1.622120 0.777090
 H 3.071950 3.344041 0.595759
 C 3.007234 2.271595 -1.290215
 H 2.744564 1.286926 -1.681255
 H 4.071260 2.425097 -1.479451
 H 2.454416 3.018502 -1.863086
 H 1.268505 0.429344 -0.310383

 Calculated Energies and Coordinates TS(1_INT_A_SI) at PBE0-
 D4(CPCM=DCM)/def2-TZVP level of theory

Electronic energy ... -3969.80591658 Eh
 Total Enthalpy ... -3969.38299325 Eh
 Final Gibbs free energy ... -3969.50463621 Eh

CARTESIAN COORDINATES (ANGSTROEM)

Si -0.488255 -1.038130 -0.110509
 O -1.777341 -1.420063 -1.084116
 O 0.519356 -0.757576 -1.409744
 O 0.249532 -2.263897 0.722447
 O -1.247174 -0.433298 1.247001
 C -1.574941 -1.204818 -2.437453
 C 0.024802 -1.263665 -2.611367
 C -2.418798 -2.251351 -3.238079
 F -2.188729 -3.488485 -2.826741
 F -2.153629 -2.177139 -4.537683
 F -3.717640 -2.028566 -3.072535
 C -2.176679 0.223644 -2.693736
 F -2.166915 0.566237 -3.973412
 F -1.485332 1.122506 -1.993329
 F -3.424228 0.293542 -2.253241
 C 0.590241 -2.727516 -2.708403
 F 1.903484 -2.726126 -2.524113
 F 0.332506 -3.288694 -3.882390
 F 0.076678 -3.483955 -1.742486
 C 0.636630 -0.426995 -3.783686
 F 1.941355 -0.648185 -3.893127
 F 0.480976 0.872519 -3.584752
 F 0.073067 -0.751707 -4.941645
 C 0.040283 -2.256574 2.094849
 C -1.284437 -1.345658 2.299107
 C -0.044122 -3.740534 2.592818
 F -0.909931 -4.450603 1.888612

11. Appendix – Dissertation Florian Tschernuth

```

F -0.394255 -3.781478 3.873597
F 1.129875 -4.349270 2.471967
C 1.348229 -1.619569 2.692564
F 1.358311 -1.630650 4.018667
F 1.476025 -0.365784 2.265364
F 2.423427 -2.265790 2.264326
C -2.634830 -2.141588 2.118045
F -2.599318 -2.870866 1.007732
F -3.648923 -1.298605 1.978688
F -2.895050 -2.937045 3.147771
C -1.386742 -0.537126 3.635116
F -2.539572 0.120813 3.694955
F -0.426739 0.366702 3.743578
F -1.323402 -1.351601 4.682316
Si 1.168159 2.185825 0.333294
C 0.908528 2.829437 2.073744
C 0.477162 3.376507 -0.935878
C 2.970019 1.776083 0.034033
H -0.165748 2.869690 2.279604
C 1.542416 4.205433 2.284482
H 1.329313 2.111797 2.782282
H 1.126472 4.952605 1.603819
H 2.622708 4.179640 2.120213
H 1.375979 4.563229 3.303852
C -0.904988 3.929456 -0.595970
H 0.471876 2.890836 -1.915183
H 1.201384 4.197060 -1.015447
H -1.639066 3.132099 -0.460578
H -1.276235 4.585792 -1.387346
H -0.884346 4.510678 0.328848
H 3.285228 1.052911 0.793439
H 3.514901 2.701271 0.262742
C 3.342562 1.284249 -1.360086
H 2.889659 0.315155 -1.570953
H 4.425086 1.172097 -1.462814
H 3.010024 1.978609 -2.135685
H 0.355980 0.887426 0.210418

```

```

C 1.397928 -1.808350 2.801129
F 1.328162 -1.897631 4.122945
F 1.764150 -0.571360 2.464684
F 2.379977 -2.602725 2.392537
C -2.563543 -1.647292 1.912099
F -2.560507 -2.254555 0.730595
F -3.423822 -0.639024 1.809488
F -3.032061 -2.490614 2.827632
C -1.213297 -0.402175 3.654750
F -2.213369 0.473712 3.690588
F -0.113127 0.275520 3.951134
F -1.417064 -1.298808 4.616422
Si 1.132367 2.286525 0.268273
C 1.147768 2.473221 2.111764
C -0.248935 3.241036 -0.520465
C 2.820349 2.405439 -0.491148
H 0.195637 2.130311 2.515291
C 1.373304 3.944347 2.482577
H 1.928788 1.847813 2.547029
H 0.576872 4.586565 2.099888
H 2.323336 4.324808 2.099664
H 1.389173 4.056046 3.569010
C -1.640834 3.002515 0.058438
H -0.236112 3.119126 -1.602846
H 0.057444 4.282536 -0.340473
H -1.985244 1.984187 -0.126032
H -2.364599 3.683283 -0.394697
H -1.662034 3.167032 1.137869
H 3.451595 1.662489 0.008169
H 3.182637 3.381738 -0.137678
C 2.943387 2.308003 -2.005649
H 2.689178 1.308683 -2.358506
H 3.966900 2.521593 -2.321331
H 2.285739 3.018307 -2.511169
H 0.801752 0.676186 -0.038931

```

Calculated energies and coordinates of INT_A_Si at PBE0-D4(CPCM=DCM)/def2-TZVP level of theory

```

Electronic energy ... -3969.80988667 Eh
Total Enthalpy ... -3969.38569342 Eh
Final Gibbs free energy ... -3969.50849320 Eh

```

CARTESIAN COORDINATES (ANGSTROEM)

```

Si -0.049211 -0.716556 -0.107526
O -1.363990 -0.588310 -1.141505
O 0.947879 -1.166112 -1.437573
O 0.376994 -2.107496 0.735100
O -0.856516 -0.141775 1.297133
C -1.136561 -0.855399 -2.482093
C 0.241958 -1.695020 -2.495914
C -2.413801 -1.544256 -3.078750
F -2.880919 -2.498511 -2.291761
F -2.159561 -2.068202 -4.274177
F -3.400969 -0.662594 -3.232810
C -0.991580 0.542343 -3.176315
F -0.980883 0.449260 -4.502169
F 0.129229 1.143581 -2.786464
F -1.986225 1.348207 -2.825924
C 0.045013 -3.237534 -2.212367
F 1.185936 -3.766846 -1.787788
F -0.341930 -3.903030 -3.299598
F -0.851099 -3.452899 -1.257802
C 1.125370 -1.605322 -3.789641
F 2.119427 -2.490324 -3.730242
F 1.687076 -0.415477 -3.937182
F 0.418352 -1.870487 -4.883974
C 0.055311 -2.180091 2.072753
C -1.127673 -1.094417 2.254850
C -0.283053 -3.664891 2.430289
F -1.270366 -4.151424 1.694896
F -0.621661 -3.770702 3.713529
F 0.766435 -4.453265 2.217768

```

Calculated energies and coordinates of TS(INT_A_3*_Si) at PBE0-D4(CPCM=DCM)/def2-TZVP level of theory

```

Electronic energy ... -3969.79415802 Eh
Total Enthalpy ... -3969.37080317 Eh
Final Gibbs free energy ... -3969.49109157 Eh

```

CARTESIAN COORDINATES (ANGSTROEM)

```

Si 0.247401 -0.734093 -0.346059
O -1.158133 -0.502826 -1.251995
O 0.997394 -1.464050 -1.730886
O 0.485499 -2.128988 0.561835
O -0.400078 0.017716 1.169952
C -1.101288 -0.841283 -2.592624
C 0.134108 -1.882255 -2.706634
C -2.511962 -1.355414 -3.040317
F -2.980367 -2.305503 -2.247408
F -2.465905 -1.830059 -4.283239
F -3.412996 -0.374486 -3.017395
C -0.825653 0.501645 -3.356974
F -0.868688 0.363263 -4.677437
F 0.366132 0.992782 -3.019646
F -1.717300 1.428422 -3.017859
C -0.267278 -3.371218 -2.371763
F 0.819251 -4.090774 -2.108004
F -0.917785 -3.963550 -3.374725
F -1.027444 -3.436851 -1.286561
C 0.915969 -1.919942 -4.067219
F 1.826696 -2.892938 -4.050462
F 1.580033 -0.794903 -4.294366
F 0.111461 -2.144876 -5.103112
C 0.254993 -2.118174 1.914868
C -0.765783 -0.890982 2.150469
C -0.237498 -3.546049 2.328654
F -1.298757 -3.922624 1.632003
F -0.544339 -3.602925 3.621306
F 0.710373 -4.451772 2.100318
C 1.678414 -1.893511 2.547791
F 1.694242 -2.026084 3.868839

```

11. Appendix – Dissertation Florian Tschernuth

```

F 2.140594 -0.681280 2.226821
F 2.548527 -2.760077 2.043272
C -2.277712 -1.245720 1.877982
F -2.425954 -1.892541 0.732005
F -2.987621 -0.125178 1.776544
F -2.815998 -1.979900 2.849433
C -0.712168 -0.261323 3.580561
F -1.620525 0.703718 3.715466
F 0.467283 0.277754 3.848267
F -0.955571 -1.175094 4.514107
Si 0.888703 2.179435 0.762564
C 0.673695 2.761607 2.505810
C -0.370678 2.869699 -0.391880
C 2.676305 2.231725 0.263019
H -0.300699 2.488523 2.904486
C 0.807772 4.294495 2.485662
H 1.440608 2.327069 3.147115
H 0.009651 4.766069 1.909213
H 1.764108 4.628584 2.076710
H 0.742449 4.671624 3.508502
C -1.832886 2.764520 0.020649
H -0.200608 2.515932 -1.405737
H -0.054498 3.926750 -0.402928
H -2.180878 1.733902 -0.031697
H -2.456318 3.367190 -0.642659
H -1.991308 3.120610 1.040947
H 3.208733 1.459451 0.828013
H 3.014523 3.186872 0.690573
C 3.001206 2.164026 -1.221293
H 2.724409 1.199051 -1.650345
H 4.073032 2.298053 -1.381053
H 2.480639 2.941714 -1.783921
H 1.200470 0.425046 -0.347560

```

Calculated energies and coordinates of Et₃SiH at PBE0-D4(CPCM=DCM)/def2-TZVP level of theory

```

Electronic energy ... -527.47794089 Eh
Total Enthalpy ... -527.26095375 Eh
Final Gibbs free energy ... -527.30955265 Eh

```

CARTESIAN COORDINATES (ANGSTROEM)

```

Si -8.707706 2.248089 0.288698
C -7.234249 3.042892 -0.567388
C -8.214948 1.534636 1.957132
C -9.481178 0.928363 -0.804467
H -6.778513 3.754545 0.130201
H -6.481327 2.263204 -0.735862
C -7.574093 3.742204 -1.881307
H -6.691688 4.202032 -2.335238
H -8.314517 4.533037 -1.730941
H -7.990147 3.043610 -2.611965
C -7.632872 2.554894 2.932329
H -7.495592 0.726216 1.777728
H -9.098530 1.056767 2.395249
H -6.718508 3.007973 2.540457
H -7.384981 2.099172 3.895122
H -8.339662 3.366803 3.125920
H -8.723534 0.156064 -0.985384
H -9.689126 1.378868 -1.781717
C -10.751932 0.300611 -0.238168
H -11.523184 1.055987 -0.062494
H -11.173081 -0.445101 -0.918449
H -10.563209 -0.197908 0.716313
H -9.735931 3.317661 0.523044

```

Calculated energies and coordinates of Et₃SiH at PBE0-D4(CPCM=acetonitrile)/def2-TZVP level of theory

```

Electronic energy ... -527.47814599 Eh
Total Enthalpy ... -527.26125033 Eh
Final Gibbs free energy ... -527.30985532 Eh

```

CARTESIAN COORDINATES (ANGSTROEM)

```

Si -8.705984 2.246198 0.288291
C -7.233612 3.041709 -0.568696
C -8.213177 1.534256 1.957173
C -9.480123 0.926167 -0.803774
H -6.775647 3.751207 0.129647
H -6.482312 2.261104 -0.740176
C -7.575179 3.744009 -1.880642
H -6.692733 4.202391 -2.336049
H -8.313209 4.536525 -1.727056
H -7.994939 3.047543 -2.611248
C -7.633971 2.555687 2.932901
H -7.491701 0.727750 1.777621
H -9.095948 1.054043 2.394402
H -6.720985 3.011617 2.541076
H -7.384746 2.099998 3.895411
H -8.343130 3.365451 3.127080
H -8.723292 0.152198 -0.980955
H -9.684893 1.375018 -1.782474
C -10.753206 0.301930 -0.238694
H -11.523931 1.058924 -0.067434
H -11.173571 -0.445366 -0.917789
H -10.567447 -0.193723 0.717884
H -9.734776 3.315984 0.522312

```

Calculated energies and coordinates of [MeCN→Et₃Si]⁺ at PBE0-D4(CPCM=DCM)/def2-TZVP level of theory

```

Electronic energy ... -659.40109109 Eh
Total Enthalpy ... -659.13947027 Eh
Final Gibbs free energy ... -659.19731608 Eh

```

CARTESIAN COORDINATES (ANGSTROEM)

```

Si 0.460150 -0.004765 -0.256712
N -1.326818 -0.011546 0.157921
C -2.442228 -0.001290 0.413515
C -3.835502 0.009823 0.728861
H -4.307075 -0.869231 0.283155
H -3.956399 -0.012221 1.814355
H -4.283987 0.919272 0.321982
C 1.269931 -0.002775 1.416255
H 0.920556 0.872123 1.973742
H 0.930178 -0.882928 1.971409
C 2.795756 0.005743 1.300513
H 3.163003 -0.873462 0.765121
H 3.153344 0.890448 0.767659
H 3.259872 0.006894 2.288959
C 0.680698 -1.562988 -1.243136
H 0.056185 -1.484831 -2.139636
H 1.717988 -1.551279 -1.600171
C 0.665964 1.558121 -1.239213
H 1.703180 1.556309 -1.596714
H 0.041710 1.476610 -2.135582
C 0.366834 2.846119 -0.476553
H 1.018872 2.956287 0.392896
H 0.516337 3.720020 -1.114222
H -0.666258 2.872127 -0.120854
C 0.392369 -2.855440 -0.483781
H 0.549110 -3.726415 -1.123720
H 1.045363 -2.962482 0.385348
H -0.640438 -2.890908 -0.128084

```

Calculated energies and coordinates of [MeCN→Et₃Si]⁺ at PBE0-D4(CPCM=acetonitrile)/def2-TZVP level of theory

```

Electronic energy ... -659.40790905 Eh
Total Enthalpy ... -659.14636791 Eh
Final Gibbs free energy ... -659.20410583 Eh

```

CARTESIAN COORDINATES (ANGSTROEM)

```

Si 0.458256 -0.005492 -0.255322
N -1.325307 -0.013063 0.158303
C -2.441073 -0.001210 0.412641
C -3.834217 0.011886 0.725905
H -4.305439 -0.867059 0.279545

```


H -3.955827 -0.009453 1.811347
H -4.279983 0.922037 0.317524
C 1.271738 -0.003308 1.415868
H 0.922202 0.871373 1.973642
H 0.932977 -0.883905 1.970969
C 2.797297 0.006246 1.297604
H 3.163720 -0.872591 0.760862
H 3.152884 0.891277 0.763771
H 3.263658 0.007522 2.285177
C 0.681784 -1.563190 -1.241876
H 0.057099 -1.484219 -2.138238
H 1.719546 -1.551847 -1.597430
C 0.665545 1.557354 -1.237539
H 1.703122 1.556661 -1.593894
H 0.040889 1.474853 -2.133585
C 0.363551 2.844446 -0.474179
H 1.015118 2.954767 0.395708
H 0.511346 3.719301 -1.111217
H -0.669702 2.867108 -0.118679
C 0.391136 -2.851511 -0.482263
H 0.546776 -3.726842 -1.121775
H 1.043517 -2.962253 0.387424
H -0.641918 -2.887914 -0.126980

Calculated energies and coordinates of Me₃SiH at PBE0-D3/def2-TZVPP

Electronic energy ... -409.65093967 Eh
Total Enthalpy ... -409.52383724 Eh
Final Gibbs free energy ... -409.56248516 Eh

CARTESIAN COORDINATES (ANGSTROEM)

Si 0.000000 -0.000691 -0.369206
H -0.000000 0.000800 -1.863390
C 1.538522 -0.887019 0.228598
H 1.559308 -1.922108 -0.118581
H 2.443485 -0.394280 -0.132867
H 1.577937 -0.899397 1.320733
C -1.538521 -0.887019 0.228598
H -1.577931 -0.899408 1.320733
H -2.443485 -0.394274 -0.132857
H -1.559312 -1.922105 -0.118591
C -0.000001 1.773125 0.232764
H 0.882553 2.310460 -0.120600
H -0.882548 2.310462 -0.120610
H -0.000007 1.811454 1.324998

Calculated energies and coordinates of Me₃SiF at PBE0-D3/def2-TZVPP

Electronic energy -508.92439829 Eh
Total Enthalpy -508.80180456 Eh
Final Gibbs free energy -508.84275550 Eh

CARTESIAN COORDINATES (ANGSTROEM)

Si 0.000000 -0.000696 0.011616
C -0.000000 1.773410 0.570554
H 0.883505 2.301611 0.205969
H -0.883510 2.301607 0.205976
H 0.000004 1.834268 1.661777
C 1.538663 -0.887273 0.566638
H 1.597062 -0.911164 1.657753
H 1.551666 -1.918631 0.208160
H 2.436166 -0.388781 0.194594
C -1.538663 -0.887271 0.566638
H -2.436166 -0.388785 0.194586
H -1.551663 -1.918633 0.208170
H -1.597067 -0.911152 1.657753
F 0.000002 0.001490 -1.601685

Calculated energies and coordinates of Me₃Si⁺ at PBE0-D3/def2-TZVPP

Electronic energy ... -408.77063889 Eh
Total Enthalpy ... -408.65298264 Eh
Final Gibbs free energy ... -408.69323035 Eh

CARTESIAN COORDINATES (ANGSTROEM)

Si 0.000200 0.000381 0.272820
C 1.574957 -0.916094 0.281046
H 1.439742 -1.996915 0.274653
H 2.175624 -0.617559 -0.585751
H 2.155888 -0.627777 1.165098
C -1.580645 -0.905301 0.273412
H -1.611589 -1.585573 1.132088
H -2.449608 -0.249031 0.296212
H -1.629843 -1.542176 -0.617923
C 0.005615 1.821875 0.265349
H 1.008367 2.246538 0.241903
H -0.566142 2.184442 -0.596527
H -0.523065 2.187182 1.153771

Calculated energies and coordinates of C₆H₅C(CH₃)-CH₂ at PBE0-D4(CPCM=DCM)/def2-TZVP level of theory

Electronic energy ... -348.67930941 Eh
Total Enthalpy ... -348.50860159 Eh
Final Gibbs free energy ... -348.54980691 Eh

CARTESIAN COORDINATES (ANGSTROEM)

C 6.998511 16.657443 6.464318
C 7.913759 16.576471 7.433194
H 6.216591 17.407760 6.471157
H 7.020327 15.974182 5.622694
C 7.890974 17.488014 8.598196
C 9.018971 15.566769 7.361350
H 8.867195 14.890013 6.520245
H 9.079810 14.978865 8.281646
H 9.991156 16.051540 7.230792
C 9.063480 17.794202 9.292346
C 9.050895 18.669607 10.368739
C 7.861547 19.247035 10.787087
C 6.682861 18.935937 10.120359
C 6.698257 18.065447 9.044164
H 10.004231 17.355815 8.981934
H 9.977320 18.898231 10.883924
H 7.849545 19.926428 11.631853
H 5.743009 19.365998 10.448538
H 5.766502 17.813432 8.551203

Calculated energies and coordinates of PhC(H)(CH₃)-CH₂SiEt₂ at PBE0-D4(CPCM=DCM)/def2-TZVP level of theory

Electronic energy ... -876.20163736 Eh
Total Enthalpy ... -875.80789303 Eh
Final Gibbs free energy ... -875.87394682 Eh

CARTESIAN COORDINATES (ANGSTROEM)

C 0.578366 0.739710 0.902179
C 1.001924 1.758990 -0.169543
C 1.631291 -0.317752 1.149736
C 0.084642 1.422733 2.166978
Si 2.588710 2.794035 -0.072762
H 1.074609 1.248644 -1.137927
H 0.179895 2.476196 -0.291050
C 2.047904 -1.128038 0.092161
C 2.192218 -0.546150 2.402644
H -0.323508 0.699242 2.876967
H -0.707843 2.131387 1.917338
H 0.877713 1.977183 2.671943
C 2.367192 4.129177 -1.389758
C 2.860697 3.642511 1.587905
C 4.143949 1.822839 -0.536017
C 2.992522 -2.123665 0.276013
H 1.619812 -0.976626 -0.893591
C 3.138005 -1.547179 2.594987
H 1.893596 0.060799 3.248469

H	1.476301	4.718511	-1.144162
C	2.264657	3.600646	-2.818430
H	3.216923	4.818239	-1.306303
C	1.823262	4.700807	1.952759
H	3.857931	4.098556	1.547548
H	2.920104	2.878336	2.370816
H	4.792079	2.536443	-1.060999
H	3.869118	1.068464	-1.281752
C	4.921673	1.172803	0.603067
C	3.544052	-2.339486	1.533605
H	3.297796	-2.738225	-0.563938
H	3.559303	-1.702928	3.582245
H	1.400500	2.942095	-2.940853
H	3.151864	3.024885	-3.096363
H	2.161272	4.410677	-3.546513
H	1.815498	5.516065	1.224960
H	2.021054	5.141478	2.934314
H	0.813227	4.284180	1.980936
H	4.323776	0.419035	1.116737
H	5.227930	1.911892	1.348222
H	5.829632	0.681777	0.239894
H	4.282778	-3.119183	1.681248
H	-0.284051	0.201365	0.485229

Calculated energies and coordinates of B(C ₆ F ₅) ₃ at PBE0-D4(CPCM=benzene)/def2-TZVP level of theory			
Electronic energy	...	-2207.04435998 Eh	
Total Enthalpy	...	-2206.85835763 Eh	
Final Gibbs free energy	...	-2206.94390926 Eh	

CARTESIAN COORDINATES (ANGSTROEM)			
B	3.092101	5.834674	1.723721
N	1.882290	6.397605	2.558964
F	3.314507	4.210446	-0.798340
F	2.731055	1.647022	-1.030344
F	1.882808	0.217796	1.110638
F	1.629577	1.437419	3.523425
F	2.221437	4.014866	3.791249
F	5.423893	7.078766	0.300452
F	5.290098	8.522426	-1.907097
F	2.914888	8.949322	-3.141208
F	0.649986	7.870640	-2.102996
F	0.754306	6.404690	0.109553
F	5.351083	3.949983	2.371676
F	7.411323	4.501093	3.927466
F	7.675830	6.945923	5.064561
F	5.796179	8.850334	4.605578
F	3.714403	8.329652	3.037772
C	1.010496	6.816180	3.160322
C	-0.089674	7.344249	3.915723
C	2.749907	4.259785	1.503416
C	2.877092	3.587602	0.297464
C	2.590886	2.239797	0.148951
C	2.160721	1.506059	1.237653
C	2.029744	2.131587	2.464177
C	2.329851	3.476083	2.569064
C	3.084156	6.710628	0.351989
C	4.214226	7.264039	-0.230538
C	4.176150	8.013486	-1.395309
C	2.968651	8.230441	-2.030843
C	1.816724	7.682711	-1.496781
C	1.900483	6.937682	-0.336040
C	4.395577	6.100085	2.662379
C	5.390103	5.167559	2.915838
C	6.489871	5.432855	3.716345
C	6.630733	6.678301	4.297219
C	5.669867	7.644818	4.062958
C	4.590989	7.339566	3.255669
H	-0.369086	6.630090	4.692483
H	-0.936271	7.512118	3.247261
H	0.209941	8.288722	4.373934

Calculated energies and coordinates of MeCN-B(C ₆ F ₅) ₃ at PBE0-D4(CPCM=benzene)/def2-TZVP level of theory			
Electronic energy	...	-2339.72502805 Eh	
Total Enthalpy	...	-2339.48685703 Eh	
Final Gibbs free energy	...	-2339.58041533 Eh	

11.5 Licenses for the reprint of publications

The three published articles in this cumulative dissertation are available open access with the following license agreement:

“This is an open access article under the terms of the [Creative Commons Attribution-NonCommercial](#) License, which permits use, distribution and reproduction in any medium, provided the original work is properly cited and is not used for commercial purposes.”

This involves the following publications:

- “Bis(perfluoropinacolato)silane: A Neutral Silane Lewis Superacid Activates Si–F Bonds” by F. S. Tschernuth, T. Thorwart, L. Greb, F. Hanusch and S. Inoue *Angew. Chem. Int. Ed.* **2021**, 60, 25799–25803.
<https://doi.org/10.1002/anie.202110980>
- “Catalytic Degradation of Aliphatic Ethers using the Lewis Superacidic Bis(perfluoropinacolato)silane” by F. S. Tschernuth, L. Bichlmaier and S. Inoue *ChemCatChem* **2023**, 15, e202300281.
<https://doi.org/10.1002/cctc.202300281>
- “Tuning the Lewis Acidity of neutral Silanes using perfluorinated Aryl- and Alkoxy Substituents” by F. S. Tschernuth, L. Bichlmaier, S. Stigler and S. Inoue *Eur. J. Inorg. Chem.* **2023**, e202300388
<https://doi.org/10.1002/ejic.202300388>

The following article was published as an Accepted Manuscript in the Journal *Dalton Transactions* (RSC) on the 14th November 2023. The license agreement permits the use of the article within academic purposes such as dissertations:

“Use in submissions of grant applications, or academic requirements such as theses or dissertations*”; *You may include your article in the electronic version of your thesis or dissertation as long as it is not made available as a separate document.” Available under:

<https://www.rsc.org/journals-books-databases/author-and-reviewer-hub/authors-information/licences-copyright-permissions/> (19.11.2023)

- “A Neutral Germanium-centered Hard and Soft Lewis Superacid and its Unique Reactivity towards Hydrosilanes” by F. S. Tschernuth, A. Kostenko, S. Stigler, A. Gradenegger and S. Inoue

Dalton Trans. **2023**, Accepted Manuscript

DOI: 10.1039/D3DT03626J